ENGINEERING ELECTRONIC DIVERSITY AND SYNTHETIC VERSATILITY INTO BOREPIN-BASED PI-CONJUGATED ORGANOBORON MATERIALS

by
David Robert Levine

A dissertation submitted to the Johns Hopkins University in conformity with the requirements for the degree of Doctor of Philosophy

Baltimore, Maryland
March, 2016

Abstract

Embedding tricoordinate boron atoms within carbon-based π-conjugated networks has emerged as a powerful strategy for property-tuning owing to the characteristic electron-deficient properties associated with the vacant p_z-orbital of boron. The borepin ring – a formally Hückel-aromatic 6π-electron heterocycle – has recently begun to be reinvestigated as a promising architectural motif to install boron functionality into extended, synthetically modifiable ladder-type polycyclic π-electron systems. However, a thorough elucidation of structure-property relationships in borepin-based materials and the development of robust synthetic methods to access a wider variety of such materials is an area requiring further work. This dissertation presents the synthesis, characterization, and further functionalization of novel polycyclic aromatics featuring benzo- and thieno-fused borepin rings.

To orient the reader, Chapter 1 features a brief introduction to the field of boron-containing polycyclic aromatic materials.

Chapter 2 describes the synthesis of parent and functionalized analogues of the "*meta-B*-entacene" scaffold, a pentacyclic ladder-type structure containing two fused borepin rings. The work provides insight into the electronic impact of positing two boron atoms within a rigid, polycyclic array in a *meta*-arrangement, leading to narrowed optical bandgaps and more difficult electrochemical reductions than for the isomeric *para-B*-entacene.

Chapter 3 describes the synthesis and characterization of a series of isomeric dithieno[*b*,*f*]borepins (DTBs), wherein the flanking thiophene rings are fused to the central borepin in different orientations. These studies feature a new, scalable synthetic

approach to construct borepin rings, relying on direct condensation of dimetalated intermediates with a mesityl boronic ester instead of traditional tin-boron exchange chemistry. Theoretical, structural, electronic, and redox analyses demonstrated DTBs possess several desirable properties of typical π-conjugated organoboranes and that the conjugation pattern of each isomer influenced molecular properties.

Chapter 4 details the investigation of the chemical reactivity of DTBs introduced in Chapter 3 and the development of synthetic methods for late-stage functionalization and property-tuning. Cross-coupling of synthetically primed DTBs led to a series of π-extended derivatives with diverse properties (including highly polarizable electronic structures and multi-electron accepting capacity), which could be tuned based upon the electronics of the appended substituent and the conjugation pattern of the DTB backbone.

Chapter 5 describes studies of other thiophene-annulated borepins wherein the borepin ring lacks a formally Hückel-aromatic π-electron arrangement. This includes the synthesis and characterization of a stable trithieno[*b,d,f*]borepin (TTB) and preliminary efforts to access DTBs with a quinoidal π-electron structure.

Chapter 6 describes early stage efforts to construct extended ladder-type thiophene-fused borepin arrays featuring thiophene rings. Suggestions for future directions in borepin-based materials research are provided.

Research Advisor:

John D. Tovar

Dissertation Readers:

Marc M. Greenberg and John P. Toscano

Acknowledgments

This dissertation is the result of the contributions of many individuals. The lion's share of thanks is owed to my advisor Professor John D. Tovar, who has given me the opportunity and resources to pursue a truly interesting and multifaceted research project dealing with several aspects of fundamental and applied organic materials chemistry. J. D. has provided me freedom to explore whichever avenues of research I felt were the most promising and impactful while giving key guidance and mentorship at the appropriate times. This balanced approach has fostered in me both the independent spirit and knowledge necessary to successfully conduct original research – for that I am very grateful. J. D. has also provided financial support to enable me to travel and present work at conferences in locations ranging from Newark, N. J. to Taipei, Taiwan(!); such rare opportunities are evidence of his firm commitment to the professional and intellectual development of his group members. In addition to J. D., I would also like to thank my other readers, Professors Marc M. Greenberg and John P. Toscano, for their advice throughout the Ph.D. process and during the preparation of this document.

The Tovar group has always featured a highly colorful cast of characters – both the scientific discussions and irrevent banter will be missed. I thank those members that I have had the privilege of overlapping with: Dr. Christopher Harvey, Dr. Anthony Caruso Jr., Dr. Stephen Diegelmann, Dr. Alicia Fraind, Dr. Brian Wall, Dr. Benjamin Streifel, Dr. Allix Sanders, Herdeline Ardona ("Digs"), Justin DeFrancisco, Reid Messersmith, Garvin Peters, Dr. Tejaswini Kale, and Dr. Wathsala Liyanage. I give special thanks to Anthony for his mentorship during my early days on the borepin project and for providing a solid foundation of work for me to build upon; to Brian for his genuine enthusiasm toward discussing research problems and brainstorming solutions, no matter how far removed from his own area of interest; to Digs for being reliable lab company when working the "night shift" and for her incredible good nature; and to Reid for being a near ideal labmate to share a project and a workspace with. I also wish to thank JHU undergraduate researchers Christie Checketts and Tiffani Chance, who assisted me with aspects of the synthesis and characterization for the work in Chapters 2 and 4.

This research could not have been done without the staff members of the JHU chemistry department. My gratitude goes to Dr. Maxime Siegler for the collection and refinement of several single crystal X-ray structures presented herein, to Dr. Cathy Moore and Dr. Joel Tang for their NMR support and expertise, to Dr. Phil Mortimer for the collection of high resolution mass spectral data on the many compounds I have prepared, and to facilities manager Boris Steinberg for unfailingly keeping our laboratories functioning properly, often going the extra mile to see emergent issues resolved swiftly. I also thank departmental administrative assistants Jean Goodwin, Lauren McGhee, and Rosalie Elder for always keeping me informed and on task with respect to the requirements necessary for fulfillment of the degree.

The importance of a strong personal support system cannot be overstated, and I am extremely grateful to all the family and friends who have been there for me throughout this journey. Words are not sufficient to express the particular thanks to which I owe my parents and sister, Dr. Stephen, Jeanne, and Valerie Levine, who have supported me in myriad ways through the years, not least of which when I was deciding to take the leap and return to pursue graduate studies after several years removed from the academic sphere.

Finally, I would like to thank my undergraduate advisor Professor Christopher J. Smart (Vassar College), without whose engaging lectures, good humor, and infectious enthusiasm for chemistry many years ago I would likely not be here today.

Dedicated to my parents, Stephen and Jeanne

Table of Contents

List of Figures

List of Schemes

List of Tables

Chapter 1: An Introduction to Boron-Containing Polycyclic Aromatic Materials

Subjects of longstanding interest in fundamental physical organic chemistry, polycyclic aromatic hydrocarbons (PAHs) have recently arisen as a class of compounds showing considerable promise for application as the working elements in organic electronic devices (Figure 1.1). Buoyed by the extreme interest generated by the remarkable electronic, mechanical, and chemical properties exhibited by the planar, extended, all-sp^2 hybridized carbon allotrope known as graphene,[1-3] studies on smaller, atom-precise PAHs are advancing at a rapid pace in order to elucidate the structure-property relationships behind these so-called "nanographenes"[4,5] and to identify the most promising new architectures for materials application.

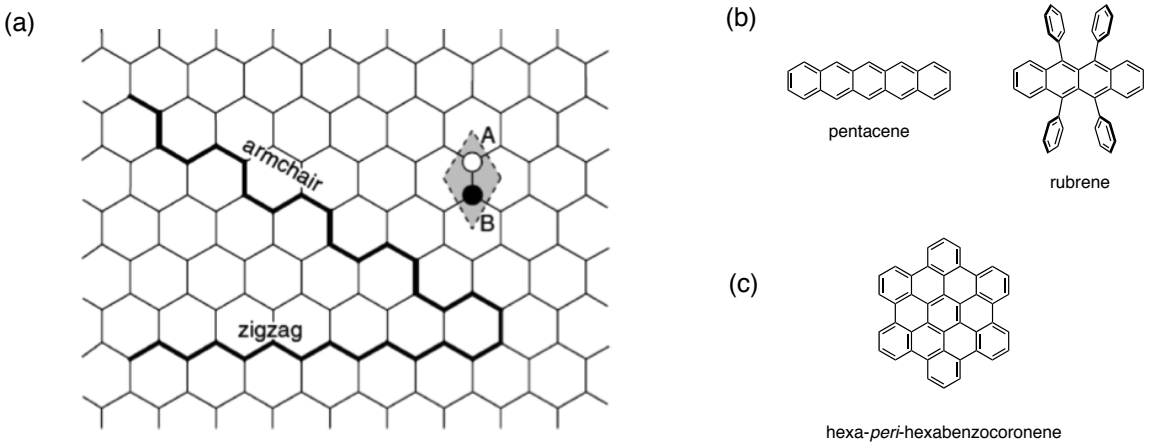

Figure 1.1. Representative PAHs of interest in contemporary organic materials science: (a) extended honeycomb structure of planar graphene, showing zigzag and armchair edge patterns;[6] (b) zigzag edge linearly fused acenes; (c) armchair edge PAH structure of hexa-*peri*-hexabenzocoronene.

Several structural and electronic aspects of PAHs are crucial to their utility as electronic materials. The extended, rigidly planar architectures of PAHs provide the ideal dihedral angle for intramolecular electronic delocalization along the π-conjugated backbone and a propensity to adopt coplanar, π-stacked networks in the solid state,

allowing for efficient intermolecular electronic coupling – a critical component of long-range electronic transport and device performance. Unlike zero-bandgap graphene, smaller, well-defined PAHs possess finite bandgaps and variable properties according to their exact sizes and edge patterns. For instance, zigzag-edged one-dimensionally fused acenes (Figure 1.1b) and their analogues have emerged as benchmark organic semiconductors,[7,8] while functionalized, disclike, armchair-edged hexa-*peri*-hexabenzocoronenes[9] (Figure 1.1c) form columnar π-stacked arrays in liquid crystalline materials showing high intrinsic charge carrier mobilities.

One of the great virtues of organic materials is the near limitless ability to modify the carbon backbone using the tools of organic synthesis. Depending on the specific synthetic alteration, it is possible to change the electronic, structural, or chemical properties of the native compound in a targeted fashion. In recent years the positional substitution of carbon atoms with main group heteroatoms has emerged as a particularly powerful strategy to tune the molecular properties of organic materials.[10] The use of main group elements – such B, N, Si, P, and Se – as atomic "dopants" has enabled not only the modulation of HOMO and LUMO levels, but also provides unique features which are typically unavailable to the all-carbon parent material (such as the reversible coordination state change[11] or irreversible covalent modification[12-16] of the heteroatoms). In particular, utilizing these heteroatoms as tethers to constrain π-conjugated arrays into a fused heteroaromatic structures takes advantage of both the inherently desirable properties of PAHs and the unique properties imbued by heteroatom substitution[10] (Figure 1.2).

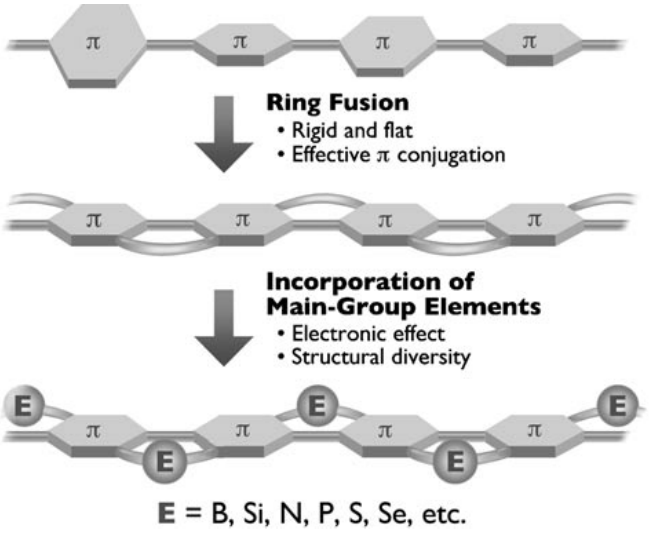

Figure 1.2. Conceptual approach for property-tuning of polycyclic aromatics via incorporation of main group heteroatoms.[10]

Among the various main group elements employed for property-tuning in organic materials, the use of tricoordinate boron for this purpose has attracted significant attention[17,18] (Figure 1.3). The incomplete valence octet of neutral, trivalent boron (envisioned as a vacant p-orbital) renders it electron-deficient, allowing it to participate in electronic delocalization with an organic π-system via $p\pi - \pi^*$ conjugation[19] ($B_p - C\pi^*$ overlap, Figure 1.3a). The electron-accepting nature of boron gives rise to conjugated systems with strong donor-acceptor character and low-lying LUMO levels, often resulting in useful linear and non-linear optical properties[20,21] and facile electrochemical reduction/ n-type charge carrier ability. Boron's empty p-orbital also provides Lewis-acidic character (Figure 1.3b), creating a basis for catalysis[22,23] and sensing schemes.[24] Importantly, sp^2-hybridized boron possesses an ideal trigonal planar geometry, allowing incorporation into conjugated organic π-systems without causing significant perturbation of orbital overlap (Figure 1.3c).

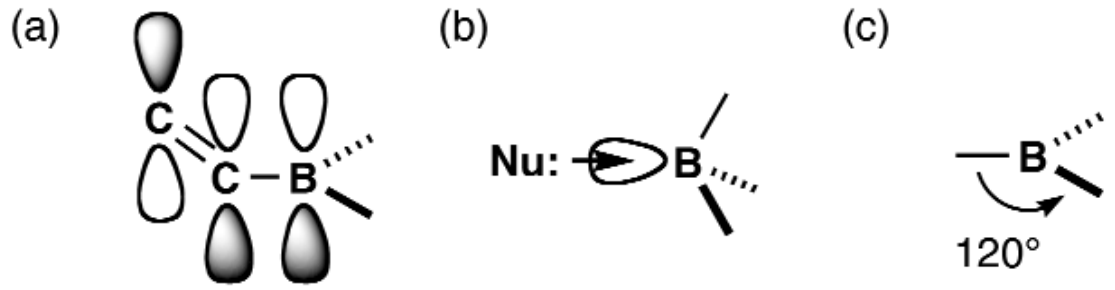

Figure 1.3. Key structural, electronic, and functional characteristics of boron-containing organic π-electron materials: (a) extended conjugation due to overlap between the organic π-system and the vacant p-orbital of boron; (b) Lewis acidity/fluxional coordination sphere of boron; (c) trigonal planar geometry of sp^2 boron.[18]

Despite the unique properties promised by boron-containing π-conjugated materials, their development has been relatively slow compared with several other classes of main-group embedded organics. This is due to the inherent chemical sensitivity of the boron center to hydrolytic and oxidative degradation, which leads to challenges in the preparation and stabilization of these materials. Thus the development of new boron-containing π-conjugated materials depends critically on advances in synthetic approach as well as effective strategies to maintain the integrity of the organoborane functionality. Three main tactics have been predominant with respect to stabilizing tricoordinate boron centers (Figure 1.4): 1) thermodynamic stabilization by the donation of a lone pair from an adjacent heteroatom (such as N or O) to boron (Figure 1.4a); 2) aggressive steric protection with bulky groups to prevent adventitious nucleophilic attack (Figure 1.4b), and most recently 3) kinetic stabilization by structural constraint,[25] whereby the boron atoms are placed within a rigid, fully-fused π-network to disfavor sp^2 - sp^3 rehybridization (Figure 1.4c).

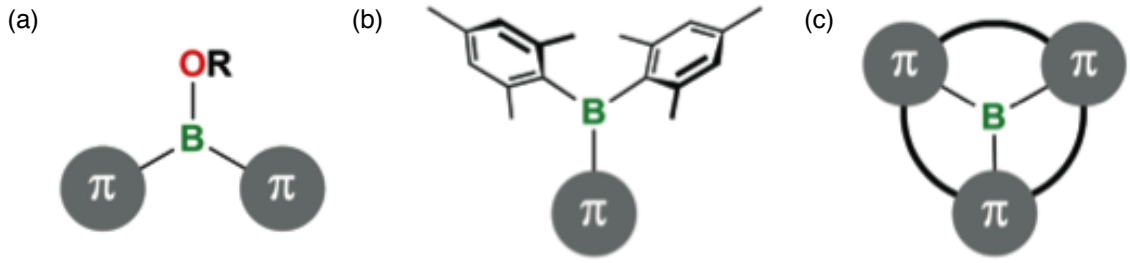

Figure 1.4. Stabilization strategies to main the integrity of boron centers in π-electron materials.[26] (a) electronic stabilization via lone-pair donation from an adjacent heteroatom. (b) kinetic stabilization via steric protection with bulky groups. (c) kinetic stabilization via structural constraint.

While organoboron moieties have been liberally employed as electron-deficient units within the main conjugated chain or as peripheral functional groups (so-called "lateral substitution) of numerous structurally unconstrained molecular and polymeric π-electron systems,[27] the synthetic methods to access PAH-based organic materials with boron atoms embedded within the polycyclic core are relatively less well-developed. However, in recent years considerable advances have been towards the latter, with breakthroughs in preparative synthetic chemistry spanning several boracyclic motifs (Figure 1.5).

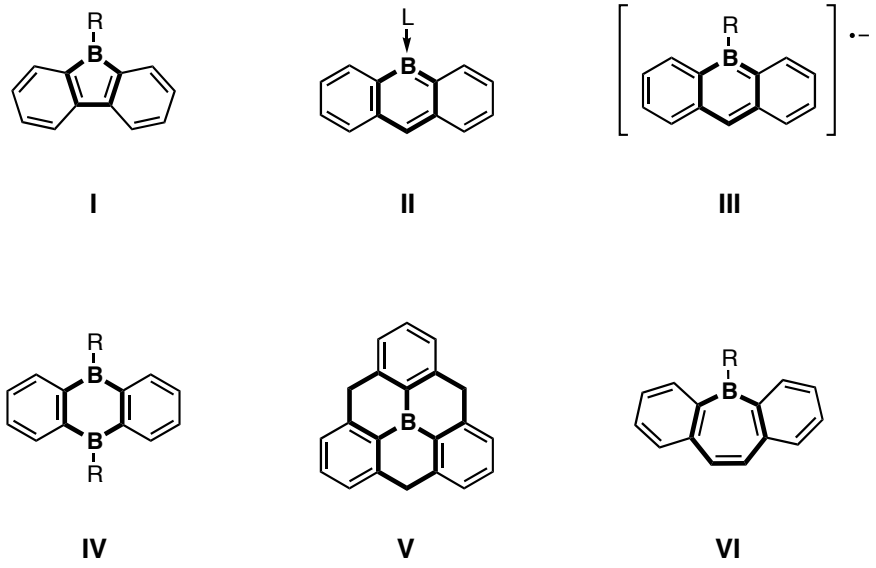

Figure 1.5. Typical boracyclic motifs encountered in boron-containing PAH materials (in **bold**): borole (**I**), borabenzene (**II**), boratabenzene (**III**), 1,4-diborin (**IV**), structurally constrained triarylborane (**IV**), borepin (**VI**).

The 5 π-electron borole ring (**I**, Figure 1.5; Figure 1.6) has long been a subject of interest due to its formally Hückel-antiaromatic character,[28] leading to strong Lewis-acid/electron-accepting properties. The fused dibenzoborole (or 9-borafluorene) structure was first synthesized by Köster and Benedikt,[29] revealing that benzannulation was crucial for stabilization of the borole core; since that time all isolable boroles have thus employed either ring fusion or perarylation[30] for stability. The development of modern borole-based PAH materials has been driven forward by the groups of Yamaguchi, Tamao, Piers, and Wagner. The strong Lewis-acidity of the borole nucleus remains a central theme in these compounds. Piers and coworkers developed perfluorinated dibenzoboroles **1** with *B*-Me (**1a**) and *B*-C_6F_6 (**1b**) functionality as structurally constrained analogues of Lewis acidic $MeB(C_6F_6)$ and $B(C_6F_6)$ compounds, respectively; the borole compounds showed enhanced Lewis acidity and promise as robust ligands for

metallocene activation in Ziegler-Natta olefin polymerization.[31] Yamaguchi and Tamao developed *B*-Tip-substituted (Tip = 2,4,6-triisopropylphenyl; tripyl) dibenzoboroles with attached π-donor groups (**2a**–**c**) as "on-off" fluorescent sensor materials for fluoride ions owing to interruption of the donor-acceptor network upon Lewis base coordination[32] (Figure 1.6); use of the more highly hindered *B*-Mes* (Mes* = 2,4,6-tri-*tert*-butylphenyl; supermesityl) protective group (**3a**–**c**) precluded any fluoride coordination but provided additional chemical robustness, allowing for reversible electrochemical reduction ($E_{1/2\ red}$ = -2.28 vs. Fc/Fc^{+}).[33] Later Yamaguchi developed synthetic routes to generate *B*-Tip thiophene- (**4**), pyrrole-, and furan-fused ladder borole compounds[34,35] based on elegant cascade cyclization chemistry; these materials were highly sensitive owing to the increased antiaromaticity of the borole ring as a result of diminished bond length alternation. Piers has developed unique photochemical and thermal rearrangements leading to the exotic fused ladder diborole **5**,[36,37] which can be considered a *bis*-boron-bridged stilbene analogue. Wagner has made several discoveries associated with the reaction chemistry of the *B*-*H* substituted borafluorene scaffold, including the ring-opening oligomerization of 9-*H*-9-borafluorene **6** to give boron-containing oligophenylenes and a structure containing a nonclassical B-C-B two-electron-three-center bond.[38,39]

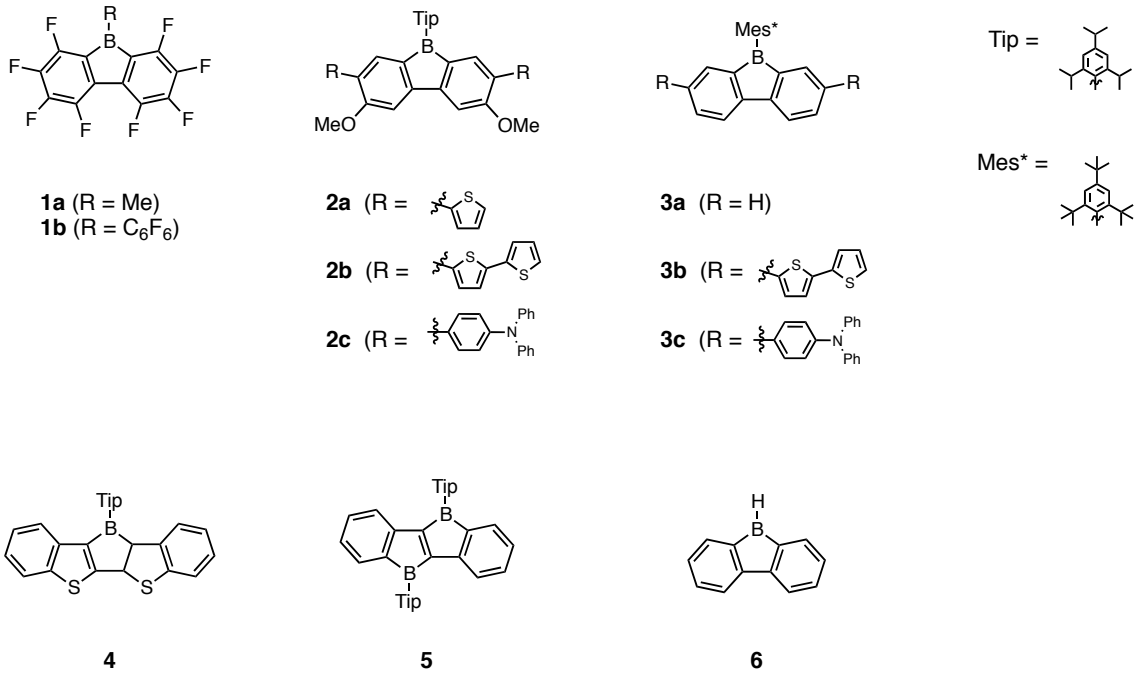

Figure 1.6. Borole-based PAHs.

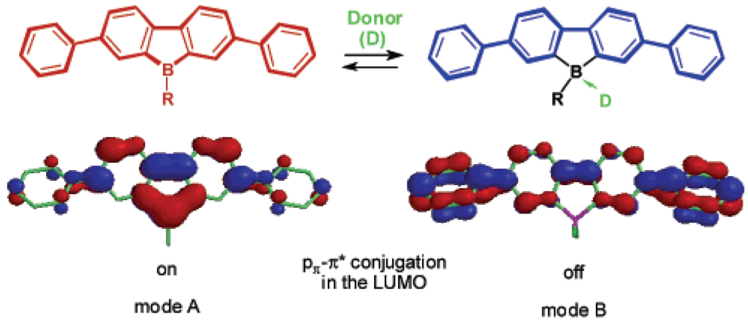

Figure 1.7. On-off switching of p_{π}-π^* conjugation in the LUMO of dibenzoborole upon Lewis base coordination.[32]

Boraacenes (**II**, Figure 1.5 and Figure 1.8) can be considered as a class of molecules featuring direct substitution of one or more carbon atoms with boron in a linearly fused array of six-membered rings. Fully conjugated boraacenes with a single boron atom bridging two benzene rings feature a formal B-C π-bond and require stabilization of boron by complexation with a Lewis base. In 2009, Piers and coworkers

were able to prepare fully unsaturated boron-containing analogues of anthracene (**7**), tetracene (**8**), and pentacene (**9**) using N-heterocyclic carbenes as stabilizing ligands;[40] these compounds nonetheless remained air and moisture sensitive. Their studies showed that the boraacenes possessed relatively planar molecular backbones, slightly reduced aromatic character, and highly red-shifted absorption spectra compared to all-carbon analogues. They were also more susceptible to reaction with molecular oxygen than the corresponding hydrocarbons.

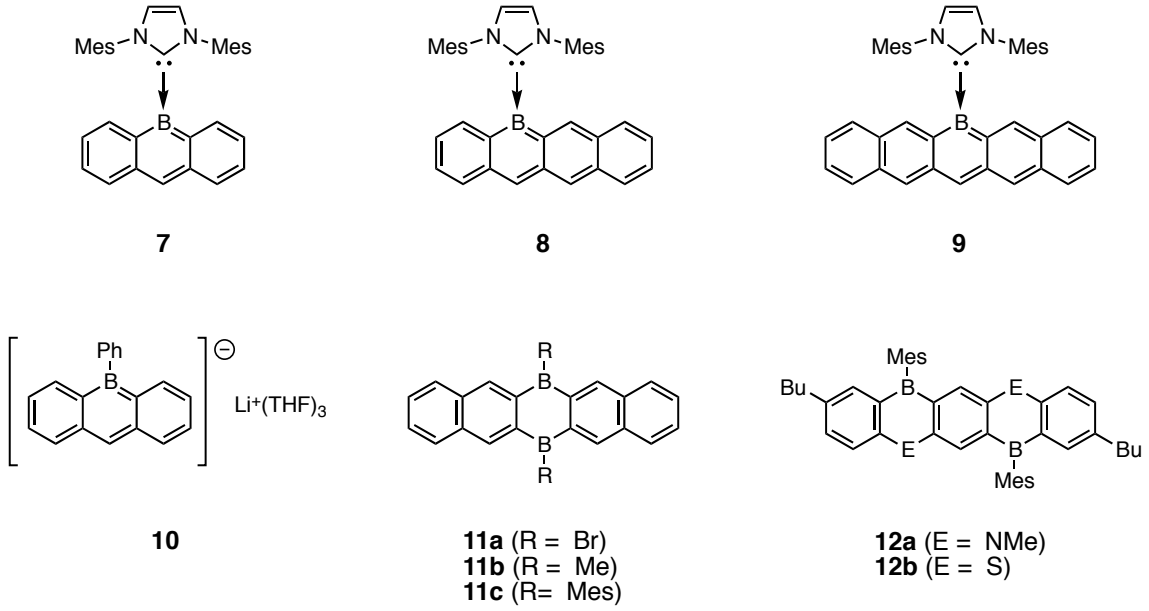

Figure 1.8. Linearly fused, acene-like PAHs with 6-membered boracycles: ligand-stabilized boraacenes (**7** – **9**), anionic borataanthracene (**10**), ladder 1,4-diborins (**11a** – **c**), and heteroborins (**12a**, **b**).

Related are to boraacenes are borataacenes, the direct isoelectronic analogues of all-carbon acenes which require the constituent boratabenzene rings to be anionic (**III**, Figure 1.5). 9-Borataanthracenes were first synthesized independently by van Veen and Bickelhaupt[41] and by Jutzi[42] in the early 1970s and the aromaticity of the boron-

containing ring was supported by spectral data and the acidity of the precursor molecules. Later, Bazan and coworkers showed that reaction of $Li(THF)_3$[9-phenyl-9-borataanthracene] (**10**, Figure 1.8) with Cp^*ZrCl_3 or Cp^*ZrMe_2Cl (*Cp = 1,2,3,4,5-pentamethylcyclopentadienyl) generates the corresponding Zr–borataanthracene complexes with η^6–coordinated boratabenzene rings;[43] the olefin polymerization capabilities of these and other related Zr-borataanthracene complexes were evaluated.

Diboraacenes (acenes containing diborin rings; **IV**, Figure 1.5) have been studied by several groups. Variously *B*-substituted 6,13-diborapentacenes (**11a – c**, Figure 1.8) were synthesized by Ashe,[44] which showed similar C-C bond lengths (C-C = 1.37 – 1.45 Å) to native pentacene (C-C = 1.34 – 1.46 Å) but very long internal B-C bonds (1.54 – 156 Å), consistent with the formulation of the diborin ring as an antiaromatic 4 π-electron subunit. *B*-Br (**11a**) and *B*-Me (**11b**) diborapentacenes showed slipped cofacial stacking π–π stacking in the crystal, which was remarkable because native pentacene instead adopts a herringbone packing pattern. Electrochemical reduction was found to be quite facile for **11c** ($E_{1/2\ red}$ = -1.23 V vs. Fc/Fc^+), showing a half-wave reduction value comparable to the effective n-type semiconductors perfluoropentacene[45] (-1.13 V) and C_{60}. (-1.14 V).

Related to the diborin motif in diboraacenes are 1,4-heteroborins (containing boron and another heteroatom situated in the 6-membered ring; **12a**, **b**, Figure 1.8). A variety of ladder-type heteroborins containing N (**12a**), P, O, and S (**12b**) atoms in the polycyclic core have been investigated extensively by Kawashima and coworkers;[46-49] it was found that the optical properties and Lewis acidity of these materials could be

modulated depending on the identity of the heteroelement employed alongside boron and by altering the location of the heteroatoms within the scaffold.

The most recent developments in design, synthesis, and property evaluation of cutting-edge boron-containing PAHs as unique materials revolve around two-dimensionally extended π-systems, with boron situated either in the center of the polycyclic core (Figure 1.9; **13** and **14**) or at the edge of the PAH (**15** – **17**). Such systems are of particular interest as well-defined molecular models of (and potential building blocks for) atom-precise boron-doped nanographenes.

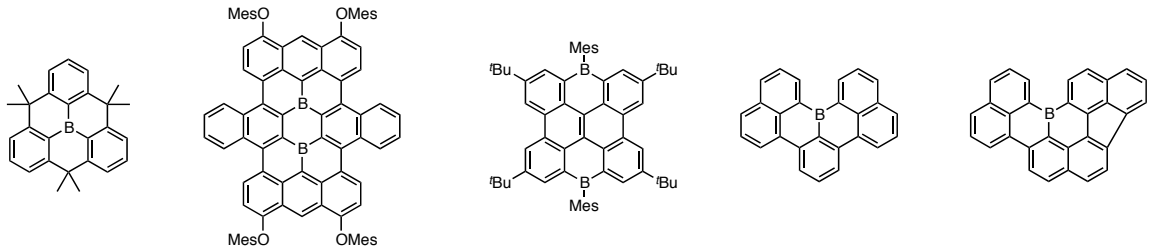

Figure 1.9. Two-dimensionally extended PAHs with boron either at the center of the fused array (**13**, **14**) or at the molecular edge (**15** – **17**).

Synthetic approaches towards PAHs with centrally embedded boron atoms have largely been pioneered by Yamaguchi and coworkers, relying on intramolecular Scholl-type or radical cyclizations to fuse the extended carbon scaffold. Utilizing this chemistry it was possible to construct the planarized triarylborane **13**[25] as well as several fully-conjugated PAH-type structures, including boron-doped nanographene **14**.[50] Notably, structural constraint of boron within the core of the PAHs provided sufficient kinetic stabilization (Figure 1.4c) to render the triarylborane moieties robust without additional steric protection. Despite being embedded within the polycyclic cores, the boron centers maintained typical Lewis base coordination ability, undergoing a plane-to-bowl

geometric perturbation of the PAH backbone geometry. A similar structural reorganization was correlated with electronic excitatations of the planarized triarylboranes, leading to unusual dual-fluorescence properties.[51] Boron-doped nanographene **14** showed several properties unique from its all carbon relatives, including a closed-shell ground state electronic structure, considerably red-shifted absorption and emission spectra, and oxidative and reductive electrochemical behavior (Figure 1.10).[50] From an application perspective, an alkoxy-substituted derivative of **14** (possessing $-OC_4H_9$ groups instead of –OMes groups) was employed as the active material in a Li battery electrode,[52] showing stable charge/discharge characteristics over ten cycles in the 1.5 – 4.0 V range with a first discharge capacity of 160 mA h g^{-1}. Related to small molecule nanographene structures are boron-doped graphene nanoribbons prepared via annealing of 9,10-dibora-9,10-dihydroanthracene at 180 °C / 400 °C on an Au surface (Figure 1.11).[53] The resulting nanoribbons were structurally resolved by high-resolution force microscopy, showing not only a well-defined, regular arrangement of the boron-doped sites but persistent Lewis acidity, enabling adsorption of NO gas and offering promise as a solid-state sensor material.

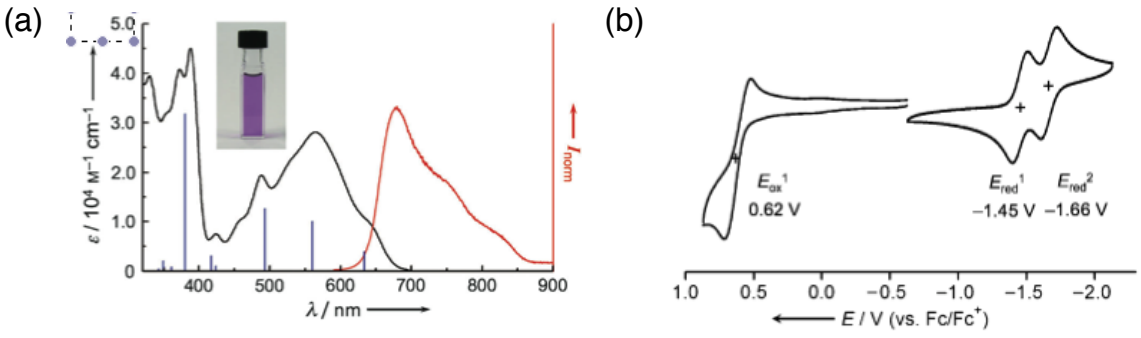

Figure 1.10. (a) electronic spectra and (b) cyclic voltammograms for boron-doped nanographene **14**.

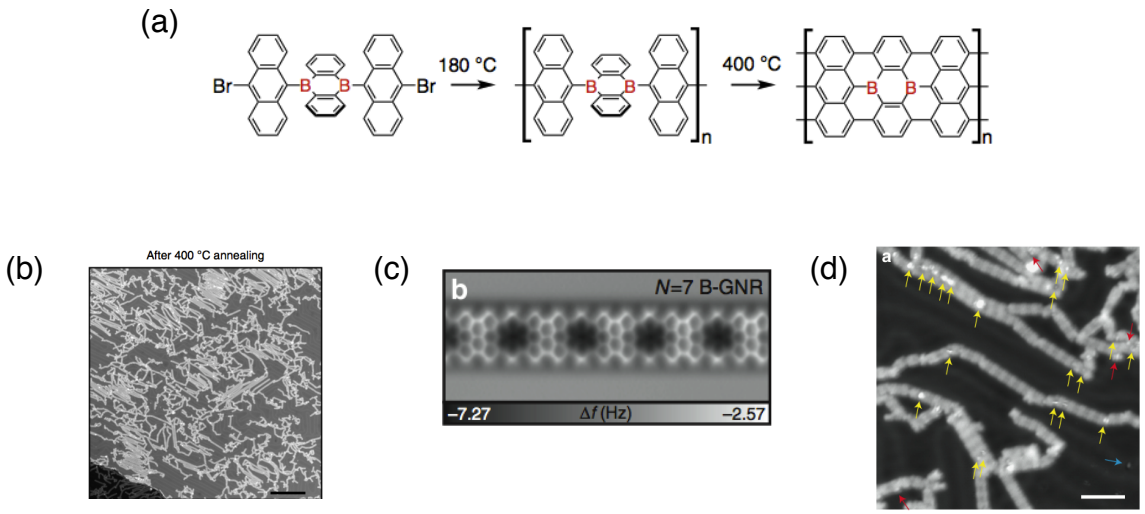

Figure 1.11. On-surface synthesis and microscopy images boron-doped nanoribbons prepared by on-surface annealing.[53] (a) Schematic of the on-surface reaction. (b) STM image of graphene nanoribbons following 400 °C annealing. (c) frequency-shift map showing the well-defined boron-doped sites and edge-structure. (d) STM image showing the sites of NO-boron complexation (yellow arrows).

The investigation of two-dimensionally fused structures with edge-situated boron atoms has been spearheaded by the groups of Wagner, Hatakeyama, and Yamaguchi. Wagner has demonstrated that boron-doped PAHs (such as **15**) can be prepared via a late stage Si-B exchange reaction following a tandem Peterson olefination/photocyclization.[54] The evaluation of electronic and redox properties of **15** revealed both cathodic and anodic electrochemical behavior and a high photoluminescence quantum yield of Φ_{PL} = 0.78. Wagner and Hatakeyama have independently developed syntheses of the helical, *B*-doped PAH **16** via Ni(0)-catalyzed Yamamoto coupling[55] and intramolecular Friedel-Crafts-type borylation,[56] respectively. Partially-constrained *B*-containing PAH **17**[57] was serendipitously obtained by Yamaguchi and coworkers during an attempt to construct a fully-fused array via the Scholl-type methods discussed above; in this partially fused analogue the dual-fluorescence phenomenon observed previously for the fully fused

systems could be attenuated by varying the coordination strength of added pyridine Lewis bases. Notably, **17** featured columnar π-stacking in the solid state.

One of the least explored boracyclic motifs in organic electronic materials is the borepin ring. In contrast to the 4 π-electron borole, the borepin possesses a formally Hückel-aromatic electronic sextet and is isoelectronic with the well-known non-benzenoid aromatics hinokitiol and the tropylium cation[58] (Figure 1.11). Though the parent borepin structure was predicted to have aromatic character by Vol'pin in 1960[59], it was not until 1992 that Ashe succeeded in synthesizing the parent compound,[60] which had to be prepared and studied *in situ* due to its sensitivity. Arguments for the aromaticity of the borepin were made based on the high frequency ^{1}H NMR chemical shifts of the parent compound and the single crystal data of the *B*-Cl substituted analogue,[61] which showed a bond length alternation value of ±0.058 Å. Prior to Ashe's work, all known borepins had relied on heteroatom-to-boron lone pair donation, ring annulation, or exhaustive substitution with aryl groups to stabilize the structure. Van Tamelen synthesized the first borepin in the form of *B*-OH dibenzo[*b*,*f*]borepin (DBB) **18** in 1960 by dehydrohalogenation of a partially saturated borepin ring,[62] while Leusink constructed the *B*-Ph benzo[*d*]borepin **19** in 1967 via tin-boron exchange chemistry.[63] Later Gronowitz and Sugihara and Murata reported the construction of thiophene annulated borepins such as borepino[3,2-*b*:6,7-*b*']dithiophenes[64] (**20a** – **c**) and 1-phenylthieno[3,4-*d*]borepin (**21**),[65] respectively. Gronowitz's dithienoborepins (DTBs) were found to be more stable than the corresponding DBBs as a result of the ability of the electron-donating thiophene rings to stabilize boron, but nonetheless decomposed when subjected to electrophilic aromatic substitution chemistry. Sugihara and Murata's 1-

phenylthieno[3,4-*d*]borepin was found to have a polarized electronic structure, in effect it was a dipole-reversed analogue of azulene; this material, too, was not highly robust, undergoing slow acid-catalyzed ring opening from adventitious H^+ in chloroform solution.

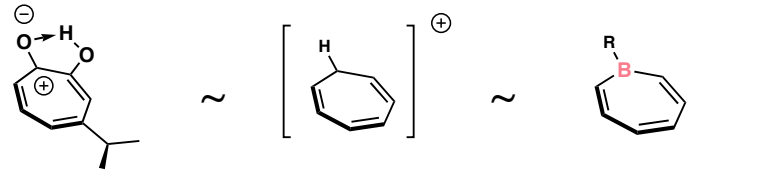

Figure 1.12. The formally Hückel-aromatic borepin ring and its isoelectronic analogues.

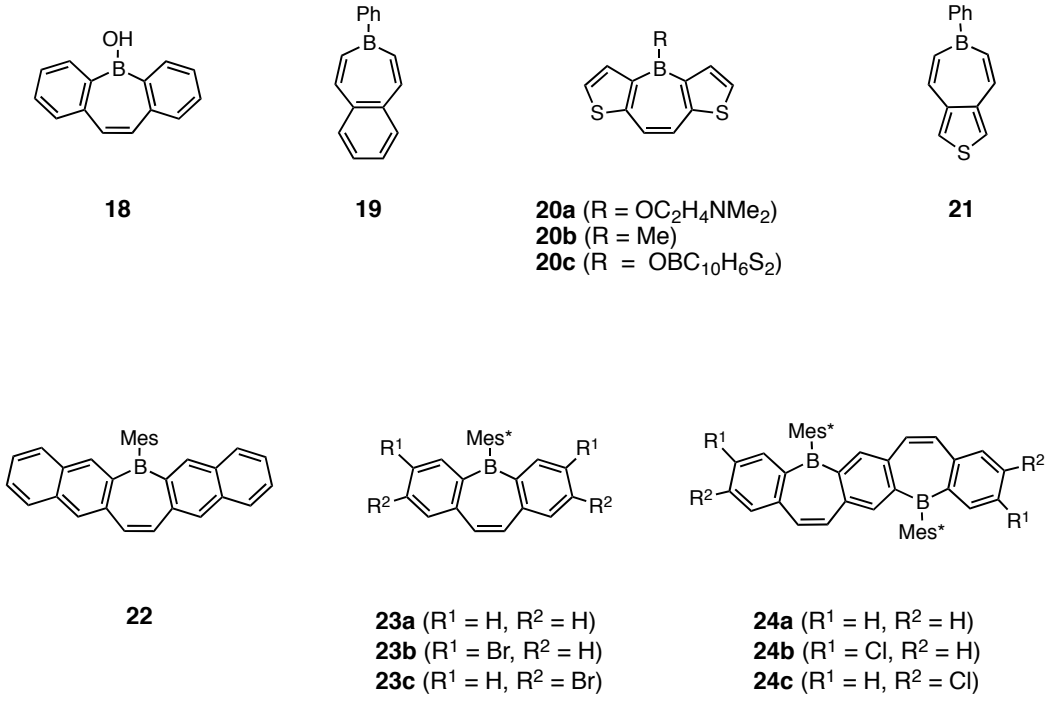

Figure 1.13. Borepin-containing PAHs.

Since its inception, the Tovar research group has maintained a continuous interest in exploring the use of unusual aromatic motifs for the construction of novel organic electronic materials. Thus the borepin framework offered an intriguing structure for further investigation. Independently, the Piers group[66] and our own[67-69] devised synthetic routes to several benzo- and naphtho-fused borepin motifs of enhanced stability compared to early generations of fused borepins. The syntheses relied upon the so-called "Wittig route", utilizing Wittig olefination to construct *ortho*-halogenated cis-stilbenes which were converted into the corresponding stannocycles by lithium-halogen exchange/Me_2SnCl_2 quench, and finally to the borepin-containing materials by tin-boron exchange with BCl_3 and treatment with a sterically-protective ArLi group (Ar = Mes, Mes*) to displace the third *B*-Cl ligand (Scheme 1.1). Piers' use of *B*-Mes steric shielding (as in dinaphthoborepin **22**) provided moderate stability to the borepin-containing structures, allowing full characterization; however, slow degradation was subsequently observed under ambient conditions. In contrast, the more hindered *B*-Mes* protective group utilized by Tovar allowed for the synthesis of several DBBs (**23a – c**) and *B*-entacenes (extended, pentacyclic ladder structures containing two fused borepin rings; **24a – c**) which were fully stable to air and moisture. Characterization of these materials indicated electron-accepting capacity via cathodic cyclic voltammetry and the presence of weak, low energy UV-vis bands characteristic of intramolecular charge-transfer. The robustness of the *B*-Mes borepin materials also enabled synthetic modification by appropriate prefunctionalization of the aryl precursors with chloride (**23b**, **c**) or bromide (**24b**, **c**) handles, allowing late-stage functionalization of the fully constructed borepin materials via transition metal-catalyzed cross-couplings. Installation

of extended π-functionality at these sites showed that π-conjugated substituents *para* to boron modified the LUMO level, while substituents *meta*- to boron narrowed the optical bandgap.[68]

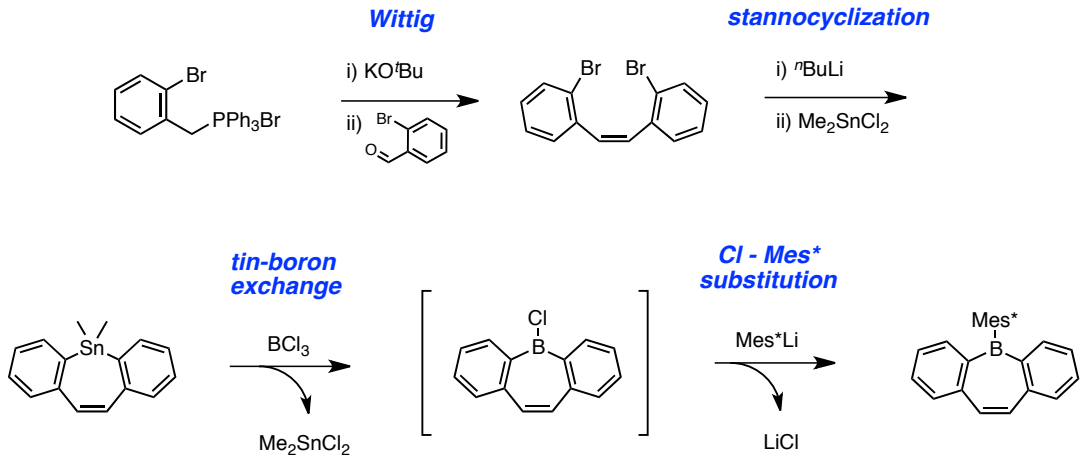

Scheme 1.1. Construction of *B*-Mes* dibenzo[*b,f*]borepins via the "Wittig route": 1) Wittig olefination, 2) Li-Br exchange/stannocycle formation, and 3) borepin formation through tin-boron exchange / Cl – Mes* substitution.

These initial research forays revealed that the borepin was a promising nucleus upon which to build stable, electronically tunable boron-doped polycyclic aromatic electronic materials. The work contained in the following chapters of this dissertation describes my efforts to 1) further expand the structure-space of synthetically accessible and highly robust borepin-containing materials; 2) fully characterize the obtained materials to elucidate key structure-property relationships and provide design principles for future borepin-based materials; and 3) to develop facile methods to tune the molecular properties of through late-stage synthetic modification.

References:

(1) Geim, A. K.; Novoselov, K. S. *Nat. Mater*. **2007**, *6*, 183–191.
(2) Rao, C. N. R.; Sood, A. K.; Subrahmanyam, K. S.; Govindaraj, A. *Angew. Chem. Int. Ed.* **2009**, *48,* 7752–7777.
(3) Allen, M. J.; Tung, V. C.; Kaner, R. B. *Chem. Rev.* **2010,** *110,* 132–145.
(4) Chen, L.; Hernandez, Y.; Feng, X.; Müllen, K. *Angew. Chem. Int. Ed.* **2012***, 51*, 7640–7654.
(5) Narita, A.; Wang, X.-Y.; Feng, X.; Müllen, K. *Chem. Soc. Rev.,* **2015***, 44,* 6616–6643.
(6) Yazyev, O. V. *Rep. Prog. Phys*. **2010**, *73,* 056501.
(7) Anthony, J. E. *Chem. Rev.* **2006,** *106*, 5028−5048.
(8) Anthony, J. E. *Angew. Chem. Int. Ed.* **2008**, *47*, 452–483.
(9) Seyler, H.; Purushothaman, B.; Jones, D. J.; Holmes, A. B.; Wong, W. W. H. *Pure Appl. Chem.* **2012**, *84*, 1047–1067.
(10) Fukazawa, A.; Yamaguchi, S. *Chem. Asian J.* **2009**, *4*, 1386–1400.
(11) Yamaguchi, S.; Akiyama, S.; Tamao, K. *J. Organomet. Chem*. **2002**, *652*, 3–9.
(12) Shefer, N.; Harel, T.; Rozen, S. *J. Org. Chem.* **2009**, *74*, 6993–6998.
(13) Durben, S.; Baumgartner, T. *Inorg. Chem.* **2011**, *50*, 6823–6836.
(14) Lorbach, A.; Bolte, M.; Li, H.; Lerner, H.-W.; Holthausen, M. C.; Jäkle, F.; Wagner, M. *Angew. Chem. Int. Ed.* **2009**, *48*, 4584–4588.
(15) Su, H.-C.; Fadhel, O.; Yang, C.-J.; Cho, T.-Y.; Fave, C.; Hissler, M.; Wu, C.-C.; Réau, R. *J. Am. Chem. Soc.* **2006**, *128*, 983–995.
(16) Ren, Y.; Baumgartner, T. *J. Am. Chem. Soc.* **2011**, *133*, 1328–1340.
(17) Entwistle, C. D.; Marder, T. B. *Chem. Mater.* **2004**, *16*, 4574–4585.
(18) Yamaguchi, S.; Wakamiya, A. *Pure Appl. Chem.* **2006**, *78*, 1413–1424.
(19) Yamaguchi, S.; Tamao, K. *Chem. Lett*. **2005**, *34*, 2–7.
(20) Yuan, Z.; Collings, J. C.; Taylor, N. J.; Marder, T. B.; Jardin, C.; Halet, J.-F. *J. Solid State Chem*. **2000**, *154*, 5–12.
(21) Entwistle, C. D.; Marder, T. B. *Angew. Chem. Int. Ed.* **2002**, *41*, 2927–2931.
(22) Jäkle, F. *Coord. Chem. Rev*. **2006**, *250*, 1107–1121.
(23) Dimitrijević, E.; Taylor, M. S. *ACS Catal.* **2013***, 3,* 945−962.
(24) Wade, C. R.; Broomsgrove, A. E. J.; Aldridge, S.; Gabbaï, F. P. *Chem. Rev.* **2010,** *110*, 3958–3984.
(25) Zhou, Z.; Wakamiya, A.; Kushida, T.; Yamaguchi, S. *J. Am. Chem. Soc.* **2012**, *134*, 4529−4532.
(26) Lorbach, A.; Hübner, A.; Wagner, M. *Dalton Trans.* **2012**, *41*, 6048–6063.
(27) Jäkle, F. *Chem. Rev.* **2010,** *110*, 3985–4022.
(28) Braunschweig, H.; Kupfer, T. *Chem. Commun.* **2011**, *47*, 10903–10914.
(29) Köster, R.; Benedikt, G. *Angew. Chem.* **1963**, *75*, 419.
(30) Eisch, J. J.; Galle, J. E.; Kozima, S. *J. Am. Chem. Soc.* 1986, *108*, 379-38**5**.
(31) Chase, P. A.; Piers, W. E.; Patrick, B. O. *J. Am. Chem. Soc.* **2000,** *122*, 12911-12912.
(32) Yamaguchi, S.; Shirasaka, T.; Akiyama, S.; Tamao, K. *J. Am. Chem. Soc*. **2002**, *124*, 8816–8817.
(33) Wakamiya, A.; Mishima, K.; Ekawa, K.; Yamaguchi, S. *Chem. Commun.,* **2008**, 579–581.
(34) Iida, A.; Yamaguchi, S. *J. Am. Chem. Soc.* **2011**, *133*, 6952–6955.
(35) Iida, A.; Sekioka, A.; Yamaguchi, S. *Chem. Sci.,* **2012***, 3,* 1461–1466.
(36) Araneda, J. F.; Neue, B.; Piers, W. E.; Parvez, M. *Angew. Chem. Int. Ed.* **2012***, 51,* 8546 –8550.
(37) Araneda, J. F.; Piers, W. E.; Sgro, M. J.; Parvez, M. *Chem. Sci.* **2014**, *3*, 1461–1466.
(38) Hübner, A.; Qu, Z.-W.; Englert, U.; Bolte, M.; Lerner, H.-W.; Holthausen, M. C.; Wagner, M. *J. Am. Chem. Soc.* **2011**, *133*, 4596–4609.
(39) Hübner, A.; Diefenbach, M.; Bolte, M.; Lerner, H.-W.; Holthausen, M. C.; Wagner, M. *Angew. Chem. Int. Ed.* **2012**, *51*, 12514–12518.
(40) Wood, T. K.; Piers, W. E.; Keay, B. A.; Parvez, M. *Chem. Eur. J.* **2010**, *16*, 12199–12206.
(41) Van Veen, R.; Bickelhaupt, F. *J. Organomet. Chem*. **1971**, *30*, C51–C53.
(42) Jutzi, P. *Angew. Chem. Int. Ed.* **1972***, 11,* 53–54.
(43) Lee, R. A.; Lachicotte, R. J.; Bazan, G. C. *J. Am. Chem. Soc.* **1998**, *120,* 6037–6046.
(44) Chen, J.; Kampf, J. W.; Ashe, A. J. *Organometallics* **2008***, 27,* 3639–3641.
(45) Youichi Sakamoto; Toshiyasu Suzuki; Masafumi Kobayashi; Yuan Gao; Yasushi Fukai; Youji

Inoue; Fumio Sato, A.; Tokito, S. *J. Am. Chem. Soc.* **2004***, 126,* 8138–8140.
(46) Agou, T.; Kobayashi, J.; Kawashima, T. *Org. Lett.* **2005,** *7,* 4373–4376.
(47) Agou, T.; Kobayashi, J.; Kawashima, T. *Org. Lett.* **2006,** *8,* 2241–2244.
(48) Agou, T.; Kobayashi, J.; Kawashima, T. *Inorg. Chem.* **2006***, 45,* 9137−9144.
(49) Agou, T.; Kobayashi, J.; Kawashima, T. *Chem. Eur. J.* **2007**, *13*, 8051 – 8060.
(50) Dou, C.; Saito, S.; Matsuo, K.; Hisaki, I.; Yamaguchi, S. *Angew. Chem. Int. Ed.* **2012***, 51,* 12206 –12210.
(51) Kushida, T.; Camacho, C.; Shuto, A.; Irle, S.; Muramatsu, M.; Katayama, T.; Ito, S.; Nagasawa, Y.; Miyasaka, H.; Sakuda, E.; Kitamura, N.; Zhou, Z.; Wakamiya, A.; Yamaguchi, S. *Chem. Sci.,* **2014,** *5,* 1296–1304.
(52) Osumi, S.; Saito, S.; Dou, C.; Matsuo, K.; Kume, K.; Yoshikawa, H.; Awaga, K.; Yamaguchi, S. *Chem. Sci.* **2016,** *7,* 219–227.
(53) Kawai, S.; Saito, S.; Osumi, S.; Yamaguchi, S.; Foster, A. S.; Spijker, P.; Meyer, E. *Nat. Comms.* **2015**, *6*, 8098–8103.
(54) Hertz, V. M.; Bolte, M.; Lerner, H.-W.; Wagner, M. *Angew. Chem. Int. Ed.* **2015**, *54,* 8800–8804.
(55) Schickedanz, K.; Trageser, T.; Bolte, M.; Lerner, H.-W.; Wagner, M. *Chem. Commun.* **2015***, 51,* 15808–15810.
(56) Miyamoto, F.; Nakatsuka, S.; Yamada, K.; Nakayama, K.-I.; Hatakeyama, T. *Org. Lett.* **2015**, *17,* 6158−6161.
(57) Matsuo, K.; Saito, S.; Yamaguchi, S. *J. Am. Chem. Soc.* **2014***, 136,* 12580−12583.
(58) Doering, W.; Knox, L. *J. Am. Chem. Soc*. **1954**, *76*, 3203–3206.
(59) Vol'pin, M. E. *Russ. Chem. Rev*. **1960**, *29,* 129–160.
(60) Ashe, A. J.; Kampf, J. W.; Nakadaira, Y.; Pace, J. M. *Angew. Chem. Int. Ed.* **1992***, 31*, 1255–1258.
(61) Ashe, A. J.; Klein, W.; Rousseau, R. *Organometallics* **1993***, 12,* 3225–3231.
(62) Van Tamelen, E.; Brieger, G.; Untch, K. G. *Tetrahedron Lett*., **1960**, *6*, 14–15.
(63) Leusink, A.; Drenth, W.; Noltes, J.; van der Kerk, G. J. M. *Tetrahedron Lett*. **1967**, *8*, 1263–1266.
(64) Jeffries III, A. T.; Gronowitz, S. *Chem. Script*. **1973**, *4,*183–187.
(65) Sugihara, Y.; Yagi, T.; Murata, I.; Imamura, A. *J. Am. Chem. Soc.* **1992**, *114*, 1479–1481.
(66) Mercier, L. G.; Piers, W. E.; Parvez, M. *Angew. Chem. Int. Ed.* **2009,** *48,* 6108 –6111.
(67) Caruso, A.; Siegler, M. A.; Tovar, J. D. *Angew. Chem. Int. Ed.* **2010***, 49,* 4213 –4217.
(68) Caruso, A.; Tovar, J. D. *J. Org. Chem.* **2011***, 76,* 2227–2239.
(69) Caruso, A.; Tovar, J. D. *Org. Lett*. **2011**, *13*, 3106–3109.

Chapter 2: Polycyclic Aromatics Containing Two *meta*-Oriented Boron Centers – Synthesis and Characterization of "*Meta-B*-entacenes"

Introduction

As discussed in Chapter 1, boron-containing ladder-type polycyclic aromatic hydrocarbons (PAHs) have emerged as promising candidate materials to serve as the active materials in organic electronic devices. Amongst such PAHs, structures featuring formally Hückel aromatic borepin rings have recently begun to elicit interest as novel architectures for boron-based π-electron materials. Previous work in the Tovar research group has focused on the development of ladder-type pentacyclic compounds containing two borepin subunits, dubbed "*B*-entacenes"[1,2] as a nod to their *B*-containing, pentacene-like architectures (Figure 2.1). The structural hallmark of the original *B*-entacene system **1** (hereafter termed *para*-*B*-entacene) was that the borepin rings were situated such that the two boron centers (as well as the extended phenylene-vinylene functionalities) were oriented in a linearly-conjugated, *para*-orientation across the central benzene ring[1] (Figure 2.1, center). Photophysical analyses revealed that the UV-vis and photoluminescence (PL) spectra of **1** were considerably red-shifted in relation to the shorter, tricyclic dibenzoborepin (DBB) species, testament to enhanced electronic delocalization in the π-extended *para*-*B*-entacene. Furthermore, the presence of two boron atoms in the polycyclic backbone led to two separate, well-behaved electrochemical reduction events with more facile first reduction than the single boron-containing DBB. By preinstalling chloride handles on the benzene rings used to construct the *para*-*B*-entacene skeleton it was possible to later carry out cross-coupling reactions to further tune chemical properties.[1,2]

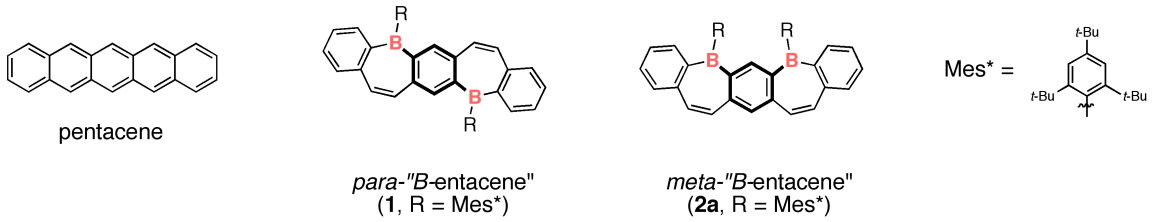

Figure 2.1. Structures of ladder-type pentacyclic aromatics: pentacene, previously prepared parent *para-B*-entacene, and the proposed *meta-B*-entacene. The *para*- and *meta*- boron-boron conjugation motifs in the *B*-entacenes are highlighted in bold.

To further utilize *B*-entacenes as potentially useful materials, a comprehensive understanding of structure-property relationships is required. Therefore we sought to elucidate the impacts of *B*-entacene structural variation on electronic properties. The following chapter details efforts to construct *B*-entacene skeletons in which the two boron centers (and the phenylene vinylene moieties) are instead situated in a cross-conjugated, *meta*-fashion relative to one another (hereafter termed "*meta-B*-entacene", **2a**, Figure 2.1) and the corresponding characterization of these compounds by empirical and computational methods.

Results and Discussion

The synthetic route developed to prepare parent *meta-B*-entacene **2a** is shown in Scheme 2.1. This path utilized the same general approach previously employed to synthesize para-*B*-entacene **1**; radical bromination of 1,5-dibromo-2,4-dimethylbenzene **3** provided 1,5-dibromo-2,4-bis(bromomethyl)benzene **4**, which was converted in the following step to diphosphonium salt **5** *via* Arbuzov-type chemistry. A subsequent *cis*-selective Wittig reaction with between **5** and two equivalents of 2-bromobenzaldehyde **6a** gave key tetrabrominated *Z,Z*-oligophenylenevinylene (OPV)-type compound **7a**,

completing the main carbon backbone of the targeted *B*-entacene structure. To install the bridging heteroatoms and complete the synthesis, two further steps were required. **7a** was subjected to a tetra-lithium-bromine exchange with *sec*-butyllithium (*s*-BuLi) in the presence of tetramethylethylenediamine (TMEDA), followed by quenching with dimethyltin dichloride (Me_2SnCl_2) to give pentacyclic compound **8a** containing two stannepin rings. The stannepins of **8a** were converted to the corresponding *B*-Cl borepins via a tin-boron exchange reaction[3,4] with BCl_3 and the final chloride was displaced with a large excess (16 equiv) of supermesityllithium (Mes*Li) to give *B*-Mes* *meta*-*B*-entacene **2a**. Dichlorinated *meta*-*B*-entacene analogues **2b** and **2c** were also prepared in an analogous manner by using chlorinated bromobenzaldehydes **6b** and **6c** in the Wittig step. The Cl atoms appended at sites either *para*- (**2b**) or *meta*- (**2c**) to the boron centers were included to allow for further site-selective functionalization of the *meta*-*B*-entacene core through cross-coupling chemistry (*vide infra*). The sterically demanding *B*-Mes* groups of **2a**–**2c** provided kinetic stabilization of the boron centers, allowing for purification under ambient laboratory conditions by silica gel chromatography and trituration with MeOH.

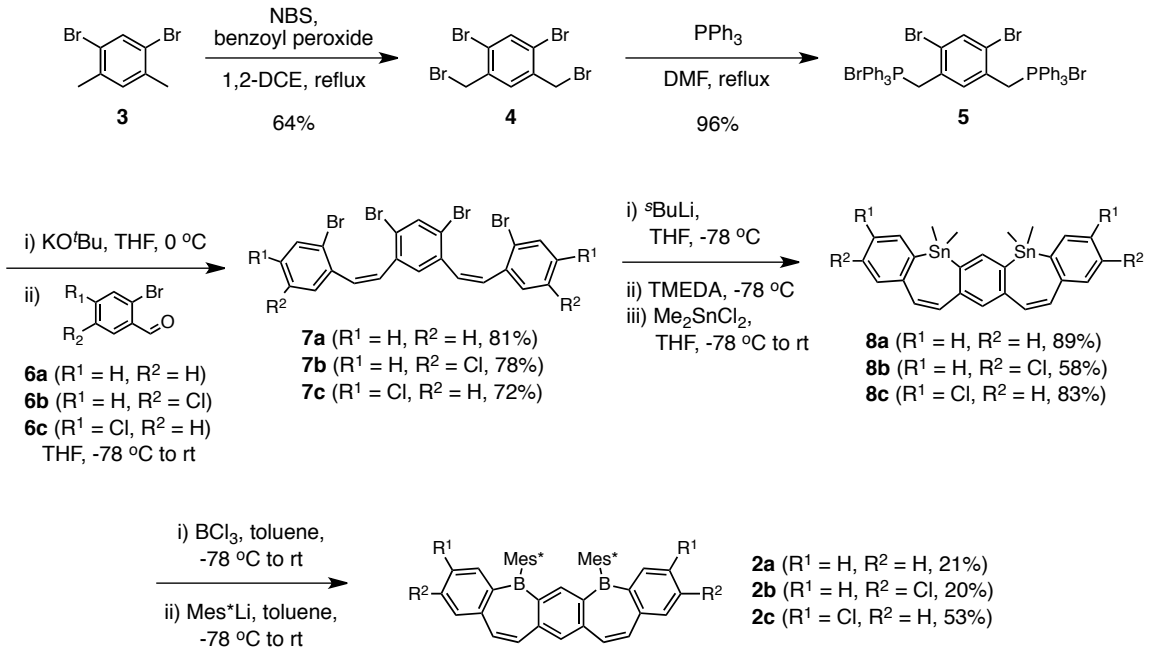

Scheme 2.1. Synthesis of parent (**2a**) and chlorinated (**2b**, **2c**) *meta-B*-entacenes.

The identity and purity of the *meta-B*-entacenes were confirmed through ^{1}H / ^{13}C NMR spectroscopy and high-resolution mass spectrometry. The ^{1}H NMR spectrum of **2a** in CD_2Cl_2 solution revealed a clear indication of the electronic impact of the *meta*-orientation of the embedded boron centers: the proton on the central benzene ring situated *ortho* to both electron-accepting boryl moieties appeared as a characteristic, strongly deshielded singlet at $\delta = 9.24$ ppm while the signal for the proton *meta* to both boryl moieties appeared as a lower frequency singlet at $\delta = 7.89$ ppm. In contrast, the two magnetically equivalent protons (both *para* to one B center and *meta* to the other) on the central benzene ring of **1** show up approximately at the halfway point between these values as a singlet at 8.27 ppm.[1]

Single crystals of parent *meta-B*-entacene **2a** suitable for X-ray crystallography were grown from slow diffusion of water into a concentrated THF solution of **2a**, providing unambiguous product identification and detailed structural information (Figure

2.2a–c). The unit cell of **2a** contained two crystallographically independent molecules within the asymmetric unit, as well as a relatively large void of approximately 145 $Å^3$ which was occupied by a THF solvent molecule. Similar, but larger voids (221 $Å^3$), were observed in the crystal structure of *para-B*-entacene **1**.[1] Unlike *para-B*-entacene, the sterically demanding *B*-Mes* groups in *meta-B*-entacene **2a** are placed in close spatial proximity on the same edge of the curved acene core, forcing the molecule to adopt a slightly twisted backbone geometry with an 18 – 20° angle between the planes defined by the terminal benzo rings (Figure 2.2b,c). This twist was well-reproduced in the DFT calculated structure (Figure 2.2d); replacement of the *B*-Mes* groups by *B*-Ph led instead to a highly planar calculated geometry (Figure 2.2e), confirming that the twist motif of **2a** was indeed caused by Mes–Mes* steric interactions.

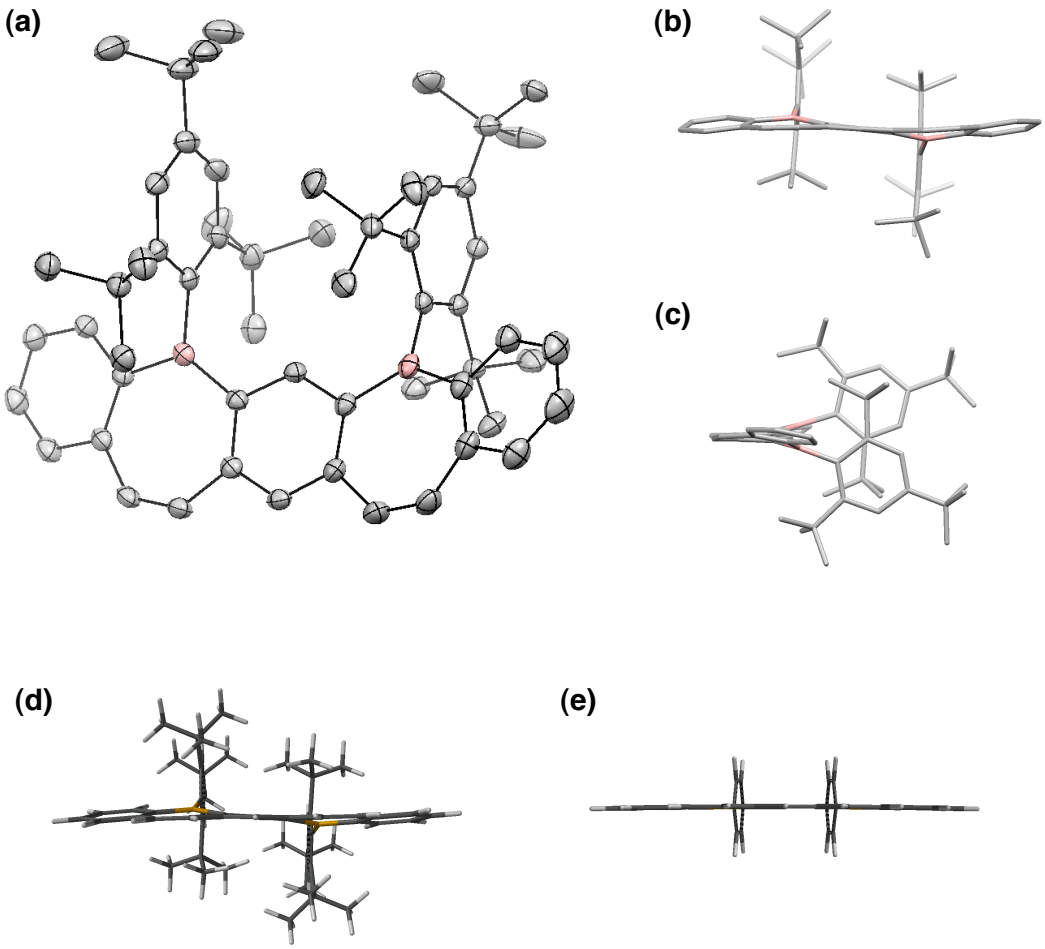

Figure 2.2. (a), (b), (c) X-ray and (d), (e) DFT-calculated structures for *meta-B*-entacene **2a**. (a) Displacement ellipsoid plot of the X-ray single crystal structure of **2a** at 110(2) K (50% probability level, H atoms omitted). (b), (c) Stick depictions of the X-ray structure of **2a** along the (b) bottom edge and (c) side edge of the PAH core, highlighting the backbone twist motif. (d), (e) DFT (B3LYP / 6-31G*) optimized structures for (d) **2a** and (e) instead with a *B*-Ph group, illustrating the influence of steric bulk of the Mes* groups in **2a**.

Though limited intermolecular face-to-face and edge-to-face close-contacts could be observed at the unhindered periphery of **2a** molecules in the crystal structure, occlusion of the central π-faces by the Mes* groups in **2a** prevented the formation of significant π–π stacking or herringbone packing motifs typically observed for unhindered acenes. [5,6]

Bond lengths in the crystal structure of **2a** were examined to determine the participation of boron in the conjugated π-electron network and to glean insight into the aromatic character of the borepin rings. The C–C bond distances in the borepin rings of **2a** were generally consistent with those observed in *para*-*B*-entacene[1], ranging from 1.339(3) to 1.453(3) Å. This resulted in a bond length alternation (BLA) value of ±0.114 Å, nearly twice as large as that of Ashe's monocyclic *B*-Cl borepin (±0.058 Å)[7] and suggestive of a decrease in borepin aromaticity due to extended benzo-fusion. Nucleus-independent chemical shift (NICS)[8,9] calculations corroborate this: the borepin NICS(1) value for values for **2a** (using *B*-2,6-dimethylphenyl in place of *B*-Mes* for computational efficiency) was found to be -0.51, indicating essentially non-aromatic character for the borepin rings.[10] Though this number is slightly less negative than the borepin NICS(1) value calculated for the *para*-*B*-entacene (-1.65),[1] the values do not differ greatly and therefore imply that the *B*-entacene isomers do not differ considerably in the extent of local borepin aromaticity.

The photophysical properties of **2a** were examined with UV-vis and PL spectroscopy (Figure 2.3 / Table 2.1). The UV-vis spectrum of **2a** in $CHCl_3$ revealed weak, low energy feature at 407 nm and intense, vibronically coupled higher energy bands at 263 and 340 nm; the low energy band at 407 nm was attributed to intramolecular charge transfer, consistent with the DFT calculated shift in the location of orbital density from the HOMO (centered mainly on the arene rings and alkene bridges) to the LUMO (centered mainly on the boron centers; Figure 2.4). Generally, the spectral features of **2a** were reminiscent of those observed in *para*-*B*-entacene **1**,[1] with the major difference being the significant hypsochromic shift of the *meta*-*B*-entacene UV-vis spectrum

compared to *para-B*-entacene, with the Abs λ_{onset} occurring at 32 nm shorter wavelength. This is consistent with diminished electron delocalization due to the shortened length of the longest all-carbon conjugation pathway in the *meta*-isomer (compare the *meta*-OPV-like conjugation of *meta-B*-entacene with the *para*-OPV-like conjugation of *para-B*-entacene, Figure 2.1).

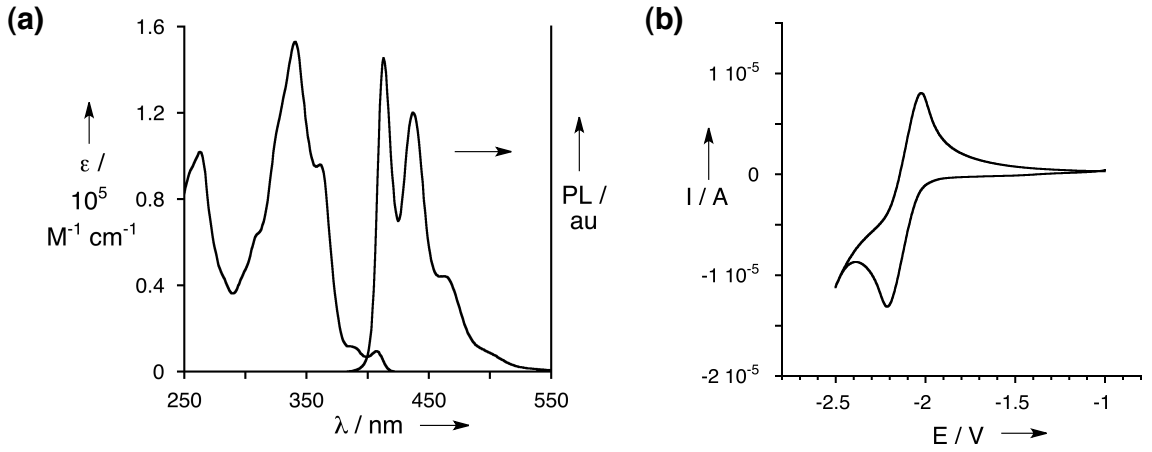

Figure 2.3. Photophysical and electrochemical data for **2a**. (a) UV-vis and PL spectra of **2a** acquired in $CHCl_3$ solution at room temperature. (b) Cyclic voltammogram of **2a**, obtained at an analyte concentration of 2.5 mM in 0.1 M *n*-Bu_4PF_6 / THF electrolyte solution; potentials are referenced to Ag/Ag^+ (= 0.00 V).

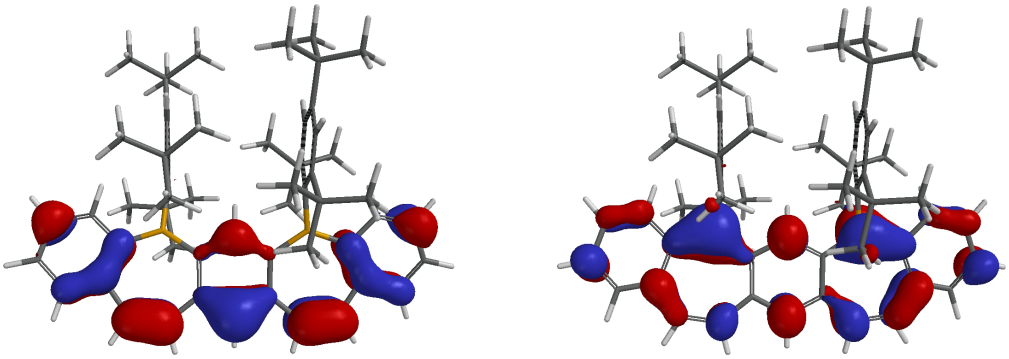

Figure 2.4. DFT calculated (B3LYP/6-31G*) frontier molecular orbitals of **2a**.

The PL spectrum of **2a** in $CHCl_3$ is shown in Figure 2.3.a. Unlike *para-B*-entacene **1**, the PL spectrum of **2a** exhibited substantial fine structure (PL λ_{max} = 413, 437 nm; shoulder at 462 nm). The structured emission spectrum was attributed to enhanced chromophore rigidity of the *meta*-isomer caused by the close proximity of the Mes* groups. This is also consistent with the observation of a high photoluminescence quantum yield for **2a** (Φ_{PL} = 0.80) and a small Stokes shift, both of which are typical of conformationally rigid systems whose excited states have low rates of non-radiative decay. The highly emissive character of **2a** was evident both in solution and in the solid state, with samples exhibiting intense, visually apparent light-blue photoluminescence upon irradiation with 360 nm UV light. This property could make the *meta-B*-entacenes (and *para-B*-entacenes) intriguing candidates as blue "dopants" in the active layers of organic light-emitting diodes (OLEDs), whose development is of interest due to a relative lack of very high-efficiency pure blue-light emitters.[11]

The redox behavior of **2a** was characterized through cyclic voltammetry (CV). Despite the fact that **2a** possesses two potentially redox-active boron centers, only a single reversible reduction wave was observed at $E_{1/2\ red}$ = -2.12 V (vs. Ag/Ag^+) in THF solution (Figure 2.3b). This contrasts with the redox behavior of *para-B*-entacene **1**, which exhibited two reversible reductions ($E_{1/2\ red}$ = -1.89 V, -2.46 V) with the first reduction event occurring 0.23 V earlier than for **2a**. Earlier onset of the first reduction event in **1** can be attributed again to the differences in conjugation between the boryl moieties – the *para B-B* arrangement in **1** provides linear conjugation between the boron centers, thus enhancing the electron deficiency of the system, whereas *B-B* cross-conjugation in **2a** does not provide the same degree of acceptor-acceptor cooperativity.

This is also in agreement with a higher DFT calculated LUMO level for **2a** compared to **1**. The trends in the onset of first reduction for the *B*-entacene isomers mirrors the behavior of unfused arylborane isomers 1,4- bis(dimesitylboryl)phenylene[12] and 1,3-bis(dimesitylboryl)phenylene,[13] with the 1,3-diborylated system also being more difficult to reduce. The absence of a second cathodic wave for **2a** was surprising, especially since Rajca's 1,3-bis(dimesitylboryl)phenylene[13] did in fact exhibit a second one-electron reduction. One possible explanation for this is that there is a large barrier to the second reduction for **2a**. Since significant conformational change can accompany the gain or loss of an electron (such as pyramidalization or planarization),[14] it is plausible that the second boron center in the rigid, highly sterically occluded environment of **2a** cannot easily accept an electron due to an unfavorable associated geometry change.

To explore the electronic influences of extended π-conjugation on the *meta-B*-entacene core, we sought to develop a repertoire for the further synthetic modification of dichloro analogues **2b** and **2c**. **2b** (chlorinated *para* to boron) was successfully subjected to late-stage functionalization *via* cross coupling chemistry, utilizing highly active Pd catalyst systems developed by Buchwald and Fu.[15,16] Stille- and Sonogashira-type reactions were used to install thienyl and 4-dimethylaminophenylacetylene substituents at the positions *para* to boron, giving **9** and **10**, respectively (Scheme 2.2). Unfortunately, *meta*-chlorinated **2c** did not show reactivity under these cross-coupling conditions, as previously observed for the analogous *meta*-chlorinated *para-B*-entacene derivative.[2]

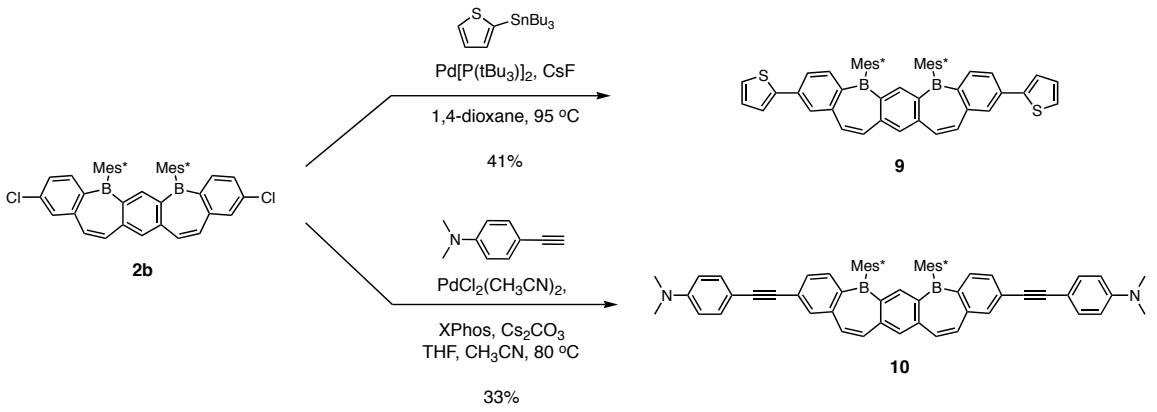

Scheme 2.2. Synthesis of donor-acceptor-type π-extended *meta-B*-entacenes **9a** and **9b** via Pd-catalyzed cross-couplings.

UV-vis and PL spectra and DFT calculations for **2b**, **9**, and **10** in $CHCl_3$ revealed the electronic impacts of placing chlorine atoms or π-substituents at the positions *para* to the *B*-centers (Table 2.1). Similar to the parent *meta*- and *para-B*-entacenes, the electronic spectra of the *para*-substituted *meta-B*-entacene remained hypsochromically shifted with respect to the identically substituted *para-B*-entacene analogues. Compared to the parent system **2a**, little change in the wavelengths of the longest absorption maximum and absorption onset were observed when substituting H with either chlorine atoms (**2b**) or moderately electron-donating thienyl groups (**9**), suggesting that these substituents do not strongly perturb the delocalization of electron density in the π-system when appended at the positions *para* to boron. However, when strongly electron-donating 4-dimethylaminophenylacetylene substituents were instead attached at the same site (**10**), there was a >40 nm bathochromic shift of the absorption onset, indicating significant enhancement in electronic delocalization. The DFT calculated frontier molecular orbital surfaces for **10** suggested that the donor-acceptor electronic structure was the basis of this phenomenon, with the HOMO being nearly entirely localized on the electron-donating *N,N*-dimethylaminophenylacetylene substituents and the LUMO

centered on the boron-containing core (Figure 2.5b, c). To glean additional insight into the electronic character of **10**, electronic spectra were also collected in solvents of different polarities (cyclohexane, chloroform, THF). The data series revealed that, while the absorption spectra were essentially unchanged, the PL spectra showed large positive solvatochromic shifts and a loss of fine structure in solvents with increasing E_T30 values (Figure 2.5a), consistent with the enhanced stabilization of polarized excited states. It is noteworthy that the degree of shift within this series (> 100 nm) is larger than that observed for the similarly functionalized *para*-*B*-entacene analogue,[2] showing that the *meta*- molecular architecture facilitates somewhat greater polarization than the *para*-isomer. This may be attributable either to electronic decoupling of the boryl acceptor units from one another in **10** or possibly the larger molecular dipole of the *meta* isomer caused by its lower degree of molecular symmetry.

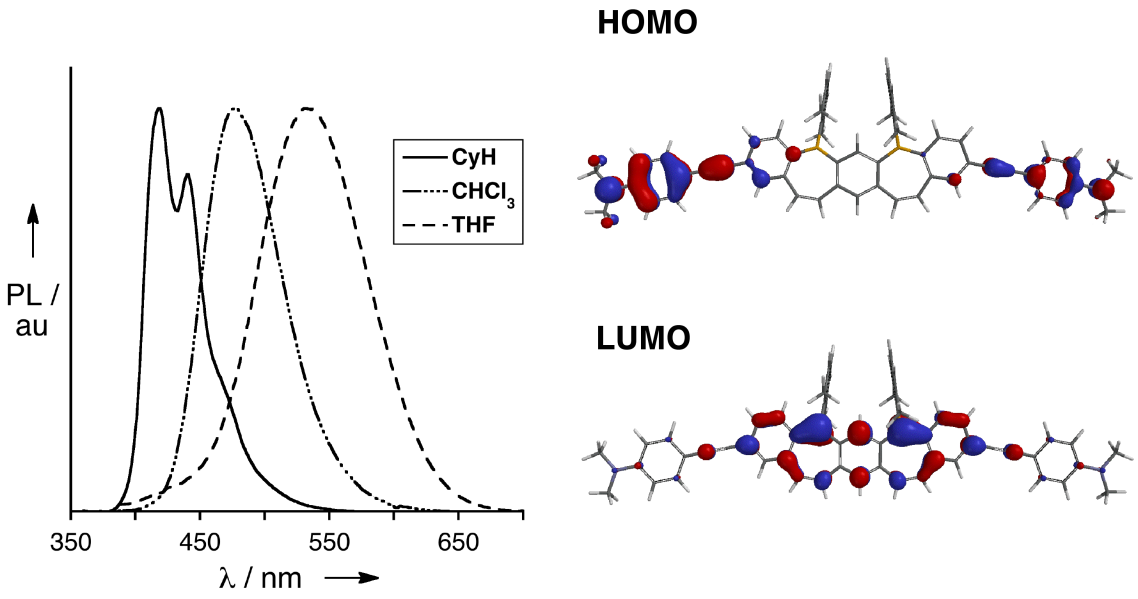

Figure 2.5. (**a**) PL spectra of **10** in cyclohexane, $CHCl_3$, and THF and (**b**) DFT-calculated frontier molecular orbitals of **10** (*B*-2,6-dimethylphenyl used in place of Mes*; B3LYP/6-31G*)

Table 2.1. Photophysical, electrochemical, and theoretical data for parent para-B-entacene **1**[a] and parent (**2a**) and *para*-functionalized *meta-B*-entacenes (**2b**, **9**, **10**).

Cmpd.	Abs λ_{max} (nm) [b,c]	Abs λ_{onset} (nm) [b]	PL λ_{max} (nm) [b]	Φ [b,d]	τ (ns) [b,e]	$E_{1/2\ red}$ [f] (eV)	HOMO (eV) [g]	LUMO (eV) [g]
1[a]	439	458	456	0.71	9.3	-1.89, -2.46		
2a	407	421	413	0.80	13.2	-2.12	-5.65	-1.88
2b	407	421	411	0.38	8.9	--	-6.02[h]	-2.30 [h]
9	411	425	441	0.39	8.8	--	-5.68 [h]	-2.15 [h]
10	400	461	477	0.48	2.8	--	-4.97 [h]	-1.97 [h]

[a] Data from reference 1
[b] Photophysical data collected in $CHCl_3$ solution
[c] Longest wavelength absorption maximum
[d] Quantum yields measured relative to a standard solution of quinine sulfate in 0.05 M H_2SO_4 (Φ = 0.55)
[e] Lifetime data fitted to a single exponential decay
[f] CV scans collected in THF solution containing 2.5 mM analyte and 0.1 M n-BuPF6 electrolyte. Potentials referenced to the Ag/Ag^+ redox couple
[g] Calculated at the DFT level (B3LYP/6-31G*)
[h] Calculations performed using *B*-2,6-dimethylphenyl groups in place of *B*-Mes*

Concluding Remarks

The successful synthesis of the *meta-B*-entacene scaffolds (in addition to previous dibenzo[*b*,*f*]borepins and *para-B*-entacenes) demonstrates the general utility of the tin-boron exchange / Mes*Li treatment protocol for the construction of air- and moisture-stable extended PAH compounds bearing alternant benzene-borepin motifs. Remarkably the double borepin formation/Mes* installation proceeded to give the targeted *meta-B*-entacenes despite the engineering of substantial steric strain into the molecular architecture (as evidenced by the out-of-plane twist of polycyclic backbone and outward splaying of the pendant Mes* groups in the crystal structure of **2a**). The demanding sterics of this transformation might offer a partial explanation for the relatively low yields obtained in comparison to the *para-B*-entacene isomer **1** (**1**: 43%; **2a**: 21%). In the future it would be desirable to further optimize the yields and develop scalable syntheses of the

B-entacene compounds to enhance their viability as candidates for optoelectronic materials.

Comparison of structural, redox, and electronic characterization data for the *para*-(**1**) and *meta*-*B*-entacene (**2a**) isomers revealed that **2b** possessed a unique, slightly twisted polycyclic skeleton, lowered electron-accepting ability, and significantly lessened electronic delocalization compared to **1**. The differences in redox and electronic properties are fully consistent with the placement of two electron-deficient boryl moieties in a *meta*-arrangement, thereby reducing the "cooperation" of the electron-accepting boron centers and shortening the longest effective conjugation pathway (i.e. – the extended OPV-like all-carbon conjugation pathway). The lack of an observable second reduction wave in the cyclic voltammogram of **2a** suggested that stereoelectronic effects may not be the only factor affecting redox behavior, and that the more congested steric environment of **2a** might also play a role (e.g. possibly by affecting reorganization energy, *vide supra*). From a materials standpoint, it is interesting to note that both *para*- and *meta*-*B*-entacenes exhibit high photoluminescence quantum yields and blue-colored emission, which suggests their possible candidacy as luminophores in light-emitting applications, as well as large void volumes in the single crystal, which may be of interest for host-guest-type applications (e.g., gas capture/storage or sensing).

Synthesis of π-extended *meta*-*B*-entacene analogues allowed for further tuning of electronic structure. Electronic spectra of *para*-donor-substituted *meta*-*B*-entacenes **9** and **10** showed that appending moderate electron donor groups had minimal impact (**9**), but that strong electron donating groups could be used to create highly polarizable electronic structures, confirmed by the large positive solvatochromic effects for **10**. The magnitude

of solvatochromism was larger than for corresponding, identically substituted *para-B*-entacene isomer, suggesting that the electronic "decoupling" of the two boron centers in *meta-B*-entacene and/or the lessened centrosymmetry of the molecular geometry can facilitate enhanced electronic polarizability. These design principles may be useful to maximize the polarizability of future extended borepin-based π-electron systems for possible application in linear or non-linear optical materials.

The work in this chapter has been published as communication in the Royal Society of Chemistry journal Chemical Communications in 2012.[17]

Experimental Section

General considerations. Unless otherwise specified, all reactions were carried out in flame- or oven-dried glassware under an atmosphere of prepurified nitrogen or argon using standard Schlenk techniques. Diethyl ether (Et_2O) and tetrahydrofuran (THF) were distilled under nitrogen from sodium/benzophenone ketyl prior to use. Toluene and acetonitrile (MeCN) were purified with an Innovative Technology, Inc. SPS-400-6 solvent purification system, stored over 3Å molecular sieves, and sparged thoroughly with nitrogen prior to use. Dimethylformamide (DMF) was obtained from Aldrich (99.8%, redistilled) and used without further purification. 1,2-Dichloroethane (1,2-DCE) and 1,4-dioxane were dried over 3Å molecular sieves and sparged thoroughly with nitrogen prior to use. Palladium catalysts were obtained from Strem Chemicals. Unless specified, all other chemicals were obtained from Alfa-Aesar, Fisher Scientific, Oakwood Chemicals, Sigma-Aldrich, Strem Chemicals, or TCI America and used as received.

1,5-dibromo-2,4-dimethylbenzene (**3**),[18] 2-bromo-4-chlorobenzaldehyde (**6c**),[19] and 4-ethynyl-*N,N*-dimethylaniline[20] were prepared according to the literature. 2,4,6-tri-*tert*-butylphenyllithium (supermesityllithium, Mes*Li) was freshly prepared before use by treatment of 1-bromo-2,4,6-tri-*tert*-butylbenzene[21] with *n*-butyllithium (1.6 M in hexanes) in THF at -78 °C for 2 h, followed by warming to room temperature and direct removal of the THF solvent on the Schlenk line under high vacuum (complete removal of THF was critical due to incompatibility of ethereal solvents with boryl halides);[22] the remaining off-white solids were resuspended in toluene and used without further purification. An alternative preparation of MesLi* in refluxing hexanes has been reported by Yamaguchi.[22]

^{1}H NMR and ^{13}C NMR spectra were obtained with a Bruker Avance 400 MHz FT-NMR spectrometer in deuterated chloroform ($CDCl_3$) or deuterated dichloromethane (CD_2Cl_2) obtained from Cambridge Isotope Laboratories, Inc. Chemical shifts are reported in parts per million (ppm, δ). ^{1}H NMR spectra were referenced to the residual proton solvent peaks ($CHCl_3$, δ = 7.26; CH_2Cl_2, δ = 5.32). ^{13}C NMR spectra were referenced to the carbon solvent peak ($CDCl_3$, δ = 77.16; CD_2Cl_2, δ = 53.84). Efforts to obtain ^{13}C NMR for *B*-entacene compounds were unsuccessful due to quadrupolar relaxation of boron. High-resolution mass spectra were obtained using a VG Instruments VG70S/E magnetic sector mass spectrometer EI (70 eV) and FAB ionization (matrix for FAB was 3-nitrobenzyl alcohol).

Photophysical considerations. Unless otherwise specified, spectroscopic measurements were conducted in $CHCl_3$ solution at room temperature. UV-visible (UV-vis) absorption spectra were obtained on a Varian Cary50 Bio UV-Visible spectrophotometer.

Photoluminescence (PL) spectra were obtained on a PTI QuantaMaster spectrofluorometer with a 75 W Xenon lamp, maintaining optical densities below 0.1 au. Photoluminescence lifetime data were collected with a PTI Timemaster LED system, maintaining optical densities below 0.1 au. Quantum yields were determined relative to quinine sulfate in 0.1 N H_2SO_4 (55%), maintaining optical densities below 0.05 au.

Electrochemical considerations. Cyclic voltammetry (CV) measurements were performed in a one-chamber, three-electrode cell using a PGSTAT302 potentiostat. A 2 mm^2 Pt button electrode was used as the working electrode with a platinum wire counter electrode relative to a quasi-internal Ag wire reference electrode submerged in 0.01 M $AgNO_3$/0.1 M *n*-Bu_4PF_6 in anhydrous acetonitrile. Measurements were taken in 0.1 M *n*-Bu_4PF_6 (in THF) electrolyte solution recorded at a scan rate of 100 mV/s. Potentials are reported relative to Ag/Ag^+ to which the Fc/Fc^+ couple was measured to be +200 mV.

X-ray crystallography. Single crystals of **2a** suitable for X-ray crystallography were grown by slow diffusion, layering a concentrated solution of **2a**/THF over water. The structure was solved/refined at the Johns Hopkins University (JHU) Chemistry Department X-ray facility by Dr. Maxime A. Siegler. All reflection intensities were measured at 110(2) K using a KM4/Xcalibur (detector: Sapphire3) with enhanced graphite-monochromated Mo *K*α radiation (λ = 0.71073 Å) under the program CrysAlisPro (Version 1.171.35.11 Oxford Diffraction Ltd., 2011). The program CrysAlisPro (Version 1.171.35.11, Oxford Diffraction Ltd., 2011) was used to refine the cell dimensions. Data reduction was done using the program CrysAlisPro (Version 1.171.35.11, Oxford Diffraction Ltd., 2011). The structure was solved with the program SHELXS-97 and was refined on F^2 with SHELXL-97.[23] Analytical numeric absorption corrections based on a multifaceted crystal model were applied using CrysAlisPro (Version 1.171.35.11, Oxford Diffraction Ltd., 2011). The temperature of the data collection was controlled using the system Cryojet (manufactured by Oxford Instruments). The H atoms were placed at calculated positions using the instructions AFIX 43 or AFIX 137 with isotropic displacement parameters having values 1.2 or 1.5 times *U*eq of the attached C atoms. X-ray structures were modeled graphically using Mercury 2.4.6 (Cambridge Crystallographic Data Centre, CCDC).[24]

2a, Fw = 790.78 (including disordered THF molecules), colorless block, 0.47 × 0.39 × 0.14 mm^3, triclinic, *P*-1 (no. 2), a = 13.6095(2), b = 19.4173(4), c = 19.7515(4) Å, α = 109.1855(18), β = 95.4448(15), γ = 96.2210(15)°, V = 4853.03(16) $Å^3$, Z = 4, D_x = 1.082 g cm^{-3},* μ = 0.060 mm^{-1},* abs. corr. range: 0.977–0.997.* 51627 Reflections were measured up to a resolution of $(\sin \theta/\lambda)_{max}$ = 0.59 $Å^{-1}$. 17073 Reflections were unique (R_{int} = 0.0428), of which 12870 were observed [$I > 2\sigma(I)$]. 1148 Parameters were refined using 114 restraints. $R1/wR2$ [$I > 2\sigma(I)$]: 0.0510/0.1404. $R1/wR2$ [all refl.]:

0.0693/0.1485. S = 1.076. Residual electron density was found between −0.29 and 0.44 e $Å^{-3}$. The asymmetric unit contains two crystallographically independent formula units (*i.e.*, *Z'* = 2). The structure is mostly ordered, except for one *tert*-butyl group which is disordered over two orientations [occupancy factor for the major component of the disorder = 0.553(3)]. The structure contains one relatively large void of 145 $Å^3$ (electron count = 42) located at (0 0.5 0.5) (and at equivalent positions). Such voids contain one THF molecule symmetrically constrained to be disordered over an inversion center. The contribution of such solvent molecules was then taken out for the final stages of the refinement using the program SQUEEZE. Compound ID code in JHU Crystallographic database: x871a; compound ID code in CCDC database: 875568.

Theoretical considerations. Geometry optimization and frontier molecular orbital calculations were performed at the DFT level (B3LYP/6-31G*) using Spartan '04 (Wavefunction Inc., Irvine, CA). Nucleus-independent chemical shift (NICS) calculations were performed with Gaussian '03 (Gaussian, Inc., Wallingford, CT)[25] on B3LYP/6-31G* optimized geometries using the GIAO method at the DFT level (B3LYP/6-31+G*) level.

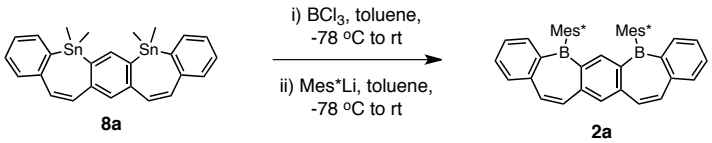

***Meta-B*-entacene (2a).** A solution of fused stannocycle **8a** (90.0 mg, 0.156 mmol) in toluene (5 mL) was cooled to -78 °C with stirring in a dried 25 mL Schlenk flask under nitrogen. A solution of BCl_3 in hexanes (1.0 M, 0.39 mL, 0.39 mmol) was added dropwise to the reaction mixture, which was then allowed to slowly warm to room temperature. After 1.5 h, the mixture was cooled to -78 °C and a suspension of freshly prepared Mes*Li (631 mg, 2.50 mmol) in toluene (11 mL) was added dropwise. The resulting mixture was allowed to warm to room temperature with continued stirring for 16 h. The mixture was partitioned between Et_2O and H_2O (1:1) and the organic layer was removed. The remaining aqueous layer was extracted with Et_2O (2x) and the combined organics were washed with brine, then dried over $MgSO_4$, filtered, and concentrated under reduced pressure to give a yellow solid which was purified by column chromatography (SiO_2, 5% CH_2Cl_2 in hexanes.) The resulting amorphous yellow solid was further purified by triturating with 10 mL methanol (sonicating for 5 min, centrifuging, and decanting the liquid phase) to provide 25.4 mg (0.0321 mmol, 21%) of **2a** as a powdered white solid. ^{1}H NMR (400 MHz, CD_2Cl_2) δ: 9.24 (s, 1H), 7.89 (s, 1H), 7.62 (d, J = 6.8 Hz, 2H), 7.59 (dd, J = 8.0 Hz, 1.6 Hz, 2H), 7.53 (td, J = 7.2 Hz, J = 1.6 Hz, 2H), 7.30 (s, 4H), 7.26 (d, J = 10.4 Hz, 4H), 7.22 (d, J = 8.4 Hz, 2H), 1.39 (s, 18H), 0.76 (s, 36H). UV-vis ($CHCl_3$), λ/nm (log ε): 263 (5.00), 340 (5.18), 361 (4.98), 388 (4.06), 407 (3.98). HRMS (EI): found *m/z* = 790.5811 ± 0.1 ppm; calculated for $C_{58}H_{72}B_2$ [M^+]: 790.5820.

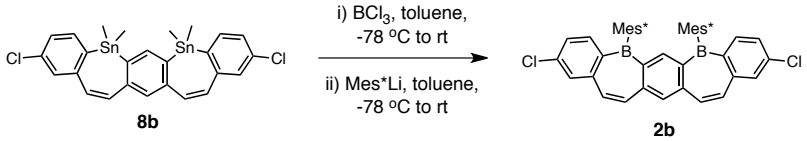

***Para*-dichloro-*meta-B*-entacene (2b).** A solution of fused stannocycle **8b** (129 mg, 0.200 mmol) in toluene (4 mL) was cooled to -78 °C with stirring in a dried 25 mL Schlenk tube under nitrogen. A solution of BCl_3 in hexanes (1.0 M, 0.50 mL, 0.50 mmol) was added dropwise to the reaction mixture, which was then allowed to slowly warm to room temperature. After 1.5 h, the mixture was cooled to -78 °C and a suspension of freshly prepared Mes*Li (808 mg, 3.20 mmol) in toluene (8 mL) was added dropwise. The resulting mixture was allowed to warm to room temperature with continued stirring for 16 h. The mixture was partitioned between Et_2O and H_2O (1:1) and the organic layer was removed. The remaining aqueous layer was extracted with Et_2O (2x) and the combined organics were washed with brine, then dried over $MgSO_4$, filtered, and concentrated under reduced pressure to give a yellow solid which was purified by column chromatography (SiO_2, 5% CH_2Cl_2 in hexanes) to give 35.2 mg (0.0409 mmol,

21%) of **2b** as an amorphous yellow solid, which was used without further purification. Analytically pure material for characterization was obtained by triturating with 10 mL methanol (sonicating for 5 min, centrifuging, and decanting the liquid phase) to provide 8.0 mg of **1b** as a powdered white solid. ^{1}H NMR (400 MHz, CD_2Cl_2) δ: 9.21 (s, 1H), 7.89 (s, 1H), 7.61 (d, J = 2.4 Hz, 2H), 7.52 (d, J = 8.4 Hz, 2H), 7.33 (s, 1H), 7.30 (s, 4H), 7.19 (dd, J = 8.4 Hz, J = 2.0 Hz, 2H), 7.13 (d, J = 12.8 Hz, 2H), 1.38 (s, 18H), 0.75 (s, 36H). UV-vis ($CHCl_3$), λ/nm (log ε): 268 (3.86), 340 (4.03), 361 (3.83), 388 (4.06), 407 (2.85). HRMS (EI): found m/z = 858.5028 ± 0.0 ppm; calculated for $C_{58}H_{70}B_2Cl_2$ [M^+]: 858.5026.

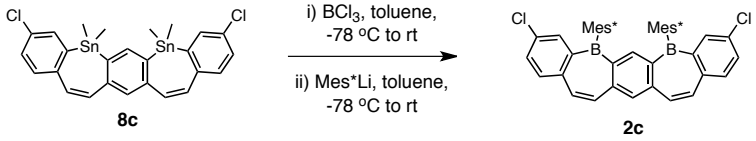

8c **2c**

***Meta*-dichloro-*meta-B*-entacene (2c).** A solution of fused stannocycle **8c** (50 mg, 0.078 mmol) in toluene (3 mL) was cooled to -78 °C with stirring in a dried 25 mL Schlenk tube under nitrogen. A solution of BCl_3 in hexanes (1.0 M, 0.193 mL, 0.193 mmol) was added dropwise to the reaction mixture, which was then allowed to slowly warm to room temperature. After 1.5 h, the mixture was cooled to -78 °C and a suspension of freshly prepared Mes*Li (313 mg, 1.24 mmol) in toluene (6 mL) was added dropwise. The resulting mixture was allowed to warm to room temperature with continued stirring for 18 h. The mixture was partitioned between Et_2O and H_2O (1:1) and the organic layer was removed. The remaining aqueous layer was extracted with Et_2O (2x) and the combined organics were washed with brine, then dried over $MgSO_4$, filtered, and concentrated under reduced pressure to give a yellow solid which was purified by column chromatography (SiO_2, 5% CH_2Cl_2 in hexanes.) The resulting material was further purified by triturating with 10 mL methanol (sonicating for 5 min, centrifuging, and decanting the liquid phase) to provide 35.5 mg of **2c** (0.0413 mmol, 53%) as an amorphous yellow solid, which was used without further purification. ^{1}H NMR (400 MHz, CD_2Cl_2) δ: 9.22 (s, 1H), 7.90 (s, 1H), 7.53 (m, 4H), 7.34 (s, 1H), 7.31 (s, 4H), 7.20 (m, 4H), 1.39 (s, 18H), 0.76 (s, 36H).

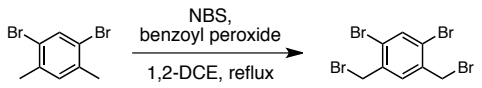

3 **4**

1,5-dibromo-2,4-bis(bromomethyl)benzene (4). A solution of 1,5-dibromo-2,4-dimethylbenzene (**3**, 3.246 g, 12.30 mmol) in 1,2-dichloroethane (120 mL) was stirred under nitrogen in a 250-mL 2-necked round-bottomed flask equipped with a reflux condenser. The mixture was stirred at room temperature and benzoyl peroxide (63 mg, 0.25 mmol) and *N*-bromosuccinimide (7.506 g, 25.83 mmol) were added in single

portions. The mixture was heated to reflux and an additional portion of benzoyl peroxide (180 mg, 0.75 mmol) was added. The reaction was allowed to continue stirring at reflux for 16 h and then cooled to room temperature. The reflux condenser was removed and the flask was stoppered and placed in a -20 °C freezer for 24 h, after which the precipitated solids were filtered off and rinsed with hexanes (150 mL.) The combined filtrates were concentrated under reduced pressure and purified via column chromatography (SiO_2, hexanes) to give 3.32 g of **4** as a white solid (7.87 mmol, 64%) ^{1}H NMR (400 MHz, $CDCl_3$) δ: 7.82 (s, 1H), 7.54 (s, 1H), 4.53 (s, 4H). HRMS (EI): found *m/z* = 338.8020, calculated for $C_8H_6Br_3$ [M^+ - Br]: 338.8020.

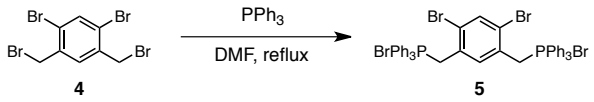

4 **5**

((4,6-dibromo-1,3-phenylene)bis(methylene))bis(bromotriphenylphosphorane) (5). To a stirring solution of **4** (4.000 g, 9.48 mmol) in DMF (20 mL) in a 50-mL 2-necked flask equipped with reflux condenser under nitrogen was added triphenylphosphine (6.219 g, 23.71 mmol) in a single portion. The mixture was heated at reflux with continued stirring for 20 h. After cooling to room temperature, the mixture was diluted with an additional 75 mL of DMF and poured into 300 mL stirring toluene. The precipitated solids were filtered off and washed with 200 mL toluene, then 200 mL Et_2O. The solid material was collected and dried under high vacuum to provide 8.62 g of diphosphonium salt **5** as a powdered white solid (8.28 mmol, 96%). ^{1}H NMR (400 MHz, $CDCl_3$) δ: 7.85-7.80 (m, 6H), 7.71-7.65 (m, 24H), 7.46 (s, 1H), 7.43 (s, 1H), 5.36 (d, *J* = 14.4 Hz, 4H). ^{13}C NMR (100 MHz, $CDCl_3$) δ: 137.3, 125.0, 32.0. HRMS (FAB): found *m/z* = 862.9819, calculated for $C_{44}H_{36}Br_3P_2$ [M^+ - Br]: 862.9842.

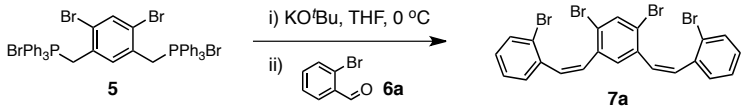

5 **7a**

2,2'-((1*Z*,1'*Z*)-(4,6-dibromo-1,3-phenylene)bis(ethene-2,1-diyl))bis(bromobenzene) (7a). To a stirring suspension of diphosphonium salt **5** (2.400 g, 2.54 mmol) in THF (25 mL) in a 2-necked round-bottomed flask under nitrogen at 0 °C was added potassium *tert*-butoxide (684 mg, 6.10 mmol) as a solid in a single portion. The mixture immediately turned a bright orange color and was stirred at 0 °C for 30 min, then cooled to -78 °C. A solution of 2-bromobenzaldehyde (**6a**, 893 mg, 4.83 mmol) in THF (25 mL) was added dropwise to the reaction mixture via cannula over 20 min. The reaction mixture was allowed to gradually warm to room temperature with continued stirring for 17 h, then partitioned between Et_2O and H_2O (1:1). The organic layer was removed and the aqueous layer was extracted with Et_2O (2x,) after which the combined organic layers were dried over $MgSO_4$, filtered, and concentrated under reduced pressure. The resulting

solid was purified by column chromatography (SiO_2, hexanes) to give 1.17 g of **7a** as a white solid (1.95 mmol, 81%). ^{1}H NMR (400 MHz, $CDCl_3$) δ: 7.77 (s, 1H), 7.51 (dd, J = 8.0 Hz, J = 1.2 Hz, 2H), 7.04 (td, J = 8.0 Hz, J = 1.6 Hz, 2H), 6.96 (td, J = 8.0 Hz, J = 1.6 Hz, 2H), 6.81, (dd, J = 7.6 Hz, J = 1.6 Hz, 2H), 6.68 (s, 1H), 6.62 (d, J = 12.0 Hz, 2H), 6.48 (d, J = 12.0 Hz). ^{13}C NMR (100 MHz, $CDCl_3$) δ: 136.5, 135.9, 133.0, 132.0, 132.0, 131.8, 130.4, 129.2, 129.2, 127.1, 123.9, 123.2. HRMS (FAB): found m/z = 597.7793 ± 0.0001, calculated for $C_{22}H_{14}{}^{79}Br_2{}^{81}Br_2$ [M^+]: 597.7788.

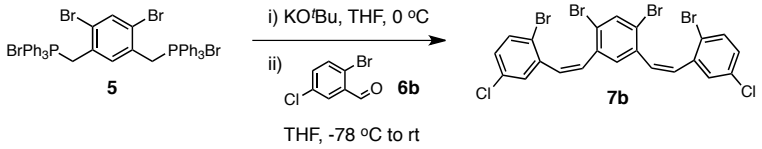

2,2'-((1*Z*,1'*Z*)-(4,6-dibromo-1,3-phenylene)bis(ethene-2,1-diyl))bis(1-bromo-4-chlorobenzene) (7b). To a stirring suspension of diphosphonium salt **5** (1.00 g, 1.06 mmol) in THF (10 mL) in a 50-mL Schlenk flask under nitrogen at 0 °C was added potassium *tert*-butoxide (684 mg, 6.10 mmol) as a solid in a single portion. The mixture immediately turned a bright orange color and was stirred at 0 °C for 30 min, then cooled to -78 °C. A solution of 2-bromo-5-chlorobenzaldehyde (**6b**, 452 mg, 2.06 mmol) in THF (10 mL) was added dropwise to the reaction mixture via cannula over 20 min. The reaction mixture was allowed to gradually warm to room temperature with continued stirring for 22 h, then partitioned between Et_2O and H_2O (1:1). The organic layer was removed and the aqueous layer was extracted with Et_2O (2x,) after which the combined organic layers were dried over $MgSO_4$, filtered, and concentrated under reduced pressure. The resulting solid was purified by column chromatography (SiO_2, hexanes) to give 535 mg of **7b** as a white solid (0.804 mmol, 81%). ^{1}H NMR (400 MHz, $CDCl_3$) δ: 7.32 (s, 1H), 7.42 (d, J = 8.4 Hz, 2H), 7.04 (d, J = 8.4 Hz, 2H),), 6.86, (s, 2H), 6.54 (d, J = 4.0 Hz, 4H). ^{13}C NMR (100 MHz, $CDCl_3$) δ: 138.2, 136.5, 135.3, 134.0, 133.2, 131.5, 130.5, 130.3, 130.0, 129.3, 123.6, 121.7. HRMS (FAB): found m/z = 665.6984 ± 0.0001; calculated for $C_{22}H_{12}{}^{79}Br_4{}^{37}Cl_2$ [M^+]: 665.6991.

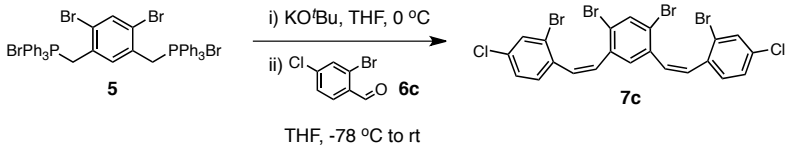

4,4'-((1*Z*,1'*Z*)-(4,6-dibromo-1,3-phenylene)bis(ethene-2,1-diyl))bis(3-bromo-1-chlorobenzene) (7c). To a stirring suspension of diphosphonium salt **5** (1.14 g, 1.20 mmol) in THF (10 mL) in a 50-mL 2-necked round-bottomed flask under nitrogen at 0 °C was added potassium *tert*-butoxide (323 mg, 2.88 mmol) as a solid in a single portion. The mixture immediately turned a bright orange color and was stirred at 0 °C for 30 min, then cooled to -78 °C. A solution of 2-bromo-4-chlorobenzaldehyde (**6c**[2], 501 mg, 2.27

mmol) in THF (10 mL) was added dropwise to the reaction mixture via cannula over 20 min. The reaction mixture was allowed to gradually warm to room temperature with continued stirring for 16 h, then partitioned 1:1 between Et_2O and H_2O. The organic layer was removed and the aqueous layer was extracted with Et_2O (2x,) after which the combined organic layers were dried over $MgSO_4$, filtered, and concentrated under reduced pressure. The resulting solid was purified by column chromatography (SiO_2, hexanes) to give 544 mg of **7c** as a white solid (0.816 mmol, 72%). ^{1}H NMR (400 MHz, $CDCl_3$) δ: 7.80 (s, 1H), 7.56 (d, *J* = 2.4 Hz, 2H), 6.96 (dd, *J* = 8.0 Hz, *J* = 2.0, 2H), 6.76 (d, *J* = 8.4 Hz, 2H), 6.67 (s, 1H), 6.54 (d, *J* = 4.8 Hz, 4H). ^{13}C NMR (100 MHz, $CDCl_3$) δ: 136.2, 135.5, 134.9, 133.9, 132.6, 132.5, 130.7,130.5, 129.5, 127.3, 124.0, 123.3. HRMS (EI): found *m/z* = 665.6999 ± 0.0 ppm; calculated for $C_{22}H_{12}{}^{79}Br_3{}^{81}Br^{35}Cl^{37}Cl$ [M^+]: 665.6999.

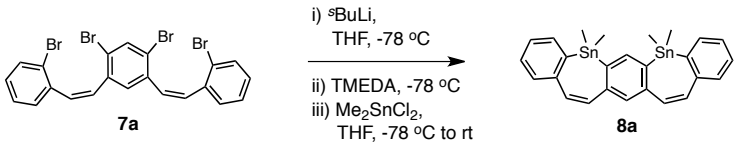

fused stannocycle (8a). To a stirring solution of **7a** (245 mg, 0.410 mmol) in THF (50 mL) at -78 °C in a 100-mL Schlenk flask under nitrogen was added dropwise a solution of *s*-BuLi in cyclohexane (1.425 M, 2.30 mL, 3.28 mmol), followed by TMEDA (0.492 mL, 3.28 mmol). The reaction was held at -78 °C for 2.5 h, after which a solution of Me_2SnCl_2 (185 mg, 0.841 mmol) in THF (12 mL) was added dropwise to the deep green reaction mixture over 30 min. The mixture was allowed to continue stirring with gradual warming to room temperature over 18 h, after which it was partitioned between Et_2O and H_2O (1:1). The organic layer was removed and the aqueous layer was extracted 2x with Et_2O. The combined organics were washed with 1 M HCl (aq), then brine, and dried over $MgSO_4$. After filtration and concentration under reduced pressure, the crude organic product was pushed through a short pad of SiO_2, eluting with of 4:1/hexanes:EtOAc (150 mL). The eluent was concentrated under reduced pressure and the resulting yellow-orange material was triturated 2x with 10 mL methanol (sonicating for 5 min, centrifuging, and decanting the liquid phase) and dried under high vacuum to provide 210 mg of **8a** as a pale yellow solid (0.352 mmol, 89%) that was used without further purification. HRMS (FAB): found *m/z* = 579.0142; calculated for $C_{26}H_{27}Sn_2$: 579.0157 [$M+H^+$].

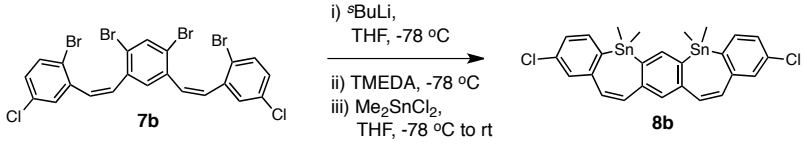

***para*-dichloro fused stannocycle (8b).** To a stirring solution of **7b** (334 mg, 0.501 mmol) in THF (50 mL) at -78 °C in a 100-mL Schlenk flask under nitrogen was added

dropwise a solution of *s*-BuLi in cyclohexane (1.4 M, 2.86 mL, 4.01 mmol), followed by TMEDA (0.601 mL, 4.01 mmol). The reaction was held at -78 °C for 2.5 h, after which a solution of Me_2SnCl_2 (184.6 mg, 0.841 mmol) in THF (10 mL) was added dropwise to the deep green reaction mixture over 30 min. The mixture was allowed to continue stirring with gradual warming to room temperature over 18 h, after which it was partitioned between Et_2O and H_2O (1:1). The organic layer was removed and the aqueous layer was extracted 2x with Et_2O. The combined organics were washed sequentially with 1 M HCl (aq) and brine, dried over $MgSO_4$, filtered, and concentrated under reduced pressure. The resulting yellow-orange material was triturated 2x with 10 mL methanol (sonicating for 5 min, centrifuging, and decanting the liquid phase) and dried under high vacuum to provide 188 mg of **8b** as a pale yellow solid (0.291 mmol, 58%) that was used without further purification.

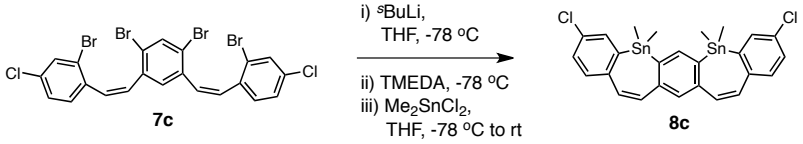

***meta*-dichloro fused stannocycle (8c).** To a stirring solution of **7c** (267 mg, 0.401 mmol) in THF (50 mL) at -78 °C in a 100-mL Schlenk flask under nitrogen was added dropwise a solution of *s*-BuLi in cyclohexane (1.4 M, 2.26 mL, 3.21 mmol), followed by TMEDA (0.494 mL, 3.21 mmol). The reaction was held at -78 °C for 2.5 h, after which a solution of Me_2SnCl_2 (180.6 mg, 0.822 mmol) in THF (10 mL) was added dropwise to the deep green reaction mixture over 30 min. The mixture was allowed to continue stirring with gradual warming to room temperature over 16 h, after which it was partitioned between Et_2O and H_2O (1:1). The organic layer was removed and the aqueous layer was extracted 2x with Et_2O. The combined organics were washed sequentially with 1 M HCl (aq) and brine, dried over $MgSO_4$, filtered, and concentrated under reduced pressure. The resulting yellow-orange material was triturated 2x with 10 mL methanol (sonicating for 5 min, centrifuging, and decanting the liquid phase) and dried under high vacuum to provide 213 mg of **8c** as a pale yellow solid (0.331 mmol, 83%) that was used without further purification.

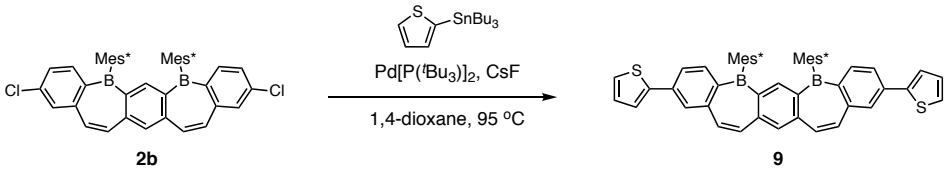

Bis(2-thienyl) *meta-B*-entacene (9). To a stirring solution of **2b** (31.5 mg, 0.0366 mmol), Pd[P(*t*-Bu)$_3$]$_2$ (2.0 mg, 0.0037 mmol), and CsF (34.5 mg, 0.227 mmol) in 1,4-dioxane (2 mL) in a dried 25-mL Schlenk tube under nitrogen was added 2-tributylstannylthiophene (30 μL, 36 mg, 0.095 mmol) dropwise *via* syringe. The mixture

was then heated to 95 °C and allowed to continue stirring for 18 h. After cooling to room temperature, the mixture was diluted with EtOAc and pushed through a short pad of SiO_2, eluting with EtOAc (150 mL). The eluent was concentrated under reduced pressure and purified by by flash column chromatography (SiO_2, gradient elution: 5% CH_2Cl_2 in hexanes - 10% CH_2Cl_2 in hexanes) to provide 14.5 mg (0.0152 mmol, 41%) of **9** as an off-white/yellow solid. ^{1}H NMR (400 MHz, CD_2Cl_2) δ: 9.24 (s, 1H), 7.90 (s, 1H), 7.87 (d, *J* = 2.0 Hz, 2H), 7.60 (d, *J* = 8.4 Hz, 2H), 7.51-7.48 (m, 4H), 7.37 (dd, *J* = 4.8 Hz, *J* = 0.8 Hz, 2H), 7.33 (d, *J* = 13.2 Hz, 2H), 7.31 (s, 4H), 7.27 (d, *J* = 13.2 Hz, 2H), 7.12 (dd, *J* = 4.8 Hz, *J* = 2.0 Hz), 1.40 (s, 18H), 0.79 (s, 36H). UV-vis ($CHCl_3$) λ/nm (log ε): 268 (3.90), 349 (4.42), 410 (2.82). HRMS (FAB): found *m/z* = 954.5589 ± 0.2 ppm; calculated for $C_{66}H_{76}B_2S_2$ [M^+]: 954.5575.

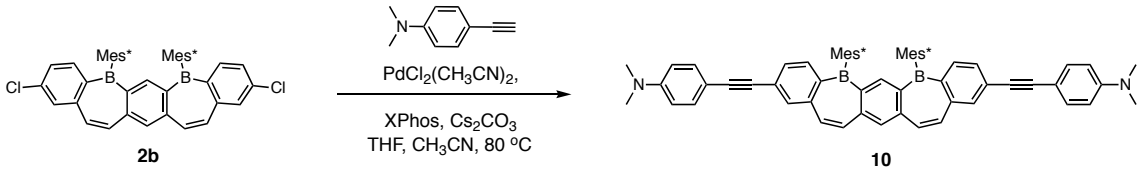

Bis(4-*N,N*-dimethylaminophenyl ethynyl) *meta-B*-entacene (10). To a stirring solution of **2b** (25.6 mg, 0.0298 mmol), $PdCl_2(CH_3CN)_2$ (2.2 mg, 0.0060 mmol), XPhos (8.3 mg, 0.018 mmol), and Cs_2CO_3 (58.3 mg, 0.179 mmol) in THF (1.0 mL) and CH_3CN (1.5 mL) in a dried 25-mL Schlenk tube under nitrogen was added a solution of 4-ethynyl-*N,N*-dimethylaniline (13.0 mg, 0.0895 mmol) in CH_3CN (0.5 mL) dropwise via syringe. The mixture was then heated to 80 °C and allowed to continue stirring for 18 h. After cooling to room temperature, the mixture was partitioned between Et_2O and H_2O (1:1) and the organic layer was removed. The remaining aqueous layer was extracted with Et_2O (2x) and the combined organics were dried over $MgSO_4$, filtered, and concentrated under reduced pressure to give a solid which was purified by column chromatography (SiO_2, gradient elution: 5% EtOAc in hexanes – 10% EtOAc in hexanes.) to provide 10.6 mg (0.00984 mmol, 33%) of **10** as a yellow solid. ^{1}H NMR (400 MHz, CD_2Cl_2) δ: 9.20 (s, 1H), 7.89 (s, 1H), 7.73 (s, 2H), 7.54 (d, *J* = 8.4 Hz, 2H), 7.40 (d, *J* = 9.2 Hz, 4H), 7.33 (d, *J* = 13.2 Hz, 2H), 7.31 (s, 4H), 7.29 (s, 2H), 7.20 (d, *J* = 4.0 Hz, 2H), 6.67 (d, *J* = 8.8 Hz, 4H), 2.99 (s, 12H), 1.39 (s, 18H), 0.77 (s, 36H). UV-vis ($CHCl_3$) λ/nm (log ε): 289 (3.92), 352 (4.10), 377 (4.10). HRMS (FAB): found *m/z* = 1076.7321 ± 2.9 ppm; calculated for $C_{78}H_{90}B_2N_2$ [M^+]: 1076.7290.

References

(1) Caruso, A.; Siegler, M. A.; Tovar, J. D. *Angew. Chem. Int. Ed.* **2010***, 49,* 4213–4217.
(2) Caruso, A.; Tovar, J. D. *Org. Lett*. **2011**, *13*, 3106–3109.
(3) Nöth, H.; Vahrenkamp, H. *J. Organomet. Chem*. **1968**, *11*, 399–405.
(4) Eisch, J. J.; Kotowicz, B. W. *Eur. J. Inorg. Chem.* **1998***,* 761–769.
(5) Curtis, M. D.; Cao, J.; Kampf, J. W. *J. Am. Chem. Soc.* **2004***, 126,* 4318–4328.
(6) Anthony, J. E. *Chem. Rev.* **2006,** *106*, 5028−5048.
(7) Ashe, A. J.; Klein, W.; Rousseau, R. *Organometallics* **1993***, 12,* 3225–3231.
(8) Schleyer, P. V. R.; Maerker, C.; Dransfeld, A.; Jiao, H.; Hommes, N. J. R. V. E. *J. Am. Chem. Soc.* **1996,** *118*, 6317–6318.
(9) Chen, Z.; Wannere, C. S.; Corminboeuf, C.; Puchta, R.; Schleyer, P. V. R. *Chem. Rev.* **2005,** *105,* 3842−3888.
(10) Subramanian, G.; Schleyer, P. V. R.; Jiao, H. *Organometallics* **1997,** *16,* 2362–2369.
(11) Zhu, M.; Yang, C. *Chem. Soc. Rev*. **2013**, *42*, 4963–4976.
(12) Kaim, W.; Schulz, A. *Angew. Chem. Int. Ed.* **1984***, 23,* 615–616.
(13) Rajca, A.; Rajca, S.; Desai, S. R. *J. Chem. Soc. Chem. Commun.* **1995**, 1957–1958.
(14) Grabowski, Z. R.; Rotkiewicz, K.; Rettig, W. *Chem. Rev.* **2003,** *103,* 3899−4031.
(15) Hundertmark, T.; Littke, A. F.; Buchwald, S. L.; Fu, G. C. *Org. Lett.* **2000,** *2,* 1729–1731.
(16) Littke, A. F.; Schwarz, L.; Fu, G. C. *J. Am. Chem. Soc.* **2002***, 124,* 6343–6348.
(17) Levine, D. R.; Caruso, A.; Siegler, M. A.; Tovar, J. D. *Chem. Commun.,* **2012***, 48,* 6256–6258.
(18) Bonifacio, M. C.; Robertson, C. R.; Jung, J.-Y.; King, B. T. *J. Org. Chem.* **2005***, 70,* 8522–8526.
(19) Čapková, K.; Yoneda, Y.; Dickerson, T. J.; Janda, K. D. *Bioorg. Med. Chem. Lett.* **2007***, 17,* 6463–6466.
(20) Rodriguez, J. G.; Tejedor, J. L.; Rumbero, A.; Canoira, L. *Tetrahedron* **2006**, *62*, *3075–3080.*
(21) Knorr, R.; Pires, C.; Behringer, C.; Menke, T; Freudenreich, J; Rossmann, E. C., A.; Böhrer, P. *J. Am. Chem. Soc.* **2006***, 128,* 14845–14853.
(22) Wakamiya, A.; Mishima, K.; Ekawa, K.; Yamaguchi, S. *Chem. Commun.,* **2008**, 579–581.
(23) Sheldrick, G. M. *Acta Cryst.* **2008**, *A64,* 112–122.
(24) Macrae, C. F.; Edgington, P. R.; McCabe, P.; Pidcock, E.; Shields, G. P.; Taylor, R.; Towler, M.; van de Streek, J. *J Appl. Cryst*. **2006**, *39*, 453–457.
(25) Gaussian 03, Revision C.01, Frisch, M. J.; Trucks, G. W.; Schlegel, H. B.; Scuseria, G. E.; Robb, M. A.; Cheeseman, J. R.; Montgomery, Jr., J. A.; Vreven, T.; Kudin, K. N.; Burant, J. C.; Millam, J. M.; Iyengar, S. S.; Tomasi, J.; Barone, V.; Mennucci, B.; Cossi, M.; Scalmani, G.; Rega, N.; Petersson, G. A.; Nakatsuji, H.; Hada, M.; Ehara, M.; Toyota, K.; Fukuda, R.; Hasegawa, J.; Ishida, M.; Nakajima, T.; Honda, Y.; Kitao, O.; Nakai, H.; Klene, M.; Li, X.; Knox, J. E.; Hratchian, H. P.; Cross, J. B.; Bakken, V.; Adamo, C.; Jaramillo, J.; Gomperts, R.; Stratmann, R. E.; Yazyev, O.; Austin, A. J.; Cammi, R.; Pomelli, C.; Ochterski, J. W.; Ayala, P. Y.; Morokuma, K.; Voth, G. A.; Salvador, P.; Dannenberg, J. J.; Zakrzewski, V. G.; Dapprich, S.; Daniels, A. D.; Strain, M. C.; Farkas, O.; Malick, D. K.; Rabuck, A. D.; Raghavachari, K.; Foresman, J. B.; Ortiz, J. V.; Cui, Q.; Baboul, A. G.; Clifford, S.; Cioslowski, J.; Stefanov, B. B.; Liu, G.; Liashenko, A.; Piskorz, P.; Komaromi, I.; Martin, R. L.; Fox, D. J.; Keith, T.; Al-Laham, M. A.; Peng, C. Y.; Nanayakkara, A.; Challacombe, M.; Gill, P. M. W.; Johnson, B.; Chen, W.; Wong, M. W.; Gonzalez, C.; and Pople, J. A.; Gaussian, Inc., Wallingford CT, **2004**.

Chapter 3: The Synthesis and Characterization of Several Isomeric Air- and Moisture-stable Dithienoborepins

Introduction

From the early investigations of van Tamelen,[1] Leusink,[2] and Axelrad and Halpern[3] to more recent experimental and theoretical work by Ashe,[4] Schleyer,[5] Schulman,[6] Sashida,[7] Piers,[8] Tovar,[9-12] and Yamaguchi,[13] published research concerning borepin-containing polycyclic aromatic hydrocarbons (PAHs) has focused mainly on systems with benzo-fused borepin rings. A fewer number of studies have been devoted to a different structural theme – the borepin-thiophene fusion (Figure 3.1). In the late 1960s and early 1970s, Gronowitz and coworkers reported the synthesis of a series of dithieno-fused borepins featuring *B*-O-*B*, *B*-OR, and *B*-alkyl motifs (Figure 3.1, **i** – **iv**)[14,15] as isoelectronic, boron-containing analogues of thiophene-annulated tropylium cations.[16-18] This was of interest because thiophene-fusion had been shown to provide more stability to the tropylium cation than benzo-fusion, a consequence of the electron-rich, polarizable character of thiophene. Gronowitz's dithienoborepins (DTBs) proved stable enough to obtain UV-vis spectroscopic data,[15] revealing electronic properties similar to tropone-based analogues. Evidence for aromatic delocalization in the borepin rings was provided based on the downfield ^{1}H NMR chemical shifts of the *B*-Me DTB relative to compounds where the 7-membered ring contained a saturated center. Although these studies provided benchmark characterization data for DTBs, Parkanyii later reported that DTB **i** was susceptible to B-C bond cleavage under electrophilic aromatic bromination conditions and decomposed entirely during attempted proton-deuterium exchange in DMSO/D_2SO4.[19]

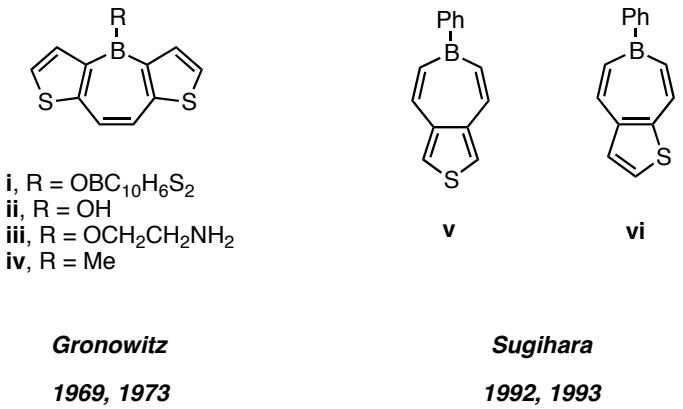

Figure 3.1. Structures of previously studied thiophene-fused borepins.

In the early 1990s, Sugihara and Murata reported the synthesis and characterization of monothieno-annelated borepins (Figure 3.1).[20-22] The initial report described the synthesis of 1-phenylthieno[3,4-*d*]borepin **v**,[20] and its characterization as an isoelectronic, dipole-reversed analogue of azulene. NMR data for this compound suggested that π-electron density resembled a 10-π electron circuit delocalized around the periphery of the fused bicyclic skeleton; on the other hand, the isomeric 1-phenylthieno[2,3-*d*]borepin **vi**, featured more localized conjugation in the individual borepin and thiophene rings.[21] Both compounds displayed redox properties characteristic for thiophene and arylborane components (anodic and cathodic behavior, respectively) as well as moderately intense fluorescence.[22] The chemical sensitivity of these compounds was however also evident as samples in $CHCl_3$ solution underwent slow cleavage of the B-C bonds over the course of a week by adventitious H^+, which could be accelerated to completion within a few hours by adding acetic acid.

Since these early thiophene-fused borepin studies, the development of π-conjugated materials for organic electronics has become an area of intense research, with thiophene-based systems occupying a priveleged position in terms of utility and

performance.[23] This is due to several properties of thiophene which have proven highly desirable, including polarizable electron density, excellent conjugation and solid-state ordering characteristics, and facile, regioselective synthetic chemistry. Many extended polycyclic ladder-type compounds featuring thiophene rings[24-26] as embedded subunits and/or terminal moieties have shown characteristics unique from all-benzenoid acenes. Namely, they tend to exhibit increased chemical and oxidative stability due to widened HOMO-LUMO gaps, greater propensity for cofacial molecular π-stacking and close S–S contacts, and ease of derivatization. Thiophene-containing PAHs (Figure 3.2) range from simple bicyclic benzothiophene (**vii**, **viii**) and thienothiophene (**ix – xii**) compounds (of which the isomers are numerous due to the different possible fusion orientations of benzene and thiophene rings) to more extended, ladder-type compounds. Notable examples among these are thieno-"end-capped" acenedithiophenes (**xiii**),[27,28] elongated linear (**xiv**)[29] and helical (**xv**)[30,31] all-thienoacenes, and core all-thienoacene units fused to terminal benzenoid structures (**xvi**).[32] Such thiophene- containing acenes have been employed most prominently as active layers several high-perfoming organic field-effect transistor (OFET) devices, as well as for other applications.

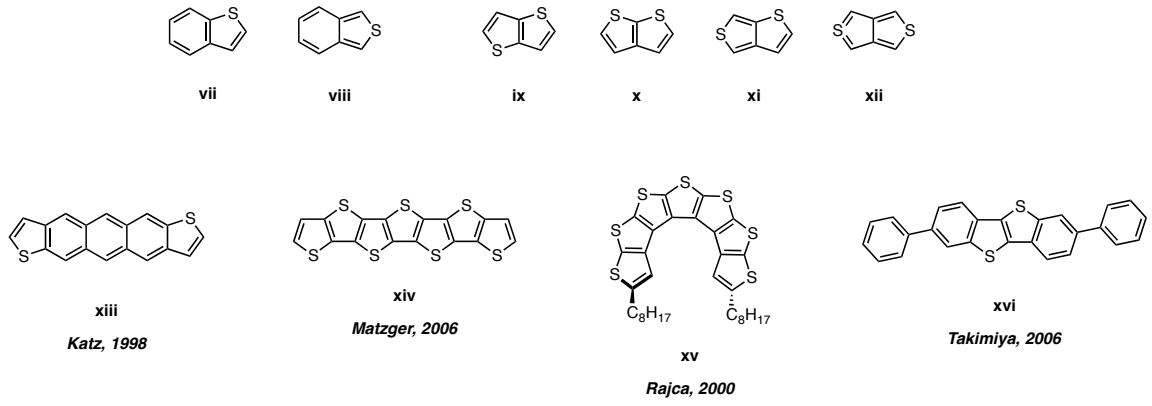

Figure 3.2. Selected small-molecule and extended, ladder-type fused heteroarenes containing thiophene rings.

In view of the paramount importance of thiophene-containing compounds in organic electronic materials development, revisiting the study of thiophene-fused borepins was identified as an area of prime interest to the Tovar group. The main objective was to establish robust synthetic methods to access these compounds in more highly stable forms to elucidate their fundamental properties as well and explore prospects for further derivatization and possible applications. Preliminary work by former Tovar group member Dr. Anthony Caruso Jr. demonstrated that a successful synthesis of *B*-phenyl dithieno[2,3-*b*:3,2-*f*]borepin could be achieved via tin-boron exchange between $PhBCl_2$ and the corresponding dithienostannepin substrate (Scheme 1). This *B*-Ph DTB possessed moderate stability toward atmospheric oxygen and moisture without rigorous kinetic protection (no bulky Mes* group) and exhibited reversible cathodic electrochemical redox behavior at a less negative potential than *B*-Mes* dibenzoborepin (DBB). However, exposure of *B*-Ph DTB to coordinating solvents resulted in deleterious Lewis acid – Lewis base interactions with the boron center and therefore – like the early systems studied by Gronowitz and Sugihara/Murata – this compound was generally unsuitable for further property-tuning through synthetic modification or for solution processing to yield functional materials.

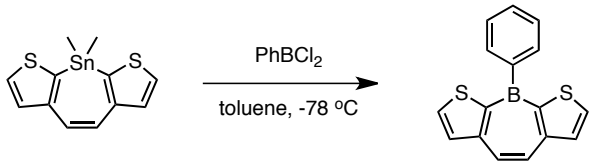

Scheme 3.1. Caruso's synthesis of a *B*-Ph DTB via the tin-boron exchange method.

This chapter describes the development of synthetic routes towards DTB scaffolds with high levels of chemical stability, allowing for the elucidation of fundamental

properties and evaluation of their promise as candidates for organic electronics. Four isomerically unique *B*-Mes DTBs (**1** – **4**, Figure 3.3) were prepared, showing several desirable features exhibited by typical boron-containing π-electron systems, including electron-accepting character, photoluminescence, and Lewis-acidic coordination of boron to fluoride ions. Spectroscopic, electrochemical, and theoretical characterization established that the position of boron in relation to the fused, conjugated thiophene rings was of key significance in dictating the properties of the different structural isomers. Studies regarding the reactivity and further functionalization of these *B*-Mes DTBs are described in Chapter 4.

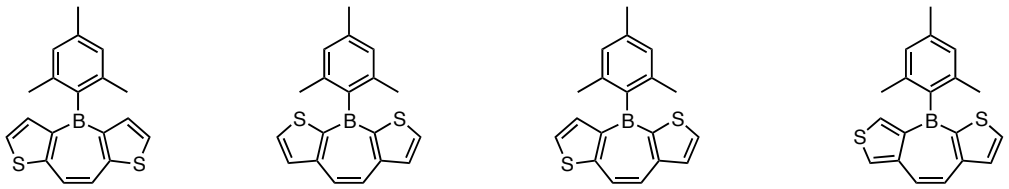

Figure 3.3. Isomeric *B*-Mes-stabilized DTBs discussed in this chapter.

Results and Discussion

Polycyclic π-electron systems based on fused thiophene-borepin core structures were envisioned to offer several advantages relative to the benzo-fused borepins previously studied in our lab. In addition to providing extra boron-stabilizing ability due to the electron-rich nature of thiophene, further opportunities for electronic tuning might be offered by generating several DTB isomers with different ring fusion motifs (Figure 3.4). Symmetrical DTB structural isomers of types **I** and **II** were initially targeted as they were viewed to offer fundamentally different conjugation relationships between the thiophene rings and boron based on the typical extension of π-conjugation at the thiophene α-position (adjacent to sulfur). Thus in **I** the main conjugation pathway runs between the thiophene α-positions and the olefinic portion of the borepin (i.e. dithienylethene-like conjugation), while the boron atom is weakly conjugated at the β-positions. Conversely, in structure **II** the boron atom is strongly conjugated via the thiophene α-positions (i.e. dithienylborane-like conjugation), while the olefinic portion of the borepin ring serves as a weakly β-conjugated ethene bridge. Hybrid "unsymmetrical" DTB structure **III** was envisioned to possibly provide aspects of both strong/weak boron-thiophene and strong/weak ethene-thiophene conjugation (a "middle ground" between **I** and **II**). Contrasting more starkly with **I-III**, DTB **IV** (featuring fusion between the *c*-edge of the thiophene rings and the *b* and *f* edges of borepin) would lack a formally Hückel-aromatic π-electron arrangement within the borepin ring, instead bearing a "radialene-line" arrangement of double bonds around the molecular periphery. Depending on whether this pattern promotes enhanced delocalization or more localized,

thiophene-centered aromatic sextets (as represented in Figure 4), the resultant electronic properties of the system could be differ quite dramatically.

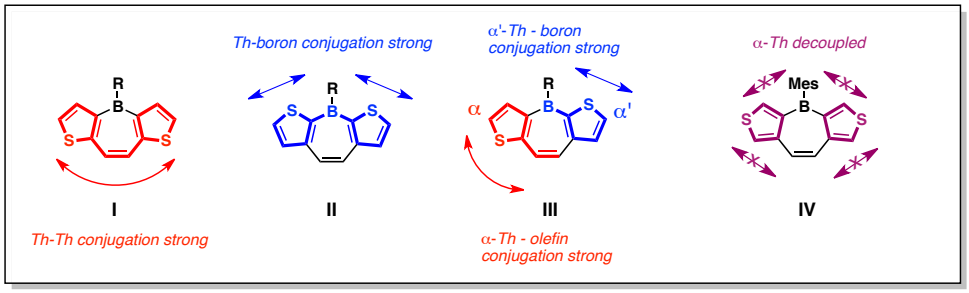

Figure 3.4. Isomeric DTB archetypes, showing envisioned major conjugation paths between the thiophene (Th) rings and the borepin due to ring fusion orientation.

Preliminary synthetic efforts towards DTBs were focused on employing tin-boron exchange chemistry (Scheme 3.2a), the traditional method of choice for borepin formation.[33] After confirming that Caruso's sterically unprotected *B*-Ph DTB could not withstand rigorous purification via silica gel chromatography or further synthetic manipulation, efforts were made to access more stable DTB compounds through the installation of bulkier boron-protective groups [such as mesityl (= 2,4,6-trimethylphenyl; Mes), tripyl (= 2,4,6-tri-isopropyl-phenyl; Tip), and supermesityl (= 2,4,6-tri-tert-butylphenyl; Mes*)], while maintaining the overall tin-boron exchange synthetic approach. Unfortunately, in contrast to the facile generation of *B*-Ph DTB, attempts to directly generate the *B*-Mes substituted DTB via tin-boron exchange by treatment of the stannocycle with $MesBBr_2$ were not successful, while related attempts to employ variants of tin-boron exchange based on sequential BX_3 / ArLi treatments (X = Cl, Br; Ar = Mes, Tip, Mes*), such as those previously used to construct *B*-Mes* DBBs and *B*-entacenes, led only to complex, intractable mixtures. Believing that the potentially aggressive aryllithium reagents might be causing undesired side-reactions (such as α-proton

abstraction or ring-opening), efforts to utilize milder reagents for aryl-group installation such as MesMgBr and MesCu[34-36] were also attempted, but to no avail.

To rule out the possibility of that the Lewis acidic BX_3 reagents could be undergoing side-reactions with the electron-rich thiophene rings, the dithienostannepin precursor **9** with electron-poor, "bromine-blocked" thiophene rings was prepared in a four-step protocol from 5-bromo-2-iodothiophene-3-carbaldehyde **5** by the typical Wittig route (Scheme 3.2b). The bromide handles were also anticipated to provide additional benefit as springboards for late-stage synthetic modification following borepin formation. Alas, all efforts attempts to convert **9** to the corresponding DTB through tin-boron exchange methods as described above remained unsuccessful.

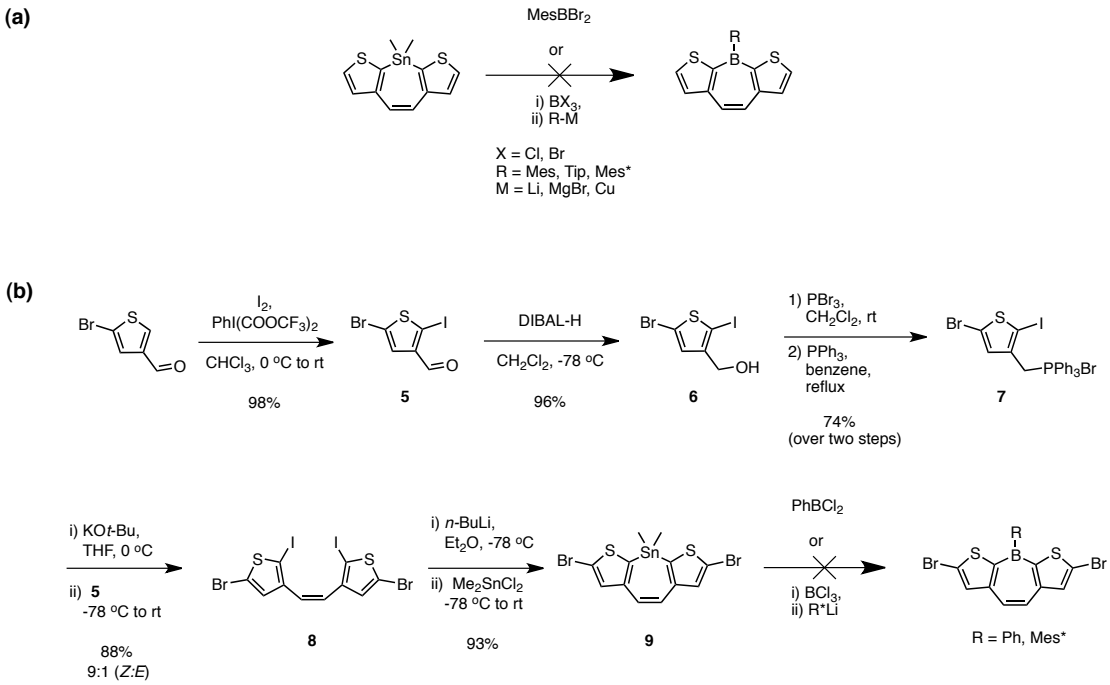

Scheme 3.2. Summary of unsuccessful attempts to utilize tin-boron exchange methods to prepare DTBs. **(a)** Attempted syntheses of *B*-Ar DTBs with bulkier Ar protective groups using stannocycle **DTSn**. **(b)** Multistep synthesis of precursor stannepin **9** with "halogen-blocked" α-positions and subsequent attempts to convert **9** to dibrominated *B*-Ph or *B*-Mes* DTBs.

Due to the persistent failure of normally reliable tin-boron exchange methods to prepare DTBs with more rigorous steric protection than *B*-Ph, alternative synthetic tactics had to be evaluated. In general, three major methods exist for the installation of BR_3 units (R = aryl, alkyl) in conjugated systems: 1) metathesis transformations (i.e. Sn-B or Si-B exchange), 2) hydro/haloboration, or 3) nucleophilic substitution of leaving groups from a borane substrate. With respect to the third method, a recent publication by Kobayashi, Kawashima, and coworkers was found to be quite encouraging.[37] The authors reported the synthesis of bis(2-thienyl)mesitylborane (**BTMB**), a compound bearing considerable structural homology to the desired DTBs, albeit in a torsionally unconstrained framework. **BTMB** was accessed by condensation of 2-thienyllithium with mesityl boronic ester $MesB(OMe)_2$ (Scheme 3.3). Notably, **BTMB** was fully stable to air and moisture both as a solid and in solution with the protection of only a single *B*-Mes protective group, while typically two Mes groups (or a single, more bulky aryl group such as Tip or Mes*) are normally required to impart stability to triarylboranes. Further investigation revealed that similar strategies exploiting boronic ester condensation have been employed to prepare other π-conjugated boron-containing polycycles, including ladder-type 1,4-heteroborins[38,39] and benzo- and thieno-annulated boroles.[40-42]

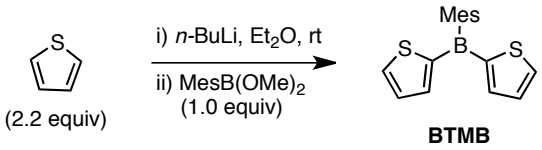

Scheme 3.3. Kawashima and coworkers' synthesis of **BTMB**.

Using a variation of the directed lithiation/mesityl boronic ester condensation procedure it was finally possible to synthesize several isomeric variants of the desired DTB compounds. Borepin formation was achieved by direct quenching of dimetallated

dithienylethenes (generated via lithium-halogen exchange through treatment of dibrominated *Z*-dithienylethenes with *t*-BuLi in Et_2O at -78 °C) with $MesB(OMe)_2$. In this manner, DTBs **1**, **2**, and **3** (types **I**, **II**, and **III** in Figure 3.4) containing *B*-Mes protective groups were prepared in moderate to good yields on scales up to an excess of one gram from dithienylethenes **10**, **11**, and **12**, respectively (Scheme 3.4). In contrast to tin-boron exchange methods, direct boronic ester condensation presented the additional advantages of not requiring extra transmetalation/isolation steps (no stannocyclic intermediate) or the use of highly toxic boron/tin halide reagents such as BCl_3 or Me_2SnCl_2 during the synthetic route. It is interesting to note that the synthetic method used here for DTB formation was previously reported by Piers and coworkers to be inapplicable for the preparation of the analogous benzo-fused DBB compounds.[8] Like Kawashima's **BTMB**, the *B*-Mes group was sufficient to render DTBs fully robust towards air, moisture, and silica gel, allowing aqueous reaction workup and facile chromatographic purification at the bench. This contrasts with DBBs, which require protection by the extremely bulky *B*-Mes* group to provide long-term stability towards ambient conditions.[9]

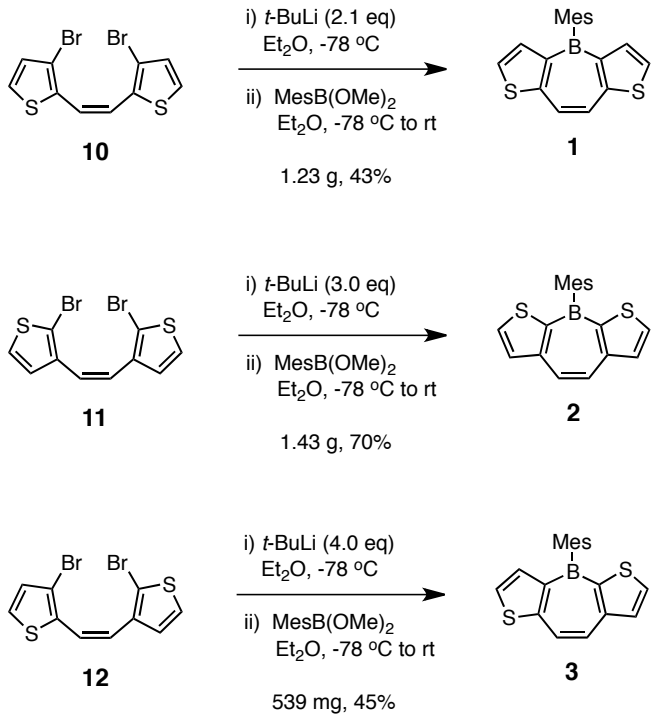

Scheme 3.4. Synthesis of *B*-Mes DTBs **1**, **2**, and **3** by the Li-Br exchange – boronic ester condensation method.

A screen of different DTB preparative conditions revealed that the use of alternative metal-halogen exchange reagents (such as *n*-BuLi or *i*-PrMgCl•LiCl[43]) generally gave inferior yields compared to *t*-BuLi and that Et_2O was a superior reaction solvent to THF. Running the reaction under high dilution conditions (≤0.01 M) also gave markedly reduced yields compared with a typical 0.1 M substrate concentration. Notably, an attempt to install the more hindered *B*-Tip group by condensation with $TipB(OMe)_2$ instead of $MesB(OMe)_2$ (as employed by Yamaguchi for the preparation of dibenzoboroles)[40] appeared to only provide extreme trace amounts of the desired product according to a crude ^1H NMR analysis, suggesting an upper limit on the allowable steric bulk present in the $ArB(OMe)_2$ reagent for successful borepin formation with this preparative method.

The dibrominated *Z*-dithienylethene precursors to DTBs were synthesized using two different strategies. For compounds **10** and **11** (precursors to DTBs **1** and **2**, respectively) Wittig reactions between brominated thienyl phosphonium salts **13** and **15** and thienyl carbaldehydes **14** and **16** provided the targeted dithienylethenes with good *Z*-selectivity (Scheme 3.5).

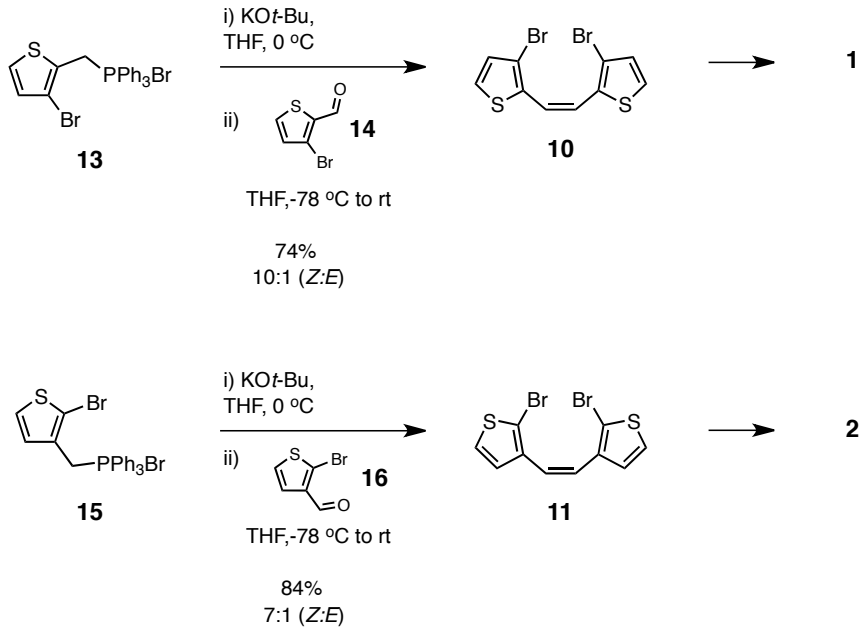

Scheme 3.5. Synthetic routes to *Z*-dithienylethenes **10** and **11** (precursors to DTBs **1** and **2**) by the Wittig route.

However, when the Wittig approach was attempted to synthesize the unsymmetrical dithienylethene **12** (the precursor to DTB **3**) poor stereoselectivity was observed and separation of the *E*/*Z* mixtures proved problematic, thus necessitating an alternative preparatory method. A literature search identified Sato's Ti–mediated reduction of disubstituted alkynes to the corresponding *cis*, *vic*-vinylic dianion equivalents[44,45] (Scheme 3.6) as a highly promising option. Employing a slight modification of Sato's original conditions, dibrominated dithienylethyne **17**[46] was converted to desired *Z*-dithienylethene **12** in high yield with no detectable *E*-isomer

contamination (^{1}H NMR analysis) upon H_2O quench (Scheme 3.7). This "alkyne reduction route" possessed several other attractive features: i) the diarylalkyne starting material was easily prepared via modular, reliable Sonogashira cross-coupling reactions; ii) the crucial thienyl bromide handles were left untouched by the mild reducing conditions; and iii) quenching of the intermediate vinyl dianion with electrophiles other than "H^+" could prove useful for constructing borepins with additional functionality installed (as in Scheme 3.6).

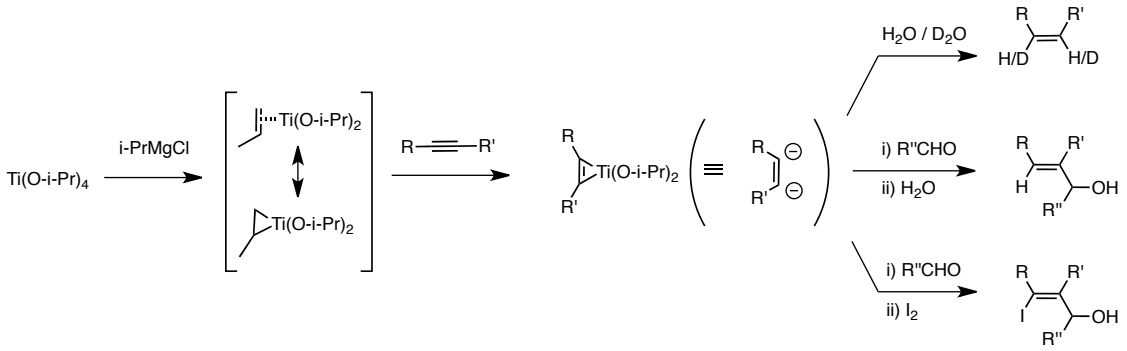

Scheme 3.6. Sato's Ti(O-^{i}Pr)$_4$ / ^{i}PrMgCl–mediated conversion of disubstituted alkynes to the corresponding *cis*, *vic*-vinylic dianion equivalents and subsequent functionalization with various electrophiles.

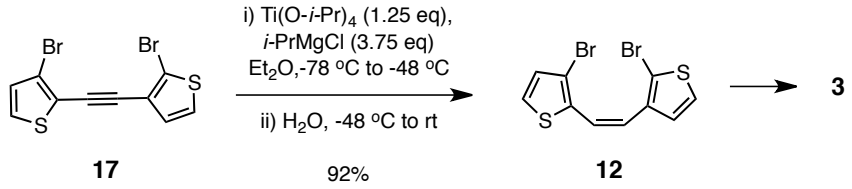

Scheme 3.7. Synthesis of *Z*-dithienylethene **12** by alkyne reduction.

The synthetic economy of the alkyne reduction route was further showcased with a streamlined 3-step formal synthesis of DTB **1** from commercially available materials. Regioselective Stille cross-coupling of bis(tri-*n*-butylstannyl)acetylene and 2 equivalents of 2,3-dibromothiophene gave dithienylethyne **18**, which was subsequently converted to

Z-dithienylethene **10** (the direct precursor to **1** as shown in Scheme 3.4) via the reduction protocol (Scheme 3.8). This short sequence gave access to DTB **1** in two fewer steps than previously achieved by the Wittig route in comparable overall yield.

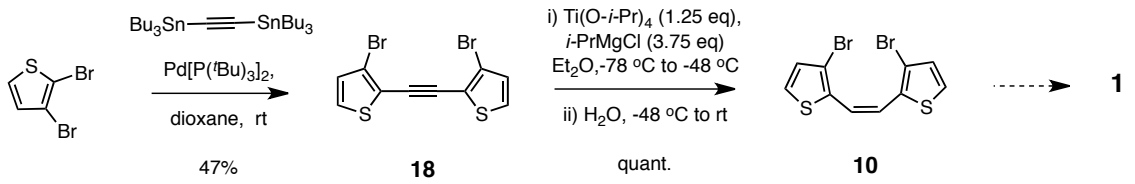

Scheme 3.8. A streamlined 3-step formal synthesis of DTB **1** from commercially available materials via the alkyne reduction route.

Alkyne reduction was also employed to convert dithienylethyne **19**[47] to *Z*-dithienylethene **20** (Scheme 3.9), a precursor designed to lead to the proposed DTB structure **IV-Mes** containing a formally "nonaromatic" borepin ring. However, attempts to carry out borepin formation under the typical conditions (metal-halogen exchange with 2.5 – 4.0 equiv of metalating agent/$MesB(OMe)_2$ quench) did not lead to the desired product. Surprisingly, previously synthesized DTB isomer **2** was observed among the crude reaction products when excess *t*-BuLi was used (Scheme 3.9). Presumably, this was a result of overlithiation of the dilithio intermediate via α-thieno proton abstraction following initial Li-Br exchange, a phenomenon previously reported by Tsuchiya and coworkers while pursuing the synthesis of related heteropins.[47] In an attempt to minimize this side reaction, *n*-BuLi was employed in place of *t*-BuLi so that a near-stoichiometric (2.1 equiv) amount reagent could be used. However, even in this case the desired compound was not observed; instead, a small amount of **4**, another unexpected (and previously unknown) DTB structural isomer, was detected in the product mixture. It was

assumed that **4** arose from an overlithiation process as described above or by small amounts of thermodynamically favored β-to-α Li migration prior to ring closure**.** Though it is not completely clear why the initially targeted DTB **IV-Mes** was never observed among the products, it is reasonable to speculate that with relatively modest *B*-Mes kinetic protection, such a compound might suffer from insufficient electronic stabilization due to a lack of strong boron-thiophene conjugation or borepin-centered aromaticity.

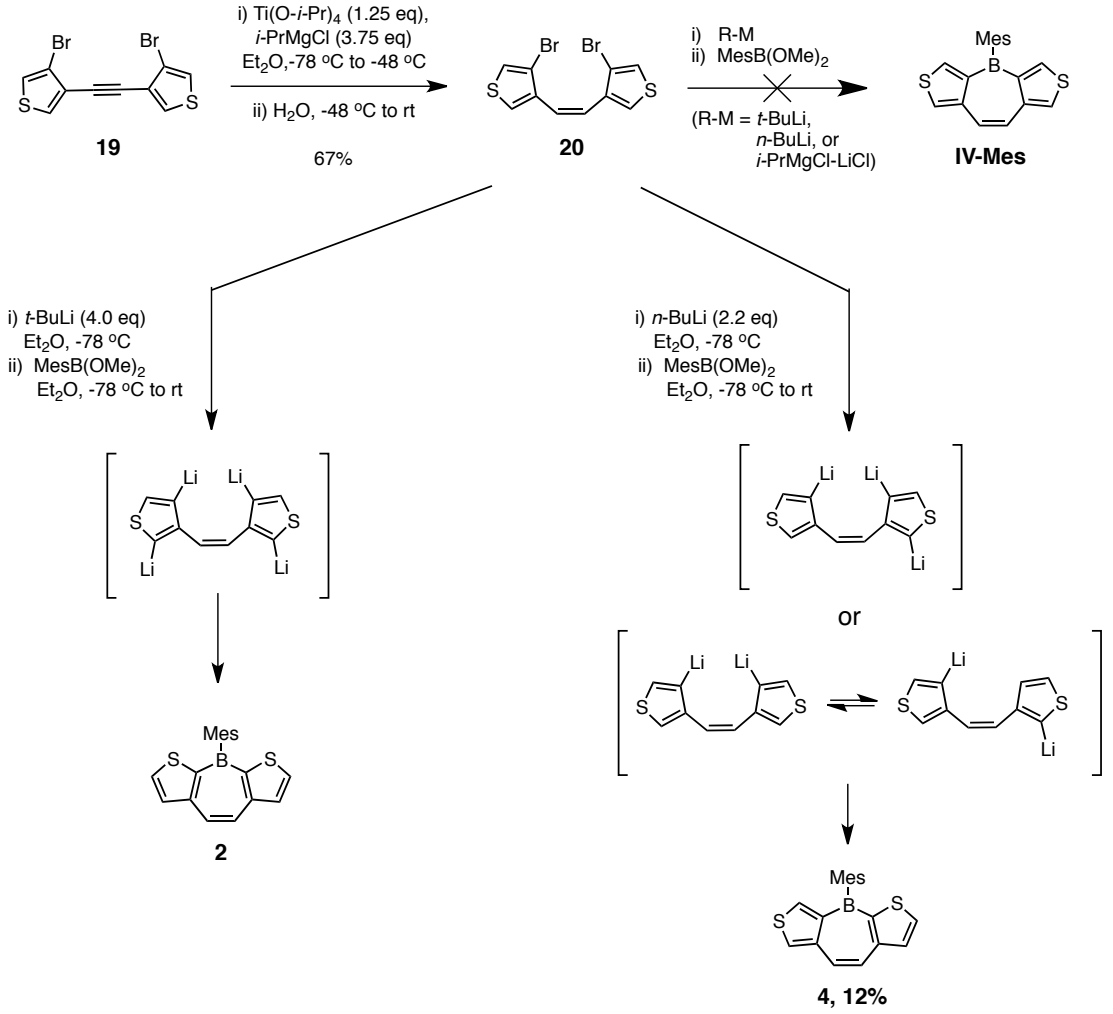

Scheme 3.9. Serendipitous formation of known DTB **2** and previously unknown DTB **4** during attempted syntheses of **IV-Mes**; plausible lithiated intermediates for the formation of **2** and **4** are given in brackets.

Following the serendipitous isolation of **4**, a rational synthesis of this compound was formulated to obtain sufficient material for further study (Scheme 3.10). Sonogashira coupling of 4-bromo-3-iodothiophene and 2-bromo-3-ethynylthiophene gave dithienylethyne **21** in 86%; subsequent Ti-mediated alkyne reduction provided *Z*-dithienylethene **22** in 67%. The final borepin formation reaction proceeded to give **4** in an improved yield of 36% (Scheme 3.10). It is of particular interest to note that **4** was robust towards aqueous, ambient, and chromatographic conditions despite lacking the formally aromatic borepin π-electron arrangement present in the other stable *B*-Mes DTB isomers (**1** – **3**). It is possible that the combination of a single strong boron-α-thieno conjugation motif and concatenation of boron within the cyclic structure of **4** imbue the triarylborane motif with sufficient electronic stabilization in lieu of any weak borepin aromaticity.

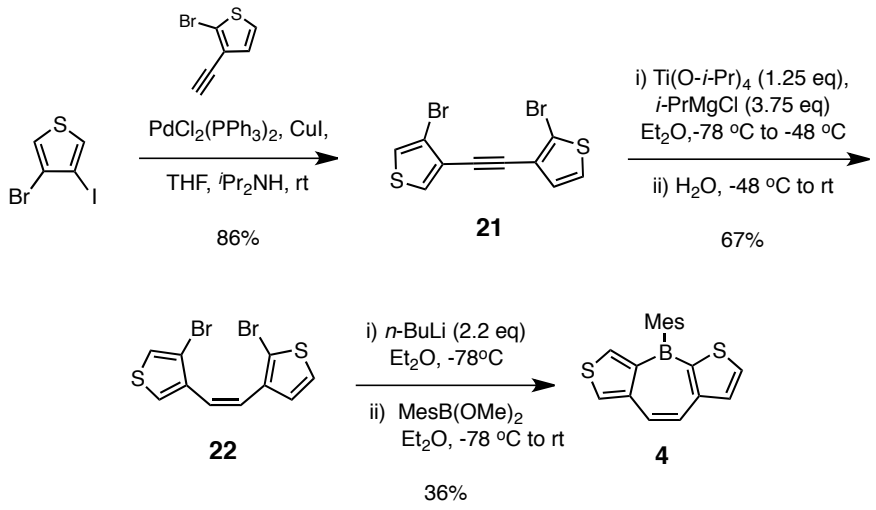

Scheme 3.10. Targeted synthesis of DTB **4.**

The identity and purity of the DTB compounds were confirmed with multinuclear NMR spectroscopy (^{1}H, ^{11}B, ^{13}C) and high-resolution mass spectrometry (HRMS). Unambiguous structural assignments were made by X-ray crystallography. UV−vis and photoluminescence (PL) spectroscopy were utilized to elucidate DTB electronic properties, and electrochemical properties were examined by cyclic voltammetry (CV). Theoretical calculations were carried out at the Density Functional Theory (DFT) / time-dependent Density Functional Theory (TD-DFT) levels to obtain optimized geometries, molecular orbital surfaces/energies, optical transitions, and nucleus-independent chemical shift (NICS) values.

The ^{1}H and ^{11}B NMR chemical shift data for **1** – **4** and related compounds *B*-Mes DBB (**DBB**)[8] and **BTMB**[37] are given in Table 3.1. ^{11}B NMR signals for the DTBs appear as broad peaks from 48.7 to 53.6 ppm, falling within the expected range for tri(hetero)arylborane structures with an sp^2 boron center. These signals are shifted considerably upfield (approx. -11 to -15 ppm) relative to the ^{11}B resonance of **DBB**, suggesting that the thiophene rings of DTBs more effectively donate π-electron density to boron than the benzene rings of **DBB**. The ^{11}B resonance of **2** occurs 6.2 ppm upfield of the signal for unconstrained congener **BTMB**, indicating that the donor-acceptor relationship is aided by the rigid, planar geometry created by the centrally fused borepin ring. Based on the ^{11}B shifts of the different DTB isomers, the amount of π-electron density at boron generally increases proportionally with the number of strongly α-*B*-conjugated thiophene rings (^{11}B upfield shift: **1** > **3** > **2** > **4**), as conceptually envisioned in Figure 3.4. This is also consistent with the dramatic downfield shift of the ^{1}H NMR peaks for the strongly α-boron-conjugated thieno rings in **2** and **3** (^{1}Hα', ^{1}Hβ') compared

to the β-boron conjugated rings in **1** and **3** (^{1}Hα, ^{1}Hβ). It was noted that in the unsymmetrical isomer **3** the ^{1}H shifts for the individual strongly/weakly boron-conjugated thiophene rings match closely with the ^{1}H chemical shifts for the symmetrical isomers **1** and **2** with the same thieno-borepin fusion motif. Despite possessing only β-conjugation with the borepin core, the uniquely *c*-edge-fused thieno ring of **4** exhibited strongly deshielded ^{1}H signals (^{1}Hα'', ^{1}Hα'''), providing an indication of the unique electronics of this isomer. This may be due in part to a lack of stabilizing cyclic π-electron current in the central, nonaromatic borepin ring (*vide infra*), encouraging stronger electron accepting behavior by boron.

Table 3.1. Selected ^{1}H/^{11}B NMR chemical shifts and calculated NICS(1) values for DTBs **1** – **4** and related compounds.

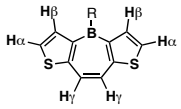

1

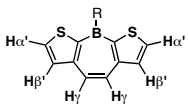

2

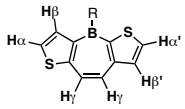

3

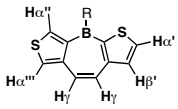

4

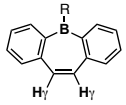

DBB

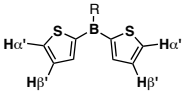

BTMB

	1[a]	**2**[a]	**3**[a]	**4**[a]	**DBB**[b]	**BTMB**[c]
^{11}B	51.9	48.7	50.1	53.6	64.3	54.9
^{1}Hα	7.47	—	7.50	—	—	—
^{1}Hβ	7.38	—	7.36	—	—	—
^{1}Hα'	—	7.95	7.94	7.87	—	7.81
^{1}Hβ'	—	7.70	7.68	7.49	—	7.29
^{1}Hα''	—	—	—	8.00	—	—
^{1}Hα'''	—	—	—	7.81	—	—
^{1}Hγ	7.69	7.74	7.65, 7.79	7.35, 7.15	7.37	—
NICS(1)[d]	-4.93	-4.90	-5.03	-1.63	-2.90	—

[a] ^{11}B/^{1}H NMR spectra collected in $CDCl_3$ solution at room temperature. R = Mes
[b] Reference 8
[c] Reference 37
[d] NICS(1) values calculated for the borepin rings; GIAO method, DFT, (B3LYP/6-31+G*). R = H.

^{1}H NMR chemical shifts, nucleus-independent chemical shift (NICS) calculations (Table 3.1), and X-ray crystallographic data were used to evaluate the degree of aromatic character of the borepin rings in DTBs. The ^{1}Hγ NMR signals for borepin ring protons in **1** – **3** fell within the "aromatic" range of the spectrum (7.65 – 7.79 ppm) and were approximately 0.3 – 0.4 ppm downfield of the corresponding ^{1}Hγ shifts for *B*-Mes DBB, suggesting greater diamagnetic ring currents within the borepin subunits of the DTBs. Theoretical NICS calculations for the borepin rings in model DTB and DBB analogues (with *B*-*H* in place of *B*-Mes) gave NICS(1) values between -4.90 and -5.03 for DTBs **1** – **3** but a considerably less negative NICS(1) value of -2.90 for **DBB**, consistent with greater local borepin aromaticity in DTBs. A plausible rationale for this is the reduced localization of Clar sextets within thiophene compared to benzene, allowing the borepin rings in DTBs greater access to π-electron density. While the experimental and theoretical data for DTBs **1** – **3** pointed toward borepin aromaticity (albeit weak), the data for **4** suggested an essentially nonaromatic borepin ring. The ^{1}Hγ signals of **4** were strongly shifted upfield by -0.4 to -0.6 ppm compared with the other DTB isomers and the calculated NICS(1)$_{borepin}$ value was -1.63. These observations are in line with the canonical resonance structure of **4** as depicted, which lacks the requisite π-electron sextet.

X-ray quality single crystals of DTBs **1** – **4** were grown via slow diffusion/slow evaporation methods by layering MeOH over concentrated solutions of the DTBs in either $CHCl_3$ (for **1**) or CH_2Cl_2 (for **2** – **4**). Crystallography provided key structural metrics for the DTB compounds (Figure 3.5). The C-B-C bond angles for **1** – **4** fell in the range 118.5 – 123.0°, confirming the sp^2 hybridization of the boron centers. In contrast to the slight bowing of the borepin ring observed in the crystal structures of **DBB**[8] and *B*-

entacenes,[9] DTBs all exhibited highly planar polycyclic core geometries with angles between the mean planes of the terminal thieno rings of less than 3.0°. The protective Mes groups in DTBs were oriented in near-perpendicular fashion to the polycyclic backbones, with borepin-Mes dihedral angles ranging from 76.6(2)° to 82.5(2)°. Optimized molecular geometries at the DFT level (B3LYP/6-31G*) generally well-reproduced the crystallographically determined structures.

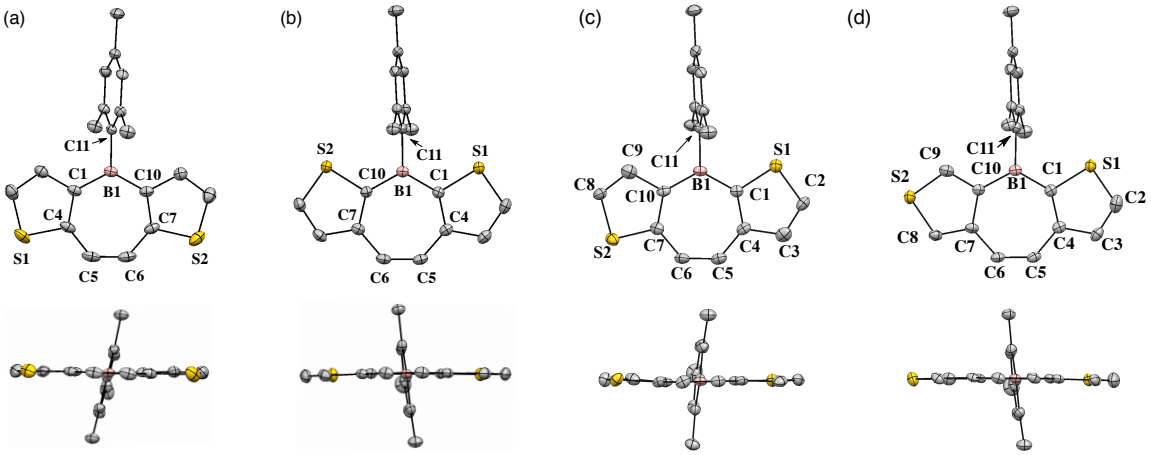

Figure 3.5. Single crystal X-ray structures of (a) **1**, (b) **2**, (c) **3**, and (d) **4** at 110(2) K (displacement ellipsoids shown at the 50% probability level) with views perpendicular (top) and parallel to (bottom) the polycyclic planes (H atoms omitted for clarity). Selected bond lengths (A): **1**: B1–C1 = 1.533(2), B1–C10 = 1.538(2), B1−C11 = 1.581(2), C1−C4 = 1.409(2), C4−C5 = 1.426(2), C5−C6 = 1.348(2), C6−C7 = 1.426(2), C7−C10 = 1.404(2); **2**: B1−C1 = 1.522(2), B1−C10 = 1.521(2), B1−C11 = 1.583(2), C1−C4 = 1.406(2), C4−C5 = 1.440(2), C5−C6 = 1.353(2), C6−C7 = 1.441(2), C7−C10 = 1.403(2); **3** (given for crystallographically independent molecule "B" in the structure): B1–C1 = 1.542(5), B1–C10 = 1.542(5), B1−C11 = 1.587(5), C1−C4 = 1.409(5), C4−C5 = 1.435(4), C5−C6 = 1.353(5), C6−C7 = 1.435(5), C7−C10 = 1.405(4); **4**: B1–C1 = 1.525(5), B1–C10 = 1.543(5), B1−C11 = 1.586(3), C1−C4 = 1.398(5), C4−C5 = 1.451(5), C5−C6 = 1.350(4), C6−C7 = 1.452(5), C7−C10 = 1.455(5).

1 – **4** showed tight packing of DTB molecules within the crystal lattices, as evidenced by the lack of incorporated solvent in the structures (in contrast to the large, solvent occupied voids seen in the crystals of *B*-Mes* *B*-entacenes).[9] Close

intermolecular π-stacking motifs were not observed, however, presumably due to occlusion of the polycyclic faces by the perpendicularly oriented Mes groups. Instead, the predominant intermolecular interactions were comprised of C-H—π and CH—HC close contacts. While the steric profiles of **1 – 4** were generally quite similar, the packing pattern of **1** was relatively distinct from the other systems. In the crystal of **1**, a slipped 1-D herringbone-like stacking pattern was observed between adjacent DTB cores with C-H—π close contacts of 2.896 Å (Figure 3.6a). In contrast, no core-to-core close-contacts were observed within the lattices of **2**, **3**, or **4**; only Mes–Mes and Mes–core close-contacts were evident between the molecules in these cases, with qualitatively similar packing patterns (Figure 3.6b – d).

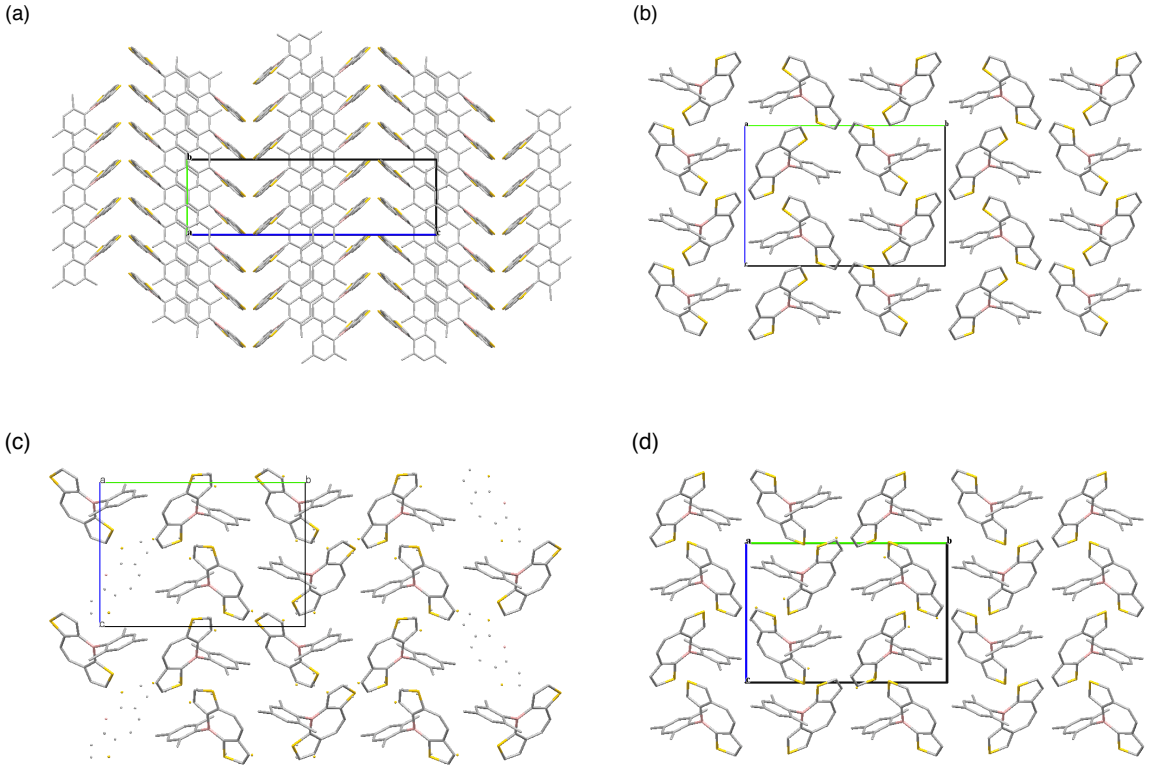

Figure 3.6. Crystal packing motifs for (a) **1**, (b) **2**, (c) **3**, and (d) **4** with unit cells shown for reference.

Crystal bond lengths provided further insight into the nature of π-bonding in the DTB skeletons. The endocyclic borepin B-C bonds (1.52-1.54 Å) for **1 – 4** were significantly shortened in comparison to the exocyclic *B*-Mes bonds (1.58-159 Å), indicative of enhanced B-C π-overlap in the planarized cores. The core B-C bonds of **l** were slightly lengthened compared to those in **2**, consistent with stronger B-C conjugation in the *B*-α-thieno linkages of **2** than the *B*-β-thieno linkages of **1**. Due to orientational disorder in the crystal, a statistically significant distinction could not be made between the *B*-α-thieno and *B*-β-thieno bonds of unsymmetrical DTB **3**; however, unsymmetrical DTB **4** showed a 0.02 Å shortening of the *B*-α-C_{thieno} bonds (1.525(5) Å) relative to the *B*-β-thieno bonds (1.543(5) Å), consistent with the trends seen in symmetrical isomers **1** and **2**.

Comparison of the DTB endocyclic bonds to those of other structurally related triarylboranes revealed that both enforced planarization and thiophene fusion were important factors leading to effective B-C π-overlap. For instance, the *B*-C_{thieno} bonds in DTB **2** are 0.02 – 0.03 Å shorter than in **BTMB**, the latter possessing identical boron-thiophene connectivity but lacking the enforced planarization afforded by extended polycyclic structure in **2**. This suggests that the B-C π-overlap in DTBs is indeed augmented by the extended ring fusion motif provided by the central borepin ring. Additionally, the polarizable nature of the thiophene rings in **1 – 4** leads to shorter core B-C bonds in DTBs compared with the same bonds in the benzene-fused *B*-Mes **DBB** [1.563(3) – 1.564(3) Å]. The reduced C-$C_{borepin}$ bond length alternation values for DTBs **1 – 3** (±0.078 – 0.088 Å) compared to *B*-Mes DBB (±0.111 Å) also indicate enhance borepin aromaticity in the former, corroborating the NMR and NICS data. X-ray bond

lengths also confirmed the π-electron arrangement shown in the canonical structure of **4**, showing the lack of formally Hückel-aromatic borepin sextet.

The electronic properties of DTBs were probed through UV-vis and PL spectroscopy in $CHCl_3$ solution (Figures 3.7 and 3.8 and Table 3.2). To facilitate structure-property analysis, the data are considered in two sets, one including the "aromatic" borepins **1** – **3** and the other containing "nonaromatic" borepin **4**. UV-vis and PL spectra are shown for each individual isomer (Figure 3.7) and as overlays of all isomers (Figure 3.8) for comparative value.

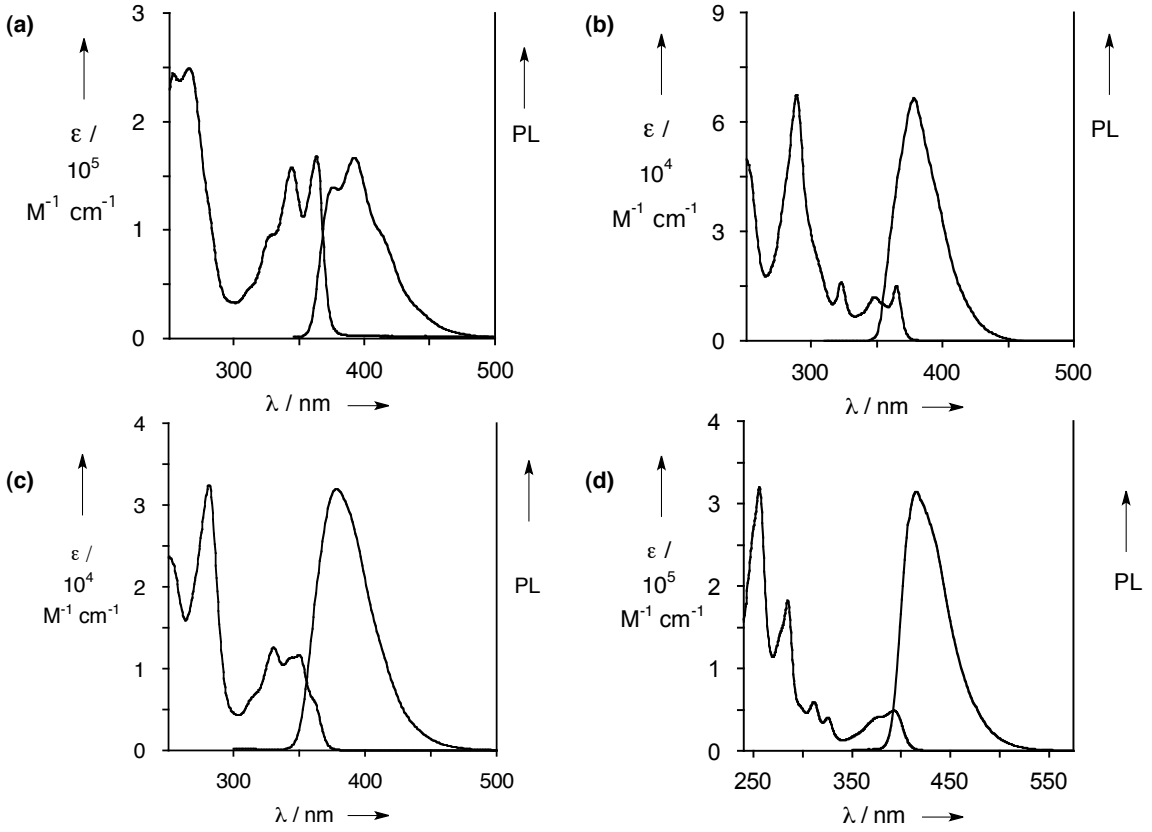

Figure 3.7. UV-vis and PL spectra of (a) **1**, (b) **2**, (c) **3**, and (d) **4** acquired in $CHCl_3$ solution at room temperature.

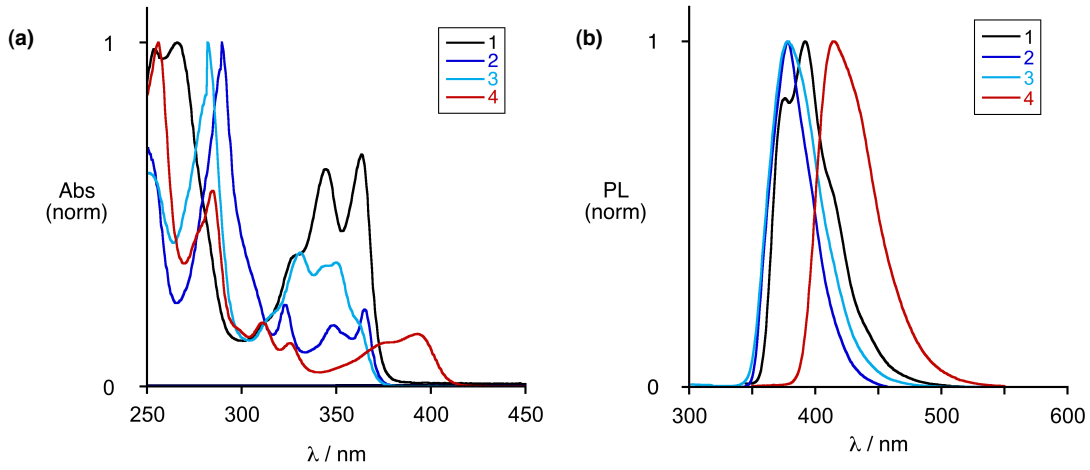

Figure 3.8. Overlaid, normalized (a) UV-vis and (b) PL spectra of **1** – **4** acquired in $CHCl_3$ solution at room temperature.

The UV-vis spectra of **1** – **3** show intense short wavelength bands in the <300 nm region and less intense long wavelength absorptions in the ~300-390 nm range. The relative intensities of the short versus long wavelength bands varied considerably among the isomers, with additional α-C_{thieno}-olefin-conjugation motifs leading to an increase in the intensity of the long wavelength absorptions (**2** < **3** < **1**). Molar extinction coefficients of the long wavelength bands were roughly an order of magnitude larger for isomer **1** than for **2** and **3**, consistent with the trends observed in the oscillator strength of the low-energy optical transitions calculated by TD-DFT. A bathochromic shift in the absorption onset was observed in the order **2** ~ **3** < **1**, reflecting an increase in effective conjugation length for the DTB isomers with longer major all-carbon conjugation pathways.

PL spectra showed trends similar to the UV-vis, with the PL emission maxima showing a slight red-shift in the order **2** < **3** < **1**. Typically small Stokes shifts were observed for all DTBs, suggesting considerable conformational rigidity in the chromophore. The PL spectra for **2** and **3** were relatively featureless but **1** exhibited

some vibronic features. PL quantum yields (Φ_{PL}) for **1** – **3** were rather low, in the range of 0.04 – 0.06. Qualitatively, a visually detectable blue emission was observed for solid samples and dilute solutions under 340 nm light. The low Φ_{PL} values of **1** – **3** are in stark contrast with **DBB**, which exhibits a much higher Φ_{PL} value of 0.70.[8] Thus the borepin-thiophene ring fusion motifs in **1** – **3** appear to enhance the efficiency of non-radiative decay pathways of the excited state compared with borepin-benzene fusion.

The UV-vis/PL spectra of **4** diverged considerably from other DTB species, confirming the uniqueness of the electronic structure (Figure 3.7d, Figure 3.8). Although the UV-vis spectrum of **4** showed high-energy, high intensity features similar to other DTBs, the absorption onset was bathochromically shifted by approx. 20 nm with respect to **1** – **3** due to a broad, low-to moderate intensity band extending from 340 to 414 nm. The emission spectrum was featureless and also bathochromically shifted relative to the other DTBs (PL λ_{max} = 415 nm). The most remarkable photophysical feature of DTB **4** was the near tenfold enhancement in PL quantum yield (Φ_{PL} = 0.53) compared to **1** – **3**, engendered visually as bright blue emission in solution and the solid state.

Theoretical calculations were carried out at the DFT level (B3LYP/6-31G*) to further elucidate the electronic structure of the DTB isomers (Figure 3.9). In accordance with the relative onsets of absorption in the UV-vis spectra, the calculated HOMO – LUMO energy gaps of the DTBs increased in the order **4** < **1** < **3** < **2**. TD-DFT calculated oscillator strengths for the low energy optical transitions reproduced the differences observed experimentally for the extinction coefficients (ε) of the DTB isomers, suggesting that the low ε values of **2** and **3** compared to **1** are a result of weak transition moments for the lowest energy allowed excitations. It is noteworthy that in

several cases the lowest energy $S_0 \rightarrow S_1$ and/or $S_0 \rightarrow S_2$ transitions are forbidden or very weakly allowed due to orbital symmetry considerations.

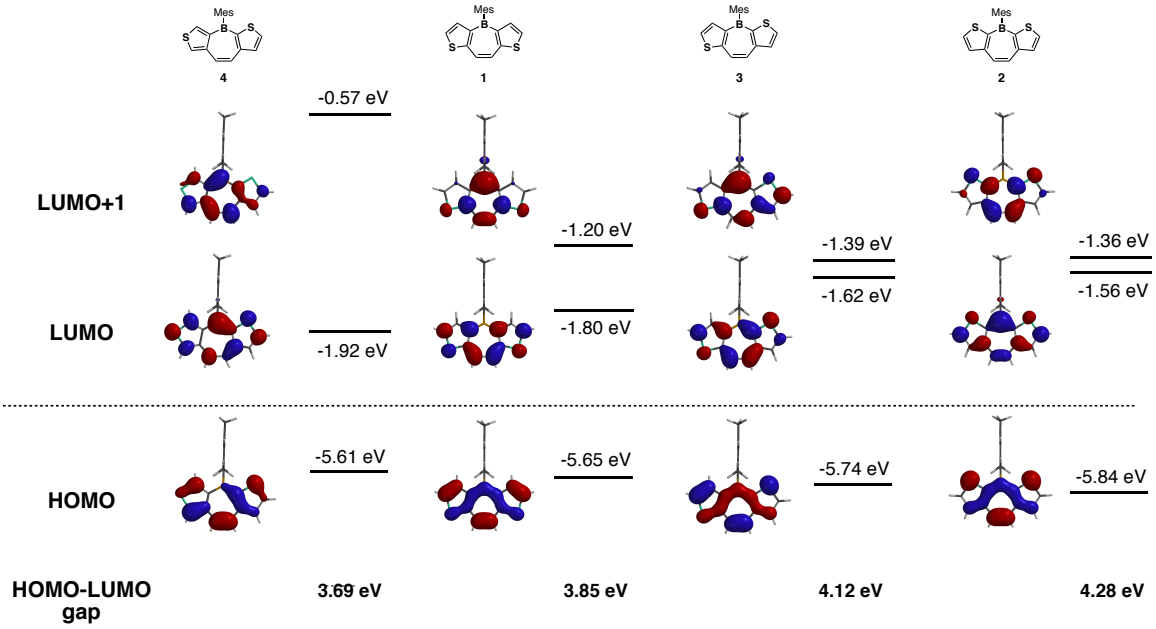

Figure 3.9. DFT calculated FMO surfaces and energy levels of DTBs **1** - **4** at the B3LYP/6-31G* level, shown from left to right in order of increasing HOMO-LUMO gap (**4** < **1** < **3** < **2**).

Calculations revealed that the distributions of frontier molecular orbitals (FMO) were dependent on the conjugation scheme of each individual isomer. For instance, the HOMOs of **1** – **3** showed significant contributions from nearly all of the core atoms, including boron. This is a rather unusual result with respect to typical π-conjugated organoboranes, in which boron contribution is normally evident in the LUMO (p-π – π* conjugation) but not the HOMO. It appears that p-π – π conjugation in the HOMO is a unique aspect of borepin electronic structure in DTBs. In contrast, the HOMO surface of DTB isomer **4** reveals a node between the boron-bound carbon of the thiophene ring fused to borepin in the 3,4-orientation, suggesting electronic decoupling at this site.

Impacts of the different conjugation schemes are also evident in the LUMOs. When B is "strongly" α-conjugated to a thiophene ring (as in the LUMO of **2**, **3**, and **4**) typical B_p-π -Cπ* overlap can be observed, but thieno β-conjugation to boron instead results in destructive overlap. The latter effect is most clearly displayed in **1** where boron does not contribute at all to the LUMO (a highly atypical situation for conjugated organoboranes); the LUMO of **1** instead reflects the π*-orbital of the dithienylethene moiety while the B-C p-π – π* conjugation is only present in the higher energy LUMO+1. These observations are general for DTBs **1** – **3**: when boron-α-thieno conjugation present in the DTBs, it is manifest as boron contribution to the LUMO, while boron-β-thieno conjugation is instead engendered as boron contribution in the higher energy LUMO+1 levels. In the case of the "aromatic" borepin isomers (**1** – **3**), a relative inversion of energy levels can be observed for the strongly boron-centered UOs, which comprise the LUMO+1 of **1** and **3** but instead the LUMO of **2**. Interestingly, increased levels of strong boron-α-thieno conjugation led to an *increase* in the overall energies of DTB LUMOs (E_{LUMO}: **1** < **3** < **2**) while strong olefin-α-thieno conjugation instead tends to lower the LUMO. This was somewhat counter to the conventional notion that boron exerts a LUMO lowering effect when embedded within the conjugation pathways of π-electron materials, and may be an inherent feature of the 6 π-electron borepin ring. This is supported by the fact that the LUMO of **4** (containing the nonaromatic borepin ring), features strong boron contribution but possesses the lowest LUMO of all the DTBs.

Electrochemical characterization demonstrated that DTBs possess the electron-accepting behavior typical of conjugated organoboranes. Cyclic voltammograms of **1** – **4** in THF showed single, reversible electrochemical reduction waves for each compound

with half-wave reduction values ($E_{1/2\ red}$) in the range -2.13 V to -2.42 V (vs. Ag/Ag^+). These reductions are somewhat more difficult to achieve than for the majority of triarylboranes reported, perhaps due to interruption of the weak borepin aromaticity upon electron injection. It was observed that increasing amounts of "strong" boron-thiophene conjugation led to more difficult reductions, with **2** requiring the most negative potential to reduce ($E_{1/2}$ red: **2** < **3** < **1** < **4**). Isomer **4** was an exception to the trend, being the easiest to reduce despite possessing one strong B-α-thieno conjugation motif. This is consistent with the idea that the 3,4-fused thieno ring this structure is much less effective in donating electron density to boron. Overall, the reduction potentials obtained from the CV scans demonstrated good agreement with the relative LUMO level energies of the different isomers obtained from DFT calculations. It is noteworthy that the reduction potentials of the DTBs do not differ strongly from *B*-Mes DBB ($E_{1/2}$ red = -2.36 V vs. Ag/Ag^+),[8] suggesting that thienannulation does not reduce the overall electron-accepting character of the borepin core compared to benzannulation.

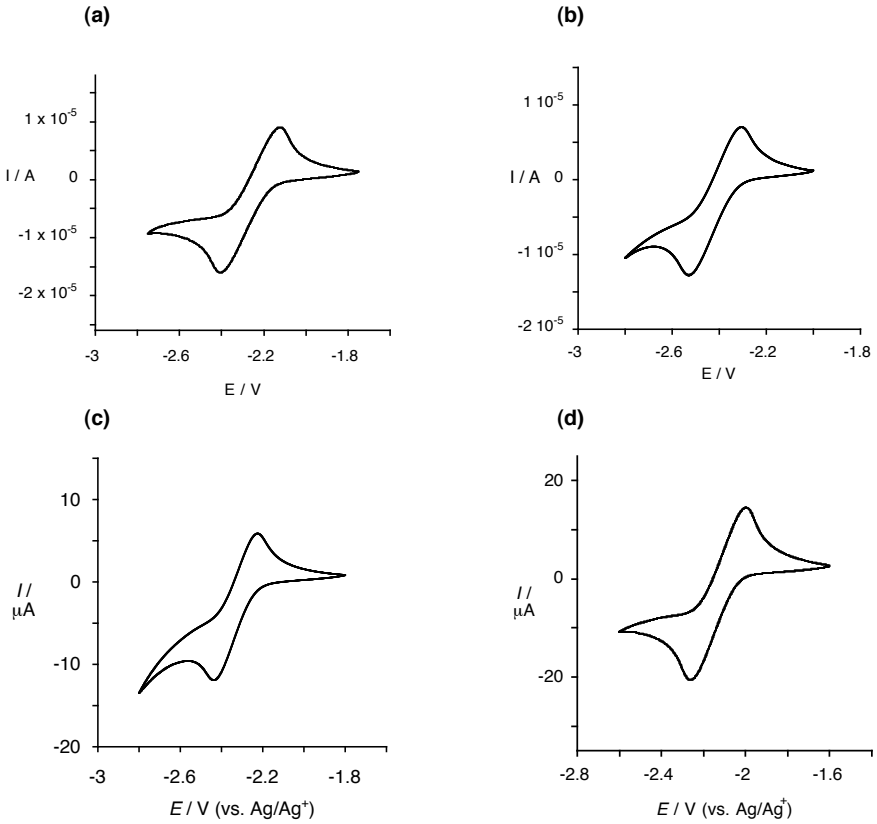

Figure 3.10. Cyclic voltammograms for (a) **1**, (b) **2**, (c) **3**, and (d) **4** in the cathodic regime. Scans acquired in 0.1 M *n*-Bu_4NPF_6 /THF solution at a 2.5 mM analyte concentration and referenced to the Ag/Ag^+ redox couple (= 0.00 V).

In contrast to the cleanly reversible reductions of DTBs, the presence of electron-deficient boron rendered them quite difficult to oxidize electrochemically. No anodic waves were seen up to the limit of the solvent window in THF (~0.9 V) and only ill-defined, irreversible anodic processes in the 1.4 – 1.6 V range were observed in CH_2Cl_2 for **1**, **3,** and **4** (Figure 3.11; Table 3.2) with E_{pa} values **4** < **1** < **3**. DTB **2** did not show oxidation under any of these conditions. The relative oxidation potentials were consistent with the ordering of the HOMO energy levels as calculated by DFT. No electropolymerization of the DTBs was observed during the measurements.

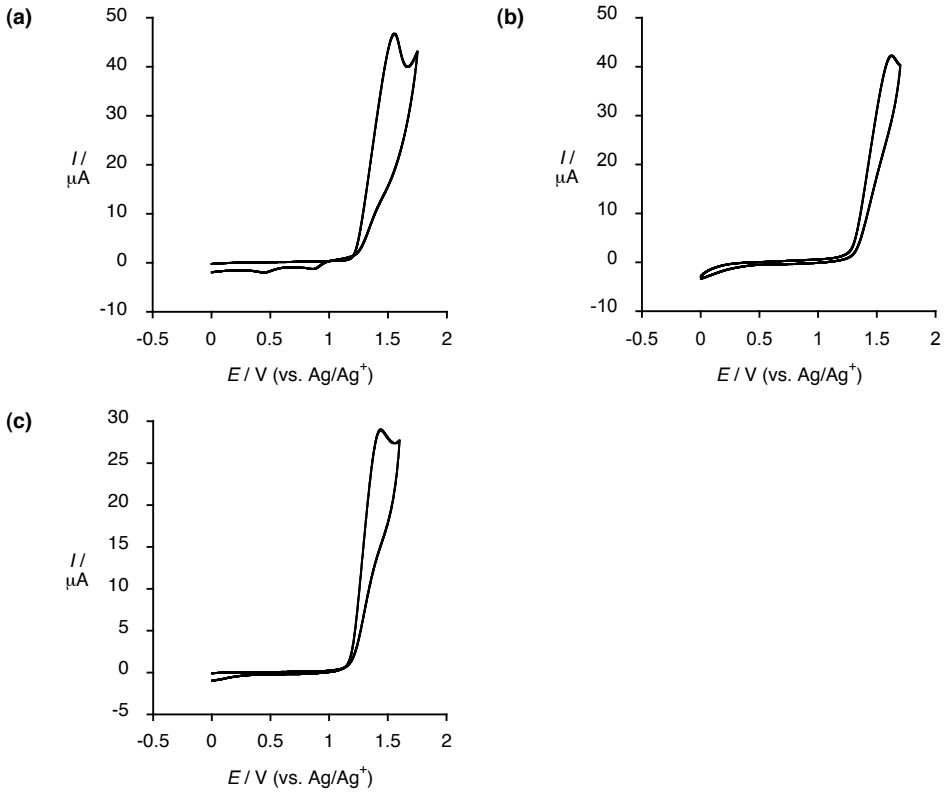

Figure 3.11. Cyclic voltammograms for (a) **1**, (b) **3**, and (c) **4** in the anodic regime (oxidation of **2** not observed). Scans acquired in 0.1 M *n*-Bu_4NPF_6 /CH_2Cl_2 solution at a 2.5 mM analyte concentration and referenced to the Ag/Ag^+ redox couple (= 0.00 V).

A key functional aspect of π-conjugated organoboron materials is their Lewis acidity, whereby the vacant p-orbital serves as an electron-pair acceptor. This acidity not only enables facile chemical or electrochemical reduction, but also for coordination to Lewis bases providing a foundation for chemical sensing schemes[48] and catalysis.[49,50] The sensing events are based on colorimetric or luminescent changes due to perturbation of the electronic structure during Lewis acid-Lewis base complexation, attributed to interruption of the p-π—π* overlap between boron and extended conjugated network. Previously, we observed that DBBs and *B*-entacenes were unable to undergo anion-binding due to the extreme steric bulk presented by the protective Mes* group. It was

therefore of particular interest to determine if the less hindered *B*-Mes DTBs could demonstrate the coordination ability lacking in DBBs.

NMR and UV-vis data revealed that the *B*-Mes DTBs could bind to Lewis basic fluoride, an anion well-documented to bind strongly and selectively with hindered triarylboranes.[48] The ^{11}B NMR spectra collected upon addition of increasing amounts of tetra-*n*-butylammonium fluoride (TBAF) to solutions of **1** and **2** in $CDCl_3$ resulted in disappearance of the native peaks at 50 ppm and the emergence of sharper peaks near 0 ppm (Figure 3.12), typical of a change in coordination state from trivalent arylboranes to corresponding tetravalent fluoroborates. Clear changes were also observed in UV-vis spectra of DTBs **1** – **4** before and after fluoride addition (Figure 3.13). Notably, these processes were reversible; addition of a stronger Lewis acid ($BF_3 \cdot Et_2O$) removed the bound fluoride ions and returned the electronic spectra to the state of the native DTB. Though the binding strength of the DTBs for fluoride was not evaluated quantitatively in terms of association constants (K_a), the requirement for a considerable excess of fluoride ion to achieve complete quenching of the parent DTB ^{11}B peaks in the NMR spectra suggests that DTBs are relatively weak fluoride binders relative to typical triarylboranes, which can show very high K_a values on the order of $10^5 - 10^7$ as determined by UV-vis titration methods.[48] The weak fluoride binding capacity of DTBs may be attributable to unfavorable interruption of aromatic character in the borepin rings or other stabilizing conjugation between boron and the extended π-systems.

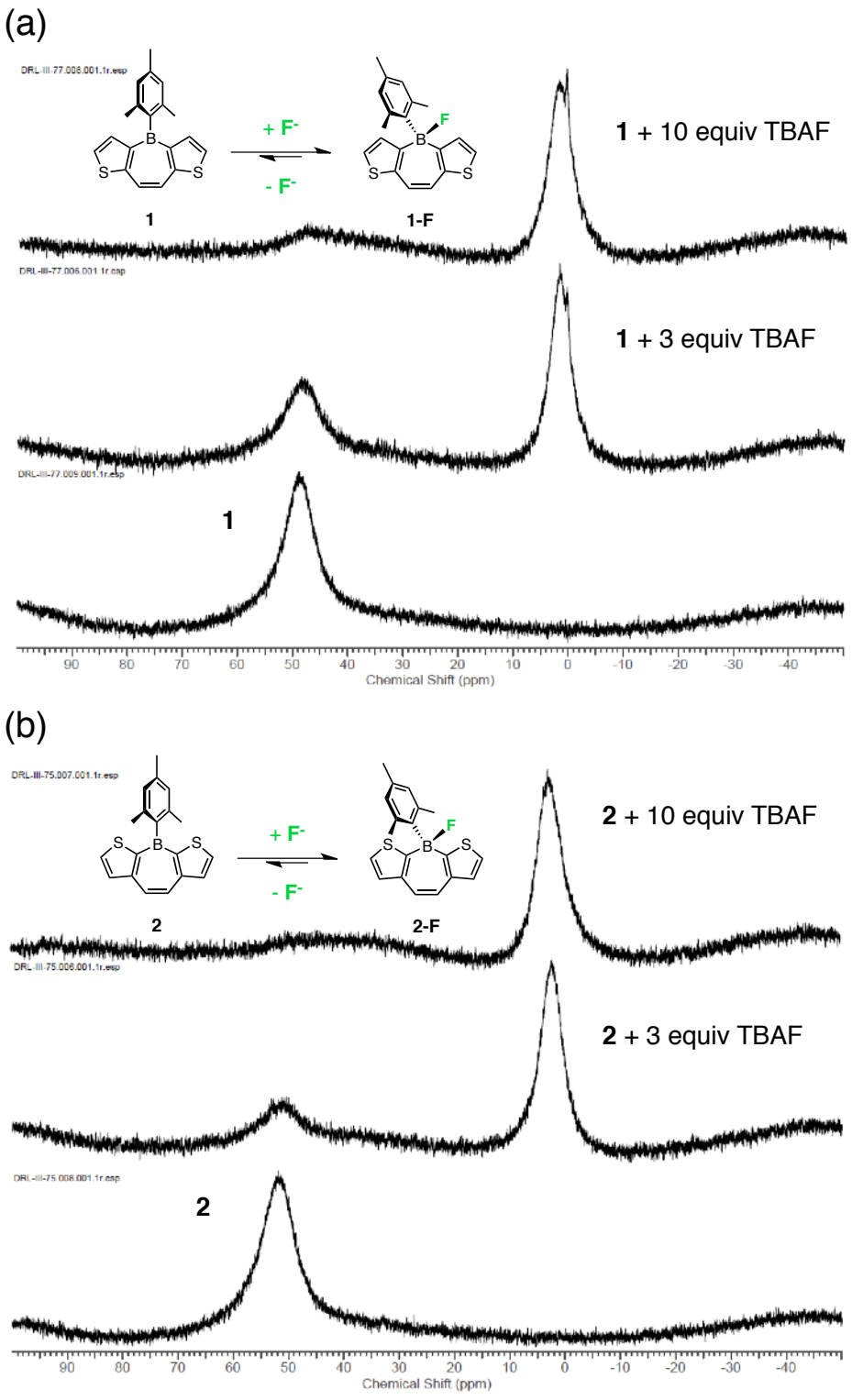

Figure 3.12. ^{11}B NMR spectra of (a) **1** and (b) **2** in $CDCl_3$ upon addition of increasing molar equivalents of TBAF.

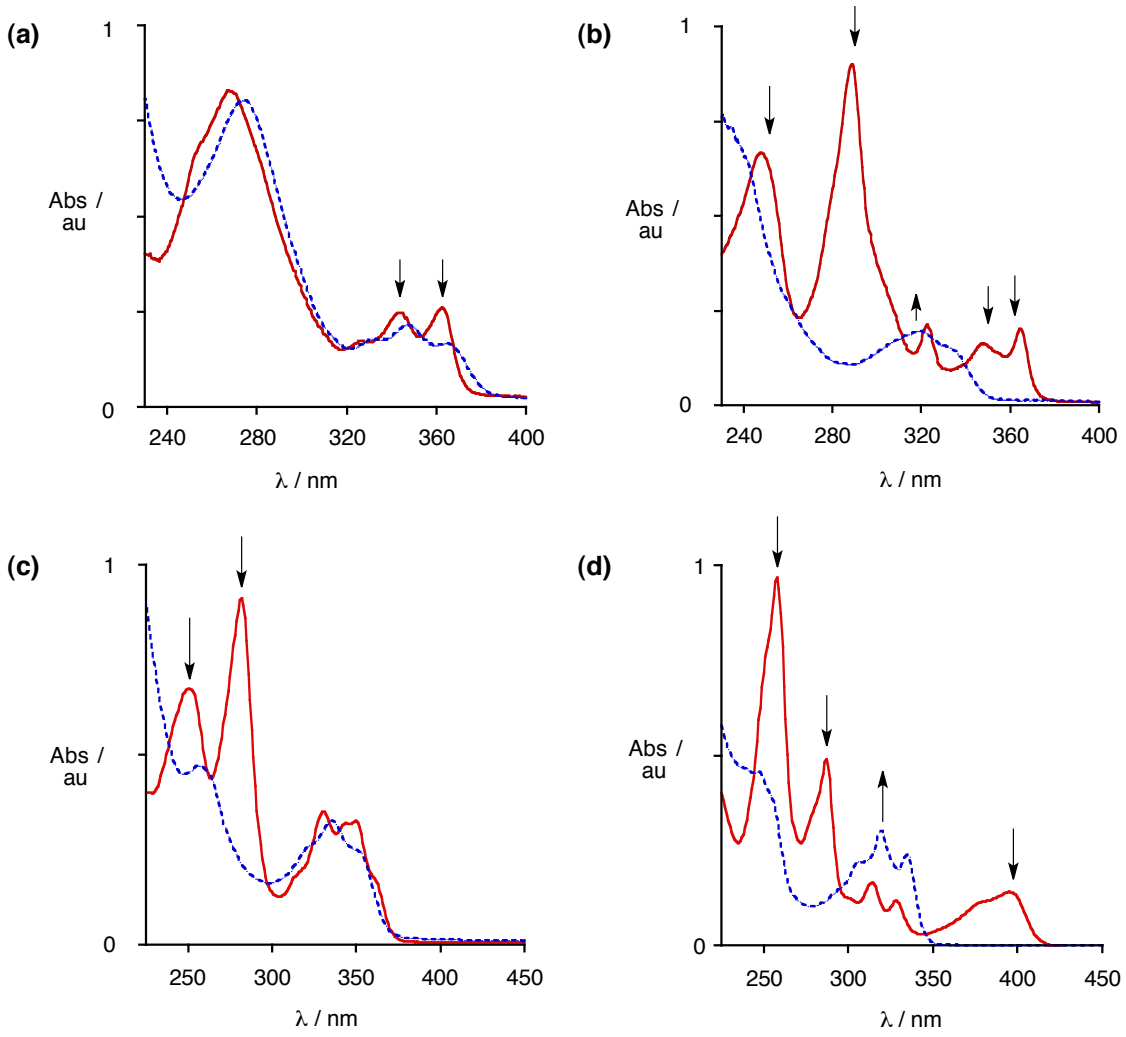

Figure 3.13. UV-vis spectra for (a) **1**, (b) **2**, (c) **3**, and (d) **4** in THF before and after addition of excess fluoride ion (TBAF). Arrows indicate major changes in peak intensity upon fluoride binding.

Among several candidate Lewis bases tested, binding was only observed in the case of added fluoride; no changes in UV-vis spectroscopic signatures were observed upon addition of other halides (Cl^-, Br^-, I^-), hydroxide ions, or nucleophilic pyridines (pyridine, *N,N*-dimethylaminopyridine). It should be noted that the cyanide binding behavior of DTBs was not evaluated, though this anion is also well-known to bind strongly to sp^2 boron centers.

The most unique aspect of the fluoride binding behavior of **1** – **4** is that the nature and degree of the induced changes in UV-vis spectra varied widely among the DTB isomers. Generally, more dramatic changes were correlated with an increase in the number of strong α-thiophene-boron conjugation motifs, which is consistent with larger expected contributions from intramolecular charge transfer (ICT) in the excited state of these isomers. Thus a sample of **1** (containing no strong boron-α-thiophene conjugation motifs) showed only very subtle changes in the location and intensity of the absorption bands after fluoride addition (Figure 3.12a). In contrast, DTB **2** (containing two strong boron-α-thiophene conjugation motifs) showed very large changes in absorption spectrum, including strong suppression of the intense short wavelength bands near 250 and 290 nm as well as the weaker longer wavelength absorptions between 350 and 380 nm (Figure 3.12b). The "mixed" strong/weak boron-thiophene conjugation motifs in **3** showed changes that appeared qualitatively intermediate between **1** and **2**, including strong suppression of the intense short wavelength bands at 250 and 282 nm, but much subtler changes in the long wavelength region from 300 to 375 nm (Figure 3.12c). DTB **4** showed the most dramatic changes of all: the intense short wavelength bands at 258 and 286 nm and the characteristic, broad, long wavelength absorptions between 350 and 415 nm disappeared completely, while the intensity of the features between 300 and 350 increased noticeably (Figure 3.12d). Thus despite possessing only one strong boron-α-thiophene conjugation motif the differences in photophysical properties of **4** and it's fluoride-bound state are quite large, indicating that ICT plays a major role in the photophysical behavior of **4**. Although Jäkle and coworkers previously reported on the impacts of isomerism on anion-binding induced electronic responses for vinyl side-chain

borylated thiophene compounds,[51] the DTBs in this study represent a rare case of such phenomena being caused by differences in boron-π-conjugation within the main chain of the structure.

Table 3.2. Photophysical, electrochemical, and theoretical data for DTBs **1** – **4**.

DTB	Abs λ_{onset} [a] / nm	Abs λ_{max} [a] / nm (log ε)	PL λ_{max} [a] / nm	Φ_{PL} [a, b]	$E_{1/2\ red}$ [c, d] / V	$E_{pa\ ox}$ [c, e, f] / V	HOMO[g] / eV	LUMO[g] / eV
1	390	254 (5.39) 266 (5.40) 344 (5.20) 363 (5.23)	376 392 411[h]	0.06	-2.26	1.57	-5.65	-1.80
2	378	289 (4.83) 323 (4.20) 349 (4.08) 365 (4.18)	378	0.05	-2.42	— [i]	-5.84	-1.56
3	378	252 (4.37) 282 (4.51) 316[h] (3.83) 331 (4.10) 343[h] (4.05) 350 (4.07) 361[h] (3.80)	378	0.04	-2.33	1.62	-5.74	-1.62
4	414	256 (550) 285 (5.26) 311 (4.77) 326 (4.61) 377[h] (4.61) 393 (4.69)	415	0.53	-2.13	1.43	-5.61	-1.92

[a] UV-vis/ PL/ Φ_{PL} collected in $CHCl_3$ solution.
[b] Φ_{PL} values determined relative to quinine sulfate in 0.05 M H_2SO_4 (Φ_{PL} = 0.55).
[c] redox potentials determined by CV and referenced to the Ag/Ag^+ redox couple (0.00 V).
[d] cathodic CV scans taken in N_2-sparged, anhydrous 0.1 M THF/*n*-Bu_4PF_6 solution containing 2.5 mM DTB
[e] anodic CV scans taken in 0.1 M CH_2Cl_2/*n*-Bu_4PF_6 solution containing 2.5 mM DTB
[f] irreversible redox process; value given is the anodic peak potential (E_{pa})
[g] calculated at the DFT level (B3LYP/6-31G*)
[h] shoulder band
[i] no oxidation observed

Concluding Remarks

The preparation of several air- and moisture-stable isomers of the DTB scaffold was achieved through key advancements in molecular design and synthetic approach. Despite the failure of several variations of previously relied upon tin-boron exchange chemistry to provide chemically robust DTBs, the development of an alternative strategy based upon lithium-halogen exchange and direct treatment with a mesityl boronic ester reproducibly provided *B*-Mes DTBs on gram scales. Unlike *B*-Ph substitution, the *B*-Mes group provided sufficient kinetic stabilization to boron to render these materials robust enough for manipulation in coordinating solvents and purification by silica gel chromatography. Additionally, utilization of Sato's stereospecific Ti-mediated reduction of alkynes to their *vic*, *cis*-vinyl dianion equivalents provided an expeditious path towards to the *Z*-dithienylethene precursors of DTBs, streamlining synthetic routes and giving access to a broader range of fused borepin architectures (such as **3** and **4**). The isolation of DTB types **I** – **III** (**1** – **3**) as air- and water-stable species, but not type **IV**, suggested rough guidelines regarding the electronic stability provided to the borepin ring by various thiophene-fusion orientations when supplemented with *B*-Mes kinetic protection.

Characterization of the DTBs revealed that these systems maintain several attractive features typical of π-conjugated organoboranes, including reversible electron-accepting behavior, polarizable electronic structures, and fluoride-binding ability. In general, thiophene-fused borepins exhibited enhanced stability, polarizability, and borepin-centered aromaticity (except in the case of **4**) compared to their benzo-fused analogues. Correlation of the properties of different DTB isomers with their unique conjugation schemes revealed the importance of strong vs. weak conjugation between the

boron center and the extended π-conjugated array. While DTB isomers **1** – **3** (containing a formally aromatic borepin ring) appear to show properties which vary in continuum-like manner according to extent of boron-π-interaction, the "non-aromatic" DTB **4** diverged more sharply, resulting in unique features such as a relatively narrow HOMO-LUMO gap, more highly-allowed low-energy optical transitions, and a tenfold increase in photoluminescence quantum yield. The structure-property relationships obtained from the study of these DTB isomers should provide useful guidelines for the design of boron-containing polycyclic aromatic structures which can capitalize on aspects of enhanced/attenuated aromaticity, the strength of boron-π electronic interactions, and/or desymmetrization of the molecular structure for targeted tuning of molecular properties.

The work in this chapter was published in part as a full article in the Journal of the American Chemical Society in 2014.[52]

Experimental Section

General considerations. Unless otherwise specified, all reactions were carried out in flame- or oven- dried glassware under an atmosphere of prepurified nitrogen or argon using standard Schlenk techniques and magnetic stirring. Acetonitrile (MeCN), dichloromethane (CH_2Cl_2), diethyl ether (Et_2O), toluene and tetrahydrofuran (THF) were purified using an Innovative Technology, Inc. SPS-400-6 solvent purification system, dried over 3Å molecular sieves, and sparged thoroughly with nitrogen prior to use. Chloroform ($CHCl_3$) and 1,4-dioxane were dried over 3Å molecular sieves and sparged thoroughly with nitrogen prior to use. Anhydrous dimethylformamide (DMF) and anhydrous benzene were obtained from Sigma-Aldrich and used without further purification. All other organic solvents were obtained from commercial sources and used as received. Palladium catalysts were obtained from Strem Chemicals. *Tert*-butyllithium (1.7 M solution in pentane) and *n*-butyllithium (1.6 M or 2.5 M solution in hexanes) from Sigma-Aldrich and titrated with diphenylacetic acid in THF prior to use. Isopropyl magnesium chloride (2.0 M in Et_2O) was obtained from Sigma-Aldrich and titrated with salicaldehyde phenylhydrazone[53] in THF prior to use. Unless otherwise noted, all other chemicals were obtained from Alfa-Aesar, Fisher Scientific, Oakwood Chemicals, Sigma-Aldrich, Strem Chemicals, or TCI America and used as received.

The following compounds were prepared according to the literature: 5-bromo-3-thiophenecarbaldehyde,[54] bromo((2-bromothiophen-3-yl)methyl)triphenylphosphorane,[55] 2-bromo-3-(bromomethyl)thiophene,[55] 2-bromo-3-((3-bromothiophen-2-yl)ethynyl)thiophene (**17**),[46] 1,2-bis(4-bromothiophen-3-yl)ethyne **(19)**,[47] 2-bromo-3-ethynylthiophene,[47] and **4**-bromo-3-iodothiophene.[56] Dimethoxymesitylborane ($MesB(OMe)_2$) was prepared by adapting a literature method for the preparation of dimethoxytripylborane ($TipB(OMe)_2$),[57] using MesMgBr in place of TipMgBr (the product was purified by fractional distillation at 140 torr; clean $MesB(OMe)_2$ distilled at 160-200 °C+). 9,9-dimethyl-stannepino[2,3-*b*:7,6-*b'*]dithiophene and 9-phenyl-borepino[2,3-*b*:7,6-*b'*]dithiophene (Scheme 3.1) were prepared according to the doctoral thesis of former Tovar group member Anthony Caruso Jr.[58]

^1H NMR (400 MHz) and ^{13}C NMR (100 MHz) spectra were obtained using a Bruker Avance 400 MHz FT-NMR spectrometer in deuterated chloroform ($CDCl_3$) or dichloromethane (CD_2Cl_2), obtained from Cambridge Isotope Laboratories, Inc. ^{11}B NMR spectra (96 MHz) were obtained using a Bruker Avance 300 MHz FT-NMR spectrometer in deuterated $CDCl_3$. All chemical shifts are reported in parts per million (ppm, δ): ^1H NMR spectra were referenced to the residual proton solvent peaks ($CHCl_3$, δ = 7.26; CH_2Cl_2, δ = 5.32); ^{13}C NMR spectra were referenced to the carbon solvent peak ($CDCl_3$, δ = 77.16; CD_2Cl_2, δ = 53.84); ^{11}B NMR spectra were referenced to an external

boron trifluoride • diethyl etherate standard in $CDCl_3$, (BF_3•Et_2O, $\delta = 0.0$). Boron-bound carbons were typically not observed in ^{13}C NMR spectra due to quadrupolar relaxation of boron. High-resolution mass spectra were obtained using a VG Instruments VG70S/E magnetic sector mass spectrometer with EI (70 eV) or FAB ionization (matrix for FAB was 3-nitrobenzyl alcohol).

Photophysical considerations. Spectroscopic measurements were collected in $CHCl_3$ or THF solution at room temperature. UV-visible (UV-vis) absorption spectra were obtained on a Varian Cary50 Bio UV-visible spectrophotometer. Photoluminescence (PL) spectra were obtained on a PTI QuantaMaster spectrofluorometer with a 75 W Xenon lamp, maintaining optical densities below 0.1 au. PL quantum yields were measured relative to a standard solution of quinine sulfate in 0.05 M aqueous H_2SO_4 while maintaining optical densities below 0.05 au.

Electrochemical considerations. Cyclic voltammetry (CV) measurements were performed under air- and moisture-free conditions in a one-chamber, three electrode cell using a PGSTAT302 potentiostat. A 2 mm^2 Pt button electrode was used as the working electrode with a Pt wire counter electrode relative to a quasi-internal Ag wire reference electrode submersed in 0.01 M $AgNO_3$/0.1M *n*-Bu_4NPF_6 in anhydrous acetonitrile. Cathodic cyclic voltammograms were taken in dry, air-free 0.1 M *n*-Bu_4NPF_6 / THF electrolyte solutions at analyte concentrations of 2.5 mM (scan rate = 100 mV/s). Anodic cyclic voltammograms were taken 0.1 M *n*-Bu_4NPF_6 / CH_2Cl_2 electrolyte solutions at analyte concentrations of 2.5 mM (scan rate = 100 mV/s). Potentials are reported relative to the Ag/Ag^+ redox couple (0.00 V) against which the Fc/Fc^+ couple was measured to be +200 mV in THF and +260 mV in CH_2Cl_2.

X-ray crystallography. Single crystals of **1**, **2**, **3**, and **4** suitable for X-ray crystallography were grown by slow diffusion/slow evaporation methods, layering MeOH over concentrated solutions of **1**/$CHCl_3$, **2**/CH_2Cl_2, **3**/CH_2Cl_2, and **4**/CH_2Cl_2. The stuctures were solved at the Johns Hopkins University (JHU) Chemistry Department X-ray facility by Dr. Maxime A. Siegler. Reflection intensities were measured at 110(2) K using a SuperNova diffractometer (equipped with Atlas detector) with Cu *K*α radiation (mirror optics, λ = 1.5418 Å) under the program CrysAlisPro (Version 1.171.36.24 Agilent Technologies, 2012). The program CrysAlisPro (Version 1.171.36.24 Agilent Technologies, 2012) was used to refine the cell dimensions. Data reduction was done using the program CrysAlisPro (Version 1.171.36.24 Agilent Technologies, 2012). The structures were solved with the program SHELXS-97 and was refined on F^2 with SHELXL-97.[59] Analytical numeric absorption corrections based on a multifaceted crystal model were applied using CrysAlisPro (Version 1.171.36.24 Agilent Technologies, 2012). The temperature of the data collection was controlled using the

system Cryojet (manufactured by Oxford Instruments). The H atoms were placed at calculated positions using the instructions AFIX 43, AFIX 123 or AFIX 137 with isotropic displacement parameters having values 1.2 or 1.5 times *U*eq of the attached C atoms. Graphical representations of crystal structures were generated using Mercury 3.6.1 (Cambridge Crystallographic Data Centre, CCDC).[60]

1: Fw = 320.26, irregular colorless block, 0.45 × 0.32 × 0.14 mm^3, monoclinic, *C*2/*c* (no. 15), a = 15.2727(2), b = 8.01478(12), c = 26.8254(4) Å, β = 97.6459(16)°, V = 3254.43(8) $Å^3$, Z = 8, D_x = 1.307 g cm^{-3}, μ = 0.319 mm^{-1}, abs. corr. range: 0.901–0.968. 15795 Reflections were measured up to a resolution of $(\sin \theta/\lambda)_{max}$ = 0.65 $Å^{-1}$. 3744 Reflections were unique (R_{int} = 0.0250), of which 3274 were observed [$I > 2\sigma(I)$]. 200 Parameters were refined. *R*1/*wR*2 [$I > 2\sigma(I)$]: 0.0343/0.0923. *R*1/*wR*2 [all refl.]: 0.0402/0.0962. S = 1.036. Residual electron density found between -0.28 and 0.37 e $Å^{-3}$. The structure is ordered. Compound ID code in JHU Crystallographic database: x1066a; compound ID code in CCDC database: 1003195.

2: Fw = 320.26, yellow block, 0.55 × 0.36 × 0.22 mm^3, monoclinic, $P2_1/c$ (no. 14), a = 8.47709(9), b = 16.63717(15), c = 11.91527(12) Å, β = 102.7901(10)°, V = 1638.77(3) $Å^3$, Z = 4, D_x = 1.298 g cm^{-3}, μ = 2.856 mm^{-1}, abs. corr. range: 0.387–0.624. 9606 Reflections were measured up to a resolution of $(\sin \theta/\lambda)_{max}$ = 0.61 $Å^{-1}$. 3190 Reflections were unique (R_{int} = 0.0143), of which 3073 were observed [$I > 2\sigma(I)$]. 202 Parameters were refined. *R*1/*wR*2 [$I > 2\sigma(I)$]: 0.0297/0.0791. *R*1/*wR*2 [all refl.]: 0.0305/0.0795. S = 1.072. Residual electron density found between -0.23 and 0.32 e $Å^{-3}$. The structure is ordered. Compound ID code in JHU Crystallographic database: xs0002a; compound ID code in CCDC database: 1003196.

3: Fw = 320.25, colorless lath, 0.33 × 0.12 × 0.06 mm^3, monoclinic, *Pc* (no. 7), a = 8.56203(19), b = 16.6074(3), c = 11.9213(2) Å, β = 102.492(2)°, V = 1655.00(6) $Å^3$, Z = 4, D_x = 1.285 g cm^{-3}, μ = 2.828 mm^{-1}, T_{min}-T_{max}: 0.606–0.862. 10974 Reflections were measured up to a resolution of $(\sin \theta/\lambda)_{max}$ = 0.62 $Å^{-1}$. 4759 Reflections were unique (R_{int} = 0.0237), of which 4599 were observed [$I > 2\sigma(I)$]. 515 Parameters were refined using 950 restraints. *R*1/*wR*2 [$I > 2\sigma(I)$]: 0.0292/0.0742. *R*1/*wR*2 [all refl.]: 0.0305/0.0752. S = 1.044. Residual electron density found between −0.16 and 0.28 e $Å^{-3}$. The structure is partly disordered. The thiophene-fused borepin fragments of the two crystallographically independent molecules (denoted by A and B) are found to be disordered over two orientations (the two mesityl groups are however ordered). Positional disorder of the S atom within the thiophene ring may occur because the two different orientations (up-down or down-up) have similar space-filling requirement in the crystal lattice. The molecule A is found to be more disordered (the occupancy factor of the major component

refines to 0.512(3)), whereas the molecule B is found to be more ordered (the occupancy factor of the major component refines to 0.838(3)). The structure is racemically twinned in the non-centrosymmetric space group *Pc*, and the BASF scale factor refines to 0.13(2). Compound ID code in JHU Crystallographic database: xs0316a.

4: Fw = 320.25, colorless lath, 0.41 × 0.16 × 0.108 mm^3, monoclinic, $P2_1/c$ (no. 14), a = 8.5425(3), b = 16.6388(5), c = 11.8273(3), β = 102.982(3)°, V = 1638.13(9) $Å^3$, Z = 4, D_x = 1.299 g cm^{-3}, μ = 2.857 mm^{-1}, T_{min}–T_{max}: 0.532–0.840. 10706 Reflections were measured up to a resolution of $(\sin \theta/\lambda)_{max}$ = 0.62 $Å^{-1}$. 3213 Reflections were unique (R_{int} = 0.0288), of which 2970 were observed [$I > 2\sigma(I)$]. 301 Parameters were refined using 547 restraints. $R1/wR2$ [$I > 2\sigma(I)$]: 0.0341/0.0893. $R1/wR2$ [all refl.]: 0.0367/0.0915. S = 1.044. Residual electron density found between -0.21 and 0.27 e $Å^{-3}$. The structure is partly disordered. The core B1→C10 is disordered over two orientations as the molecule has a pseudo two-fold axis (symmetry is broken because the positions of the S atoms cannot be related by a two-fold axis). The occupancy factor of the major component of the disorder refines to 0.7894(15). Compound ID code in JHU Crystallographic database: xs0522a.

Theoretical considerations. Geometry optimizations/molecular orbital calculations were performed at the Density Functional Theory (DFT) level (B3LYP/6-31G*) and optical transitions for the optimized structures were calculated using time-dependent DFT (TD-DFT) at the same theory level using Spartan '04 (Wavefunction Inc., Irvine, CA). Nucleus independent chemical shifts (NICS) for model compounds of **1**, **2**, **3**, **4**, and **DBB-Mes** (replacing the *B*–Mes groups with *B*–H) were calculated with Gaussian '03 (Gaussian, Inc., Wallingford, CT)[61] at the DFT level (B3LYP/6-31+G*) using the GIAO method.

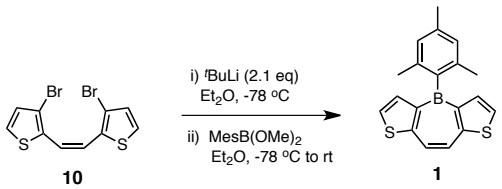

***B*-mesityl-dithieno[3,2-*b*:2',3'-*b*]borepin (1).** To a stirring solution of dithienylethene **10** (3.15 g, 9.00 mmol) in Et_2O (90 mL) at -78 °C in a 250-mL Schlenk flask under nitrogen was added *t*-BuLi (10.9 mL, 1.82 M in pentane, 19.8 mmol) dropwise over 10 min via syringe, whereupon the reaction mixture became olive-green. After 45 min, a solution of $MesB(OMe)_2$ (1.81 g, 1.88 mL, 9.45 mmol) in 45 mL Et_2O was added dropwise via cannula over 25 min and the reaction mixture was allowed to gradually warm to room temperature with continued stirring. After 16 h, saturated aq. NH_4Cl and a small amount of brine were added to the dark-brown reaction mixture, which was then partitioned between Et_2O and H_2O (1:1). The organic layer was removed and the aqueous layer was extracted 4x with EtOAc. The combined organics were dried over $MgSO_4$, filtered, and concentrated under reduced pressure to a orange-brown oil/solid which was purified by column chromatography (SiO_2, gradient elution: 5% $CHCl_3$ in hexanes → 10% $CHCl_3$ in hexanes) to give 1.23 g of DTB **1** (3.83 mmol, 43%) as a pale yellow solid. ^{1}H NMR (400 MHz, $CDCl_3$) δ: 7.69 (s, 2H), 7.47 (d, 2H, *J*= 5.2 Hz), 7.38 (d, 2H, *J*= 5.2 Hz), 6.91 (m, 2H), 2.39 (s, 3H), 1.94 (s, 6H); ^{11}B NMR (96 MHz, $CDCl_3$) δ: 51.9; ^{13}C NMR (100 MHz, $CDCl_3$) δ: 156.1, 138.4, 138.1, 127.1, 126.7, 123.0, 22.9, 21.4 (boron-bound carbons not observed). HRMS (FAB): found *m/z* = 320.0872 ± 2.3 ppm; calculated for $C_{19}H_{17}{}^{11}BS_2$ [M^+]: 320.0865. m.p. = 160.5 °C.

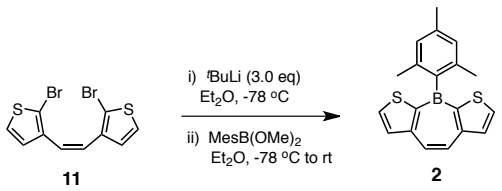

***B*-mesityl-dithieno[2,3-*b*:3',2'-*f*]borepin (2).** To a stirring solution of dithienylethene **11** (2.22 g, 6.34 mmol) in 63 mL Et_2O at -78 °C in a 250-mL Schlenk flask under nitrogen was added *t*-BuLi (10.4 mL, 1.82 M in pentane, 19.0 mmol) dropwise over 10 min via syringe, whereupon the reaction mixture became yellow-orange. After 1 h, a solution of $MesB(OMe)_2$ (1.33 mL, 1.28 g, 6.66 mmol) in 34 mL Et_2O was added dropwise via cannula over 20 min and the reaction mixture was allowed to gradually warm to room temperature. After 16 h, saturated aq. NH_4Cl and a small amount of brine were added to the orange-red reaction mixture, which was then partitioned between Et_2O and H_2O (1:1). The organic layer was removed and the aqueous layer was extracted 4x with EtOAc. The combined organics were dried over $MgSO_4$, filtered, and concentrated

under reduced pressure to a orange-red solid which was purified by column chromatography (SiO_2, gradient elution: 5% $CHCl_3$ in hexanes → 10% $CHCl_3$ in hexanes → 15% $CHCl_3$ in hexanes) to give 1.43 g of DTB **2** (4.46 mmol, 70%) as a pale yellow solid. ^{1}H NMR (400 MHz, $CDCl_3$) δ: 7.95 (d, J = 4.8 Hz, 2H), 7.74 (s, 2H), 7.70 (d, J = 4.8 Hz, 2H), 6.95 (m, 2H), 2.41 (s, 3H), 2.04 (s, 6H); ^{11}B NMR (96 MHz, $CDCl_3$) δ: 48.7; ^{13}C NMR (100 MHz, $CDCl_3$) δ: 150.4, 139.1, 137.5, 135.9, 133.1, 127.3, 126.4, 22.7, 21.6 (boron-bound carbons not observed). HRMS (EI): found m/z = 320.0868 ± 1.0 ppm; calculated for $C_{19}H_{17}{}^{11}BS_2$ [M^+]: 320.0865. m.p. = 164.3 °C.

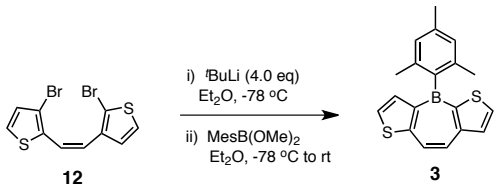

12 **3**

***B*-mesityl-dithieno[3,2-*b*:3',2'-*f*]borepin (3).** To a stirring solution of dithienylethene **12** (1.320 g, 3.770 mmol) in 38 mL Et_2O -78 °C in a 100-mL Schlenk tube under nitrogen was added *t*-BuLi (1.59 M in pentane, 9.48 mL, 15.1 mmol) dropwise via syringe. After 1 h, a solution of dimethoxymesitylborane (0.811 mL, 4.03 mmol) in 21 mL Et_2O was added dropwise via cannula and the mixture was allowed to continue stirring at -78 °C with gradual warming to room temperature. After 16 h, saturated aq. NH_4Cl and a small amount of brine were added to the red-brown reaction mixture, which was then partitioned between Et_2O and H_2O (1:1). The organic layer was removed, and the aqueous layer was extracted 4x with EtOAc. The combined organics were dried over $MgSO_4$, filtered, and concentrated under reduced pressure to give an oily brown residue which was purified by column chromatography (SiO_2, gradient elution: hexanes → 5% $CHCl_3$ in hexanes → 10% $CHCl_3$ in hexanes) to give 539 mg of DTB **3** (1.68 mmol, 45%) as an off-white solid. ^{1}H NMR (400 MHz, $CDCl_3$) δ: 7.94 (d, J = 4.8 Hz, 1H), 7.79 (d, J = 11.6 Hz, 1H), 7.69 (d, J = 4.8 Hz, 1H), 7.65 (d, J = 11.6 Hz, 1H), 7.50 (d, J = 5.2 Hz, 1H), 7.36 (d, J = 5.2 Hz, 1H), 6.94 (s, 2H), 2.41, (s, 3H), 2.01 (s, 6H); ^{11}B NMR (96 MHz, $CDCl_3$) δ: 50.1; ^{13}C NMR (100 MHz, $CDCl_3$) δ: 156.4, 150.2, 138.6, 137.6, 137.0, 136.2, 132.9, 127.2, 126.8. 124.9, 124.4, 22.8, 21.5 (boron-bound carbons not observed); HRMS (EI): found m/z = 320.0858 ± 2.3 ppm; calculated for $C_{19}H_{17}{}^{11}BS_2$ [M^+]: 320.0865.

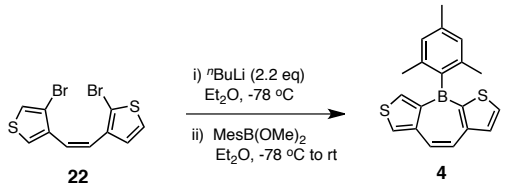

22 4

***B*-mesityl-dithieno[3,4-*b*:3',2'-*f*]borepin (4).** To a stirring solution of dithienylethene **22** (33.0 mg, 0.0943 mmol) in 2.5 mL Et_2O at -78 °C in a 25-mL Schlenk tube under nitrogen was added *n*-BuLi (2.57 M in hexanes, 0.081 mL, 0.21 mmoL) dropwise via syringe. After 20 m, a solution of dimethoxymesitylborane (0.048 mL, 0.24 mmol) in 1 mL Et_2O was added dropwise via syringe. After stirring for another 1 h at -78 °C, the mixture was allowed to warm slowly to room temperature. After 6 h, sat. aq. NH_4Cl was added and the mixture was partitioned between Et_2O and H_2O (1:1), adding a small amount of brine. The organic layer was removed, and the aqueous layer was extracted 2x with Et_2O. The combined organics were dried over $MgSO_4$, filtered, and concentrated under reduced pressure that was purified by column chromatography (SiO_2, gradient elution: hexanes → 5% $CHCl_3$ in hexanes → 10% $CHCl_3$ in hexanes) to give 11.0 mg of DTB **4** (0.0343 mmol, 36%) as a yellow solid. ^{1}H NMR (400 MHz, $CDCl_3$) δ: 8.01 (dd, J = 4.0 Hz, 1.2 Hz, 1H), 7.88 (d, J = 6.4 Hz, 1H), 7.82 (d, J = 4.4 Hz, 1H), 7.49 (d, J = 6.4 Hz, 1H), 7.36 (d, J = 15.6 Hz, 1H), 7.16 (d, J = 15.6 Hz, 1H), 6.91 (d, J = 0.8 Hz, 2H), 2.38, (s, 3H), 2.03 (s, 6H); ^{11}B NMR (96 MHz, $CDCl_3$) δ: 53.6; ^{13}C NMR (100 MHz, $CDCl_3$) δ: 150.8, 143.3, 138.8, 137.1, 133.6, 128.0, 127.1, 126.3, 122.3, 22.8, 21.5 (boron-bound carbons not observed); HRMS (EI): found m/z = 320.0863 ± 0.5 ppm; calculated for $C_{19}H_{17}{}^{11}BS_2$ [M^+]: 320.0865.

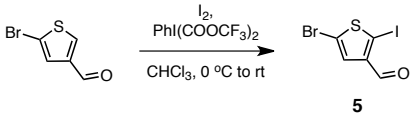

5

5-bromo-2-iodothiophene-2-carbaldehyde (5). A 250-mL Schlenk flask was charged with 5-bromo-3-thiophenecarbaldehyde[54] (7.343 g, 38.43 mmol) under nitrogen and 120 mL $CHCl_3$ was added. The mixture was cooled to 0 °C with stirring then iodine (6.048 g, 23.83 mmol), followed by bis-trifluoroacetoxyiodobenzene (10.910 g, 25.37 mmol,) were added portionwise under a purge of nitrogen and the reaction mixture was allowed to continue stirring with gradual warming to room temperature. After 20 h, saturated aqueous sodium thiosulfate was added and the mixture was partitioned between $CHCl_3$ and H_2O (1:1). The organic phase was separated and the aqueous phase was extracted 3x with $CHCl_3$. The combined organics were dried over $MgSO_4$, filtered, and concentrated under reduced pressure to give a solid which was purified by column chromatography (SiO_2, gradient elution: 35% CH_2Cl_2 in hexanes → 50% CH_2Cl_2 in hexanes → 65% CH_2Cl_2 in hexanes) to provide 11.29 g of aldehyde **5** as a canary yellow crystalline solid (35.63 mmol, 93%.) ^{1}H NMR (400 MHz, $CDCl_3$) δ: 9.56 (s, 1H), 7.27 (s, 1H). HRMS

(EI): found *m/z* = 315.8053 ± 0.4 ppm; calculated for $C_5H_2{}^{79}BrIOS$ [M^+]: 315.8054. Characterization data matched the literature.[62]

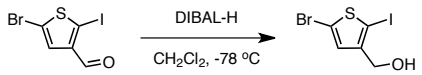

5 **6**

(5-bromo-2-iodothiophen-3-yl)methanol (6). A 250-mL Schlenk flask was charged with 5-bromo-2-iodo-3-thiophenecarbaldehyde (**5**, 3.112 g, 9.82 mmol) under nitrogen and 98 mL CH_2Cl_2 was added. The mixture was cooled to -78 °C with stirring and 1.50 mL of DIBAL-H (1.0 M solution in hexanes, 1.5 mmol) was added dropwise to the reaction mixture over 10 min, during which time the mixture turned from a turbid white suspension to bright yellow, then finally resulting in a transparent, colorless solution. The mixture was allowed to stir for a further 20 min then H_2O was added, followed by warming to room temperature. The mixture was partitioned between CH_2Cl_2 and H_2O (1:1); brine was then added and the mixture was extracted 4x with CH_2Cl_2. The combined organics were dried over $MgSO_4$, filtered, and concentrated under reduced pressure to provide 2.951 g of **6** as a white solid (9.25 mmol, 94%) that was used without further purification. ^{1}H NMR (400 MHz, $CDCl_3$) δ: 6.79 (s, 1H), 4.53 (d, J = 6.0 Hz, 2H), 1.69 (s, br, 1H). ^{13}C NMR (100 MHz, $CDCl_3$) δ: 146.5, 130.9, 116.0, 62.3. HRMS (EI): found *m/z* = 317.8206 ± 1.5 ppm; calculated for $C_5H_4{}^{79}BrIOS$ [M^+]: 317.8211.

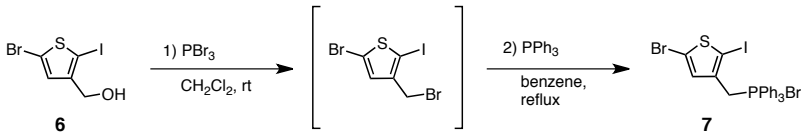

6 **7**

bromo((5-bromo-2-iodothiophen-3yl)methyl)triphenylphosphorane (7). To a 50-mL round-bottomed flask charged with 5-bromo-2-iodo-3-thiophenemethanol (**6,** 402 mg, 1.26 mmol) under nitrogen was added 12 mL of CH_2Cl_2 and stirred at room temperature. Phosphorus tribromide (0.24 mL, 2.52 mmol) was added dropwise to the mixture over 3 min via syringe and the resulting mixture was allowed to continue stirring overnight. After 20 h, solvent was removed directly from the mixture under high vacuum. The reaction vessel was placed in an ice-water batch and the remaining yellow residue was carefully quenched with saturated aqueous sodium bicarbonate then partitioned between CH_2Cl_2 and H_2O (1:1). The organic layer was removed and the aqueous layer was extracted 3x with CH_2Cl_2. The combined organics were dried over $MgSO_4$, filtered, and concentrated under reduced pressure to give the crude 5-bromo-3-(bromomethyl)-2-iodothiophene, which was used immediately without further purification due to material instability. ^{1}H NMR (400 MHz, $CDCl_3$) δ: 6.96 (s, 1H), 4.35 (s, 2H). To a 2-necked 50-mL round-bottomed flask fitted with reflux condenser under nitrogen was added the

crude 5-bromo-3-(bromomethyl)-2-iodothiophene (assumed 1.26 mmol), triphenylphosphine (347 mg, 1.32 mmol), and 25 mL benzene. The mixture was heated to reflux and stirred for 14 h, resulting in the formation of a white precipitate. After cooling to room temperature, the precipitated material was filtered off and washed 2x with 30 mL portions of Et_2O. The solids were dried under high vacuum to provide 601 mg of phosphonium salt **7** as a white solid (0.932 mmol, 74% over 2 steps from **6**) that was used without further purification. ^{1}H NMR (400 MHz, $CDCl_3$) δ: 7.85-7.73 (m, 9H), 7.71-7.64 (m, 6H), 6.81 (s, 1H), 5.54 (d, J = 14.0 Hz, 2H). HRMS (FAB): found m/z = 562.9098 ± 0.5 ppm; calculated for $C_{23}H_{18}{}^{79}BrIPS$ [M^+-^{79}Br]: 562.9095.

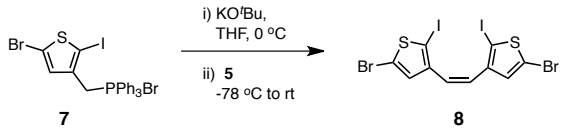

(*Z*)-1,2-bis(5-bromo-2-iodothiophen-3-yl)ethene (8). To a stirring suspension of phosphonium salt **7** (400 mg, 0.621 mmol) in 6 mL THF at 0 °C under nitrogen was added. potassium *tert*-butoxide (70 mg, 0.621) in a single portion. The mixture immediately became resulting orange mixture and was stirred for 30 min at 0 °C, then cooled to -78 °C. A solution of aldehyde **5** (164 mg, 0.518 mmol) in 6 mL THF was added dropwise via syringe and the mixture was allowed to stir with gradual warming to room temperature over 18 h. The mixture was partitioned between H_2O and Et_2O (1:1) and a small amount of brine was added. The organic layer was removed and the aqueous layer was extracted 2x with Et_2O. The combined organics were dried over $MgSO_4$, filtered, and concentrated under reduced pressure, then pushed through a short pad of SiO_2, eluting 5% EtOAc in hexanes. The eluent was concentrated under reduced pressure to provide 273 mg of **8** as a yellow-orange solid that was used without further purification (0.453 mmol, 88%, 9:1 / *Z:E.*) ^{1}H NMR (400 MHz, $CDCl_3$) δ: 6.60 (s, 2H), 6.30 (s, 2H). ^{13}C NMR (100 MHz, $CDCl_3$) δ: 142.8, 130.5, 126.5, 115.8, 77.9. HRMS (FAB): found m/z = 601.6193 ± 0.4 ppm; calculated for $C_{10}H_4{}^{79}Br^{81}Br\ I_2S_2$ [M^+]: 601.6190.

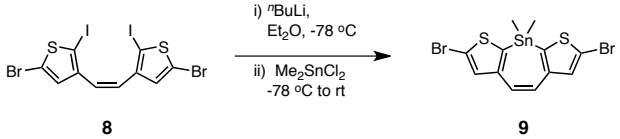

2,7-dibromo-9,9-dimethyl-9*H*-stannepino[2,3-*b*:7,6-*b*']dithiophene (9). A solution of dithienylethene **8** (60 mg, 0.100 mmol) in THF (11 mL) was cooled to -78 °C with stirring in a 25-mL Schlenk flask under nitrogen. A solution of *n*-BuLi in hexanes (1.64

M, 0.125 mL) was added dropwise to the mixture, which was allowed to continue stirring for 30 m. A solution of Me_2SnCl_2 (22.0 mg, 0.100 mmol) in THF (5 mL) was added dropwise to the reaction mixture over 10 min and allowed to continue stirring with gradual warming to room temperature over 21 h. The mixture was partitioned between Et_2O and H_2O (1:1); the organic layer was removed and the aqueous layer was extracted 2x with Et_2O. The combined organic layers were dried over $MgSO_4$, filtered, and concentrated under reduced pressure to give an orange-brown oil-solid mixture. The mixture was transferred to a scintillation vial and triturated 2x with methanol (sonicating, centrifuging, and decanting the supernatant) to provide 49 mg of **9** as a sticky maroon solid which was used without further purification (0.098 mmol, 98%). ^{1}H NMR (400 MHz, $CDCl_3$) δ: 7.11 (s, 2H), 6.61 (s, 2H), 0.60 (s, 2H). ^{13}C NMR (100 MHz, CDCl3) δ: 146.5, 134.1, 133.9, 125.5, 116.5, -8.0. MS (EI/CI): found *m/z* = 495.8; calculated for $C_{12}H_{10}{}^{79}Br_2S_2Sn$ [M^+]: 495.8.

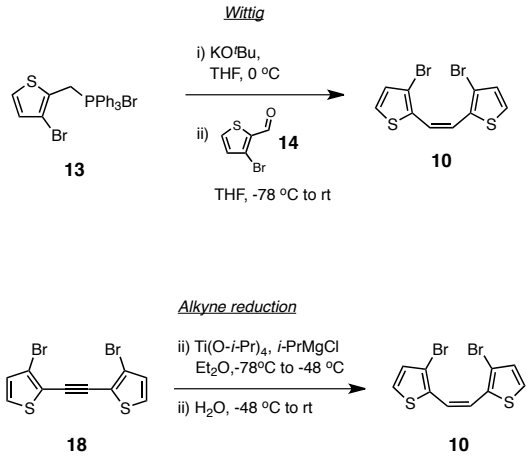

(*Z*)-1,2-bis(3-bromothiophen-2-yl)ethene (10).

Via Wittig olefination: To a stirring suspension of phosphonium salt **13** (3.40 g, 6.56 mmol) in 65 mL THF at 0 °C in 250-mL 3-necked round-bottomed flask under nitrogen was added potassium *tert*-butoxide (803 mg, 7.16 mmol) in a single portion. The mixture immediately became a deep red color and was stirred for a further 30 min at 0 °C, then cooled to -78 °C. A solution of aldehyde **14** (1.14 g, 5.97 mmol) in 60 mL THF was added dropwise over 20 min via cannula and the mixture was allowed to continue stirring with gradual warming to room temperature over 16 h. The mixture was partitioned between Et_2O and H_2O (1:1) and a small amount of brine was added. The organic layer was removed and the aqueous layer was extracted 2x with Et_2O. The combined organics were dried over $MgSO_4$, filtered, and concentrated under reduced pressure to a volume of approx. 10 mL, then pushed through a short pad of SiO_2, eluting with 10% EtOAc in hexanes. The eluent was concentrated under reduced pressure to give 1.94 g of an isomeric *E / Z* (1:10.3) mixture of the product as (5.54 mmol, 85%) as a deep orange oil/solid. Further purification via column chromatography (SiO_2, 1% $CHCl_3$ in hexanes)

provided 1.70 g of isomerically pure *Z*-dithienylethene **10** as a light yellow solid (4.85 mmol, 74%). ^{1}H NMR (400 MHz, $CDCl_3$) δ: 7.27 (d, J = 6.0 Hz, 2H), 6.99 (d, J = 5.2 Hz, 2H), 6.71 (s, 2H); ^{13}C NMR (100 MHz, $CDCl_3$) δ: 133.2, 130.2, 127.3, 123.7, 113.0; HRMS (EI): found m/z = 349.8261 ± 1.1 ppm; calculated for $C_{10}H_6{}^{79}Br^{81}BrS_2$ [M^+]: 349.8257. *Via alkyne reduction:* To a stirring solution of dithienylethyne **18** (24.3 mg, 0.0698 mmol) in 1 mL Et_2O at -78 °C in a 25-mL Schlenk tube under nitrogen was added dropwise via syringe titanium (IV) isopropoxide (0.026 mL, 0.0873 mmol) then isopropyl magnesium chloride (2.0 M in Et_2O, 0.137 mL, 0.262 mmol) to give a bright yellow solution. After stirring for 5 min at -78 °C, the solution was warmed to -48 °C and held at this temperature for 3 h, during which time the reaction mixture became deep red-orange. Water (0.5 mL) was added dropwise via syringe and the mixture was allowed to warm to room temperature with stirring for 1 h. After partitioning the mixture between Et_2O and H_2O (1:1), the organic layer was removed and the aqueous layer was extracted 2x with Et_2O. The combined organics were washed sequentially with 1 M HCl (aq) and brine, dried over $MgSO_4$, filtered, and concentrated under reduced pressure to give 24.4 mg of **10** as a yellow solid/film (0.0698 mmol, quant.) without further purification. The ^{1}H NMR spectrum matched that of isomerically pure *Z*-dithienylethene **10** as prepared by the Wittig olefination method.

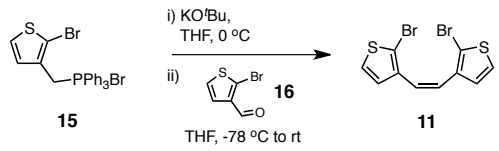

(*Z*)-1,2-bis(2-bromothiophen-3-yl)ethene (11). To a stirring suspension of phosphonium salt **15**[55] (5.21 g, 10.1 mmol) in 100 mL THF at 0 °C in 500-mL Schlenk flask under nitrogen was added potassium *tert*-butoxide (1.22 g, 10.9 mmol) in a single portion. The mixture immediately became a bright orange color and was stirred for a further 30 min at 0°C, then cooled to -78 °C. A solution of aldehyde **16** (1.60 g, 8.38 mmol) in 85 mL THF was added dropwise over 20 min via cannula and the mixture was allowed to warm to room temperature with continued stirring for 16 h. The mixture was partitioned between Et_2O and H_2O (1:1) and a small amount of brine was added. The organic layer was removed and the aqueous layer was extracted 2x with Et_2O. The combined organics were washed 2x with brine, dried over $MgSO_4$, filtered, and concentrated under reduced pressure to a volume of approx. 30 mL. The concentrated mixture was then pushed through a short pad of SiO_2, eluting with 500 mL of 5% EtOAc in hexanes. The eluent was concentrated under reduced pressure to give 2.89 g of an isomeric *E* / *Z* (1 : 6.7) mixture of dithienylethene **11** (8.29 mmol, 99%) as an orange oil/solid. Further purification via column chromatography (SiO_2, hexanes) provided 2.46 g of isomerically pure *Z*-dithienylethene **4** (7.02 mmol, 84%) as an off-white solid. ^{1}H

NMR (400 MHz, $CDCl_3$) δ: 7.12 (d, *J*= 5.6 Hz, 2H), 6.71 (d, *J* = 5.6 Hz, 2H), 6.50 (s, 2H); ^{13}C NMR (100 MHz, $CDCl_3$) δ: 137.4, 128.0, 125.5, 123.9, 113.0; HRMS (EI): found *m/z* = 349.8253; calculated for $C_{10}H_6{}^{79}Br^{81}BrS_2$ [M^+]: 349.8257.

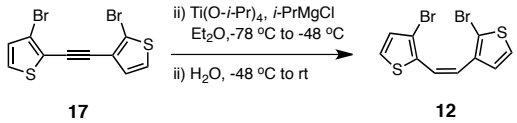

17 **12**

(*Z*)-2-bromo-3-(2-(3-bromothiophen-2-yl)vinyl)thiophene (12). To a stirring solution of dithienylethyne **17** (1.428 g, 4.103 mmol) in 41 mL Et_2O at -78 °C in a 100-mL Schlenk tube under nitrogen was added dropwise via syringe titanium (IV) isopropoxide (1.52 mL, 5.13 mmol) then isopropyl magnesium chloride (2.0 M in Et_2O, 7.64 mL, 15.38 mmol) to give a bright yellow solution. After stirring for 30 min at -78 °C, the solution was warmed to -48 °C and held at this temperature for 3 h, during which time the reaction mixture became deep red-brown. Water (5 mL) was added dropwise and the mixture was allowed to continue stirring with gradual warming to room temperature over 12 h. After partitioning the mixture between Et_2O and H_2O (1:1), the organic layer was removed and the aqueous layer was extracted 3x with Et_2O. The combined organics were washed sequentially with 1 M HCl (aq) and brine, dried over $MgSO_4$, filtered, and concentrated under reduced pressure to an orange oil which was purified by column chromatography (SiO_2, hexanes) to give 1.320 g of *Z*-dithienylethene **12** (4.103 mmol, 92%) as a yellow oil. ^1H NMR (400 MHz, CD_2Cl_2) δ: 7.27 (d, *J* = 6.0 Hz, 1H), 7.21 (d, *J* = 5.2 Hz, 1H), 6.96 (d, *J* = 5.2 Hz, 1H), 6.82 (d, *J* = 11.6 Hz, 1H), 6.82 (d, *J* = 6.0 Hz, 1H), 6.44 (d, *J* = 11.6 Hz, 1H); ^{13}C NMR (100 MHz, CD_2Cl_2) δ: 137.5, 130.0, 128.5, 127.0, 126.7, 124.2, 124.1, 113.2, 113.0; HRMS (EI): found *m/z* = 349.8264 ± 1.9 ppm; calculated for $C_{10}H_6{}^{79}Br^{81}BrS_2$ [M^+]: 349.8257.

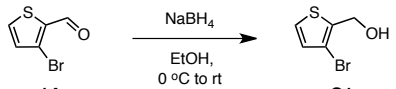

14 **S1**

(3-bromothiophen-2-yl)methanol (S1). To a stirring 0 °C solution of aldehyde **14** (6.91g, 36.2 mmol) in 140 mL EtOH in under N_2 in a 250-mL Schlenk flask was added $NaBH_4$ (2.36 g, 62.3 mmol) portionwise. The mixture was allowed to stir with gradual warming to room temperature over 22 h, then the volatile components were removed under reduced pressure by rotary evaporation to give a cloudy oil. Saturated aq NH_4Cl was added dropwise to the residue and the mixture was partitioned between EtOAc and H_2O (1:1). The organic layer was removed and the aqueous layer was extracted 3x with EtOAc. The combined organics were dried over $MgSO_4$, filtered, and concentrated under reduced pressure to give a yellow oil which was purified by column chromatography (SiO_2, gradient elution: 5% EtOAc in hexanes – 10% EtOAc in hexanes) to provide 6.30 g (32.6 mmol, 90%) of alcohol **S1** as a colorless oil. ^1H NMR (400 MHz, $CDCl_3$) δ: 7.27

(d, J = 5.2 Hz, 1H), 6.97 (d, J = 5.2 Hz, 1H), 4.81 (d, J = 6.4 Hz, 2H), 1.94 (s, br, 1H). Characterization data matched the literature.[63]

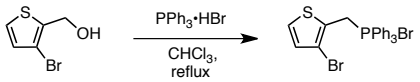

S1 **13**

bromo((3-bromothiophen-2-yl)methyl)triphenylphosphorane) (13). To a 100-mL 2-necked round-bottomed flask fitted with reflux condenser and charged with (3-bromothiophen-2-yl)methanol **S1** (6.10 g, 31.6 mmol) under nitrogen was added 25 mL $CHCl_3$ and the mixture was stirred at room temperature. Solid PPh_3•HBr (10.8 g, 31.6 mmol) was added portionwise under a purge of nitrogen and then the mixture was heated to reflux. After 20 h, the mixture was allowed to cool to room temperature, transferred to a 250-mL round-bottomed flask, and concentrated under reduced pressure. The resulting residue was dissolved in a minimal amount of $CHCl_3$, then poured over 150 mL Et_2O to precipitate a white-orange solid which was filtered off and rinsed with 300 mL Et_2O. The solid material was collected and dried under high vacuum to provide 16.3 g of phosphonium salt **13** (31.6 mmol, quant) as a powdered white solid. ^{1}H NMR (400 MHz, $CDCl_3$) δ: 7.82 – 7.77 (m, 9H), 7.68 – 7.63 (m, 6H), 7.24 (q, J = 2.8 Hz, 1H), 6.82 (d, J = 5.2 Hz, 1H), 5.86 (d, J = 13.2, 2H); HRMS (FAB): found m/z = 439.0112 ± 0.9 ppm; calculated for $C_{23}H_{19}{}^{81}BrPS$ [M^+-^{79}Br]: 439.0108.

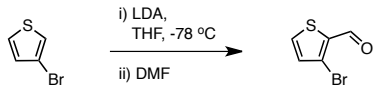

14

3-bromothiophene-2-carbaldehyde (14). To a stirring solution of i-Pr_2NH (12.0 mL, 85.0 mmol) in THF (150 mL) at 0 °C in a 500-mL 2-necked round-bottomed flask under nitrogen was added n-BuLi (53.1 mL, 1.6 M in hexanes, 85.0 mmol) dropwise over 20 min. After stirring for an additional 20 min at 0 °C, the mixture was cooled to -78 °C and a solution of 3-bromothiophene (13.9 g, 85.0 mmol) in 90 mL THF was added dropwise over 35 min via cannula. After stirring for 1 h at -78 °C, the mixture was allowed to warm to 0 °C for 30 min before cooling again to -78 °C. A solution of DMF (6.83 g, 93.5 mmol) in 55 mL THF was then added dropwise over 20 min via cannula and the mixture was allowed to gradually warm to room temperature with stirring for 20 h. Saturated aq NH_4Cl and brine were added and the mixture was partitioned between Et_2O and H_2O. The organic layer was removed and the aqueous layer was extracted 1x with Et_2O. The combined organics were washed with brine (1x) then dried over $MgSO_4$, filtered, and concentrated under reduced pressure to give an orange oil which was purified by column chromatography (SiO_2, gradient elution: 5% EtOAc in hexanes → 10% EtOAc in hexanes) to give 14.2 g of aldehyde **4** (74.5 mmol, 88%) as a yellow oil.

^{1}H NMR (400 MHz, $CDCl_3$) δ: 9.99 (s, 1H), 7.71 (dd, J = 0.8, 2.0 Hz, 1H), 7.15 (d, J = 2.0, 1H). Characterization data matched the literature.[64]

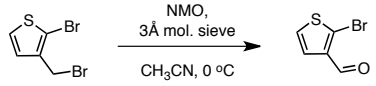

16

2-bromothiophene-3-carbaldehyde (16). To a stirring mixture of *N*-methylmorpholine-*N*-oxide (NMO; 3.86 g, 31.8 mmol) and 3Å molecular sieves (25.5 g) in MeCN (80 mL) at 0 °C under nitrogen was added dropwise 2-bromo-3-(bromomethyl)thiophene[55] (2.63 g, 10.3 mmol) over 5 min via syringe. After 2 h, the reaction mixture was filtered directly through a short pad of SiO_2, eluting with 600 mL EtOAc. The eluent was concentrated under reduced pressure to give 1.66 g of aldehyde **16** as a yellow oil (8.72 mmol, 85%), which became an off-white solid after storage at 5 °C. This material was used without further purification. ^{1}H NMR (400 MHz, $CDCl_3$) δ: 9.95 (s, 1H), 7.36 (d, J = 6.0 Hz, 1H), 7.29 (d, J = 6.0 Hz, 1H). Characterization data matched the literature.[65]

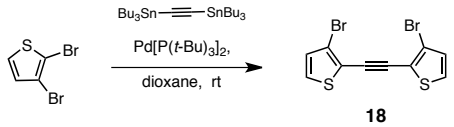

18

1,2-bis(3-bromothiophen-2-yl)ethyne (**18**). To a 25-mL Schlenk tube charged with $Pd[P(t\text{-}Bu)_3]_2$ (5.2 mg, 0.0102 mmol) and a stir bar under nitrogen was added 1 mL 1,4-dioxane and 2,3-dibromothiophene (32.1 mg, 0.339 mmol) and the mixture was stirred at room temperature. Bis(tri-*n*-butylstannyl)acetylene (0.087 mL, 0.17 mmol) was added dropwise to the reaction mixture via syringe and the walls of the tube were rinsed down with an additional 0.5 mL 1,4-dioxane to ensure quantitative reagent transfer. The mixture was stirred at room temperature for 18 h, during which time it became a deep brown-red color. CsF (350 mg) was then added and the mixture was vigorously stirred for 30 m. The mixture was pushed through a short pad of SiO_2, eluting Et_2O (~125 mL), and the eluent was concentrated under reduced pressure to an oily brown residue that was purified by column chromatography (SiO_2, hexanes) to give 27.3 mg of dithienylethyne **18** (0.0784 mmol, 47%) as a pale yellow oil. ^{1}H NMR (400 MHz, $CDCl_3$) δ: 7.28 (d, J = 5.2 Hz, 2H), 7.02 (d, J = 5.6 Hz, 2H); ^{13}C NMR (100 MHz, $CDCl_3$) δ: 130.5, 128.1, 120.3, 117.1, 88.4; HRMS (EI): found m/z = 347.8096 ± 1.4 ppm; calculated for $C_{10}H_4{}^{79}Br^{81}BrS_2$ [M^+]: 347.8101.

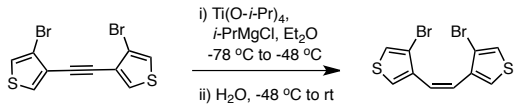

19 **20**

(*Z*)-1,2-bis(4-bromothiophen-3-yl)ethene (20). To a stirring solution of dithienylethyne **19** (210 mg, 0.603 mmol) in Et_2O (6 mL) at -78 °C in a 25-mL Schlenk tube under nitrogen was added dropwise via syringe titanium (IV) isopropoxide (0.223 mL, 0.754 mmol) then isopropyl magnesium chloride (1.91 M in Et_2O, 1.18 mL, 2.26 mmol) to give a bright yellow solution. After stirring for 5 min at -78 °C, the solution was warmed to -48 °C and held at this temperature for 2 h, during which time the reaction mixture became deep red-orange. Water (2 mL) was added dropwise via syringe and the mixture was allowed to warm to room temperature with stirring for 16 h. After partitioning the mixture between Et_2O and H_2O (1:1), the organic layer was removed and the aqueous layer was extracted 3x with Et_2O. The combined organics were washed sequentially with 1 M HCl (aq) and brine, dried over $MgSO_4$, filtered, and concentrated under reduced pressure to give a viscous orange oil that was purified by column chromatography (SiO_2, hexanes) to give 141 mg of *Z*-dithienylethene **20** (0.403 mmol, 67%) as a pale yellow oil. ^{1}H NMR (400 MHz, $CDCl_3$) δ: 7.27 (d, J = 3.2 Hz, 2H), 7.06 (d, J = 3.2 Hz, 2H), 6.56 (s, 2H); ^{13}C NMR (100 MHz, $CDCl_3$) δ: 136.7, 125.1, 123.4, 123.0, 112.8; HRMS (EI): found m/z = 349.8260 ± 0.9 ppm; calculated for $C_{10}H_6{}^{79}Br^{81}BrS_2$ [M^+]: 349.8257.

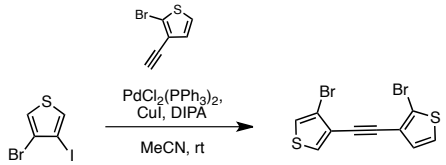

21

2-bromo-3-((4-bromothiophen-3-yl)ethynyl)thiophene (21). To a stirring solution of 4-bromo-3-iodothiophene (532 mg, 1.84 mmol), $PdCl_2(PPh_3)_2$ (38 mg, 0.055 mmol), and CuI (21 mg, 0.11 mmol) in THF/diisopropylamine (1:1, 40 mL) under nitrogen was added a nitrogen sparged solution of 2-bromo-3-ethynylthiophene in THF (5 mL) dropwise via cannula. The mixture was allowed to stir for at room temperature 18 h then pushed through a short pad of SiO_2, eluting 10% EtOAc in hexanes. The eluent was concentrated under reduced pressure to an orange oil that was further purified by column chromatography (SiO_2, hexanes) to give 550 mg of **21** (1.58 mmol, 86%) as an off-white solid. ^{1}H NMR (400 MHz, $CDCl_3$) δ: 7.55 (d, J = 3.6 Hz, 1H), 7.28 (d, J = 3.2 Hz, 1H), 7.22 (d, J = 6.0 Hz, 1H), 7.05 (d, J = 5.6 Hz, 1H). ^{13}C NMR (100 MHz, $CDCl_3$) δ: 130.0, 129.4, 126.1, 124.4, 123.2, 117.6, 113.8, 86.4, 85.9; HRMS (EI): found m/z = 347.8094 ± 2.0 ppm; calculated for $C_{10}H_4{}^{79}Br^{81}BrS_2$ [M^+]: 347.8101.

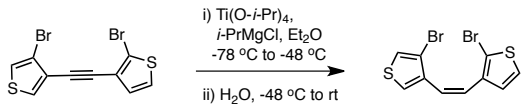

21 22

(*Z*)-2-bromo-3-(2-(4-bromothiophen-3-yl)vinyl)thiophene (22). To a stirring solution of dithienylethyne **21** (629 mg, 1.81 mmol) in 18 mL Et_2O at -78 °C in a 50-mL Schlenk flask under nitrogen was added dropwise via syringe titanium (IV) isopropoxide (0.669 mL, 2.26 mmol) then isopropyl magnesium chloride (1.91 M in Et_2O, 3.55 mL, 6.78 mmol) to give a bright yellow solution. After stirring for 10 min at -78 °C, the solution was warmed to -48 °C and held at this temperature for 3 h, during which time the reaction mixture became deep red-brown. Water (3 mL) was added dropwise and the mixture was allowed to continue stirring with gradual warming to room temperature over 15 h. After partitioning the mixture between Et_2O and H_2O (1:1), the organic layer was removed and the aqueous layer was extracted 2x with Et_2O. The combined organics were washed sequentially with 1 M HCl (aq) and brine, dried over $MgSO_4$, filtered, and concentrated under reduced pressure to a viscous orange oil which was purified by column chromatography (SiO_2, hexanes) to give 443 mg of *Z*-dithienylethene **22** (1.27 mmol, 70%) as a pale yellow oil that became a white solid upon prolonged standing at room temperature. ^{1}H NMR (400 MHz, $CDCl_3$) δ: 7.28 (d, J = 3.6 Hz, 1H), 7.11 (dd, J = 6.0 Hz, 0.4 Hz,1H), 7.08 (dd, J = 3.6 Hz, J = 0.4 Hz, 1H), 6.70 (d, J = 5.6 Hz, 1H), 6.54 (d, J = 12.0 Hz, 1H), 6.50 (dd, J = 12.0, 0.8 Hz, 1H); ^{13}C NMR (100 MHz, $CDCl_3$) δ: 137.2, 136.7, 127.3, 125.7, 124.8, 124.1, 124.0, 124.0, 122.9, 112.8, 105.1; HRMS (EI): found m/z = 349.8253 ± 1.2 ppm; calculated for $C_{10}H_6{}^{79}Br^{81}BrS_2$ [M^+]: 349.8257.

References

(1) Van Tamelen, E.; Brieger, G.; Untch, K. G. *Tetrahedron Lett*., **1960**, 6, 14–15.
(2) Leusink, A.; Drenth, W.; Noltes, J.; van der Kerk, G. J. M. *Tetrahedron Lett*. **1967**, *8*, 1263–1266.
(3) Axelrad, G.; Halpern, D. *J. Chem. Soc. D: Chem. Commun*. **1971**, 291.
(4) Ashe, A. J.; Kampf, J. W.; Kausch, C. M.; Konishi, H.; Kristen, M. O.; Kroker, J. *Organometallics* **1990**, *9***,** 2944–2948.
(5) Subramanian, G.; Schleyer, P. V. R.; Jiao, H. *Organometallics* **1997,** *16,* 2362-2369.
(6) Schulman, J.; Disch, R. *Organometallics*. **2000**, *19,* 2932–2936.
(7) Sashida, H.; Kuroda, A. *J. Chem. Soc., Perkin Trans. 1*, **2000**, 1965–1969.
(8) Mercier, L. G.; Piers, W. E.; Parvez, M. *Angew. Chem. Int. Ed.* **2009,** *48,* 6108 –6111.
(9) Caruso, A.; Siegler, M. A.; Tovar, J. D. *Angew. Chem. Int. Ed.* **2010***, 49,* 4213 –4217.
(10) Caruso, A.; Tovar, J. D. *J. Org. Chem.* **2011***, 76,* 2227–2239.
(11) Caruso, A.; Tovar, J. D. *Org. Lett*. **2011**, *13*, 3106–3109.
(12) Levine, D. R.; Caruso, A.; Siegler, M. A.; Tovar, J. D. *Chem. Commun.,* **2012***, 48,* 6256–6258.
(13) Iida, A.; Saito, S.; Sasamori, T.; Yamaguchi, S. *Angew. Chem. Int. Ed.* **2013***, 52,* 3760 –3764.
(14) Gronowitz, S.; Gassne, P.; Yom-Tov, B. *Acta Chem Scand*. **1969**, *23,* 2927–2930.
(15) Jeffries III, A. T.; Gronowitz, S. *Chem. Script*. **1973**, *4,*183–187.
(16) Sullivan, D.; Pettit, R. *Tetrahedron Lett*. **1963**, *4*, 401–403.
(17) Turnbo, R. G.; Sullivan, D. L.; Pettit, R. *J. Am. Chem. Soc.* **1964**, *86*, 5630–5632.
(18) Gronowitz, S.; Yom-Tov, B.; Michael, U. *Acta Chem. Scand*. **1973**, *27,* 2257–2270.
(19) Jeffries III, A.; Párkányi, C. *J. Phys. Chem*. **1976**, *80*, 287–291.
(20) Sugihara, Y.; Yagi, T.; Murata, I.; Imamura, A. *J. Am. Chem. Soc.* **1992**, *114*, 1479-1481.
(21) Sugihara, Y.; Miyatake, R.; Yagi, T. *Chem. Lett*. **1993**, 933–936.
(22) Sugihara, Y.; Miyatake, R.; Yagi, T.; Murata, I.; Jinguji, M.; Nakazawa, T.; Imamura, A. *Tetrahedron*. **1994**, *50*, 6495–6504.
(23) *Handbook of Thiophene-based Materials: Applications in Organic Electronics and Photonics.* Perepichka, I. F.; Perepichka, Eds.. D. F. John Wiley and Sons, 2009.
(24) Anthony, J. E. *Chem. Rev.* **2006,** *106*, 5028−5048.
(25) Takimiya, K.; Nakano, M.; Kang, M. J.; Miyazaki, E.; Osaka, I. *Eur. J. Org. Chem.* **2013***,* 217–227.
(26) Cinar, M. E.; Ozturk, T. *Chem. Rev.* **2015***, 115,* 3036−3140.
(27) Laquindanum, J. G.; Katz, H. E.; Lovinger, A. J. *J. Am. Chem. Soc.* **199***8, 120,* 664–672.
(28) Payne, M. M.; Odom, S. A.; Parkin, S. R.; Anthony, J. E. *Org. Lett.* **2004,** *6,* 3325–3328.
(29) Zhang, X.; Côté, A. P.; Matzger, A. J. *J. Am. Chem. Soc.* **2005***, 127,* 10502–10503.
(30) Rajca, A.; Wang, H.; Pink, M.; Rajca, S. *Angew. Chem. Int. Ed.* **2000***, 39,* 4481–4483.
(31) Rajca, A.; Miyasaka, M.; Pink, M.; Wang, H.; Rajca, S. *J. Am. Chem. Soc.* **2004**, *126*, 15211–15222.
(32) Takimiya, K.; Osaka, I.; Mori, T.; Nakano, M. *Acc. Chem. Res.* **2014***, 47,* 1493−1502.
(33) Ashe, A. J.; Kampf, J. W.; Nakadaira, Y.; Pace, J. M. *Angew. Chem. Int. Ed.* **1992***, 31*, 1255–1258.
(34) Tsuda, T.; Yazawa, T.; Watanabe, K. *J. Org. Chem.* **1981**, *46*, 192–194.
(35) Jäkle, F.; Manners, I. *Organometallics* **1999,** *18,* 2628–2632.
(36) Sundararaman, A.; Jäkle, F. *J.Organomet. Chem.* **2003**, *681,* 134–142.
(37) Miyasaka, S.; Kobayashi, J.; Kawashima, T. *Tetrahedron Lett*. **2009**, *50*, 3467–3469.
(38) Agou, T.; Kobayashi, J.; Kawashima, T. *Org. Lett.* **2006,** *8,* 2241–2244.
(39) Agou, T.; Kobayashi, J.; Kawashima, T. *Chem. Eur. J.* **2007**, *13*, 8051–8060.
(40) Yamaguchi, S.; Shirasaka, T.; Akiyama, S.; Tamao, K. *J. Am. Chem. Soc*. **2002**, *124*, 8816–8817..
(41) Kim, S.; Song, K.-H.; Kang, S. O.; Ko, J. *Chem. Commun.,* **2004**, 68–69.
(42) Iida, A.; Yamaguchi, S. *J. Am. Chem. Soc.* **2011**, *133*, 6952–6955.
(43) Krasovskiy, A.; Knochel, P. *Angew. Chem. Int. Ed.* **2004***, 43*, 3333–3336.
(44) Harada, K.; Urabe, H.; Sato, F. *Tetrahedron Lett.* **1995**, *36*, 3203–3206.
(45) Sato, F.; Okamoto, S. *Adv. Synth. Catal.* **2001***, 343,* 759–784.
(46) Fukazawa, A.; Kishi, D.; Tanaka, Y.; Seki, S.; Yamaguchi, S. *Angew. Chem. Int. Ed.* **2013***, 52*,

12091 –12095.
(47) Yasuike, S.; Nakashima, F.; Kurita, J.; Tsuchiya, T. *Heterocycles*. **1997**, *45*, 1899–1902.
(48) Wade, C. R.; Broomsgrove, A. E. J.; Aldridge, S.; Gabbaï, F. P. *Chem. Rev.* **2010,** *110*, 3958–3984.
(49) Jäkle, F. *Coord. Chem. Rev*. **2006**, *250*, 1107–1121.
(50) Dimitrijević, E.; Taylor, M. S. *ACS Catal.* **2013***, 3,* 945−962.
(51) Pammer, F.; Jäkle, F. *Chem. Sci*. **2012**, *3*, 2598–2606.
(52) Levine, D. R.; Siegler, M. A.; Tovar, J. D. *J. Am. Chem. Soc*. **2014**, *136*, 7132−7139.
(53) Love, B. E.; Jones, E. G. *J. Org. Chem.* **1999,** *64,* 3755-3756.
(54) Amishiro, N.; Nagamura, S.; Kobayashi, E.; Okamoto, A.; Gomi, K.; Saito, H. *Chem. Pharm. Bull*. **1999**, *47*, 1393—1403.
(55) Ngwendson, J. N.; Atemnkeng, W. N.; Schultze, C. M.; Banerjee, A. *Org. Lett*. **2006**, *8*, 4085–4088.
(56) Spagnolo, P.; Zanirato, P.; Gronowitz, S. *J. Org. Chem.* **1982**, *47*, 3177–3180.
(57) Pelter, A.; Smith, K.; Buss, D.; Jin, Z. *Heteroatom Chem*. **1992**, *3*, 275–277.
(58) Caruso Jr., A. The Synthesis and Characterization of Boron-Containing Pi-Electron Materials that Incorporate Formally Aromatic Borepin Rings. Ph.D. Thesis, Johns Hopkins University, May 2011.
(59) Sheldrick, G. M. *Acta Cryst.* **2008**, *A64,* 112–122.
(60) Macrae, C. F.; Edgington, P. R.; McCabe, P.; Pidcock, E.; Shields, G. P.; Taylor, R.; Towler, M.; van de Streek, J. *J Appl. Cryst*. **2006**, *39*, 453–457.
(61) Gaussian 03, Revision C.01, M. J. Frisch, G. W. Trucks, H. B. Schlegel, G. E. Scuseria, M. A. Robb, J. R. Cheeseman, J. A. Montgomery, Jr., T. Vreven, K. N. Kudin, J. C. Burant, J. M. Millam, S. S. Iyengar, J. Tomasi, V. Barone, B. Mennucci, M. Cossi, G. Scalmani, N. Rega, G. A. Petersson, H. Nakatsuji, M. Hada, M. Ehara, K. Toyota, R. Fukuda, J. Hasegawa, M. Ishida, T. Nakajima, Y. Honda, O. Kitao, H. Nakai, M. Klene, X. Li, J. E. Knox, H. P. Hratchian, J. B. Cross, C. Adamo, J. Jaramillo, R. Gomperts, R. E. Stratmann, O. Yazyev, A. J. Austin, R. Cammi, C. Pomelli, J. W. Ochterski, P. Y. Ayala, K. Morokuma, G. A. Voth, P. Salvador, J. J. Dannenberg, V. G. Zakrzewski, S. Dapprich, A. D. Daniels, M. C. Strain, O. Farkas, D. K. Malick, A. D. Rabuck, K. Raghavachari, J. B. Foresman, J. V. Ortiz, Q. Cui, A. G. Baboul, S. Clifford, J. Cioslowski, B. B. Stefanov, G. Liu, A. Liashenko, P. Piskorz, I. Komaromi, R. L. Martin, D. J. Fox, T. Keith, M. A. Al-Laham, C. Y. Peng, A. Nanayakkara, M. Challacombe, P. M. W. Gill, B. Johnson, W. Chen, M. W. Wong, C. Gonzalez, and J. A. Pople, Gaussian, Inc., Wallingford CT, 2004.
(62) Lee, K. H.; Morino, K.; Sudo, A.; Endo, T. *J. Polym. Sci. A. Polym.Chem*. **2011**, *49,* 1190–1194.
(63) Hagen, S. E.; Domagala, J.; Gajda, C.; Lovdahl, M.; Tait, B. D.; Wise, E.; Holler, T.; Hupe, D.; Nouhan, C.; Urumov, A.; Zeikus, G.; Zeikus, E.; Lunney, E. A.; Pavlovsky, A.; Gracheck, S. J.; Saunders, J.; Van der Roest, S.; Brodfuehrer, J. *J. Med. Chem.* **2001**, *44,* 2319–2332.
(64) Zhao, H.; Dankwardt, J. W.; Koenig, S. G.; Singh, S. P. *Tetrahedron Lett*. **2012**, *53*, 166–169.
(65) Christophersen, C.; Begtrup, M.; Ebdrup, S.; Petersen, H.; Vedsø, P. *J. Org. Chem.* **2003**, *68*, 9513–9516.

Chapter 4: The Chemical Reactivity of Dithienoborepins and the Synthesis and Characterization of Electronically Diverse π-Extended Analogues

Introduction

The thiophene ring has several attractive features that have positioned it as a highly useful structural motif to build organic electronic materials. Beyond high stability and desirable electronic and redox properties, another key element is its synthetic versatility,[1,2] undergoing facile and typically regioselective functionalization. Thus when employed as a terminal ring in an extended π-array, thiophene's reactivity can be used advantageously to construct new C-C and C-heteroatom bonds, providing great scope for property-tuning. It was envisioned, therefore, that the robust dithienoborepin (DTB) systems described in Chapter 3 might be well-suited for the construction of extended boron-containing π-conjugated materials via direct synthetic manipulation of the thiophene rings. This would constitute a distinct advantage over many other boron containing polycyclic aromatics (including *B*-Mes* DBBs) which are often incompatible with more aggressive metalation or halogenation chemistries and typically require preinstallation of synthetic handles (such as halides) at an early stage to later carry out regioselective transformations on the final boron-containing material.

The following chapter describes experiments aimed at assessing the stability and reactivity of DTBs under typical conditions used to functionalize thiophene rings, with the ultimate goal of utilizing synthetic chemistry for targeted property-tuning of the DTB cores. Herein it is demonstrated that the robustness of DTBs enabled a broad range of synthetic transformations to be carried out and that the derivatives generated by these manipulations permitted advantageous adjustments to DTB photophysical and redox properties.

Results and Discussion

The main question to be answered, particularly in view of the sensitivity of early DTBs synthesized by Gronowitz[3] and our lab,[4] was whether or not *B*-Mes DTBs were robust enough to survive more aggressive conditions used to modify the unfunctionalized thiophene rings. Thus an initial screen was carried out to determine the amenability of the DTB scaffolds towards two types of standard thiophene synthetic modification: 1) electrophilic aromatic substitution (S_EAr) with a "Br^+" source and 2) directed α-metalation with an alkyllithium reagent.

To test the feasibility of S_EAr, ~20 mg amounts of DTBs **1** and **2** were treated with 2+ equiv of N-bromosuccinimide (NBS) in *N,N*-dimethylformamide (DMF) at room temperature (Scheme 4.1, condition a). Unlike DTBs with lesser steric protection (*B*-OR or *B*-Ph), the *B*-Mes systems survived the S_EAr bromination conditions and maintained the structural integrity of the triarylborane motif. It was observed that the regioselectivity of bromination depended upon the specific DTB architecture. For **1**, bromine was incorporated at the usual thiophene α-positions to give the dibrominated **1-Br$_2$** in 52% and a lesser amount of the singly α-monobrominated **1-Br** (30%). To achieve reasonable conversion to **1-Br$_2$** on larger scales (up to 200 mg), the addition of $CHCl_3$ as a cosolvent and heating the reaction to 60 °C was necessary (presumably due to the reduced solubility of the brominated material; Scheme 4.1, condition b).

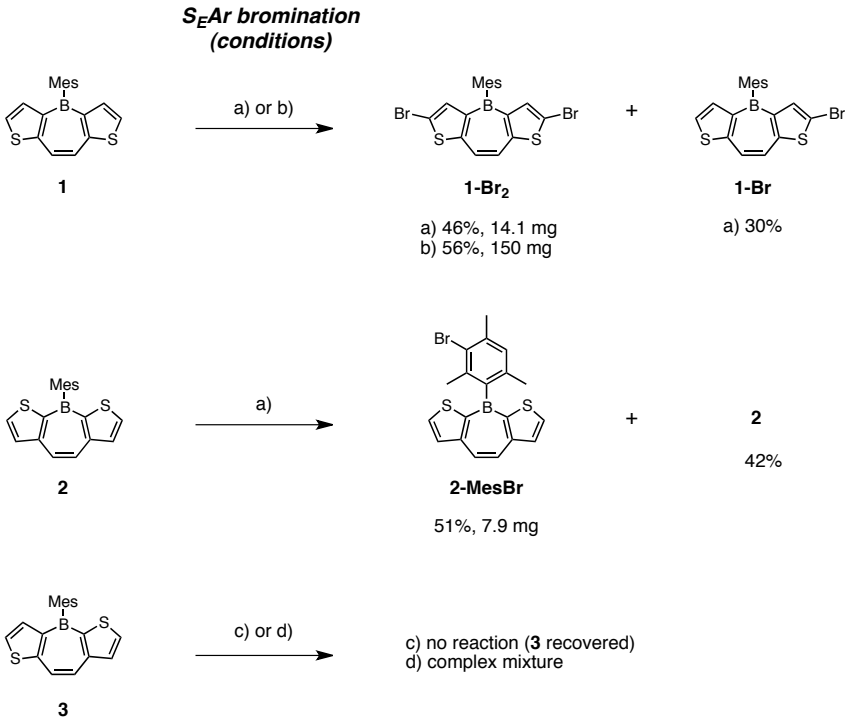

Scheme 4.1. S_EAr bromination trials of DTBs **1** – **3**. Reaction conditions: (a) NBS (2.0 equiv), DMF, r.t., 12 h. (b) NBS (3.4 equiv), DMF:$CHCl_3$ (1:1), 60 °C, 2 d. (c) NBS, $CHCl_3$, 0 °C to r.t, 24 h. (d) NBS, $CHCl_3$, 60 °C, 2 d.

Because DTB **1** demonstrated selective dibromination of the thiophene α-positions, an attempt was made to determine if more reactive iodide handles could also be installed via S_EAr. However, treatment of **1** with molecular iodine and bis(trifluoroacetoxy)iodobenzene as a mild oxidant[5] resulted in a different different halogentation regioselectivity pattern, giving a mixture of Mes-iodinated compound **1-Mes-I** (28%) and the diiodo compound **1-I-Mes-I** (43%) with iodo substitution at the Mes ring and at one thiophene α-position (Scheme 4.2).

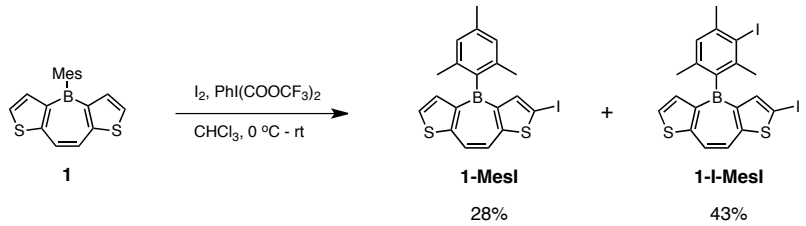

Scheme 4.2. S_EAr iodination of **1**.

It was found that DTB electronics exerted an influence on S_EAR regioselectivity during NBS bromination of DTB isomer **2**. Here bromination of the thiophene rings was not observed at all; monobromination occurred instead on the pendant mesityl (Mes) ring, giving **2-MesBr** in 51% (Scheme 4.1, condition a). The non-reactive nature of the thiophene rings in DTB **2** toward S_EAr was attributed to strong conjugation of the typically reactive α-thieno positions to π-accepting boron center, leading to passivation of these sites towards bromination. It is important to note that with 42% of starting material **2** was recovered, indicating that the reaction conditions did not cause appreciable DTB decomposition.

The reactivity of DTB **3** was of particular interest, since it contained two inequivalent thiophene rings. Unfortunately, bromination trials of **3** with 1 equiv of NBS at room temperature returned mostly unreacted starting material (Scheme 4.1, condition c), while the use of excess NBS under more forcing conditions led to a complex assortment of products (Scheme 4.1, condition d); this suggested that S_EAr was not a viable method to functionalize **3** in a site-selective manner. Overall, the results of the various S_EAr trials revealed that the success/regioselectivity of DTB halogenation was sensitive to several parameters, including the specific electronic structure of each DTB isomer as well as the halogenating reagent employed.

In contrast to S_EAr halogenations, directed metalation with >2 equiv of an alkyllithium reagent was found to be a very reliable method to selectively generate α, α'–thieno-difunctionalized analogues of all three DTB isomers (Scheme 4.2). Treatment of **1** and **2** with *tert*-butyllithium (*t*-BuLi) at -78 °C in Et_2O (generating the putative reactive dilithio species) followed by quenching with a deuterium labeling source (D_2O or MeOD) incorporated deuterium exclusively at the thiophene α and α' positions of **1** and **2** to give **1-*d*$_2$** and **2-*d*$_2$** in good to high yields (^{1}H NMR analysis of the crude products). ^{1}H NOE NMR experiments confirmed this result unambiguously, showing the presence of thieno α– and β-protons in the parent DTB cores and the absence of the α-protons after the lithiation/deuteration. Dilithiation of unsymmetrical DTB **3** was similarly reliable, giving α, α'-dideuterio product **3-*d*$_2$** in 81% after D^+ quench; it was noted that slightly higher levels of conversion to **3-*d*$_2$** (92%) were achieved when a larger excess of *t*-BuLi was used (3.0 equiv) and the lithiated mixture was allowed to warm to room temperature prior to quenching (Table 4.1., entries 1 and 2).

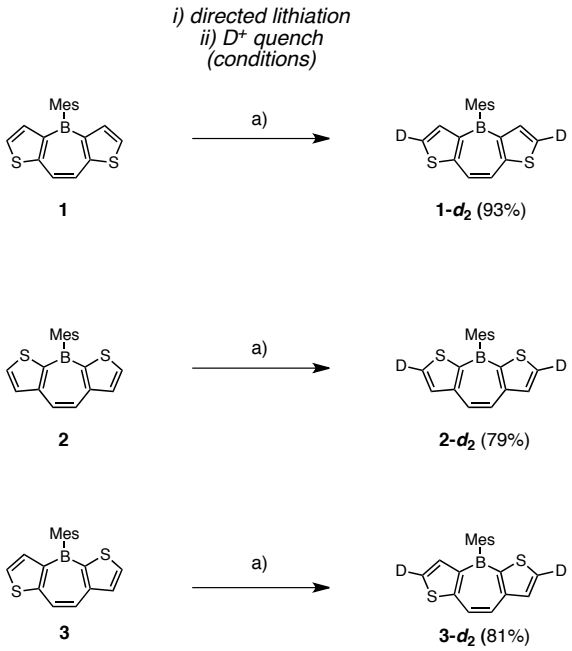

Scheme 4.3. Directed lithiation of **1, 2,** and **3** followed by D^+ quench, showing high α,α'-dimetalation regioselectivity. Reaction conditions: (a) i) *t*-BuLi (2.5 eq), Et_2O -78 °C, 10 min, ii) D_2O or MeOD, -78 °C to rt.

To determine if there was a regiopreference for lithiation of the different thieno rings in **3**, monolithiation experiments were carried out using 1.1 equiv *t*-BuLi, followed by MeOD quench (Table 4.2, entries 3-5) and the product distribution was analyzed by ^{1}H NMR. Under kinetic conditions (lithiation and quench at -78 °C), a moderate 2.3:1 bias for lithiation at the α'-position of the "weakly" boron-conjugated thieno ring over the "strongly" boron-conjugated α-position was observed (entry 3). This preference was essentially nullified (1:1) when the lithiated mixture was allowed to warm to room temperature for 1 h prior to quench, signaling little difference in relative thermodynamic acidity of the α-sites (entry 4). Heating the lithiates to reflux prior to D^+ quench led only to recovery of starting material **3**, suggesting lithiate instability at elevated temperatures (entry 5). It should be noted that the NMR spectra appeared to show small amounts of

doubly deuterated material during the monolithiation experiments, however accurate quantification of these amounts were not achieved due to overlapping resonances.

Table 4.1. Regioselectivity of directed lithiation for **3** during dilithiation (entries 1, 2) and monolithiation (entries 3-5) experiments.

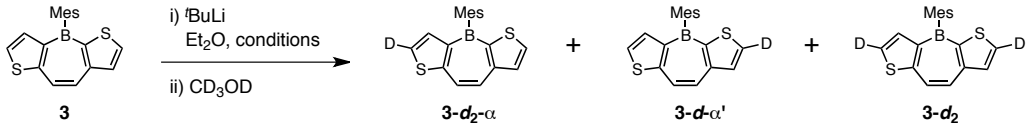

3 **3-*d*$_2$-α** **3-*d*-α'** **3-*d*$_2$**

Entry	***t*-BuLi (eq)**	**Conditions**	**rel. Ratio** [a]		
			3-*d*-α	**3-*d*-α'**	**3-*d*$_2$**
1	2.5	-78 °C, 10 m	0.16	0.03	0.81
2	3.0	-78 °C – r.t., 1 h	0.04	0.04	0.92
3	1.1	-78 °C, 20 m	0.69	0.31	— [c]
4	1.1	-78 °C – r.t., 1 h	0.53	0.47	— [c]
5 [b]	1.1	-78 °C – 35 °C, 2 h	—	—	—

[a] based on integration of ^{1}H NMR signals of the product mixture.
[b] decomposition of lithiate; only starting material recovered.
[c] unquantifiable due to closely overlapping ^{1}H signals.

Having shown that directed lithiation chemistry was a reliable tool to regioselectively modify DTBs at the thiophene α-positions, focus was shifted to the installation of synthetically relevant functional handles for further elaboration of the π-system. It was determined that the dilithiation/quench protocol was suitable for the installation of several types of unique functionality (Scheme 4.3). Quenching of the dilithio species with elemental bromine or iodine provided dibromo- (**1-Br$_2$**, **2-Br$_2$**, **3-Br$_2$**) and diiodo-functionalized (**1-I$_2$**, **2-I$_2$**) DTBs, respectively. Quenching instead with tri-*n*-butylstannyl chloride gave bis-stannylated derivatives **1-Sn$_2$** and **2-Sn$_2$**; use of DMF as the electrophile provided DTB dialdehydes **1-(CHO)$_2$** and **2-(CHO)$_2$.** The brominated

and formylated derivatives were purified by column chromatography; due to the very poor solubility of diiodinated DTBs (even in powerful solvents such as $CHCl_3$, chlorobenzene, and *ortho*-dichlorobenzene), **1-I$_2$** and **2-I$_2$** were purified in a cursory manner by trituration with $CHCl_3$. The identities of the halogenated and formylated DTBs were verified by NMR and HRMS. Due to the sensitivity of the stannane groups towards silica gel, **1-Sn$_2$** and **2-Sn$_2$** were used directly in subsequent reactions without purification.

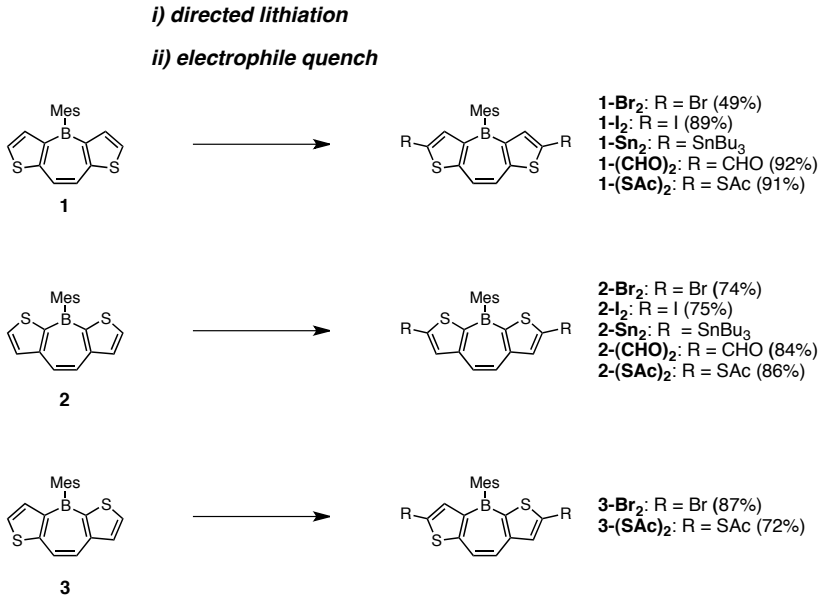

Scheme 4.4. Synthesis of DTBs with synthetically or functionally useful handles installed via directed lithiation / quench methods. Lithiation conditions: *t*-BuLi (2.2-2.5 equiv), Et_2O, -78 °C, 30 m or -78 °C to rt, 1 h. Electrophile quench conditions: For **1-Br$_2$** – **3-Br$_2$**: Br_2 (2.2 equiv) -78 °C to rt; For **1-I$_2$**, **2-I$_2$**: I_2 (4.0 equiv), Et_2O, -78 °C to rt; For **1-Sn$_2$**, **2-Sn$_2$**: *n*-BuSnCl (3.0 equiv), 78 °C to rt; For **1-(CHO)$_2$**, **2-(CHO)$_2$**: DMF (3.0 equiv), -78 °C to rt; For **1-(SAc)$_2$** – **3-(SAc)$_2$**: i) S_8 (2.5 equiv), 78 °C to rt, ii) acetyl chloride (6.0 equiv), -78 °C to rt.

Lithiation chemistry also allowed for the synthesis DTB dithioacetates via a one-pot, multistep protocol. Here, directed lithiation was followed by sequential treatment with elemental sulfur and acetyl chloride, providing **1-(SAc)$_2$**, **2-(SAc)$_2$**, and **3-(SAc)$_2$**.

The thioacetate functional group was of interest since it has proven a useful Au electrode-anchoring group[6,7] to allow the study of single molecule conductance properties in π-conjugated small molecules via scanning tunneling microscopy-break junction (STM-BJ) and mechanically controlled break junction (MC-BJ) methods.[8-10] A collaborative effort between our group and the Electrochemical Nanoscience group (Prof. Thomas Wandlowski, Associate Prof. Wenjing Hong and graduate researcher Masoud Baghernejad) at the University of Bern is currently underway to investigate the electronic behavior of these isomeric DTB dithioacetates in terms of their conductance, quantum interference,[9] and stimulus-induced switchability[10] when employed in single molecule junctions (as envisioned in Figure 4.1). Preliminary results from Wandlowski and coworkers have indicated that the conductance properties of different DTBs are isomer-dependent, suggesting that the unique conjugation pathways in each isomer can influence conductance at the single molecule level. Further, fluoride treatment was observed to induce a switching in DTB single molecule conductance as a result of fluoride complexation with boron. Elaboration of these results via further experimentation and supplemental theoretical calculations are underway, with a manuscript in preparation.

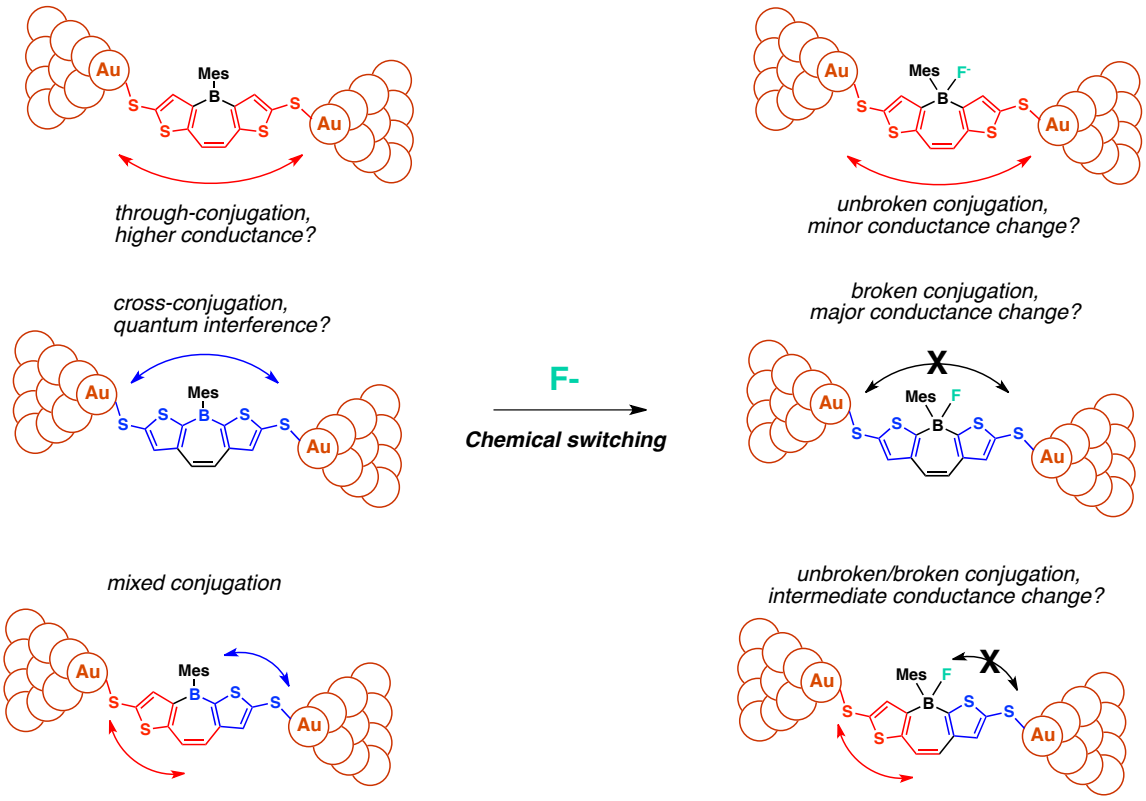

Figure 4.1. Schematic representation showing conceptual conjugation/conductance pathways and fluoride-induced switching in DTB dithioacetate isomers.

Synthetically primed dibromo- and distannylated-DTBs were employed as substrates in Pd-catalyzed cross-couplings to access a broad range of π-extended DTB derivatives (Table 4.2). These reactions established the key features of the DTB scaffolds with respect to cross-coupling capabilities: 1) good compatibility of the DTB synthons with both mild (i.e. Suzuki, Sonogashira, Stille) and more aggressive (Kumada) coupling conditions, 2) successful construction of several types of new DTB C-C bonds (DTB-arene, DTB-heteroarene, DTB-alkyne), 3) ability to use the DTB core as either the electrophilic (**1-Br$_2$**, **2-Br$_2$, 3-Br$_2$**) or nucleophilic (**1-Sn$_2$**, **2-Sn$_2$**) cross-coupling partner, and 4) that successful cross-coupling of DTBs could be achieved with both electron-rich (**4**, **5**) and electron-poor (**6**, **7**) substrates.

Table 4.2. Pd-catalyzed cross-couplings for the synthesis of π-extended DTB analogues.

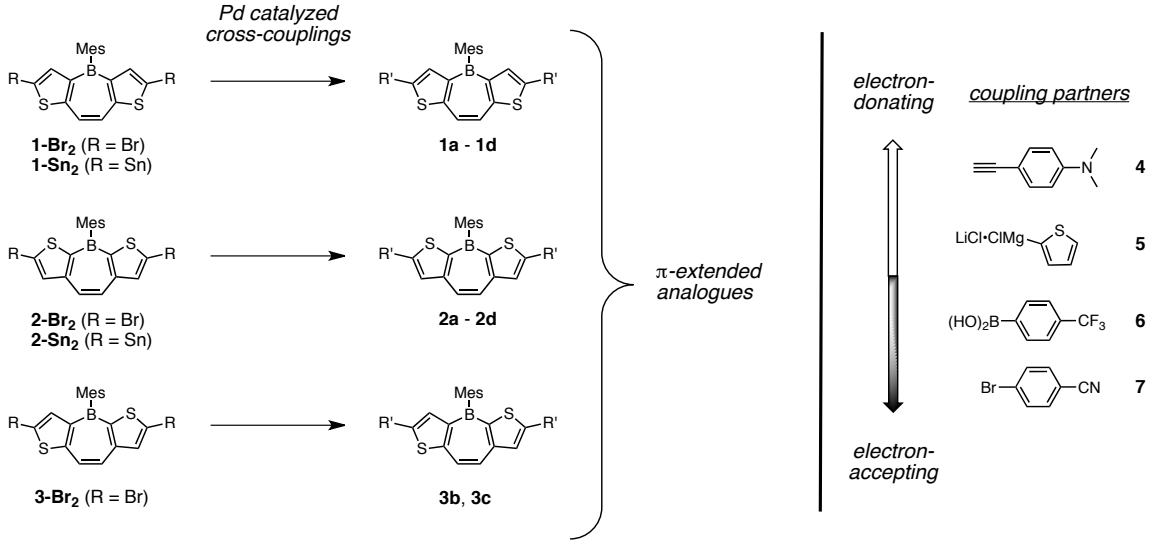

Entry	DTB	Conditions	Product	R'	Yield
1	**1-Br$_2$**	*Sonogashira*	**1a**	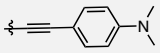	quant.
2	**2-Br$_2$**	*Sonogashira*	**2a**	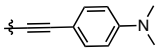	quant.
3	**1-Br$_2$**	*Kumada*	**1b**		63%
4	**2-Br$_2$**	*Kumada*	**2b**		67%
5	**3-Br$_2$**	*Kumada*	**3b**		61%
6	**1-Br$_2$**	*Suzuki*	**1c**	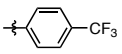	77%
7	**2-Br$_2$**	*Suzuki*	**2c**	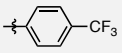	quant.
8	**3-Br$_2$**	*Suzuki*	**3c**	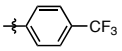	60%
9	**1-Sn$_2$**	*Stille*	**1d**	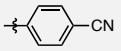	quant.
10	**2-Sn$_2$**	*Stille*	**2d**	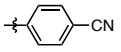	86%

Reaction conditions: *Sonogashira:* **4** (2.4 equiv)**,** Pd[P(*t*-Bu)$_3$]$_2$ (0.1 equiv), CuI (0.08 equiv), diisopropylamine (2.4 equiv), toluene, r.t. *Kumada*: **5** (3.0 equiv)**,** Pd-PEPPSI-IPr (0.1 equiv), THF, 50 °C. *Suzuki:* **6** (3.0 equiv)**,** Pd(OAc)$_2$ (0.1 equiv), SPhos (0.25 equiv), K_3PO_4 (4.0 equiv), toluene, r.t. *Stille:* **7** (2.2 equiv)**,** Pd(PPh$_3$)$_4$ (0.1 equiv), 1,4-dioxane, reflux.

π-Extended donor-acceptor-donor (D–A–D) type DTB analogues were constructed through Sonogashira and Kumada cross-couplings of dibromo-DTBs **1-Br$_2$** – **3-Br$_2$** (Table 4.2, entries 1 – 5). Sonogashira cross-couplings under Fu's conditions[11] with

alkyne **4** gave DTB compounds **1a** and **2a**, featuring strongly electron-donating *N*,*N*-dimethylaminophenylacetylene substituents appended to the electron-deficient DTB core (entries 1, 2). More moderately electron-donating thienyl substituents (**1b** – **3b**) were installed via Kumada couplings of thienyl Grignard **5** using Organ's Pd-PEPPSI-IPr catalyst (entries 3 – 5).[12] It is noteworthy that the potentially aggressive arylmagnesium reagents used for the Kumada couplings did not disturb the boron centers of the DTBs, even at 60 °C.

Acceptor-acceptor-acceptor (A'–A–A')-type DTBs were also synthesized through Pd-catalyzed methods (entries 6 – 10). The bis-(trifluoromethylphenyl)-subtituted DTBs **1c** – **3c** were generated through Suzuki couplings of dibromo DTBs **1-Br$_2$** – **3-Br$_2$** with trifluoromethylphenyl boronic acid under Buchwald's conditions (entries 6 – 8).[13] It is useful to recognize that the robust DTB triarylborane motif withstood the basic conditions required to activate the arylboronic acid cross-coupling partner, which is of interest since it has been demonstrated that even highly hindered triarylboranes can undergo Suzuki activation.[14] Finally, to construct DTB skeletons with even more powerful electron-accepting functionality, PhCN groups (**1d** – **2d**) were installed under mild Stille conditions from bis-stannylated DTBs **1-Sn$_2$** and **2-Sn$_2$** with 4-bromobenzonitrile **7** (entries 9, 10).

The synthetic utility of DTB dialdehydes were realized through a separate reaction manifold, Schiff base formation. **1-(CHO)$_2$** and **2-(CHO)$_2$** were subjected to trifluoroacetic acid-catalyzed condensation with 4-*tert*-butylaniline in $CHCl_3$ to generate the corresponding conjugated imines **1e** and **2e** in 87% and 51% (Scheme 4.5). The compatibility of the DTB cores with the strong Brønsted acid employed (CF_3COOH) in

these transformations is noteworthy. Product identities were confirmed through NMR and HRMS; however, electronic and redox characterization were hampered by the apparent instability of these species in dilute solution, possible due to the reversibility of imine formation. The ability to carry out inherently reversible imine formation suggests that DTB dialdehydes may be suitable for the construction complex organoboron networks (such as polymers or macrocycles) through equilibrium-driven, self-correcting dynamic covalent chemistry (DCC).[15,16]

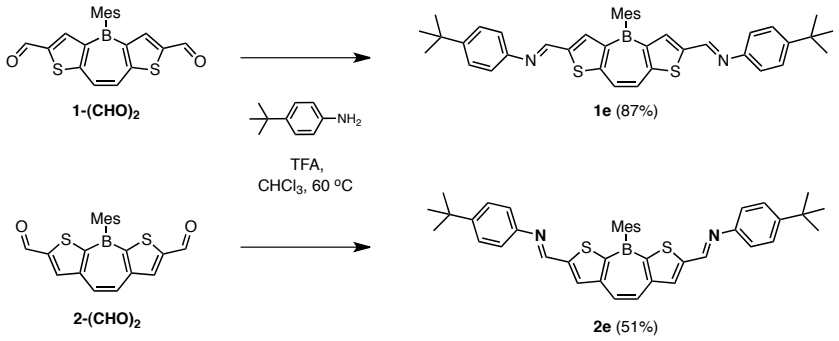

Scheme 4.5. Functionalization of DTB-dialdehydes through imine formation.

Not all DTB functionalization efforts were successful. Attempts to carry out Sonogashira-type chemical copolymerization of DTB diiodides **1-I$_2$** / **2-I$_2$** with comonomer 1,4-bis(decyloxy)-2,5-diethynylbenzene (Scheme 4.6) led to the formation of tough films (Figure 4.2c), which were virtually insoluble in several organic solvents despite the deliberate inclusion of greasy decyloxy side chains. Although the UV-vis and photoluminescence (PL) spectra of a small amount of soluble material obtained via THF rinse of the films (Figure 4.2a, b) revealed spectroscopic profiles similar to spectra of the aryl-acetylene functionalized small-molecule DTBs compounds **1a** and **2a** (Figure 4.3, *vide infra*), suggesting some degree of coupling, attempted GPC analysis indicated that the soluble fraction was of very low molecular weight (monomer-to-dimer length).

These results indicate that future DTB polymerization efforts should focus on engineering more powerful solubilizing features into the precursor materials, such as longer linear or branched alkyl chains. It may be beneficial to consider modifying the DTB core itself; one possible approach might be to incorporate alkyl side-chains at the free borepin ring positions. This could be executed, for example, during the titanium-mediated alkyne reduction (Scheme 4.7a),[17] or through Miyaura's Pt-catalyzed protocol for the diborylation of disubstituted alkynes[18] (followed by subsequent cross-coupling and borepin formation; Scheme 4.7).

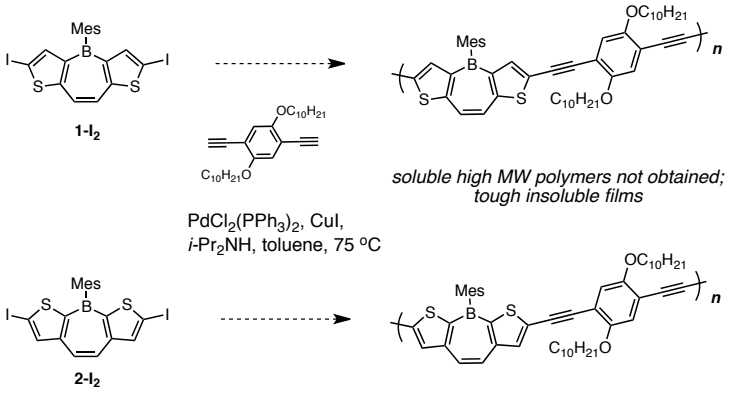

Scheme 4.6. Attempted Sonogashira-type chemical copolymerization of DTB diiodides with 1,4-bis(decyloxy)-2,5-diethynylbenzene.

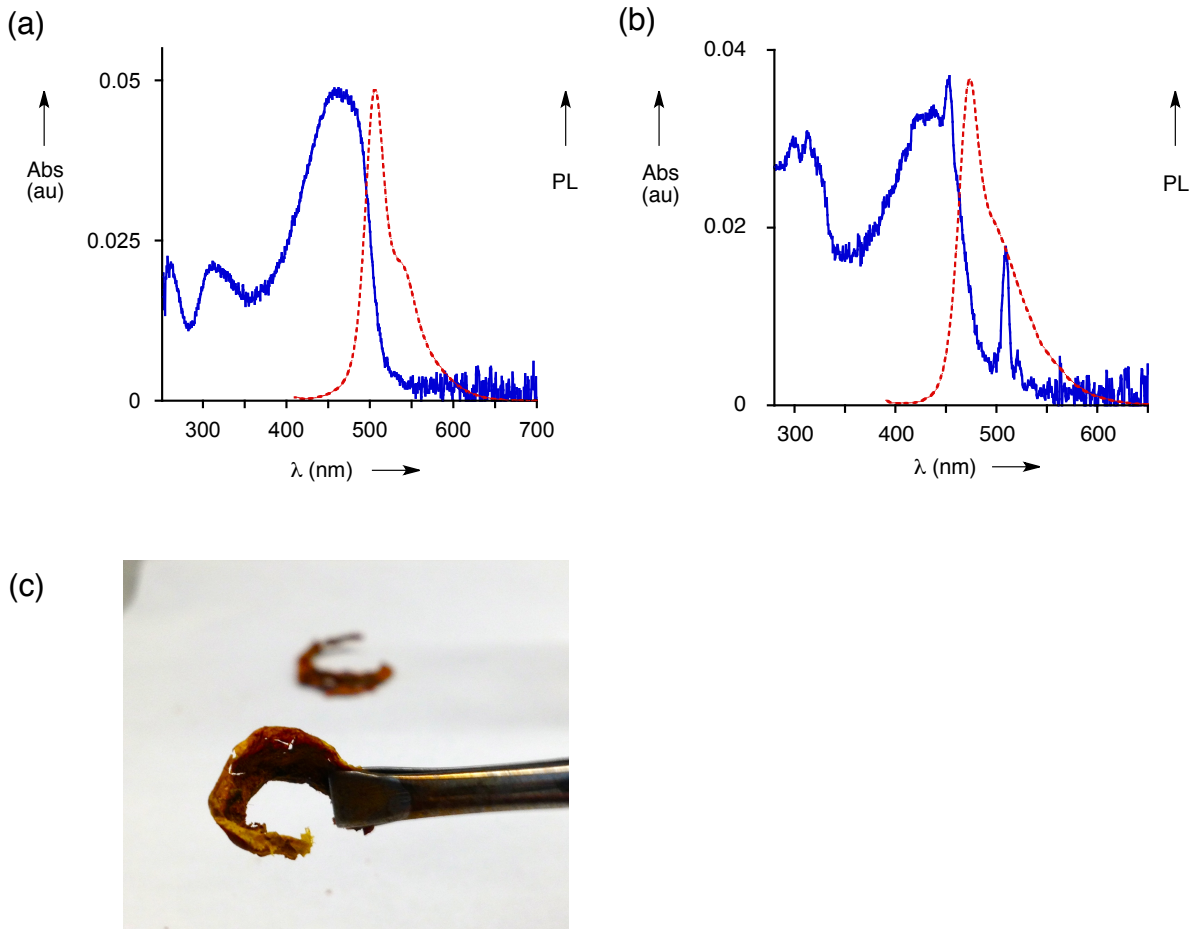

Figure 4.2. UV-vis (blue spectra) and PL (red dotted spectra) data for the soluble material obtained from attempted copolymerizations of (a) **1-I$_2$** or (b) **2-I$_2$** with 1,4-bis(decyloxy)-2,5-diethynylbenzene. (c) Photograph of the insoluble films obtained from the reactions.

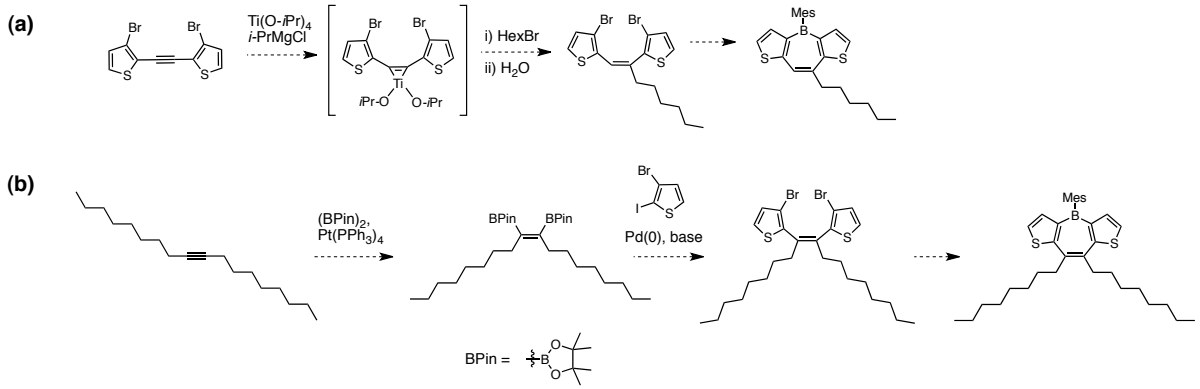

Scheme 4.7. Proposed synthetic approaches towards DTBs with solubilizing alkyl chains (a) during the Ti-mediated alkyne-reduction step or (b) via a separate route utilizing Miyaura's diborylation of dialkylacetylenes.

Attempts were also made to carry out direct, Pd-catalyzed C-H arylation of parent DTBs, a synthetic strategy which had made a substantial impact in contemporary synthetic materials chemistry.[19] Unfortunately, methods for the direct arylation of thiophenes with aromatic bromides or iodides, such as those developed by the groups of Fagnou and Itami,[20,21] were not successful when applied in preliminary trials with DTBs **1** and **2**, yielding either unreacted starting materials or complex, intractable mixtures (Scheme 4.8). While it is not possible to fully rule out the prospects for C-H activation of DTBs, it is likely that the development of any such methods will entail extensive testing and optimization.

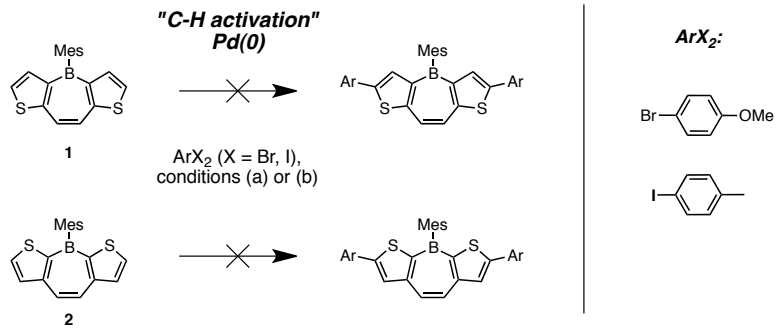

Scheme 4.8. Unsuccessful attempts to carry out direct arylation of parent DTBs via C-H activation methods. Reaction conditions: (a) 4-bromo-anisole, $Pd(OAc)_2$, PCy_3-HBF_4, PivOH, K_2CO_3, toluene, 115 °C (Fagnou's protocol). (b) iodobenzene, $PdCl_2$, 2,2'-bipyridyl, Ag_2CO_3, *m*-xylene, 120 °C (Itami's protocol).

The π-extended DTB derivatives were characterized with UV-Vis and PL spectroscopy, cyclic voltammetry (CV), and supplemented with theoretical calculations at the density functional theory (DFT) level (B3LYP/6-31G*). Electronic spectra and CV scans for functionalized derivatives of DTBs **1** and **2** are presented in Figures 4.2 and 4.3 and discussed with regard to structure-property implications; the data is collated in Table 4.3 at the end of the section.

Electronic properties of the π-extended DTBs were characterized though UV-vis and PL spectroscopy in $CHCl_3$ solution; spectra for the series **1a** – **1d** and **2a** – **2d** are shown in Figure 4.2. Compared to the parent systems, considerable bathochromic shifts in absorption and emission onsets were observed for the functionalized DTBs, consistent with DFT calculations showing narrowed HOMO-LUMO gaps in the extended analogues (Table 4.3). In accord with trends observed for the parent compounds, the functionalized DTBs with longer all-carbon main conjugation pathways (strong thiophene-thiophene conjugation via the α-positions over the olefinic portion of the borepin rings) possessed absorption spectra that were bathochromically shifted relative to those with shorter ones (Abs λ_{onsets} **2x** < **1x**, for any analogue "x"). Generally, the D–A–D-type DTB analogues showed red-shifted absorption spectra compared with the A'–A–A'-type DTBs, consistent with the enhancement of intramolecular charge transfer in the former. Particularly noteworthy were the spectra of strong D–A–D analogues **1a** and **2a**, which showed markedly longer absorption onsets relative to the other compounds. Interestingly, though the PL spectra for the "weakly" boron-conjugated strong D–A–D compound **1a** was not shifted strongly compared with the other functionalized analogues **1b** – **1d**, the "strongly" boron-conjugated **2a** showed a bathochromic shift in PL λ_{max} of approx. 80 nm compared with **2b** – **2d**, suggesting a highly polarizable character due to the integral role of boron in the D-A chromophore of **2a**. The photoluminescence quantum yields varied widely among the π-extended DTBs (between Φ_{PL} = 0.02 for **2c** and **2d** to Φ_{PL} = 0.49 for **1c**) with no particularly discernible trend with respect to functional group identifity or backbone isomer, though the values for most of the compounds were relatively low (Φ_{PL} < 0.10).

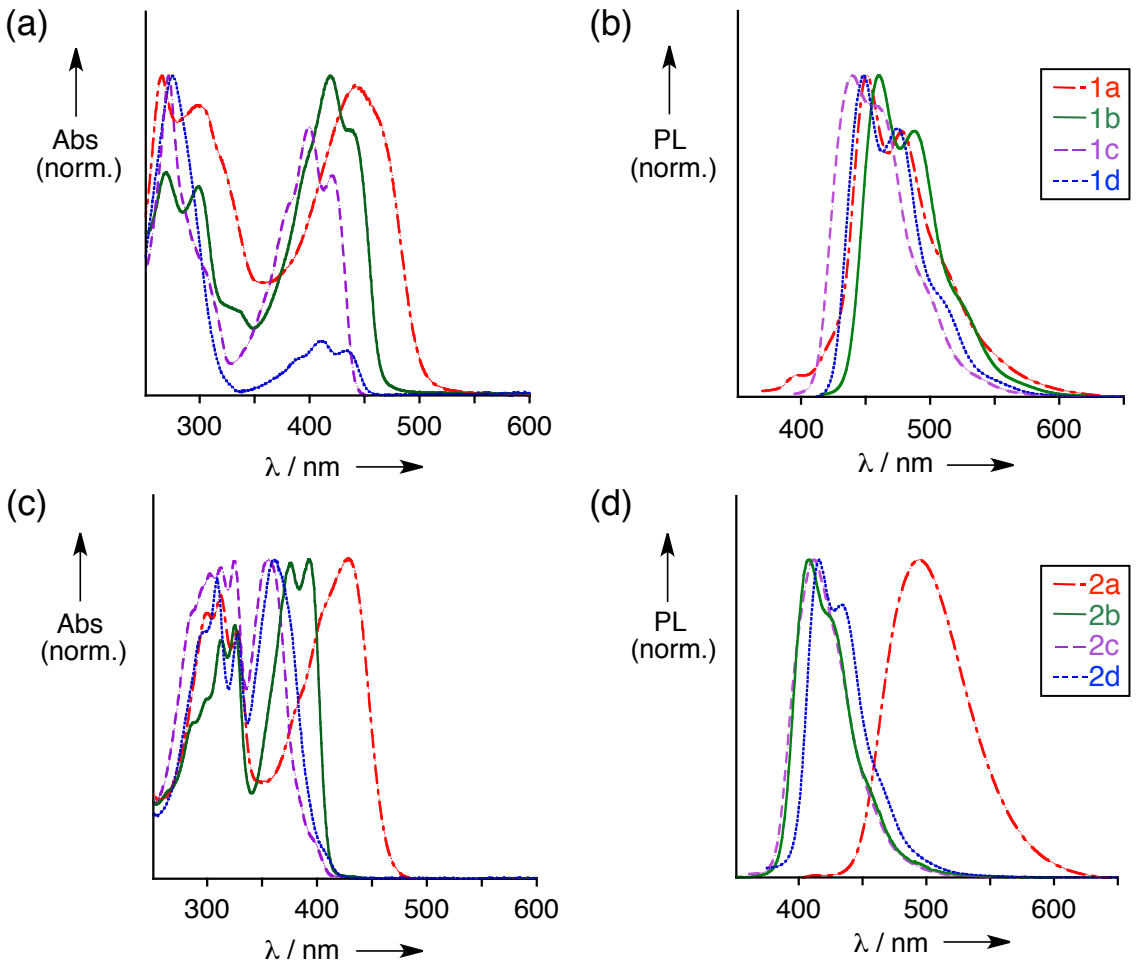

Figure 4.3. Normalized UV-vis and PL spectra for π-functionalized DTBs in $CHCl_3$ at room temperature: (a) UV-vis and (b) PL spectra for **1a**, **1b**, **1c**, and **1d**; (c) UV-vis and (d) PL spectra for **2a**, **2b**, **2c**, and **2d**.

CV was used to probe the electrochemical properties of the functionalized DTBs (Figure 4.4, Table 4.3). The CV scans showed that π-extended DTBs underwent more facile electrochemical reduction than the corresponding parent compounds, regardless of substituent electronics. This is consistent with DFT calculations showing lowered LUMO levels for the substituted DTBs (Table 4.3). As anticipated, the analogues possessing substituents with stronger electron-accepting character (**1c, 2c, 1d**, **2d**) showed the most facile electrochemical reductions. Comparison of different DTB

isomers with the same π-substituents indicated that the analogues possessing stronger α-conjugation between boron and the extended π-system (**1a** – **1d**) were relatively more difficult to reduce than those with weaker boron–β-thieno conjugation (**2a** – **2d**). This is in agreement with the same general trend observed for the parent compounds and is also consistent with the lower relative LUMO levels for the "**1x**" analogues predicted by DFT.

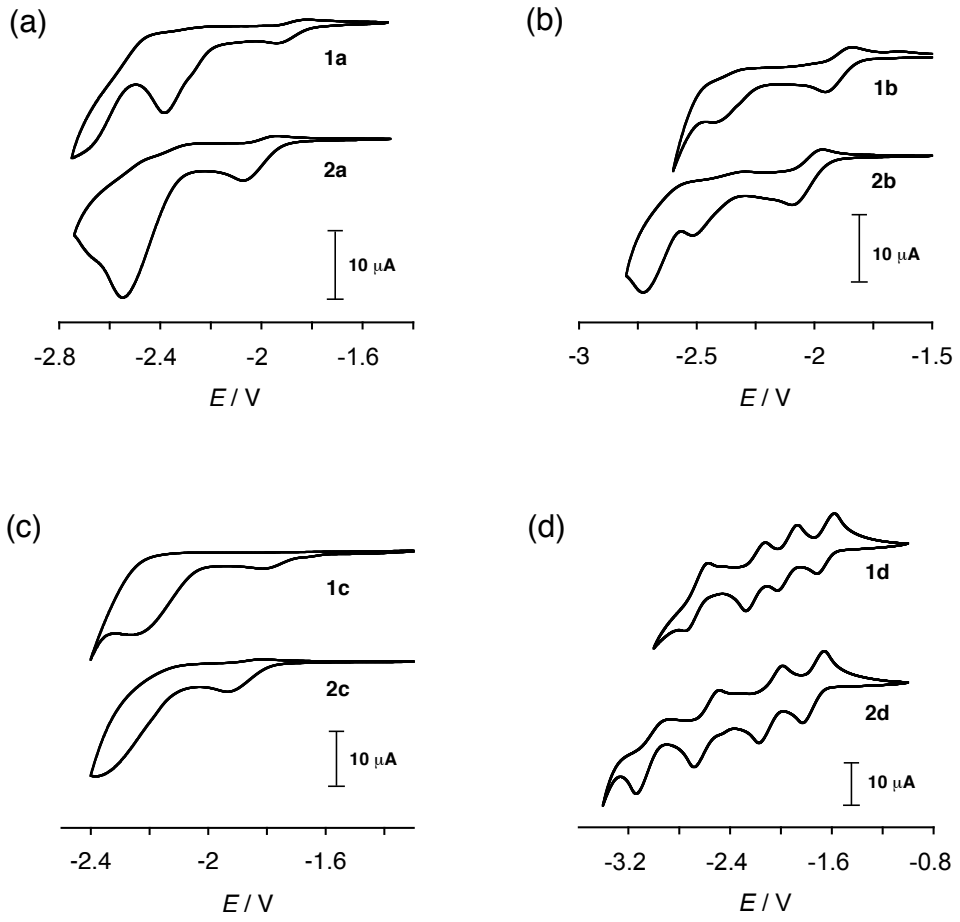

Figure 4.4. Cathodic CV scans for π-extended DTBs (a) **1a** and **2a**, (b) **1b** and **2b**, (c) **1c** and **2c**, (d) **1d** and **2d**. Scans acquired in 1.0 M *n*-Bu_4NPF_6 / THF electrolyte solution at an analyte concentration of 2.5 mM; potentials referenced to Ag/Ag^+ (= 0.00V).

The most unique aspect of the redox chemistry was that all π-extended DTBs underwent multiple cathodic processes (Figure 4.4), despite the fact that the parent DTBs (and even π-functionalized DBB compounds)[22] showed only single reduction waves for

each compound. The reversibility and number of these reductions varied based on the DTB substituent and on the DTB backbone isomer. With respect to substituent identity, the *N,N*-dimethylphenylalkynyl- (**1a**, **2a**), thienyl- (**1b**, **2b**), and PhCN-substituted (**1c**, **2c**) DTBs showed clearly reversible first reduction waves (Figure 4.4a, b, d); however, the corresponding first reductions for the $PhCF_3$-substituted analogues were irreversible (Figure 4.4c). Cyclic voltammograms of strong donor-substituted **1a** and **2a** showed two reductions, with strong irreversible processes following the first reversible process (Figure 4.4a), while the thienyl-substituted systems **1b** and **2b** showed one to two irreversible reductions after the first reversible wave. Even the irreversibly reducible trifluoromethylphenyl-substituted **1c** exhibited a second cathodic wave near -2.4 V.

The cathodic behavior exhibited by PhCN-disubstituted DTBs **1d**/**2d** was of particular interest. These compounds showed up to four fully-reversible reduction waves, indicating a powerful synergy between the peripheral electron-accepting PhCN units the boron-containing core (Figure 4.4d). The individual redox steps were attributed to two separate PhCN-centered single-electron reductions and two single-electron reductions at the boron center. The ability to reversibly access tetraanionic states in stepwise fashion is quite rare within the realm of organic small molecules and suggests that such acceptor-functionalized DTBs might be of interest as capacitive elements for multistate switching in n-type logic[23-25] or memory applications.[26]

Strong donor-acceptor type conjugated organoboranes have shown particular utility as chemoselective colorimetric and luminescent sensing agents for Lewis bases.[27,28] The extended conjugation and strong D-A motifs in DTBs **1a** and **2a** thus suggested that these compounds may show enhanced photophysical responses to fluoride-

binding compared with the parent DTBs. Indeed, treatment of THF solutions of **1a** and **2a** with tetra-*n*-butylammonium fluoride (TBAF) led to distinct changes that, unlike the parent compounds, could be observed not only spectroscopically but also visually (Figure 4.5). Similar to the parent DTBs, the responses of **1a** and **2a** varied according to conjugation scheme of the each isomer. The UV-vis spectrum of **1a** with strong donor groups weakly conjugated to boron showed only small hypsochromic shifts in the major absorption bands upon fluoride addition, while the color of the solution changed slightly from an orange to faint yellow (Figure 4.5b). Similarly, the initially featureless PL spectrum of **1a** showed a corresponding hypsochromic PL λ_{max} shift of 66 nm accompanied by the emergence of fine structure in response to added fluoride (Figure 4.5c). Notably, the visually observable color of emission for this sample under 365 nm light changed from yellow-orange to a teal color. Overall, the changes could be considered colorimetric in nature.

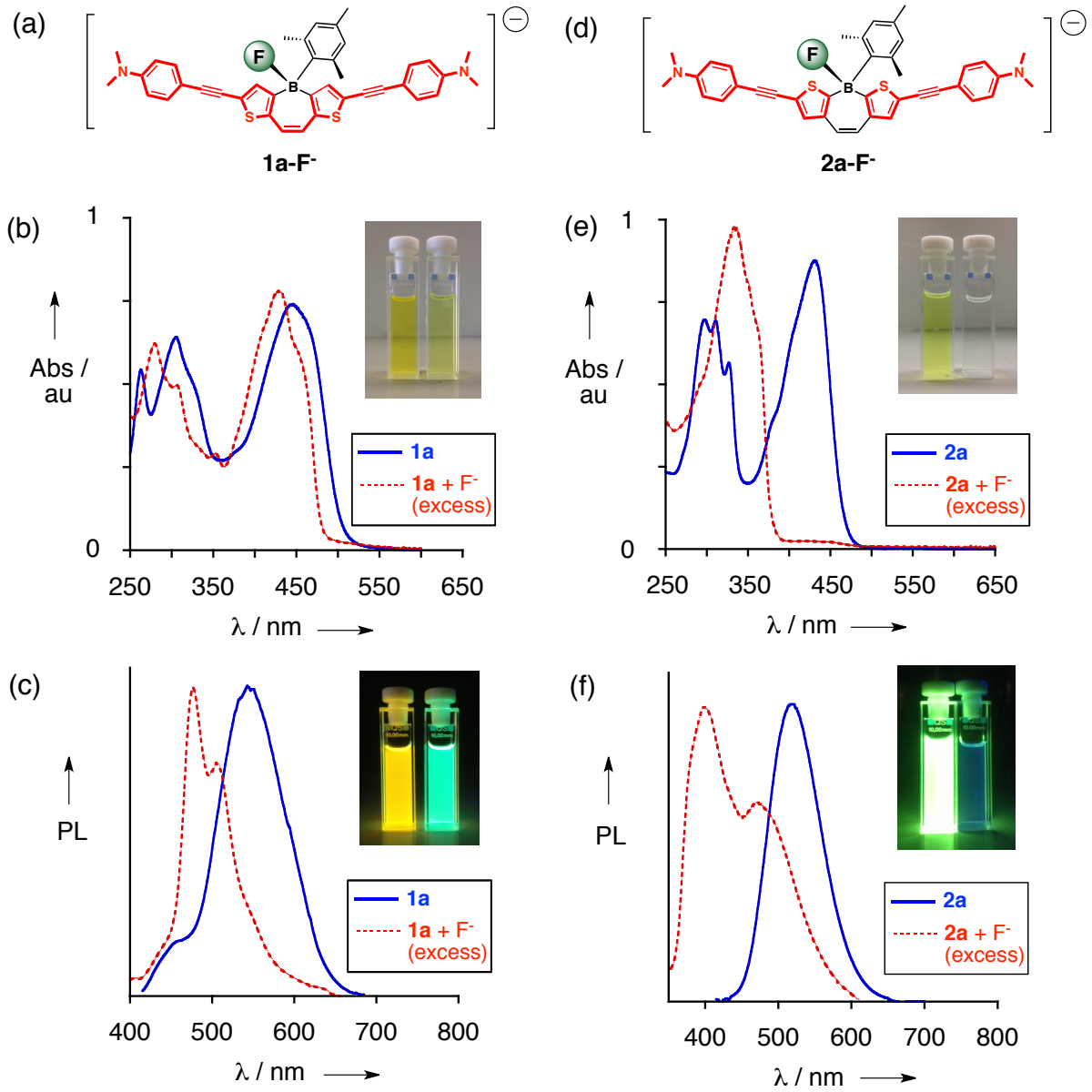

Figure 4.5. Photophysical response to fluoride treatment of D-A DTBs **1a** and **2a** in THF solution. (a) Representation of fluoride-bound **1a-F**$^-$, with unbroken "major" conjugation pathway depicted in red. (b) UV-vis and (c) normalized PL spectra before and after TBAF addition to **1a**. (d) Representation of fluoride bound **2a-F**$^-$ with broken "major" conjugation pathway in red. (e) UV-vis spectra and (f) normalized PL spectra before and after TBAF addition. Photo insets illustrate sample appearance before (left) and after (right) addition of fluoride under (b, e) ambient light and upon (e, f) 365 nm irradiation in the dark.

The response of DTB **2a** to fluoride addition was much more dramatic. A large hypsochromic shift of 95 nm for the Abs λ_{max} was accompanied by a visually observable color change in solution from yellow to completely colorless (Figure 4.5e). An associated very large hypsochromic shift of over 118 nm of the PL λ_{max} was also observed with strong quenching of the emission intensity (Figure 4.4f). As opposed to the color-change response of **1a**, here the visual effect of fluoride complexation was an "on-off" switching of sample luminescence to the naked eye (blue-green to nonemissive).

The differences in the electronic response of the strong D–A–D DTB isomers can be rationalized in terms of the role of boron in the major π-conjugation pathways (Figure 4.5a, d). While fluoride binding to **1a** does not greatly influence the electronic structure in the major all-carbon conjugation pathway due to the peripheral role of boron (weak β-thieno–boron conjugation, Figure 4.5a), the intramolecular charge-transfer pathway in **2a** (strong α-thieno–boron conjugation) is effectively shut down upon coordination of fluoride to the empty p_z orbital of boron (Figure 4.5b). While similar trends were observed spectroscopically for the parent DTB compounds (Chapter 3), the extended π-systems of the donor-functionalized DTBs shift the electronic spectra further into the visible range, allowing for visually observable differences between the bound and unbound states in the different isomers thereby providing a basis for colorimetric/ luminescent sensing. The application of the concept of "strong vs. weak" conjugation in donor-acceptor π-conjugated organoboranes should allow for the construction of other sensor-type materials with tunable absorption/emission properties based on easily functionalizable DTB cores.

Table 4.3. Photophysical, electrochemical, and theoretical data for π-functionalized DTBs.

DTB	Abs λ_{onset} [a] /nm (log ε)	Abs λ_{max} [a] /nm (log ε)	PL λ_{max} [a] /nm (log ε)	Φ_{PL} [b]	$E_{½\ red}$ [c] /V	HOMO [d] /eV	LUMO [d] /eV
1a	578	265 (4.43) 297 (4.40) 440 (4.44)	450 478 509[e]	0.08	-1.89 -2.35[f]	-4.64	-1.92
1b	501	270 (3.88) 299 (3.85) 335[e] (3.46) 419 (4.03) 439 (3.95)	465 488 528[e]	0.13	-1.89 -2.43	-5.17	-2.17
1c	455	272 (4.57) 306[e] (4.16) 381[e] (4.35) 400 (4.50) 421 (4.41)	439 460 496	0.49	-1.76 -2.26[f]	-5.67	-2.50
1d	460	275 (4.46) 392[e] (3.48) 409 (3.66) 439 (3.56)	449 475 507[e]	0.04	-1.64 -1.94 -2.20 -2.66	-5.85	-2.78
2a	493	300 (4.49) 312 (4.52) 328 (4.46) 428 (4.57)	495	0.33	-2.01 -2.55[f]	-4.81	-1.76
2b	448	285[e] (3.39) 299[e] (3.46) 312 (3.59) 325 (3.61) 375 (3.71) 392 (3.71)	408 424[e]	0.08	-2.02 -2.50[f] -2.72[f]	-5.54	-2.02
2c	418	285[e] (4.56) 303 (4.62) 312 (4.63) 325 (4.64) 355 (4.64) 398[e] (3.70)	411	0.02	-1.87 -2.36[f]	-6.04	-2.28
2d	431	296[e] (4.90) 309 (4.98) 328 (4.90) 361 (5.01)	416 434 462[e]	0.02	-1.73 -2.08 -2.58 -3.00	-6.18	-2.66

[a] UV-vis/ PL/ Φ_{PL} collected in $CHCl_3$ solution.
[b] Φ_{PL} values determined relative to quinine sulfate in 0.05 M H_2SO_4 (Φ_{PL} = 0.55).
[c] CV scan taken in N_2-sparged, anhydrous 0.1 M THF/*n*-Bu_4PF_6 solution containing 2.5 mM DTB and referenced to the Ag/Ag^+ redox couple (0.00 V).
[d] calculated at the DFT level (B3LYP/6-31G*)
[e] shoulder band
[f] irreversible redox process; cathodic peak potential (E_{pc}) value given

Concluding Remarks

B-Mes substituted DTBs **1**, **2**, and **3** demonstrated generally excellent levels of stability towards typical S_EAr halogenation and lithiation/quench methods used to functionalize thiophene rings, not undergoing the deleterious B-C bond cleavage reactions which plagued earlier generations of DTB molecules with lesser steric protection (*B*-Ph, *B*-alkyl, *B*-OR). Owing to differences in conjugation between boron and the thiophene rings, each DTB isomer showed unique regioselectivity preferences during S_EAr trials; in contrast, directed lithiation occurred exclusively at the thiophene α-positions for all parent DTB isomers, enabling the site-selective installation of several functional groups (Br, I, CHO, $SnBu_3$, and SAc).

Tuning of the electronic and redox properties of the DTB π-systems was achieved by carrying out Pd-catalyzed cross-couplings of synthetically primed Br-/ $SnBu_3$-functionalized DTBs with an electronically diverse range of π-conjugated substrates. Regardless of the particular electronic nature of each π-substituent or DTB backbone isomer, it was shown that functionalization led to bathochromic shifts in absorption and fluorescence spectra and improved electron-accepting capacity in all cases due to narrowing of the HOMO-LUMO gaps and elevation of the LUMOs, respectively. Appending strong-electron-donating substituents could be used to generate strongly polarizable donor-acceptor materials with isomer-dependent responses to fluoride treatment, while strong electron-withdrawing substituents led to DTB analogues with reversible, four-electron accepting capacity. Access to this broad range of properties through DTB functionalization chemistry (as well as the possibilities for further fine-tuning based on the specifics of boron-π-conjugation patterns) suggests that DTBs will be

versatile vehicles to generate highly stable boron-containing π-electron systems for future organic materials development. The further molecular engineering of DTB cores with solubility-enhancing features (e.g. – alkyl or silyl side-chains) is envisioned as the next benchmark towards this goal, potentially allowing access to DTB-based solution-processible polymers and copolymers. Such modifications are also likely to be important for the successful synthesis of large, extended DTB-based PAHs.

The work in this chapter has been published in part as a full article in the Journal of the American Chemical Society in 2014.[29]

Experimental Section:

General considerations. Unless otherwise specified, all reactions were carried out in flame- or oven-dried glassware under an atmosphere of prepurified nitrogen or argon using standard Schlenk techniques and magnetic stirring. Acetonitrile (MeCN), dichloromethane (CH_2Cl_2), diethyl ether (Et_2O), toluene, and tetrahydrofuran (THF) were purified using an Innovative Technology, Inc. SPS-400-6 solvent purification system, dried over 3Å molecular sieves, and sparged thoroughly with nitrogen prior to use. Anhydrous dimethylformamide (DMF) was obtained from Sigma-Aldrich (99.8%, redistilled) and used without further purification. All other organic solvents were obtained from commercial sources, dried over 3Å molecular sieves, and sparged thoroughly with nitrogen prior to use. Palladium catalysts were obtained from Strem Chemicals. *Tert*-butyllithium was obtained as a 1.7 M solution in pentane from Sigma-Aldrich and titrated with diphenylacetic acid in THF prior to use. Unless otherwise noted, all other chemicals were obtained from Alfa-Aesar, Fisher Scientific, Oakwood Chemicals, Sigma-Aldrich, Strem Chemicals, or TCI America and used as received. DTB compounds **1**, **2**, and **3** were prepared as described in Chapter 3.

The following compounds were prepared according to literature procedures: 4-ethynyl-*N,N*-dimethylaniline.[30] 2-Thienylmagnesium chloride·lithium chloride was prepared by treatment of 2-bromothiophene with *i*PrMgCl·LiCl at room temperature in THF (Knochel's procedure).[31]

^{1}H NMR (400 MHz) and ^{13}C NMR (100 MHz) spectra were obtained using a Bruker Avance 400 MHz FT-NMR spectrometer in deuterated chloroform ($CDCl_3$) and deuterated dichloromethane (CD_2Cl_2) obtained from Cambridge Isotope Laboratories, Inc. All chemical shifts are reported in parts per million (ppm, δ): ^{1}H NMR spectra were referenced to the residual proton solvent peaks ($CHCl_3$, δ = 7.26; CH_2Cl_2, δ = 5.32); ^{13}C NMR spectra were referenced to the carbon solvent peak ($CDCl_3$, δ = 77.16; CD_2Cl_2, δ = 53.84). Boron-bound carbons were typically not observed in ^{13}C NMR spectra due to quadrupolar relaxation of boron. High-resolution mass spectra were obtained using a VG Instruments VG70S/E magnetic sector mass spectrometer with EI (70 eV) and FAB ionization (matrix for FAB was 3-nitrobenzyl alcohol).

Photophysical considerations. Spectroscopic measurements were collected in $CHCl_3$ or THF solution at room temperature. UV-visible (UV-vis) absorption spectra were obtained on a Varian Cary50 Bio UV-visible spectrophotometer. Photoluminescence (PL) spectra were obtained on a PTI QuantaMaster spectrofluorometer with a 75 W Xenon lamp, maintaining optical densities below 0.1 au. PL quantum yields were measured relative to a standard solution of quinine sulfate in 0.05 M aqueous H_2SO_4 while maintaining optical densities below 0.05 au.

Electrochemical considerations. Cyclic voltammetry (CV) measurements were performed under air- and moisture-free conditions in a one-chamber, three electrode cell using a PGSTAT302 potentiostat. A 2 mm^2 Pt button electrode was used as the working electrode with a Pt wire counter electrode relative to a quasi-internal Ag wire reference electrode submersed in 0.01 M $AgNO_3$/0.1M *n*-Bu_4NPF_6 in anhydrous acetonitrile. Cyclic voltammograms were taken 0.1 M *n*-Bu_4NPF_6 / THF electrolyte solutions at analyte concentrations of 2.5 mM (scan rate = 100 mV/s). Potentials are reported relative to the Ag/Ag^+ redox couple (0.00 V) against which the Fc/Fc^+ couple was measured to be +200 mV.

Theoretical considerations. Geometry optimizations/molecular orbital calculations were performed at the Density Functional Theory (DFT) level (B3LYP/6-31G*) and electronic transitions for the optimized structures were calculated using time-dependent DFT (TD-DFT) at the same level with Spartan '04 software (Wavefunction Inc., Irvine, CA).

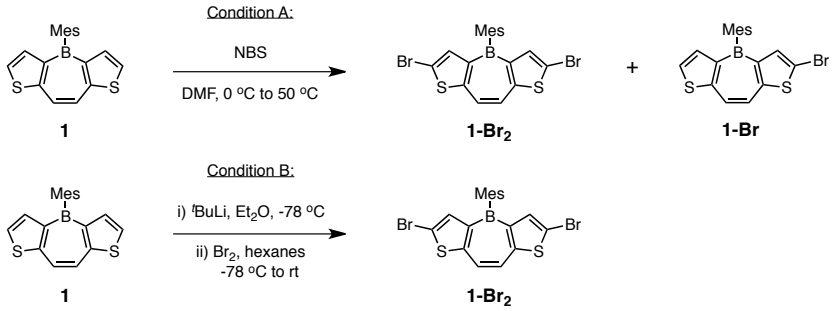

1-Br$_2$. *Condition A*: To a stirring solution of **1** (20.8 mg, 0.0649 mmol) in 1 mL DMF at 0 °C in a 25-mL Schlenk tube under nitrogen was added NBS (25.8 mg, 0.130 mmol) in a single portion. The sides of the flask were rinsed with an additional 1 mL DMF and the mixture was allowed to come to room temperature and stirred in the absence of light; after 12 h an additional portion of NBS (6.3 mg, 0.035 mmol) was added and the mixture stirred at 50 °C for 1 h and at room temperature for a further 12 h. The volatile components were removed under reduced pressure and the residue was purified by column chromatography (SiO_2, 5% $CHCl_3$ in hexanes → 10% $CHCl_3$ in hexanes) to afford 14.1 mg of **1-Br$_2$** as a white solid (0.0294 mmol, 46%). The monobrominated side-product **1-Br** (8.1 mg) was isolated as a white solid (0.020 mmol, 31%).

Condition B: To a stirring solution of **1** (10.1 mg, 0.0315 mmol) in 1.5 mL Et_2O at -78 °C in a 25-mL Schlenk tube under nitrogen was added *t*-BuLi (1.59 M in pentane, 0.044 mL, 0.069 mmoL) dropwise via syringe. The colorless solution immediately became a pink-colored suspension and after stirring for 1 h a solution of Br_2 (0.044 mL, 0.069 mmol) in 0.069 mL hexanes was added dropwise to the mixture. The mixture was allowed to stir for 20 h with gradual warming to room temperature then saturated aq $Na_2S_2O_3$ was added. After partitioning the mixture between Et_2O and H_2O (1:1), the organic layer was removed and the aqueous layer was extracted 1x with Et_2O. The combined organics were dried over $MgSO_4$, filtered, and concentrated under reduced pressure to give an orange-brown solid which was purified by column chromatography ((SiO_2, hexanes → 5% $CHCl_3$ in hexanes → 10% $CHCl_3$ in hexanes) to give 7.4 mg of **1-Br$_2$** (0.015 mmol, 49%) as a white solid.

1-Br$_2$: ^{1}H NMR (400 MHz, CD_2Cl_2) δ: 7.56 (s, 2H), 7.25 (s, 2H), 6.92 (m, 2H), 2.37, (s, 3H), 1.92 (s, 6H); ^{13}C NMR (100 MHz, CD_2Cl_2) δ: 158.0, 140.7, 127.6, 122.6, 22.5, 21.5; HRMS (EI): found *m/z* = 477.9050 ± 0.9 ppm; calculated for $C_{19}H_{15}{}^{11}BS_2{}^{79}Br^{81}Br$ [M^+]: 477.9055.

1-Br: ^{1}H NMR (400 MHz, CD_2Cl_2) δ: 7.73 (d, *J*= 11.6 Hz, 1H), 7.55 (d, *J*= 11.6 Hz, 1H), 7.54 (d, *J*= 5.2 Hz, 1H), 7.33 (d, *J*= 5.2 Hz, 1H), 7.24 (s, 1H), 6.91 (s, 2H), 2.36, (s, 3H), 1.91 (s, 6H); ^{13}C NMR (100 MHz, CD_2Cl_2) δ: 157.9, 140.5, 138.5, 136.9, 127.9, 127.4, 123.9, 121.8, 114.7, 22.8, 21.3; HRMS (EI): found *m/z* = 397.9962 ± 2.1 ppm; calculated for $C_{19}H_{16}{}^{11}BS_2{}^{79}Br$ [M^+]: 397.9970.

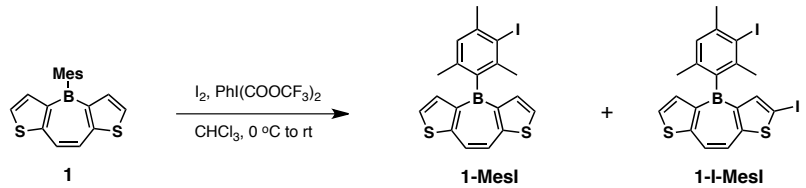

1 1-MesI 1-I-MesI

1-MesI, **1-I-MesI**. To a stirring solution of **1** (10.7 mg, 0.0334 mmol) in 1 mL $CHCl_3$ at 0 °C in a 25-mL Schlenk tube under nitrogen were added iodine (8.9 mg, 0.0351 mmol) and [bis(trifluoroacetoxy)iodo]benzene (15.8 mg, 0.0367 mmol) in single portions. The mixture was allowed to come to room temperature with continued stirring. After 24 h, additional portions of iodine (8.9 mg, 0.0351 mmol) and [bis(trifluoroacetoxy)iodo]benzene (15.8 mg, 0.0367 mmol) were added. After 10 h of further stirring, sat. aq. $Na_2S_2O_3$ was added to the mixture and allowed to stir for 1 h. The organic layer was removed and the aqueous layer was extracted 2x with $CHCl_3$. The combined organics were dried over $MgSO_4$, filtered, and concentrated under reduced pressure to a dark oil that was purified by column chromatography (SiO_2, 5% CHCl3 in hexanes) to give 4.1 mg of **1-MesI** (0.00919 mmol, 28%) and 8.2 mg of **1-I-MesI** (0.0143 mmol, 43%) as off-white solids.

1-MesI: ^{1}H NMR (400 MHz, CD_2Cl_2) δ: 7.74 (s, 1H), 7.54 (d, *J* = 4.8 Hz, 2H), 7.32 (d, *J* = 4.8 Hz, 2H), 7.01 (m, 1H), 2.54 (s, 3H), 2.13 (s, 3H), 1.87 (s, 3H); ^{13}C NMR (100 MHz, CD_2Cl_2) δ: 160.7, 157.1, 138.2, 128.8, 127.5, 123.3, 114.8, 109.6, 30.9, 30.1, 22.2; HRMS (EI): found *m/z* = 445.9842 ± 2.4 ppm; calculated for $C_{19}H_{16}$ $^{11}BIS_2$ [M^+]: 445.9831 .

1-I-MesI: ^{1}H NMR (400 MHz, CD_2Cl_2) δ: 7.72 (dd, *J* = 11.6 Hz, *J* = 0.4 Hz, 1H), 7.63 (dd, *J* = 11.6 Hz, *J* = 0.4 Hz, 1H), 7.55 (d, *J* = 5.6 Hz, 1H), 7.44, (d, *J* = 0.4 Hz, 1H), 7.31 (dd, *J* = 5.2 Hz, *J* = 0.8 Hz, 1H), 7.01 (m, 1H), 2.54 (s, 3H), 2.12 (s, 3H), 1.86 (s, 3H); ^{13}C NMR (100 MHz, CD_2Cl_2) δ: 162.2, 147.7, 141.0, 138.3, 138.2, 128.8, 128.0, 123.7, 121.5, 30.9, 30.1, 22.2; HRMS (EI): found *m/z* = 571.8809 ± 1.9 ppm; calculated for $C_{19}H_{15}$ $^{11}BI_2S_2$ [M^+]: 571.8798.

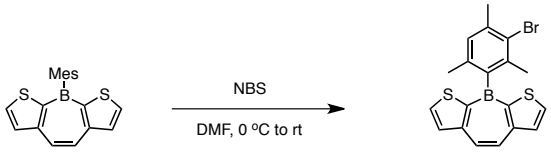

2 2-MesBr

2-MesBr. To a stirring 0 °C solution of **2** (10.8 mg, 0.0337 mmol) in 1 mL DMF under N_2 in a 25-mL Schlenk tube was added NBS (12.0 mg, 0.0674 mmol) in a single portion. The mixture was allowed to come to room temperature and stirred in the absence of light for 12 h then the volatile components were removed directly under high vacuum. The crude product was purified by column chromatography (SiO_2, gradient elution: 2% $CHCl_3$ in hexanes → 5% $CHCl_3$ in hexanes → 10% $CHCl_3$ in hexanes) to afford 7.9 mg of **2-MesBr** as a white solid (0.017 mmol, 52%, 91% brsm). The remaining starting

material **2** was recovered as 4.7 mg of a white solid (0.015 mmol, 44%). ^{1}H NMR (400 MHz, CD_2Cl_2) δ: 8.01 (d, 2H, *J*= 4.8 Hz), 7.79 (s, 2H), 7.74 (d, 2H, *J*= 4.8 Hz), 7.05 (m, 1H), 2.50 (s, 3H), 2.14 (s, 3H), 1.95 (s, 3H); ^{13}C NMR (100 MHz, CD_2Cl_2) δ: 151.3, 138.2, 136.5, 133.6, 129.9, 126.8, 125.66, 24.7, 24.3, 22.1; HRMS (EI): found *m/z* = 399.9957 ± 1.9 ppm; calculated for $C_{19}H_{16}{}^{11}BS_2{}^{81}Br$ [M^+]: 399.9955.

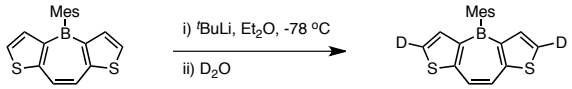

1 **1-*d*$_2$**

1-*d*$_2$. To a stirring -78°C solution of **1** (10.5 mg, 0.0328 mmol) in 1.5 mL Et_2O under N_2 in a 25-mL Schlenk tube was added *t*-BuLi (1.59 M in pentane, 0.052 mL, 0.082 mmoL) dropwise via syringe. The colorless solution immediately became a pink-colored suspension and after 10 m D_2O (0.8 mL) was added dropwise to the mixture with rapid stirring. The cooling bath was removed and the mixture was allowed to come to room temperature for 2 h then brine was added. After partitioning the mixture between Et_2O and H_2O (1:1), the organic layer was removed and the aqueous layer was extracted 1x with Et_2O. The combined organics were dried over $MgSO_4$, filtered, and concentrated under reduced pressure to give 9.8 mg of **1-*d*$_2$** (0.030 mmol, 93%) as a pale yellow solid. ^{1}H NMR (400 MHz, $CDCl_3$) δ: 7.69 (s, 2H), 7.38 (s, 2H), 6.92 m, 2H), 2.39 (s, 3H), 1.95 (s, 6H); ^{13}C NMR (100 MHz, $CDCl_3$) δ: 156.1, 138.3, 138.1, 136.4, 127.1, 123.0, 22.9, 21.4; HRMS (EI): found *m/z* = 322.0997 ± 1.9 ppm; calculated for $C_{19}H_{15}D_2{}^{11}BS_2$ [M^+]: 322.0990.

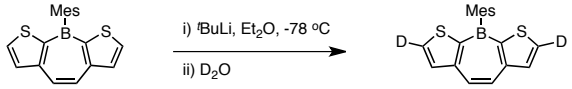

2 **2-*d*$_2$**

2-*d*$_2$. To a stirring -78°C solution of **2** (10.7 mg, 0.0334 mmol) in 1.5 mL Et_2O under N_2 in a 25-mL Schlenk tube was added *t*-BuLi (1.59 M in pentane, 0.053 mL, 0.084 mmoL) dropwise via syringe. The colorless solution immediately became a mustard-colored suspension and after 10 m D_2O (0.8 mL) was added dropwise to the mixture with rapid stirring. The cooling bath was removed and the mixture was allowed to come to room temperature for 2 h then brine was added. After partitioning the mixture between Et_2O and H_2O (1:1), the organic layer was removed and the aqueous layer was extracted 1x with Et_2O. The combined organics were dried over $MgSO_4$, filtered, and concentrated under reduced pressure to give 8.5 mg of **2-*d*$_2$** (0.026 mmol, 79%) as pale yellow solid. ^{1}H NMR (400 MHz, $CDCl_3$) δ: 7.74 (s, 2H), 7.69 (s, 2H), 6.94 m, 2H), 2.40 (s, 3H), 2.04 (s, 6H); ^{13}C NMR (100 MHz, $CDCl_3$) δ: 150.4, 139.1, 133.0, 127.3, 126.4, 22.7, 21.6; HRMS (EI): found *m/z* = 322.0990 ± 0.1 ppm; calculated for $C_{19}H_{15}D_2{}^{11}BS_2$ [M^+]: 322.0990.

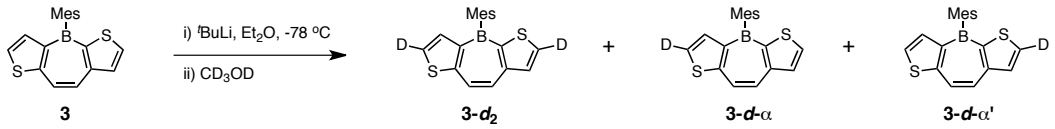

3-d_2. To a stirring solution of **3** (15.9 mg, 0.0496 mmol) in 1.5 mL Et_2O at -78 °C in a 25-mL Schlenk tube under nitrogen was added *t*-BuLi (1.59 M in pentane, 0.070 mL, 0.124 mmoL) dropwise via syringe. The colorless solution immediately became a mustard-colored suspension and after 10 m CD_3OD (0.8 mL) was added dropwise to the mixture with rapid stirring. The cooling bath was removed and the mixture was allowed to come to room temperature for 1 h then brine was added. After partitioning the mixture between Et_2O and H_2O (1:1), the organic layer was removed and the aqueous layer was extracted 1x with Et_2O. The combined organics were dried over $MgSO_4$, filtered, and concentrated under reduced pressure to give 16.9 mg of a yellow solid which was estimated by ^{1}H NMR to be 81% **3-d_2**, 16% **3-*d*-α** , and 3% **3-*d*-α'**.

3-d_2: ^{1}H NMR (400 MHz, CD_2Cl_2) δ: 7.79 (d, J = 11.6 Hz, 1H), 7.69 (s, 1H), 7.65 (d, J = 11.6 Hz, 1H), 7.36 (s, 1H), 6.94, (s, 2H), 2.40, (s, 3H), 2.00 (s, 6H).

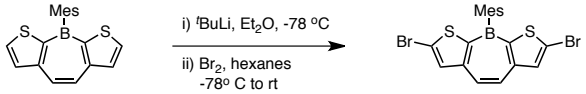

2-Br_2. To a stirring solution of **2** (10.3 mg, 0.0322 mmol) in 1.5 mL Et_2O at -78 °C in a 25-mL Schlenk tube under nitrogen was added *t*-BuLi (1.59 M in pentane, 0.045 mL, 0.071 mmoL) dropwise via syringe. The colorless solution immediately became a mustard-colored suspension. After stirring for 30 m, a solution of Br_2 (0.036 mL, 0.071 mmol) in 0.071 mL hexanes was added dropwise to the mixture. The mixture was allowed to stir for 20 h with gradual warming to room temperature and saturated aq $Na_2S_2O_3$ was added. After partitioning the mixture between Et_2O and H_2O (1:1), the organic layer was removed and the aqueous layer was extracted 1x with Et_2O. The combined organics were dried over $MgSO_4$, filtered, and concentrated under reduced pressure to give a yellow solid which was purified by column chromatography (SiO_2, hexanes) to give 8.5 mg of **2-Br_2** (0.024 mmol, 74%) as an off-white solid. ^{1}H NMR (400 MHz, CD_2Cl_2) δ: 7.66 (s, 2H), 7.61 (s, 2H), 6.94 (m, 2H), 2.38, (s, 3H), 2.01 (s, 6H); ^{13}C NMR (100 MHz, CD_2Cl_2) δ: 151.1, 139.4, 138.6, 136.1, 127.8, 126.6, 125.2, 22.5, 21.5; HRMS (EI): found m/z = 477.9055 ± 0.0 ppm; calculated for $C_{19}H_{15}{}^{11}BS_2{}^{79}Br^{81}Br$ [M^+]: 477.9055.

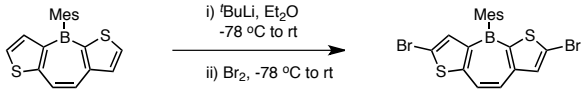

3 **3-Br_2**

3-Br_2. To a stirring solution of **3** (63.1 mg, 0.197 mmol) in 5 mL Et_2O at -78 °C in a 25-mL Schlenk tube under nitrogen was added *t*-BuLi (1.59 M in pentane, 0.310 mL, 0.493 mmoL) dropwise via syringe. The colorless solution immediately became a mustard-colored suspension. After stirring for 10 m at -78 °C the mixture was allowed to stir at room temperature for 1 h, then cooled to -78 °C and neat Br_2 (0.026 mL, 0.512 mmol) was added dropwise via syringe. The mixture was allowed to stir for 8 h with gradual warming to room temperature and saturated aq Na_2HCO_3 was added. After partitioning the mixture between Et_2O and H_2O (1:1), the organic layer was removed and the aqueous layer was extracted 2x with Et_2O. The combined organics were dried over $MgSO_4$, filtered, and concentrated under reduced pressure to give a yellow solid which was purified by column chromatography (SiO_2, gradient elution: hexanes → 2% $CHCl_3$ in hexanes) to give 83.2 mg of **3-Br_2** (0.174 mmol, 87%) as an off-white solid. ^{1}H NMR (400 MHz, $CDCl_3$) δ: 7.60 (s, 1H), 7.59 (d, *J* = 11.6 Hz, 1H)), 7.48 (d, *J* = 11.6 Hz, 1H), 7.25 (s, 1H), 6.93 (s, 2H), 2.39, (s, 3H), 1.99 (s, 6H); ^{13}C NMR (100 MHz, CD_2Cl_2) δ: 157.5, 150.5, 139.5, 138.6, 137.6, 135.4, 127.4, 125.6, 124.5, 124.0, 115.4, 22.8, 21.5; HRMS (EI): found *m/z* = 477.9061 ± 1.3 ppm; calculated for $C_{19}H_{15}{}^{11}BS_2{}^{79}Br^{81}Br$ [M^+]: 477.9055.

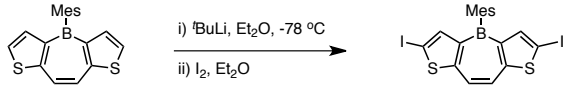

1 **1-I_2**

1-I_2. To a stirring solution of **1** (14.4 mg, 0.0450 mmol) in 2 mL Et_2O at -78 °C in a 25-mL Schlenk tube under nitrogen was added *t*-BuLi (1.82 M in pentane, 0.062 mL, 0.11 mmoL) dropwise via syringe. The colorless solution immediately became a pink suspension and after stirring for 30 m a solution of I_2 (45.6 mg, 0.180 mmol) in 1.5 mL Et_2O was added dropwise to the mixture via syringe (a yellow precipipate was noted immediately upon addition of I_2). The mixture was allowed to stir for 17 h with gradual warming to room temperature and saturated aq. $Na_2S_2O_3$ was added. After partitioning the mixture between Et_2O and H_2O (1:1), the organic layer was removed and the aqueous layer was extracted 3x with $CHCl_3$. The combined organics were dried over $MgSO_4$, filtered, and concentrated under reduced pressure to give a yellow solid which was triturated with MeOH and then rinsed with a small amount of $CHCl_3$ to give 22.8 mg of **1-I_2** (0.0399 mmol, 89%) as an off-white solid (note: **1-I_2** exhibited very low solubility in most organic solvents). ^{1}H NMR (400 MHz, $CDCl_3$) δ: 7.53 (s, 2H), 7.46 (s, 2H), 6.92 (s, 2H), 2.40, (s, 3H), 1.93 (s, 6H); HRMS (EI): found *m/z* = 571.8806 ± 1.4 ppm; calculated for $C_{19}H_{15}{}^{11}BI_2S_2$ [M^+]: 571.8798.

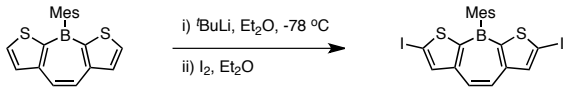

2 **2-I_2**

2-I_2. To a stirring solution of **2** (14.4 mg, 0.0450 mmol) in 2 mL Et_2O at -78 °C in a 25-mL Schlenk tube under nitrogen was added *t*-BuLi (1.82 M in pentane, 0.062 mL, 0.11 mmol) dropwise via syringe. The colorless solution immediately became a mustard-colored suspension and after stirring for 30 m a solution of I_2 (45.6 mg, 0.180 mmol) in 1.5 mL Et_2O was added dropwise to the mixture via syringe. The resulting red-brown solution was allowed to stir for 17 h with gradual warming to room temperature and saturated aq. $Na_2S_2O_3$ was added. After partitioning the mixture between Et_2O and H_2O (1:1), the organic layer was removed and the aqueous layer was extracted 3x with Et_2O. The combined organics were dried over $MgSO_4$, filtered, and concentrated under reduced pressure to give a yellow solid which was triturated with MeOH to give 19.2 mg of **2-I_2** (0.0336 mmol, 75%) as an off-white solid (note: **2-I_2** exhibited low solubility in most organic solvents). ^{1}H NMR (400 MHz, $CDCl_3$) δ: 7.79 (s, 2H), 7.58 (s, 2H), 6.93 (s, 2H), 2.39 (s, 3H), 2.03 (s, 6H); ; ^{13}C NMR (100 MHz, $CDCl_3$) δ: 151.4, 142.7, 139.1, 138.1, 127.5, 125.5, 22.6, 21.6; HRMS (EI): found *m/z* = 571.8808 ± 1.8 ppm; calculated for $C_{19}H_{15}{}^{11}BI_2S_2$ [M^+]: 571.8798.

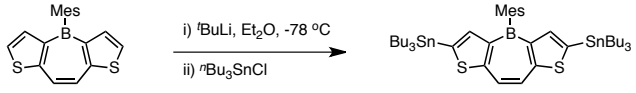

1 **1-Sn_2**

1-Sn_2. To a stirring -78 °C solution of **1** (20.2 mg, 0.0631 mmol) in 3.0 mL Et_2O under N_2 in a 25-mL Schlenk tube was added *t*-BuLi (1.88 M in pentane, 0.084 mL, 0.16 mmol) dropwise via syringe. The colorless solution immediately became a pink-colored suspension. After stirring for 30 m, neat Bu_3SnCl (0.051 mL, 0.19 mmol) was added dropwise to the mixture. The mixture was allowed to stir for 8 h with gradual warming to room temperature then was partitioned between Et_2O and H_2O (1:1) and a few drops of brine were added. The organic layer was removed and the aqueous layer was extracted 3x with Et_2O. The combined organics were dried over $MgSO_4$, filtered, and concentrated under reduced pressure to give 105 mg of crude **1-Sn_2** as yellow-orange oil, which was used directly without further purification. ^{1}H NMR (400 MHz, $CDCl_3$) δ: 7.68 (s, 2H), 7.43 (s, 2H), 6.89 (m, 2H), 2.38, (s, 3H), 1.95 (s, 6H), 1.57-1.45 (m, 12H), 1.39-1.24 (m, 24H), 0.94-0.79 (m, 18H).

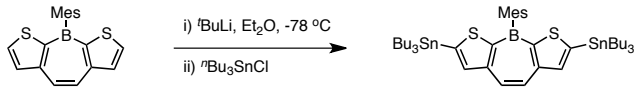

2 **2-Sn$_2$**

2-Sn$_2$. To a stirring -78 °C solution of **2** (20.6 mg, 0.0643 mmol) in 3.0 mL Et_2O under N_2 in a 25-mL Schlenk tube was added *t*-BuLi (1.88 M in pentane, 0.084 mL, 0.16 mmol) dropwise via syringe. The colorless solution immediately became a mustard-colored suspension and after stirring for 30 m neat Bu_3SnCl (0.051 mL, 0.19 mmol) was added dropwise to the mixture. The mixture was allowed to stir for 8 h with gradual warming to room temperature then was partitioned between Et_2O and H_2O (1:1) and a few drops of brine were added. The organic layer was removed and the aqueous layer was extracted 3x with Et_2O. The combined organics were dried over $MgSO_4$, filtered, and concentrated under reduced pressure to give 111 mg of crude **2-Sn$_2$** as a yellow oil, which was used directly without further purification. ^{1}H NMR (400 MHz, $CDCl_3$) δ: 7.74 (s, 2H), 7.72 (s, 2H), 6.95 (m, 2H), 2.42, (s, 3H), 2.04 (s, 6H), 1.57-1.45 (m, 12H), 1.39-1.24 (m, 12H), 1.19-1.09 (m, 12H), 0.94-0.79 (m, 24H).

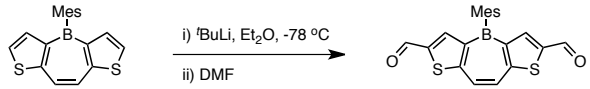

1 **1-(CHO)$_2$**

1-(CHO)$_2$. To a stirring solution of **1** (13.1 mg, 0.0409 mmol) in 2.0 mL Et_2O at -78 °C in a 25-mL Schlenk tube under nitrogen was added *t*-BuLi (1.82 M in pentane, 0.049 mL, 0.090 mmol) dropwise via syringe. The colorless solution immediately became a pink-colored suspension and after stirring for 30 m neat anhydrous DMF (0.010 mL, 0.131 mmol) was added dropwise to the mixture, whereupon the suspension became yellow-colored. The mixture was allowed to stir for 5 h with gradual warming to room temperature and then 1 mL of saturated aq NH_4Cl was added. After stirring for a further 15 min, the mixture was neutralized with saturated aq $NaHCO_3$ and partitioned between EtOAc and H_2O (1:1). The organic layer was removed and the aqueous layer was extracted 4x with EtOAc and 1x with $CHCl_3$. The combined organics were dried over $MgSO_4$, filtered, and concentrated under reduced pressure to an orange solid which was purified by column chromatography (SiO_2, gradient elution: 5% EtOAc in hexanes → 10% EtOAc in hexanes) to give 14.2 mg of **1-(CHO)$_2$** (0.0377 mmol, 92%) as a yellow-orange solid. ^{1}H NMR (400 MHz, CD_2Cl_2) δ: 9.96 (s, 2H), 7.99 (s, 2H), 7.77 (s, 2H), 6.98 (s, 2H), 2.42, (s, 3H), 1.97 (s, 6H); ^{13}C NMR (100 MHz, $CDCl_3$) δ: 183.9, 161.2, 147.5, 144.5, 137.9, 137.6, 127.7, 126.6, 23.1, 21.4; HRMS (EI): found *m/z* = 376.0767 ± 1.0 ppm; calculated for $C_{21}H_{17}{}^{11}BO_2S_2$ [M^+]: 376.0763.

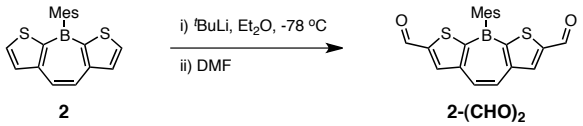

2 **2-(CHO)$_2$**

2-(CHO)$_2$. To a stirring solution of **2** (13.5 mg, 0.0422 mmol) in 2.0 mL Et_2O at -78 °C under nitrogen in a 25-mL Schlenk tube was added *t*-BuLi (1.82 M in pentane, 0.051 mL, 0.093 mmol) dropwise via syringe. The colorless solution immediately became a mustard-colored suspension and after stirring for 30 min neat anhydrous DMF (0.010 mL, 0.131 mmol) was added dropwise to the mixture, whereupon the suspension became gray-colored. The mixture was allowed to stir for 5 h with gradual warming to room temperature and then 1 mL of saturated aq NH_4Cl was added. After stirring for a further 15 min, the mixture was neutralized with saturated aq $NaHCO_3$ and partitioned between EtOAc and H_2O (1:1). The organic layer was removed and the aqueous layer was extracted 4x with EtOAc and 1x with $CHCl_3$. The combined organics were dried over $MgSO_4$, filtered, and concentrated under reduced pressure to a yellow-orange solid which was purified by column chromatography (SiO_2, gradient elution: 10% EtOAc in hexanes → 20% EtOAc in hexanes → 30% EtOAc in hexanes) to give 13.4 mg of **2-(CHO)$_2$** (0.0356 mmol, 84%) as a yellow solid. ^{1}H NMR (400 MHz, $CDCl_3$) δ: 10.14 (s, 2H), 8.29 (s, 2H), 7.77 (s, 2H), 6.94 (s, 2H), 2.39, (s, 3H), 2.01 (s, 6H); ^{13}C NMR (100 MHz, CD_2Cl_2) δ: 183.7, 151.0, 150.3, 139.7, 138.9, 138.7, 127.7, 127.5, 22.7, 21.5; HRMS (EI): found *m/z* = 376.0763 ± 0.1 ppm; calculated for $C_{21}H_{17}{}^{11}BO_2S_2$ [M^+]: 376.0763.

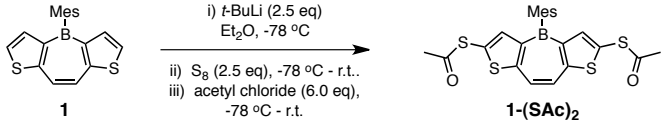

1 **1-(SAc)$_2$**

1-(SAc)$_2$. To a stirring solution of **1** (19.8 mg, 0.0618 mmol) in 2 mL Et_2O at -78 °C in a 25-mL Schlenk tube under nitrogen was added *t*-BuLi (1.61 M in pentane, 0.096 mL, 0.155 mmol) dropwise via syringe. The colorless solution immediately became a pink-colored suspension and was allowed to stir at -78 °C for 1 h, then warmed to room temperature for 1 h (the suspension became yellow in color). The mixture was then cooled to -78 °C and elemental sulfur (5.0 mg, 0.155 mmol) was added as a solid in a single portion under a purge of nitrogen (the sides of the flask were rinsed down with an additional 1 mL Et_2O to ensure quantitative transfer of solids into the reaction mixture). The mixture was allowed to warm to room temperature for 1 h, whereupon the suspension became orange in color, then cooled to -78 °C. Neat acetyl chloride (0.026 mL, 0.37 mmol) was added dropwise to the mixture via syringe, giving an orange solution, and the reaction mixture was allowed to continue stirring with gradual warming to room temperature over 15 h. Saturated aq. NH_4Cl was added, then the mixture was partitioned between Et_2O and H_2O (1:1), adding a small amount of brine. The organic layer was removed and the aqueous layer was extracted 2x with Et_2O. The combined organics were dried over $MgSO_4$, filtered, and concentrated under reduced pressure to

give a orange-brown solid which was purified by column chromatography (SiO_2, gradient elution: 25% CH_2Cl_2 in hexanes → 50% CH_2Cl_2 in hexanes → 75% CH_2Cl_2 in hexanes) to give 26.4 mg of **1-(SAc)$_2$** (0.0562 mmol, 91%) as a bright yellow solid. ^{1}H NMR (400 MHz, $CDCl_3$) δ: 7.61 (s, 2H), 7.33 (s, 2H), 6.90 (s, 2H), 2.42 (s, 6H), 2.38, (s, 3H), 1.94 (s, 6H); ^{13}C NMR (100 MHz, $CDCl_3$) δ: 192.9, 160.2, 145.3, 138.2, 136.8, 127.7, 127.3, 123.2, 30.0, 23.1, 21.4; HRMS (EI): found *m/z* = 468.0530 ± 2.6 ppm; calculated for $C_{23}H_{21}{}^{11}BO_2S_4$ [M^+]: 468.0518.

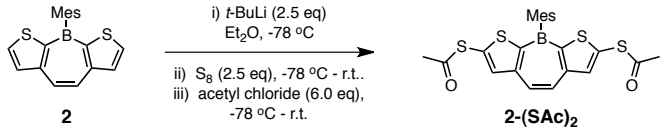

2 **2-(SAc)$_2$**

2-(SAc)$_2$. To a stirring solution of **2** (20.1 mg, 0.0628 mmol) in 2 mL Et_2O at -78° C in a 25-mL Schlenk tube under nitrogen was added *t*-BuLi (1.61 M in pentane, 0.096 mL, 0.155 mmol) dropwise via syringe. The colorless solution immediately became a mustard-colored suspension and was allowed to stir at -78 °C for 1 h, then warmed to room temperature for 1 h (the suspension became yellow in color). The mixture was then cooled to -78 °C and elemental sulfur (5.0 mg, 0.155 mmol) was added as a solid in a single portion under a purge of nitrogen (the sides of the flask were rinsed down with an additional 1 mL Et_2O to ensure quantitative transfer of solids into the reaction mixture). The mixture was allowed to warm to room temperature for 1 h, whereupon the suspension became orange in color, then cooled to -78 °C. Neat acetyl chloride (0.026 mL, 0.37 mmol) was added dropwise to the mixture via syringe, giving an orange solution, and the reaction mixture was allowed to continue stirring with gradual warming to room temperature over 15 h. Saturated aq. NH_4Cl was added, then the mixture was partitioned between Et_2O and H_2O (1:1), adding a small amount of brine. The organic layer was removed and the aqueous layer was extracted 2x with Et_2O. The combined organics were dried over $MgSO_4$, filtered, and concentrated under reduced pressure to give a yellow-brown solid which was purified by column chromatography (SiO_2, gradient elution: 25% CH_2Cl_2 in hexanes → 50% CH_2Cl_2 in hexanes → 75% CH_2Cl_2 in hexanes) to give 25.3 mg of **2-(SAc)$_2$** (0.0562 mmol, 86%) as a yellow solid. ^{1}H NMR (400 MHz, $CDCl_3$) δ: 7.71 (s, 2H), 7.66 (s, 2H), 6.91 (m, 2H), 2.44, (s, 6H), 2.43 (s, 3H), 2.05 (s, 6H); ^{13}C NMR (100 MHz, $CDCl_3$) δ: 191.9, 150.1, 139.5, 139.1, 137.9, 137.1, 127.4, 126.5, 30.1, 22.8, 21.5; HRMS HRMS (EI): found *m/z* = 468.0517 ± 0.1 ppm; calculated for $C_{23}H_{21}{}^{11}BO_2S_4$ [M^+]: 468.0518.

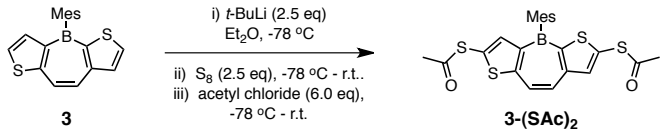

3-(SAc)$_2$. To a stirring solution of **3** (22.0 mg, 0.0687 mmol) in 2 mL Et_2O at -78 °C in a 25-mL Schlenk tube under nitrogen was added *t*-BuLi (1.59 M in pentane, 0.108 mL, 0.172 mmol) dropwise via syringe. The colorless solution immediately became a tan-colored suspension and was allowed to stir at -78 °C for 1 h, then warmed to room temperature for 1 h. The mixture was then cooled to -78 °C and elemental sulfur (5.5 mg, 0.172 mmol) was added as a solid in a single portion under a purge of nitrogen (the sides of the flask were rinsed down with an additional 1 mL Et_2O to ensure quantitative transfer of solids into the reaction mixture). The mixture was allowed to warm to room temperature for 1 h, whereupon the suspension became bright yellow in color, then cooled to -78 °C. Neat acetyl chloride (0.029 mL, 0.41 mmol) was added dropwise to the mixture via syringe, giving a yellow-orange solution, and the reaction mixture was allowed to continue stirring with gradual warming to room temperature over 15 h. Saturated aq. NH_4Cl was added, then the mixture was partitioned between Et_2O and H_2O (1:1), adding a small amount of brine. The organic layer was removed and the aqueous layer was extracted 2x with Et_2O. The combined organics were dried over $MgSO_4$, filtered, and concentrated under reduced pressure to give a yellow solid which was purified by column chromatography (SiO_2, gradient elution: 25% CH_2Cl_2 in hexanes → 50% CH_2Cl_2 in hexanes → 75% CH_2Cl_2 in hexanes) to give 23.3 mg of **3-(SAc)$_2$** (0.0497 mmol, 72%) as a yellow solid. ^{1}H NMR (400 MHz, $CDCl_3$) δ: 7.72 (s, 1H), 7.68 (d, *J* = 11.6 Hz, 1H), 7.57 (d, J = 11.6 Hz, 1H), 7.33 (s, 1H), 6.91 (s, 1H), 2.43 (s, 3H), 2.42 (s, 3H), 2.38 (s, 3H), 2.00 (s, 6H); ^{13}C NMR (100 MHz, $CDCl_3$) δ: 192.9, 191.8, 160.8, 149.8, 144.5, 139.5, 138.7, 137.4, 137.3, 127.5, 127.3, 125.7, 124.1, 30.1, 29.9, 22.9, 21.5; HRMS (EI): found *m/z* = 468.0527 ± 2.1 ppm; calculated for $C_{23}H_{21}{}^{11}BO_2S_4$ [M^+]: 468.0518.

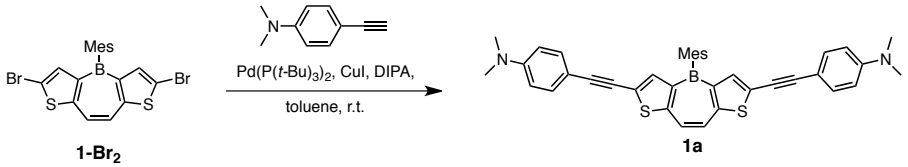

1a. To a stirring solution of **1-Br$_2$** (21.0 mg, 0.0439 mmol), $Pd(P(t\text{-}Bu)_3)_2$ (2.2 mg, 0.0044 mmol), and CuI (0.7 mg, 0.004 mmol) in 2.0 mL toluene under N_2 in a 25-mL Schlenk tube was added sequentially neat diisopropylamine (0.015 mL, 0.11 mmoL) then a solution of 4-ethynyl-*N,N*-dimethylaniline (15.2 mg, 0.105 mmol) in 1.25 mL toluene dropwise via syringe. The orange solution immediately became dark brown and was stirred at room temperature for 16 h. The volatile components were removed directly from the reaction vessel under high vacuum and the remaining residue was purified by column chromatography (SiO_2, gradient elution: 5% to 50% EtOAc in hexanes → 100%

EtOAc → 5% MeOH in EtOAc → 10% MeOH in EtOAc) to give 26.6 mg of **1a** (0.0439 mmol, quant.) as dark orange solid. ^{1}H NMR (400 MHz, $CDCl_3$) δ: 7.54 (s, 2H), 7.41 (s, 2H), 7.37 (d, *J* = 8.8 Hz,), 6.93 (s, 2H), 6.64 (d, *J* = 8.8 Hz, 4H), 2.99 (s, 12H), 2.40 (s, 3H), 1.98 (s, 6H); ^{13}C NMR (100 MHz, $CDCl_3$) δ: 156.0, 150.5, 142.0, 138.1, 136.5, 132.9, 127.2, 125.6, 122.8, 111.9, 109.2, 100.1, 97.4, 80.8, 40.3, 23.0, 21.4; HRMS (EI): found *m/z* = 606.2344 ± 1.5 ppm; calculated for $C_{39}H_{35}{}^{11}BN_2S_4$ [M^+]: 606.2335.

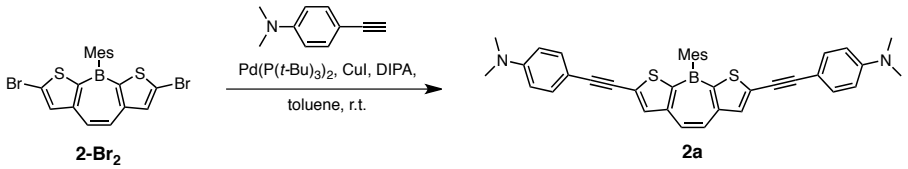

2a. To a stirring solution of **2-Br$_2$** (22.1 mg, 0.0462 mmol), Pd(P(*t*-Bu)$_3$)$_2$ (2.4 mg, 0.0046 mmol), and CuI (0.7 mg, 0.004 mmol) in 2.0 mL toluene under N_2 in a 25-mL Schlenk tube was added sequentially neat diisopropylamine (0.015 mL, 0.11 mmoL) then a solution of 4-ethynyl-*N,N*-dimethylaniline (16.1 mg, 0.111 mmol) in 1.25 mL toluene dropwise via syringe. The orange solution immediately became dark brown and was stirred at room temperature for 16 h. The volatile components were removed directly from the reaction vessel under high vacuum and the remaining residue was purified by column chromatography (SiO_2, gradient elution: 50% $CHCl_3$ in hexanes → 75% $CHCl_3$ in hexanes → 90% $CHCl_3$ in hexanes) to give 28.0 mg of **2a** (0.0462 mmol, quant.) as golden yellow solid. ^{1}H NMR (400 MHz, $CDCl_3$) δ: 7.69 (s, 2H), 7.58 (s, 2H), 7.36 (d, *J* = 9.2 Hz,), 6.93 (s, 2H), 6.64 (d, *J* = 9.2 Hz, 4H), 3.00 (s, 12H), 2.39 (s, 3H), 2.07 (s, 6H); ^{13}C NMR (100 MHz, $CDCl_3$) δ: 150.5, 150.0, 138.9, 137.8, 135.5, 134.2, 132.9, 127.5, 126.2, 111.8, 108.9, 98.7, 80.9, 40.6, 22.8, 21.8; HRMS (EI): found *m/z* = 606.2336 ± 0.3 ppm; calculated for $C_{39}H_{35}{}^{11}BN_2S_4$ [M^+]: 606.2335.

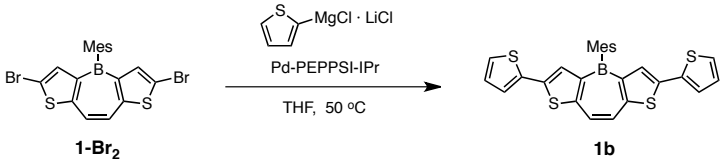

1b. To a stirring solution of **1-Br$_2$** (14.8 mg, 0.0310 mmol) and Pd-PEPPSI-IPr (1.6 mg, 0.0024 mmol) in 2.0 mL THF at 0 °C in a 25-mL Schlenk tube under nitrogen was added a solution of thiophen-2-ylmagnesium chloride·lithium chloride (0.19 M in THF, 0.49 mL, 0.093 mmol) dropwise via syringe. The cooling bath was removed and the mixture was heated to 50 °C with continued stirring for 16 h, at which point an additional portion of 2-thienylmagnesium bromide·lithium chloride solution (0.25 mL, 0.047 mmol) was added. After stirring for a further 4 h, the mixture was cooled to room temperature and partitioned between EtOAc and brine (1:1). The organic layer was removed and the aqueous layer was extracted 3x with EtOAc. The combined organics were dried over $MgSO_4$, filtered, and concentrated under reduced pressure to give a solid that was

purified by column chromatography (SiO_2, gradient elution: 10% $CHCl_3$ in hexanes → 15% $CHCl_3$ in hexanes → 20% $CHCl_3$ in hexanes) to give 9.4 mg of **1b** (0.019 mmol, 63%) as a yellow-orange solid. ^{1}H NMR (400 MHz, CD_2Cl_2) δ: 7.57 (s, 2H), 7.35 (s, 2H), 7.26-7.23 (m, 4H), 7.02 (dd, J = 5.2 Hz, J = 3.6 Hz), 6.93 (s, 2H), 2.41, (s, 3H), 2.00 (s, 6H); ^{13}C NMR (100 MHz, $CDCl_3$) δ: 155.1, 138.5, 138.0, 136.9, 136.5, 134.1, 128.1, 127.3, 125.8, 125.4, 122.9, 23.0, 21.5; HRMS (EI): found m/z = 484.0625 ± 1.3 ppm; calculated for $C_{27}H_{21}{}^{11}BS_4$ [M^+]: 484.0619.

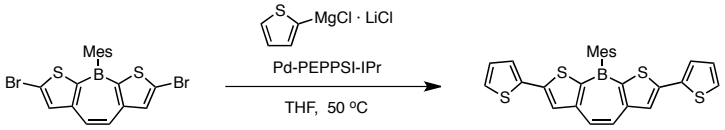

2-Br$_2$ **2b**

2b. To a stirring solution of **2a** (18.5 mg, 0.0387 mmol) and Pd-PEPPSI-IPr in 2.0 mL THF at 0 °C in a 25-mL Schlenk tube under nitrogen was added a solution of 2-thienylmagnesium chloride·lithium chloride (0.19 M in THF, 0.61 mL, 0.12 mmol) dropwise via syringe. The cooling bath was removed and the mixture was heated to 50 °C with continued stirring for 16 h, at which point an additional portion of thiophen-2-ylmagnesium bromide·lithium chloride solution (0.31 mL, 0.060 mmol) was added. After stirring for a further 4 h, the mixture was cooled to room temperature and partitioned between EtOAc and brine (1:1). The organic layer was removed and the aqueous layer was extracted 3x with EtOAc. The combined organics were dried over $MgSO_4$, filtered, and concentrated under reduced pressure to give a solid that was purified by column chromatography (SiO_2, gradient elution: 10% $CHCl_3$ in hexanes → 15% $CHCl_3$ in hexanes → 20% $CHCl_3$ in hexanes) to give 14.6 mg of **2b** (0.030 mmol, 78%) as a pale yellow solid. ^{1}H NMR (400 MHz, $CDCl_3$) δ: 7.71 (s, 2H), 7.62 (s, 2H), 7.32 (dd, J = 6.4 Hz, J = 1.2 Hz 2H), 7.31 (dd, J = 8.0 Hz, J = 1.2 Hz), 7.04 (dd, J = 5.2 Hz, J = 4.0 Hz, 2H), 6.98 (s, 2H), 2.43 (s, 3H), 2.11 (s, 6H); ^{13}C NMR (100 MHz, $CDCl_3$) δ: 151.0, 146.7, 139.3, 136.9, 128.9, 128.3, 127.4, 126.7, 126.5, 126.0, 22.7, 21.6; HRMS (EI): found m/z = 484.0619 ± 0.1 ppm; calculated for $C_{27}H_{21}{}^{11}BS_4$ [M^+]: 484.0619.

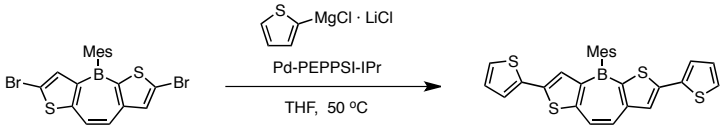

3-Br$_2$ **3b**

(3b). To a stirring solution of **3-Br$_2$** (20.8 mg, 0.0435 mmol) and Pd-PEPPSI-IPr (2.4 mg, 0.00348 mmol) in 2.0 mL THF at 0 °C in a 25-mL Schlenk tube under nitrogen was added a solution of 2-thienylmagnesium chloride·lithium chloride (0.163 M in THF, 0.804 mL, 0.131 mmol) dropwise via syringe. The cooling bath was removed and the mixture was heated to 50 °C with continued stirring for 16 h and then cooled to room

temperature. After partitioning the mixture between EtOAc and brine (1:1), the organic layer was removed and the aqueous layer was extracted 3x with EtOAc. The combined organics were dried over $MgSO_4$, filtered, and concentrated under reduced pressure to give a solid that was purified by column chromatography (SiO_2, gradient elution: 10% $CHCl_3$ in hexanes → 15% $CHCl_3$ in hexanes → 20% $CHCl_3$ in hexanes) to give 12.9 mg of **3b** (0.0266 mmol, 61%) as a canary yellow solid. ^{1}H NMR (400 MHz, $CDCl_3$) δ: 7.70 (s, 1H), 7.65 (d, J = 11.6 Hz, 1H), 7.53 (d, J = 11.6 Hz, 1H), 7.32, (s, 1H), 7.32 (m, 2H), 7.25 (d, J = 4.4 Hz, 2H), 7.03 (m, 2H), 6.96 (s, 2H), 2.43 (s, 3H), 2.06 (s, 6H); ^{13}C NMR (100 MHz, $CDCl_3$) δ: 155.0, 151.1, 147.1, 138.7, 138.6, 137.1, 136.9, 133.0, 128.6, 128.3, 128.1, 127.3, 126.5, 126.1, 125.8, 125.3, 125.1, 124.4, 22.8, 21.6; HRMS (EI): found m/z = 484.0626 ± 1.4 ppm; calculated for $C_{27}H_{21}{}^{11}BS_4$ [M^+]: 484.0619.

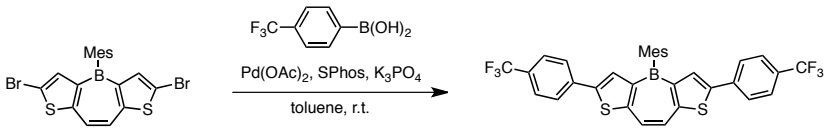

1-Br$_2$ **1c**

1c. A 25-mL Schlenk tube was charged with **1-Br$_2$** (21.5 mg, 0.0450 mmol), 4-(trifluoromethyl)phenylboronic acid (25.6 mg, 0.135 mmol), palladium (II) acetate (3.0 mg, 0.0045 mmol), SPhos (4.6 mg, 0.011 mmol), and potassium phosphate tribasic (38.2 mg, 0.180 mmol) under nitrogen. Toluene (3 mL) was added and the resulting orange solution was stirred at room temperature for 14 h. The volatile components were removed directly under high vacuum and the remaining residue was purified by column chromatography (SiO_2, gradient elution: hexanes → 2.5% $CHCl_3$ in hexanes → 5% $CHCl_3$ in hexanes → 10% $CHCl_3$ in hexanes → 25% $CHCl_3$ in hexanes) to give 20.7 mg of **1c** (0.0346 mmol, 77%) as a canary-yellow solid. ^{1}H NMR (400 MHz, $CDCl_3$) δ: 7.72 (d, J = 8.0 Hz, 4H), 7.68 (s, 2H), 7.62 (d, J = 8.0 Hz, 4H), 7.60 (s, 2H), 6.96 (m, 2H), 2.44 (s, 3H), 2.02 (s, 6H) ; ^{13}C NMR (100 MHz, CD_2Cl_2) δ: 156.4, 143.5, 138.1, 135.2, 133.4, 127.5, 126.9, 126.1, 123.6, 123.3, 23.1; HRMS (EI): found m/z = 608.1252 ± 2.1 ppm; calculated for $C_{33}H_{23}{}^{11}BF^6S_2$ [M^+]: 608.1238.

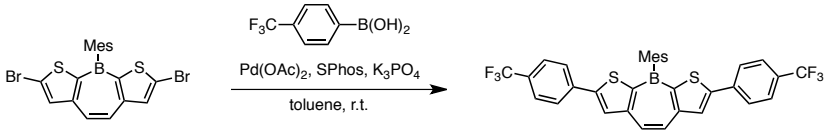

2-Br$_2$ **2c**

2c. A 25-mL Schlenk tube was charged with **2-Br$_2$** (25.6 mg, 0.0535 mmol), 4-(trifluoromethyl)phenylboronic acid (30.6 mg, 0.161 mmol), palladium (II) acetate (3.6 mg, 0.0054 mmol), SPhos (5.3 mg, 0.013 mmol), and potassium phosphate tribasic (45.4 mg, 0.214 mmol) under nitrogen. Toluene (3 mL) was added and the resulting orange solution was stirred at room temperature for 14 h. The volatile components were removed directly under high vacuum and the remaining residue was purified by column

chromatography (SiO_2, gradient elution: hexanes → 2.5% $CHCl_3$ in hexanes → 5% $CHCl_3$ in hexanes → 25% $CHCl_3$ in hexanes) to give 32.6 mg of **2c** (0.0535 mmol, quant.) as a yellow solid. ^{1}H NMR (400 MHz, $CDCl_3$) δ: 7.95 (s, 2H), 7.84 (d, J = 8.0 Hz, 4H), 7.73 (s, 2H), 7.66 (d, J = 8.0 Hz, 4H), 6.99 (m, 2H), 2.44 (s, 3H), 2.12 (s, 6H); ^{13}C NMR (100 MHz, CD_2Cl_2) δ: 152.0, 151.3, 139.2, 130.0, 1275. 127.1, 127.0, 126.2, 126.1, 22.7, 21.6. HRMS (EI): found m/z = 608.1253 ± 2.4 ppm; calculated for $C_{33}H_{23}{}^{11}BF^6S_2$ [M^+]: 608.1238.

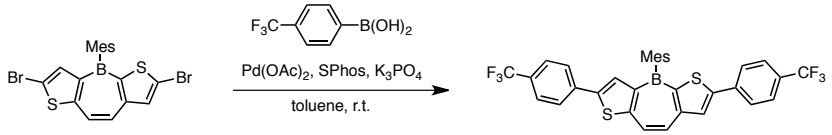

3-Br$_2$ **3c**

3c. A 25-mL Schlenk tube was charged with **3-Br$_2$** (22.0 mg, 0.0460 mmol), 4-(trifluoromethyl)phenylboronic acid (26.2 mg, 0.138 mmol), palladium (II) acetate (3.1 mg, 0.0046 mmol), SPhos (4.7 mg, 0.012 mmol), and potassium phosphate tribasic (39.1 mg, 0.184 mmol) under nitrogen. Toluene (3 mL) was added and the resulting orange solution was stirred at room temperature for 14 h. The volatile components were removed directly under high vacuum and the remaining residue was purified by column chromatography (SiO_2, gradient elution: hexanes → 5% $CHCl_3$ in hexanes → 10% $CHCl_3$ in hexanes) to give 28.0 mg of **3c** (0.0278 mmol, 60%) as a yellow solid. ^{1}H NMR (400 MHz, $CDCl_3$) δ: 7.93 (s, 1H), 7.83 (d, J = 8.0 Hz, 2H), 7.75 (d, J = 11.2 Hz, 1H), 7.73 (d, J = 8.0 Hz, 2H), 7.65 (d, J = 8.0 Hz, 2H), 7.64 (d, J = 11.6 Hz, 1H), 7.62 (d, J = 8.0 Hz, 2H), 7.58 (s, 1H), 6.99 (s, 2H), 2.44 (s, 3H), 2.07 (s, 6H); ^{13}C NMR (100 MHz, CD_2Cl_2) δ: 156.6, 152.2, 151.1, 143.6, 138.7, 137.4, 137.2, 134.2, 129.8, 127.4, 127.1, 126.9, 126.1, 126.1, 126.0, 125.8, 124.7, 22.9, 21.6. HRMS (EI): found m/z = 608.1236 ± 0.4 ppm; calculated for $C_{33}H_{23}{}^{11}BF^6S_2$ [M^+]: 608.1238.

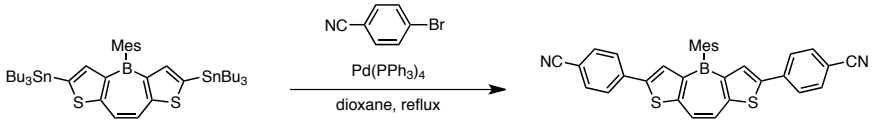

1-Sn$_2$ **1d**

1d. To a stirring solution of 4-bromobenzonitrile (25.3 mg, 0.139 mmol) and $Pd(PPh_3)_4$ (3.6 mg, 0.0032 mmol) in 1 mL toluene under argon in a 25-mL Schlenk tube under argon was added a solution of crude **1-Sn$_2$** (56.7 mg, ~0.0631 mmol) in 2.5 mL toluene dropwise via syringe. The mixture was heated to reflux (~110°C) for 48 h and then allowed to cool to room temperature. The volatile components were removed directly from the reaction vessel under high vacuum and the remaining residue was pushed through a pad of celite, eluting with 100 mL $CHCl_3$. The filtrate was concentrated under reduced pressure and the resulting crude material purified by column chromatography (SiO_2, gradient elution: 5% $CHCl_3$/10% EtOAc/85% hexanes → 5% $CHCl_3$/15% EtOAc/80% hexanes) to give 28.3 mg of **1d** (0.0541 mmol, 86% in two steps from **1**) as a

yellow-orange solid. ^{1}H NMR (400 MHz, $CDCl_3$) δ: 7.70 (d, J = 8.8 Hz, 4H), 7.68 (s, 2H), 7.65 (d, J = 8.8 Hz, 4H), 6.96 (s, 2H), 2.44 (s, 3H), 2.00 (s, 6H); ^{13}C NMR (100 MHz, $CDCl_3$) δ: 156.7, 143.0, 138.0, 137.9, 136.9, 135.8, 132.9, 127.5, 127.0, 123.8, 118.8, 111.5, 23.1, 21.5; HRMS (EI): found m/z = 522.1405 ± 1.7 ppm; calculated for $C_{33}H_{23}N_2\,{}^{11}BS_2$ [M^+]: 522.1396.

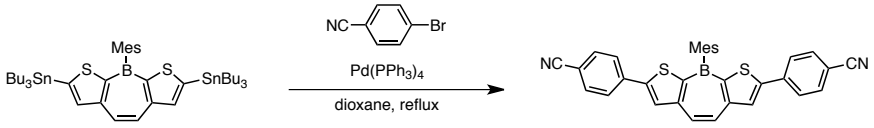

2d. To a stirring solution of 4-bromobenzonitrile (25.7 mg, 0.141 mmol) and $Pd(PPh_3)_4$ (3.6 mg, 0.0032 mmol) in 1 mL toluene under argon in a 25-mL Schlenk tube under argon was added a solution of crude **2-Sn$_2$** (57.8 mg, ~0.0643 mmol) in 2.5 mL toluene dropwise via syringe. The mixture was heated to reflux (~110°C) for 48 h and then allowed to cool to room temperature. The volatile components were removed directly from the reaction vessel under high vacuum and the remaining residue was pushed through a pad of celite, eluting with 100 mL $CHCl_3$. The filtrate was concentrated under reduced pressure and the resulting crude material purified by column chromatography (SiO_2, gradient elution: 5% $CHCl_3$/20% EtOAc/75% hexanes → 5% $CHCl_3$/30% EtOAc/65% hexanes) to give 33.6 mg of **2d** (0.0643 mmol, quant. in two steps from **2**) as a pale yellow solid. ^{1}H NMR (400 MHz, $CDCl_3$) δ: 7.97 (s, 2H), 7.83 (d, J = 8.4 Hz, 4H), 7.73 (s, 2H), 7.69 (d, J = 8.4 Hz, 4H), 6.99 (s, 2H), 2.43 (s, 3H), 2.10 (s, 6H); ^{13}C NMR (100 MHz, $CDCl_3$) δ: 151.3, 151.2, 139.1, 138.1, 137.9, 132.9, 130.5, 127.5, 127.2, 127.1, 118.7, 112.2, 22.7, 21.7; HRMS (EI): found m/z = 522.1404 ± 1.7 ppm; calculated for $C_{33}H_{23}N_2\,{}^{11}BS_2$ [M^+]: 522.1396.

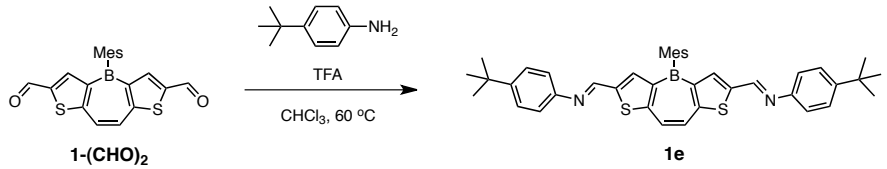

1e. To a stirring solution of **1-(CHO)$_2$** (18.2 mg, 0.0484 mmol) and 4-*tert*-butylaniline (15.2 mg, 0.102 mmol) in 1.5 mL $CHCl_3$ under N_2 in a 25-mL Schlenk tube was added a single drop of trifluoroacetic acid and the mixture was heated to 60°C for 24 h. After cooling to room temperature, the mixture was concentrated under reduced pressure and the yellow-brown residue was purified directly by column chromatography (SiO_2, 5% EtOAc / 5% $CHCl_3$ / 90% hexanes) to give 27.0 mg of **1e** (0.0423 mmol, 87%) as a yellow-orange solid. ^{1}H NMR (400 MHz, $CDCl_3$) δ: 8.58 (s, 2H), 7.72 (s, 2H), 7.67 (s, 2H), 7.40 (d, J = 8.8 Hz, 4H), 7.19 (d, J = 8.4 Hz, 4H), 6.98 (s, 2H), 2.43 (s, 3H), 2.01 (s, 6H), 1.34 (s, 18H); ^{13}C NMR (100 MHz, $CDCl_3$) δ: 158.5, 152.1, 150.0, 148.4, 144.5,

142.8, 138.2, 136.9, 127.4, 126.2, 125.2, 121.0, 34.7, 31.5, 23.1, 21.5; HRMS (EI): found *m/z* = 638.2948 ± 2.0 ppm; calculated for $C_{41}H_{43}N_2{}^{11}BS_2$ [M^+]: 638.2961.

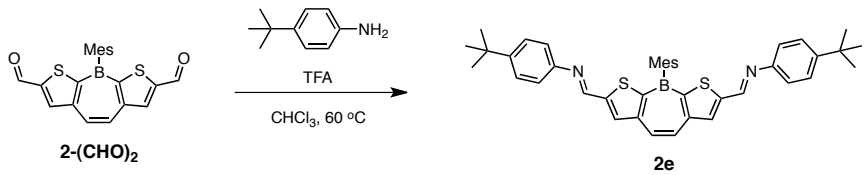

2-(CHO)$_2$ **2e**

2e. To a stirring solution of **2-(CHO)$_2$** (19.5 mg, 0.0518 mmol) and 4-*tert*-butylaniline (16.2 mg, 0.109 mmol) in 1.5 mL $CHCl_3$ under N_2 in a 25-mL Schlenk tube was added a single drop of trifluoroacetic acid and the mixture was heated to 60°C for 24 h. After cooling to room temperature, the mixture was concentrated under reduced pressure and the yellow-brown residue was purified directly by column chromatography (SiO_2, 5% EtOAc / 5% $CHCl_3$ / 90% hexanes) to give 17.0 mg of **2e** (0.0266 mmol, 51%) as a yellow-orange solid. ^{1}H NMR (400 MHz, $CDCl_3$) δ: 8.72 (s, 2H), 8.01 (s, 2H), 7.69 (s, 2H), 7.41 (d, *J* = 8.4 Hz, 4H), 7.20 (d, *J* = 8.4 Hz, 4H), 6.93 (s, 2H), 2.39 (s, 3H), 2.09 (s, 6H), 1.34 (s, 18H); ^{13}C NMR (100 MHz, CD_2Cl_2) δ: 151.8, 151.3, 150.4, 150.3, 148.4, 139.0, 137.8, 136.3, 127.6, 127.5, 126.9, 126.3, 120.9, 34.8, 31.5, 22.8, 21.5; HRMS (EI): found *m/z* = 638.2958 ± 0.4 ppm; calculated for $C_{41}H_{43}N_2{}^{11}BS_2$ [M^+]: 638.2961.

References

(1) Katz, H. E.; Bao, Z.; Gilat, S. L. *Acc. Chem. Res*. **2001,** 34, 359 – 369.
(2) *Handbook of Thiophene-based Materials: Applications in Organic Electronics and Photonics.* Perepichka, I. F.; Perepichka, Eds.. D. F. John Wiley and Sons, 2009.
(3) Jeffries III, A. T.; Gronowitz, S. *Chem. Script*. **1973**, *4,*183 – 187.
(4) Caruso Jr. A. The Synthesis and Characterization of Boron-Containing Pi-Electron Materials that Incorporate Formally Aromatic Borepin Rings. Ph.D Thesis, Johns Hopkins University, May 2011.
(5) D'Auria, M.; Mauriello, G. *Tetrahedron Lett*. **1995**, *36*, 4883 – 4884.
(6) Leary, E.; La Rosa, A.; González, M. T.; Rubio-Bollinger, G.; Agraït, N.; Martín, N. *Chem. Soc. Rev*. **2015**, *44*, 920 – 942.
(7) Aradhya, S. V.; Venkataraman, L. *Nat. Nanotech*. **2013**, *8*, 399 – 410.
(8) Sun, L.; Diaz-Fernandez, Y. A.; Gschneidtner, T. A.; Westerlund, F.; Lara-Avila, S.; Moth-Poulsen, K. *Chem. Soc. Rev*. **2014**, *43*, 7378 – 7411.
(9) Lambert, C. J. *Chem.Soc.Rev*. **2015**, *44*, 875 – 888.
(10) Zhang, J. L.; Zhong, J. Q.; Lin, J. D.; Hu, W. P.; Wu, K.; Xu, G. Q.; Wee, A. T. S.; Chen, W. *Chem. Soc. Rev*. **2015**, *44*, 2998 – 3022.
(11) Hundertmark, T.; Littke, A. F.; Buchwald, S. L.; Fu, G. C. *Org. Lett.* **2000***, 2,* 1729 – 1731.
(12) Organ, M. G.; Abdel-Hadi, M.; Avola, S.; Hadei, N.; Nasielski, J.; O'Brien, C. J.; Valente, C. *Chem. Eur. J*. **2007**, *13*, 150–157.
(13) Walker, S. D.; Barder, T. E.; Martinelli, J. R.; Buchwald, S. L. *Angew. Chem. Int. Ed.* **2004**, *43*, 1871–1876.
(14) Wang, N.; Hudson, Z. M.; Wang, S. *Organometallics* **2010**, *29*, 4007 – 4011.
(15) Rowan, S. J.; Cantrill, S. J.; Cousins, G. R. L.; Sanders, J. K. M.; Stoddart, J. F. *Angew. Chem. Int. Ed.* **2002**, *41*, 898 – 952.
(16) Jin, Y.; Yu, C.; Denman, R. J.; Zhang, W. *Chem. Soc. Rev*., **2013**, *42*, 6634 – 6654.
(17) Harada, K.; Urabe, H.; Sato, F. *Tetrahedron Lett.* **1995**, *36*, 3203 – 3206.
(18) Ishiyama, T.; Matsuda, N.; Miyaura, N.; Suzuki, A. *J. Am. Chem. Soc.* **1993**, *115*, 11018 – 11019.
(19) Segawa, Y.; Maekawa, T.; Itami, K. *Angew. Chem. Int. Ed*. **2015**, *54*, 66 – 81.
(20) Schipper, D. J.; Fagnou, K. *Chem. Mater*. **2011**, *23*, 1594 – 1600.
(21) Yanagisawa, S.; Ueda, K.; Sekizawa, H.; Itami, K. *J. Am. Chem. Soc.* **2009***, 131*, 14622 – 14623.
(22) Caruso, A.; Tovar, J. D. *J. Org. Chem.* **2011***, 76,* 2227 – 2239.
(23) Li, H.; Xu, Q.; Li, N.; Sun, R.; Ge, J.; Lu, J.; Gu, H.; Yan, F. *J. Am. Chem. Soc.* **2010***, 132*, 5542 – 5543.
(24) Gu, P.-Y.; Zhou, F.; Gao, J.; Li, G.; Wang, C.; Xu, Q.-F.; Zhang, Q.; Lu, J.-M. *J. Am. Chem. Soc.* **2013**, *135*, 14086 − 14089.
(25) Simão, C.; Mas-Torrent, M.; Casado-Montenegro, J.; Otón, F.; Veciana, J.; Rovira, C. *J. Am. Chem. Soc*. **2011**, *133*, 13256 – 13259.
(26) Scott, J. C.; Bozano, L. D. *Adv. Mater.* **2007**, *19*, 1452–1463.
(27) Zhou, G.; Baumgarten, M.; Müllen, K. *J. Am. Chem. Soc.* **2008**, *130*, 12477 – 12484.
(28) Wade, C. R.; Broomsgrove, A. E. J.; Aldridge, S.; Gabbaï, F. P. *Chem. Rev.* **2010,** *110*, 3958 – 3984.
(29) Levine, D. R.; Siegler, M. A.; Tovar, J. D. *J. Am. Chem. Soc*. **2014**, *136*, 7132 − 7139.
(30) Gonzalo Rodríguez, J.; Lafuente, A.; Martín Villamil, R.; Martínez Alcazar, M. P. *J. Phys. Org. Chem.* **2001**, *14*, 859 − 868. .
(31) Krasovskiy, A.; Knochel, P. *Angew. Chem. Int. Ed.* **2004***, 43*, 3333 – 3336.

Chapter 5: Thiophene-fused Borepins with Non-aromatic Conjugation Schemes – Towards Proaromatic and Quinoidal Systems

Introduction

Previous chapters of this dissertation discussed the investigation of borepins as building blocks for π-conjugated organic materials, seeking capitalize on the weak *aromaticity* inherent to the borepin ring for additional electronic stabilization of the electron-deficient boron center. In contrast, the investigation of *non-aromatic* borepin motifs (i.e., wherein the borepin ring does not possess a π-electron sextet) remain a relatively underexplored area. The discovery that unsymmetrical DTB **4** in Chapter 3 did not require an aromatic π-electronic arrangement within the borepin ring to remain stable to air and moisture (and that it exhibited properties unique from "aromatic" DTB compounds) provided impetus for the exploration of other such non-aromatic borepin motifs.

Disubstituted aromatic compounds of extended conjugation can be considered to exist in two resonance forms – the typical "aromatic" one and a quinoid form, the latter describing a state wherein the π-electrons are delocalized in a more "polyene-like" fashion (Figure 5.1a). Normally the quinoidal form is destabilized relative to the aromatic form but the energetic gap between the two forms can be narrowed or even reversed to favor the quinoid form by specific molecular design, such as in the classical hydrocarbons studied by Thiele and Chichibabin. Engineering quinoidal electronic structure has found application in organic electronics due to the highly delocalized electronic structure and low bandgaps exhibited by such materials; furthermore, quinoidal electronic structures have been invoked as the operative resonance form in the charge carrying units of bipolaronic polythiophenes and other conjugated polymers. Some formally quinoidal systems have even been shown to possess appreciable biradical character;[1] such high-spin materials have generated interest in the field of organic spintronics[2,3] for logic and data storage applications.

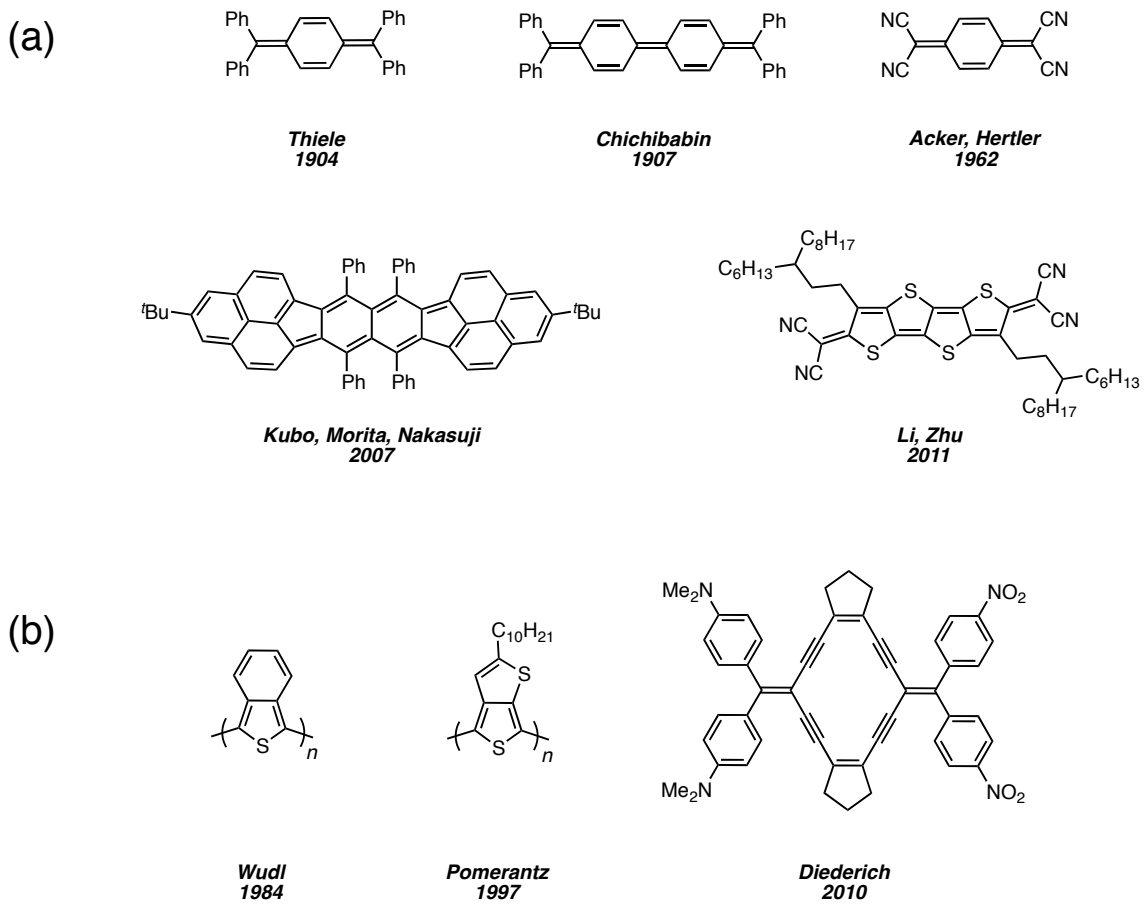

Figure 5.1. Representative (a) quinoidal and (b) proaromatic organic π-systems.

Closely tied to the singlet/ quinoid – triplet/diradical duality is the concept of "proaromaticity",[4] the tendency for quinoidal structures to return to their more stable aromatic forms (Figure 5.1b). Engineering quinoidal structure with the express intent of utilizing the inherent proaromatic character was the fundamental principle behind Wudl's iconic (poly)isothianaphthene (PITN),[5] for which the propensity to restore aromaticity in the quinoidal benzene rings led to a small optical bandgap that could be further reduced to ca. 1 eV upon doping. In addition to the construction of low-bandgap polymers (such as PITN and (poly)thieno[3,4-*b*]thiophene), proaromaticity has also found use as a design element to build non-linear optical chromophores[6] and NIR-absorbing organic dyes.[7]

The following chapter discusses progress towards borepin-based π-systems containing *non-aromatic* borepin motifs, including a trithienoborepin scaffold and preliminary work toward a disubstituted DTB system favoring a quinoidal π-electronic arrangement.

Results and Discussion

Building on the successful synthesis of DTB **4** from chapter 3, it was envisioned that other "non-aromatic" borepin cores could be accessible due to the stabilizing influence of the fused thieno rings and *B*-Mes steric protection. One particular structural modification of interest was the fusion of an additional thieno ring to the central borepin; along with prospects for unique electronic and redox properties, a third thiophene ring could offer functionality as a synthetically modifiable group for further elaboration of the core structure. Several such trithienoborepins (TTBs) were considered as possible targets (Figure 5.2a). Sugihara and Murata's successful synthesis of thieno[3,4-d]borepin **TB**[8] (Figure 5.2b) suggested that trithieno-fused variants of this compound should be synthetically feasible. Perhaps most intriguing is the potential proaromaticity of the non-aromatic borepin core within the TTB structures when incorporated in an extended π-conjugated system, similar to PITN (Figure 5.2b, c). While typical proaromatic compounds favor p-type carrier properties, the inherent electron-deficiency of the boron center in the TTB might also facilitate n-type characteristics (Figure 5.2d), possibly leading to ambipolar behavior.

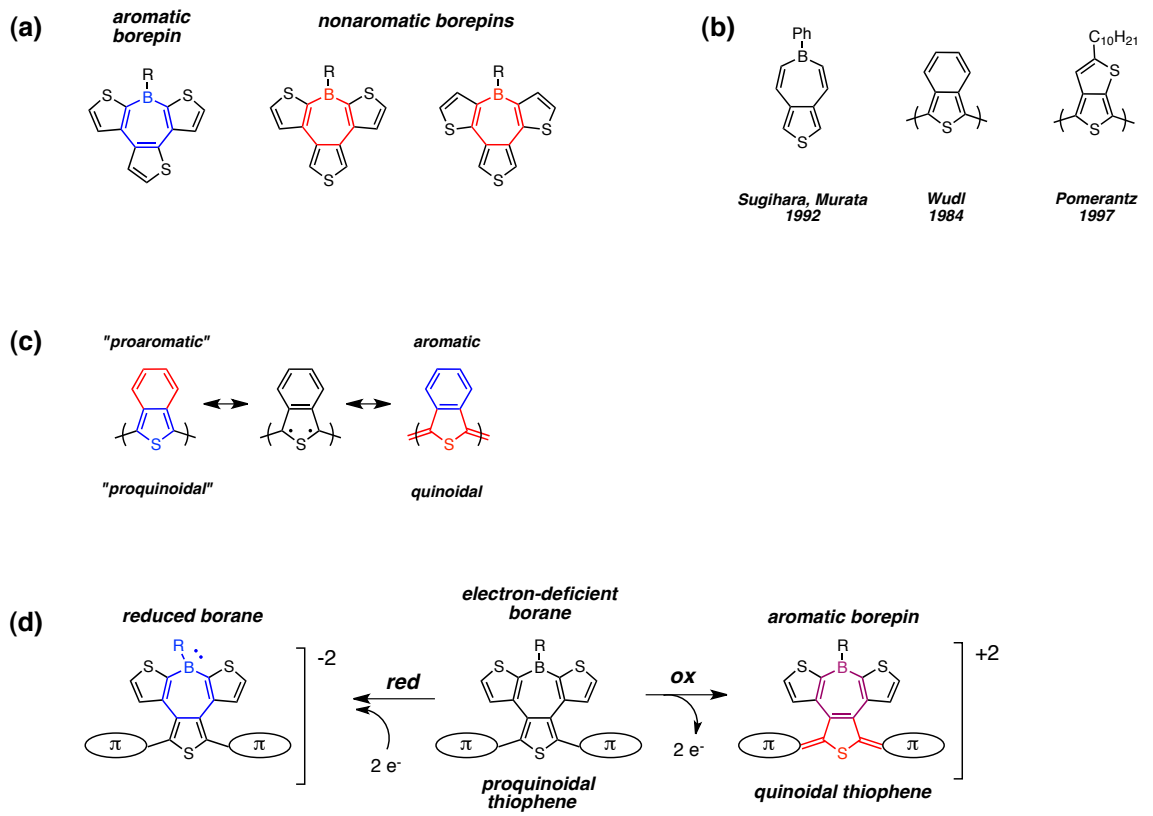

Figure 5.2. Structures and points of interest of TTB systems. (a) Structures of some envisioned TTB isomers containing either formally Hückel aromatic or nonaromatic borepin rings and (b) related compounds. (c) Resonance forms of polyisothianaphthene (PITN), illustrating proaromatic character. (d) Electronic structural basis for possible ambipolar charge carrier properties in π-extended TTB systems based on proaromaticity and electron deficiency.

A sample retrosynthetic analysis for TTBs is shown Scheme 5.1. Disconnection of the B-C bonds (standard borepin formation via $MesB(OMe)_2$ condensation) gives the key dihalogenated terthiophene precursor, which could in turn be obtained via iododesilylation of the trimethylsilyl (TMS) groups with ICl. The doubly TMS-functionalized terthiophene was considered to be potentially accessible via cross-coupling of two equivalents of a 2-silylated-3-metalated thiophene precursor (or the equivalent) with 3,4-diiodothiophene. Bäuerle has employed a similar approach for the iterative synthesis of terthiophene-based dendrimers.[9]

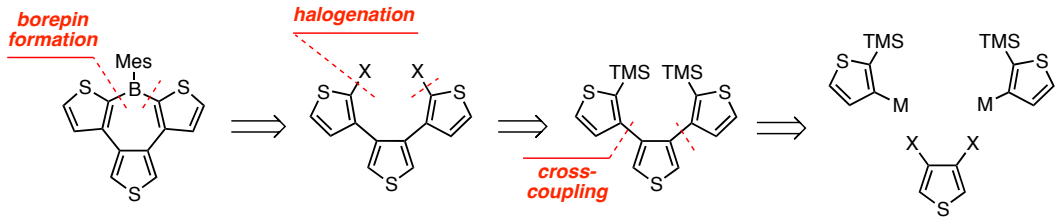

Scheme 5.1. Initial retrosynthetic approach to TTBs

Experimentally, however, this route proved problematic for the particular TTB isomer envisioned in Scheme 5.1. Upon generation of the 2-silyl-3-metalated thiophene species (either via Li-Br exchange or Mg-Br exchange), spontaneous ring-opening of thiophene occurred to give the acyclic, conjugated enyne thiol after H_2O quench as judged by ^1H NMR spectra of the crude product (Scheme 5.2). This type of side reaction has been reported previously upon generation of other 2-substituted-3-lithiothiophenes.[10]

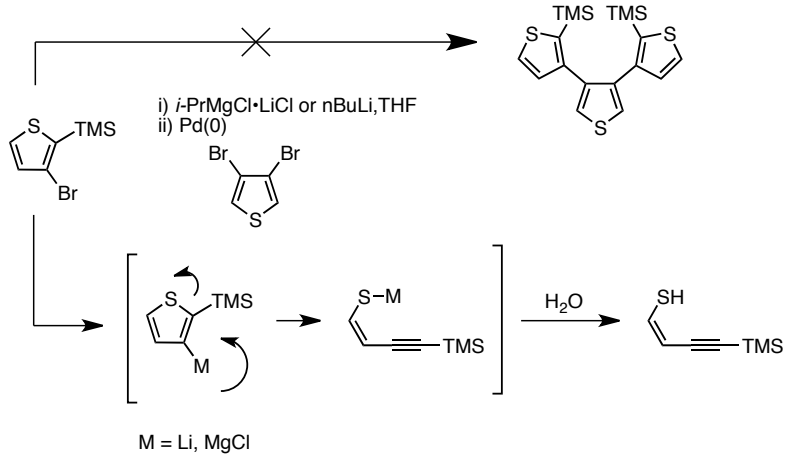

Scheme 5.2. Unsuccessful attempt to generate a terthienyl TTB precursor due to competitive ring-opening of 3-metalated-2-trimethylsilylthiophene.

The practical problems presented by the ring opening suggested that other TTB structures might constitute more tractable synthetic targets in the short term. Ultimately it was found that another TTB isomer **(1)** could be constructed in highly step-economic fashion

from easily prepared materials (Scheme 5.3). A regioselective double Stille cross-coupling of 3,4-diiodothiophene with (3-bromothiophen-2-yl)tributylstannane gave directly the desired dibrominated terthiophene precursor **2** in 25% yield. **2** was converted to TTB **1** in 60% yield via the typical borepin preparative method discussed in Chapter 3. Like the *B*-Mes DTBs, **1** was fully stable towards air, moisture, and silica gel and could be handled on the bench without special precautions.

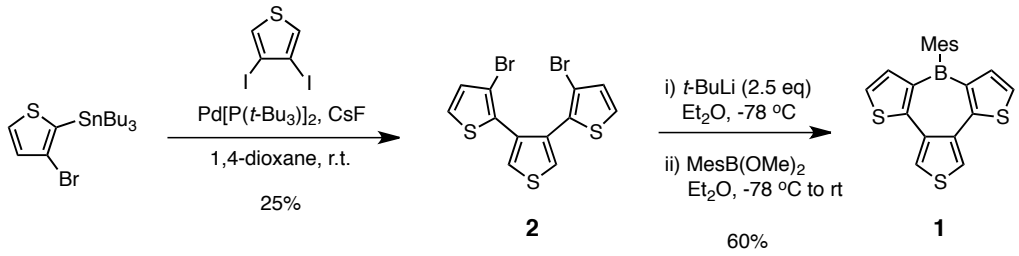

Scheme 5.3. Synthesis of TTB **1**.

NMR data for **1** and related thiophene-fused borepins **TB** and **DTB** are presented in Table 5.1. The ^{11}B signal for **1** is slightly shielded in comparison to both the related **DTB** and **TB** structures, suggesting a modest increase in π-electron density at the boron center of **1**. Perhaps most surprising is that the ^{11}B signal for **TB** is only deshielded by 1.6 ppm relative to **1**, despite **TB** lacking the two of the three electron-rich thiophene rings in **1**. The ^{1}H spectrum showed that ^{1}Hα' signals of the thiophene ring fused at the *d*-edge of the borepin in TTB **1** occur quite far downfield (8.09 ppm), while a similar deshielding is also seen for the same ^{1}Hα' signals of **TB** structure (7.75 ppm) as reported by Sugihara and Murata. This suggests a strong contribution of the *d*-fused thiophene ring in the electronic stabilization of boron in the TTB structure. Further, comparison of the corresponding thieno ^{1}Hα/^{1}Hβ signals in **DTB** and **1** reveals a relatively significant ~0.3 ppm upfield shift for **1**,

suggesting that the thiophene rings fused at the *b,f* positions of the TTB are less polarized than in the **DTB** structure.

Table 5.1. Selected $^{1}H/^{11}B$ NMR chemical shifts for TTB **1** and related compounds.

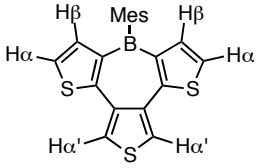

1

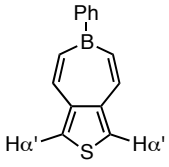

TB

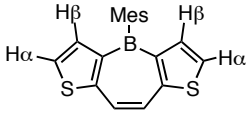

DTB

	1[a]	**TB**[a,b]	**DTB**[a]
^{11}B	49.2	50.8	51.9
^{1}Hα	7.16	—	7.47
^{1}Hβ	7.11	—	7.38
^{1}Hα'	8.09	7.75	—

[a] $^{11}B/^{1}H$ NMR spectra collected in $CDCl_3$ solution at room temperature.
[b] Reference 8.

Photophysical, theoretical, and electrochemical data for **1** are given in Figures 5.3 and 5.4. The UV-vis spectrum of **1** in $CHCl_3$ solution (Figure 5.3.a) shows distinct short [250 – 300 nm; Abs λ_{max} = 265, 291 nm] and long wavelength [325 – 400 nm; Abs λ_{max} = 361, 378 (shoulder) nm] absorption regions; an additional very weak, long wavelength band was observed near 425 nm with extended tailing to almost 500 nm (Figure 5.3b). The Abs λ_{onset} value for **1** of 484 is bathochromically-shifted nearly 90 nm compared to **DTB**, showing that the additional thieno fusion results in enhanced π-electron delocalization. DFT calculations for **1** reveal that the HOMO is comprised of the π-orbitals of the three thiophene rings without any contribution from boron (unlike DTBs which show a substantial HOMO coefficient for boron), while the LUMO is mainly delocalized over the central thieno[3,4-*d*]borepin substructure with a very strong boron contribution (Figure 5.3c); this suggests that

the HOMO-LUMO transition of **1** should have substantial intramolecular charge-transfer (ICT) character, consistent with the weak, low energy bands observed in the UV-vis spectrum. The photoluminescence (PL) spectrum of **1** extends broadly over the range 350 to 590 nm (PL λ_{max} = 407 nm; Figure 5.3a). The PL quantum yield for **1** was found to be very low (Φ_{PL} = 0.01). Cyclic voltammograms of **1** in THF in the cathodic regime demonstrated that the TTB has two-electron-accepting behavior, with a reversible reduction wave at $E_{1/2\ red}$ = -2.11 V (vs. Ag/Ag^{+}, Figure 5.4a, b) and a less reversible wave occurring at E_{pc} = -2.79 V (Figure 5.4b). This indicated that the TTB possessed greater electron accepting behavior than **DTB**, which only showed a single reduction wave at $E_{1/2\ red}$ = -2.26 V (Chapter 3).

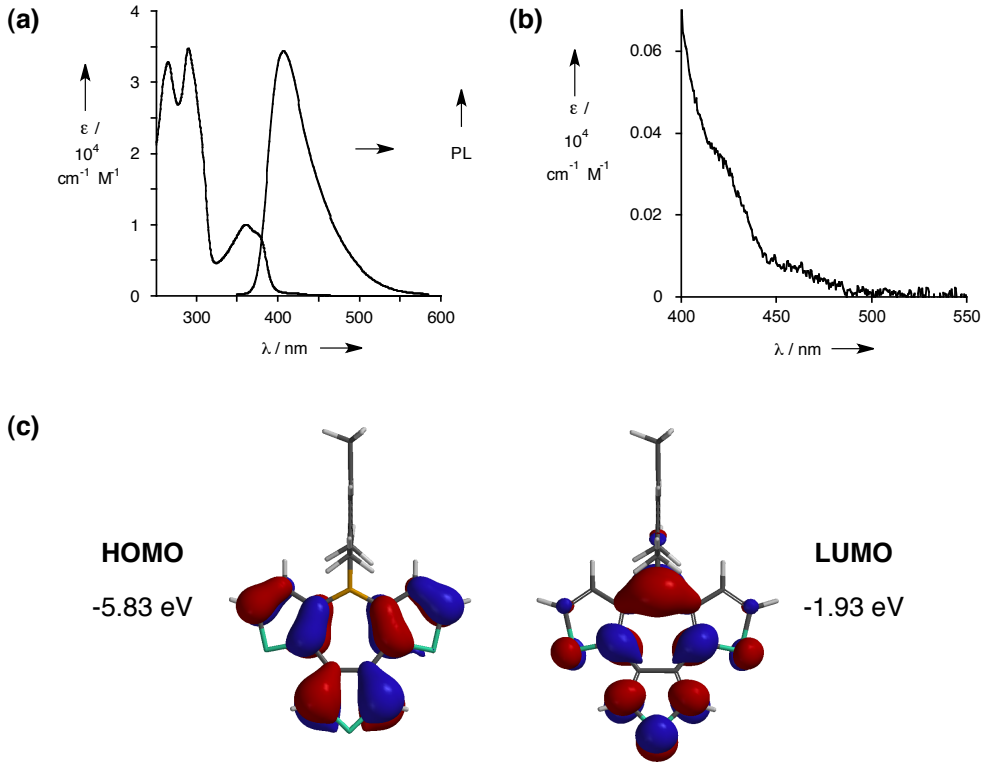

Figure 5.3. Photophysical and theoretical data for **1**. (a) UV-vis and (b) PL spectra of **1** in $CHCl_3$ solution. (b) Detail of weak long wavelength absorption bands between 400 and 500 nm. (c) DFT calculated (B3LYP/6-311G**) HOMO and LUMO surfaces of **1**.

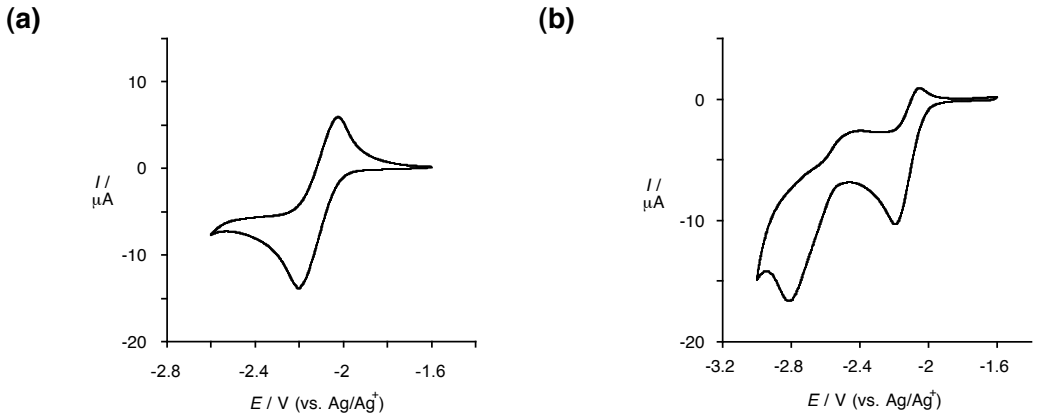

Figure 5.4. Cyclic voltammograms of **1** (c) from –1.6 V to –2.5 V and (d) from –1.6 V to –3.0 V in 0.1 M *n*-Bu_4PF_6 /THF solution at a TTB concentration of 2.5 mM; potentials referenced to Ag/Ag^+ (= 0.00 V).

The X-ray structure of TTB **1** was determined using single crystals grown via slow evaporation from a concentrated solution of **1** in CH_2Cl_2 / MeOH (Figure 5.5). The structural features of **1** (Figure 5.5a) were generally similar to those observed in DTBs, including a planar core structure (average atomic deviation of 0.087 Å from the mean plane of the tetracycle, maximum deviation = 0.19 Å for a single atom) and perpendicular orientation of the *B*-Mes group to the core (87.5°). The planarity of the TTB core is noteworthy, as analogous tribenzoborepins (TBBs) have been theoretically predicted to show pronounced puckering of the borepin ring;[11] it is likely that reduced steric hindrance in the bay regions between thiophene rings in the TTB structure allows for the planar conformation. Both the endocyclic (1.541(2) Å, 1.544(3) Å) and exocyclic (1.583(2) Å) B–C bond lengths in **1** were similar to DTBs, indicating considerable B-C π-conjugation in the borepin ring. C–C bond lengths within the borepin ring also confirmed that the conjugation scheme shown in the canonical structure of **1** is accurate, verifying the non-aromatic π-electron arrangement.

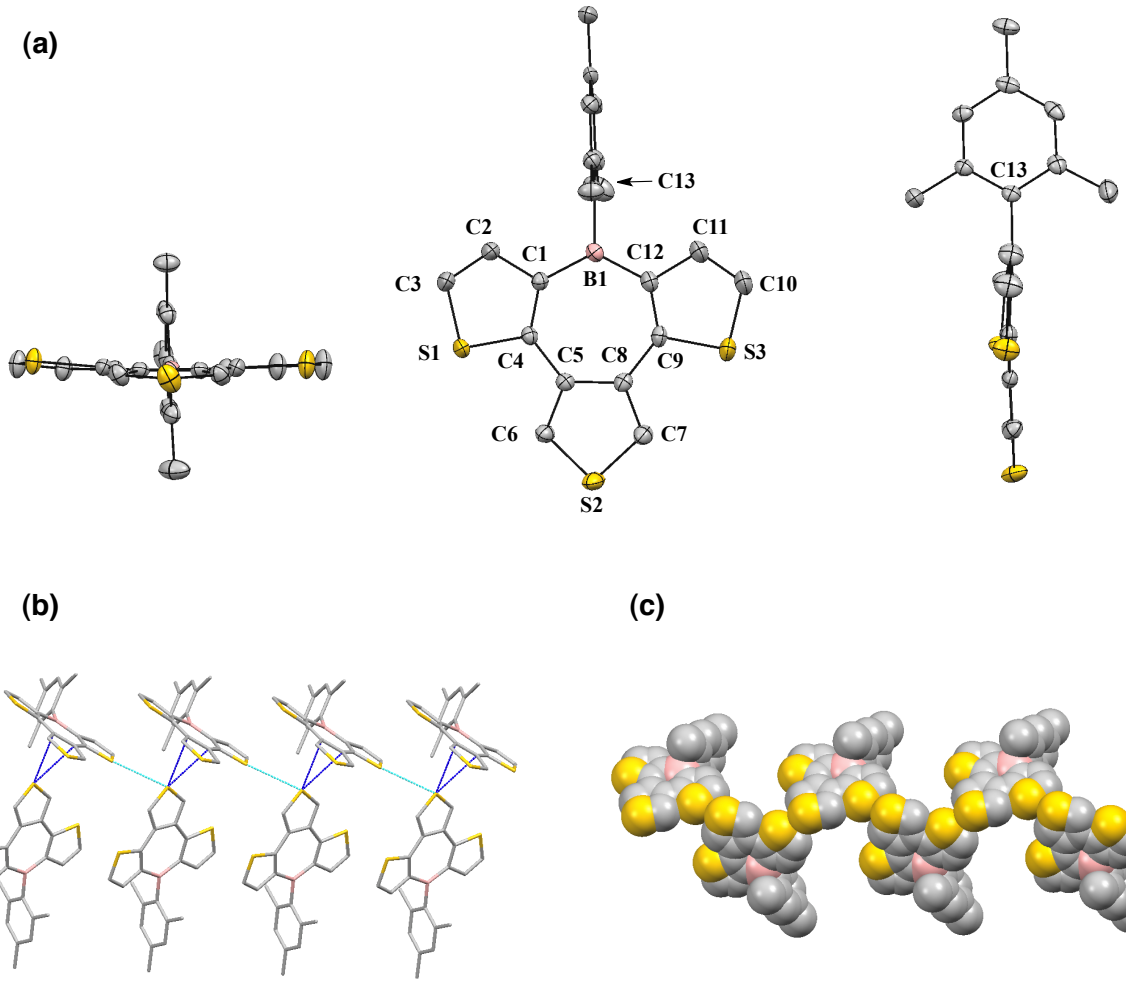

Figure 5.5. X-ray structures of TTB **1** and solid-state packing arrangements at 110(2) K. (a) X-ray structure of **1** (displacement ellipsoids shown at 50% probability level) with bottom edge (left), face-on (middle), and side edge (right) perspective views. Selected bond lengths (Å): B1–C1: 1.541(2), B1–C12: 1.544(3), B1–C13: 1.583(2), C1–C4: 1.388(2), C4–C5: 1.454(2), C5–C6: 1.383(2), C5–C8: 1.446(2), C7–C8: 1.399(2), C8–C9: 1.453(2), C9–C12: 1.391(2), C10–C11: 1.353(3). (b, c) Crystal structure packing arrangements of **1**: (b) stick depiction showing slipped herringbone motif, highlighting S-S (3.55 Å, dotted light blue lines) and S-π (3.19 Å, dotted dark blue lines) close-contacts. c) Space-filling model highlighting S-S close-contacts (yellow spheres).

In the crystal lattice, molecules of **1** pack in double layer stacks in a highly-slipped herringone pattern owing to intermolecular S-S (3.55 Å) and S-π (3.19 Å) interactions (Figure 5.5b, c). Such S-S interactions were not observed in the solid-state structures of

DTBs, demonstrating the influence of the additional thiophene ring on solid state ordering. The adjacent herringbone layers pack together with C-H—π and H—H close-contacts between the cores and Me groups on the Mes rings. Cofacial π—π stacking is not present to an appreciable degree.

Continued studies of the TTB scaffold are suggested. Besides the synthesis of other TTB isomers for structure-property evaluation, determination of the chemical reactivity patterns and functionalization prospects of **1** are indicated. A preliminary attempt to carry out NBS bromination of **1** in $CHCl_3$ at temperatures up to 60 °C resulted in a complex mixture, indicating a broad spectrum of products and/or possible degradation of the starting material. More mild bromination conditions or directed metalation chemistry could be more promising alternatives to functionalize TTBs and provide access to extended conjugated boron-containing proaromatic materials.

Extended polycyclic aromatics and oligoarenes with quinoidal electronic structures have drawn increasing interest due to the highly delocalized nature of the π-electrons and the potential for substantial diradical character due to small singlet-triplet energy gaps. Generally speaking, longer "quinoidal" oligoheteroarenes tend to favor the triplet diradical state more strongly due to the increase in aromatic stabilization energy corresponding to the larger number of arene rings in the backbone. A standard method to generate quinoidal conjugation in fused arene and oligoarene compounds is the installation of terminal dicyanomethyl groups by Takahashi coupling[12] followed by oxidation to generate the desired quinoidal electronic state. In recent Tovar group work, the quinoid form of bis-dicyanomethylene-functionalized unusual π-extended aromatic systems based on a bis-thienyl-functionalized methano-10-annulene (MTA) core was shown to generate substantial

diradical character despite a relatively small number of arene units as a result of favorable Baird aromaticity in the triplet state.[13] Accordingly, the synthesis of other unusual quinoidal aromatics (such as those containing borepin motifs) could be of particular interest. Quinoidal boron-containing π-electron systems have been subjects of fundamental interest in their reduced forms from Kaim's early studies[14] to the present day,[15] but neutral boron-containing quinoid-type structures are lesser known.

Preliminary results have suggested that the synthesis of quinoid-type DTB systems may possible through typical Takahashi conditions; treatment of dibromo-DTB **3** with malononitrile/NaH and $PdCl_2(PPh_3)_2$ (Scheme 5.4) gave a material which turned from a yellow to a deep blue color in $CHCl_3$ upon workup (Figure 5.6a), suggesting adventitious oxidation of the putative coupling product to directly give the desired quinoidal bis-dicyanomethylene-functionalized system **4**. Such *in situ* oxidations to generate similar quinoid-type compounds upon air exposure are known.[16] The UV-vis spectrum of the crude product was broad and highly bathochromically shifted (Abs λ_{onset} > 800 nm) compared with typical functionalized DTBs (Figure 5.6b); such spectra are a distinguishing characteristic of highly conjugated quinoidal compounds. Unfortunately, efforts to definitively confirm **4** as the product by NMR spectra and mass spectrometry were hampered by the material's low solubility, complicating purification and characterization efforts. Future work should be directed at optimizing the synthesis and determining the best method of purification to verify the identity of **4** and allow full characterization. Reengineering the quinoidal DTB core for greater solubility to ease purification/manipulation (e.g., with the addition of alkyl side-chains, as proposed in Chapter 4) may be useful in this regard.

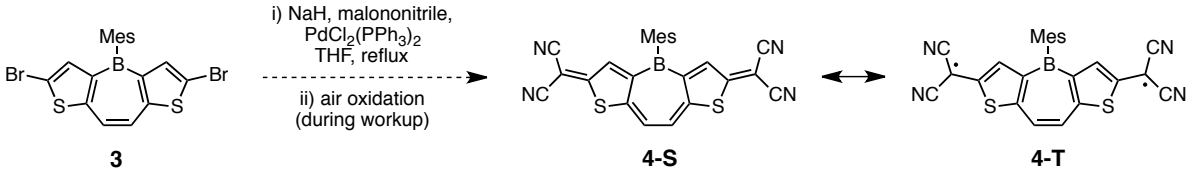

Scheme 5.4. Attempted synthesis of putative *bis*-dicyanomethylene substituted DTB **4** via a Takahashi coupling procedure, shown in canonical singlet quinoid (**4-S**) and triplet diradical (**4-T**) forms.

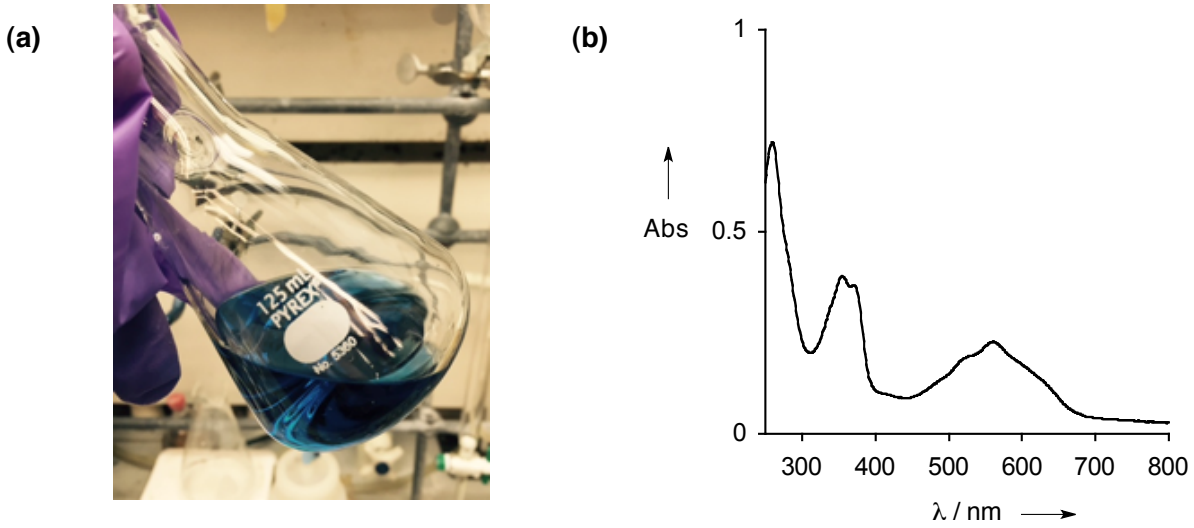

Figure 5.6. Evidence for the formation of quinoidal DTB **4**. a) Photograph showing deep-blue color of organic extract upon reaction workup. (b) UV-vis spectrum of the crude product from Takahashi coupling in $CHCl_3$ following workup.

Theoretical data for the ground state singlet (**4-S**) and triplet (**4-T**) states of **4** were calculated at the DFT (B3LYP/6-31G*) level, along with an extended, dithienyl functionalized DTB analogue **5** and are shown in Figure 5.7 and Table 5.2. The calculated frontier molecular orbital (FMO) surfaces **4-S** and **4-T** show a clear indication of a transition from a typical quinoidal HOMO in **4-S** to an aromatic SOMO in the open shell state **4-T** (Figure 5.7a,b). Both the LUMO of **4-S** and SOMO of **4-T** share identical orbital distribution, as expected. The spin density surface for **4-T** shows broad delocalization of spin over the dithienylethene core and dicyanomethylene substituents, but relatively weak spin density at boron.

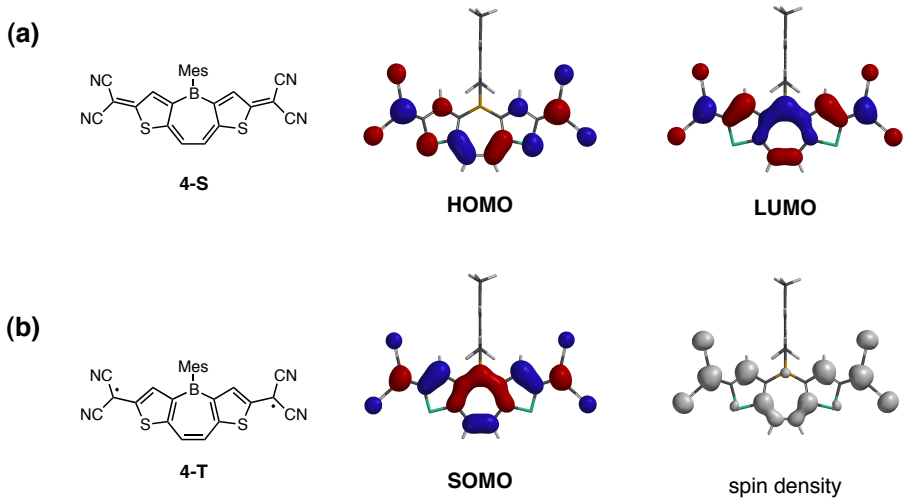

Figure 5.7. DFT calculated (B3LYP/6-31G*) surfaces for **4-S** and **4-T**. (a) HOMO and LUMO of **4-S** and (b) SOMO and spin density surface for **4-T**.

FMO energy levels and singlet-triplet energy gaps for **4** and **5**, alongside Otsubo's quinoidal benzodithiophene system **BDTQ**[17] and our group's dithienyl-subsituted quinoidal methano[10]annulene **TMTQ**,[13] are given in Table 5.2. The calculated singlet-triplet gap that of **4** is considerably larger than **BDTQ** or **TMTQ**, suggesting that **4** should have very little if any triplet population at room temperature. Nonetheless, **4** possesses a narrow bandgap in the singlet state comparable to **BDTQ**, the latter being somewhat unstable due to its benzenoid *o*-quinodimethane character. The interruption of *o*-quinodimethane character via the presence of the borepin group in **4** (and shielding Mes group) might afford additional stability and good material prospects. Interestingly, the addition of the two additional thienyl rings in the structure of **5** leads to a compound with a theoretically predicted 0.19 eV energetic preference for a triplet ground state, thus providing an intriguing diradical target for further investigation.

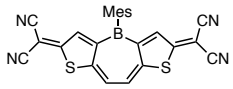

4

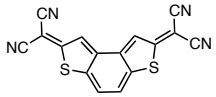

BDTQ

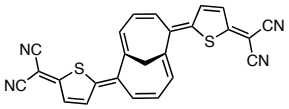

TMTQ

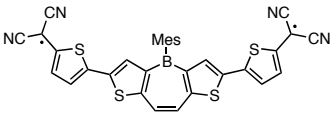

5

Compound	Singlet state (quinoid)			Triplet state (diradical)			Singlet-triplet gap
	HOMO (eV)	LUMO (eV)	E_{gap} (eV)	SOMO (eV)	LUMO (eV)	E_{gap} (eV)	$E_{SOMO} - E_{HOMO}$ (eV)
4	-6.25	-4.69	1.56	-6.05	-2.83	3.22	0.20
BDTQ	-6.36	-4.82	1.54	-6.23	-2.22	4.01	0.13
TMTQ	-5.79	-4.14	1.65	-5.68	-2.83	2.85	0.11
5	-5.45	-4.55	0.90	-5.64	-3.01	2.63	-0.19

Table 5.2. DFT calculated (B3LYP/6-31G*) energy levels for quinoidal DTBs and related compounds **BDTQ** and **TMTQ.** Resonance forms shown are the energetically favored ground state according to calculations.

Concluding Remarks

The synthesis of TTB **1** illustrates that the DTB preparative method developed in Chapter 3 is also amenable to the preparation of stable, trithieno-fused borepin structures. The presence of a formally aromatic borepin ring is not a necessary prerequisite for TTB stability under ambient conditions and furthermore might be used to elicit other desirable properties associated with proaromaticity of the borepin ring. Initial characterization data of **1** indicates that the TTB structure has greater electron-accepting capacity and bathochromically shifted electronic spectra compared to the analogous DTB, indicating that the third thieno ring plays a significant role in the electronic structure. It is anticipated that development of protocols for further synthetic elaboration of **1** could be leveraged for electronic tuning in small molecule TTB analogues or to generate oligomers displaying behavior typical of proaromatic π-electron materials.

Though in preliminary stages, the functionalization of DTBs with dicyanomethylene groups and subsequent oxidation to provide quinoidal DTB analogues should prove an intriguing area of research. Early experimental and theoretical results imply a highly delocalized electronic structure in quinoidal DTBs and open-shell ground states for the π-extended quinoidal DTB analogue **5**. The known capabilities of boron as a radical stabilizing moiety and a vehicle for unusual nonclassical bonding motifs provide further impetus for exploration of these unusual boron-containing organic diradical compounds at the fundamental level.

Experimental Section

General considerations. Unless otherwise specified, all reactions were carried out in flame- or oven- dried glassware under an atmosphere of prepurified nitrogen or argon using standard Schlenk techniques and magnetic stirring. Dichloromethane (CH_2Cl_2), diethyl ether (Et_2O), toluene and tetrahydrofuran (THF) were purified using an Innovative Technology, Inc. SPS-400-6 solvent purification system, dried over 3Å molecular sieves, and sparged thoroughly with nitrogen prior to use. Chloroform ($CHCl_3$) and 1,4-dioxane were dried over 3Å molecular sieves and sparged thoroughly with nitrogen prior to use. All other organic solvents were obtained from commercial sources and used as received. Palladium catalysts were obtained from Strem Chemicals. *Tert*-butyllithium (1.7 M solution in pentane) and *n*-butyllithium (1.6 M or 2.5 M solution in hexanes) from Sigma-Aldrich and titrated with diphenylacetic acid in THF prior to use. Unless otherwise noted, all other chemicals were obtained from Alfa-Aesar, Fisher Scientific, Oakwood Chemicals, Sigma-Aldrich, Strem Chemicals, or TCI America and used as received.

The following compounds were prepared according to the literature: 3-bromo-2-(trimethylsilyl)thiophene[18] and 3-bromo-2-(tributylstannyl)thiophene.[19] Dimethoxymesitylborane ($MesB(OMe)_2$) was prepared by adapting a literature method for the preparation of dimethoxytripylborane ($TipB(OMe)_2$)[20], using MesMgBr in place of TipMgBr (the product was purified by fractional distillation at 140 torr; clean $MesB(OMe)_2$ distilled at 160-200°C+). Dibromo-DTB **3** was prepared according to the procedure given in Chapter 4.

^1H NMR (400 MHz) and ^{13}C NMR (100 MHz) spectra were obtained using a Bruker Avance 400 MHz FT-NMR spectrometer in deuterated chloroform ($CDCl_3$) obtained from Cambridge Isotope Laboratories, Inc. ^{11}B NMR spectra (96 MHz) were obtained using a Bruker Avance 300 MHz FT-NMR spectrometer in deuterated $CDCl_3$. All chemical shifts are reported in parts per million (ppm, δ): ^1H NMR spectra were referenced to the residual proton solvent peaks ($CHCl_3$, $\delta = 7.26$; CH_2Cl_2, $\delta = 5.32$); ^{13}C NMR spectra were referenced to the carbon solvent peak ($CDCl_3$, $\delta = 77.16$); ^{11}B NMR spectra were referenced to an external boron trifluoride • diethyl etherate standard in $CDCl_3$, ($BF_3 \bullet Et_2O$, $\delta = 0.0$). Boron-bound carbons were typically not observed in ^{13}C NMR spectra due to quadrupolar relaxation of boron. High-resolution mass spectra were obtained using a VG Instruments VG70S/E magnetic sector mass spectrometer with EI (70 eV) and FAB ionization (matrix for FAB was 3-nitrobenzyl alcohol).

Photophysical considerations. Spectroscopic measurements were collected in $CHCl_3$ solution at room temperature. UV-visible (UV-vis) absorption spectra were obtained on a Varian Cary50 Bio UV-visible spectrophotometer. Photoluminescence (PL) spectra were obtained on a PTI QuantaMaster spectrofluorometer with a 75 W Xenon lamp, maintaining optical densities below 0.1 au. PL quantum yields were measured relative to a standard solution of quinine sulfate in 0.05 M aqueous H_2SO_4 while maintaining optical densities below 0.05 au.

Electrochemical considerations. Cyclic voltammetry (CV) measurements were performed under air- and moisture-free conditions in a one-chamber, three electrode cell using a PGSTAT302 potentiostat. A 2 mm^2 Pt button electrode was used as the working electrode with a Pt wire counter electrode relative to a quasi-internal Ag wire reference electrode submersed in 0.01 M $AgNO_3$/0.1M *n*-Bu_4NPF_6 in anhydrous acetonitrile. Cyclic voltammograms were taken 0.1 M *n*-Bu_4NPF_6 / THF electrolyte solutions at analyte concentrations of 2.5 mM (scan rate = 100 mV/s). Potentials are reported relative to the Ag/Ag^+ redox couple (0.00 V) against which the Fc/Fc^+ couple was measured to be +200 mV.

Theoretical considerations. Geometry optimizations/molecular orbital calculations were performed at the Density Functional Theory (DFT) level [B3LYP/6-311G** for **1**; B3LYP/ 6-31G* for **4** (singlet), **BDTQ** (singlet), **TMTQ** (singlet), and **5** (singlet); UB3LYP/6-31G* for **4** (triplet), **BDTQ** (triplet), **TMTQ** (triplet), and **5** (triplet)] using Spartan '04 (Wavefunction Inc., Irvine, CA).

X-ray crystallography. Single crystals of **1** suitable for X-ray crystallography were grown by slow diffusion/slow evaporation, layering MeOH over a concentrated solution of **1**/CH_2Cl_2. The stuctures were solved/refined at the Johns Hopkins University (JHU) Chemistry Department X-ray facility by Dr. Maxime A. Siegler. All reflection intensities were measured at 110(2) K using a SuperNova diffractometer (equipped with Atlas detector) with Cu *K*α radiation (λ = 1.54178 Å) under the program CrysAlisPro (Version 1.171.36.32 Agilent Technologies, 2013). The same program was used to refine the cell dimensions and for data reduction. The structure was solved with the program SHELXS-2013 and was refined on F^2 with SHELXL-2013[21]. Analytical numeric absorption correction based on a multifaceted crystal model was applied using CrysAlisPro. The temperature of the data collection was controlled using the system Cryojet (manufactured by Oxford Instruments). The H atoms were placed at calculated positions using the instructions AFIX 43, AFIX 123, AFIX 137 with isotropic displacement parameters having values 1.2 or 1.5 *U*eq of the attached C atoms. Graphical representations of crystal structures were generated using Mercury 3.6.1.[22] (Cambridge Crystallographic Data Centre, CCDC).

1, Fw = 376.34, pale yellow plate, 0.21 × 0.14 × 0.04 mm^3, monoclinic, $P2_1/c$ (no.14), a = 7.70318(14), b = 30.4005(5), c = 8.39458(15), β = 109.979(2)°, V = 1847.54(6) $Å^3$, Z = 4, D_x = 1.353 g cm^{-3}, μ = 3.648 mm^{-1}, T_{min}–T_{max}: 0.607–0.876. 12834 Reflections were measured up to a resolution of $(\sin \theta/\lambda)_{max}$ = 0.62 $Å^{-1}$. 3628 Reflections were unique (R_{int} = 0.0266) of which 3209 were observed [$I > 2\sigma(I)$]. 228 Parameters were refined. $R1/wR2$ [$I > 2\sigma(I)$]: 0.0329/0.0860. $R1/wR2$ [all refl.]: 0.0377/0.0896. S = 1.050. Residual electron density found between -0.27 and 0.41 e $Å^{-3}$. The structure is ordered. Compound ID code in JHU Crystallographic database: xs0590a.

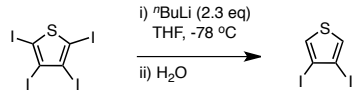

3, 4-diiodothiophene. To a stirring solution of tetraiodothiophene (5.88 g, 10.0 mmol) in THF (100 mL) at -78 °C in a 250-mL Schlenk flask under nitrogen was added *n*-BuLi (2.57 in hexanes, 8.95 mL, 23.0 mmol) over 5 m via syringe. After 1 h, H_2O (10 mL) was added and the mixture was allowed to gradually warm to room temperature. Bulk THF was removed from the mixture under reduced pressure (rotary evaporation) and the remaining material was partitioned between Et_2O and brine (1:1). The organic layer was removed and the aqueous layer was extracted 1x with Et_2O. The combined organics were washed 2x with brine then dried over $MgSO_4$, filtered, and concentrated under reduced pressure to a dark oil which was pushed through a short pad of SiO_2, eluting hexanes. The eluent was concentrated under reduced pressure to give 3.44 g of the product as a yellow oil which was used without further purification. ^{1}H NMR (400 MHz, $CDCl_3$); 7.41 (s, 2H).

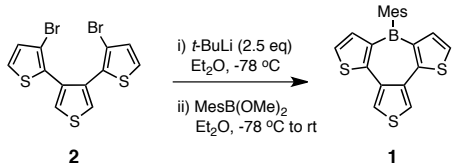

2 **1**

7-mesityl-borepino[3,2-*b*:6,7-*b′*:4,5-*c′′*]trithiophene (1). To a stirring solution of terthiophene **2** (236 mg, 0.581 mmol) in Et_2O (6 mL) at -78 °C in a 25-mL Schlenk flask under nitrogen was added *t*-BuLi (1.02 mL, 1.41 M in pentane, 1.45 mmol) dropwise via syringe, whereupon the reaction mixture became yellow-orange. After 20 min, a solution of $MesB(OMe)_2$ (123.0 mg, 0.129 mL, 0.639 mmol) in 2 mL Et_2O was added dropwise via syringe and the reaction mixture was allowed to gradually warm to room temperature with continued stirring for 20 h. Saturated aq. NH_4Cl and a small amount of brine were added to the reaction mixture, which was then partitioned between Et_2O and H_2O (1:1). The organic layer was removed and the aqueous layer was extracted 2x with Et_2O. The combined organics were dried over $MgSO_4$, filtered, and concentrated under reduced pressure to a dark orange oil which was purified by column chromatography (SiO_2, gradient elution: 5% $CHCl_3$ in hexanes → 10% $CHCl_3$ in hexanes → 15% $CHCl_3$ in hexanes) to give 131 mg of TTB **1** (0.348 mmol, 60%) as a white solid. ^{1}H NMR (400 MHz, $CDCl_3$) δ: 8.09 (s, 2H), 7.16 (d, J = 5.2 Hz, 2H), 7.11 (d, J = 5.2 Hz, 2H), 6.89 (d, J = 0.8 Hz, 2H), 2.37 (s, 3H), 1.99 (s, 6H); ^{11}B NMR (96 MHz, $CDCl_3$) δ: 49.2; ^{13}C NMR (100 MHz, $CDCl_3$) δ: 152.6, 138.0, 137.5, 136.4,134.7, 127.1, 124.0, 122.8, 22.7, 21.4. HRMS (EI): found m/z = 370.5806 ± 1.4 ppm; calculated for $C_{21}H_{17}{}^{11}BS_3[M^+]$: 376.0586.

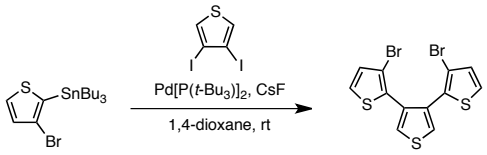

2

3,3''-dibromo-2,3':4',2''-terthiophene (2). A 25-mL Schlenk tube was charged with 3,4-diiodothiophene (702 mg, 2.09 mmol), $Pd[P(t\text{-}Bu)_3]_2$ (32 mg, 0.063 mmol), CsF (1.33 g, 8.78 mmol), and a stir bar under nitrogen. 1,4-dioxane (6 mL) was added and the mixture was stirred at room temperature. A solution of 3-bromo-2-(tri-n-butylstannyl)thiophene (323 mg, 0.714 mmol) in 4 mL 1,4-dioxane was added dropwise by syringe and the mixture was stirred for 16 h at room temperature then heated to 75 °C for 2 hr. After cooling to room temperature, mixture was poured over a short pad of SiO_2 and eluted with $CHCl_3$ (note: the fluoride salts formed a dense cake over the SiO_2 which had to be broken up manually to allow filtration). The eluent was concentrated under reduced pressure to give a dark oil that was purified by column chromatography (SiO_2, gradient elution: 5% $CHCl_3$ in hexanes → 10% $CHCl_3$ in hexanes) to give 236 mg of **2** as a yellow oil (0.581 mmol, 28%). ^{1}H NMR (400 MHz, $CDCl_3$): 7.61 (s, 2H), 7.24 (d, 2H, J = 5.6 Hz), 6.97 (d, 2H, J = 5.2 Hz); ^{13}C NMR (100 MHz, $CDCl_3$): 132.8, 132.1, 130.6, 127.1, 126.3, 111.1. HRMS (EI): found m/z = 405.7981 ± 0.7 ppm; calculated for $C_{12}H_6{}^{79}Br^{81}BrS_3[M^+]$: 405.7981.

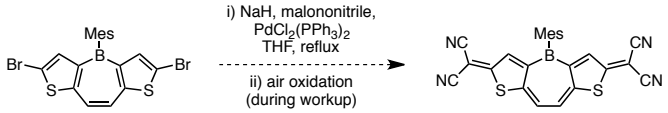

3 **4**

2,2'-(4-mesityl-2*H*-borepino[3,2-*b*:6,7-*b'*]dithiophene-2,6(4*H*)-diylidene)dimalononitrile (4). To a stirring solution of malononitrile (5.9 mg, 0.0897 mmol) in THF (1 mL) at 0 °C under nitrogen was added sodium hydride (4.3 mg, 0.179 mmol) in a single portion; the sides of the flask were rinsed with an additional 0.5 mL THF and the mixture was allowed to warm to room temperature with continued stirring for 1 h. The resulting suspension was transferred dropwise via cannula into a stirring mixture of dibromo DTB **3** (14.3 mg, 0.0299 mmol), $PdCl_2(PPh_3)_2$ (2.1 mg, 0.00299 mmol), and 1 mL THF in a 25-mL Schlenk tube under nitrogen. The mixture was heated to reflux for 7 h, during which time the mixture became deep red. After cooling to room temperature, 2 mL H_2O and 4 mL 2 M HCl (aq) were added. The mixture was partitioned between $CHCl_3$ and H_2O (1:1) under air (note: the organic phase turned from a dull brown color to a deep blue during work up) The organic layer was removed and the aqueous layer was extracted 2x with $CHCl_3$. The combined organics were dried over $MgSO_4$, filtered, and concentrated under reduced pressure to give 23.0 mg of a deep blue-black solid. UV-vis (crude, $CHCl_3$) λ/nm: 260, 354, 370, 521(sh), 558, 628 (sh). Further material purification was attempted by column chromatography [SiO_2, gradient elution: 2% MeOH in $CHCl_3$ → (5%, 10%, 15%, 20%, 25%, 50%) MeOH in $CHCl_3$ → 100% MeOH], giving 8.6 mg of a red-purple solid. This material did not provide a

reasonable signal to noise level for definitive identification via NMR spectroscopy in $CDCl_3$ or MeOD due to compound insolubility.

References

(1) Kubo, T. *Chem. Lett*. **2015**, *44*, 111–122.
(2) Sun, D.; Ehrenfreund, E.; Valy Vardeny, Z. *Chem. Commun*. **2014**, *50*, 1781–1793.
(3) Gallagher, N. M.; Olankitwanit, A.; Rajca, A. *J. Org. Chem*. **2015**, *80*, 1291−1298.
(4) Wu, Y. L.; Bureš, F.; Jarowski, P. D.; Schweizer, W. B.; Boudon, C.; Gisselbrecht, J. P.; Diederich, F. *Chem. Eur. J*. **2010**, *16*, 9592–9605.
(5) Wudl, F.; Kobayashi, M.; Heeger, A. J. *J. Org. Chem*. **1984**, *49*, 3382–3384.
(6) Andreu, R.; Blesa, M. J.; Carrasquer, L.; Garin, J.; Orduna, J.; Villacampa, B.; Alcalá, R.; Casado, J.; Ruiz Delgado, M. C.; López Navarrete, J. T.; Allain, M. *J. Am. Chem. Soc.* **2005**, *127*, 8835–8845.
(7) Brogdon, P.; Giordano, F.; Puneky, G. A.; Dass, A.; Zakeeruddin, S. M.; Nazeeruddin, M. K.; Grätzel, M.; Tschumper, G. S.; Delcamp, J. H. *Chem. Eur. J*. **2016**, *22*, 694–703.
(8) Sugihara, Y.; Yagi, T.; Murata, I.; Imamura, A. *J. Am. Chem. Soc.* **1992**, *114*, 1479–1481.
(9) Ma, C.-Q.; Mena-Osteritz, E.; Debaerdemaeker, T.; Wienk, M. M.; Janssen, R. A. J.; Bäuerle, P. *Angew. Chem. Int. Ed*. **2007**, *46*, 1679–1683.
(10) Gronowitz, S. *Chem. Heterocycl. Compd*. **1995**, *30*, 1252–1283.
(11) Schulman, J. M.; Disch, R. L. *Organometallics* **2000**, *19*, 2932–2936.
(12) Uno, M.; Seto, K.; Takahashi, S. *J. Chem. Soc. Chem. Commun.* **1984**, 932–933.
(13) Streifel, B. C.; Zafra, J. L.; Espejo, G. L.; Gómez-García, C. J.; Casado, J.; Tovar, J. D. *Angew. Chem. Int. Ed*. **2015**, *54*, 5888–5893.
(14) Schulz, A.; Kaim, W. *Chem. Ber.* **1989**, *122*, 1863–1868.
(15) Ji, L.; Edkins, R. M.; Lorbach, A.; Krummenacher, I.; Brückner, C.; Eichhorn, A.; Braunschweig, H.; Engels, B.; Low, P. J.; Marder, T. B. *J. Am. Chem. Soc*. **2015**, *137*, 6750−6753.
(16) Suzuki, Y.; Miyazaki, E.; Takimiya, K. *J. Am. Chem. Soc.* **2010**, *132*, 10453–10466.
(17) Yoshida, S.; Fujii, M.; Aso, Y.; Otsubo, T.; Ogura, F. *J.Org. Chem*. **1994**, *59*, 3077–3081.
(18) Devarie-Baez, N. O.; Shuhler, B. J.; Wang, H.; Xian, M. *Org. Lett*. **2007**, *9*, 4655–4658.
(19) Xiong, Y.; Wu, Q.; Li, J.; Wang, S.; Gao, X.; Li, H. *J. Org. Chem*. **2013**, *78*, 752−756.
(20) Pelter, A.; Smith, K.; Buss, D.; Jin, Z. *Heteroatom Chem*. **1992**, *3*, 275–277.
(21) Sheldrick, G. M. *Acta Cryst.* **2008**, *A64,* 112–122.
(22) Macrae, C. F.; Edgington, P. R.; McCabe, P.; Pidcock, E.; Shields, G. P.; Taylor, R.; Towler, M.; van de Streek, J. *J Appl. Cryst*. **2006**, *39*, 453–457.

Chapter 6: Preliminary Work Towards other Heteroarene-fused Borepins and Proposed Future Directions

Introduction

Chapters 2 - 5 of this dissertation have outlined the synthesis and characterization of several benzo- and thieno-fused polycyclic aromatic structures containing one or more borepin rings, the evaluation of their structural, electronic, and redox properties, and consideration of possible applications towards future boron-containing organic optoelectronic materials. The successful syntheses of these diverse borepin-based structures suggests that the borepin motif could be incorporated into many other compounds. The following chapter discusses preliminary efforts towards other (hetero)arene-fused borepin compounds and provides suggestions for future directions in borepin-based materials research.

Results and Discussion

In addition to the dithienoborepin (DTB) and trithienoborepin (TTB) structures thus far synthesized, several other ladder-type systems containing borepin motifs could be envisioned as interesting targets for study. One possible avenue of exploration is the extension of the DTB core with additional fused alternant borepin-thiophene segments, such as in **I** (Figure 6.1). Elucidating the properties of **I** could provide insight into the effect of creating an extended, fused polycyclic array with exclusive "strong" boron-thiophene α-conjugation. Structurally similar but torsionally unconstrained thienylboranes **BDT2** and **FBDT2** were recently reported by Jäkle and coworkers to be highly electron-deficient and air-stable owing to *B*-Mes* or *B*-FMes steric protection,[1] adding further comparative value to the preparation and study of **I**.

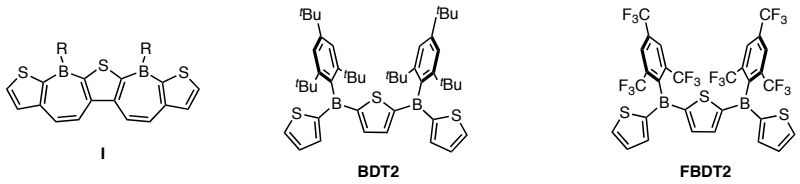

Figure 6.1. Extended ladder-type polycyclic aromatic **I** containing alternant borepin-thiophene ring fusion motif and Jäkle's structurally related thienylboranes **BDT2** and **FBDT2**.

DFT calculations at the B3LYP/6-31G* level indicate that *B*-Mes analogue **I-Mes** has a planar structure and a narrowed HOMO-LUMO gap (3.54 eV) relative to the tricyclic DTB **2** from Chapter 3 (4.25 eV) with which it shares an analogous ring fusion pattern (Figure 6.2). Bandgap reduction in **I-Mes** is mainly a result of a considerably reduced LUMO level, illustrating the impact of embedding a second boron center in the core. Like the DTB structure, **I-Mes** shows strong LUMO density at both boron centers suggesting a basis for stepwise electron accepting abilities/multistate switching. The multiple Lewis acidic sites might also support stepwise anion complexation; conjugated small molecules and polymeric species containing multiple Lewis acidic boron centers have drawn particular interest as sensor materials with amplified sensitivity, as catalysts, and as building blocks for supramolecular assemblies.[2-8]

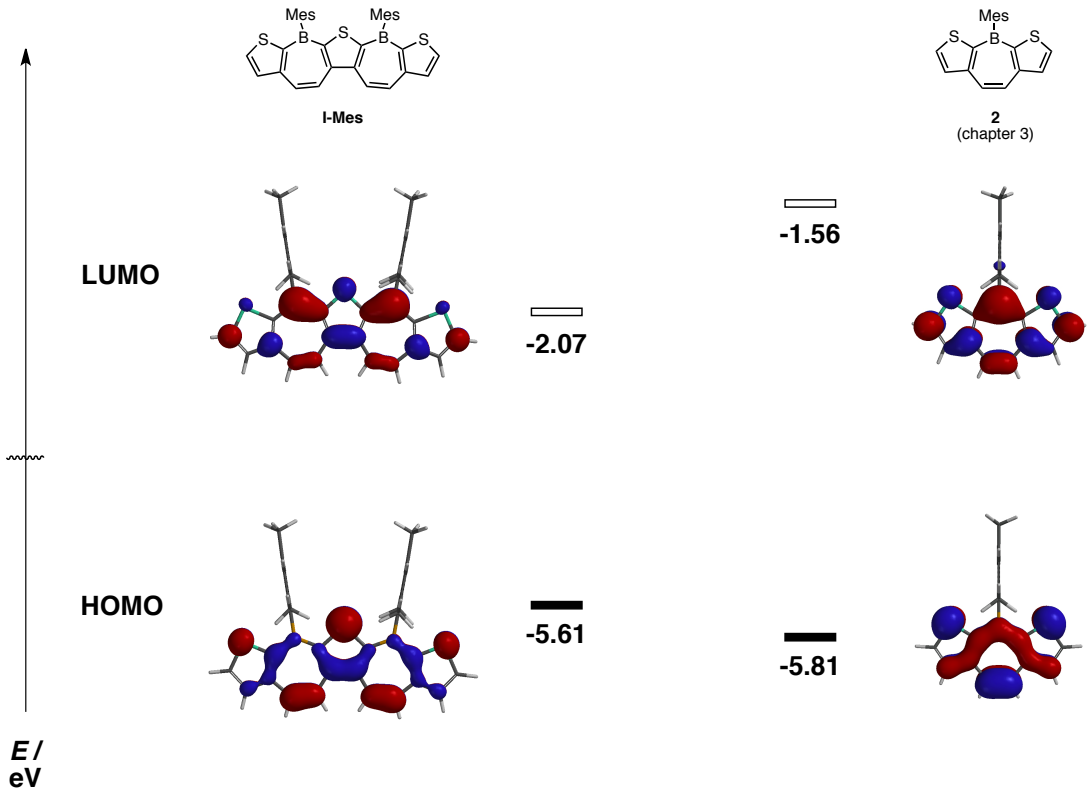

Figure 6.2. DFT calculated HOMO and LUMO levels of extended ladder compound **I-Mes** and shorter DTB congener **2** (from chapter 2).

A retrosynthetic analysis of **I** is shown in Scheme 6.1, relying on typical Sonagashira cross-couplings and stereoselective alkyne to alkene reduction to access the key trithieno-*Z*,*Z*-diene precursor which could be converted to the final borepin-containing product. Employing bulky silyl substituents (TIPS, TBDMS, etc.) as the R' groups on the terminal thiophene rings should provide good compound solubility throughout the synthetic route; the silane groups could be removed following borepin formation via acidic deprotection to generate the parent compound for direct study and to allow further functionalization of the thieno positions.

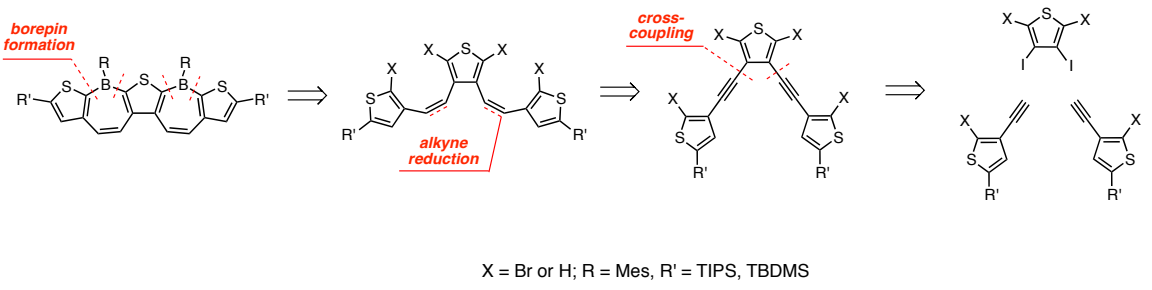

Scheme 6.1. Retrosynthetic analysis of extended, fused alternating thiophene fused borepins.

Preliminary efforts towards the preparation of the TIPS-substituted ladder borepin **1** are shown in Scheme 6.2. Unfortunately, attempts to synthesize tetrabrominated trithienodiyne **4** via Sonogashira cross coupling between 2,5-dibromo-3,4-diiodothiophene **2** and (5-bromo-4- ethynylthiophen-2-yl)triisopropylsilane **3** generated dithienyldiacetylene compound **5** as the only major product (32%) due to competitive Glaser-type alkyne homocoupling (several minor undesired cross-coupled products could be observed in the crude product mixture). In an alternative approach, **6**, a non-brominated analogue of **4**, was prepared in 49% *via* an analogous Sonogashira route (Scheme 6.2b). **6** was subsequently converted to the *Z*, *Z*-diene **7** in 56% by Ti-mediated alkyne reduction. The final transformation to target borepin compound **1** remains to be achieved. Directed tetrametalation of the free α-thieno positions of **7** with an appropriately strong and selective base (such at *t*-BuLi, BuLi/TMEDA, or Schlosser's superbase *n*-BuLi/*t*-BuOK[9-11]) followed by double ring closure via $MesB(OMe)_2$ quench could be a plausible path to the targeted borepin-containing pentacycle. If the directed tetrametalation approach is not viable, installation of bromo- or iodo- handles on precursors **6** or **7** prior to continuing the synthesis should enable borepin formation via our proven lithium-halogen exchange /$MesB(OMe)_2$ quench protocol.

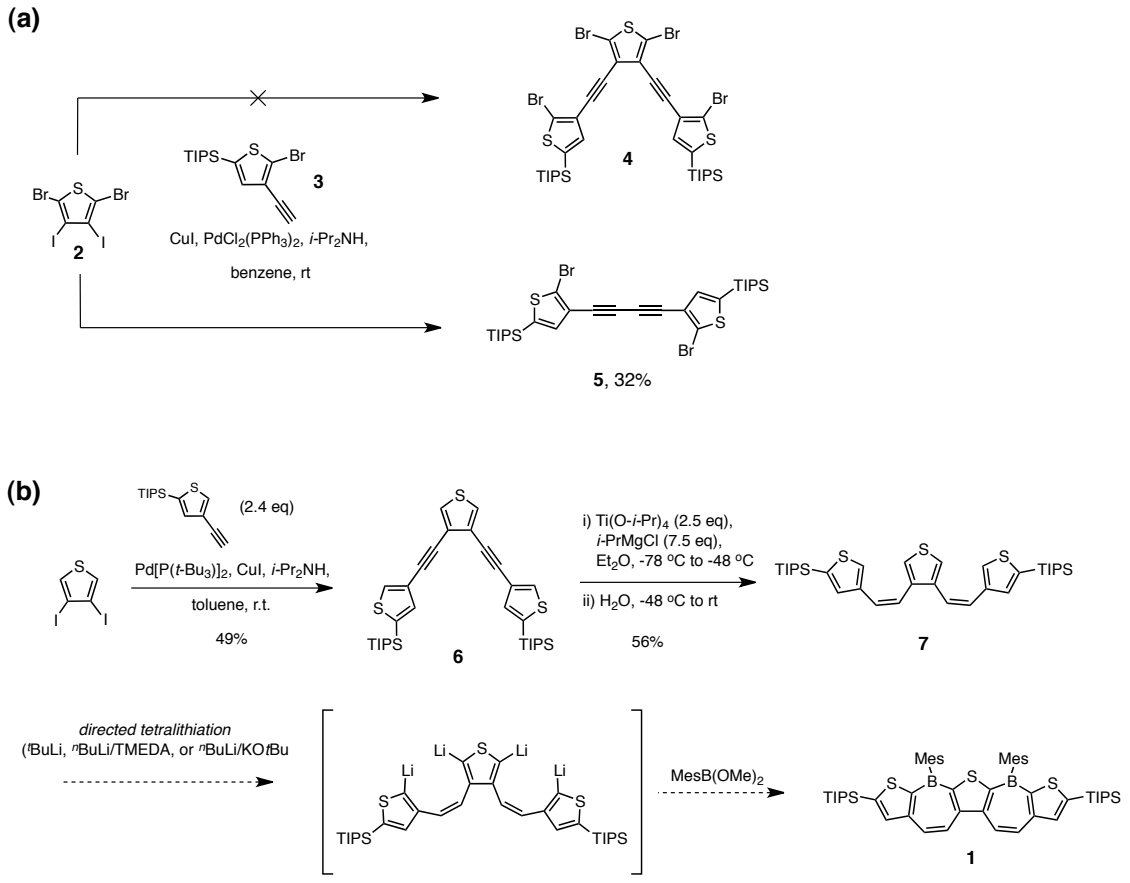

Scheme 6.2. Synthetic efforts towards extended, fused pentacyclic thienoborepin **1.** (a) unsuccessful synthesis of tetrabrominated precursor **4** due to competitive alkyne homocoupling. (b) Synthetic route to trithieno-diene **7**, with proposed final synthetic step toward **1**.

Polymers and small molecules based on thienothiophene cores[12,13] have emerged as highly promising candidates for organic materials. For instance, Takimiya and coworkers have shown that benzothieno[3,2-*b*]benzothiophenes, and related architectures[14-16] such as dinaphtho[2,3-*b*:2',3'-*f*]thieno[3,2-b]thiophene **DNTT** (Figure 5.X) are high-perfoming wide-bandgap semiconductors with excellent optical transparency.[17] Such compounds have also shown high thermal stability under medical sterilization conditions (e.g. autoclaving) without a loss in performance, enabling use in biomedical applications.[18]

The incorporation of borepin subunits within acenes containing thienothiophene units might provide additional properties of interest to this promising class of materials, such as n-type or ambipolar charge transport or sensing capability. Structures **II** and **III** (Figure 6.3) represent two such molecular motifs. Several other variations on such a core could also be envisioned (e.g. with thienothiophene/ benzene terminal units, a more highly extended thienoacene core unit, and so forth).

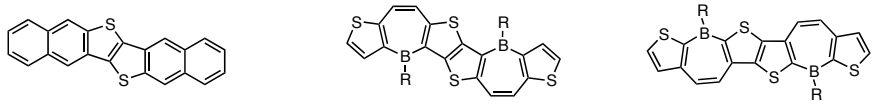

Figure 6.3. Takimiya's thienothiophene-based semiconducting material **DNTT** and proposed borepin-containing thienothiophene-based acenes **II** and **III**.

DFT calculations on *B*-Mes substituted **II-Mes** indicate a highly planar polycyclic architecture, broad delocalization of the frontier molecular orbitals over the core, and a narrowed HOMO-LUMO gap (3.07 eV) compared to structurally analogous DTB **1** from Chapter 3 (3.85 eV) of which **II-Mes** can be considered a fused "dimer" (Figure 6.4). In contrast to the alternant thiophene-borepin structure **I-Mes** in Figure 6.2, the narrowing of the bandgap in **II-Mes** is due to substantial HOMO elevation in addition to LUMO lowering. Similar to the DTB, weak β-conjugation between boron and the thiophene units in **II-Mes** results in a lack of contribution from boron to the LUMO, however boron contributions are evident in the HOMO and LUMO+1.

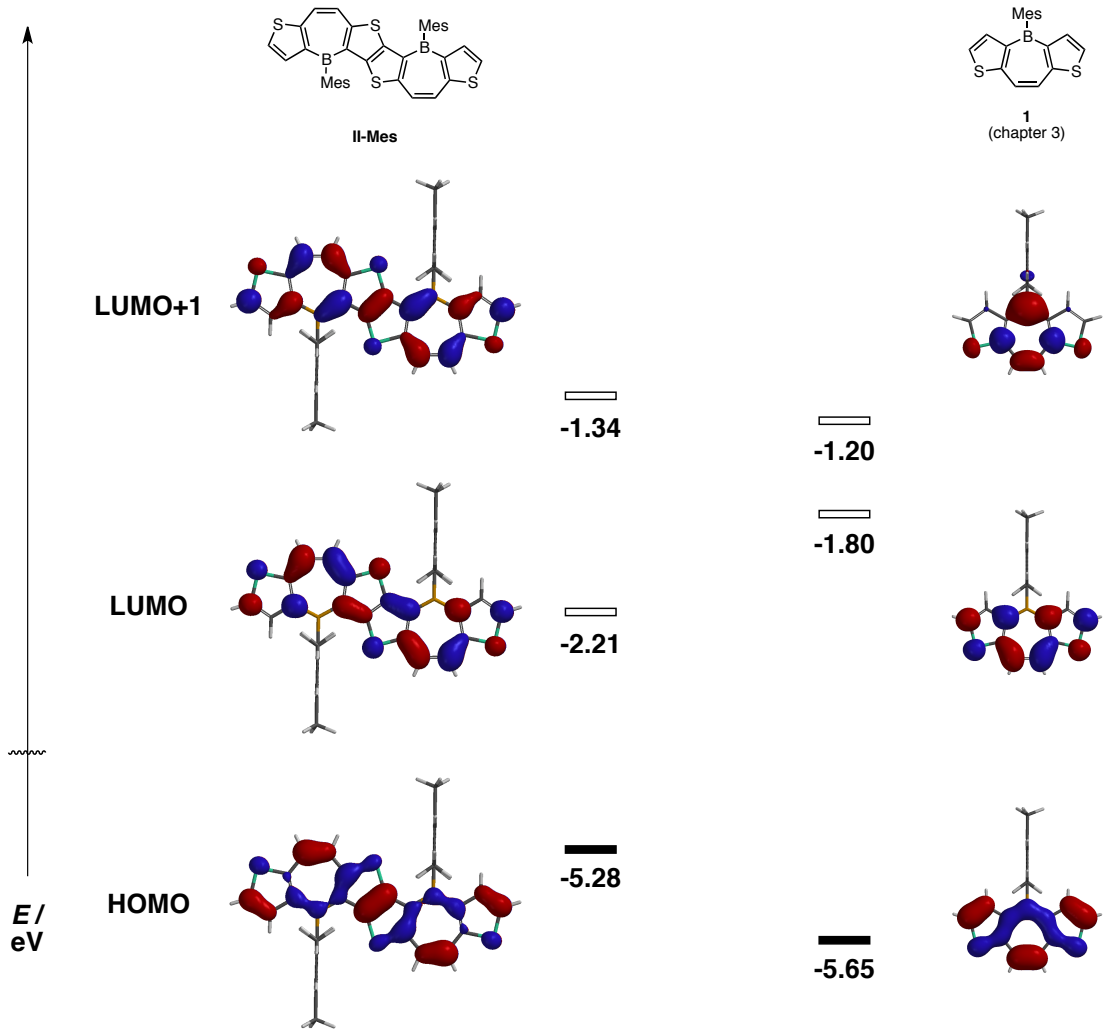

Figure 6.4. DFT calculated (B3LYP/6-31G*) frontier molecular orbitals of ladder thienothiophene-fused borepin **II-Mes** and the structurally analogous DTB **1** from chapter 3.

Scheme 6.3 provides retrosynthetic analysis of **8**, a TIPS-substituted analogue of **II-Mes**, which could be achieved by a two step sequence from the known thienothiophene compound **9**[19] via reactions employed in typical DTB preparative chemistry.

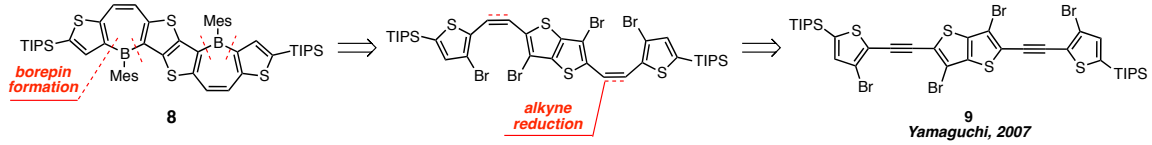

Scheme 6.3. Retrosynthetic analysis of thienothiophene-fused borepin structure **8**.

While the preceding chapters of this dissertation have demonstrated that the electron-rich thiophene ring has great utility in the creation of stable, electronically-tunable fused borepin species, the heterocyclic chemical space provides substantial scope to generate other fused borepins with unique chemical properties. One unexplored possibility is to generate borepin-based structures that feature fusion to an electron-accepting aromatic ring. Thiazole is a reasonable candidate which has featured prominently not only in natural products and bioactive synthetic compounds, but also in electron-poor organic electronic materials (Figure 6.5).[20] Dithiazole-fused borepins (DTzBs), such as **IV** or **V**, are structurally similar to DTBs, but should be electronically quite different.

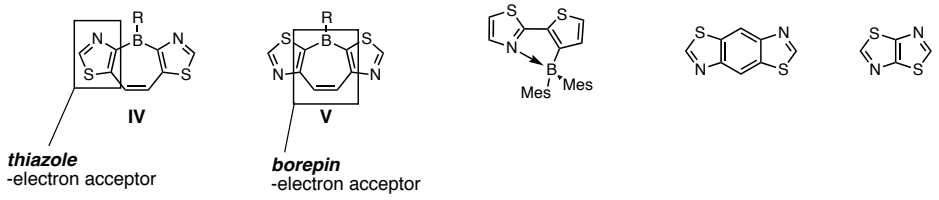

Figure 6.5. Structures of proposed fused borepins featuring electron-accepting thiazole rings (DTzBs) and some thiazole-based motifs currently employed in organic electronics.

DFT calculations on DTzBs indicate that a thiazole-for-thiophene replacement would considerably perturb molecular electronics, resulting in significant lowering of LUMO levels compared to their DTB congeners (Figure 6.6). The LUMO and LUMO+1 surfaces of DTzBs and DTBs are located on the polycyclic core and are virtually identical in their distribution; however, the electron-accepting nature of the thiazole rings causes the core-centered orbitals that comprise the HOMOs of DTBs to fall in energy, becoming the HOMO-2 of **IV-Mes** and **V-Mes** (here the HOMO and HOMO-1 levels of DTzBs are instead centered on the pendant Mes ring). The calculations corroborate the notion that

the thiazole rings could allow DTzBs to be more highly electron-accepting relative to benzo- and thieno-fused borepins studied thus far. As an added benefit, the thiazole ring can often be functionalized in a manner similar to thiophene for further tuning of molecular properties.

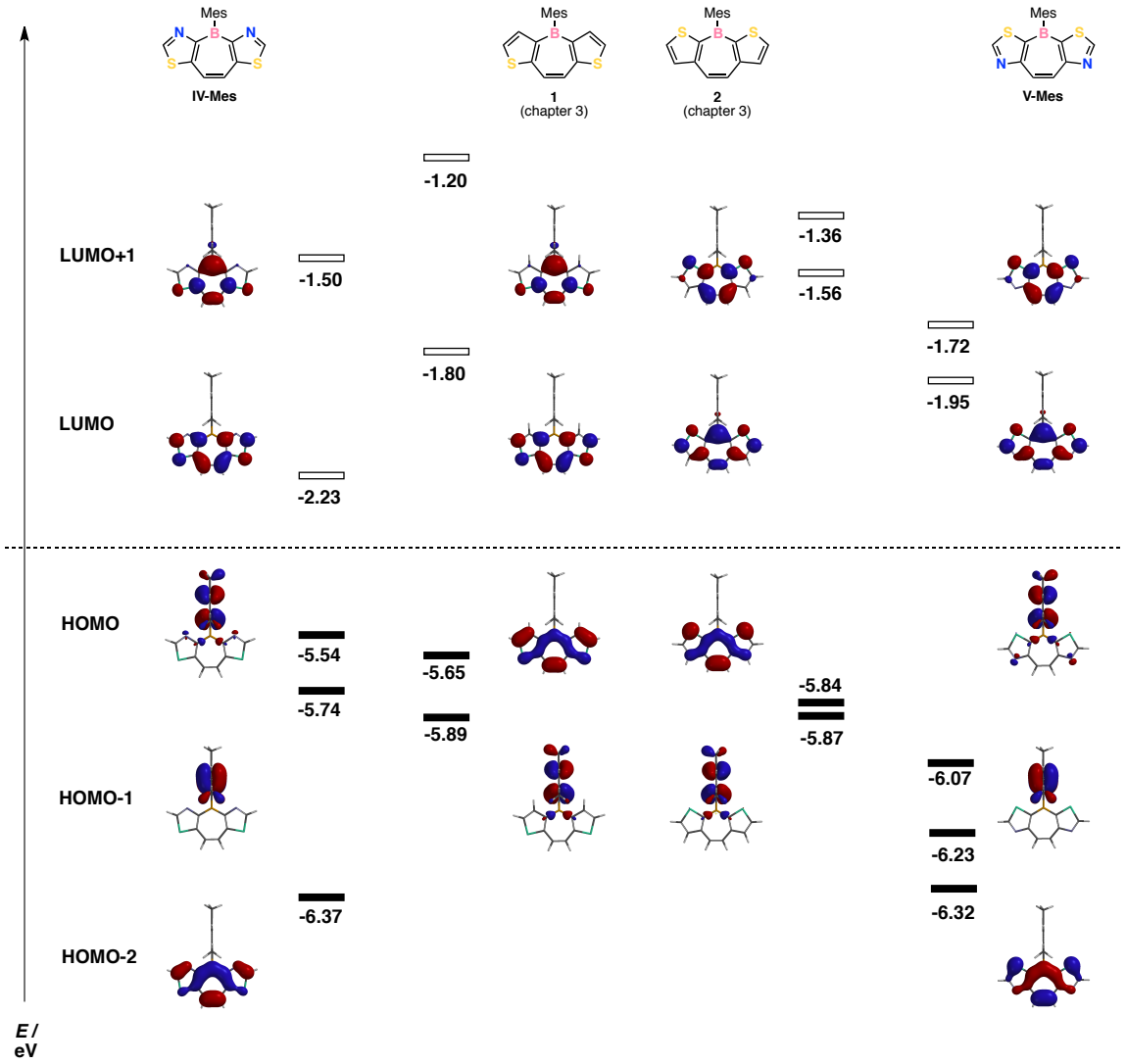

Figure 6.6. Comparison of DFT calculated frontier molecular orbitals for *B*-Mes DTzBs (**IV-Mes** and **V-Mes**) and analogous DTBs from Chapter 3.

Retrosynthetically, DTzBs could plausibly be accessed from dibrominated dithiazolylacetylenes via standard alkyne reduction route (Scheme 6.4). The dithiazolylacetylene compounds could be generated via cross-couplings with

appropriately substituted thiazoles and bis(tributylstannyl)acetylene, for instance. Substituted thiazole precursors of these types have been reported in the literature by Sammakia, Marder, and Yamaguchi[21-23] (the latter are shown as synthons in the retrosynthetic scheme).

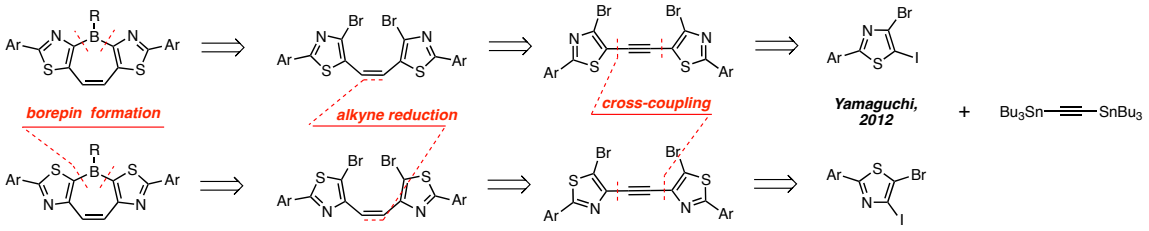

Scheme 6.4. Retrosynthetic approaches to DTzB analogues from literature precursors.

The motifs discussed above are but a few of the myriad borepin-containing π-conjugated systems that could be of interest; other unique structures are shown in Figure 6.7. These include compounds with a thus far unrealized fused diborepin motif **VI**, which could provide a counterpoint to fused diborole species recently constructed by Piers and coworkers[24,25] (Figure 6.7a). Structurally constrained, fully planarized triarylboranes containing multiple borepin rings (such as **VII**, Figure 6.7b) could also be of particular interest considering the surge of interest in large PAHs with either centrally embedded[26-29] or edge-situated[30-32] boron atoms as heteroatom-doped nanographene segments, ambipolar mesogens, and luminescent materials. Even exotic borepin compounds containing diborin motifs with B-B bonds (**VIII**) might be imagined, which have drawn interest due to their high electron-accepting capacity and aromatic character in the dianionic state[33,34] (Figure 6.7c).

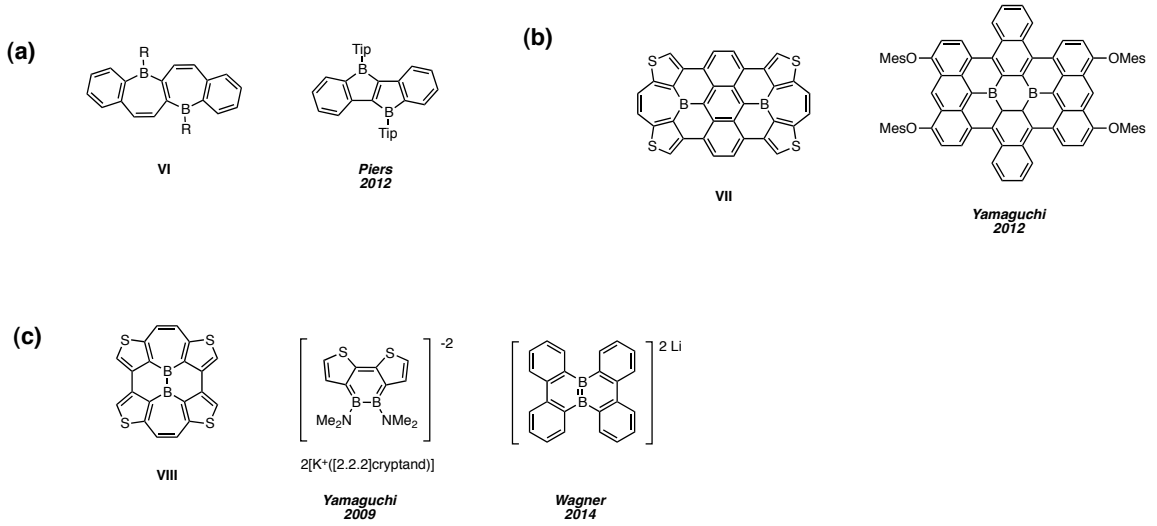

Figure 6.7. Other proposed future borepin targets and related literature compounds. (a) A ladder diborepin (**VI**) and Piers' fused diborole. (b) A fully planarized polycyclic structure containing two DTB motifs (**VII**) and Yamaguchi's boron-doped nanographene. (c) A planarized diborepin compound with an internal B-B bond (**VIII**), Yamaguchi's dianionic diborin, and Wagner's B-B bond-containing graphene flake.

Concluding Remarks

This chapter has outlined several ways in which the robust synthetic chemistry used to construct thiophene-annelated borepins (such as DTBs and TTBs in chapters 3 and 5) might be applied to generate other borepin-containing organic materials of interest. Among these are the extended ladder-type thiophene-annelated borepins whose preliminary synthetic steps have carried out. The elongated conjugated networks should provide excellent electronic delocalization and polarizability compared with benzene-fused borepin PAHs of similar size (such as *B*-entacenes), while maintaining the advantageous stability provided by thienannulation. Preparation of even more electron-deficient borepin species through ring fusion to electron-accepting heterocycles such as thiazole could be leveraged to enhance n-type characteristics. Finally, while likely to be synthetically challenging, the realization exotic targets (such as those with fused

diborepin structures or extended fully planarized 2-D systems) could generate substantial interest from both fundamental chemical and materials perspectives.

In conclusion, this dissertation has described the rational design, synthesis, characterization, and further functionalization of a variety of benzo- and thieno-fused borepin-based polycyclic aromatic compounds as prospective boron-containing organic electronic materials. The main advances can be summarized as follows: 1) the tin-boron exchange preparative approach can be used to to prepare a variety of extended benzo-fused borepin structures, as shown in the successful synthesis of the meta-*B*-entacene isomer (Chapter 2), the properties of which deviated in expected fashion from the previously studied more "highly conjugated" para-*B*-entacene; 2) The "alkyne-reduction route" to access key *Z*-alkene precursors and subsequent condensation of dimetalated substrates with $MesB(OMe)_2$ represent robust, scalable synthetic methods to access several dithieno-fused borepins (Chapters 3 and 5), with the resulting materials showing excellent stability and isomer-dependent electronic properties; 3) The facile synthetic chemistry associated with the thiophene ring can be used to modify parent DTBs, allowing a broad range of further functionalization and targeted property-tuning of the core structure (Chapter 4); 5) Thiophene-annulation, coupled with *B*-Mes steric protection, confers stability to a wide range of borepin-containing structures with non-aromatic borepin rings (such as DTB **4** from Chapter 3 and TTB **1** from Chapter 5), whose electronic properties differ from aromatic borepin-based structures. The further development of synthetic chemistry towards thiophene-fused borepins and related structures should hold many opportunities to realize boron-containing polycyclic arenes

whose beneficial stability and tunability should provide good prospects to translate into novel functional organo-main group electronic materials.

Experimental Section

General considerations. Unless otherwise specified, all reactions were carried out in flame- or oven- dried glassware under an atmosphere of prepurified nitrogen or argon using standard Schlenk techniques and magnetic stirring. Dichloromethane (CH_2Cl_2), diethyl ether (Et_2O), toluene and tetrahydrofuran (THF) were purified using an Innovative Technology, Inc. SPS-400-6 solvent purification system, dried over 3Å molecular sieves, and sparged thoroughly with nitrogen prior to use. Chloroform ($CHCl_3$) and 1,4-dioxane were dried over 3Å molecular sieves and sparged thoroughly with nitrogen prior to use. Anhydrous benzene was obtained from Sigma-Aldrich and used without further purification. All other organic solvents were obtained from commercial sources and used as received. Palladium catalysts were obtained from Strem Chemicals. *Tert*-butyllithium (1.7 M solution in pentane) and *n*-butyllithium (1.6 M or 2.5 M solution in hexanes) from Sigma-Aldrich and titrated with diphenylacetic acid in THF prior to use. Isopropyl magnesium chloride (2.0 M in Et_2O) was obtained from Sigma-Aldrich and titrated with salicaldehyde phenylhydrazone in THF prior to use. Unless otherwise noted, all other chemicals were obtained from Alfa-Aesar, Fisher Scientific, Oakwood Chemicals, Sigma-Aldrich, Strem Chemicals, or TCI America and used as received.

The following compounds were prepared according to literature procedures: ((2-bromothiophen-3-yl)ethynyl)trimethylsilane[35] and tetraiodothiophene.[36] 3,4-diiodothiophene was prepared as described in Chapter 5.

^{1}H NMR (400 MHz), and ^{13}C NMR (100 MHz) spectra were obtained using a Bruker Avance 400 MHz FT-NMR spectrometer in deuterated chloroform ($CDCl_3$) or dichloromethane (CD_2Cl_2) obtained from Cambridge Isotope Laboratories, Inc. ^{11}B NMR (96 MHz) spectra were obtained using a Bruker Avance 300 MHz FT-NMR spectrometer in deuterated $CDCl_3$. All chemical shifts are reported in parts per million (ppm, δ): ^{1}H NMR spectra were referenced to the residual proton solvent peaks ($CHCl_3$, δ = 7.26; CD_2Cl_2, δ = 5.32); ^{13}C NMR spectra were referenced to the carbon solvent peak ($CDCl_3$, δ = 77.16; CD_2Cl_2, δ = 53.84). High-resolution mass spectra were obtained using a VG Instruments VG70S/E magnetic sector mass spectrometer with EI (70 eV) and FAB ionization (matrix for FAB was 3-nitrobenzyl alcohol).

Theoretical considerations. Geometry optimizations/molecular orbital calculations were performed at the Density Functional Theory (DFT) level (B3LYP/6-31G*) using Spartan '04 (Wavefunction Inc., Irvine, CA).

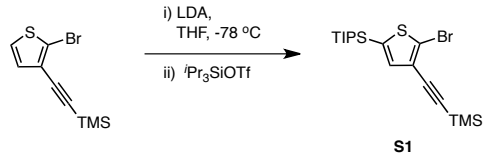

(5-bromo-4-((trimethylsilyl)ethynyl)thiophen-2-yl)triisopropylsilane S1. To a stirring solution of diisopropylamine (0.09 mL, 0.642 mmol) in THF at -78 °C in a 25-mL Schlenk tube under nitrogen at was added dropwise *n*-BuLi (1.67 M in hexanes, 0.40 mL, 0.668 mmol). After 30 m, the solution was warmed to 0 °C and transferred via cannula to a stirring solution of ((2-bromothiophen-3-yl)ethynyl)trimethylsilane (150 mg, 0.579 mmol) and triisopropylsilyl trifluoromethanesulfonate (269 mg, 0.878 mmol) in THF (4 mL) at -78 °C in a 25-mL Schlenk tube under nitrogen. The mixture was allowed to continue stirring for 18 h with gradual warming to room temperature, then concentrated under reduced pressure. 5% NH_4Cl (aq) was added, and the mixture was extracted 3x with Et_2O. The combined organics were dried over $MgSO_4$, filtered, and concentrated under reduced pressure to give a **S1** as a colorless oil (89.2 mg, 0.215 mmol, 37%) which was used without further purification. ^{1}H NMR (400 MHz, $CDCl_3$): 7.08 (s, 1H), 1.29 (sept, J = 9.2 Hz, 3H), 1.08 (d, J = 9.2 Hz, 18H), 0.27 (s, 3H).

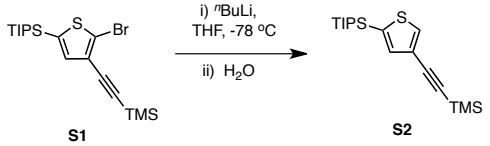

triisopropyl(4-((trimethylsilyl)ethynyl)thiophen-2-yl)silane S2. To a stirring solution of **S1** (466 mg, 1.12 mmol) in THF (6 mL) at -78 °C in a 25-mL Schlenk flask under nitrogen was added *n*-BuLi (2.57 M in hexanes, 0.523 mL, 1.34 mmol) dropwise via syringe. After 30 m, H_2O (2 mL) was added and the mixture was allowed to warm to room temperature, then partitioned between Et_2O and brine (1:1). The organic layer was removed and the aqueous layer was extracted 2x with Et_2O. The combined organics were washed with brine, dried over $MgSO_4$, filtered, and concentrated under reduced pressure to give an oil that was purified by column chromatography (SiO_2, hexanes), to give crude **S2** as a yellow oil that was used directly in the next step without further purification. ^{1}H NMR (400 MHz, CD_2Cl_2): 7.74 (d, J = 0.8 Hz, 1H), 7.26 (d, J = 0.8 Hz, 1H), 1.33 (sept, J = 7.2 Hz, 3H), 1.09 (d, J = 7.2 Hz, 18H), 0.25 (s, 3H).

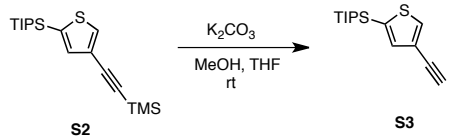

(4-ethynylthiophen-2-yl)triisopropylsilane S3. To a stirring mixture of the crude **S2** and potassium carbonate (300 mg, 2.17 mmol) in THF (3 mL) in a 15-mL round

bottomed flask under air was added 3 mL MeOH. After 16 h, the solid material was filtered off and the filtrate was concentrated under reduced pressure. The residue was taken up in Et_2O and washed with brine. The aqueous layer was was extracted 2x with Et2O and the combined organics were washed with brine, dried over MgSO4, filtered, and concentrated under reduced pressure to give an oil that was pushed through a short pad of SiO_2, eluting hexanes. The eluent was concentrated under reduced pressure to give 202 mg of **S3** (0.764 mmol, 68% over two steps from **S1**) as yellow oil that was used immediately without further purification.^{1}H NMR (400 MHz, CD_2Cl_2): 7.79, (dd, J = 1.2 Hz, J = 0.4 Hz, 1H), 7.30 (d, J = 1.2 Hz, 1H), 3.11 (s, 1H), 1.34 (sept, J = 7.6 Hz, 3H), 1.10 (d, J = 7.2 Hz, 18H).

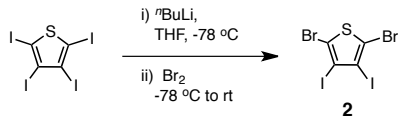

2,5-dibromo-3,4-diiodothiophene 2. To a stirring solution of tetraiodothiophene (588 mg, 1.00 mmol) in THF (10 mL) at -78 °C in a 25-mL Schlenk tube under nitrogen was added *n*-BuLi (2.5 M in hexanes, 0.84 mL, 2.1 mmol) dropwise via syringe. After 1 h, neat Br_2 (0.113 mL, 354 mg, 2.20 mmol) was added dropwise via syringe. The mixture was allowed to continue stirring for 5 h with gradual warming to room temperature. A solution of Na_2SO_3 (sat., aq.) was added, the mixture was partitioned between Et_2O and H_2O (1:1). The organic layer was removed and the aqueous layer was extracted 2x with Et_2O. The combined organics were dried over $MgSO_4$, filtered, and concentrated under reduced pressure to give a pale yellow solid which was recrystallized from EtOH to give 228 mg (0.462 mmol, 46%) **1** as yellow crystals. ^{13}C NMR (100 MHz, $CDCl_3$): 115.6, 99.0. HRMS (EI): found m/z = 493.6156 ± 0.1 ppm; calculated for $C_{12}H_6{}^{79}Br^{81}BrS_3$ [M^+]: 493.6157.

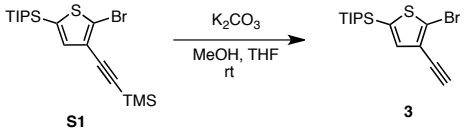

(5-bromo-4-ethynylthiophen-2-yl)triisopropylsilane 3. To a suspension of (5-bromo-4-((trimethylsilyl)ethynyl)thiophen-2-yl)triisopropylsilane **S1** (518 mg, 1.25 mmol) and potassium carbonate (346 mg, 2.50 mmol) in THF (6 mL) in a 25-mL round bottomed flask under nitrogen was added MeOH (6 mL) and the mixture was stirred at room temperature for 8 h. The solid material was filtered off, rinsing with Et_2O, and the filtrate was concentrated under reduced pressure. The resulting residue was dissolved in Et_2O, washed with H_2O and brine, concentrated under reduced pressure, and purified by column chromatography (SiO_2, hexanes) to give 331 mg of **2** (331 mg, 0.971 mmol,

78%) as a pale yellow-orange oil that was used immediately. ^{1}H NMR (400 MHz, $CDCl_3$): 7.11 (s, 1H), 3.32 (s, 1H), 1.27 (sept, J = 9.2 Hz, 3H), 1.09 (d, J = 9.2 Hz, 18H).

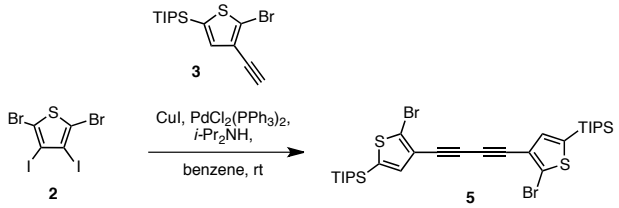

1,4-bis(2-bromo-5-(triisopropylsilyl)thiophen-3-yl)buta-1,3-diyne 5. A 25-mL Schlenk tube was charged with 2,5-dibromo-3,4-diiodothiophene (76.0 mg, 0.154 mmol), $PdCl_2(PPh_3)_2$ (7.6 mg, 0.0101 mmol), CuI (2.1 mg, 0.0101 mmol), and a stir bar under nitrogen. Benzene (1.5 mL), diisopropylamine (0.5 mL), and a solution of **2** (323 mg, 0.714 mmol) in 1.5 mL benzene was added to the vessel and the mixture was stirred for 48 h at room temperature, after which the volatile components were removed directly under high vacuum. The residue was purified by column chromatography (SiO_2, hexanes) to give 35.0 mg of **5** (0.0511 mmol, 33%) as a yellow-orange solid. ^{1}H NMR (400 MHz, $CDCl_3$): 7.14 (s, 1H), 1.28 (sept, J = 7.2 Hz, 3H), 1.09 (sept, J = 7.2 Hz, 3H); ^{13}C NMR (100 MHz, $CDCl_3$): 138.6, 137.2, 124.7, 123.9, 115.8, 105.3, 99.2, 18.7, 11.9; MS (EI): found m/z = 684.1; calculated for $C_{12}H_6{}^{79}Br^{81}BrS_3$ [M^+]: 684.1.

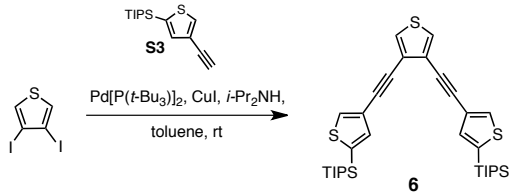

A 25-mL Schlenk tube was charged with $Pd[P(t\text{-}Bu)_3]_2$ (9.8 mg, 0.0191 mmol), CuI (3.0 mg, 0.0159 mmol), and a stir bar under nitrogen. Toluene (1 mL) was added and the mixture was stirred at room temperature. Sequentially were added 3,4-diiodothiophene (107 mg, 0.318 mmol), diisopropylamine (0.11 mL, 0.764 mmol), and a solution of **S3** (202 mg, 0.764 mmol) in 2 mL toluene dropwise via syringe and the mixture was stirred for 12 h at room temperature then heated to 75 °C for 2 hr. After cooling to room temperature, the volatile components were removed directly under high vacuum and the residue was was purified by column chromatography (SiO_2, gradient elution: hexanes → 5% CH_2Cl_2 in hexanes → 10% CH_2Cl_2 in hexanes) to give 95.3 mg of **6** (0.156 mmol, 49%) as a dark brown amorphous solid (0.581 mmol, 28%). ^{1}H NMR (400 MHz, $CDCl_3$): 7.70 (d, J = 0.8 Hz, 2H), 7.46 (s, 2H), 7.34 (d, J = 0.8 Hz, 2H), 1.34 (sept, J = 7.2 Hz, 6H), 1.10 (d, J = 7.6 Hz, 36H); ^{13}C NMR (100 MHz, $CDCl_3$): 138.3, 135.0, 134.1, 127.8, 126.2, 123.3, 83.2, 18.7, 11.9. HRMS (EI): found m/z = 608.2449 ± 1.2 ppm; calculated for $C_{34}H_{48}S_3Si_2$ [M^+]: 608.2457.

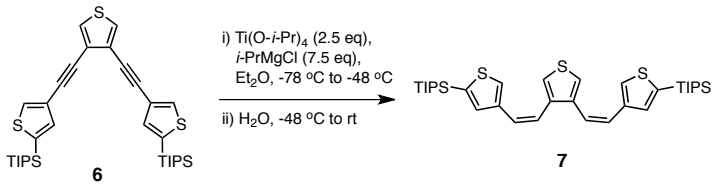

3,4-bis((*Z*)-2-(5-(triisopropylsilyl)thiophen-3-yl)vinyl)thiophene 7. To a stirring solution of **6** (41.7 mg, 0.0685 mmol) in Et_2O in a 25-mL Schlenk tube under nitrogen at -78 ^oC was added dropwise via syringe titanium (IV) isopropoxide (0.051 mL, 0.172 mmol) then isopropyl magnesium chloride (1.61 M in Et_2O, 0.32 mL, 0.51 mmol). After stirring for 5 min at -78 °C, the solution was warmed to -48 °C and held at this temperature for 3 h, during which time the reaction mixture became deep red-orange. Water (0.5 mL) was added dropwise via syringe and the mixture was allowed to warm to room temperature with stirring for 1 h. After partitioning the mixture between Et_2O and H_2O (1:1), the organic layer was removed and the aqueous layer was extracted 2x with Et_2O. The combined organics were washed sequentially with 1 M HCl (aq) and brine, dried over $MgSO_4$, filtered, and concentrated under reduced pressure to give an oily solid which was purified by column chromatography (SiO_2, hexanes) to provide **7** (23.7 mg, 0.0387 mmol, 56%) as a viscous yellow oil. ^1H NMR (400 MHz, $CDCl_3$): 7.35 (s, 2H), 7.11 (s, 2H), 7.02 (dd, J = 1.2 Hz, J = 1.2 Hz, 2H), 6.57 (d, J = 12.0 Hz, 2H), 6.27 (d, J = 12.0 Hz, 2H), 1.25 (sept, J = 7.2 Hz, 6H), 1.05 (d, J = 7.6 Hz, 36H); ^{13}C NMR (100 MHz, $CDCl_3$): 139.9, 138.4, 136.6, 134.2, 129.5, 126.0, 123.0, 122.9, 18.9, 12.0. HRMS (EI): found m/z = 612.2765 ± 0.8 ppm; calculated for $C_{34}H_{52}S_3Si_2$ [M^+]: 612.2770.

References

(1) Yin, X.; Chen, J.; Lalancette, R. A.; Marder, T. B.; Jäkle, F. *Angew. Chem. Int. Ed.* **2014**, *53*, 9761 –9765.

(2) Hoffend, C.; Schödel, F.; Bolte, M.; Lerner, H.-W.; Wagner, M. *Chem. Eur. J.* **2012**, *18*, 15394 – 15405.

(3) Bresner, C.; Haynes, C. J. E.; Addy, D. A.; Broomsgrove, A. E. J.; Fitzpatrick, P.; Vidovic, D.; Thompson, A. L.; Fallis, I. A.; Aldridge, S. *New J. Chem*., **2010**, *34*, 1652–1659.

(4) Sundararaman, A.; Venkatasubbaiah, K.; Victor, M.; Zakharov, L. N.; Rheingold, A. L.; Jäkle, F. *J. Am. Chem. Soc.* **2006**, *128*, 16554–16565.

(5) Galbraith, E.; Fyles, T. M.; Marken, F.; Davidson, M. G.; James, T. D. *Inorg. Chem*. **2008**, *47*, 6236-6244.

(6) Schmidt, H. C.; Reuter, L. G.; Hamacek, J.; Wenger, O. S. *J. Org. Chem.* **2011**, *76*, 9081−9085.

(7) Sundararaman, A.; Victor, M.; Varughese, R.; Jäkle, F. *J. Am. Chem. Soc.* **2005**, *127*, 13748–13749.

(8) Jäkle, F. *Coord. Chem. Rev*. **2006**, *250*, 1107–1121.

(9) Schlosser, M. *Pure Appl. Chem*. **1988**, *60*, 1627–1634.

(10) Fattuoni, C.; Usai, M.; Cabiddu, M. G.; Cadoni, E.; De Montis, S.; Sotgiu, F.; Cabiddu, S. *J. Heterocycl. Chem*. **2007**, *44*, 609–615.

(11) Kowalik, J.; Tolbert, L. M. *J. Org. Chem.* **2001,** *66,* 3229–3231.

(12) Cinar, M. E.; Ozturk, T. *Chem. Rev.* **2015***, 115,* 3036−3140.

(13) McCulloch, I.; Heeney, M.; Chabinyc, M. L.; DeLongchamp, D.; Kline, R. J.; Cölle, M.; Duffy, W.; Fischer, D.; Gundlach, D.; Hamadani, B. *Adv. Mater.* **2009**, *21*, 1091–1109.

(14) Yamamoto, T.; Takimiya, K. *J. Am. Chem. Soc.* **2007**, 129, 2224–2225.

(15) Mori, T.; Nishimura, T.; Yamamoto, T.; Doi, I.; Miyazaki, E.; Osaka, I.; Takimiya, K. *J. Am. Chem. Soc.* **2013**, *135*, 13900−13913.

(16) Takimiya, K.; Osaka, I.; Mori, T.; Nakano, M. *Acc. Chem. Res.* **2014**, *47*, 1493−1502.

(17) Moon, H.; Cho, H.; Kim, M.; Takimiya, K.; Yoo, S. *Adv. Mater*. **2014**, *26*, 3105–3110.

(18) Kuribara, K.; Wang, H.; Uchiyama, N.; Fukuda, K.; Yokota, T.; Zschieschang, U.; Jaye, C.; Fischer, D.; Klauk, H.; Yamamoto, T.; Takimiya, K.; Ikeda, M.; Kuwabara, H.; Sekitani, T.; Loo, Y.-L.; Someya, T. *Nat. Comms*. **2012**, *3*, 723.

(19) Okamoto, T.; Kudoh, K.; Wakamiya, A.; Yamaguchi, S. *Chem. Eur. J*. **2007**, *13*, 548 – 556.

(20) Lin, Y.; Fan, H.; Li, Y.; Zhan, X. *Adv. Mater*. **2012**, *24*, 3087–3106.

(21) Stangeland, E. L.; Sammakia, T. *J. Org. Chem.* **2004**, *69*, 2381–2385.

(22) Getmanenko, Y. A.; Tongwa, P.; Timofeeva, T. V.; Marder, S. R. *Org. Lett*. **2010**, *12*, 2136–2139.

(23) Mouri, K.; Saito, S.; Yamaguchi, S. *Angew. Chem. Int. Ed*. **2012**, *51*, 5971 –5975.

(24) Araneda, J. F.; Neue, B.; Piers, W. E.; Parvez, M. *Angew. Chem. Int. Ed.* **2012***, 51,* 8546 –8550.

(25) Araneda, J. F.; Piers, W. E.; Sgro, M. J.; Parvez, M. *Chem. Sci.* **2014**, *3*, 1461–1466.

(26) Saito, S.; Matsuo, K.; Yamaguchi, S. *J. Am. Chem. Soc*. **2012**, *134*, 9130−9133.

(27) Dou, C.; Saito, S.; Matsuo, K.; Hisaki, I.; Yamaguchi, S. *Angew. Chem. Int. Ed.* **2012***, 51,* 12206 –12210.

(28) Kushida, T.; Shuto, A.; Yoshio, M.; Kato, T.; Yamaguchi, S. *Angew. Chem. Int. Ed*. **2015,** *54*, 6922 –6925.

(29) Osumi, S.; Saito, S.; Dou, C.; Matsuo, K.; Kume, K.; Yoshikawa, H.; Awaga, K.; Yamaguchi, S. *Chem. Sci.* **2016,** *7,* 219–227.

(30) Hertz, V. M.; Bolte, M.; Lerner, H.-W.; Wagner, M. *Angew. Chem. Int. Ed.* **2015**, *54,* 8800 – 8804.

(31) Schickedanz, K.; Trageser, T.; Bolte, M.; Lerner, H.-W.; Wagner, M. *Chem. Commun.* **2015***, 51,* 15808–15810.

(32) Hertz, V. M.; Lerner, H.-W.; Wagner, M. *Org. Lett*. **2015**, *17*, 5240 – 5243.

(33) Wakamiya, A.; Mori, K.; Araki, T.; Yamaguchi, S. *J. Am. Chem. Soc.* **2009**, *131*, 10850 –10851.

(34) Hübner, A.; Bolte, M.; Lerner, H.-W.; Wagner, M. *Angew. Chem. Int. Ed*. **2014**, *53*, 10408 – 10411.

(35) O'Connor, M. J.; Yelle, R. B.; Zakharov, L. N.; Haley, M. M. *J. Org. Chem.* **2008**, *73*, 4424.

(36) Zhang, D.; Tessier, C. A.; Youngs, W. J. *Chem. Mater*. **1999**, *11*, 3050–3057.

Appendix 1. Supporting Information for Chapter 2

List of Figures

List of Tables

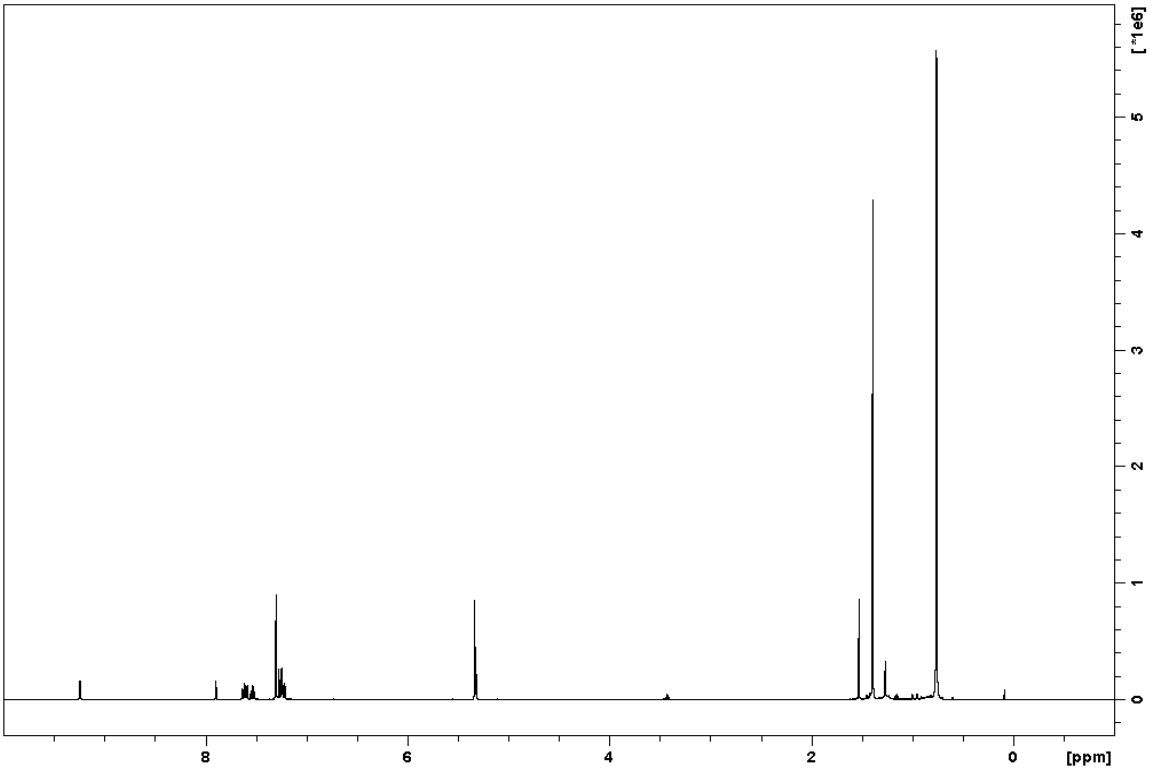

Figure A1.1. ^{1}H NMR (400 MHz, CD_2Cl_2) spectrum for **2a**.

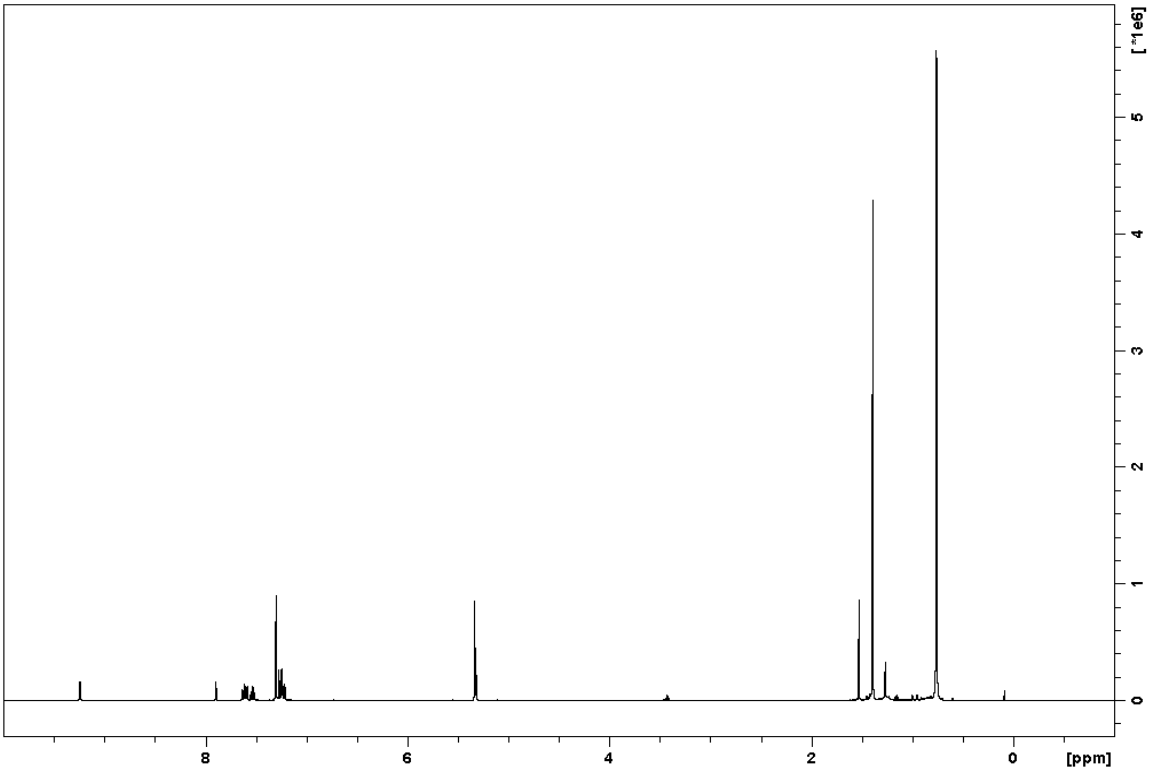

Figure A1.2. ^{1}H NMR (400 MHz, CD_2Cl_2) spectrum for **2b**.

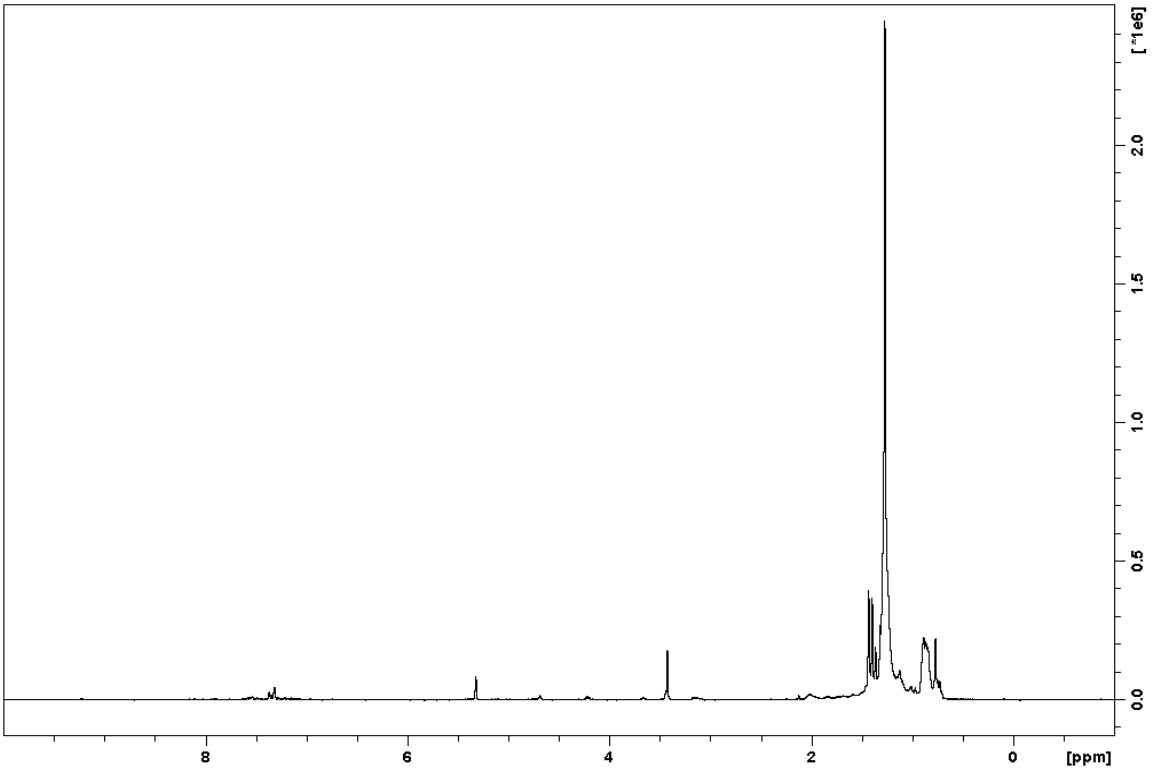

Figure A1.3. ^{1}H NMR (400 MHz, CD_2Cl_2) spectrum for **2c**.

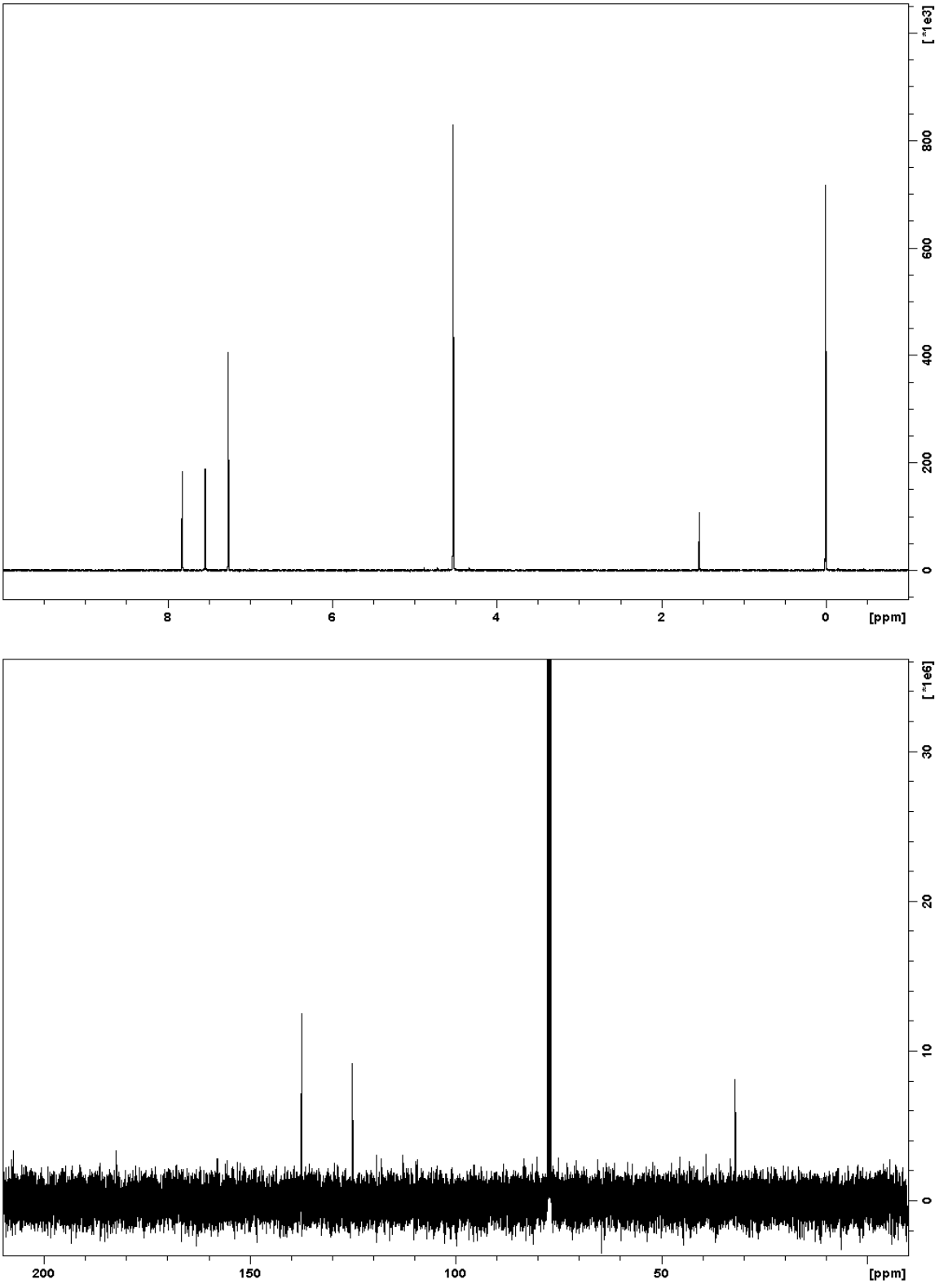

Figure A1.4. ^{1}H (400 MHz, $CDCl_3$) and ^{13}C NMR (100 MHz, $CDCl_3$) spectra for **4**.

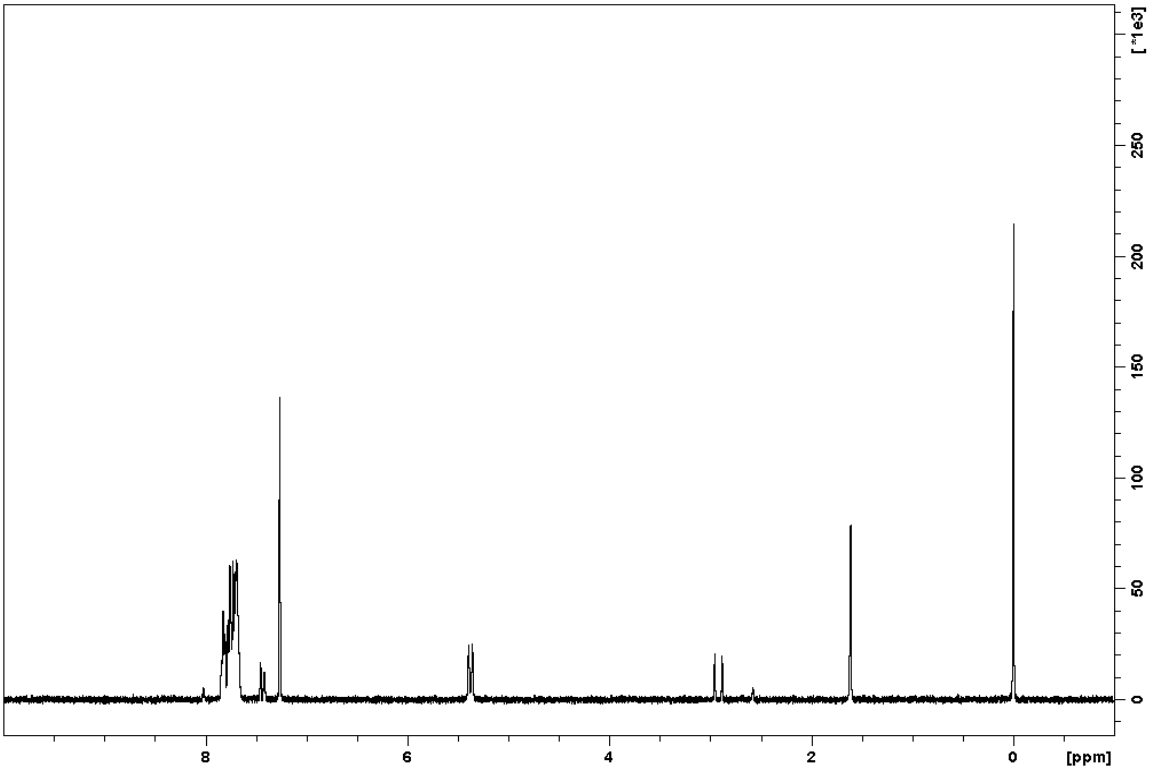

Figure A1.5. ^{1}H NMR (400 MHz, $CDCl_3$) spectrum for **5**.

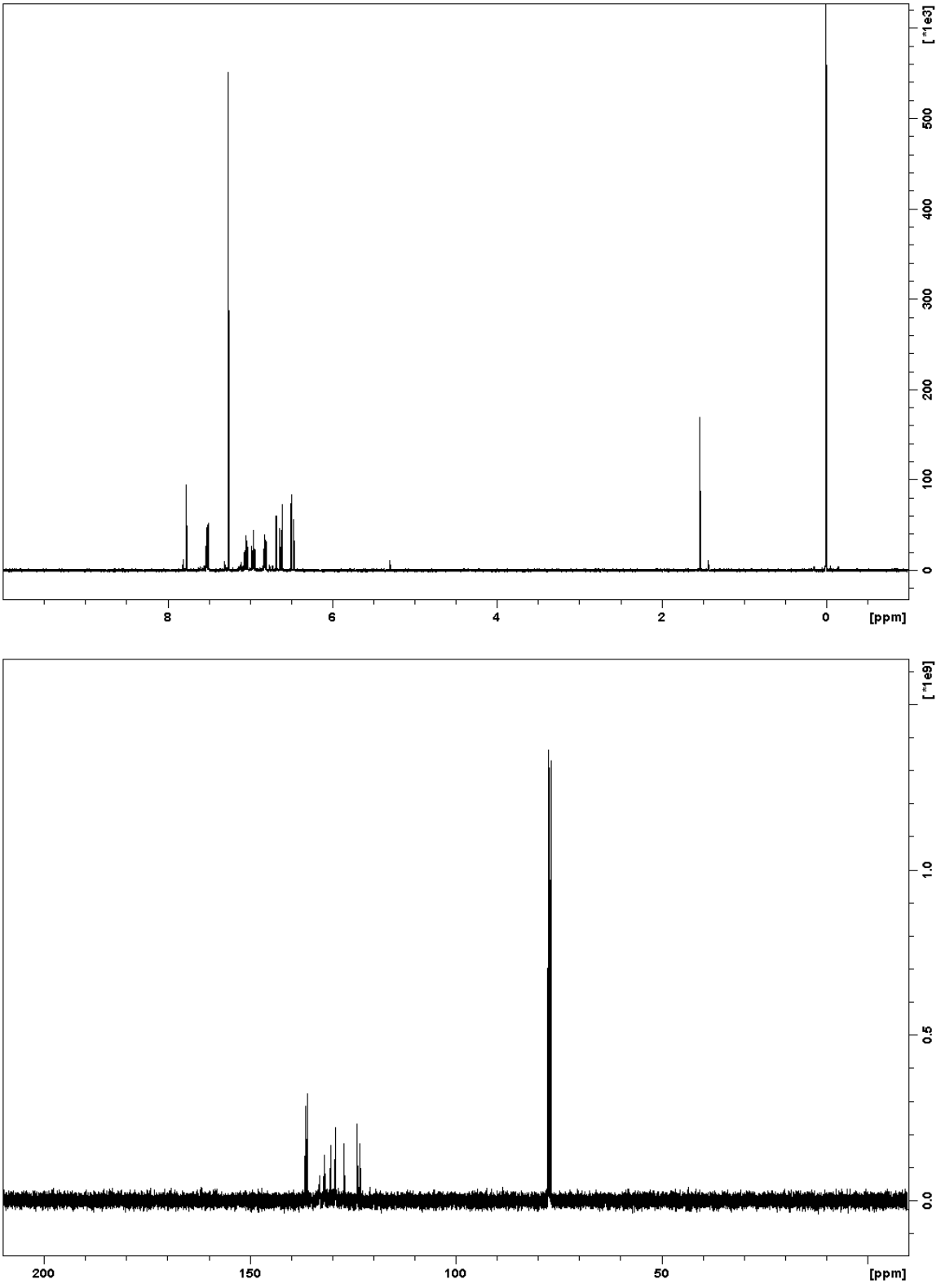

Figure A1.6. ^{1}H (400 MHz, $CDCl_3$) and ^{13}C NMR (100 MHz, $CDCl_3$) spectra for **7a**.

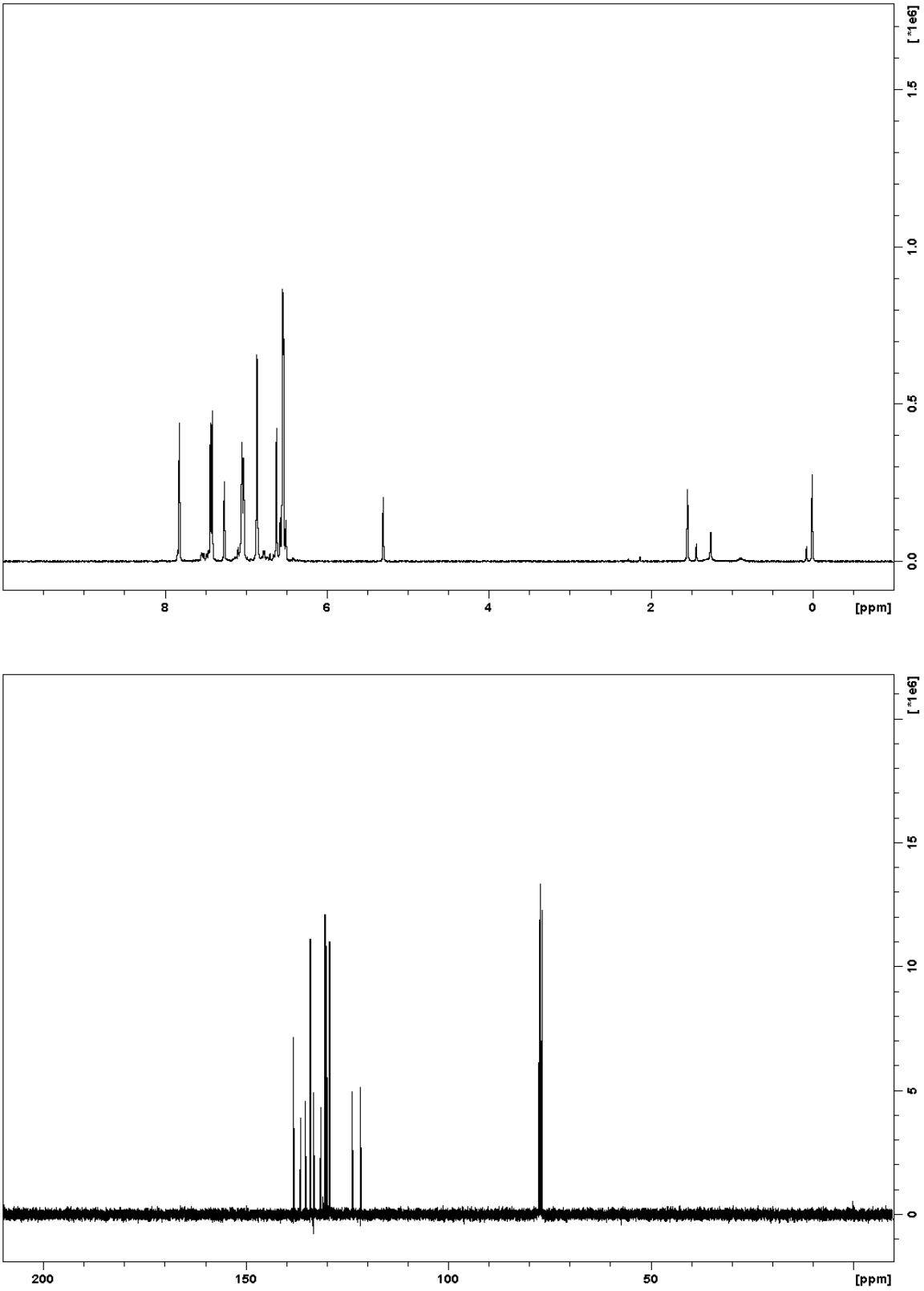

Figure A1.7. ^{1}H (400 MHz, $CDCl_3$) and ^{13}C NMR (100 MHz, $CDCl_3$) spectra for **7b**.

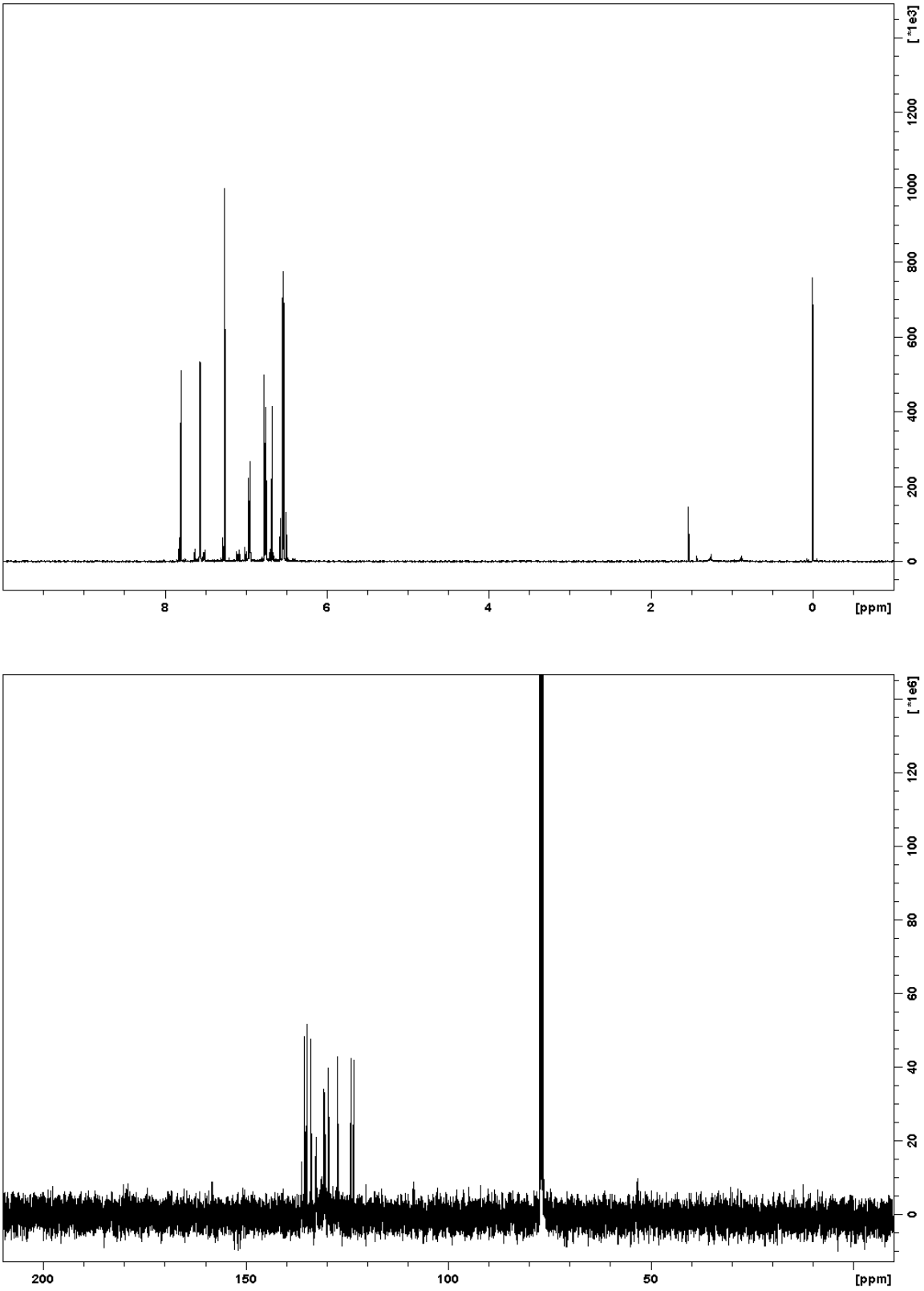

Figure A1.8. ^{1}H (400 MHz, $CDCl_3$) and ^{13}C NMR (100 MHz, $CDCl_3$) spectra for **7c**.

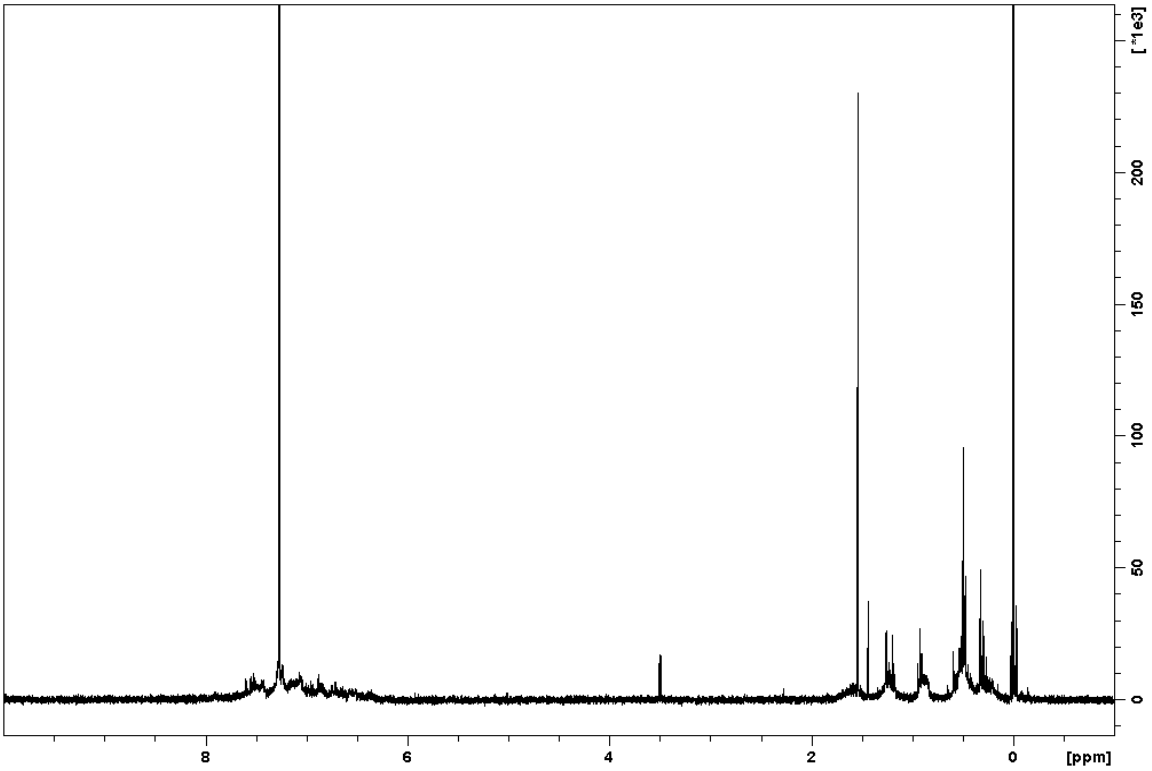

Figure A1.9. ^{1}H (400 MHz, $CDCl_3$) and ^{13}C NMR (100 MHz, $CDCl_3$) spectra for **8a**.

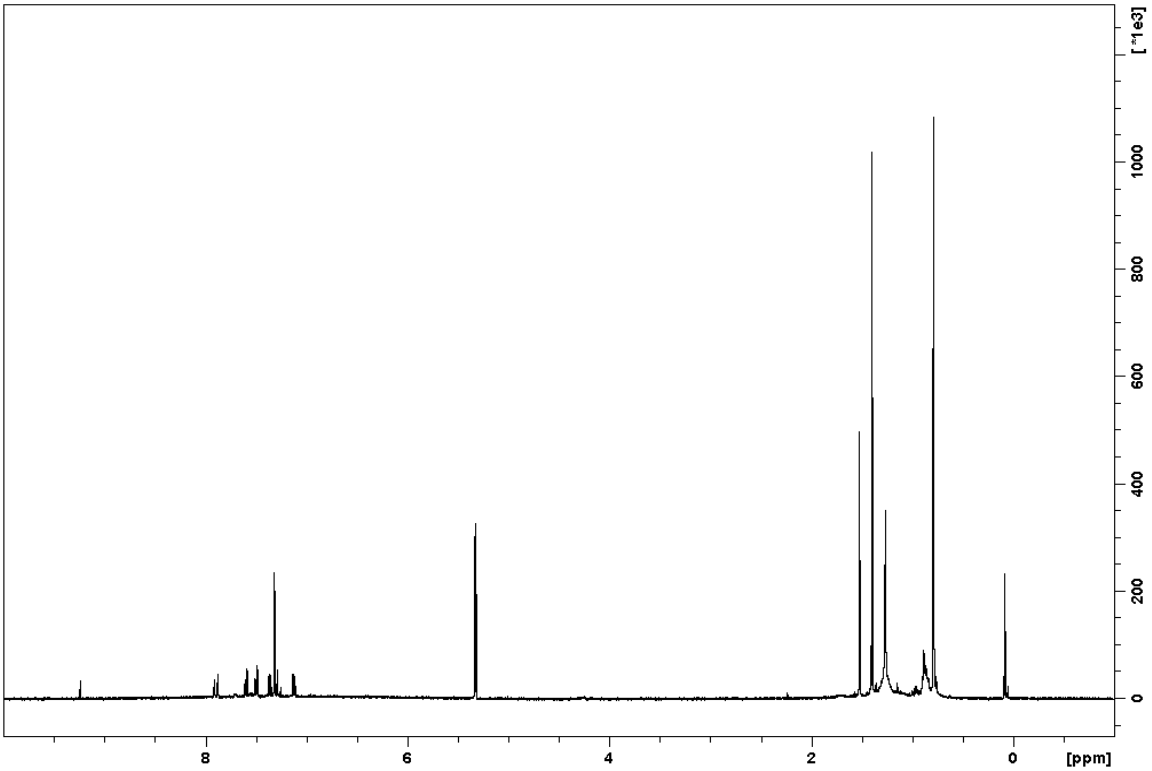

Figure A1.10. ^{1}H (400 MHz, CD_2Cl_2) spectrum for **9**.

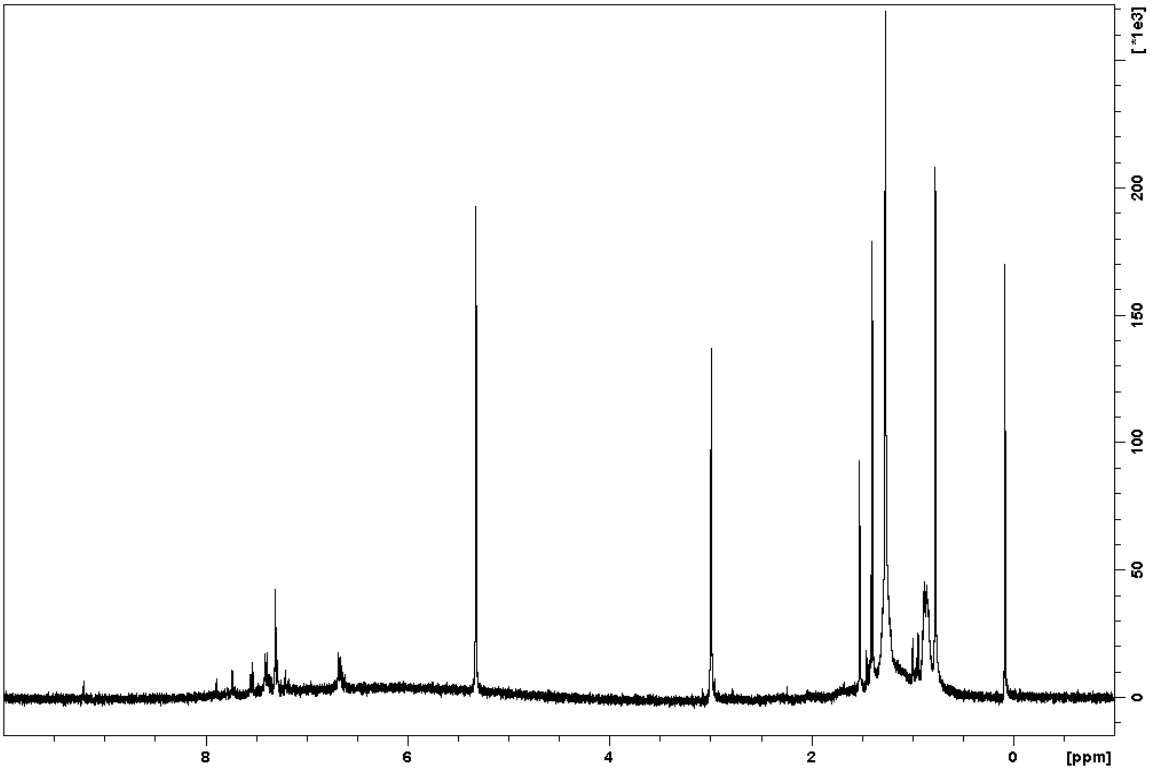

Figure A1.11. ^{1}H (400 MHz, CD_2Cl_2) spectrum for **10**.

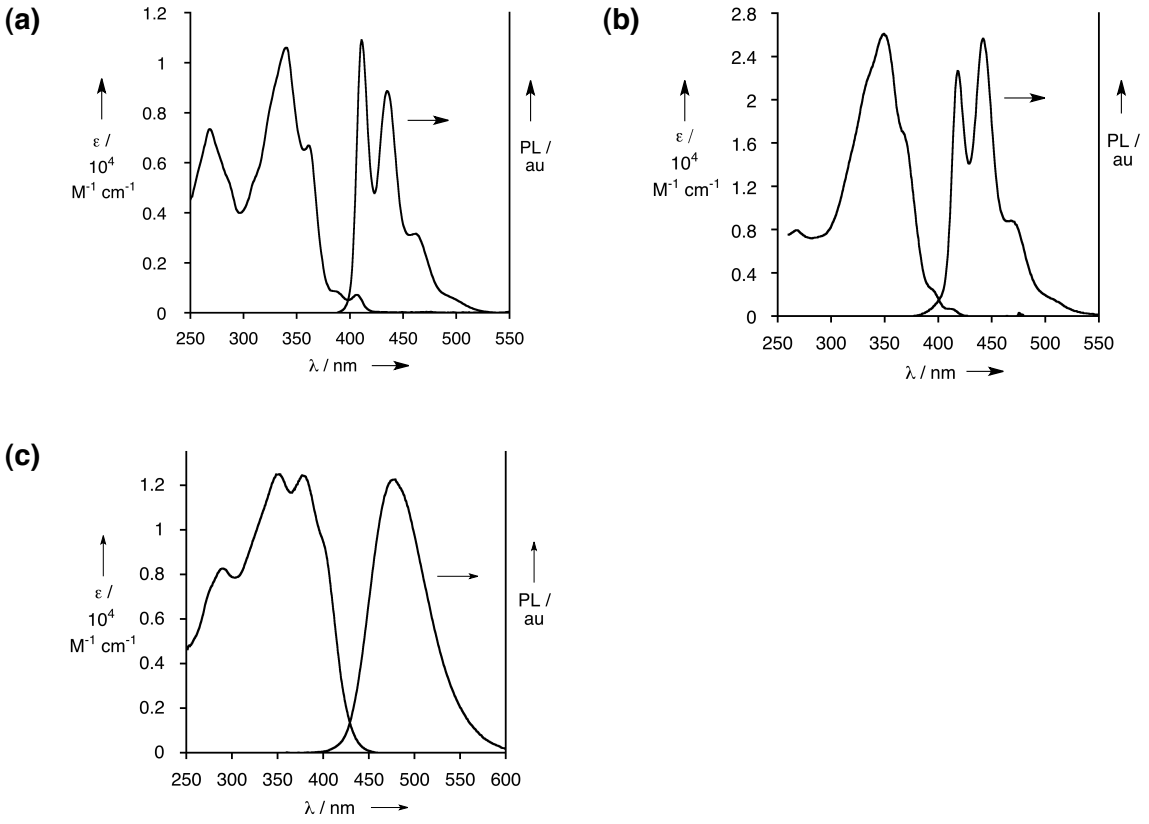

Figure A1.12. UV-vis and PL spectra for (a) **2b**, (b) **9**, and (c) **10** acquired in $CHCl_3$ at room temperature.

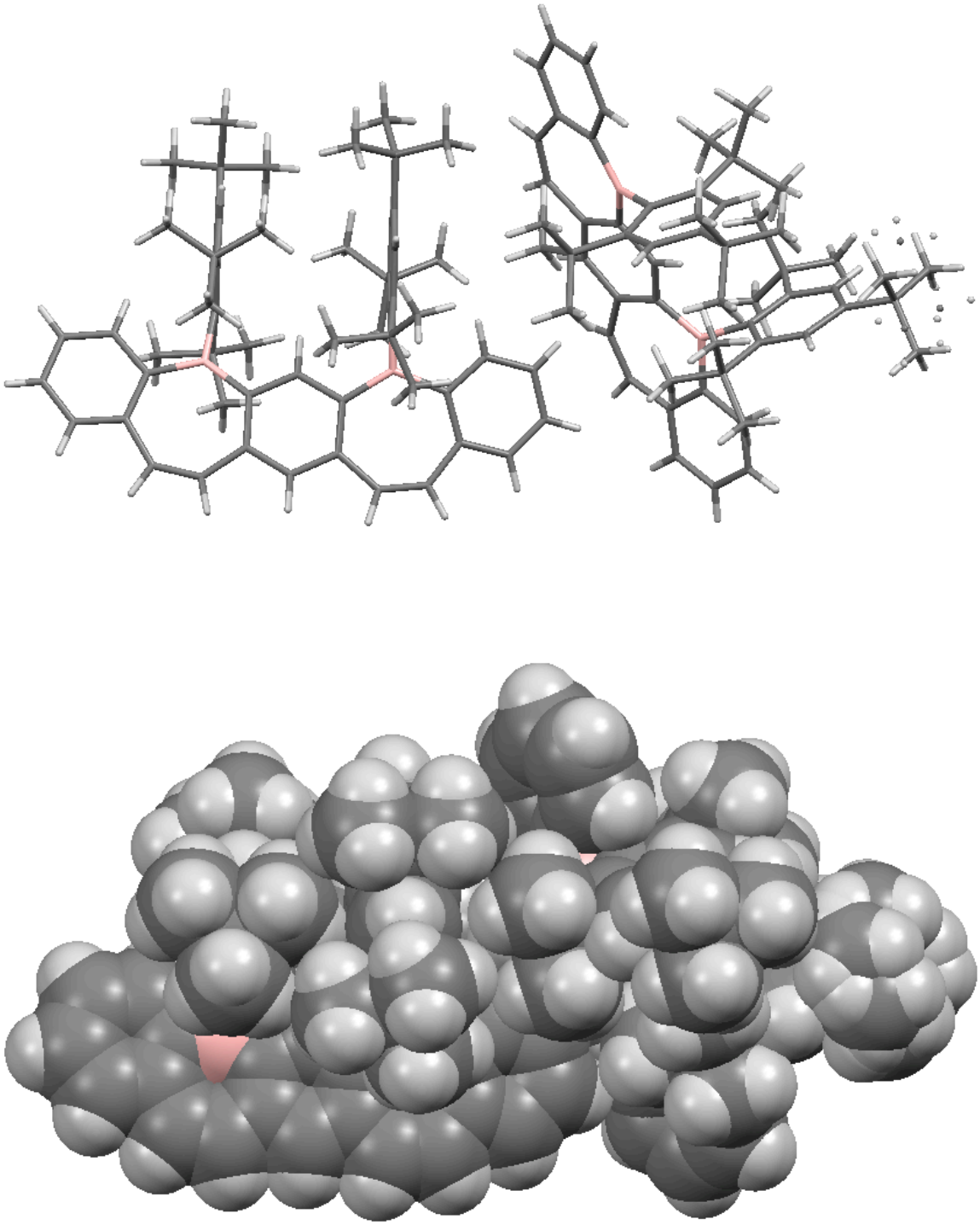

Figure A1.13. Asymmetric unit of the unit cell for the crystal structure of **2a** in capped stick (top) and space-filling representations (bottom).

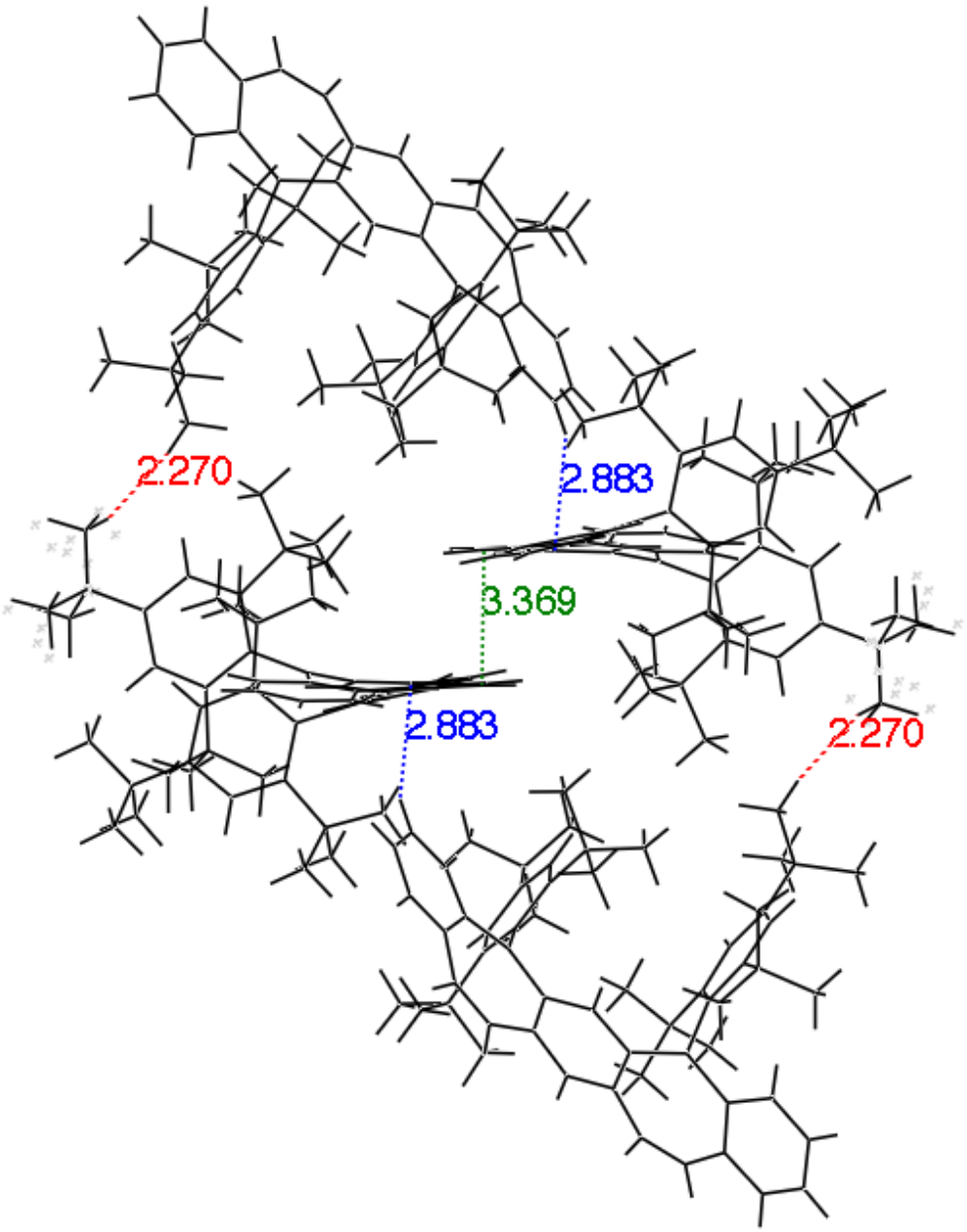

Figure A1.14. Wireframe depiction of solid-state packing motif for **2a**, illustrating intermolecular close-contacts (in Å). Green: C-C face-to-face interactions. Blue: C-H edge-to-face interactions. Red: *t*-Bu – *t*-Bu interactions.

Table A1.1. Atomic coordinates for the X-ray crystal structure of **2a**.

Number	Label	Xfrac + ESD	Yfrac + ESD	Zfrac + ESD
1	C1A	0.89383(12)	0.16090(9)	0.15120(9)
2	H1A	0.8396	0.1849	0.1416
3	C2A	0.95770(12)	0.14269(9)	0.09812(9)
4	C3A	0.99664(13)	0.14946(9)	-0.03718(10)
5	C4A	0.96458(15)	0.17751(11)	-0.09169(11)
6	H4A	0.9216	0.2139	-0.0805
7	C5A	0.99220(17)	0.15496(12)	-0.16072(12)
8	H5A	0.9671	0.1748	-0.1958
9	C6A	1.05612(17)	0.10379(12)	-0.17756(12)
10	H6A	1.0746	0.0868	-0.2248
11	C7A	1.09324(15)	0.07731(11)	-0.12519(11)
12	H7A	1.1394	0.0432	-0.1368
13	C8A	1.06559(13)	0.09872(10)	-0.05520(10)
14	C9A	1.11435(13)	0.06796(10)	-0.00586(11)
15	H9A	1.1647	0.0401	-0.0252
16	C10A	1.10302(13)	0.07070(10)	0.06152(11)
17	H10A	1.1506	0.0478	0.0815
18	C11A	1.03328(12)	0.10135(9)	0.11060(10)
19	C12A	1.04479(13)	0.08928(9)	0.17617(10)
20	H12A	1.097	0.0631	0.1846
21	C13A	0.98531(13)	0.11277(9)	0.23052(10)
22	C14A	1.01614(13)	0.09870(10)	0.29647(11)
23	H14A	1.0652	0.0668	0.2917
24	C15A	0.98900(14)	0.12184(11)	0.36266(11)
25	H15A	1.027	0.1068	0.3967
26	C16A	0.91308(13)	0.16542(10)	0.39319(10)
27	C17A	0.91852(14)	0.18723(11)	0.46851(10)
28	H17A	0.9719	0.1754	0.4952
29	C18A	0.84925(15)	0.22526(11)	0.50524(10)
30	H18A	0.8561	0.2408	0.5566
31	C19A	0.76946(15)	0.24064(10)	0.46657(10)
32	H19A	0.7197	0.2655	0.4909
33	C20A	0.76292(14)	0.21948(10)	0.39217(9)
34	H20A	0.707	0.2296	0.3664
35	C21A	0.83445(12)	0.18380(9)	0.35250(9)
36	C22A	0.90194(12)	0.14727(9)	0.21698(9)
37	C23A	0.89267(12)	0.24448(9)	0.04360(9)

38	C24A	0.94748(12)	0.31746(9)	0.07174(9)
39	C25A	0.90138(12)	0.37639(9)	0.06725(10)
40	H25A	0.94	0.4241	0.0841
41	C26A	0.80183(12)	0.36936(10)	0.03940(10)
42	C27A	0.74904(12)	0.29935(10)	0.01399(9)
43	H27A	0.6804	0.2931	-0.0046
44	C28A	0.79139(12)	0.23676(9)	0.01418(9)
45	C29A	1.06021(12)	0.33851(9)	0.10319(10)
46	C30A	1.10702(12)	0.28083(10)	0.12682(11)
47	H30A	1.0697	0.2687	0.1625
48	H30B	1.1765	0.3004	0.1485
49	H30C	1.105	0.2363	0.0847
50	C31A	1.11761(14)	0.35314(12)	0.04530(12)
51	H31A	1.1087	0.3082	0.0026
52	H31B	1.1887	0.3678	0.0644
53	H31C	1.0923	0.3928	0.0317
54	C32A	1.07511(14)	0.40865(10)	0.17079(11)
55	H32A	1.063	0.451	0.1563
56	H32B	1.1436	0.4171	0.1954
57	H32C	1.0282	0.4025	0.2038
58	C33A	0.75668(14)	0.43816(11)	0.03867(11)
59	C34A	0.81192(18)	0.47454(14)	-0.00731(15)
60	H34A	0.7822	0.518	-0.0085
61	H34B	0.8068	0.4394	-0.0567
62	H34C	0.8824	0.4896	0.0137
63	C35A	0.64632(15)	0.41887(12)	0.00717(12)
64	H35A	0.6101	0.3938	0.0351
65	H35B	0.6391	0.3863	-0.0434
66	H35C	0.619	0.4641	0.0096
67	C36A	0.76550(17)	0.49253(11)	0.11602(12)
68	H36A	0.7282	0.4695	0.1451
69	H36B	0.738	0.5369	0.1152
70	H36C	0.8359	0.506	0.1373
71	C37A	0.71913(13)	0.16307(10)	-0.02258(10)
72	C38A	0.76151(14)	0.09239(10)	-0.02687(10)
73	H38A	0.7829	0.093	0.0221
74	H38B	0.8188	0.0891	-0.0537
75	H38C	0.71	0.0497	-0.0518
76	C39A	0.68411(15)	0.15645(12)	-0.10116(10)
77	H39A	0.7418	0.1554	-0.1274
78	H39B	0.6512	0.1989	-0.1013
79	H39C	0.637	0.1109	-0.1248
80	C40A	0.62945(14)	0.16413(11)	0.01897(11)

81	H40A	0.5816	0.1192	-0.0055
82	H40B	0.5973	0.2073	0.0206
83	H40C	0.6521	0.1666	0.0684
84	C41A	0.71510(12)	0.18325(9)	0.23568(8)
85	C42A	0.63480(12)	0.12293(9)	0.20592(9)
86	C43A	0.54187(12)	0.13587(9)	0.18140(9)
87	H43A	0.49	0.095	0.1615
88	C44A	0.52020(12)	0.20482(10)	0.18419(9)
89	C45A	0.59766(12)	0.26265(10)	0.21421(9)
90	H45A	0.5848	0.3109	0.2183
91	C46A	0.69404(12)	0.25417(9)	0.23896(9)
92	C47A	0.64512(12)	0.04103(9)	0.19278(9)
93	C48A	0.72214(14)	0.02866(10)	0.24721(10)
94	H48A	0.7213	-0.0244	0.2367
95	H48B	0.706	0.0512	0.2962
96	H48C	0.7886	0.0512	0.2437
97	C49A	0.54696(14)	-0.00402(10)	0.19585(12)
98	H49A	0.4975	-0.007	0.1551
99	H49B	0.5221	0.02	0.2415
100	H49C	0.5585	-0.0538	0.1929
101	C50A	0.67291(15)	0.00884(11)	0.11620(10)
102	H50A	0.7361	0.0363	0.113
103	H50B	0.6202	0.0128	0.0809
104	H50C	0.6802	-0.0431	0.1059
105	C51A	0.41573(13)	0.21512(11)	0.15581(10)
106	C52A	0.38138(15)	0.15886(15)	0.07881(12)
107	H52A	0.315	0.1661	0.0609
108	H52B	0.3785	0.1087	0.0802
109	H52C	0.4288	0.1661	0.0465
110	C53A	0.34025(14)	0.20075(13)	0.20390(12)
111	H53A	0.3598	0.2356	0.2534
112	H53B	0.3387	0.1502	0.2041
113	H53C	0.2739	0.2072	0.1851
114	C54A	0.41363(16)	0.29112(14)	0.15149(17)
115	H54A	0.465	0.3014	0.1232
116	H54B	0.4266	0.3278	0.2004
117	H54C	0.3479	0.2935	0.1281
118	C55A	0.76747(13)	0.32785(9)	0.26971(10)
119	C56A	0.87720(13)	0.32194(10)	0.28899(10)
120	H56A	0.9022	0.2916	0.2457
121	H56B	0.8831	0.2991	0.3264
122	H56C	0.9165	0.3713	0.3072
123	C57A	0.73173(15)	0.37841(11)	0.33729(11)

124	H57A	0.7734	0.4268	0.354
125	H57B	0.7368	0.3567	0.3756
126	H57C	0.6621	0.384	0.3255
127	C58A	0.76687(14)	0.36589(11)	0.21284(11)
128	H58A	0.7854	0.3329	0.1681
129	H58B	0.8149	0.4114	0.2311
130	H58C	0.6999	0.3776	0.203
131	B1A	0.95014(14)	0.17561(11)	0.03546(11)
132	B2A	0.82062(14)	0.17008(10)	0.26856(11)
133	C1B	0.53643(12)	0.33542(9)	0.58530(9)
134	H1B	0.4958	0.3058	0.6048
135	C2B	0.49351(12)	0.34639(9)	0.52253(9)
136	C3B	0.31568(13)	0.31899(9)	0.42552(9)
137	C4B	0.21805(13)	0.27968(10)	0.40648(9)
138	H4B	0.2014	0.2428	0.427
139	C5B	0.14540(14)	0.29158(10)	0.35980(10)
140	H5B	0.0805	0.2638	0.3491
141	C6B	0.16817(14)	0.34453(10)	0.32864(10)
142	H6B	0.1184	0.3547	0.2977
143	C7B	0.26353(14)	0.38217(10)	0.34290(10)
144	H7B	0.2794	0.417	0.3198
145	C8B	0.33865(13)	0.37079(9)	0.39065(9)
146	C9B	0.43609(13)	0.41267(9)	0.39714(9)
147	H9B	0.4389	0.4395	0.3648
148	C10B	0.52297(13)	0.42149(9)	0.43912(9)
149	H10B	0.5755	0.4511	0.4285
150	C11B	0.55347(13)	0.39511(9)	0.49755(9)
151	C12B	0.65120(13)	0.42185(9)	0.53159(9)
152	H12B	0.6913	0.4527	0.513
153	C13B	0.69435(12)	0.40668(9)	0.59089(9)
154	C14B	0.79940(13)	0.43716(10)	0.61513(10)
155	H14B	0.8241	0.4695	0.5915
156	C15B	0.86825(13)	0.42885(10)	0.66389(10)
157	H15B	0.9328	0.4538	0.6652
158	C16B	0.86489(13)	0.38984(10)	0.71500(10)
159	C17B	0.95818(14)	0.38967(11)	0.75276(11)
160	H17B	1.017	0.4112	0.7407
161	C18B	0.96664(15)	0.35943(12)	0.80627(12)
162	H18B	1.0305	0.359	0.83
163	C19B	0.88139(16)	0.32961(12)	0.82530(12)
164	H19B	0.886	0.3095	0.8631
165	C20B	0.78940(14)	0.32910(10)	0.78901(10)
166	H20B	0.7316	0.3087	0.8032

167	C21B	0.77681(13)	0.35731(9)	0.73203(9)
168	C22B	0.63429(12)	0.36439(9)	0.62211(9)
169	C23B	0.34310(12)	0.23436(9)	0.50600(9)
170	C24B	0.36000(12)	0.16190(9)	0.46526(9)
171	C25B	0.31294(13)	0.10176(10)	0.47943(10)
172	H25B	0.3235	0.0539	0.4509
173	C26B	0.25200(13)	0.10737(10)	0.53224(10)
174	C27B	0.23616(13)	0.17743(11)	0.57107(10)
175	H27B	0.1945	0.1831	0.6079
176	C28B	0.27829(12)	0.24095(10)	0.55908(9)
177	C29B	0.42154(13)	0.14035(10)	0.40129(10)
178	C30B	0.48337(14)	0.20340(10)	0.38735(10)
179	H30D	0.5334	0.2299	0.4297
180	H30E	0.4395	0.2373	0.3786
181	H30F	0.5169	0.1835	0.3449
182	C31B	0.49721(16)	0.09073(11)	0.41390(11)
183	H31D	0.541	0.1166	0.4597
184	H31E	0.5374	0.079	0.3741
185	H31F	0.4613	0.045	0.4159
186	C32B	0.34823(15)	0.09779(11)	0.33199(10)
187	H32D	0.3854	0.0826	0.2907
188	H32E	0.3008	0.1297	0.3236
189	H32F	0.3118	0.0541	0.3376
190	C33B	0.20301(15)	0.03729(11)	0.54313(12)
191	C34B	0.28155(16)	-0.01098(11)	0.55315(13)
192	H34D	0.3203	-0.0211	0.5125
193	H34E	0.2481	-0.0576	0.5548
194	H34F	0.3263	0.0149	0.5985
195	C35B	0.12978(18)	-0.00782(13)	0.47416(14)
196	H35D	0.0795	0.0221	0.4658
197	H35E	0.0968	-0.0524	0.4803
198	H35F	0.1666	-0.0218	0.4326
199	C36B	0.14693(18)	0.05447(14)	0.60753(14)
200	H36D	0.1934	0.082	0.6516
201	H36E	0.1156	0.0084	0.6115
202	H36F	0.0954	0.0842	0.6013
203	C37B	0.24493(13)	0.31337(10)	0.60709(10)
204	C38B	0.27656(16)	0.32351(13)	0.68673(11)
205	H38D	0.3492	0.3263	0.6958
206	H38E	0.2441	0.2816	0.6976
207	H38F	0.2566	0.3691	0.7176
208	C39B	0.13047(14)	0.30631(12)	0.59278(12)
209	H39D	0.1087	0.3513	0.6235

210	H39E	0.1002	0.2639	0.6039
211	H39F	0.1097	0.2993	0.5418
212	C40B	0.28621(14)	0.38441(10)	0.59564(10)
213	H40D	0.2635	0.4264	0.6305
214	H40E	0.2623	0.3817	0.5463
215	H40F	0.3593	0.3907	0.6028
216	C41B	0.58150(12)	0.32765(9)	0.73655(9)
217	C42B	0.53992(12)	0.38295(9)	0.78819(9)
218	C43B	0.47381(12)	0.36233(9)	0.83027(9)
219	H43B	0.4461	0.3999	0.8638
220	C44B	0.44634(12)	0.28992(9)	0.82574(9)
221	C45B	0.48674(13)	0.23666(9)	0.77472(9)
222	H45B	0.4688	0.1865	0.7701
223	C46B	0.55203(13)	0.25269(9)	0.73003(9)
224	C47B	0.56022(12)	0.46689(9)	0.79939(9)
225	C48B	0.48920(14)	0.48264(10)	0.74296(11)
226	H48D	0.5016	0.5352	0.7493
227	H48E	0.42	0.4693	0.7493
228	H48F	0.5007	0.4535	0.6942
229	C49B	0.66731(14)	0.49413(10)	0.79284(11)
230	H49D	0.6804	0.471	0.7431
231	H49E	0.7138	0.4811	0.8261
232	H49F	0.6765	0.5478	0.8052
233	C50B	0.54133(17)	0.51459(10)	0.87417(10)
234	H50D	0.5606	0.5667	0.8807
235	H50E	0.581	0.5021	0.9114
236	H50F	0.4703	0.5055	0.8784
237	C51B	0.37392(14)	0.26920(10)	0.87358(10)
238	C52B	0.3387(4)	0.3320(2)	0.9215(3)
239	H52D	0.3958	0.3681	0.9508
240	H52E	0.2975	0.3161	0.9533
241	H52F	0.2986	0.3545	0.8929
242	C53B	0.4333(3)	0.23024(19)	0.91838(18)
243	H53D	0.4885	0.2657	0.9513
244	H53E	0.4601	0.1891	0.8854
245	H53F	0.3887	0.2115	0.9465
246	C54B	0.2904(3)	0.2104(2)	0.8229(2)
247	H54D	0.244	0.1944	0.8517
248	H54E	0.3193	0.1681	0.794
249	H54F	0.2544	0.2312	0.7907
250	C55B	0.58503(14)	0.18395(9)	0.67593(9)
251	C56B	0.49047(16)	0.13356(11)	0.62945(11)
252	H56D	0.4535	0.1607	0.6043

253	H56E	0.4482	0.1176	0.6607
254	H56F	0.5094	0.0903	0.5938
255	C57B	0.63915(16)	0.14073(11)	0.71711(10)
256	H57D	0.5955	0.1273	0.7489
257	H57E	0.7005	0.1715	0.7463
258	H57F	0.6559	0.0959	0.6824
259	C58B	0.65268(15)	0.19721(10)	0.62306(10)
260	H58D	0.6671	0.1499	0.5913
261	H58E	0.7152	0.2281	0.65
262	H58F	0.6193	0.2223	0.5938
263	B1B	0.38679(14)	0.30275(10)	0.48454(10)
264	B2B	0.66619(15)	0.35029(10)	0.69468(11)
265	C51'	0.37392(14)	0.26920(10)	0.87358(10)
266	C52'	0.3633(4)	0.1925(3)	0.8738(3)
267	H52G	0.3406	0.1582	0.8244
268	H52H	0.3143	0.1863	0.9054
269	H52I	0.4279	0.1824	0.8916
270	C53'	0.2628(3)	0.2828(3)	0.8505(3)
271	H53G	0.2379	0.2497	0.801
272	H53H	0.2643	0.3341	0.8527
273	H53I	0.2186	0.2728	0.8836
274	C54'	0.4010(5)	0.3216(3)	0.9552(3)
275	H54G	0.3501	0.3099	0.9833
276	H54H	0.4033	0.373	0.9578
277	H54I	0.4662	0.3143	0.975

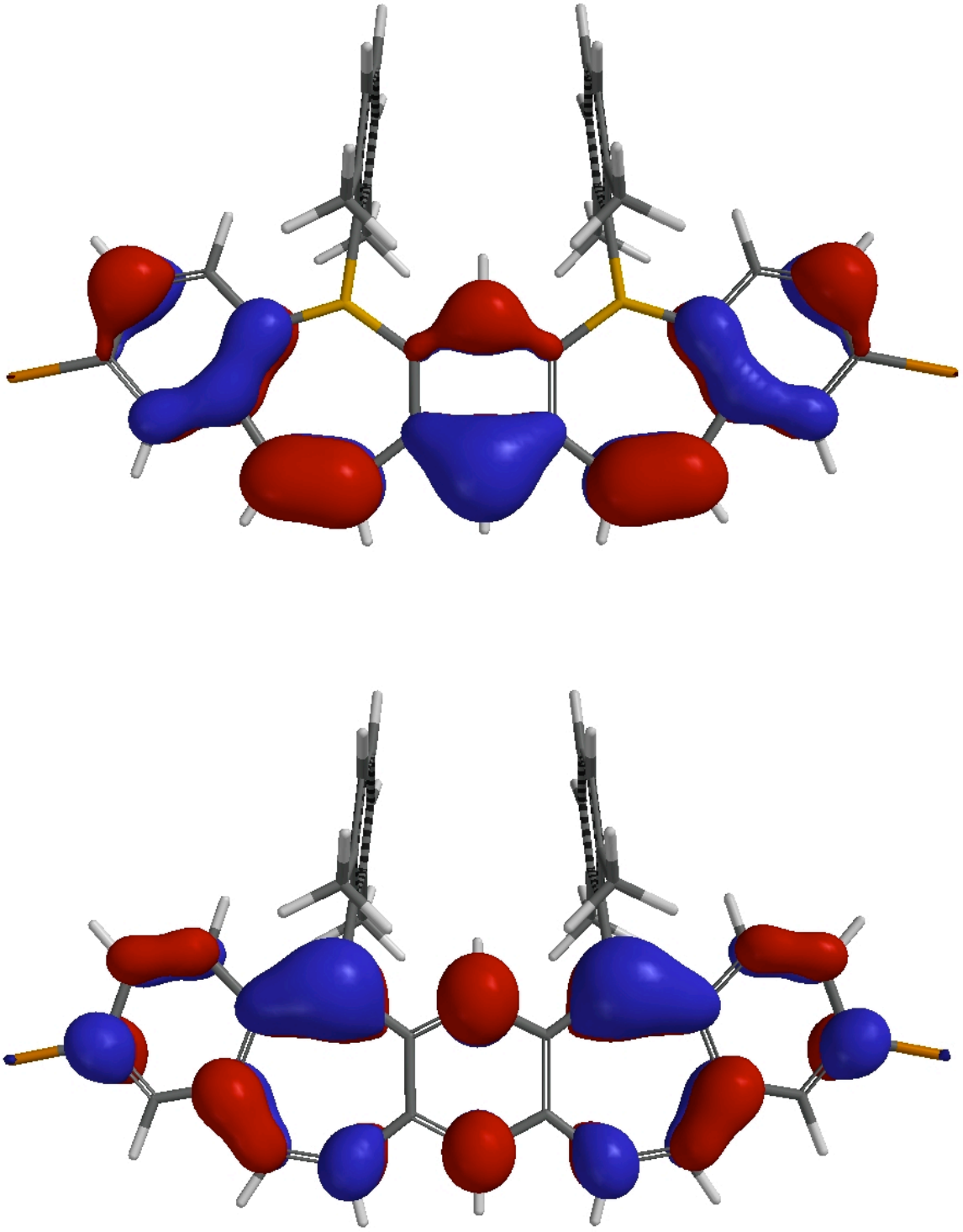

Figure A1.15. Calculated frontier molecular orbital surfaces for ***B*-(2,6-dimethylphenyl)-2b** (DFT; B3LYP/6-31G*). Top: HOMO. Bottom: LUMO.

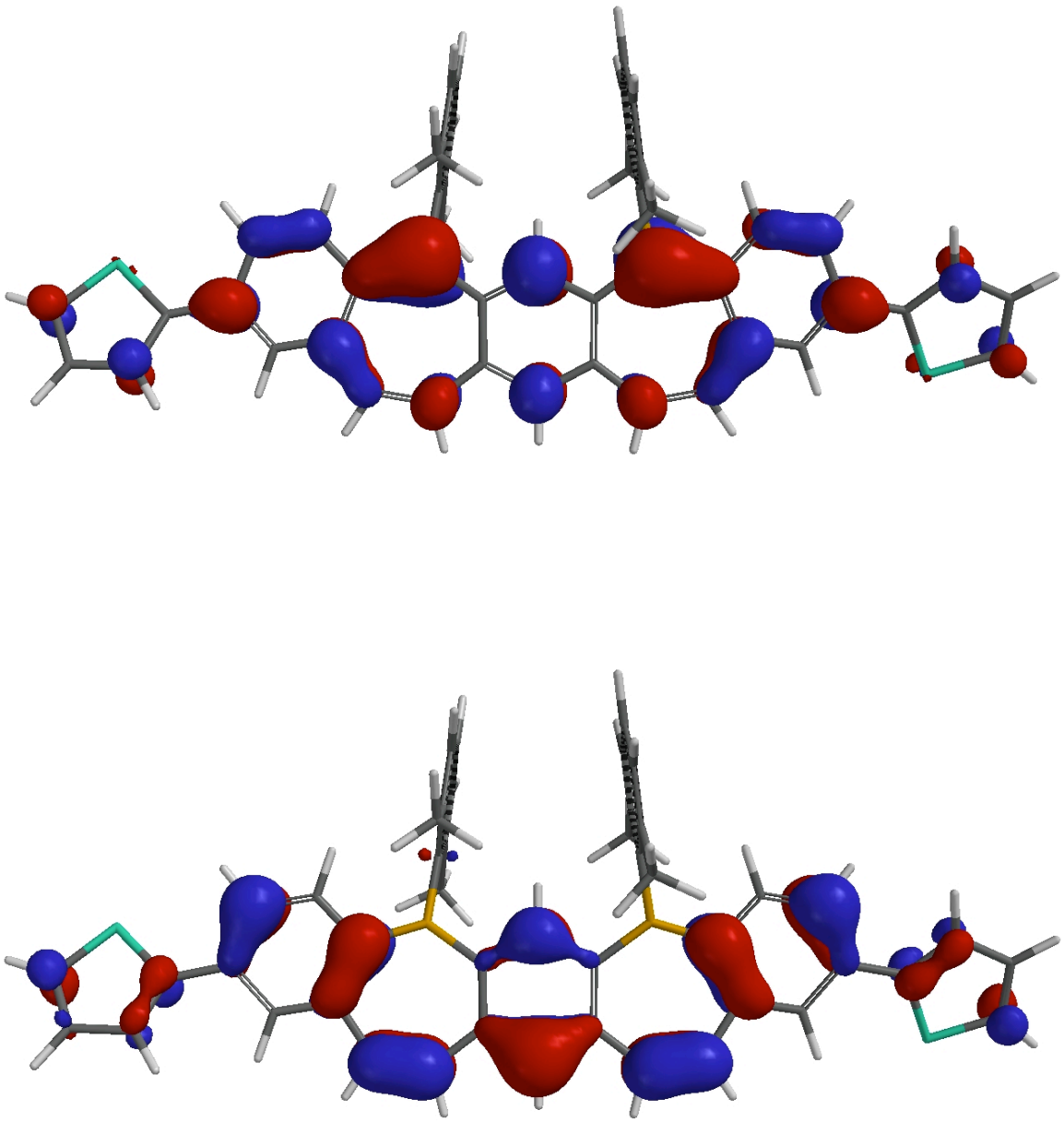

Figure A1.16. Calculated frontier molecular orbital surfaces for ***B*-(2,6-dimethylphenyl)-9** (DFT; B3LYP/6-31G*). Top: HOMO. Bottom: LUMO.

Table A1.2. Cartesian coordinates (in Å) for optimized geometries of *meta-B*-entacene compounds (***B-Ph*-2a**, **2a**, ***B*-(2,6-dimethylphenyl)-2b**, ***B*-(2,6-dimethyphenyl)-9**, and ***B*-(2,6-dimethyphenyl)-10**) calculated at the DFT (B3LYP/6-31G*) level of theory.

***B*-Ph-2a**

ATOM		X	Y	Z
1	C	0.011279	-0.740995	-4.029050
2	C	0.052227	-1.272124	-6.837165
3	C	0.008877	-2.082998	-4.524847
4	C	0.054303	0.045550	-6.373153
5	C	0.028938	-2.310689	-5.921054
6	C	-0.024608	-2.632521	-1.240508
7	C	-0.031388	-3.285744	0.000000
8	C	-0.024608	-2.632521	1.240508
9	C	-0.014352	-1.200625	1.263130
10	C	0.008877	-2.082998	4.524847
11	C	0.011279	-0.740995	4.029050
12	C	0.033308	0.287254	5.005790
13	C	0.028938	-2.310689	5.921054
14	C	0.052227	-1.272124	6.837165
15	C	0.054303	0.045550	6.373153
16	B	-0.005743	-0.289456	-2.528163
17	B	-0.005743	-0.289456	2.528163
18	H	0.071545	0.876507	-7.073141
19	H	0.068224	-1.485007	-7.902946
20	H	0.026286	-3.336871	-6.280383
21	H	-0.040259	-4.373520	0.000000
22	H	0.034286	1.316830	4.669717
23	H	0.071545	0.876507	7.073141
24	H	0.068224	-1.485007	7.902946
25	H	0.026286	-3.336871	6.280383
26	C	-0.028581	-3.515976	-2.388063
27	C	-0.014001	-3.290830	-3.723831
28	C	-0.014352	-1.200625	-1.263130
29	C	-0.011791	-0.566652	0.000000
30	C	-0.028581	-3.515976	2.388063
31	C	-0.014001	-3.290830	3.723831
32	H	-0.042984	-4.569860	2.113465
33	H	-0.018913	-4.198833	4.325787
34	H	-0.018913	-4.198833	-4.325787
35	H	-0.042984	-4.569860	-2.113465
36	H	-0.005982	0.515406	0.000000
37	C	0.033308	0.287254	-5.005790
38	C	-0.010881	1.284001	2.292343
39	C	-0.022604	4.103087	2.017729

40	C	-1.214569	2.008636	2.224871
41	C	1.186654	2.016731	2.205629
42	C	1.184691	3.406219	2.071195
43	C	-1.224115	3.398077	2.090256
44	C	-0.010881	1.284001	-2.292343
45	C	-0.022604	4.103087	-2.017729
46	C	-1.214569	2.008636	-2.224871
47	C	1.186654	2.016731	-2.205629
48	C	1.184691	3.406219	-2.071195
49	C	-1.224115	3.398077	-2.090256
50	H	2.142209	1.497189	2.252141
51	H	-2.165726	1.482626	2.286866
52	H	-2.165726	1.482626	-2.286866
53	H	0.034286	1.316830	-4.669717
54	H	2.142209	1.497189	-2.252141
55	H	2.127583	3.944314	-2.008461
56	H	-0.027110	5.185255	-1.915974
57	H	-2.171514	3.929767	-2.042688
58	H	-0.027110	5.185255	1.915974
59	H	-2.171514	3.929767	2.042688
60	H	2.127583	3.944314	2.008461

2a

ATOM		X	Y	Z
1	C	-0.507970	2.295978	4.056925
2	C	-1.150675	2.825433	6.798443
3	C	-0.844439	3.613468	4.497225
4	C	-0.798317	1.535396	6.395969
5	C	-1.161221	3.841545	5.857340
6	C	-0.391825	4.125446	1.234871
7	C	-0.286144	4.779800	0.000951
8	C	-0.101850	4.134464	-1.228125
9	C	-0.063556	2.705389	-1.253364
10	C	0.393989	3.658120	-4.490160
11	C	0.253681	2.309939	-4.036456
12	C	0.386997	1.308302	-5.030675
13	C	0.668589	3.917253	-5.853891
14	C	0.811020	2.901513	-6.784594
15	C	0.664330	1.577202	-6.366132
16	B	-0.165297	1.829930	2.580458
17	B	-0.036108	1.816175	-2.556687
18	H	-0.763847	0.721834	7.115747
19	H	-1.402063	3.035902	7.834754
20	H	-1.415666	4.852460	6.166460
21	H	-0.354878	5.865159	-0.003331
22	H	0.268544	0.272934	-4.737628

23	H	0.757892	0.759790	-7.076247
24	H	1.025471	3.136234	-7.823944
25	H	0.767585	4.951750	-6.173467
26	C	-0.634744	5.015037	2.354898
27	C	-0.846768	4.807530	3.674841
28	C	-0.253452	2.703436	1.270099
29	C	-0.121784	2.071619	0.010449
30	C	0.017115	5.038669	-2.356461
31	C	0.238314	4.848722	-3.677470
32	H	-0.063633	6.085155	-2.066253
33	H	0.309156	5.770190	-4.254162
34	H	-1.046383	5.715479	4.242552
35	H	-0.688870	6.060918	2.056063
36	H	-0.061776	0.987986	0.014369
37	C	-0.483435	1.297225	5.062968
38	C	-0.360240	0.250701	-2.442268
39	C	-0.951952	-2.559354	-2.614240
40	C	-1.704686	-0.211061	-2.645894
41	C	0.669614	-0.731775	-2.315671
42	C	0.339699	-2.096107	-2.397972
43	C	-1.947301	-1.588255	-2.725347
44	C	0.353311	0.318111	2.474688
45	C	1.289943	-2.396594	2.620825
46	C	-0.553823	-0.785207	2.347584
47	C	1.740511	0.024060	2.670692
48	C	2.155501	-1.316141	2.747154
49	C	-0.053920	-2.092330	2.415048
50	C	-2.112598	-0.716388	2.230792
51	C	2.895048	1.048722	2.940473
52	C	-2.972829	0.665146	-2.927421
53	C	2.209371	-0.476059	-2.190143
54	C	4.161328	0.680970	2.120094
55	C	3.250966	0.984991	4.448013
56	C	2.608422	2.520541	2.591482
57	C	1.750388	-3.862467	2.722013
58	C	3.271843	-3.988231	2.929986
59	C	1.381374	-4.613933	1.421463
60	C	1.044767	-4.540664	3.920563
61	C	-2.714804	0.663940	1.910534
62	C	-2.737439	-1.188099	3.569033
63	C	-2.607956	-1.660207	1.104278
64	C	-2.873509	2.160785	-2.573191
65	C	-4.193575	0.143918	-2.122717
66	C	-3.300958	0.561510	-4.439158
67	C	2.638635	0.971084	-1.895318
68	C	2.895925	-0.894004	-3.516675
69	C	2.799778	-1.337505	-1.043907

70	C	-1.301287	-4.050325	-2.772640
71	C	-0.063965	-4.960725	-2.656594
72	C	-2.313118	-4.470894	-1.681931
73	C	-1.930059	-4.282477	-4.166858
74	H	-1.235646	-3.989022	-4.962567
75	H	-2.853128	-3.708556	-4.301184
76	H	-2.174795	-5.343288	-4.303127
77	H	0.682184	-4.730938	-3.425778
78	H	0.417486	-4.876476	-1.675829
79	H	-0.361575	-6.007580	-2.788099
80	H	-2.580683	-5.528840	-1.795695
81	H	-3.236383	-3.884436	-1.734987
82	H	0.303441	-4.594416	1.230387
83	H	-1.888916	-4.332830	-0.681070
84	H	1.881759	-4.162796	0.557038
85	H	1.690551	-5.664542	1.486223
86	H	3.552381	-5.046660	2.981378
87	H	3.595496	-3.515571	3.864324
88	H	-0.044442	-4.537103	3.806956
89	H	1.285032	-4.025503	4.857919
90	H	1.366871	-5.585366	4.014554
91	H	3.834764	-3.537211	2.104820
92	H	-0.750093	-2.916882	2.325311
93	H	3.940750	0.658451	1.047843
94	H	3.201364	-1.516482	2.929203
95	H	4.594326	-0.284028	2.396669
96	H	2.287350	-1.144458	-0.097371
97	H	1.140313	-2.818927	-2.321887
98	H	2.742601	-2.411586	-1.244214
99	H	-2.960588	-1.924442	-2.908129
100	H	-4.505443	-0.864424	-2.407387
101	H	-3.986611	0.140818	-1.047645
102	H	-5.052807	0.802065	-2.298197
103	H	-3.448839	-0.479039	-4.747033
104	H	-4.220733	1.115419	-4.666709
105	H	-2.494031	0.980434	-5.049548
106	H	-2.103613	2.690930	-3.139432
107	H	-3.825373	2.644052	-2.825989
108	H	-2.397350	1.041077	0.936014
109	H	-3.807854	0.572327	1.888961
110	H	-2.485139	1.420154	2.666604
111	H	4.937207	1.437018	2.289733
112	H	-2.433190	-2.717000	1.325555
113	H	-3.690579	-1.539774	0.975259
114	H	-2.124695	-1.432383	0.149805
115	H	-2.378529	-2.182090	3.855785
116	H	-3.829427	-1.239421	3.474155

117	H	-2.505129	-0.496545	4.385227
118	H	-0.200907	0.290778	4.781095
119	H	3.540534	-0.027768	4.747651
120	H	2.401575	1.290814	5.068144
121	H	3.862071	-1.097854	-0.912237
122	H	4.090924	1.656147	4.669038
123	H	1.788776	2.949406	3.173320
124	H	3.496941	3.117362	2.831357
125	H	2.394837	2.660822	1.529144
126	H	-2.693480	2.320877	-1.507657
127	H	2.287617	1.319332	-0.921502
128	H	2.304634	1.677561	-2.659511
129	H	3.734252	1.020023	-1.888219
130	H	2.595015	-0.243718	-4.344604
131	H	2.652344	-1.925096	-3.792826
132	H	3.986197	-0.821872	-3.414146

***B*-(2,6-dimethylphenyl)-2b**

ATOM		X	Y	Z
1	C	4.022968	-0.921121	0.006989
2	C	6.814028	-1.458740	0.026442
3	C	4.514346	-2.263904	0.006358
4	C	6.372883	-0.135062	0.027410
5	C	5.907943	-2.504147	0.015811
6	C	1.229267	-2.801163	-0.008332
7	C	-0.013541	-3.450710	-0.010390
8	C	-1.251269	-2.791541	-0.007505
9	C	-1.268562	-1.359927	-0.004121
10	C	-4.532157	-2.228442	0.005152
11	C	-4.030062	-0.889703	0.006367
12	C	-5.004058	0.140727	0.014678
13	C	-5.927685	-2.457682	0.012003
14	C	-6.825437	-1.405062	0.020296
15	C	-6.373640	-0.084993	0.021818
16	B	2.525088	-0.455340	-0.001979
17	B	-2.528711	-0.435772	-0.000212
18	H	7.084867	0.683389	0.035545
19	H	6.275203	-3.525326	0.014994
20	H	-0.017764	-4.538405	-0.013540
21	H	-4.662318	1.169551	0.015750
22	H	-7.079046	0.739121	0.028233
23	H	-6.302847	-3.475996	0.010863
24	C	2.373925	-3.689027	-0.010170
25	C	3.710418	-3.471132	-0.003928
26	C	1.257754	-1.369724	-0.005053
27	C	-0.002946	-0.732081	-0.004199

28	C	-2.402931	-3.670287	-0.008491
29	C	-3.737666	-3.441899	-0.003094
30	H	-2.132087	-4.725054	-0.013624
31	H	-4.343359	-4.346870	-0.004759
32	H	4.309022	-4.380803	-0.006182
33	H	2.094775	-4.741638	-0.016430
34	H	0.001407	0.351541	-0.003254
35	C	5.005143	0.101542	0.017369
36	C	-2.284610	1.138336	-0.002291
37	C	-1.955417	3.936603	-0.006706
38	C	-2.201368	1.849362	-1.221811
39	C	-2.194675	1.852418	1.214965
40	C	-2.031230	3.242216	1.198202
41	C	-2.037892	3.239199	-1.209422
42	C	2.292949	1.120516	-0.007179
43	C	1.984762	3.921174	-0.017817
44	C	2.215501	1.829514	-1.228297
45	C	2.208524	1.837976	1.208461
46	C	2.055479	3.228929	1.188637
47	C	2.062277	3.220536	-1.218989
48	H	4.671561	1.133038	0.017838
49	H	1.987678	3.770404	2.129770
50	H	1.864826	5.001553	-0.021957
51	H	2.000052	3.755535	-2.164210
52	H	-1.827476	5.016080	-0.008423
53	H	-1.971314	3.775760	-2.153463
54	H	-1.959298	3.781080	2.140539
55	Cl	8.536220	-1.803446	0.038778
56	Cl	-8.550405	-1.735571	0.028887
57	C	2.311471	1.095157	-2.549863
58	C	2.297292	1.113092	2.535762
59	C	-2.287986	1.125177	2.540641
60	C	-2.301443	1.118565	-2.545036
61	H	3.267461	0.614008	2.658560
62	H	2.171818	1.804002	3.375679
63	H	1.527430	0.336407	2.625898
64	H	3.279150	0.588336	-2.659827
65	H	1.536837	0.323387	-2.641893
66	H	2.198648	1.781252	-3.395492
67	H	-2.160893	1.813911	3.382107
68	H	-1.521091	0.345467	2.630081
69	H	-3.260176	0.629535	2.661267
70	H	-1.532157	0.341577	-2.637904
71	H	-2.182875	1.805691	-3.389043
72	H	-3.272580	0.618901	-2.657265

***B*-(2,6-dimethylphenyl)-9**

ATOM		X	Y	Z
1	C	-3.985787	0.620084	0.084584
2	C	-6.807025	1.171272	-0.148305
3	C	-4.470305	1.959189	-0.042562
4	C	-6.332172	-0.150194	-0.031881
5	C	-5.857848	2.194972	-0.141983
6	C	-1.181717	2.475240	-0.048907
7	C	0.068432	3.105752	-0.137819
8	C	1.294857	2.426524	-0.181662
9	C	1.287540	0.995307	-0.172497
10	C	4.560908	1.791905	-0.099311
11	C	4.028598	0.465822	-0.155600
12	C	4.977926	-0.583559	-0.074227
13	C	5.952253	1.983386	0.026961
14	C	6.860718	0.927214	0.134509
15	C	6.338958	-0.379467	0.081105
16	B	-2.497445	0.158090	0.213495
17	B	2.526748	0.052665	-0.296981
18	H	-7.031230	-0.980736	-0.056276
19	H	-6.198401	3.225770	-0.200045
20	H	0.087953	4.192887	-0.174390
21	H	4.618313	-1.605571	-0.123764
22	H	7.002722	-1.235227	0.171688
23	H	6.332022	3.001087	0.020919
24	C	-2.319397	3.372926	-0.041277
25	C	-3.657551	3.161804	-0.048036
26	C	-1.226348	1.046878	0.031902
27	C	0.019207	0.388177	-0.051909
28	C	2.465267	3.279286	-0.243316
29	C	3.794171	3.020596	-0.200192
30	H	2.217642	4.338078	-0.305565
31	H	4.421575	3.910578	-0.233952
32	H	-4.251070	4.074752	-0.073483
33	H	-2.032689	4.423552	-0.060337
34	H	-0.001573	-0.694626	-0.021147
35	C	-4.975648	-0.395640	0.094477
36	C	2.246673	-1.482988	-0.617608
37	C	1.821495	-4.194028	-1.265417
38	C	2.186707	-1.898619	-1.969322
39	C	2.088544	-2.448946	0.402866
40	C	1.879355	-3.792217	0.066434
41	C	1.973835	-3.247332	-2.276429
42	C	-2.268658	-1.375381	0.585966
43	C	-1.940784	-4.078548	1.317278
44	C	-2.155792	-2.378591	-0.403898

45	C	-2.214636	-1.749800	1.949851
46	C	-2.050823	-3.095542	2.298522
47	C	-1.994626	-3.717524	-0.026374
48	C	-2.192908	-2.021112	-1.875800
49	C	-2.354797	-0.708504	3.041810
50	C	2.372008	-0.899125	-3.093042
51	C	2.128764	-2.046483	1.863060
52	C	-8.242890	1.442838	-0.258919
53	C	8.294324	1.187961	0.289990
54	C	8.915470	2.317079	0.777710
55	C	10.336183	2.230743	0.788768
56	C	10.797354	1.034837	0.309340
57	S	9.497560	-0.005875	-0.167688
58	C	-9.295376	0.654647	0.152140
59	C	-10.573946	1.224873	-0.105491
60	C	-10.495081	2.446944	-0.715747
61	S	-8.850724	2.919033	-0.989502
62	H	-11.511435	0.746980	0.157480
63	H	-9.156208	-0.297498	0.652300
64	H	-11.302326	3.096998	-1.025990
65	H	10.985865	3.022786	1.145322
66	H	8.366270	3.176768	1.145840
67	H	11.821637	0.703391	0.203802
68	H	3.015071	-1.444526	2.098641
69	H	1.251002	-1.448689	2.138765
70	H	2.139713	-2.926370	2.514332
71	H	1.757929	-4.525896	0.860159
72	H	1.659245	-5.239798	-1.514993
73	H	1.933781	-3.555967	-3.319024
74	H	-3.342254	-0.229338	3.017303
75	H	-2.227306	-1.154137	4.033866
76	H	2.230891	-1.370830	-4.070983
77	H	3.377766	-0.459310	-3.079397
78	H	-1.611995	0.092473	2.938545
79	H	-3.053004	-1.386226	-2.121747
80	H	-4.651217	-1.425509	0.195707
81	H	-2.251090	-2.919393	-2.498694
82	H	-1.291241	-1.473188	-2.176761
83	H	-1.908522	-4.479982	-0.797161
84	H	-1.816746	-5.121316	1.599267
85	H	-2.014156	-3.372539	3.350306
86	H	1.661500	-0.065998	-3.019604

***B*-(2,6-dimethylphenyl)-10**

ATOM		X	Y	Z
1	C	4.006867	-0.098379	-0.316640

2	C	6.834443	0.402187	-0.122576
3	C	4.516307	1.235699	-0.219456
4	C	6.338908	-0.916272	-0.217237
5	C	5.906150	1.450430	-0.134769
6	C	1.238341	1.807808	-0.151206
7	C	0.002338	2.460189	-0.034499
8	C	-1.232892	1.803049	0.064386
9	C	-1.250138	0.371813	0.078592
10	C	-4.510732	1.227588	0.166240
11	C	-4.000033	-0.108906	0.206426
12	C	-4.970602	-1.144805	0.203197
13	C	-5.902483	1.445247	0.132051
14	C	-6.832196	0.398397	0.120110
15	C	-6.335397	-0.922486	0.152217
16	B	2.509028	-0.532913	-0.420381
17	B	-2.500254	-0.547084	0.263129
18	H	7.034666	-1.749781	-0.217807
19	H	6.279051	2.468759	-0.072961
20	H	0.001770	3.548063	-0.017727
21	H	-4.622457	-2.171136	0.244377
22	H	-7.031771	-1.755458	0.147440
23	H	-6.275737	2.465174	0.114293
24	C	2.389812	2.686052	-0.207726
25	C	3.723749	2.452186	-0.225432
26	C	1.256801	0.377883	-0.211424
27	C	0.003619	-0.258177	-0.078151
28	C	-2.384427	2.678501	0.151453
29	C	-3.717891	2.443572	0.183939
30	H	-2.115735	3.733952	0.169564
31	H	-4.327490	3.345584	0.221021
32	H	4.333728	3.354696	-0.232268
33	H	2.120405	3.741485	-0.205731
34	H	0.003986	-1.341506	-0.097017
35	C	4.976507	-1.134947	-0.321162
36	C	-2.233202	-2.090146	0.565528
37	C	-1.839712	-4.814821	1.176671
38	C	-2.139957	-2.519508	1.910922
39	C	-2.125467	-3.049796	-0.467124
40	C	-1.930886	-4.399643	-0.149283
41	C	-1.943870	-3.874950	2.200007
42	C	2.243130	-2.060719	-0.792599
43	C	1.841038	-4.752561	-1.530837
44	C	2.128373	-3.066746	0.194239
45	C	2.152756	-2.427002	-2.156815
46	C	1.951947	-3.766713	-2.509150
47	C	1.929450	-4.399554	-0.186853
48	C	2.206263	-2.718077	1.666503

49	C	2.291552	-1.382733	-3.246071
50	C	-2.272416	-1.526505	3.047719
51	C	-2.209349	-2.631893	-1.921027
52	H	-3.103268	-2.028116	-2.121450
53	H	-1.341224	-2.029045	-2.215844
54	H	-2.239695	-3.504340	-2.581657
55	H	-1.848350	-5.128052	-0.952786
56	H	-1.689319	-5.865697	1.411726
57	H	-1.878862	-4.193802	3.238391
58	H	3.289084	-0.924460	-3.239391
59	H	2.134496	-1.820108	-4.237583
60	H	-2.115871	-2.009816	4.017691
61	H	-3.267970	-1.064284	3.063016
62	H	1.567786	-0.567227	-3.123243
63	H	3.099115	-2.124853	1.899868
64	H	4.629669	-2.158706	-0.410002
65	H	2.233730	-3.620850	2.285146
66	H	1.336363	-2.130527	1.985632
67	H	1.841325	-5.164230	0.581616
68	H	1.687558	-5.790763	-1.815039
69	H	1.887191	-4.036379	-3.561380
70	H	-1.545409	-0.708913	2.961867
71	C	-8.227351	0.662663	0.088517
72	C	-9.423935	0.890394	0.070128
73	C	8.227055	0.663863	-0.026833
74	C	9.421171	0.891375	0.053056
75	C	-10.815938	1.168370	0.051300
76	C	-13.613724	1.736493	0.018534
77	C	-11.773064	0.133973	0.062760
78	C	-11.293966	2.493870	0.019587
79	C	-12.650680	2.775438	0.001512
80	C	-13.132334	0.404606	0.045651
81	C	10.810474	1.168977	0.144160
82	C	13.602813	1.735949	0.322151
83	C	11.287385	2.494650	0.188551
84	C	11.766054	0.134100	0.190545
85	C	13.122843	0.403992	0.276386
86	C	12.641592	2.775627	0.274207
87	N	-14.967366	2.011850	0.011478
88	N	14.953030	2.010897	0.411415
89	C	15.918595	0.925487	0.411587
90	C	15.416327	3.387361	0.416016
91	C	-15.429086	3.384583	-0.099526
92	C	-15.930082	0.925067	-0.041427
93	H	-16.939463	1.339914	-0.028588
94	H	-15.830187	0.257777	0.824959
95	H	-15.822378	0.317061	-0.952042

96	H	-15.103462	3.858697	-1.037421
97	H	-16.519837	3.398499	-0.073347
98	H	-15.065990	3.999913	0.734506
99	H	-12.964862	3.811949	-0.025430
100	H	-10.579364	3.311613	0.007236
101	H	-11.434680	-0.897823	0.084006
102	H	-13.826419	-0.426969	0.052282
103	H	15.777393	0.256633	1.271841
104	H	15.855941	0.318671	-0.503328
105	H	16.925621	1.341611	0.472365
106	H	10.574105	3.312873	0.153111
107	H	12.955884	3.812080	0.302397
108	H	13.816106	-0.427736	0.307626
109	H	11.428321	-0.897599	0.157836
110	H	15.133684	3.921169	-0.503079
111	H	16.504688	3.398689	0.492316
112	H	15.012845	3.948462	1.270323

Appendix 2. Supporting Information for Chapter 3

List of Figures

List of Tables

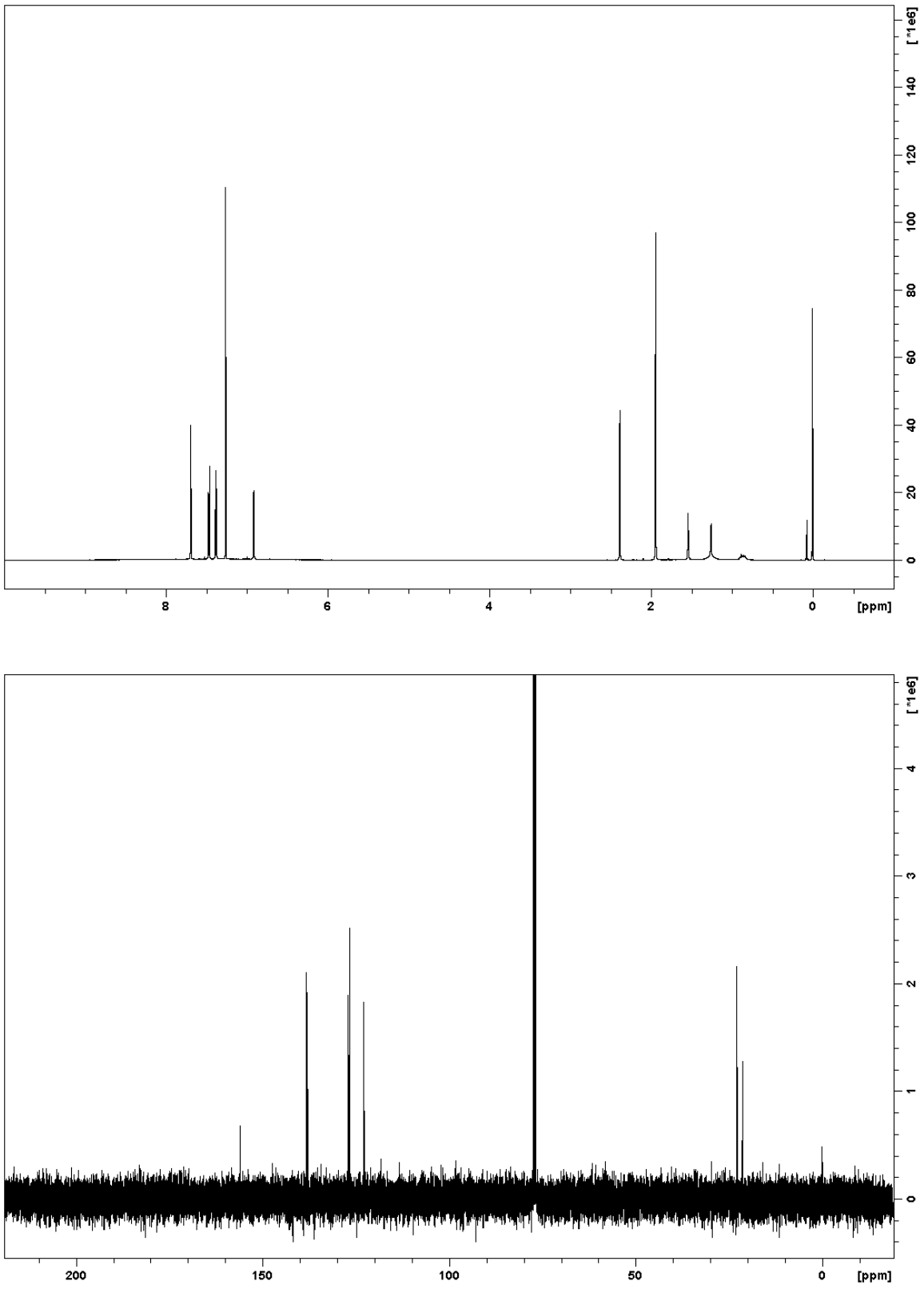

Figure A2.1. ^{1}H (400 MHz, $CDCl_3$) and ^{13}C NMR (100 MHz, $CDCl_3$) spectra for **1**.

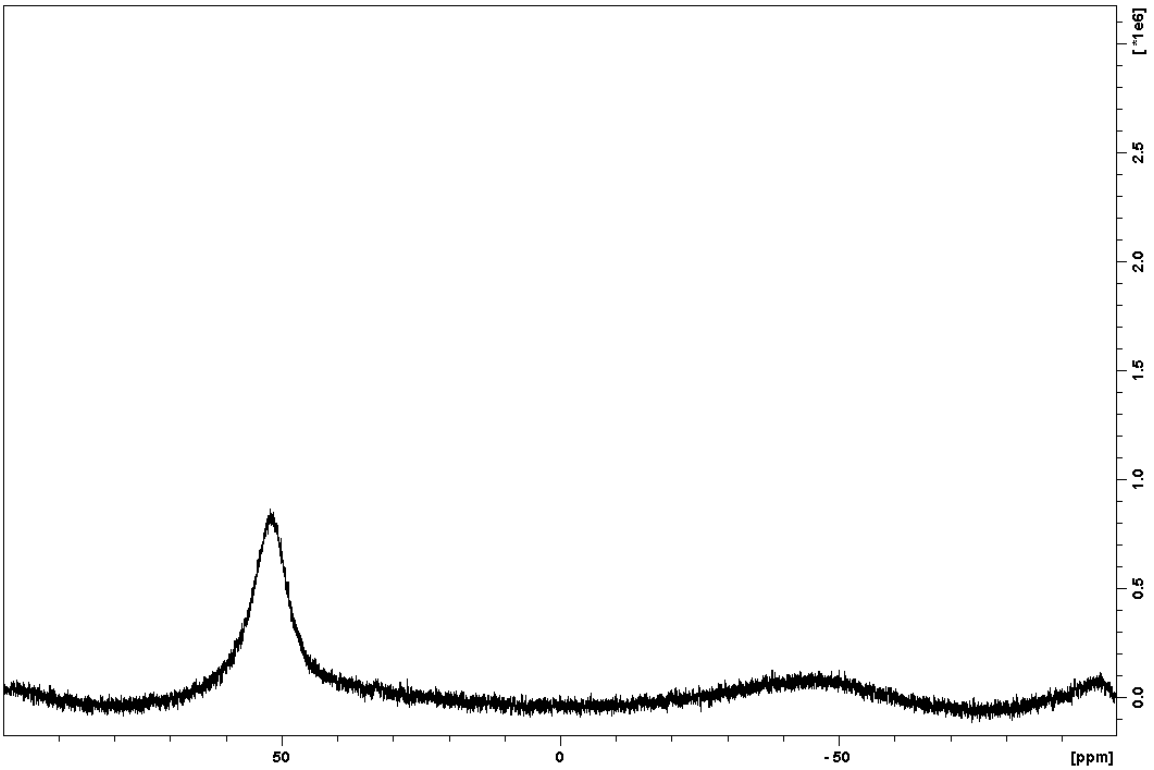

Figure A2.2. ^{11}B NMR (96 MHz, $CDCl_3$) spectrum for **1**.

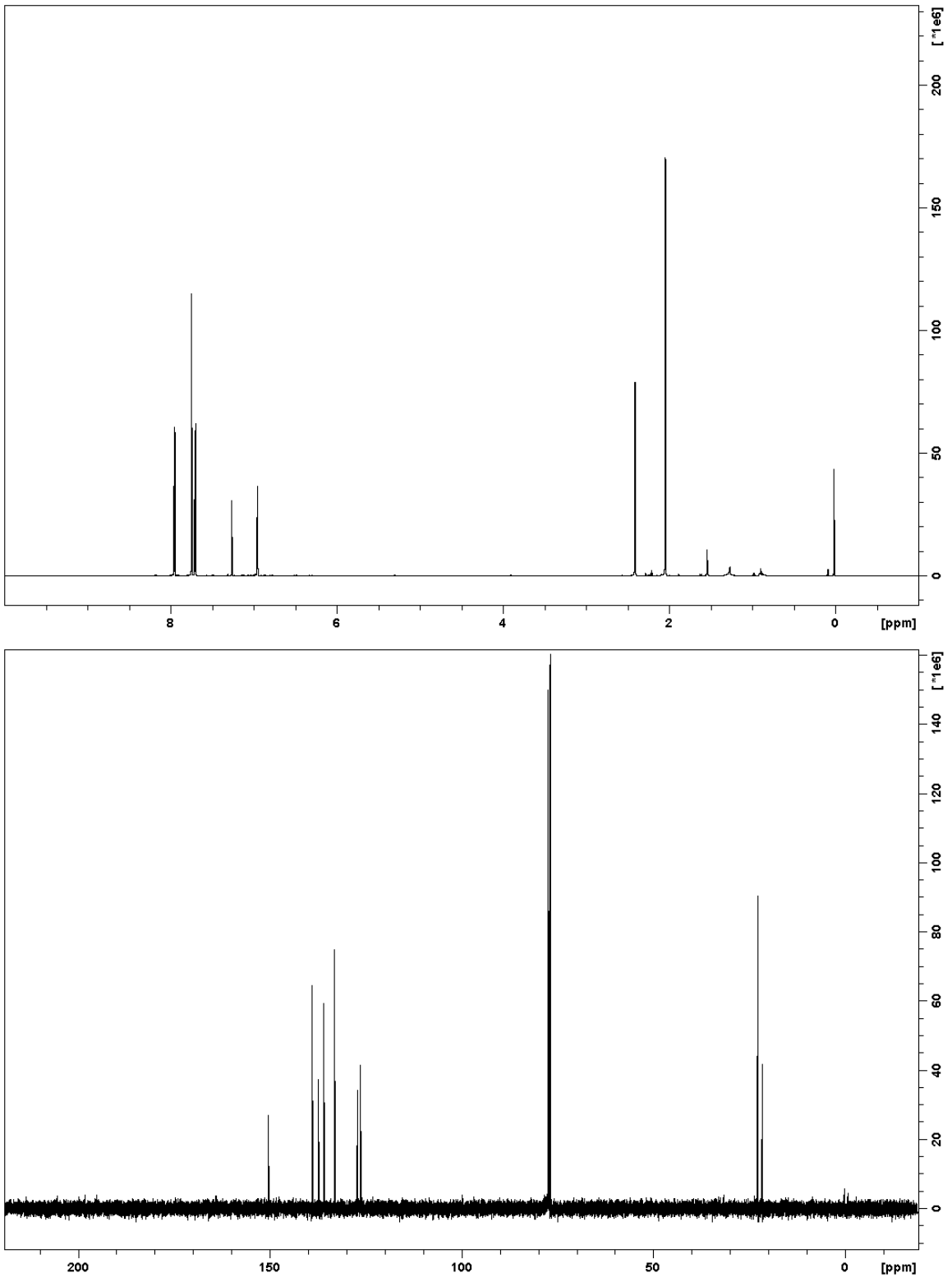

Figure A2.3. ^{1}H (400 MHz, $CDCl_3$) and ^{13}C NMR (100 MHz, $CDCl_3$) spectra for **2**.

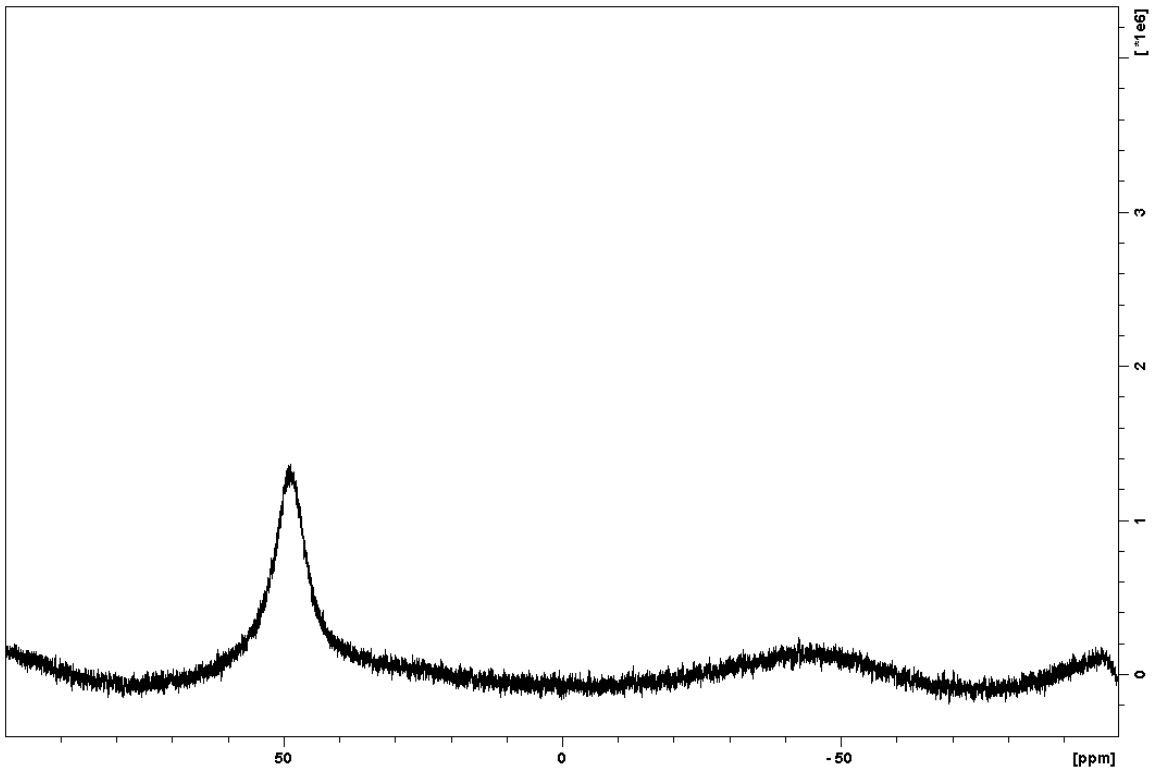

Figure A2.4. ^{11}B NMR (96 MHz, $CDCl_3$) spectrum for **2**.

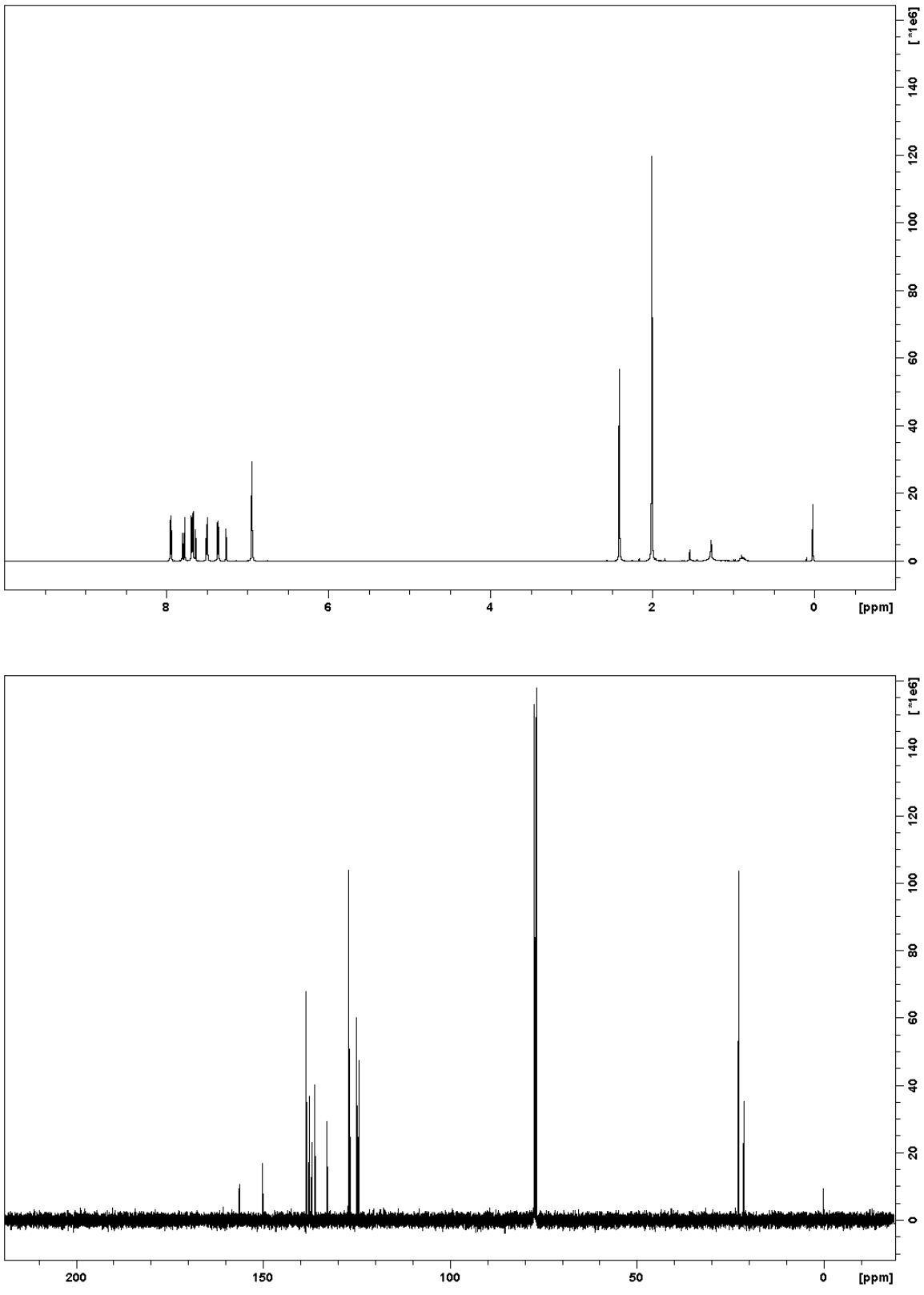

Figure A2.5. ^{1}H (400 MHz, $CDCl_3$) and ^{13}C NMR (100 MHz, $CDCl_3$) spectra for **3**.

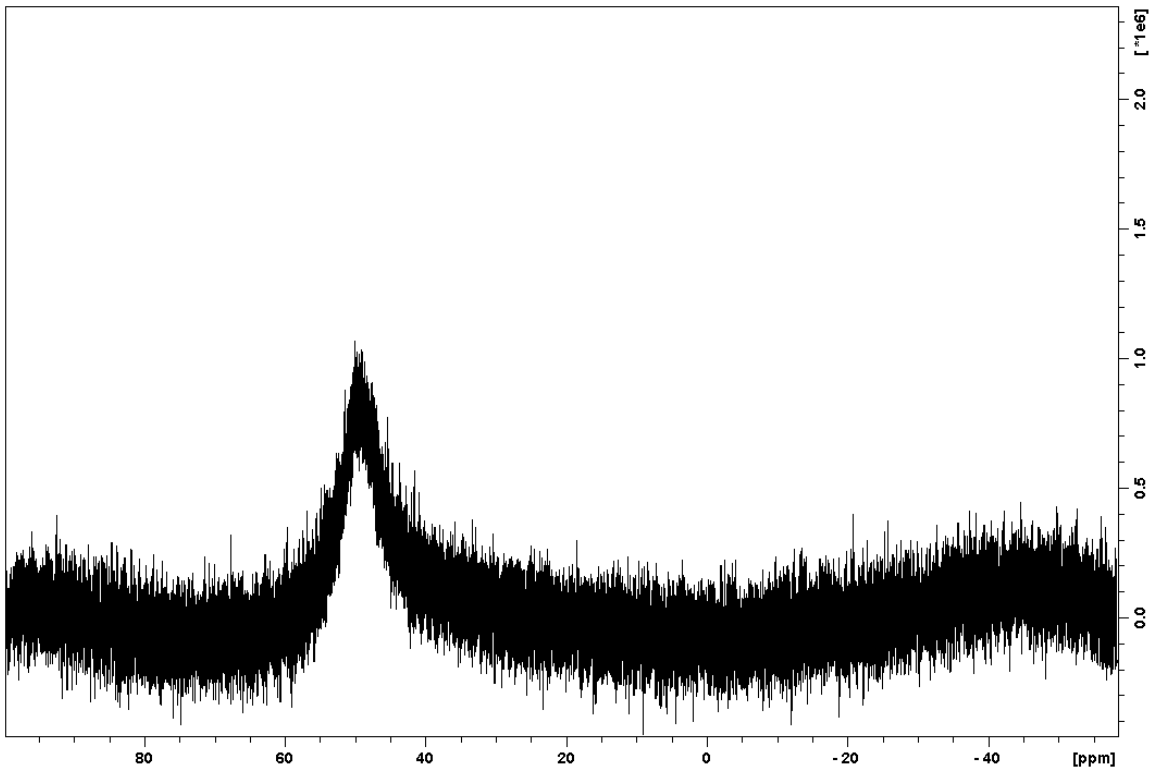

Figure A2.6. ^{11}B NMR (96 MHz, $CDCl_3$) spectrum for **3**.

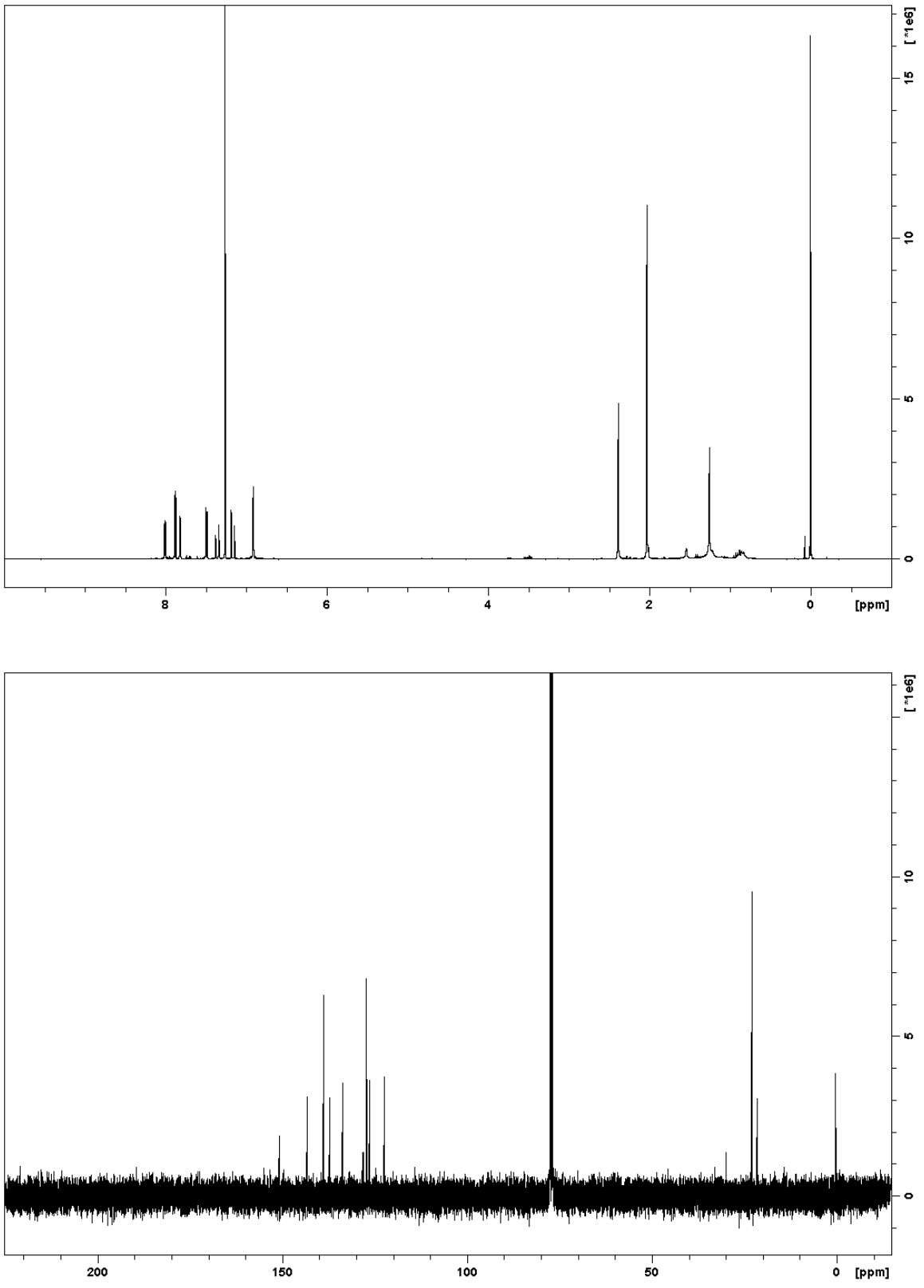

Figure A2.7. ^{1}H (400 MHz, $CDCl_3$) and ^{13}C NMR (100 MHz, $CDCl_3$) spectra for **4**.

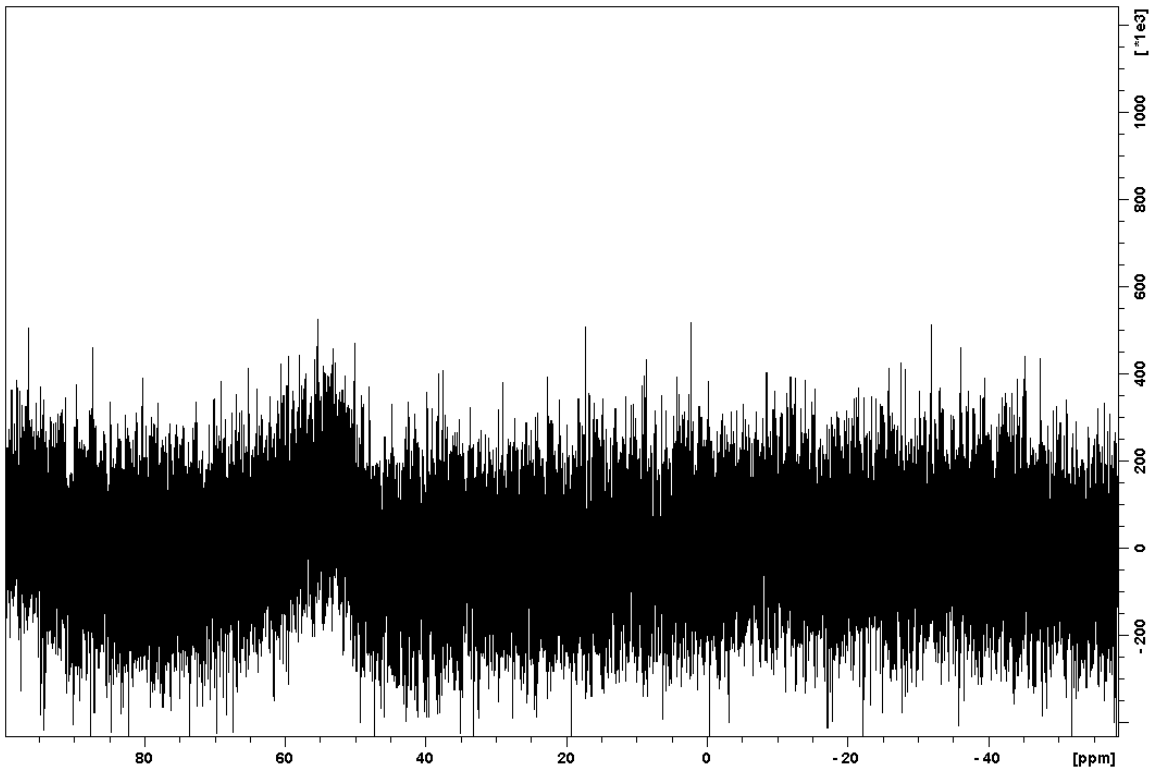

Figure A2.8. ^{11}B NMR (96 MHz, $CDCl_3$) spectrum for **4**.

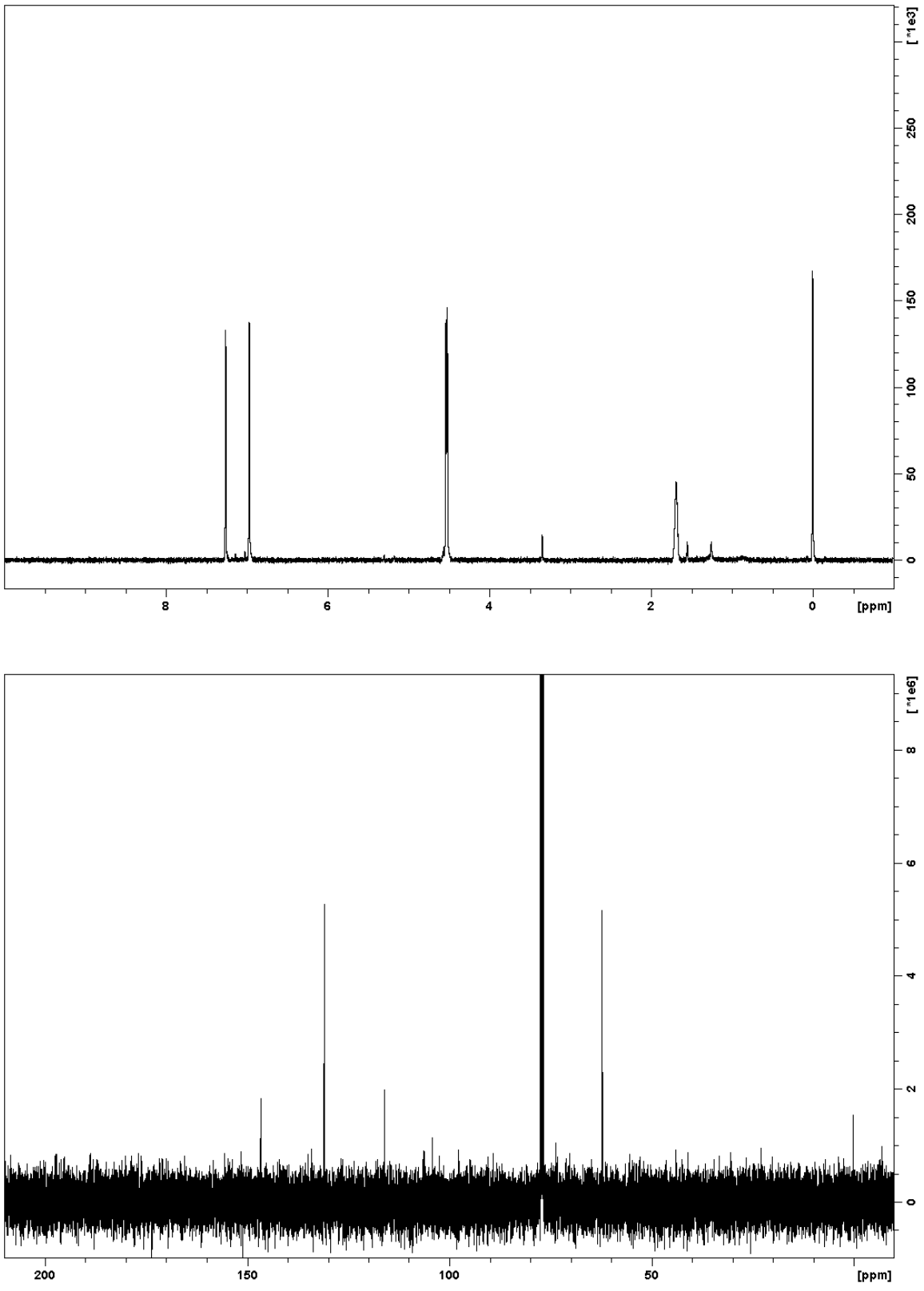

Figure A2.9. ^{1}H (400 MHz, $CDCl_3$) and ^{13}C NMR (100 MHz, $CDCl_3$) spectra for **6**.

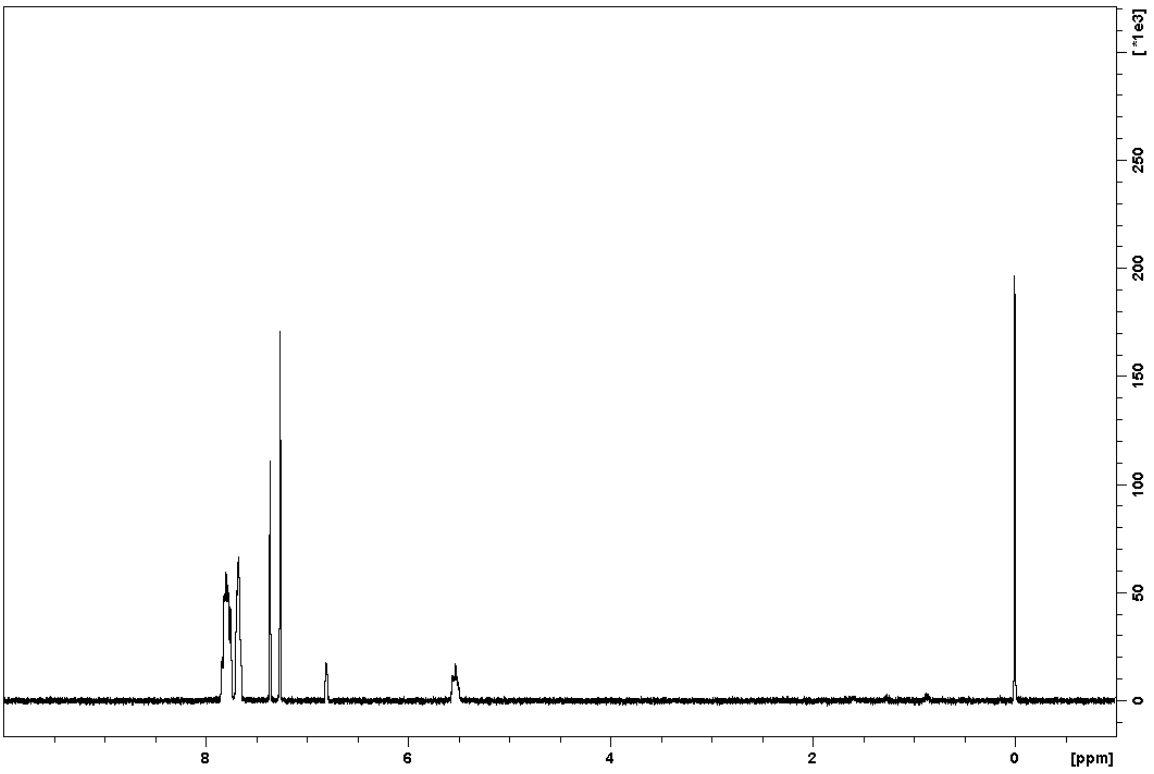

Figure A2.10. ^{1}H NMR (400 MHz, $CDCl_3$) spectrum for **7**.

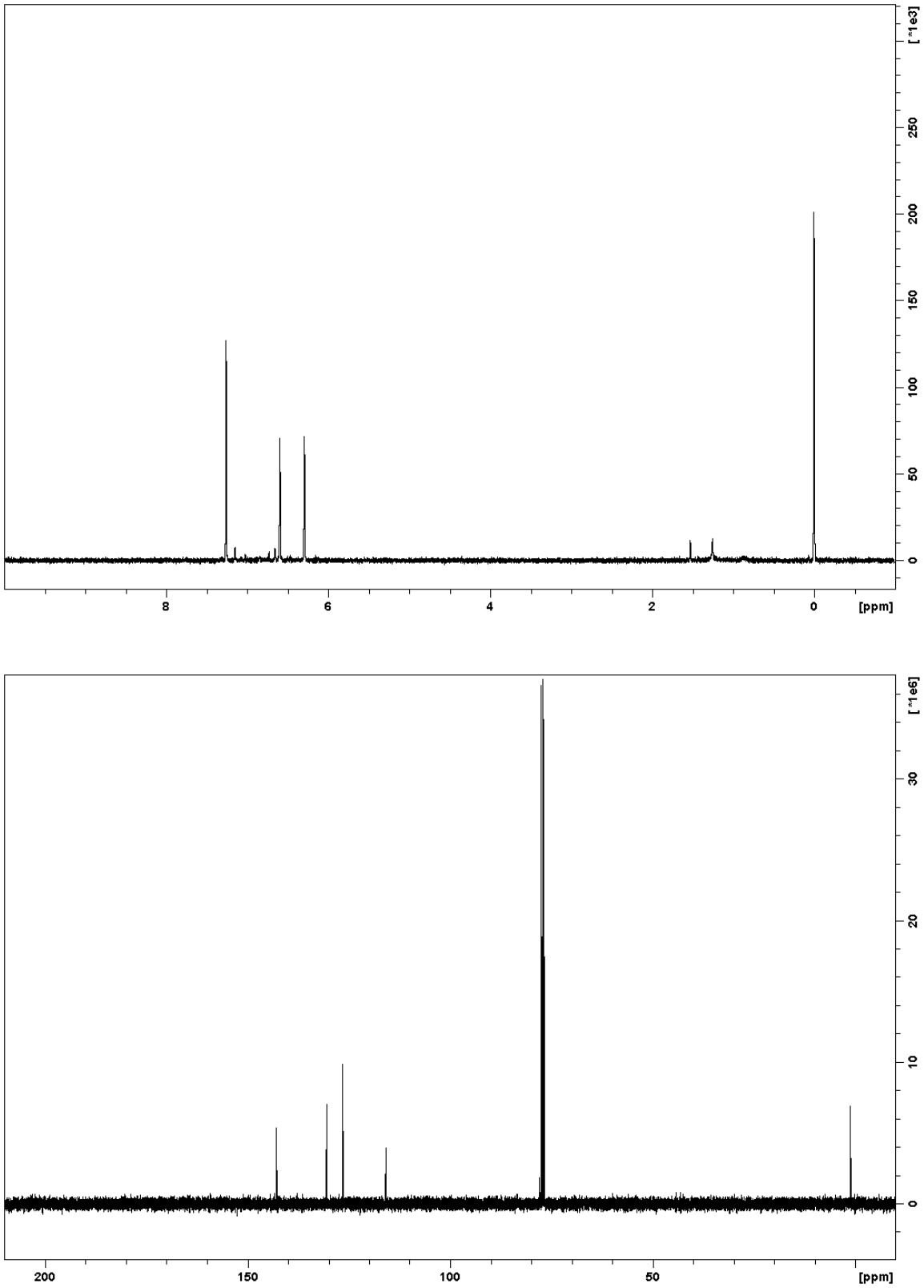

Figure A2.11. ^{1}H (400 MHz, $CDCl_3$) and ^{13}C NMR (100 MHz, $CDCl_3$) spectra for **8**.

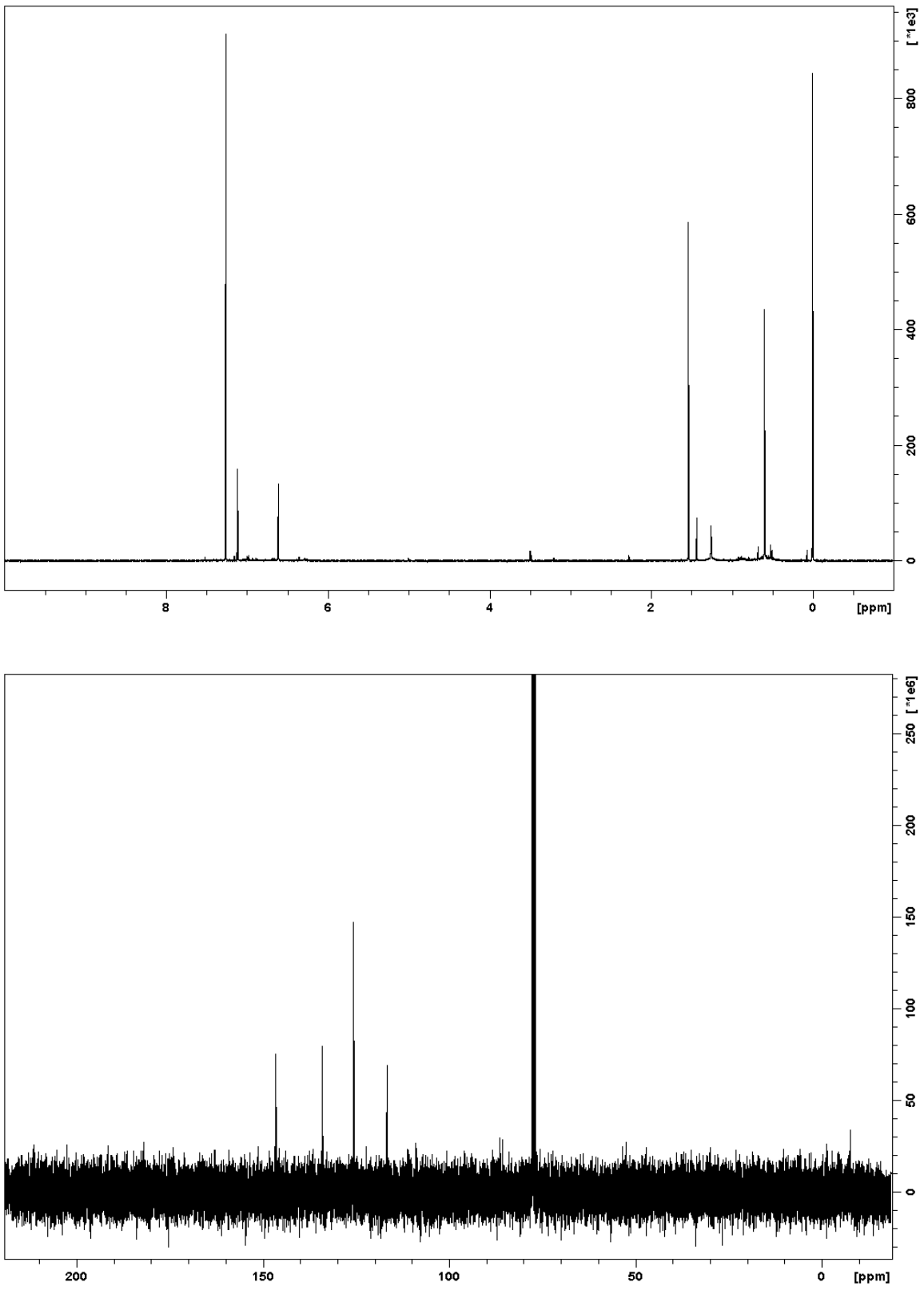

Figure A2.12. ^{1}H (400 MHz, $CDCl_3$) and ^{13}C NMR (100 MHz, $CDCl_3$) spectra for **9**.

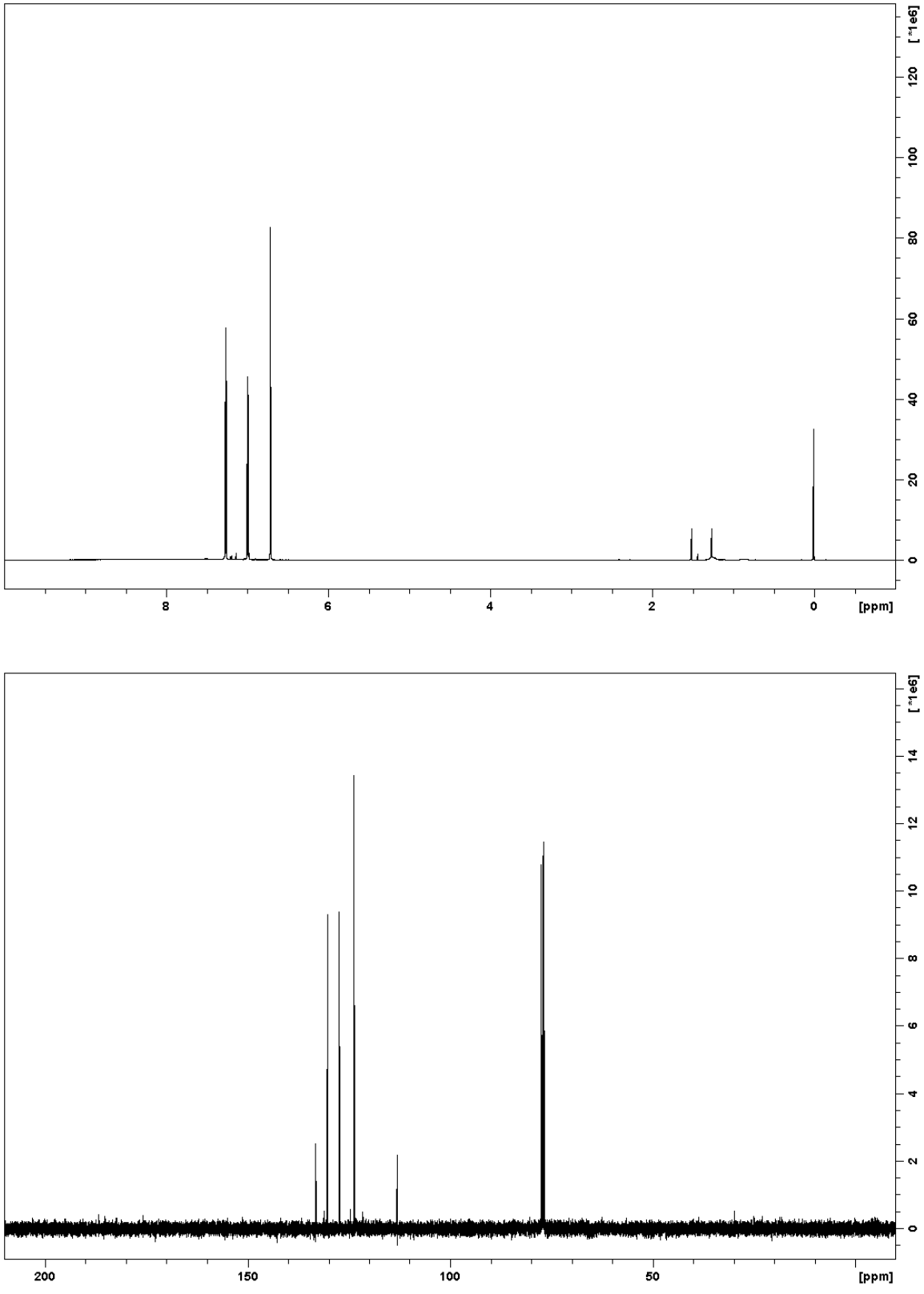

Figure A2.13. ^{1}H (400 MHz, $CDCl_3$) and ^{13}C NMR (100 MHz, $CDCl_3$) spectra for **10**.

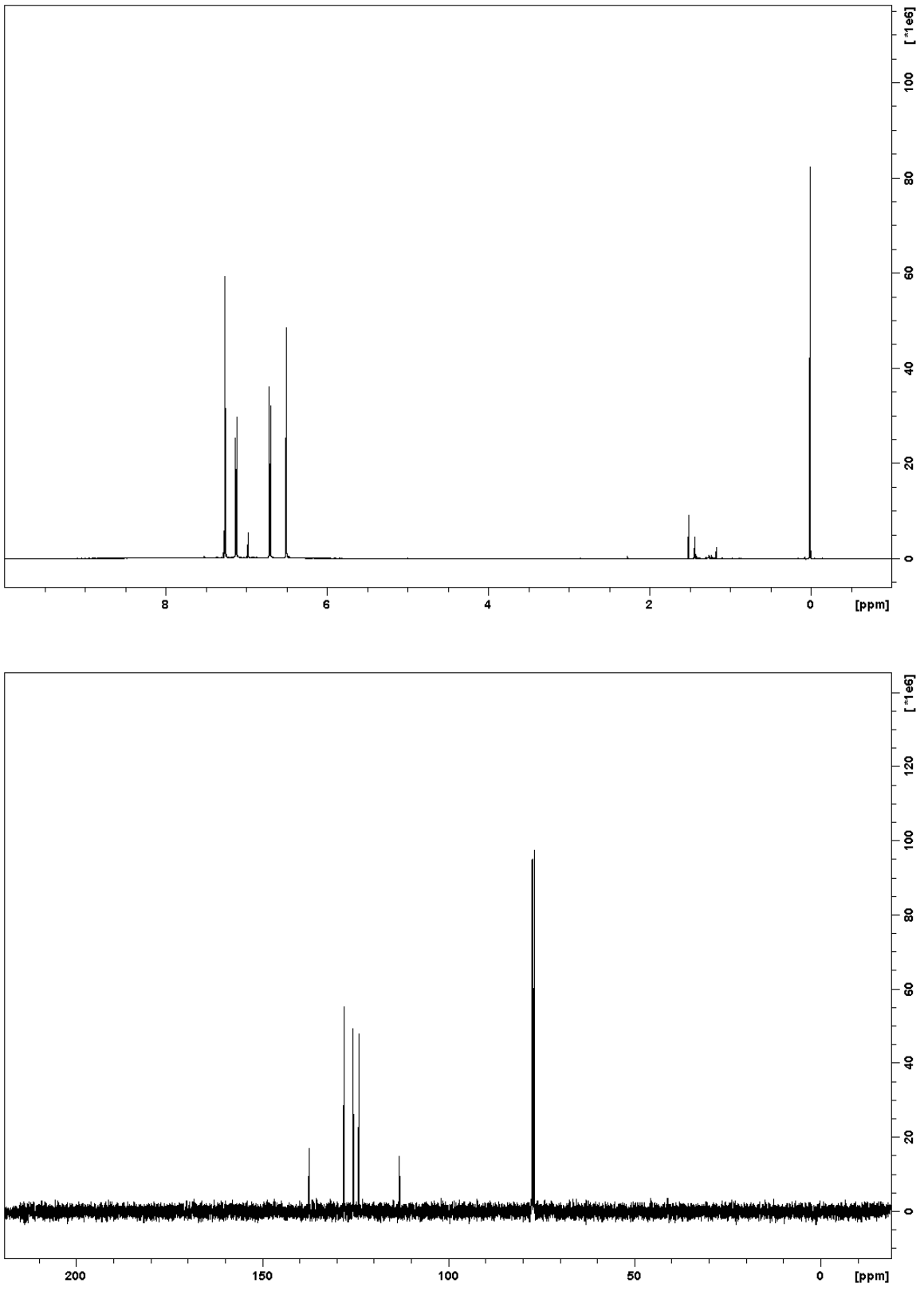

Figure A2.14. ^{1}H (400 MHz, $CDCl_3$) and ^{13}C NMR (100 MHz, $CDCl_3$) spectra for **11**.

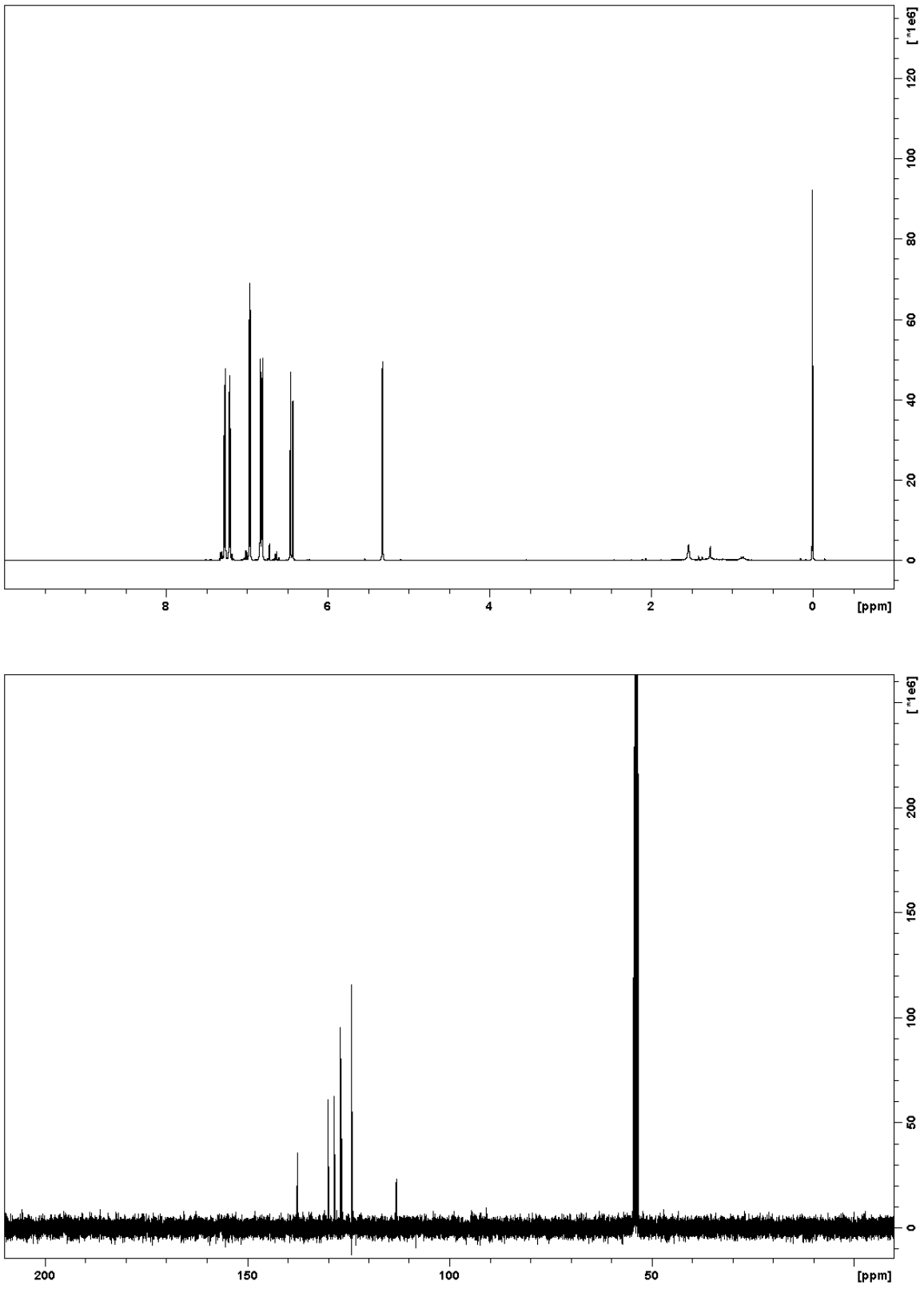

Figure A2.15. ^{1}H (400 MHz, CD_2Cl_2) and ^{13}C NMR (100 MHz, CD_2Cl_2) spectra for **12**.

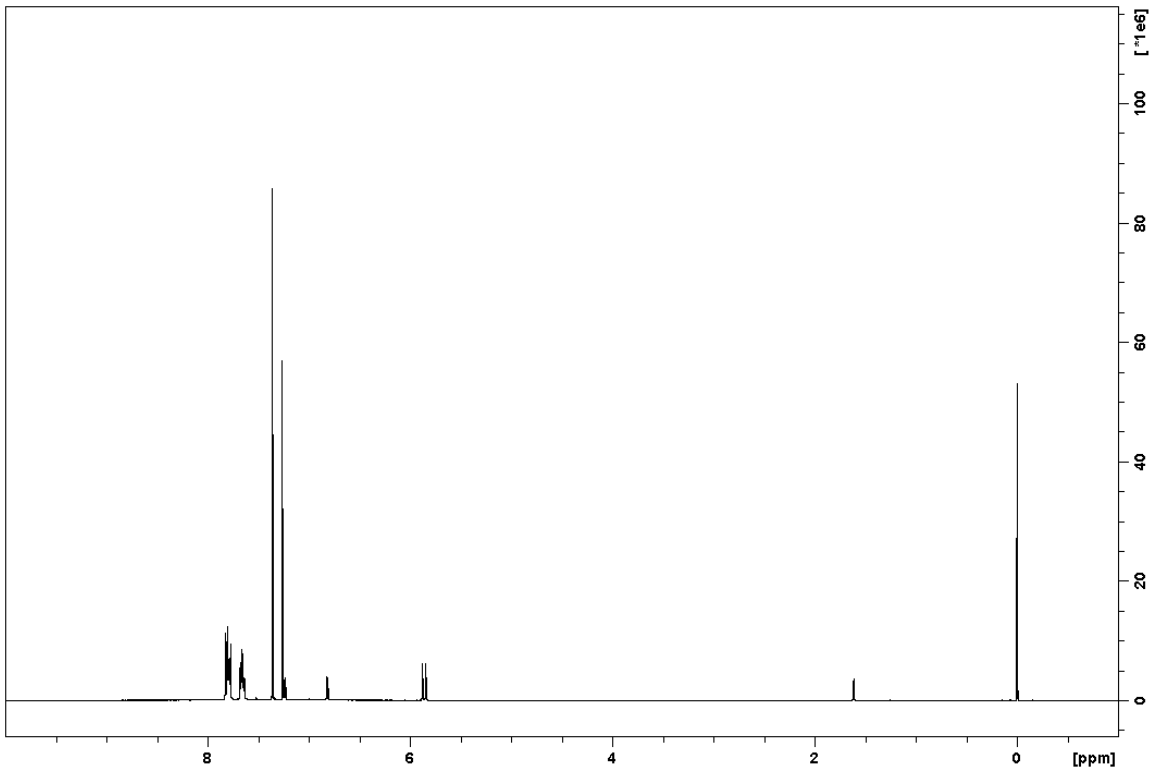

Figure A2.16. ^{1}H (400 MHz, $CDCl_3$) spectrum for **13**.

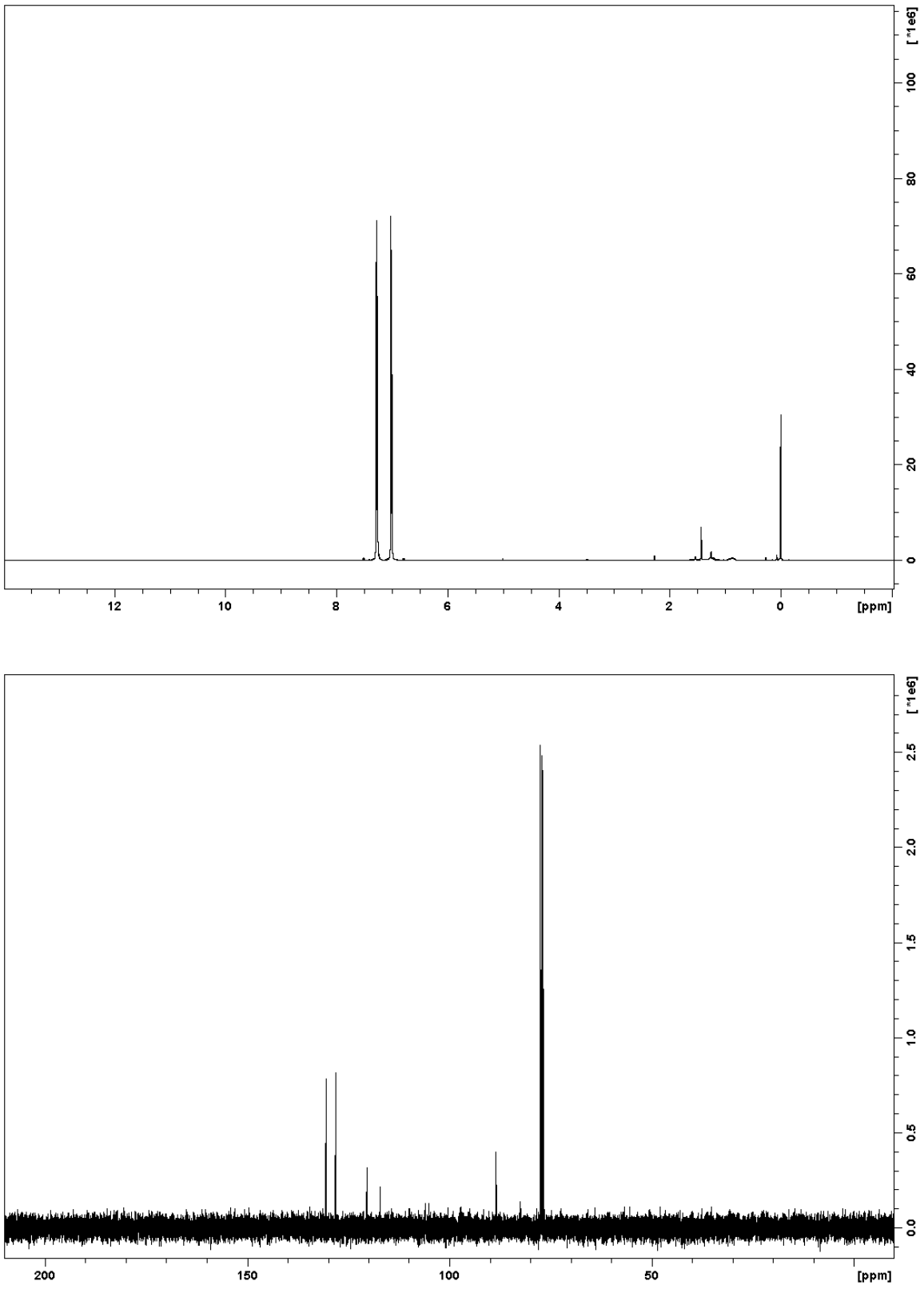

Figure A2.17. ^{1}H (400 MHz, $CDCl_3$) and ^{13}C NMR (100 MHz, $CDCl_3$) spectra for **18**.

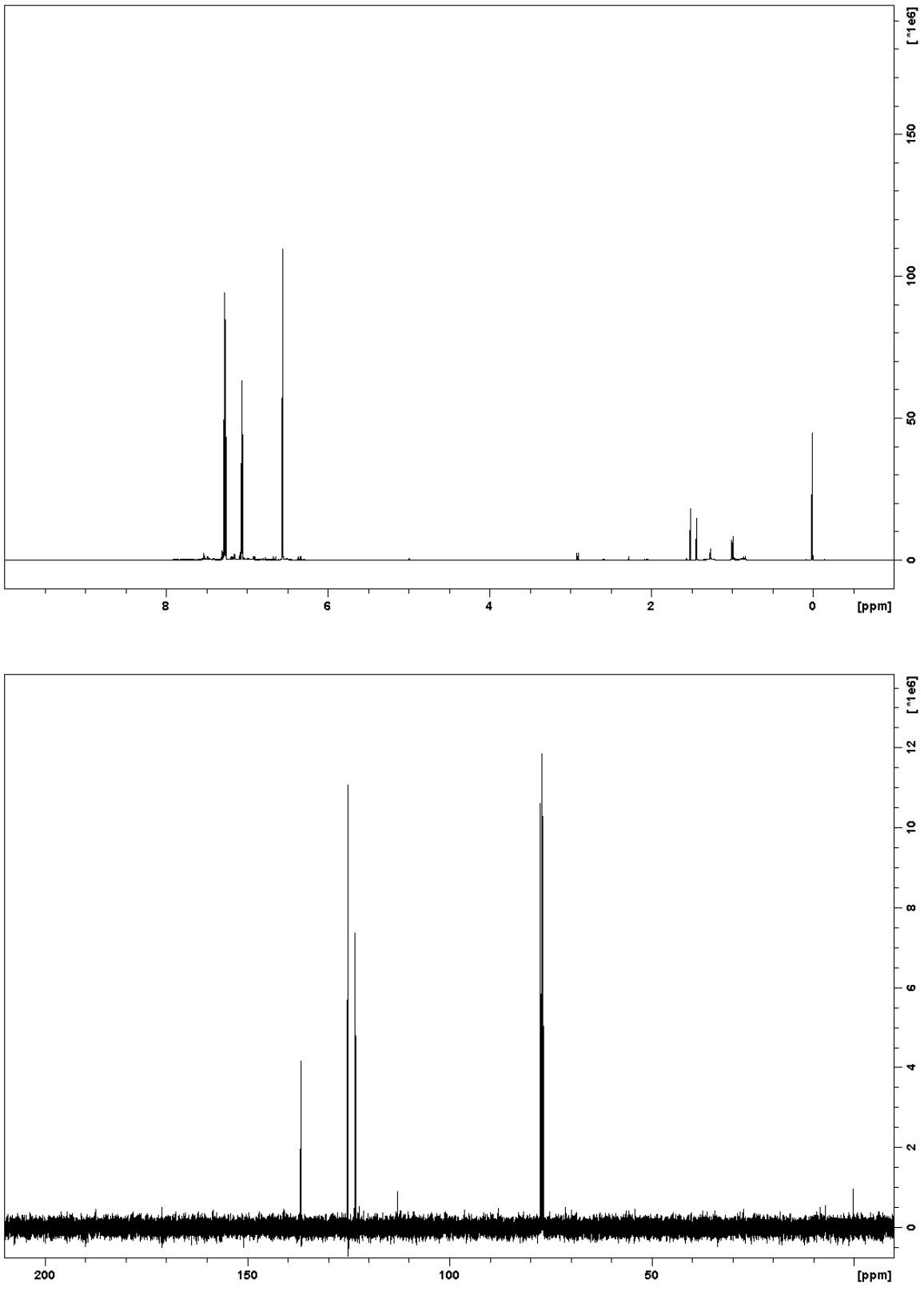

Figure A2.18. ^{1}H (400 MHz, $CDCl_3$) and ^{13}C NMR (100 MHz, $CDCl_3$) spectra for **20**.

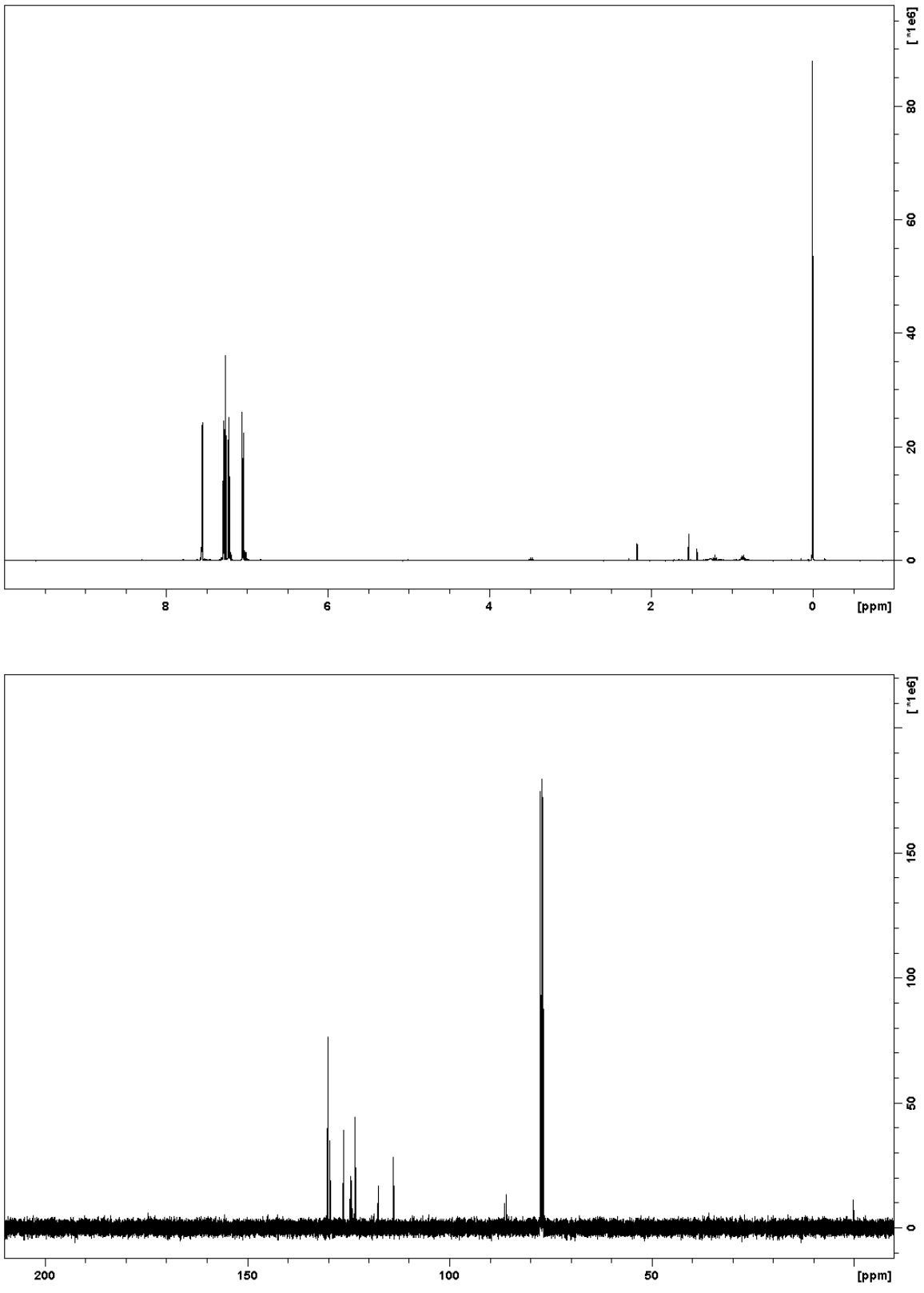

Figure A2.19. ^{1}H (400 MHz, $CDCl_3$) and ^{13}C NMR (100 MHz, $CDCl_3$) spectra for **21**.

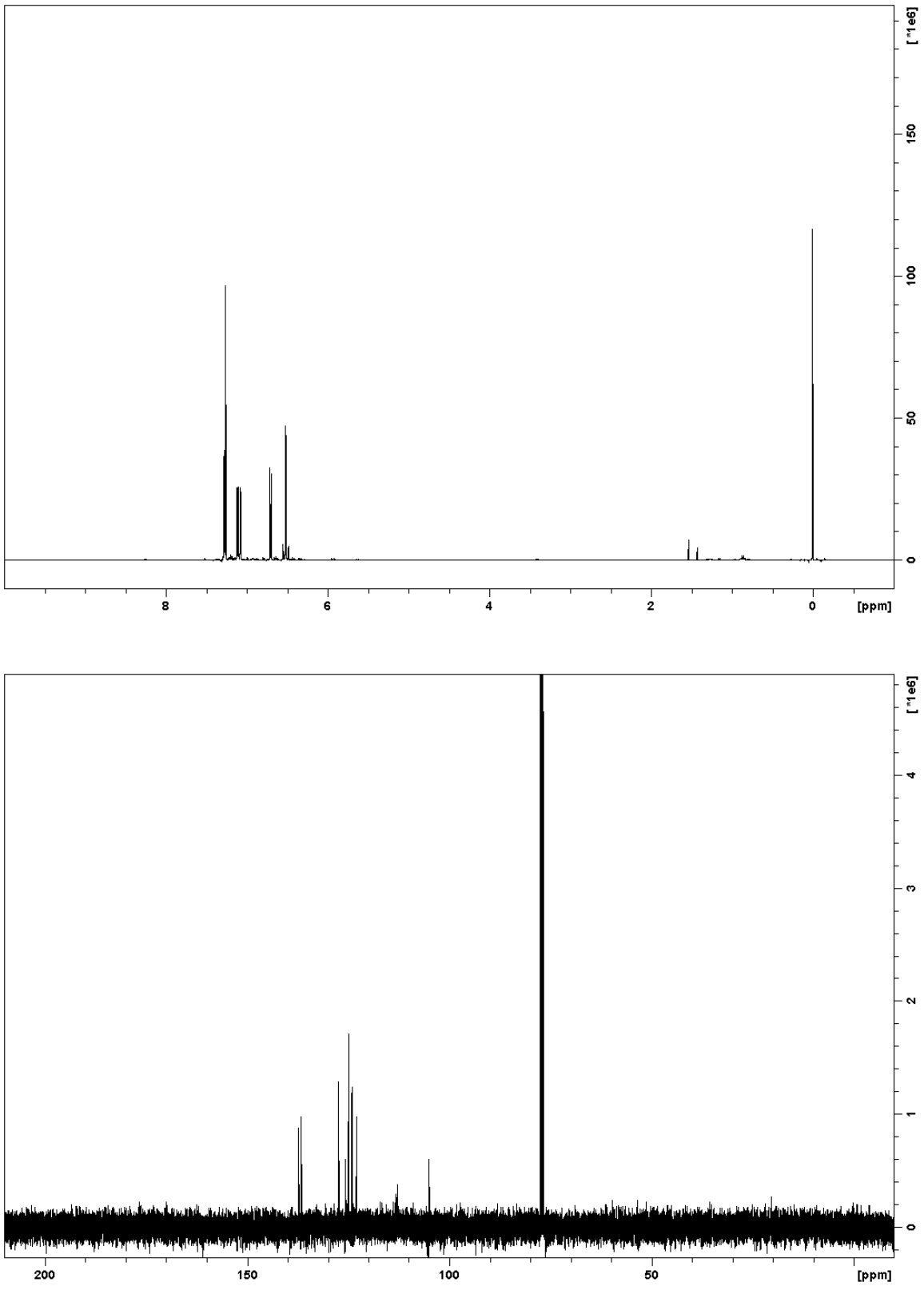

Figure A2.20. ^{1}H (400 MHz, $CDCl_3$) and ^{13}C NMR (100 MHz, $CDCl_3$) spectra for **22**.

Table A2.1. Atomic coordinates for X-ray crystal structures of **1**, **2**, **3**, and **4**.

1

Number	Label	Xfrac + ESD	Yfrac + ESD	Zfrac + ESD
1	B1	0.25131(10)	0.28451(17)	0.13268(5)
2	C1	0.35169(9)	0.25968(16)	0.13830(5)
3	C2	0.40716(9)	0.34763(17)	0.10812(5)
4	H2	0.385	0.4294	0.0841
5	C3	0.49394(10)	0.30508(19)	0.11658(6)
6	H3	0.5385	0.3531	0.0995
7	C4	0.40259(9)	0.14756(17)	0.17062(5)
8	C5	0.37919(10)	0.03499(18)	0.20782(6)
9	H5	0.4265	-0.0301	0.2242
10	C6	0.29989(11)	0.00717(17)	0.22315(5)
11	H6	0.2993	-0.0718	0.2495
12	C7	0.21676(10)	0.08076(16)	0.20497(5)
13	C8	0.05570(11)	0.1388(2)	0.19419(5)
14	H8	-0.0061	0.1453	0.1954
15	C9	0.09873(9)	0.22761(18)	0.16192(5)
16	H9	0.0695	0.3034	0.1381
17	C10	0.19189(9)	0.19782(16)	0.16679(4)
18	C11	0.20650(8)	0.39909(15)	0.08849(4)
19	C12	0.16247(8)	0.32520(15)	0.04454(5)
20	C13	0.12497(9)	0.42372(17)	0.00461(5)
21	H13	0.0946	0.3714	-0.0245
22	C14	0.13077(8)	0.59660(17)	0.00620(5)
23	C15	0.17413(8)	0.66987(16)	0.04964(5)
24	H15	0.1787	0.788	0.0514
25	C16	0.21104(8)	0.57461(16)	0.09067(5)
26	C17	0.15621(10)	0.13764(16)	0.03971(5)
27	H17A	0.1854	0.0857	0.0706
28	H17B	0.1853	0.1012	0.0111
29	H17C	0.0939	0.1043	0.0342
30	H17D	0.1244	0.1084	0.0067
31	H17E	0.1244	0.093	0.0662
32	H17F	0.2158	0.0899	0.0431
33	C18	0.09149(10)	0.7011(2)	-0.03801(6)
34	H18A	0.0639	0.628	-0.0649
35	H18B	0.1382	0.7669	-0.0504
36	H18C	0.0468	0.7763	-0.0275
37	H18D	0.102	0.8195	-0.0303
38	H18E	0.0278	0.6805	-0.0448
39	H18F	0.1192	0.6711	-0.0677

40	C19	0.25457(10)	0.66182(17)	0.13735(5)
41	H19A	0.254	0.7826	0.1316
42	H19B	0.3157	0.6232	0.1452
43	H19C	0.2222	0.6363	0.1656
44	S1	0.51298(2)	0.15425(5)	0.161765(17)
45	S2	0.12634(3)	0.01351(5)	0.232447(13)

2

Number	Label	Xfrac + ESD	Yfrac + ESD	Zfrac + ESD
1	B1	0.68994(17)	0.21854(9)	0.28472(12)
2	C1	0.71005(16)	0.14534(8)	0.36317(11)
3	C2	0.82435(19)	0.04937(9)	0.52136(13)
4	H2	0.8855	0.021	0.5857
5	C3	0.68278(18)	0.02274(8)	0.45537(12)
6	H3	0.6343	-0.0269	0.4683
7	C4	0.61356(16)	0.07671(8)	0.36426(11)
8	C5	0.46328(17)	0.05762(8)	0.28555(12)
9	H5	0.4149	0.0086	0.3012
10	C6	0.37999(17)	0.09833(8)	0.19295(12)
11	H6	0.2833	0.0727	0.1537
12	C7	0.41300(16)	0.17392(8)	0.14378(11)
13	C8	0.30731(17)	0.20401(9)	0.04196(12)
14	H8	0.2127	0.1766	0.0029
15	C9	0.35562(18)	0.27550(10)	0.00672(12)
16	H9	0.2992	0.3038	-0.0593
17	C10	0.54397(16)	0.22560(8)	0.18465(11)
18	C11	0.82357(15)	0.28664(8)	0.30231(11)
19	C12	0.96151(16)	0.27661(8)	0.25602(11)
20	C13	1.07520(16)	0.33802(9)	0.26535(11)
21	H13	1.1671	0.3307	0.233
22	C14	1.05728(17)	0.40982(8)	0.32096(12)
23	C15	0.92191(17)	0.41899(8)	0.36793(11)
24	H15	0.9089	0.4674	0.4071
25	C16	0.80478(16)	0.35904(8)	0.35900(11)
26	C17	0.98492(18)	0.19992(9)	0.19431(13)
27	H17A	0.8947	0.1633	0.1952
28	H17B	1.0866	0.1744	0.2331
29	H17C	0.9887	0.2122	0.1145
30	H17D	1.0853	0.2033	0.1666
31	H17E	0.8934	0.1922	0.1288
32	H17F	0.9913	0.1544	0.2474
33	C18	1.1830(2)	0.47515(10)	0.33128(15)

34	H18A	1.2854	0.4561	0.3792
35	H18B	1.1465	0.5228	0.3668
36	H18C	1.1987	0.489	0.2546
37	C19	0.65823(17)	0.37160(8)	0.40995(13)
38	H19A	0.6617	0.4257	0.4429
39	H19B	0.6584	0.3316	0.4704
40	H19C	0.5597	0.3656	0.3495
41	S1	0.87952(4)	0.14011(2)	0.47493(3)
42	S2	0.53048(4)	0.30867(2)	0.09540(3)

3

Number	Label	Xfrac + ESD	Yfrac + ESD	Zfrac + ESD
1	B1A	0.8435(4)	0.5309(2)	0.7093(3)
2	C1A	0.8667(4)	0.60366(19)	0.7905(3)
3	S1A	1.0315(6)	0.6055(3)	0.9018(4)
4	C2A	0.9806(15)	0.6968(7)	0.9506(14)
5	H2A	1.0437	0.7246	1.0142
6	C3A	0.841(3)	0.7246(10)	0.8884(19)
7	H3A	0.7926	0.773	0.906
8	C4A	0.7702(4)	0.6721(2)	0.7888(3)
9	C5A	0.6242(4)	0.6934(2)	0.7118(3)
10	H5A	0.5789	0.7432	0.7275
11	C6A	0.5409(4)	0.6526(2)	0.6195(3)
12	H6A	0.4452	0.6782	0.5806
13	C7A	0.5741(4)	0.5770(2)	0.5714(3)
14	S2A	0.4474(6)	0.5488(3)	0.4481(3)
15	C8A	0.5554(13)	0.4622(7)	0.4404(13)
16	H8A	0.5249	0.4219	0.3832
17	C9A	0.688(3)	0.4582(8)	0.5243(17)
18	H9A	0.7655	0.4169	0.5287
19	C10A	0.7001(4)	0.5234(2)	0.6084(3)
20	C11A	0.9750(4)	0.46265(19)	0.7267(3)
21	C12A	0.9558(4)	0.3902(2)	0.7821(3)
22	C13A	1.0715(4)	0.3297(2)	0.7916(3)
23	H13A	1.0571	0.2809	0.8297
24	C14A	1.2076(4)	0.3394(2)	0.7464(3)
25	C15A	1.2268(4)	0.4112(2)	0.6919(3)
26	H15A	1.3186	0.4186	0.6604
27	C16A	1.1138(4)	0.4733(2)	0.6822(3)
28	C17A	0.8092(4)	0.3778(2)	0.8319(4)
29	H17A	0.8265	0.3316	0.8843
30	H17B	0.7161	0.3675	0.7696

31	H17C	0.7903	0.4261	0.8741
32	C18A	1.3325(5)	0.2741(2)	0.7579(4)
33	H18A	1.3181	0.2359	0.8174
34	H18B	1.4393	0.2982	0.7792
35	H18C	1.3213	0.2458	0.6844
36	C19A	1.1392(5)	0.5505(2)	0.6229(4)
37	H19A	1.2142	0.5412	0.5728
38	H19B	1.1831	0.5913	0.6805
39	H19C	1.0368	0.5694	0.5768
40	B1B	0.4594(4)	0.0303(2)	0.6408(3)
41	C1B	0.6036(4)	0.02247(19)	0.7407(3)
42	S1B	0.61683(18)	-0.06166(7)	0.82796(13)
43	C2B	0.7908(6)	-0.0289(3)	0.9180(5)
44	H2B	0.8463	-0.0571	0.984
45	C3B	0.8383(17)	0.0443(8)	0.8804(10)
46	H3B	0.9325	0.0717	0.9179
47	C4B	0.7340(4)	0.0742(2)	0.7815(3)
48	C5B	0.7676(4)	0.1499(2)	0.7338(3)
49	H5B	0.8637	0.1752	0.7727
50	C6B	0.6845(4)	0.1911(2)	0.6422(3)
51	H6B	0.7313	0.2405	0.6262
52	C7B	0.5358(4)	0.1710(2)	0.5658(3)
53	S2B	0.45849(18)	0.24054(8)	0.45972(11)
54	C8B	0.2940(6)	0.1822(3)	0.4076(5)
55	H8B	0.2096	0.1959	0.3447
56	C9B	0.3028(13)	0.1138(8)	0.4695(10)
57	H9B	0.2224	0.0736	0.4513
58	C10B	0.4354(4)	0.1037(2)	0.5622(3)
59	C11B	0.3274(4)	-0.0383(2)	0.6233(3)
60	C12B	0.3477(4)	-0.11066(19)	0.5663(3)
61	C13B	0.2295(4)	-0.1702(2)	0.5550(3)
62	H13B	0.2417	-0.2183	0.5146
63	C14B	0.0956(4)	-0.1609(2)	0.6011(3)
64	C15B	0.0770(4)	-0.0887(2)	0.6572(3)
65	H15B	-0.0153	-0.081	0.6881
66	C16B	0.1906(4)	-0.0282(2)	0.6687(3)
67	C17B	0.4931(4)	-0.1231(2)	0.5162(3)
68	H17D	0.589	-0.1061	0.5721
69	H17E	0.4826	-0.0911	0.4459
70	H17F	0.5024	-0.1802	0.498
71	C18B	-0.0304(5)	-0.2261(2)	0.5889(4)
72	H18D	-0.1176	-0.2139	0.5231
73	H18E	-0.0725	-0.2284	0.659

74	H18F	0.0174	-0.2781	0.5768
75	C19B	0.1664(4)	0.0487(2)	0.7305(4)
76	H19D	0.0555	0.0516	0.7395
77	H19E	0.1892	0.0951	0.6856
78	H19F	0.2389	0.0494	0.8063

4

Number	Label	Xfrac + ESD	Yfrac + ESD	Zfrac + ESD
1	C1	0.7895(17)	0.1474(8)	0.6376(14)
2	S1	0.61992(9)	0.14310(6)	0.52514(8)
3	C2	0.6757(11)	0.0535(6)	0.4771(8)
4	H2	0.6148	0.0264	0.411
5	C3	0.8137(9)	0.0249(5)	0.5413(8)
6	H3	0.8605	-0.0248	0.5271
7	C4	0.8823(9)	0.0785(5)	0.6342(8)
8	C5	1.0339(10)	0.0578(5)	0.7119(6)
9	H5	1.0816	0.0095	0.693
10	C6	1.1178(10)	0.0963(4)	0.8068(8)
11	H6	1.2115	0.0687	0.8465
12	C7	1.0900(9)	0.1725(5)	0.8590(8)
13	C8	1.1936(8)	0.1994(3)	0.9579(6)
14	H8	1.2885	0.1716	0.9947
15	S2	1.13441(17)	0.28824(8)	1.00809(10)
16	C9	0.9690(10)	0.2917(3)	0.8996(7)
17	H9	0.8927	0.3341	0.8908
18	C10	0.9543(10)	0.2268(4)	0.8241(5)
19	B1	0.8094(14)	0.2190(8)	0.7200(12)
20	C11	0.67405(16)	0.28605(8)	0.69996(11)
21	C12	0.53643(16)	0.27429(9)	0.74504(11)
22	C13	0.42169(17)	0.33497(9)	0.73544(12)
23	H13	0.33	0.3267	0.767
24	C14	0.43860(17)	0.40738(9)	0.68067(12)
25	C15	0.57345(17)	0.41803(8)	0.63450(12)
26	H15	0.5855	0.4668	0.5956
27	C16	0.69148(16)	0.35881(8)	0.64385(12)
28	C17	0.51358(18)	0.19671(9)	0.80532(14)
29	H17A	0.6042	0.1607	0.8047
30	H17B	0.4135	0.171	0.7647
31	H17C	0.5082	0.208	0.8857
32	H17D	0.4131	0.1991	0.832
33	H17E	0.6038	0.1888	0.872
34	H17F	0.5091	0.1518	0.7511

35	C18	0.3124(2)	0.47200(10)	0.67077(16)
36	H18A	0.2094	0.4515	0.6262
37	H18B	0.3444	0.5189	0.6311
38	H18C	0.3015	0.4876	0.7485
39	C19	0.83723(17)	0.37263(9)	0.59364(13)
40	H19A	0.8315	0.4264	0.5592
41	H19B	0.8398	0.3322	0.5338
42	H19C	0.9348	0.3682	0.6554
43	C1'	0.951(4)	0.2287(16)	0.810(2)
44	S1'	0.9618(9)	0.3101(3)	0.8992(6)
45	C2'	1.135(3)	0.2798(14)	0.9928(19)
46	H2'	1.1868	0.3092	1.0596
47	C3'	1.187(3)	0.2113(14)	0.961(3)
48	H3'	1.2842	0.1863	0.9997
49	C4'	1.076(4)	0.1783(18)	0.861(3)
50	C5'	1.126(4)	0.1059(16)	0.813(3)
51	H5'	1.2319	0.0884	0.8469
52	C6'	1.045(4)	0.059(2)	0.727(2)
53	H6'	1.0898	0.0076	0.7224
54	C7'	0.900(4)	0.075(2)	0.641(3)
55	C8'	0.836(3)	0.023(2)	0.552(3)
56	H8'	0.8887	-0.0256	0.5409
57	S2'	0.6594(8)	0.0504(4)	0.4618(6)
58	C9'	0.6575(16)	0.1367(9)	0.5394(14)
59	H9'	0.5757	0.1763	0.5206
60	C10'	0.789(7)	0.143(3)	0.633(5)
61	B1'	0.806(5)	0.218(3)	0.711(5)

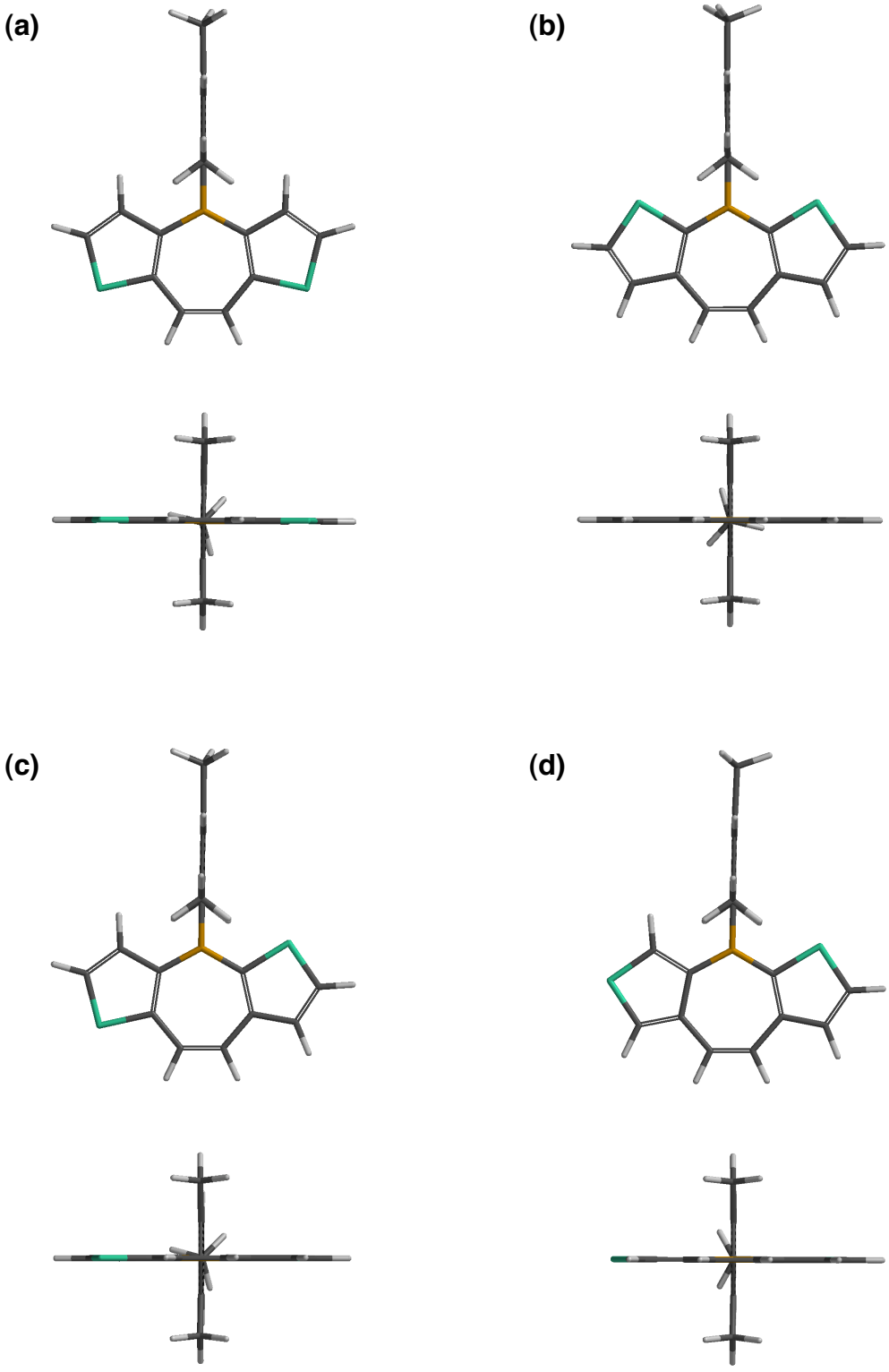

Figure A2.21. DFT optimized geometries (B3LYP/6-31G*) for (a) **1**, (b) **2**, (c) **3**, (d) **4** shown (top) perpendicular to and (bottom) parallel to the polycyclic plane.

Table A2.2. Cartesian coordinates (in Å) for optimized geometries of **1**, **2**, **3**, and **4** calculated at the DFT (B3LYP/6-31G*) level.

1

	Atom		X	Y	Z
1	C	C2	1.6730562	-1.3608897	0.0083458
2	C	C5	4.1692929	-0.6893673	0.0054649
3	H	H2	5.1515370	-1.1576556	0.0084582
4	C	C6	4.1707620	0.6792254	-0.0021241
5	H	H5	5.1540098	1.1453934	-0.0043177
6	C	C8	1.6759918	1.3560193	-0.0073872
7	B	B1	0.9459648	-0.0016851	0.0000890
8	C	C11	-0.6428425	0.0002804	-0.0012485
9	C	C12	-3.4849942	0.0102804	-0.0035398
10	C	C13	-1.3667269	0.0159792	1.2132385
11	C	C14	-1.3635730	-0.0081188	-1.2154221
12	C	C15	-2.7631761	-0.0016190	-1.1990450
13	C	C16	-2.7644937	0.0217693	1.1949334
14	H	H7	-3.3027228	-0.0045344	-2.1449486
15	H	H10	-3.3053497	0.0378890	2.1402593
16	C	C17	-0.6326646	-0.0208976	-2.5426016
17	H	H4	0.0202477	0.8545542	-2.6521385
18	H	H12	-1.3330374	-0.0216167	-3.3840664
19	H	H13	0.0080489	-0.9066917	-2.6407461
20	C	C18	-4.9962999	-0.0073954	-0.0000923
21	H	H11	-5.3855735	-1.0052603	0.2438562
22	H	H14	-5.4022195	0.2710254	-0.9783915
23	H	H15	-5.4045858	0.6861772	0.7443761
24	C	C19	-0.6363269	0.0312552	2.5406235
25	H	H1	-1.3369263	0.0378489	3.3818642
26	H	H16	0.0081470	0.9146655	2.6356788
27	H	H17	0.0129297	-0.8465072	2.6533684
28	C	C1	3.0637263	-1.5855773	0.0101139
29	C	C3	3.0671222	1.5777927	-0.0076953
30	S	S1	3.4372253	-3.3071487	0.0200153
31	S	S2	3.4442578	3.2985945	-0.0171994
32	C	C4	1.7537240	-3.7215627	0.0218109
33	C	C7	0.9614253	-2.6129578	0.0152455
34	H	H38	-0.1217145	-2.6626175	0.0151832
35	C	C9	0.9669914	2.6095896	-0.0151688
36	H	H41	-0.1160353	2.6616782	-0.0164577
37	C	C10	1.7616410	3.7165144	-0.0208321
38	H	H60	1.4616160	4.7564547	-0.0270795
39	H	H81	1.4515456	-4.7608843	0.0275771

2

	Atom		X	Y	Z
1	S	S1	-0.5123355	-2.8267484	0.0107660
2	C	C1	-1.9448237	-3.7934778	0.0144831
3	C	C2	-1.4276706	-1.3262664	0.0044272
4	C	C3	-2.8071649	-1.6184661	0.0052831
5	C	C4	-3.0743065	-3.0306972	0.0110822
6	H	H6	-4.0793763	-3.4404921	0.0127348
7	C	C5	-3.8959930	-0.6832222	0.0015565
8	H	H2	-4.8800310	-1.1496429	0.0030404
9	C	C6	-3.8960633	0.6804530	-0.0034021
10	H	H5	-4.8801685	1.1467048	-0.0052524
11	C	C7	-2.8073601	1.6158807	-0.0069774
12	C	C8	-1.4278022	1.3238551	-0.0053070
13	S	S2	-0.5126636	2.8244734	-0.0115948
14	C	C9	-1.9453447	3.7909824	-0.0164414
15	C	C10	-3.0747280	3.0280719	-0.0132072
16	H	H8	-4.0798414	3.4377655	-0.0152906
17	C	C11	0.9220729	-0.0004895	0.0014745
18	C	C12	3.7611808	0.0102152	0.0036597
19	C	C13	1.6448794	-0.0068932	-1.2149214
20	C	C14	1.6416123	0.0127735	1.2174410
21	C	C15	3.0405299	0.0193174	1.1996088
22	C	C16	3.0419143	-0.0000648	-1.1953041
23	H	H7	3.5807410	0.0333396	2.1448671
24	H	H10	3.5834730	-0.0005748	-2.1401870
25	C	C17	0.9145385	0.0217807	2.5467780
26	H	H4	0.2569892	0.8947960	2.6425489
27	H	H12	1.6194864	0.0432464	3.3839629
28	H	H13	0.2823247	-0.8669809	2.6667586
29	C	C18	5.2721369	-0.0070813	0.0003517
30	H	H11	5.6602885	-1.0089339	-0.2283135
31	H	H14	5.6781736	0.2865657	0.9740676
32	H	H15	5.6798864	0.6748158	-0.7551280
33	C	C19	0.9184914	-0.0179089	-2.5445880
34	H	H1	1.6239312	-0.0145188	-3.3816534
35	H	H16	0.2653101	0.8565580	-2.6558782
36	H	H17	0.2817997	-0.9054141	-2.6491953
37	H	H32	-1.8796627	4.8717487	-0.0212959
38	H	H40	-1.8791300	-4.8742328	0.0190365
39	B	B1	-0.6652941	-0.0012374	0.0000093

3

		Atom	X	Y	Z
1	C	C1	1.6660483	-1.1466057	0.0080859
2	C	C2	3.0647662	-1.3330819	0.0033968
3	C	C5	4.0747175	-0.3160579	-0.0060806
4	C	C6	3.9610070	1.0455460	-0.0110372
5	C	C7	2.7865833	1.8545200	-0.0079474
6	C	C8	1.4180546	1.5241389	-0.0013777
7	S	S2	3.0228462	3.6003363	-0.0128857
8	C	C9	1.3120433	3.8821410	-0.0063896
9	C	C10	0.6090925	2.7150096	-0.0006758
10	B	B1	0.8001768	0.1132550	0.0041924
11	C	C11	-0.7809276	-0.0385525	0.0041289
12	C	C12	-3.6069531	-0.3274961	0.0002670
13	C	C13	-1.4978833	-0.1138894	-1.2131111
14	C	C14	-1.5009349	-0.1021796	1.2175835
15	C	C15	-2.8929190	-0.2477034	1.1973576
16	C	C16	-2.8876364	-0.2592604	-1.1968941
17	C	C17	-0.7719046	-0.0357238	-2.5408391
18	C	C18	-0.7810361	-0.0091345	2.5476649
19	H	H2	-0.2164542	0.9056242	-2.6405837
20	H	H13	-0.0423402	-0.8476711	-2.6530641
21	H	H12	-1.4715684	-0.0998265	-3.3805098
22	H	H4	5.0943916	-0.6975159	-0.0096152
23	H	H1	4.9010275	1.5943610	-0.0179351
24	H	H9	0.9296012	4.8947538	-0.0069259
25	H	H7	-0.4742783	2.6745660	0.0039972
26	H	H5	-0.2438147	0.9427575	2.6475818
27	H	H15	-1.4821192	-0.0850087	3.3850165
28	H	H10	-3.4230317	-0.3240391	-2.1432208
29	H	H8	-3.4323381	-0.3026384	2.1417251
30	C	C19	-5.1121555	-0.4631134	-0.0081852
31	H	H16	-5.4435150	-1.2174298	-0.7317528
32	H	H11	-5.4942334	-0.7509414	0.9768977
33	H	H17	-5.5977009	0.4822949	-0.2857924
34	H	H14	-0.0368416	-0.8069493	2.6633589
35	S	S1	0.8703908	-2.7145977	0.0191176
36	C	C3	2.3731570	-3.5672436	0.0169449
37	H	H6	2.3918054	-4.6501168	0.0228012
38	C	C4	3.4408025	-2.7200594	0.0085019
39	H	H3	4.4740744	-3.0524679	0.0062034

4

	Atom		X	Y	Z
1	C	C1	1.4140628	-1.4847411	-0.0005947
2	C	C2	0.6609747	-2.6448090	-0.0022962
3	H	H5	-0.4185644	-2.7146175	-0.0030383
4	C	C3	2.8378877	-1.8009037	-0.0007475
5	C	C4	3.0711213	-3.1644333	-0.0016703
6	H	H3	4.0310327	-3.6641852	-0.0016788
7	S	S1	1.6129129	-4.0799230	-0.0032612
8	C	C5	3.9540632	-0.8816031	-0.0000671
9	H	H4	4.9271616	-1.3705204	-0.0001988
10	C	C6	3.9811672	0.4748853	0.0004151
11	H	H1	4.9740573	0.9219137	0.0004750
12	B	B1	0.7189773	-0.1009176	0.0004593
13	C	C11	-0.8663438	-0.0331476	0.0004314
14	C	C12	-3.7037585	0.0934886	-0.0003778
15	C	C13	-1.5875987	-0.0074727	1.2159204
16	C	C14	-1.5867948	-0.0046663	-1.2154594
17	C	C15	-2.9838401	0.0575932	-1.1974111
18	C	C16	-2.9845649	0.0547712	1.1971214
19	H	H9	-3.5237645	0.0777797	-2.1429189
20	H	H10	-3.5249511	0.0729929	2.1424054
21	C	C17	-0.8610276	-0.0557035	2.5447489
22	H	H2	-1.5640810	-0.0307126	3.3834481
23	H	H12	-0.1740383	0.7919128	2.6610123
24	H	H13	-0.2583526	-0.9677299	2.6403834
25	C	C18	-0.8592894	-0.0505650	-2.5438765
26	H	H7	-1.5614735	-0.0200003	-3.3831170
27	H	H14	-0.2598366	-0.9644417	-2.6422269
28	H	H15	-0.1691457	0.7949725	-2.6564051
29	C	C19	-5.2115393	0.1952685	-0.0006811
30	H	H11	-5.5413859	1.2432517	0.0053759
31	H	H16	-5.6465835	-0.2853938	0.8825518
32	H	H17	-5.6454238	-0.2749606	-0.8900333
33	C	C20	3.2206064	2.8447852	0.0017043
34	C	C21	2.1149137	3.6474470	0.0020075
35	S	S2	0.6561463	2.7309592	0.0014420
36	C	C22	1.5237898	1.2001907	0.0010226
37	C	C23	2.9081177	1.4458409	0.0007610
38	H	H33	2.0874469	4.7298899	0.0024957
39	H	H39	4.2379186	3.2235049	0.0018788

Table A2.3. TD-DFT (B3LYP/6-31G*) calculated excited states and transition energies for **1**, **2**, **3**, and **4**.

1

TDDFT/TDA Excitation Energies

Excited state 1: excitation energy (eV) = 3.4889
Total energy for state 1: -1555.393282622078
Multiplicity: Singlet
Trans. Mom.: -0.0012 X -0.0033 Y -0.0129 Z
Strength : 0.0000
HOMO-1 → LUMO amplitude = 0.9985

Excited state 2: excitation energy (eV) = 3.7363
Total energy for state 2: -1555.384188839874
Multiplicity: Singlet
Trans. Mom.: -0.0084 X 0.0035 Y 0.0005 Z
Strength : 0.0000
HOMO-2 → LUMO amplitude = 0.9978

Excited state 3: excitation energy (eV) = 3.8199
Total energy for state 3: -1555.381117344484
Multiplicity: Singlet
Trans. Mom.: 0.0037 X 2.1611 Y -0.0128 Z
Strength : 0.4371
HOMO-3 → LUMO+1 amplitude = -0.3470
HOMO → LUMO amplitude = 0.9145

Excited state 4: excitation energy (eV) = 3.8921
Total energy for state 4: -1555.378464209810
Multiplicity: Singlet
Trans. Mom.: 0.5185 X -0.0054 Y 0.0001 Z
Strength : 0.0256
HOMO-4 → LUMO amplitude = 0.2714
HOMO-3 → LUMO amplitude = 0.3253
HOMO → LUMO+1 amplitude = 0.8929

Excited state 5: excitation energy (eV) = 3.9048
Total energy for state 5: -1555.377999435622
Multiplicity: Singlet
Trans. Mom.: 0.0111 X 0.0073 Y 0.0005 Z
Strength : 0.0000
HOMO-1 → LUMO+1 amplitude = 0.9939

2

TDDFT/TDA Excitation Energies

Excited state 1: excitation energy (eV) = 3.5746
Total energy for state 1: -1555.397413884652
Multiplicity: Singlet
Trans. Mom.: 0.0110 X -0.0012 Y -0.0004 Z
Strength : 0.0000
HOMO-1 → LUMO amplitude = 0.9956

Excited state 2: excitation energy (eV) = 3.8045
Total energy for state 2: -1555.388964206992
Multiplicity: Singlet
Trans. Mom.: 0.6514 X -0.0158 Y 0.0015 Z
Strength : 0.0396
HOMO-3 → LUMO+1 amplitude = 0.2308
HOMO-2 → LUMO amplitude = 0.7060
HOMO → LUMO amplitude = -0.6348

Excited state 3: excitation energy (eV) = 3.8069
Total energy for state 3: -1555.388875942188
Multiplicity: Singlet
Trans. Mom.: -0.6551 X -0.0137 Y 0.0009 Z
Strength : 0.0400
HOMO-3 → LUMO+1 amplitude = -0.2349
HOMO-2 → LUMO amplitude = 0.7057
HOMO → LUMO amplitude = 0.6306

Excited state 4: excitation energy (eV) = 3.8529
Total energy for state 4: -1555.387186387519
Multiplicity: Singlet
Trans. Mom.: 0.0201 X 0.0013 Y -0.0211 Z
Strength : 0.0001
HOMO-1 → LUMO+2 amplitude = 0.9969

Excited state 5: excitation energy (eV) = 4.0607
Total energy for state 5: -1555.379551182434
Multiplicity: Singlet
Trans. Mom.: -0.1612 X -0.0176 Y -0.0006 Z
Strength : 0.0026
HOMO-2 → LUMO+2 amplitude = -0.9950

3

TDDFT/TDA Excitation Energies

Excited state 1: excitation energy (eV) = 3.6035
Total energy for state 1: -1555.392803381599
Multiplicity: Singlet
Trans. Mom.: 0.0053 X 0.0026 Y 0.0053 Z
Strength : 0.0000
HOMO-1 → LUMO amplitude = 0.9476
HOMO-1 → LUMO+1 amplitude = 0.3126

Excited state 2: excitation energy (eV) = 3.7722
Total energy for state 2: -1555.386604893714
Multiplicity: Singlet
Trans. Mom.: 0.0168 X 0.0103 Y 0.0049 Z
Strength : 0.0000
HOMO-1 → LUMO amplitude = -0.3139
HOMO-1 → LUMO+1 amplitude = 0.9444

Excited state 3: excitation energy (eV) = 3.8074
Total energy for state 3: -1555.385312241519
Multiplicity: Singlet
Trans. Mom.: 0.6768 X 0.4116 Y -0.0031 Z
Strength : 0.0585
HOMO-4 → LUMO amplitude = -0.2277
HOMO-3 → LUMO amplitude = -0.3055
HOMO → LUMO amplitude = 0.3725
HOMO → LUMO+1 amplitude = 0.8002

Excited state 4: excitation energy (eV) = 3.8392
Total energy for state 4: -1555.384144017414
Multiplicity: Singlet
Trans. Mom.: 0.1792 X 0.2166 Y -0.0007 Z
Strength : 0.0074
HOMO-2 → LUMO amplitude = 0.9489
HOMO-2 → LUMO+1 amplitude = 0.2263

Excited state 5: excitation energy (eV) = 3.9788
Total energy for state 5: -1555.379014284684
Multiplicity: Singlet
Trans. Mom.: -0.0956 X 1.3705 Y -0.0047 Z
Strength : 0.1840
HOMO-3 → LUMO+1 amplitude = 0.4006
HOMO → LUMO amplitude = 0.7665
HOMO → LUMO+1 amplitude = -0.3729

4

TDDFT/TDA Excitation Energies

Excited state 1: excitation energy (eV) = 3.2721
Total energy for state 1: -1555.397473006435
Multiplicity: Singlet
Trans. Mom.: 0.0027 X -0.0010 Y 0.0011 Z
Strength : 0.0000
HOMO-1 → LUMO amplitude = 0.9942

Excited state 2: excitation energy (eV) = 3.3913
Total energy for state 2: -1555.393094557601
Multiplicity: Singlet
Trans. Mom.: -1.0704 X 0.7176 Y 0.0004 Z
Strength : 0.1380
HOMO → LUMO amplitude = 0.9514

Excited state 3: excitation energy (eV) = 3.5181
Total energy for state 3: -1555.388433570173
Multiplicity: Singlet
Trans. Mom.: -0.0714 X 0.0977 Y 0.0001 Z
Strength : 0.0013
HOMO-2 → LUMO amplitude = 0.9952

Excited state 4: excitation energy (eV) = 4.1065
Total energy for state 4: -1555.366810446701
Multiplicity: Singlet
Trans. Mom.: 0.0791 X 0.8773 Y 0.0007 Z
Strength : 0.0781
HOMO-3 → LUMO amplitude = 0.8580
HOMO → LUMO+1 amplitude = 0.4584

Excited state 5: excitation energy (eV) = 4.5931
Total energy for state 5: -1555.348929777693
Multiplicity: Singlet
Trans. Mom.: -0.5063 X 0.3652 Y 0.0003 Z
Strength : 0.0439
HOMO-4 → LUMO amplitude = 0.7990
HOMO → LUMO+1 amplitude = -0.2135
HOMO → LUMO+2 amplitude = -0.49

Appendix 3. Supporting Information for Chapter 4

List of Figures

List of Tables

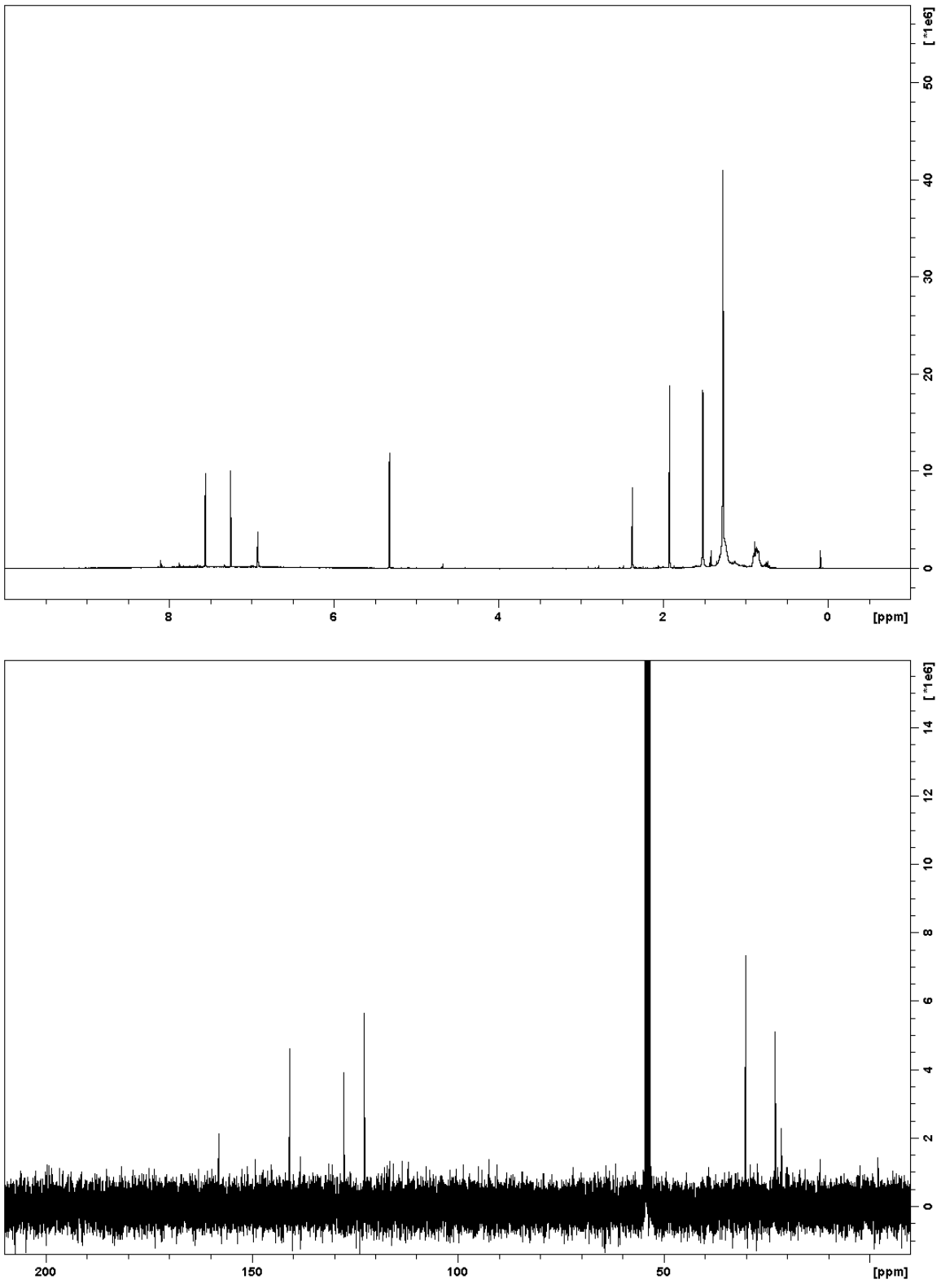

Figure A3.1. ^{1}H (400 MHz, CD_2Cl_2) and ^{13}C NMR (100 MHz, CD_2Cl_2) spectra for **1-Br$_2$**.

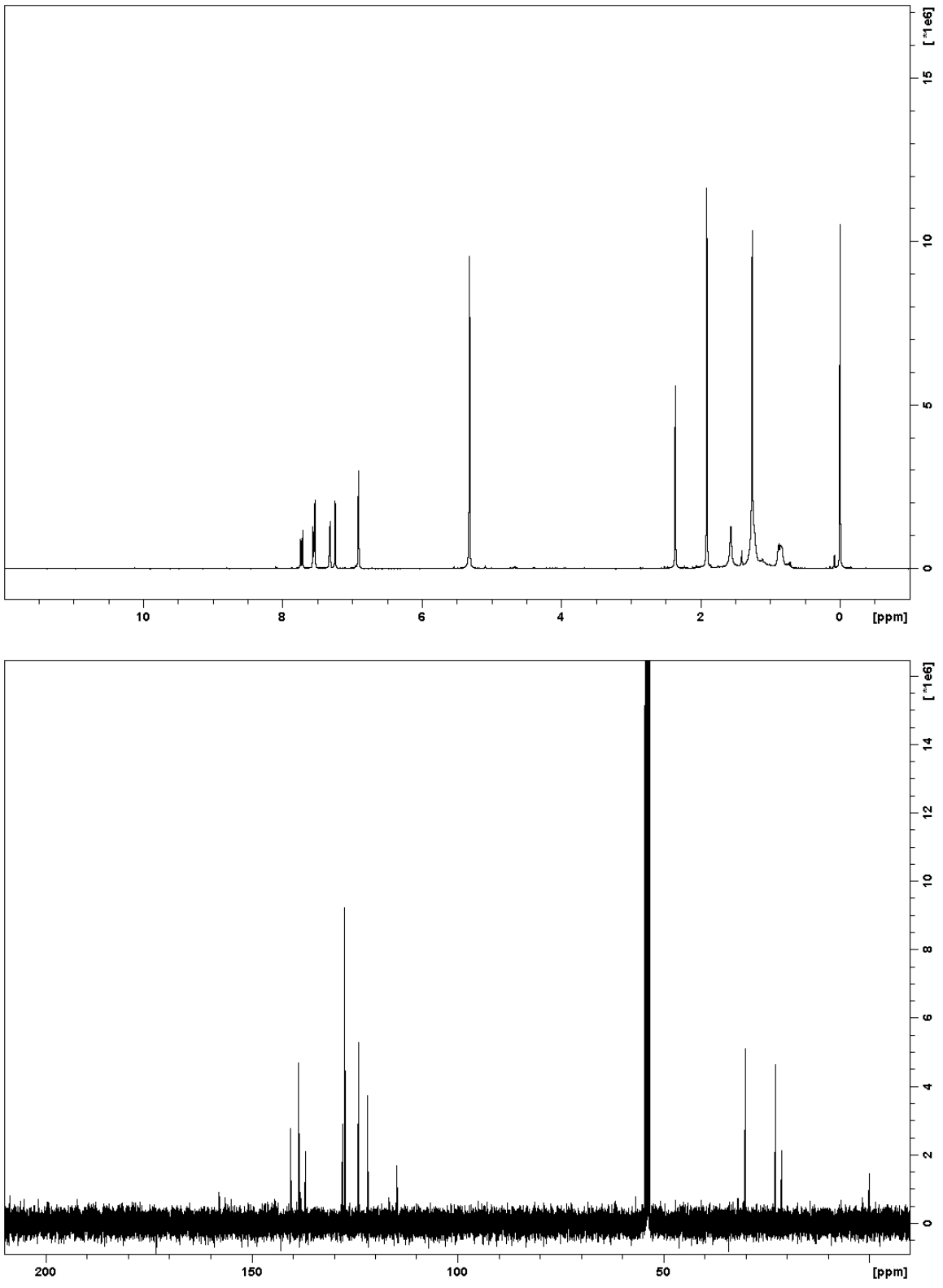

Figure A3.2. ^{1}H (400 MHz, CD_2Cl_2) and ^{13}C NMR (100 MHz, CD_2Cl_2) spectra for **1-Br**.

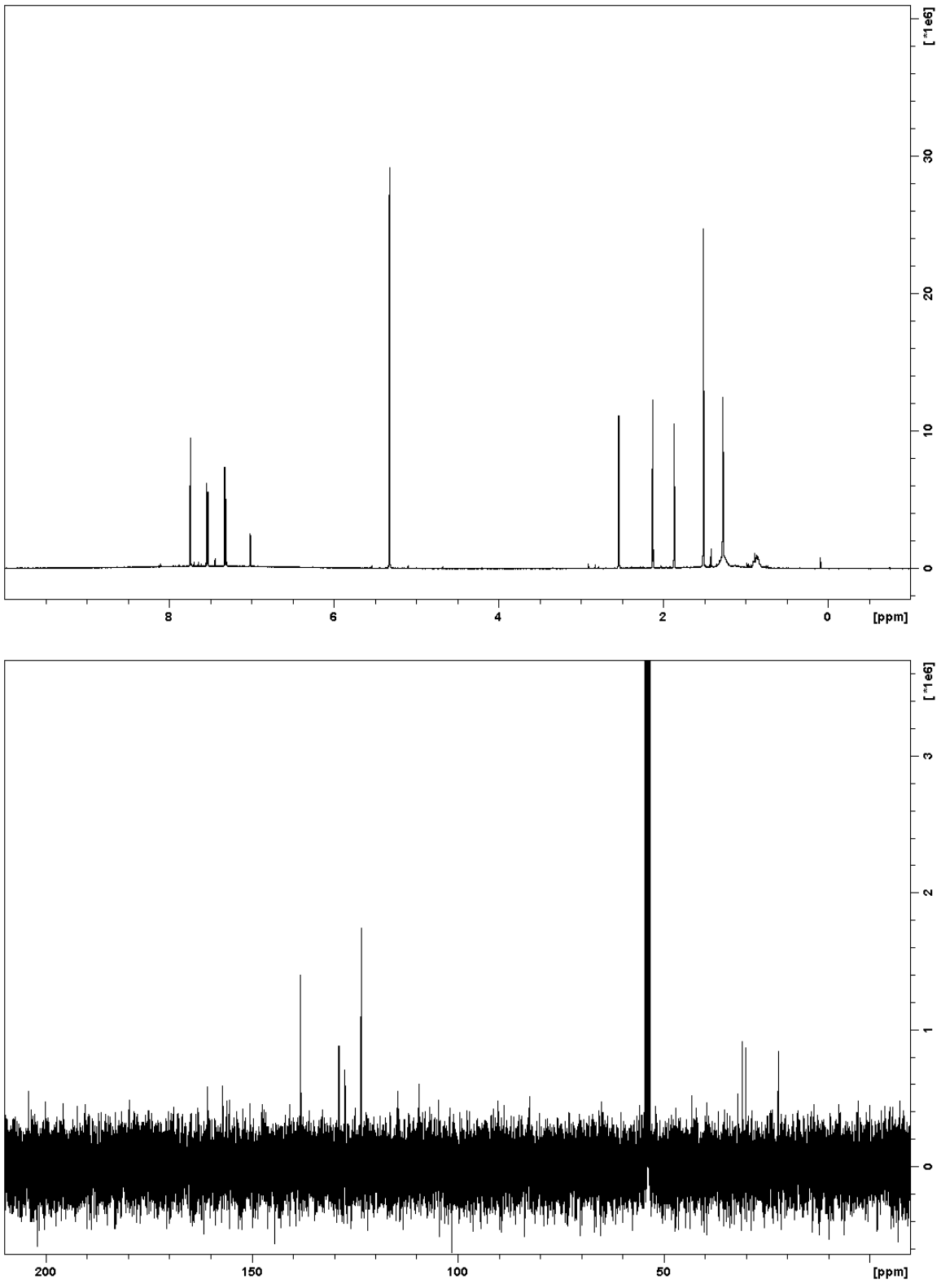

Figure A3.3. ^{1}H (400 MHz, CD_2Cl_2) and ^{13}C NMR (100 MHz, CD_2Cl_2) spectra for **1-Mes-I**.

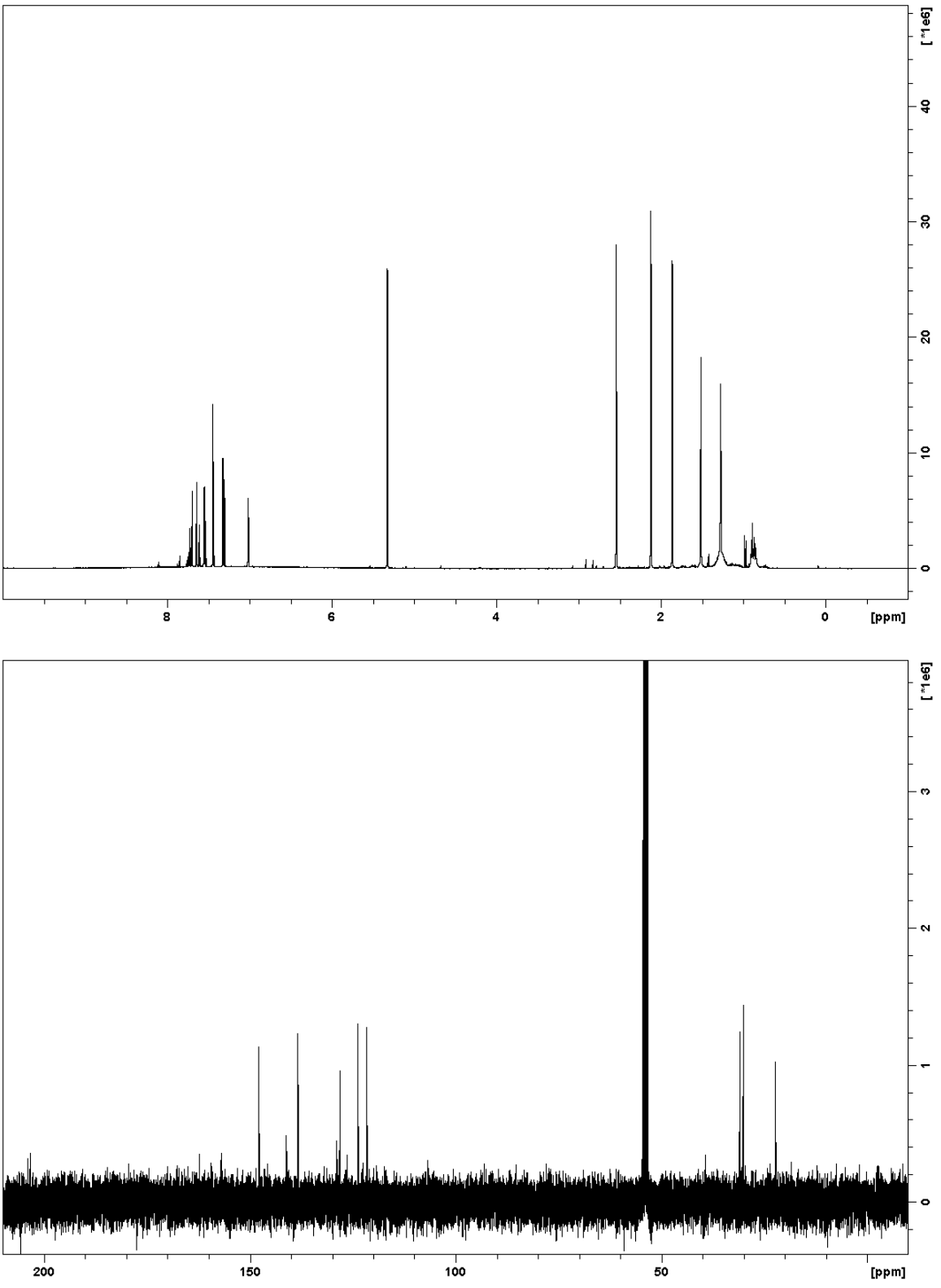

Figure A3.4. ^{1}H (400 MHz, CD_2Cl_2) and ^{13}C NMR (100 MHz, CD_2Cl_2) spectra for **1-I-Mes-I**.

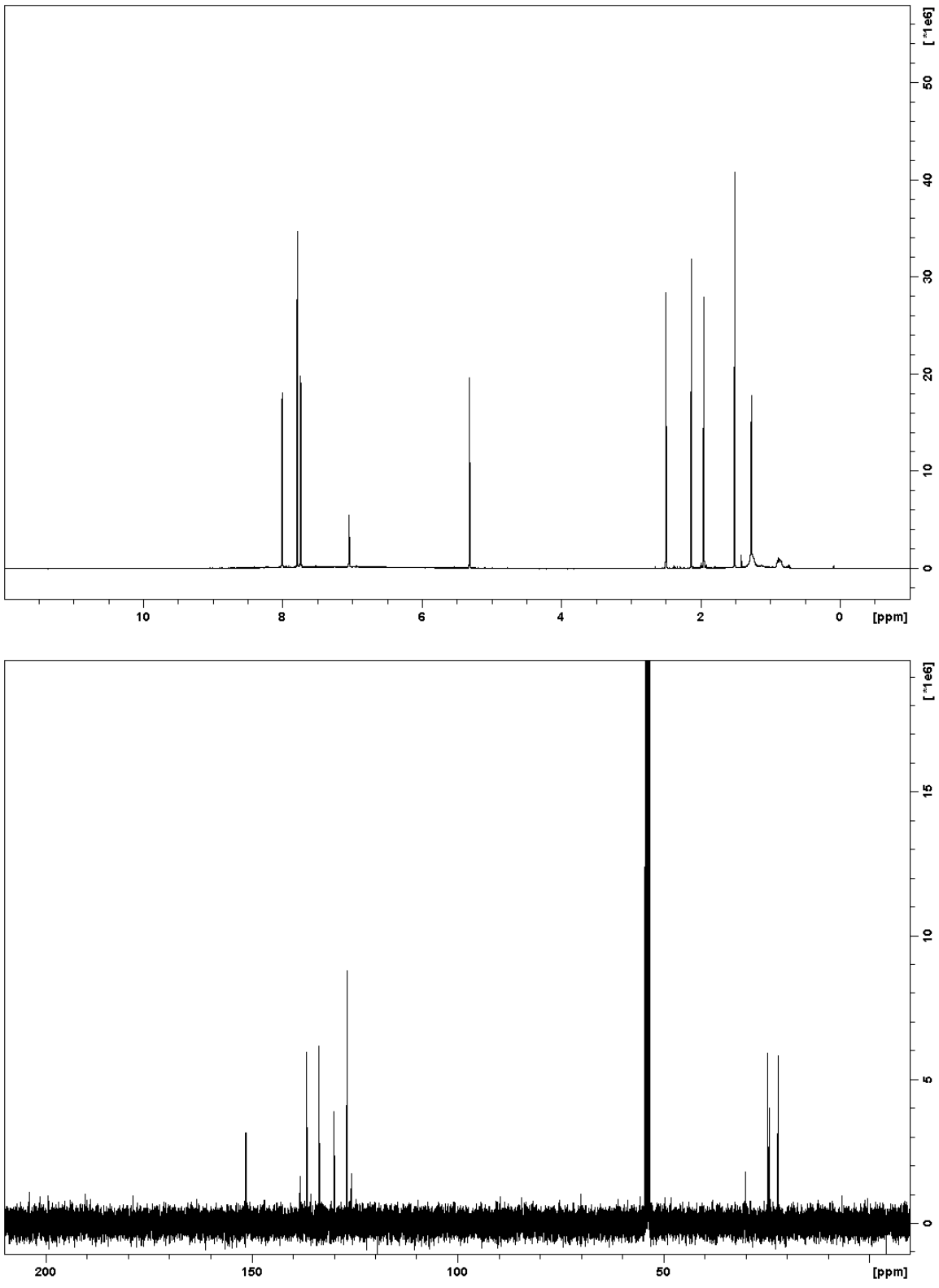

Figure A3.5. ^{1}H (400 MHz, CD_2Cl_2) and ^{13}C NMR (100 MHz, CD_2Cl_2) spectra for **2-Mes-Br**.

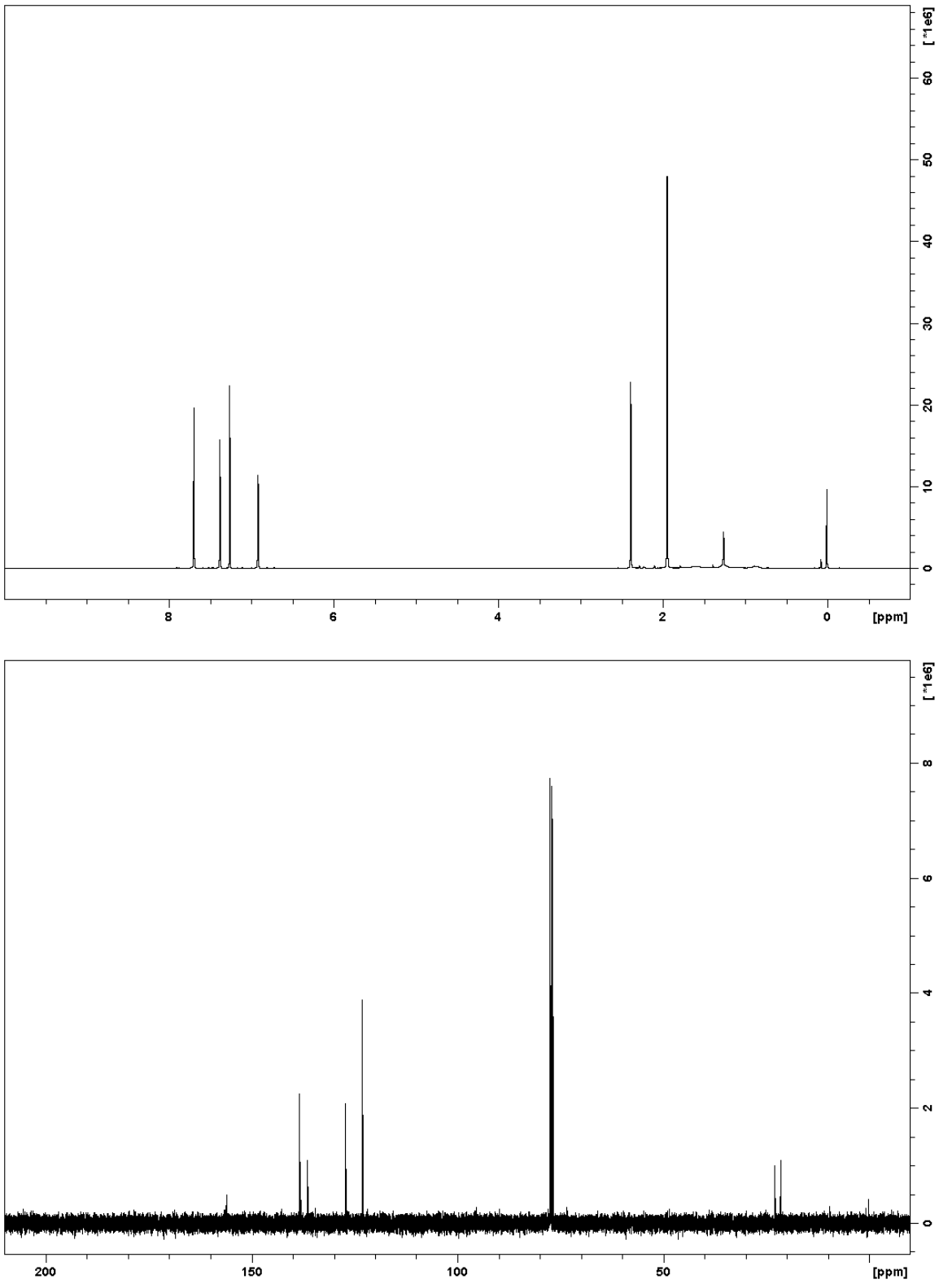

Figure A3.6. ^{1}H (400 MHz, $CDCl_3$) and ^{13}C NMR (100 MHz, $CDCl_3$) spectra for **1-*d*$_2$**.

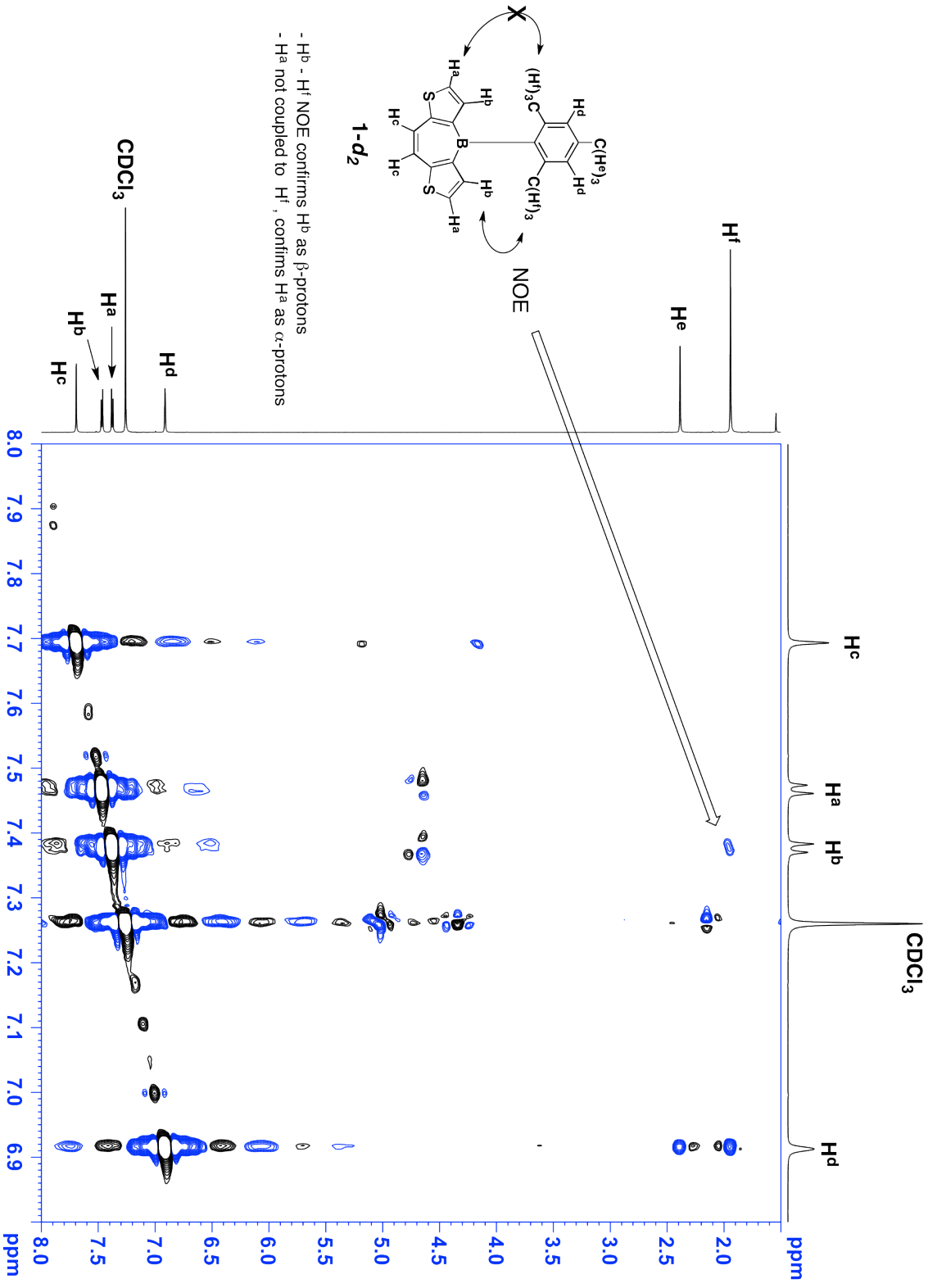

Figure A3.7. ^{1}H NOESY spectra of **1** in $CDCl_3$ (400 MHz). Negatively phased signals are shown as blue contours (NOE signals).

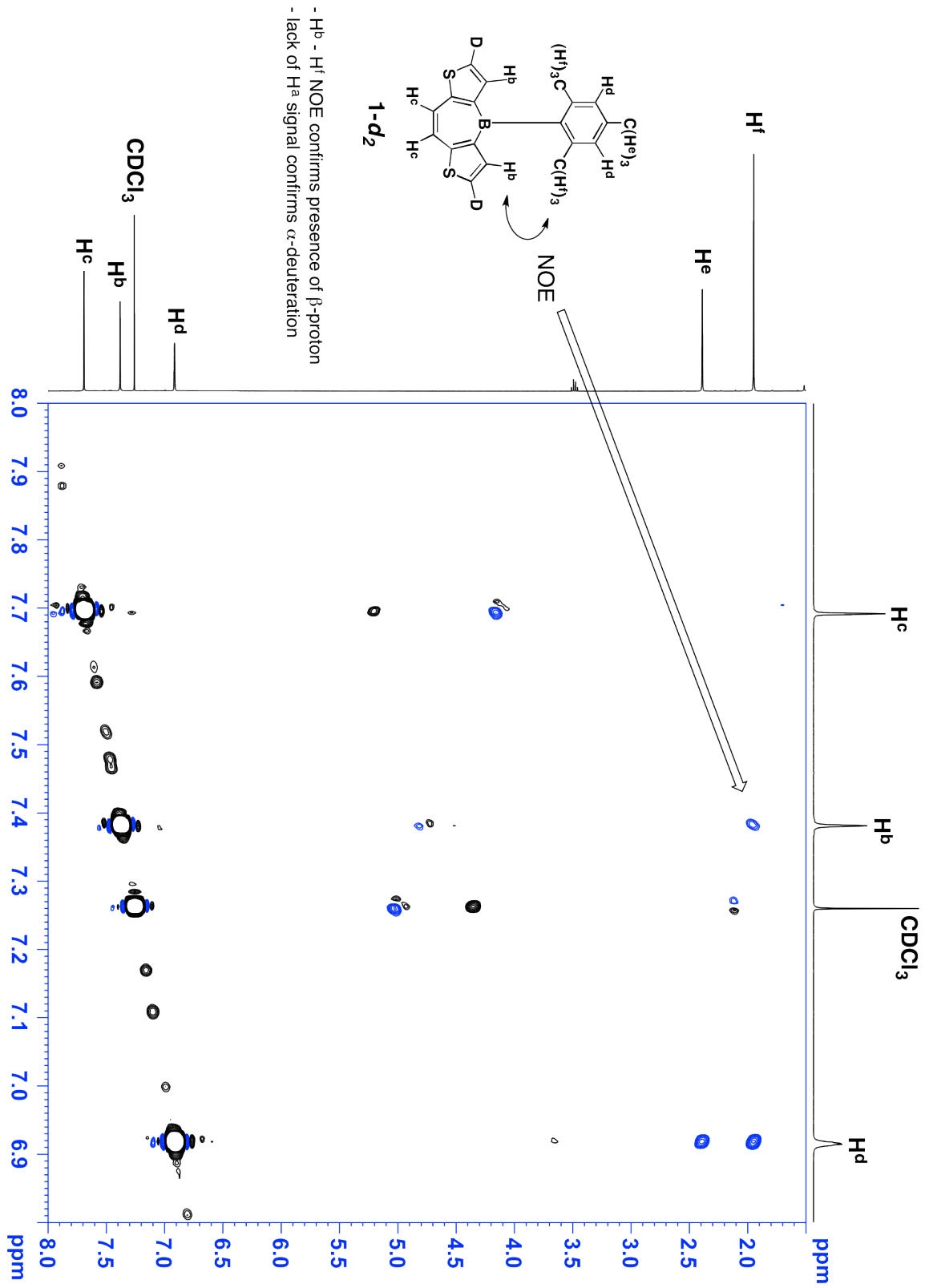

Figure A3.8. ^{1}H NOESY spectra of **1-*d*$_2$** in $CDCl_3$ (400 MHz). Negatively phased signals are shown as blue contours (NOE signals)

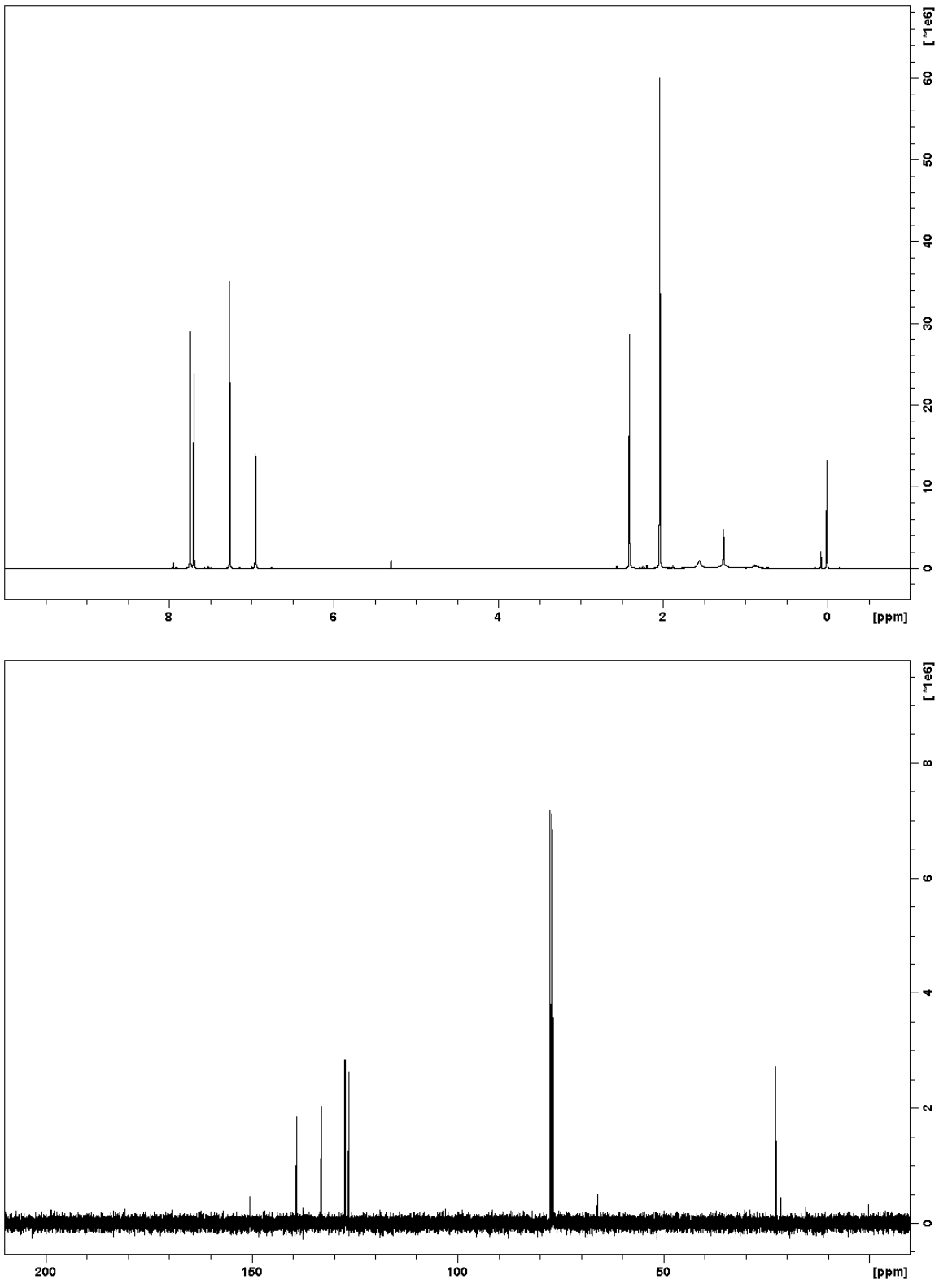

Figure A3.9. ^{1}H (400 MHz, $CDCl_3$) and ^{13}C NMR (100 MHz, $CDCl_3$) spectra for **2-*d*$_2$**.

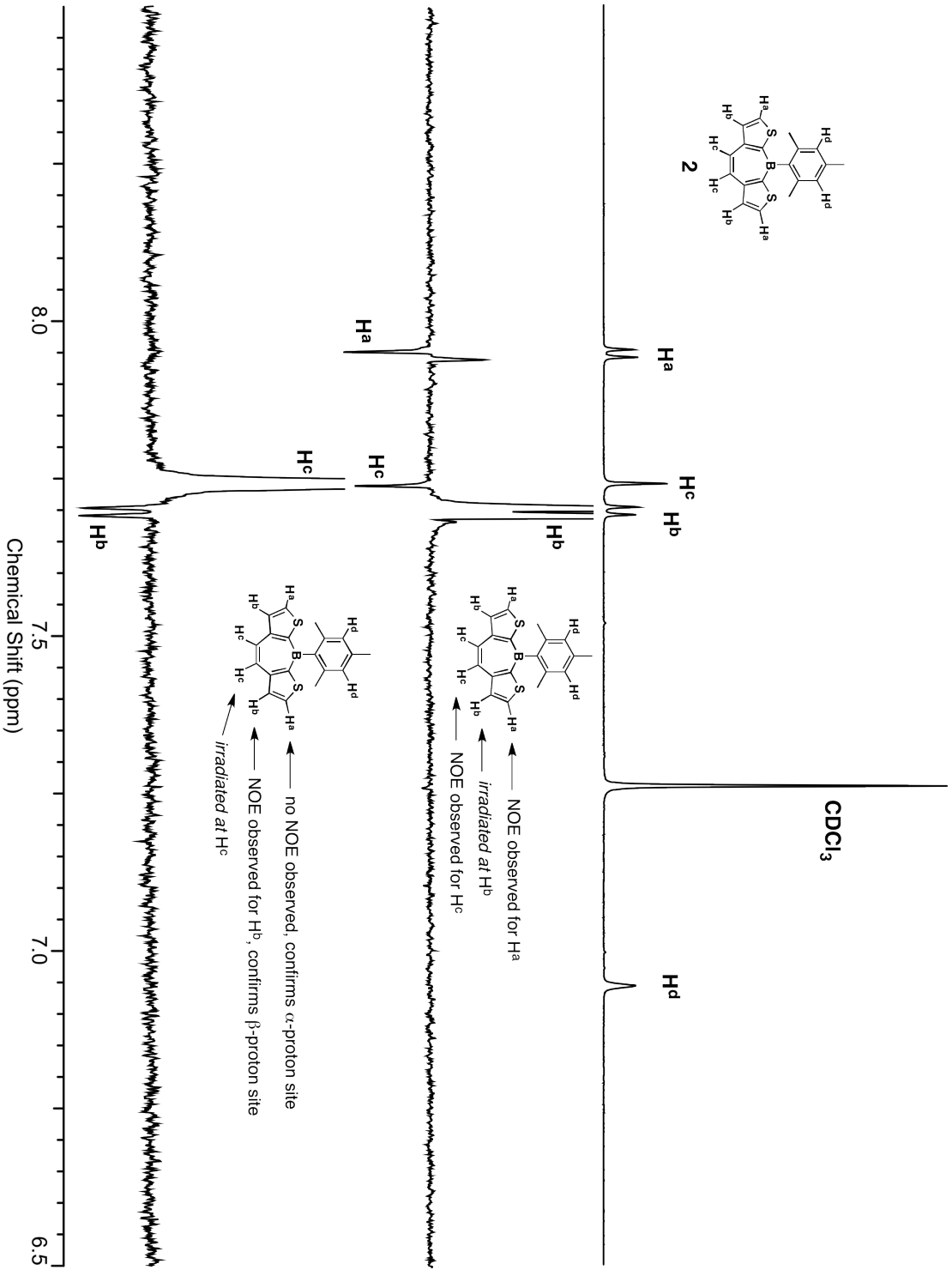

Figure A3.10. 1-D ^{1}H and ^{1}H NOE spectra of **2** in $CDCl_3$: (a) ^{1}H NMR spectrum. (b) ^{1}H NOE spectrum upon irradiation at Hb. (c) ^{1}H NOE spectrum upon irradiation at Hc.

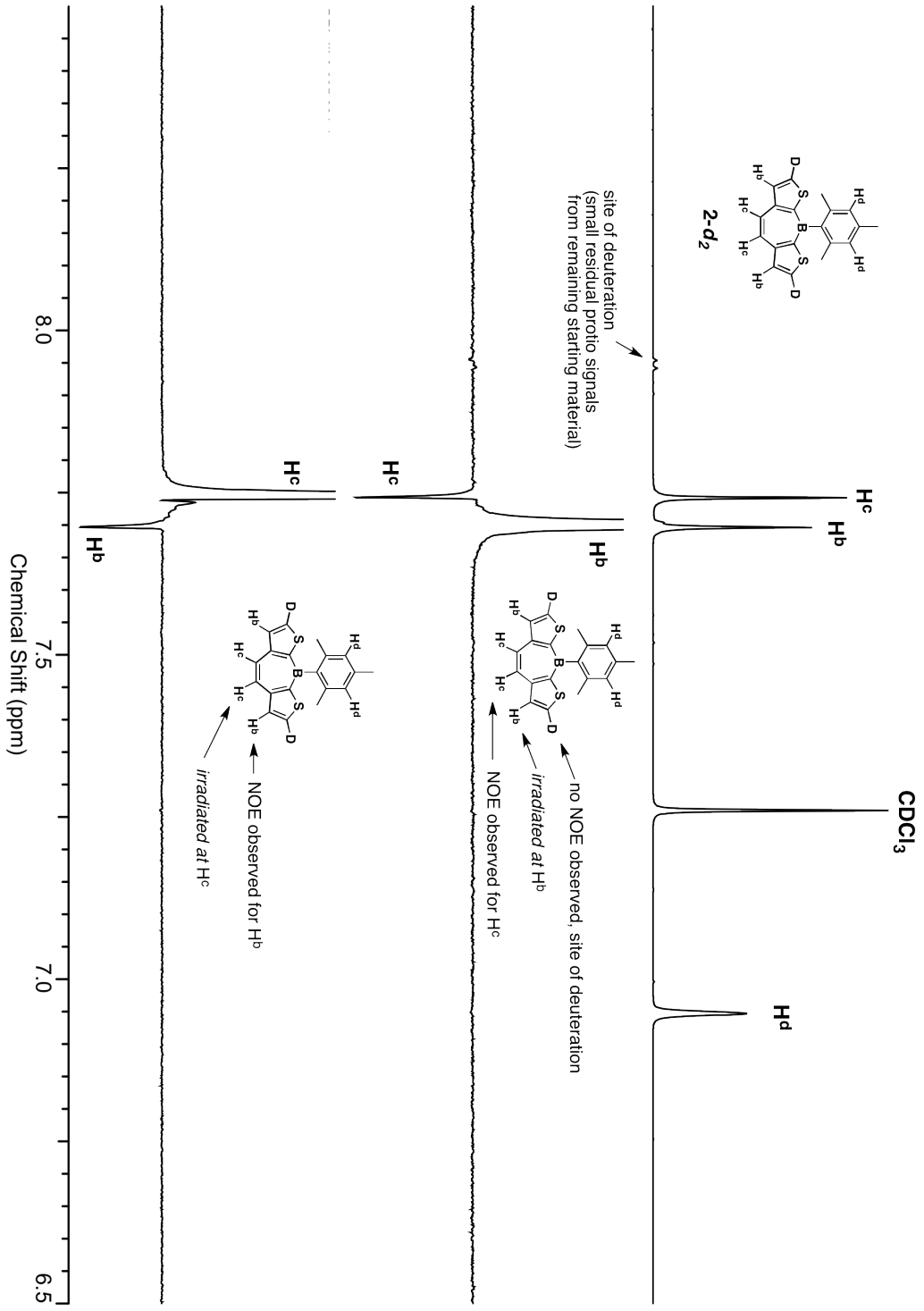

Figure A3.11. 1D ^{1}H and ^{1}H NOE spectra of **2-*d*$_2$** in $CDCl_3$: (a) ^{1}H NMR spectrum. (b) ^{1}H NOE spectrum upon irradiation at Hb. (c) ^{1}H NOE spectrum upon irradiation at Hc.

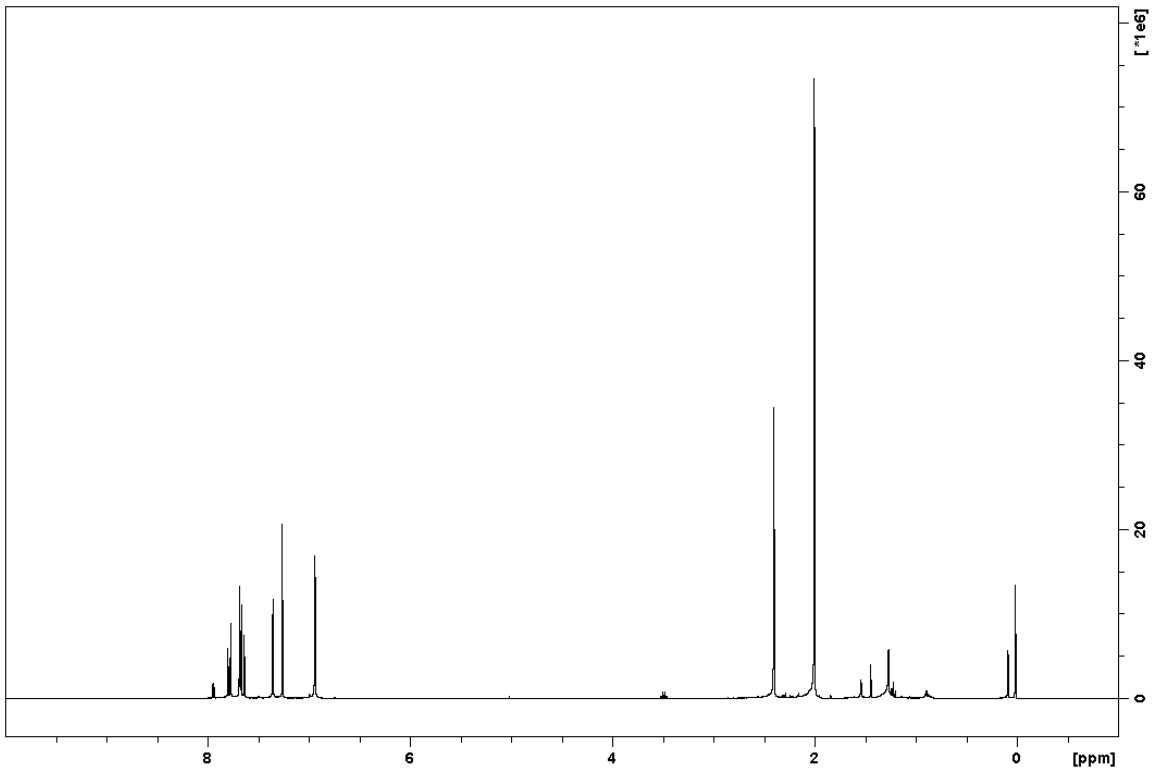

Figure A3.12. ^{1}H (400 MHz, $CDCl_3$) spectrum for **3-d_2**.

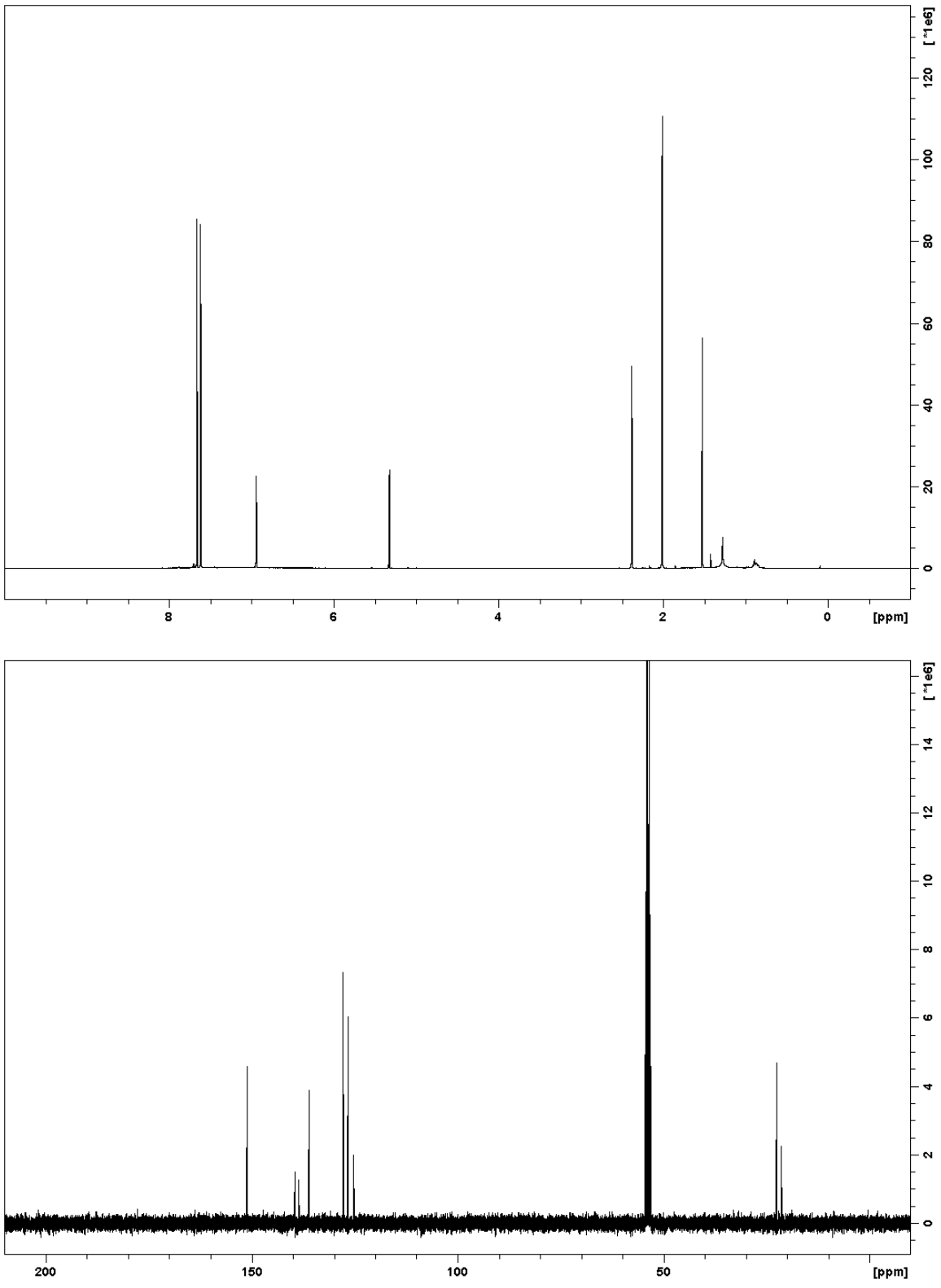

Figure A3.13. ^{1}H (400 MHz, CD_2Cl_2) and ^{13}C NMR (100 MHz, CD_2Cl_2) spectra for **2-Br$_2$**.

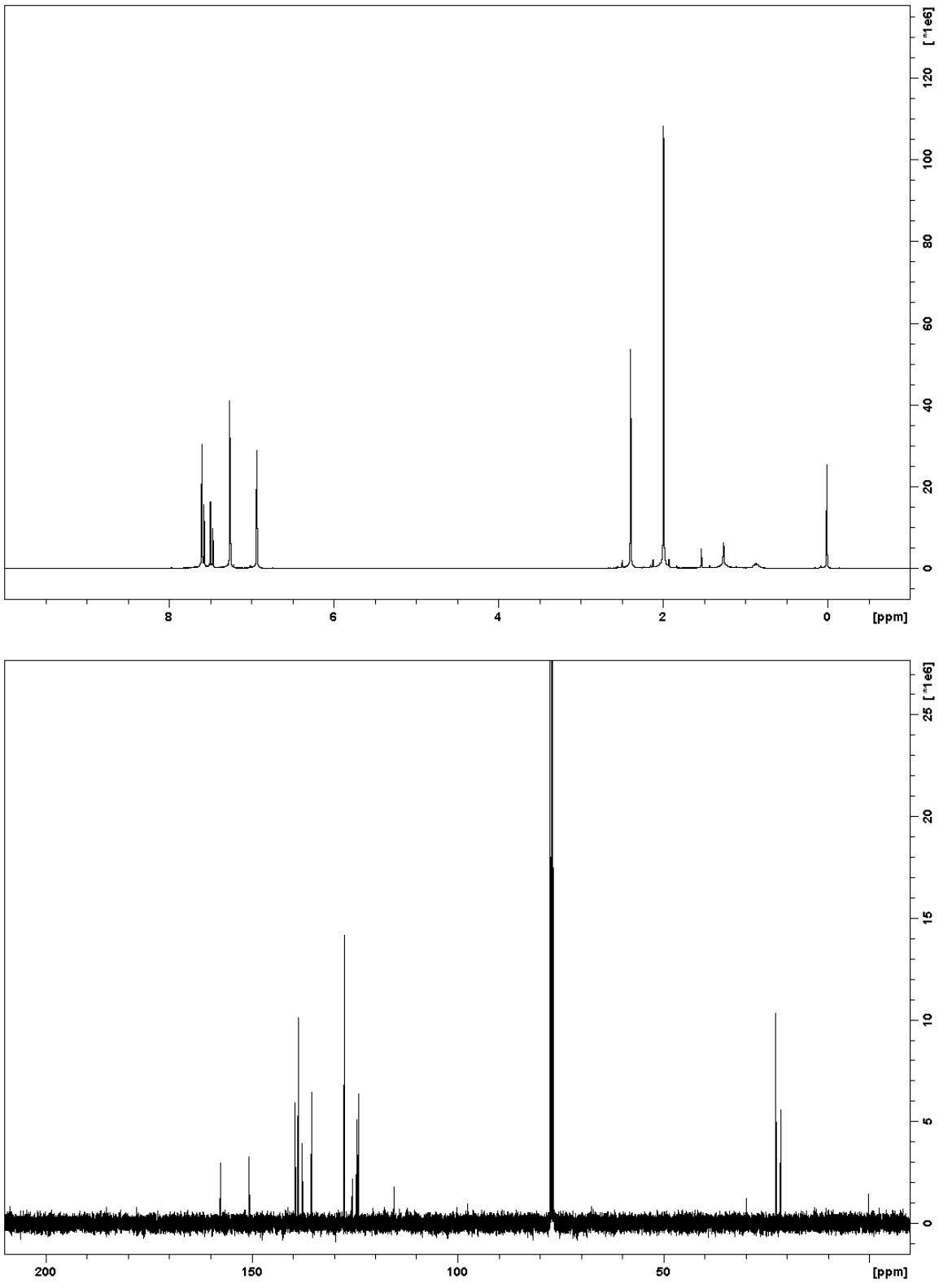

Figure A3.14. ^{1}H (400 MHz, $CDCl_3$) and ^{13}C NMR (100 MHz, $CDCl_3$) spectra for **3-Br$_2$**.

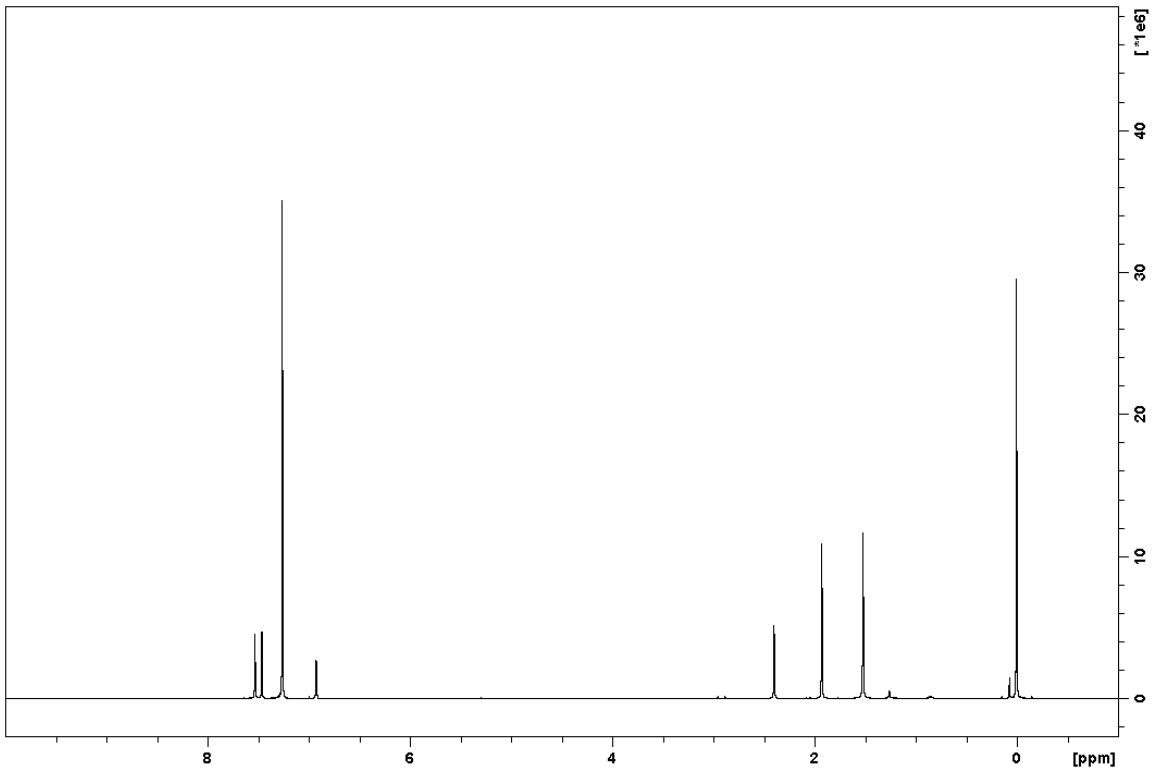

Figure A3.15. ^{1}H (400 MHz, $CDCl_3$) spectrum for **1-I_2**.

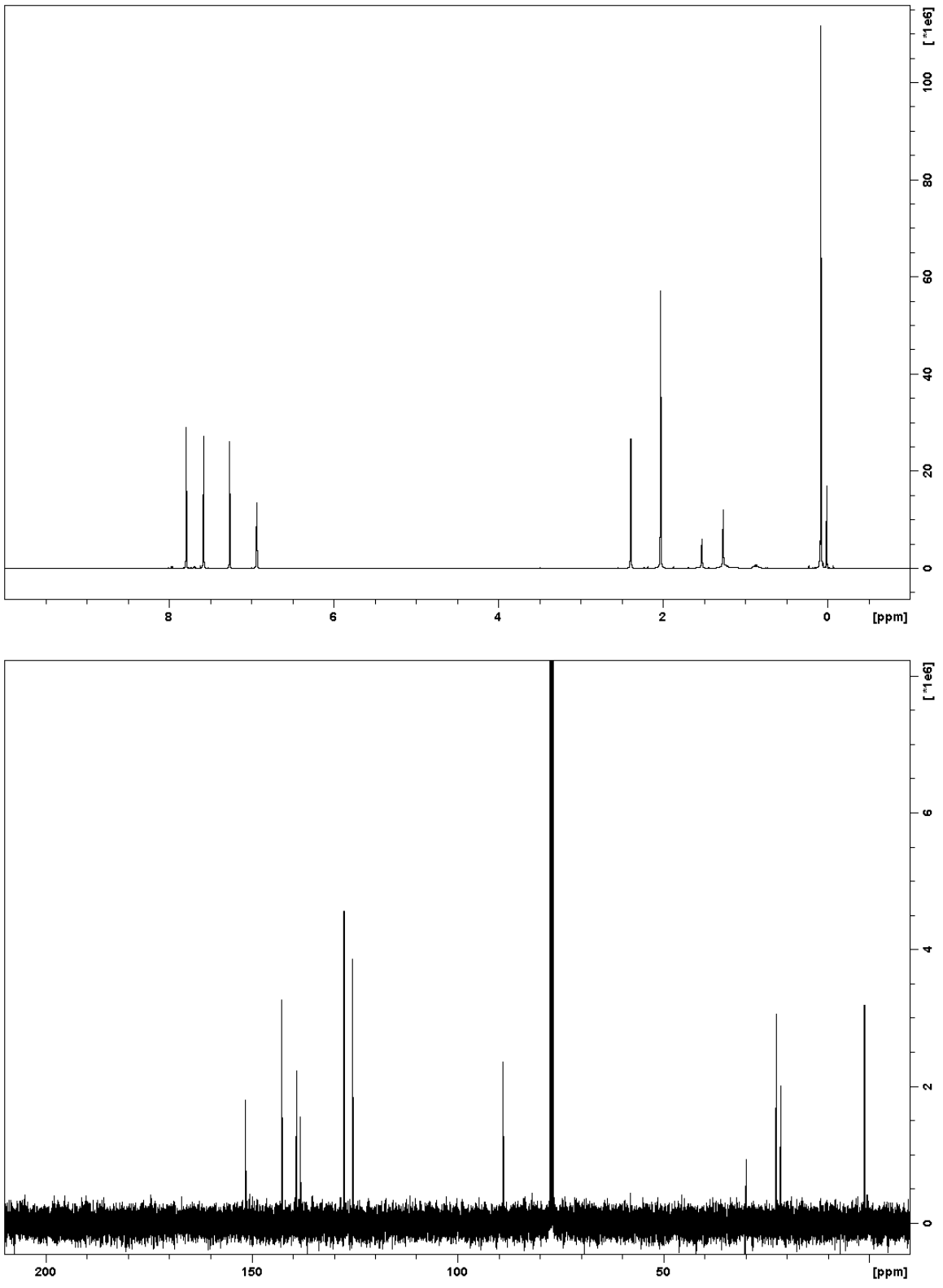

Figure A3.16. ^{1}H (400 MHz, $CDCl_3$) and ^{13}C NMR (100 MHz, $CDCl_3$) spectra for **2-I_2**.

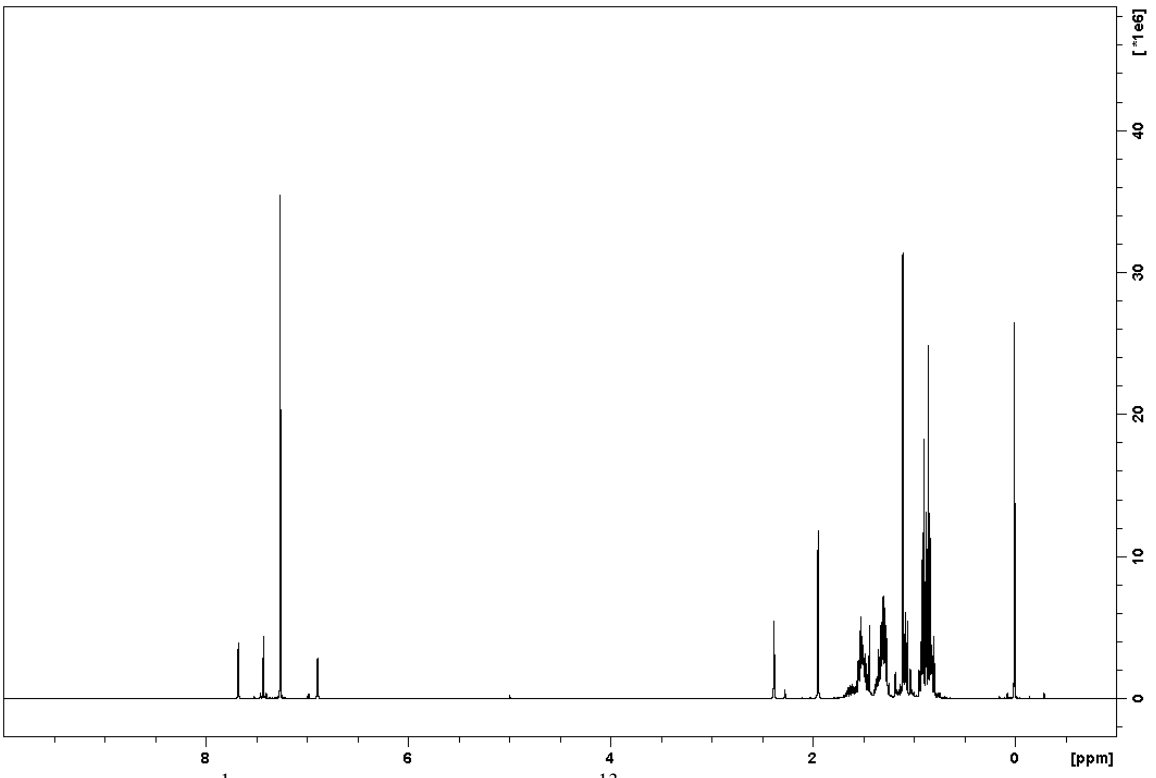

Figure A3.17. ^{1}H (400 MHz, $CDCl_3$) and ^{13}C NMR (100 MHz, $CDCl_3$) spectra for **1-Sn$_2$**.

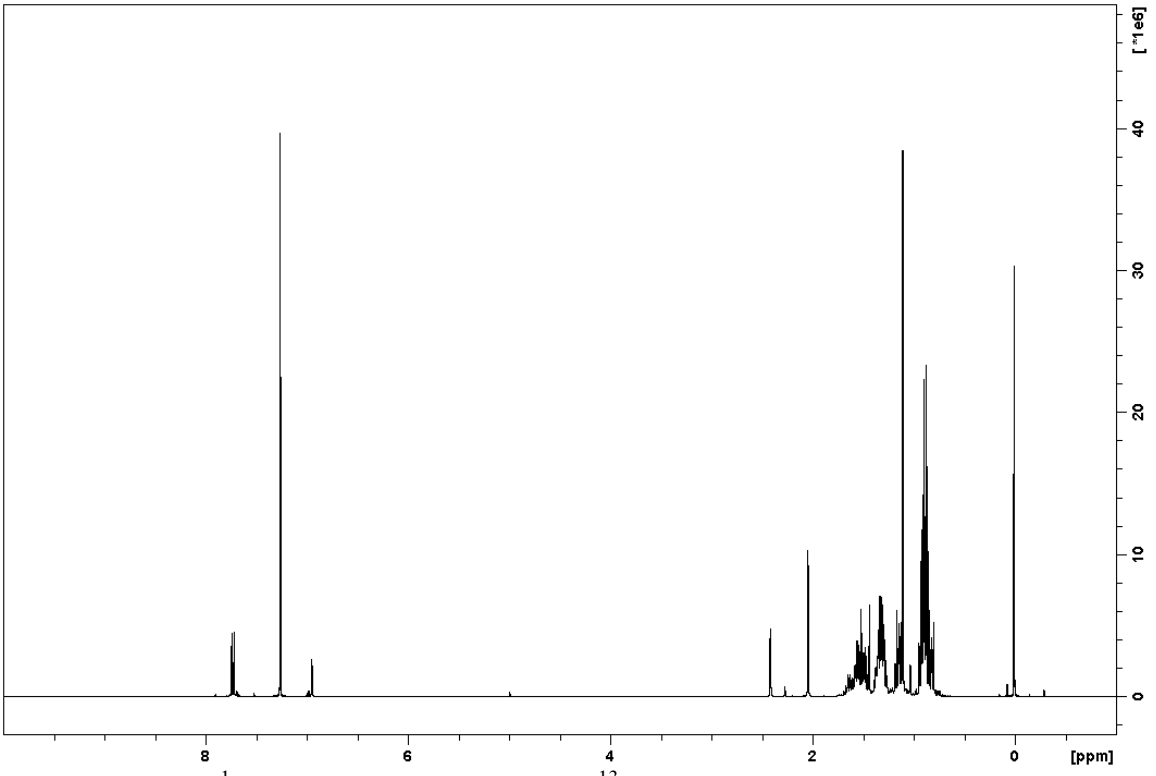

Figure A3.18. ^{1}H (400 MHz, $CDCl_3$) and ^{13}C NMR (100 MHz, $CDCl_3$) spectra for **2-Sn$_2$**.

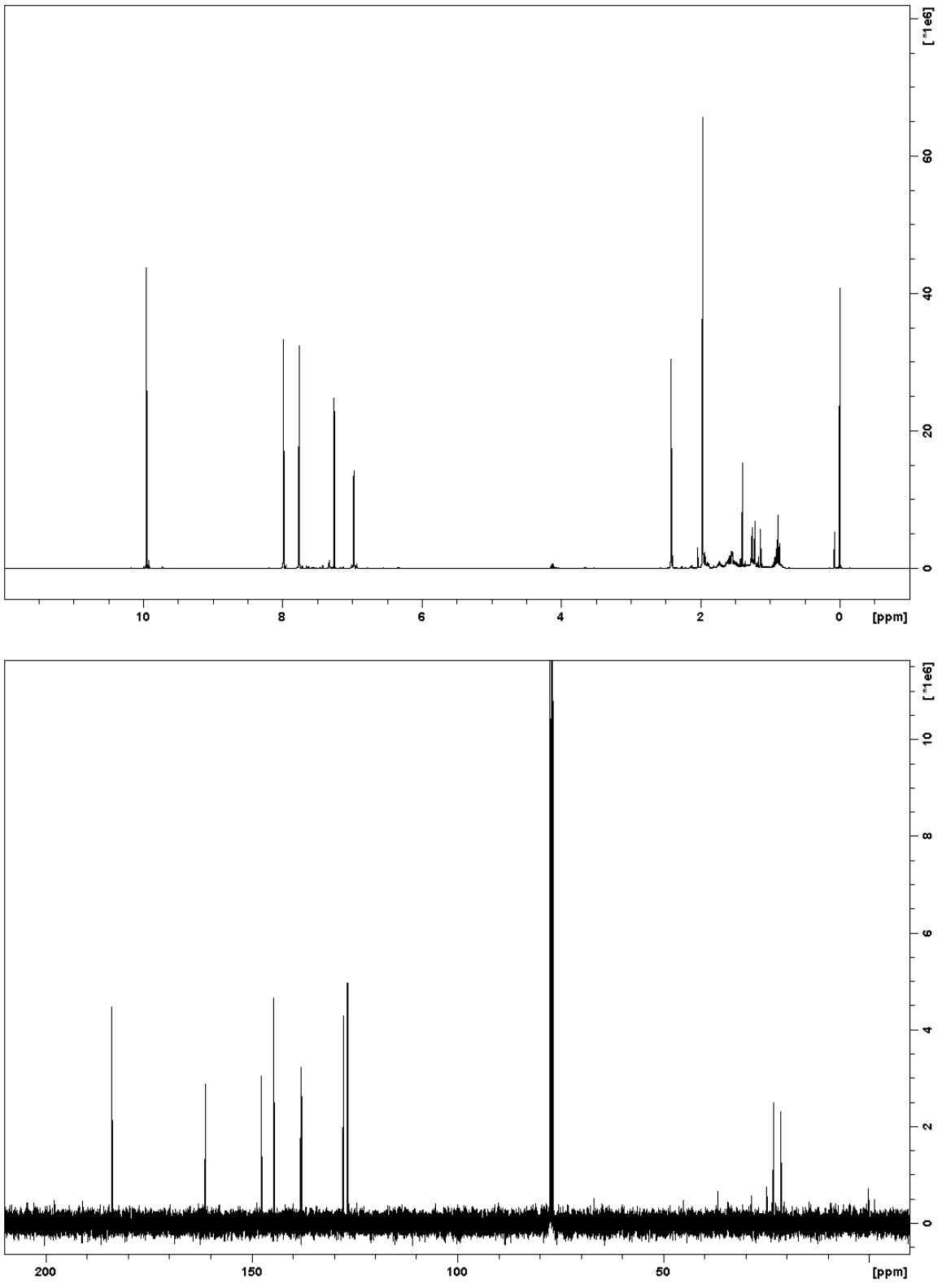

Figure A3.19. ^{1}H (400 MHz, $CDCl_3$) and ^{13}C NMR (100 MHz, $CDCl_3$) spectra for **1-(CHO)$_2$**.

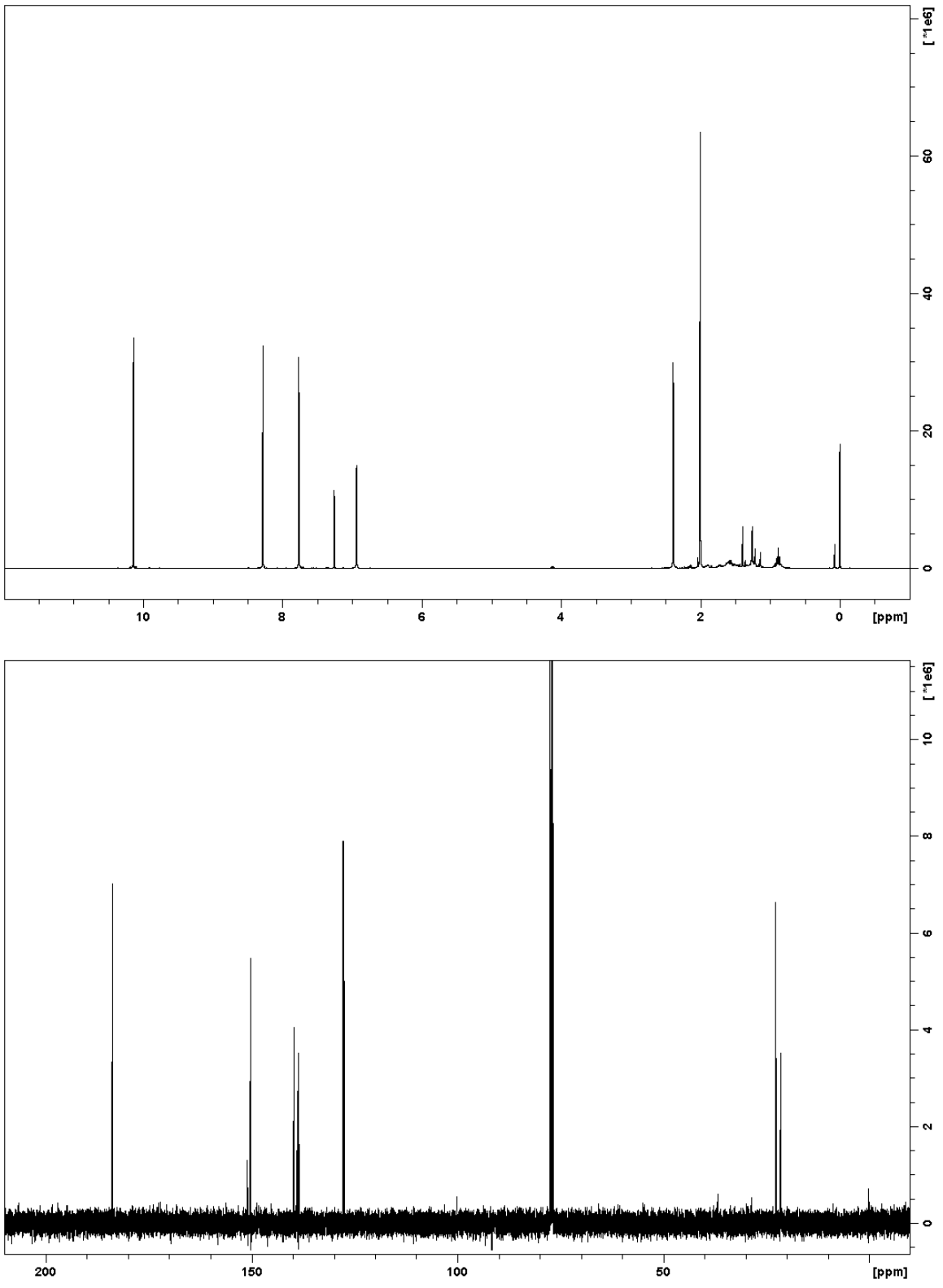

Figure A3.20. ^{1}H (400 MHz, $CDCl_3$) and ^{13}C NMR (100 MHz, $CDCl_3$) spectra for **2-$(CHO)_2$**.

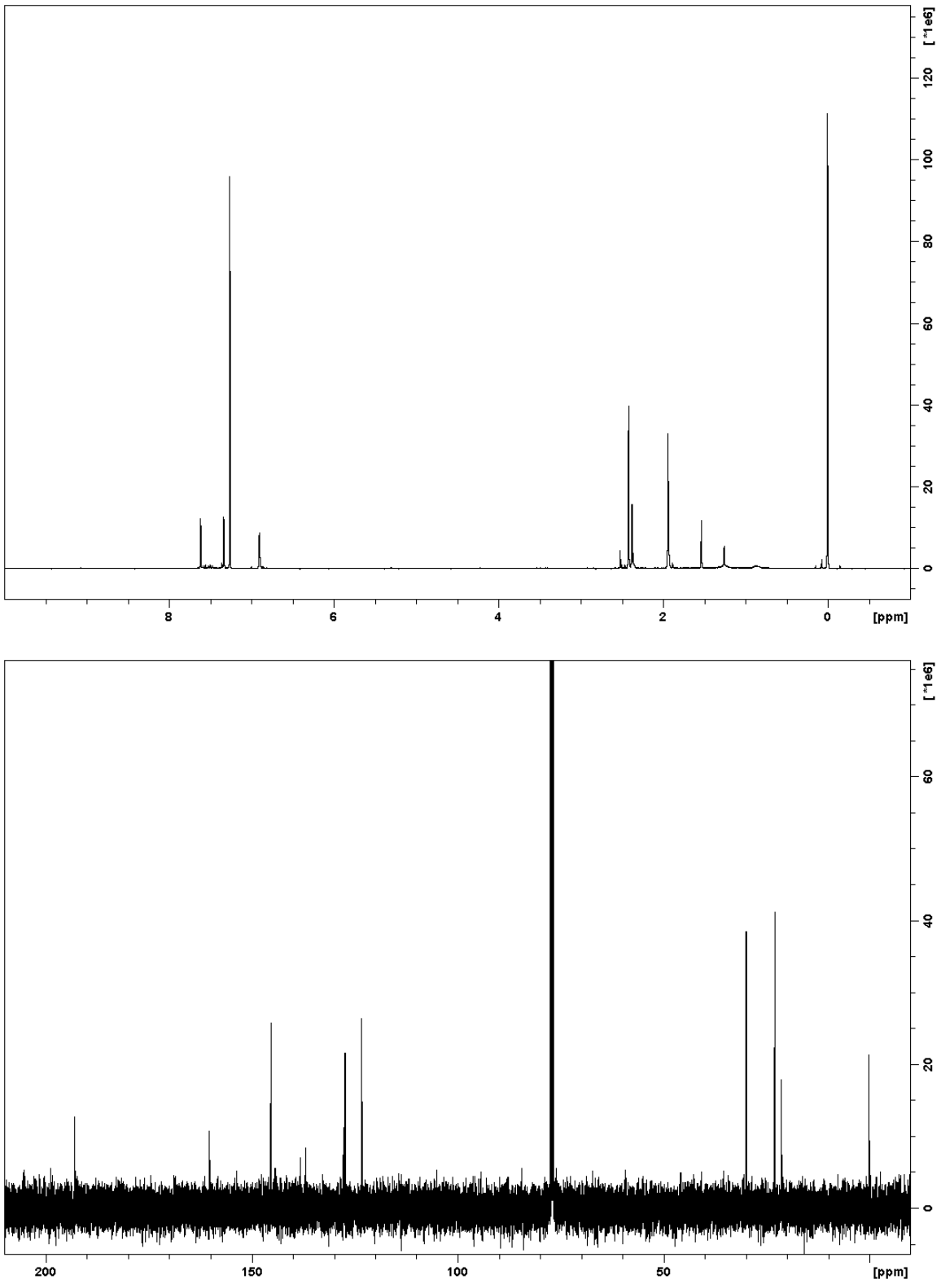

Figure A3.21. ^{1}H (400 MHz, $CDCl_3$) and ^{13}C NMR (100 MHz, $CDCl_3$) spectra for **1-(SAc)$_2$**.

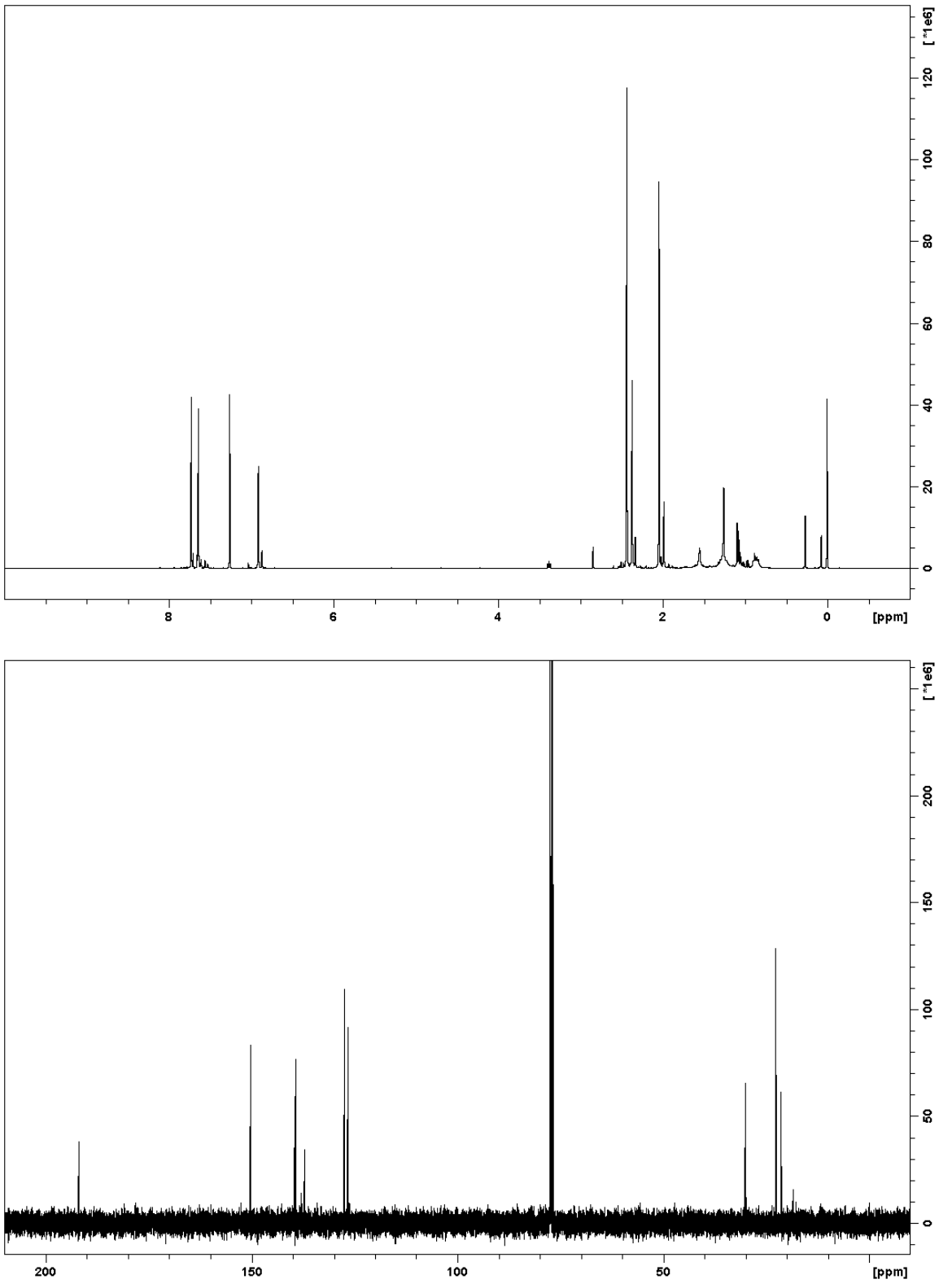

Figure A3.22. ^{1}H (400 MHz, $CDCl_3$) and ^{13}C NMR (100 MHz, $CDCl_3$) spectra for **2-(SAc)$_2$**.

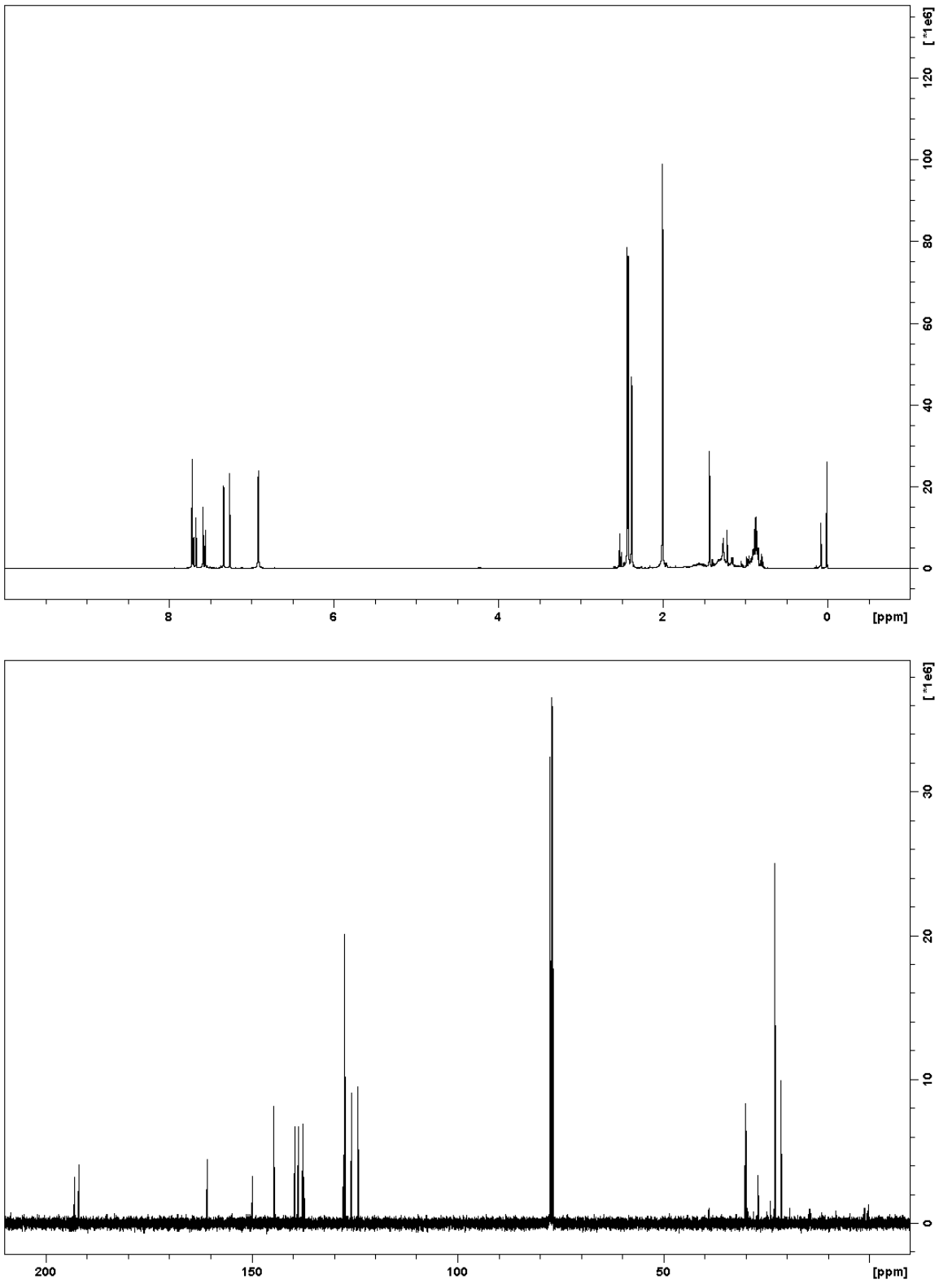

Figure A3.23. ^{1}H (400 MHz, $CDCl_3$) and ^{13}C NMR (100 MHz, $CDCl_3$) spectra for **3-(SAc)$_2$**.

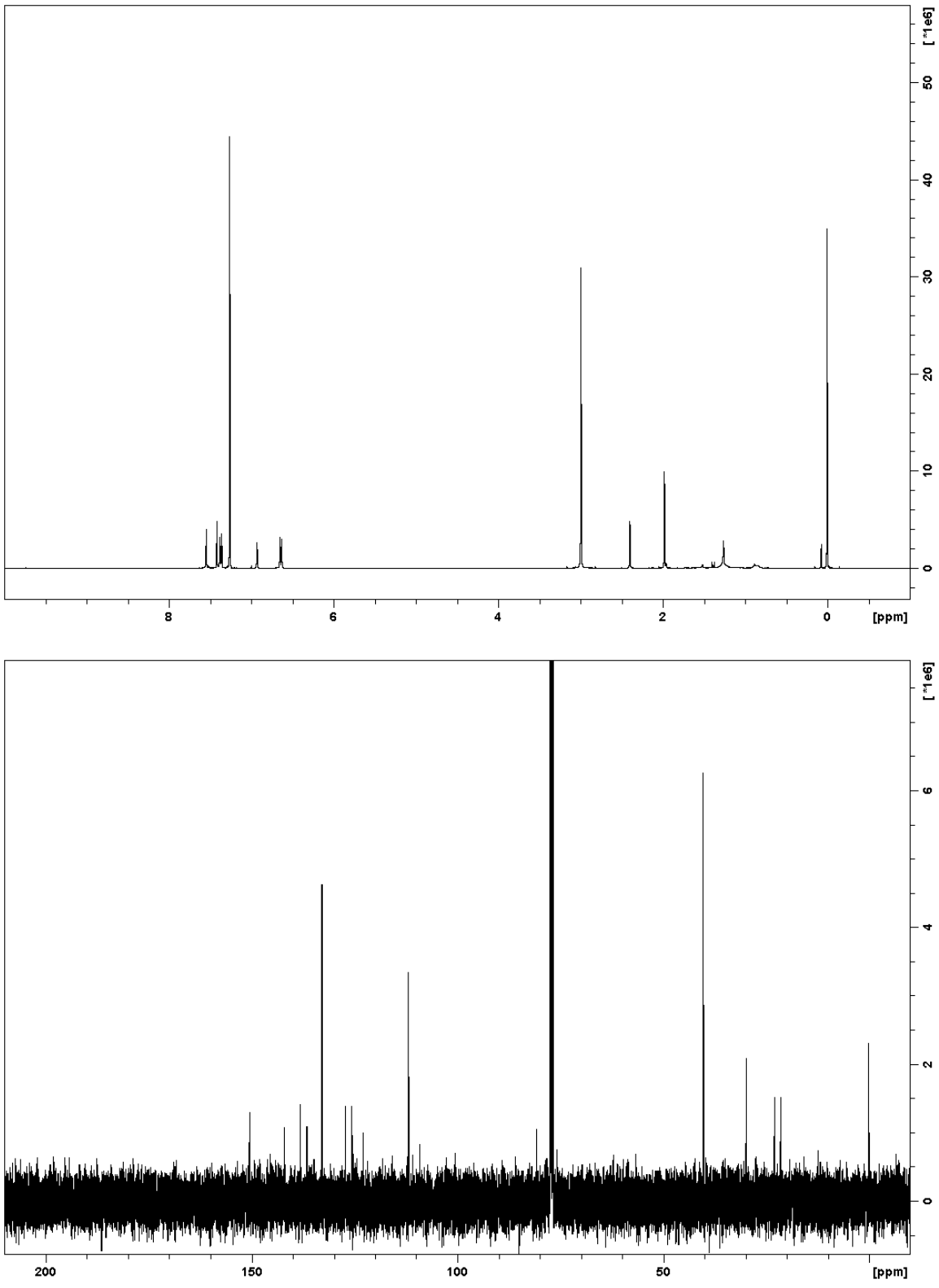

Figure A3.24. ^{1}H (400 MHz, $CDCl_3$) and ^{13}C NMR (100 MHz, $CDCl_3$) spectra for **1a**.

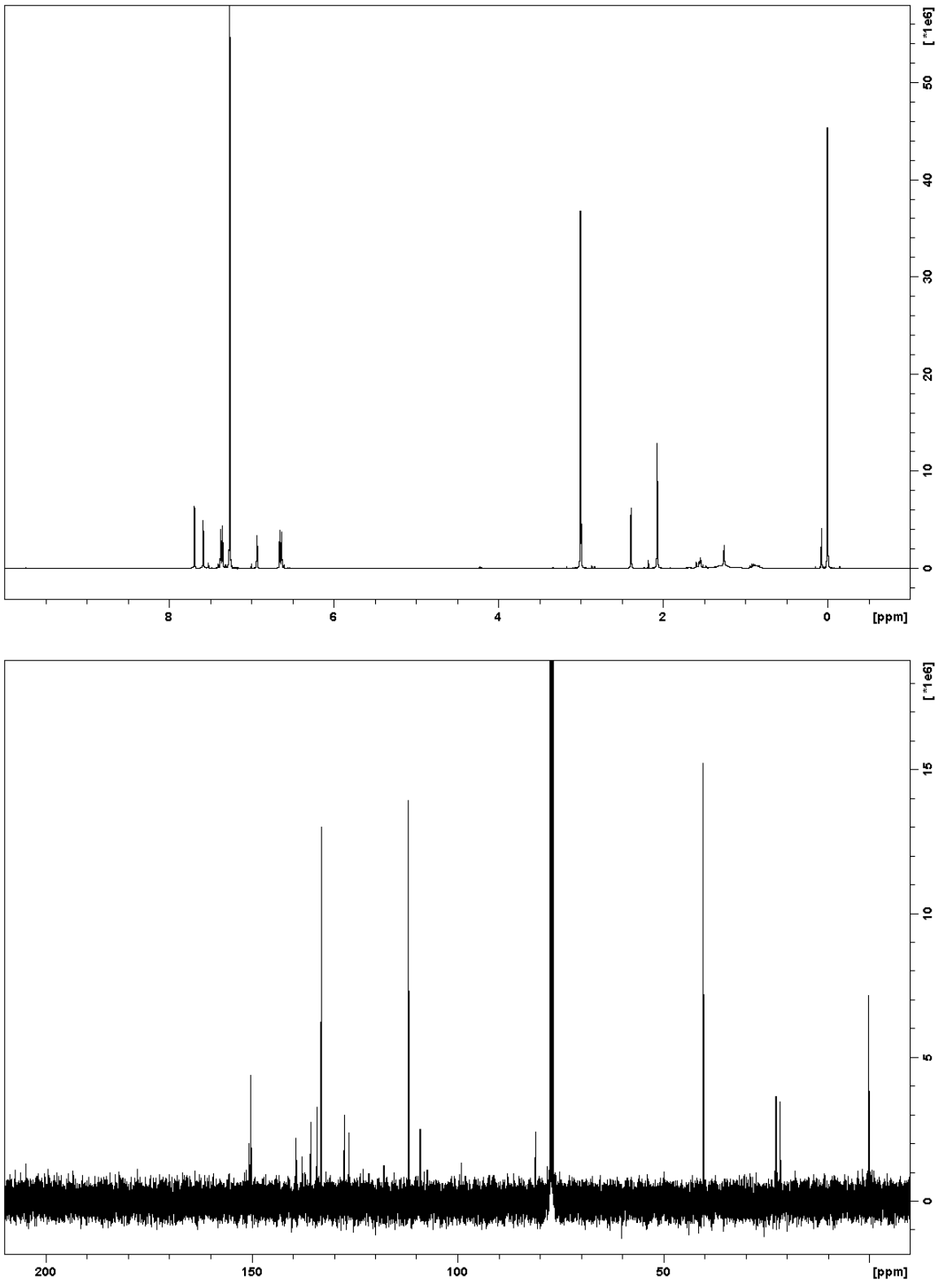

Figure A3.25. ^{1}H (400 MHz, $CDCl_3$) and ^{13}C NMR (100 MHz, $CDCl_3$) spectra for **2a**.

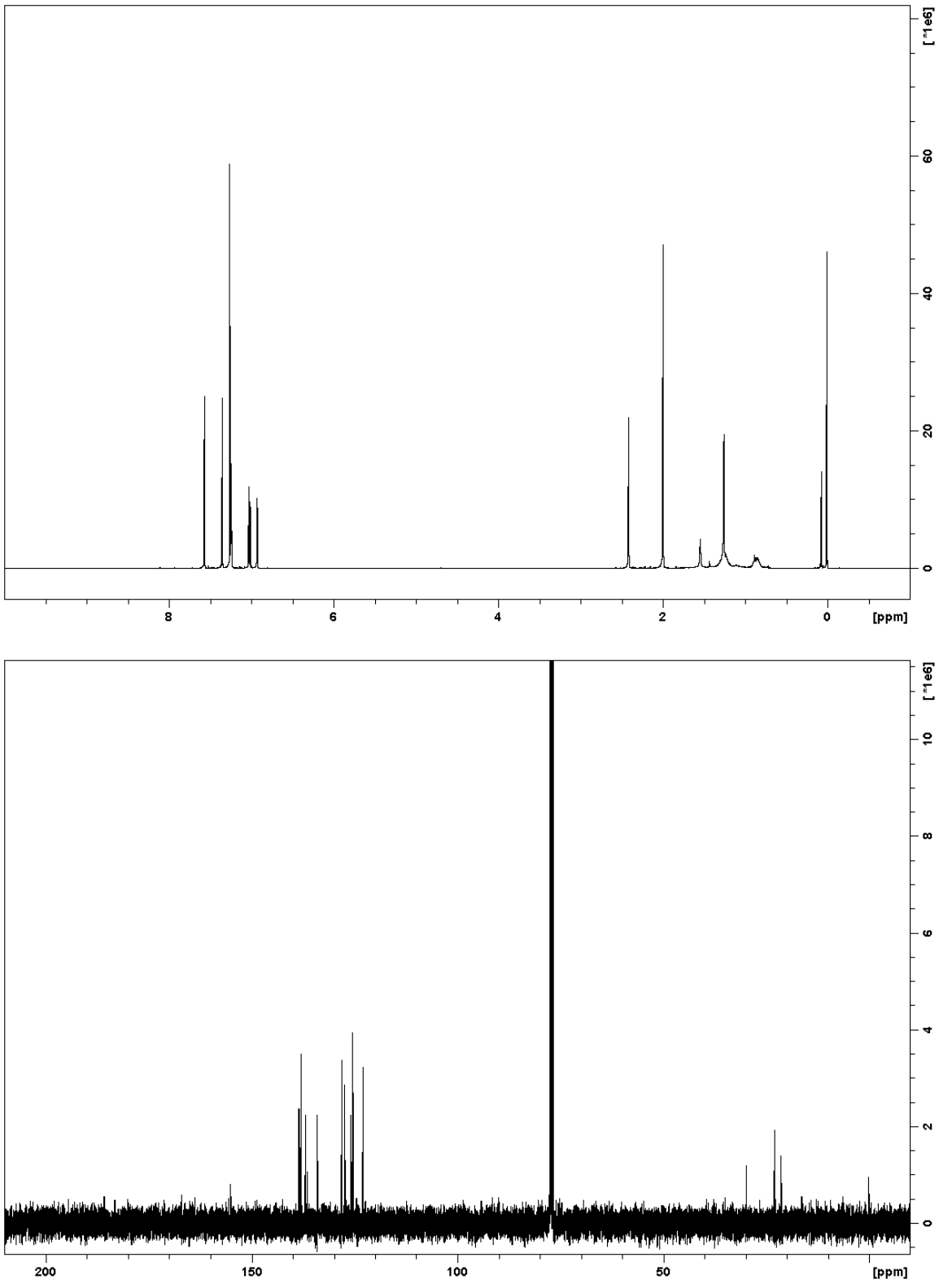

Figure A3.26. ^{1}H (400 MHz, $CDCl_3$) and ^{13}C NMR (100 MHz, $CDCl_3$) spectra for **1b**.

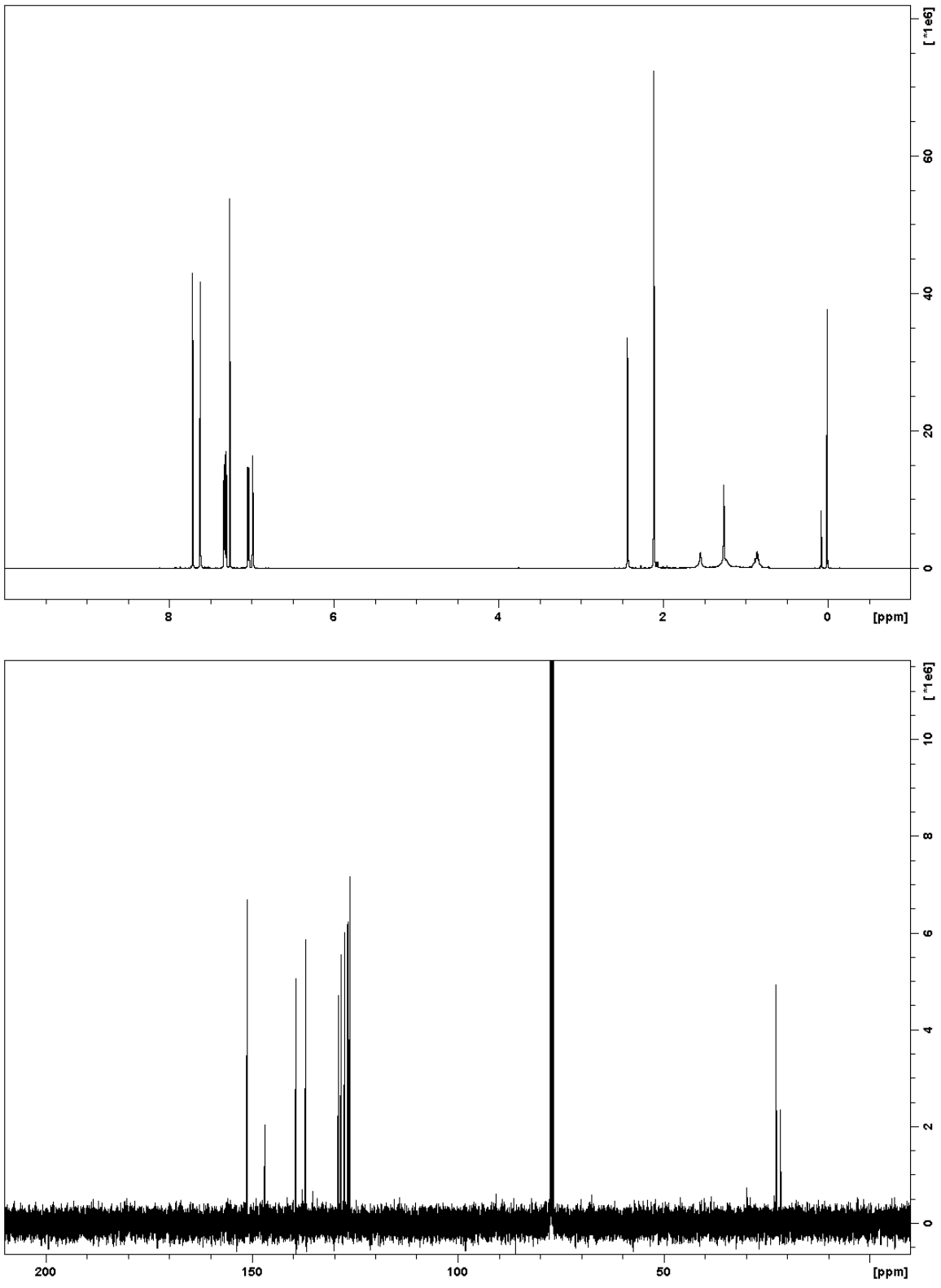

Figure A3.27. ^{1}H (400 MHz, $CDCl_3$) and ^{13}C NMR (100 MHz, $CDCl_3$) spectra for **2b**.

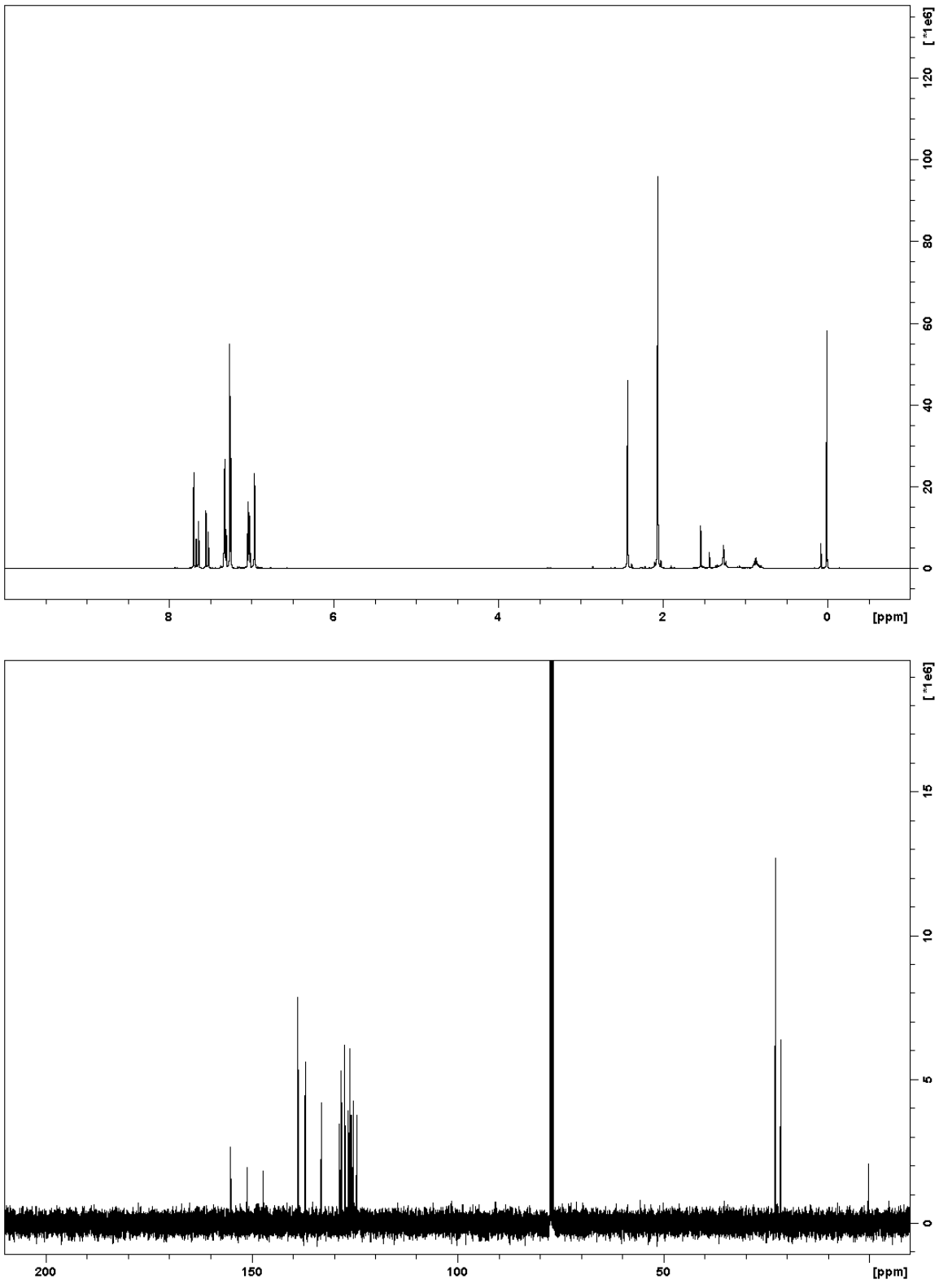

Figure A3.28. ^{1}H (400 MHz, $CDCl_3$) and ^{13}C NMR (100 MHz, $CDCl_3$) spectra for **3b**.

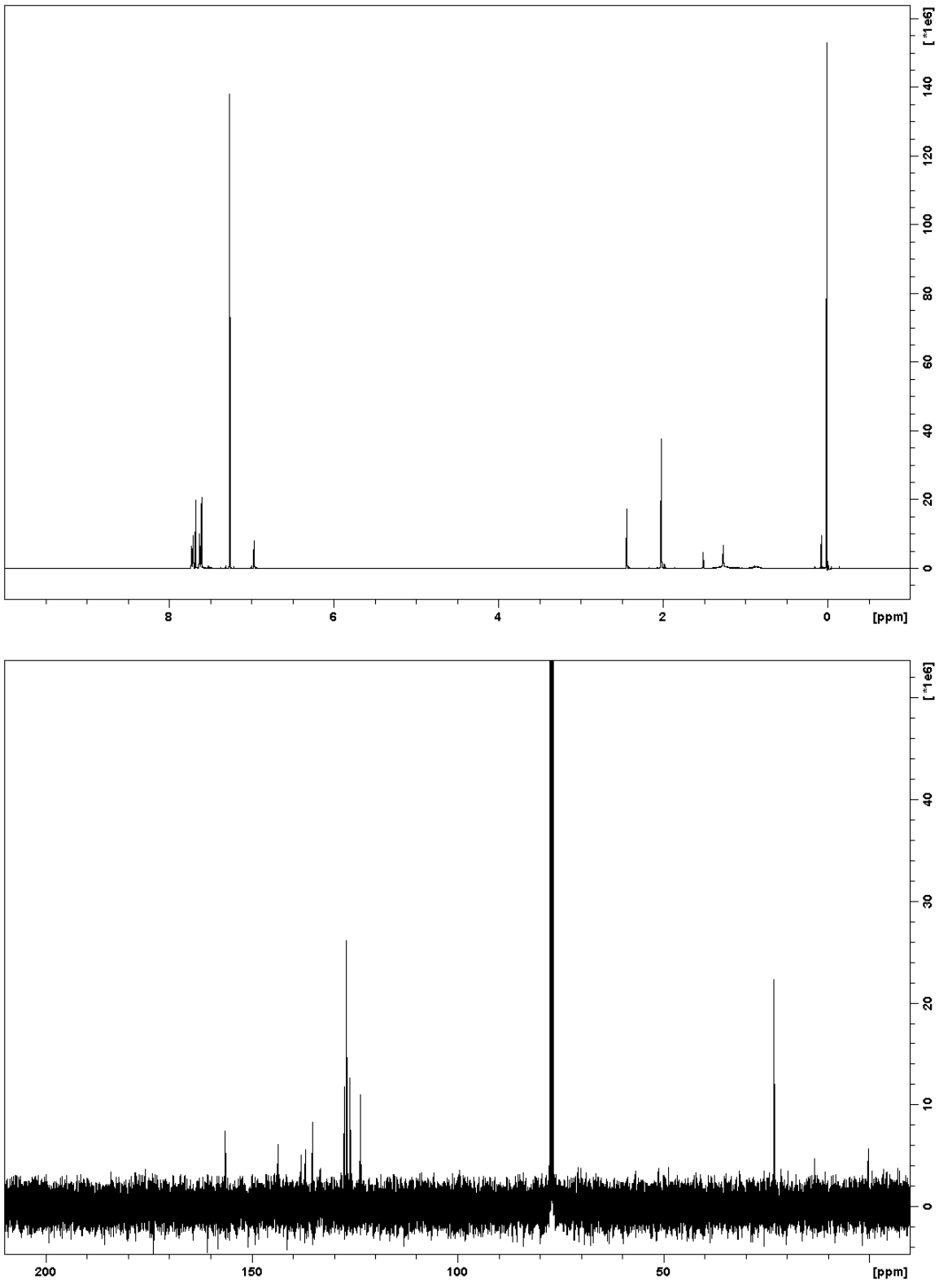

Figure A3.29. ^{1}H (400 MHz, $CDCl_3$) and ^{13}C NMR (100 MHz, $CDCl_3$) spectra for **1c**.

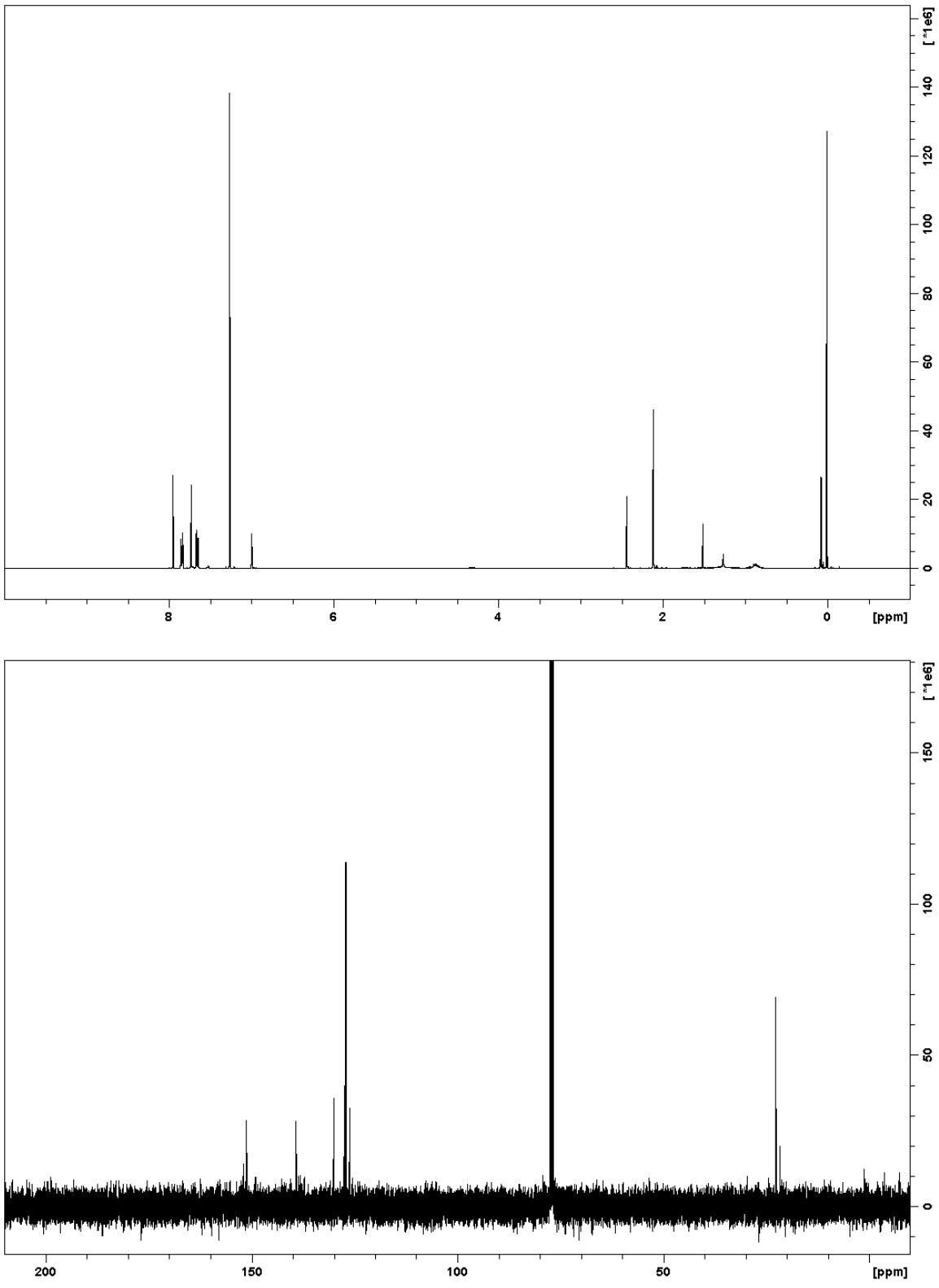

Figure A3.30. ^{1}H (400 MHz, $CDCl_3$) and ^{13}C NMR (100 MHz, $CDCl_3$) spectra for **2c**.

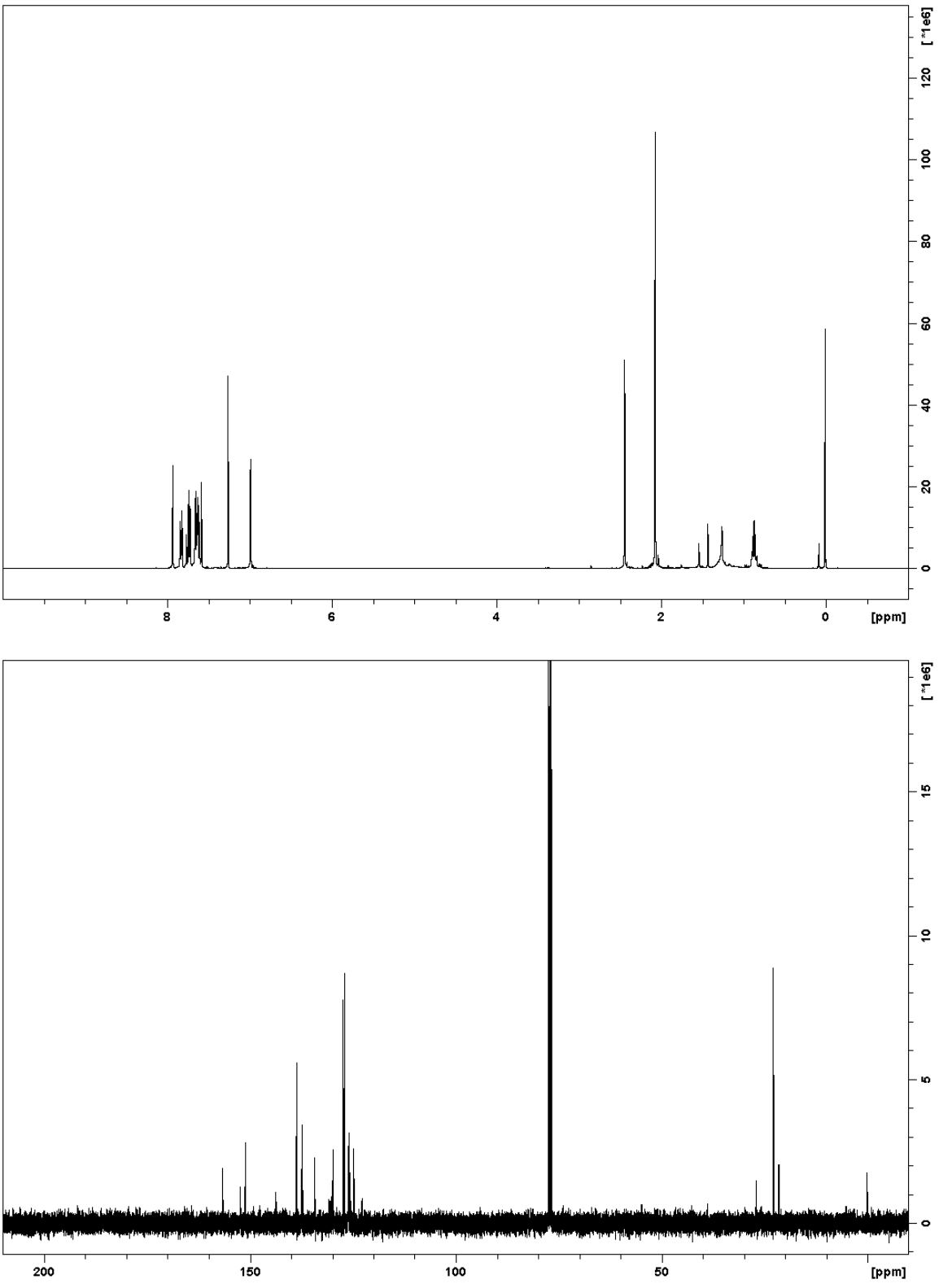

Figure A3.31. ^{1}H (400 MHz, $CDCl_3$) and ^{13}C NMR (100 MHz, $CDCl_3$) spectra for **3c**.

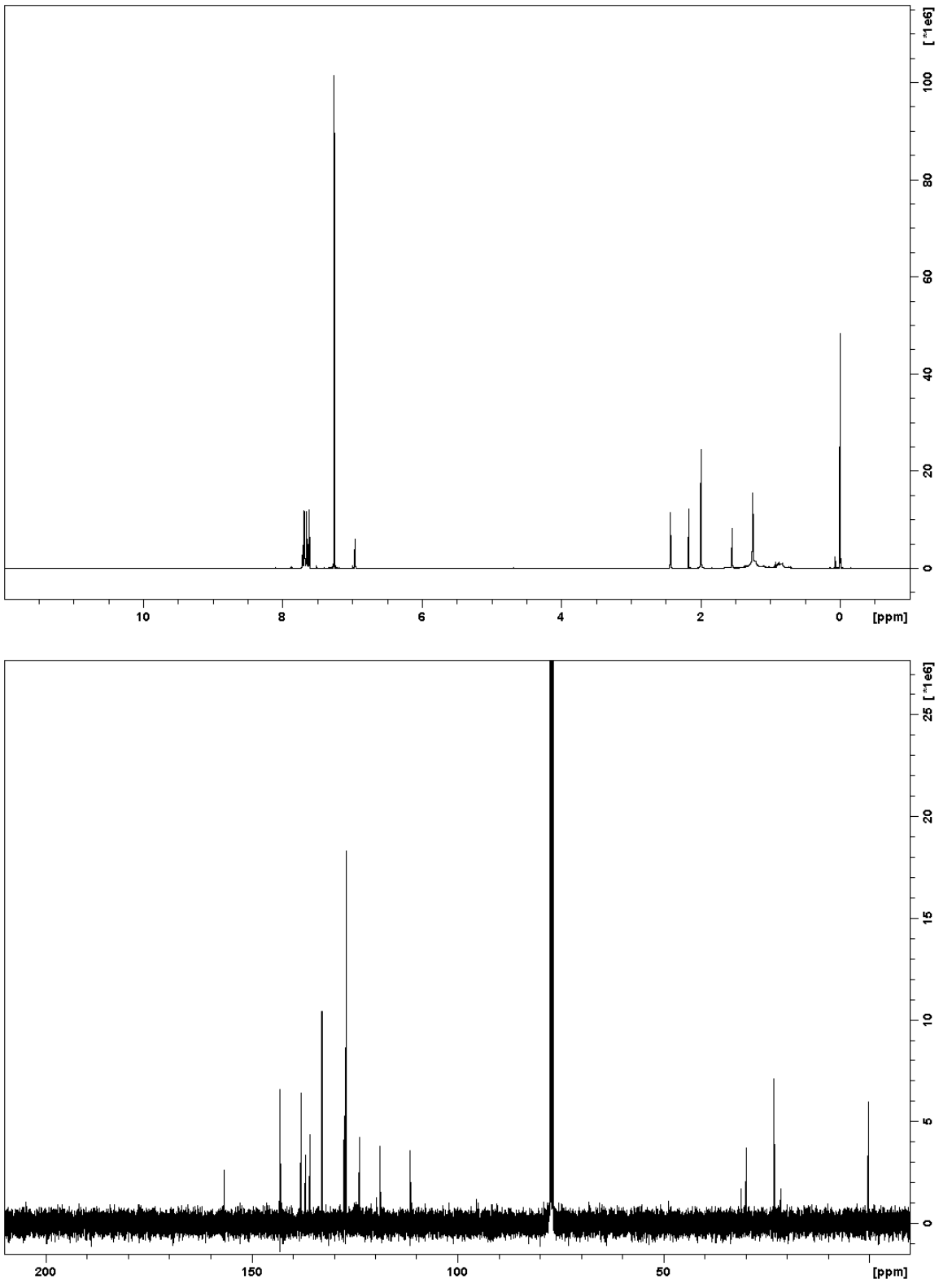

Figure A3.32. ^{1}H (400 MHz, $CDCl_3$) and ^{13}C NMR (100 MHz, $CDCl_3$) spectra for **1d**.

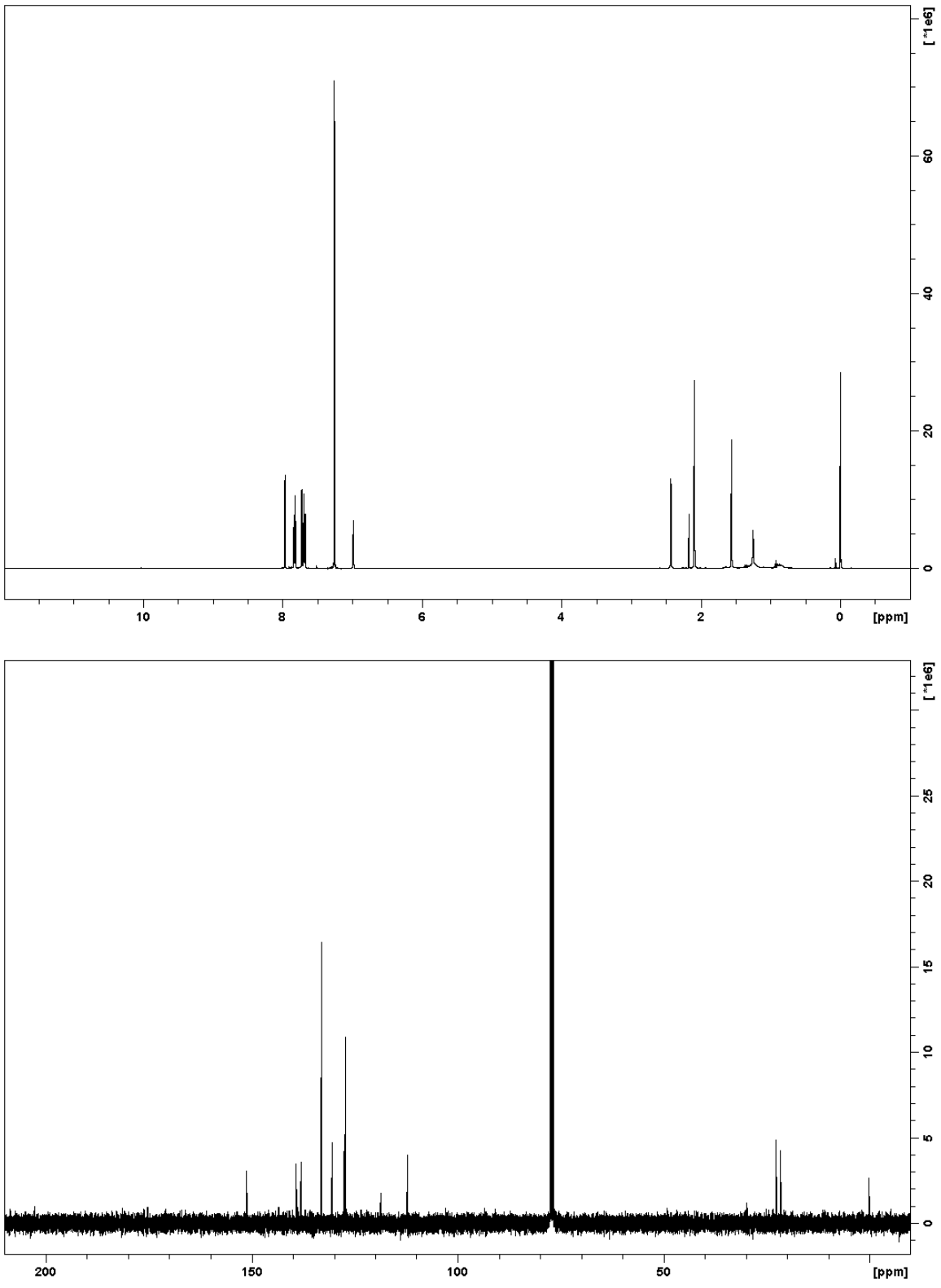

Figure A3.33. ^{1}H (400 MHz, $CDCl_3$) and ^{13}C NMR (100 MHz, $CDCl_3$) spectra for **2d**.

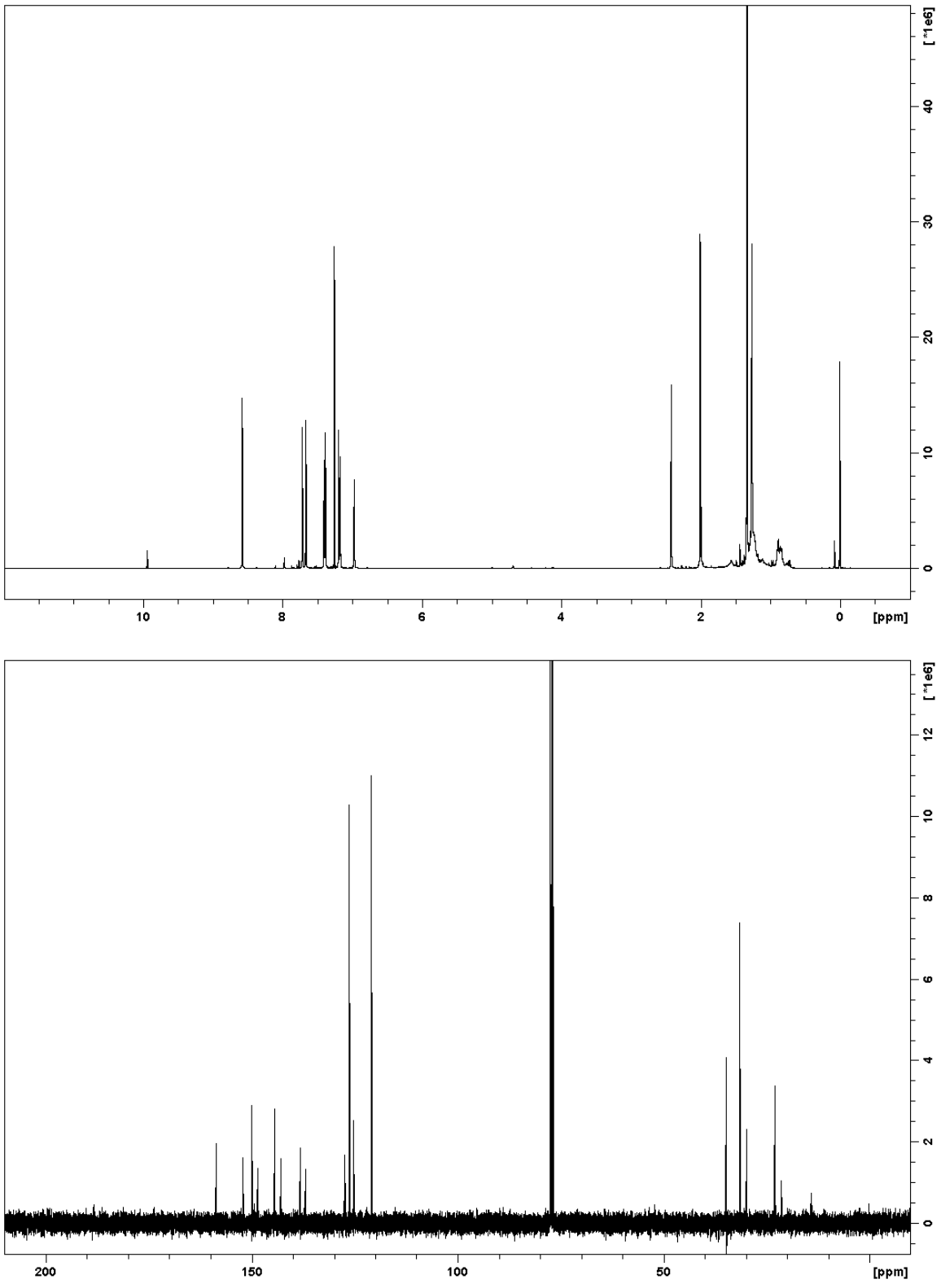

Figure A3.34. ^{1}H (400 MHz, $CDCl_3$) and ^{13}C NMR (100 MHz, $CDCl_3$) spectra for **1e**.

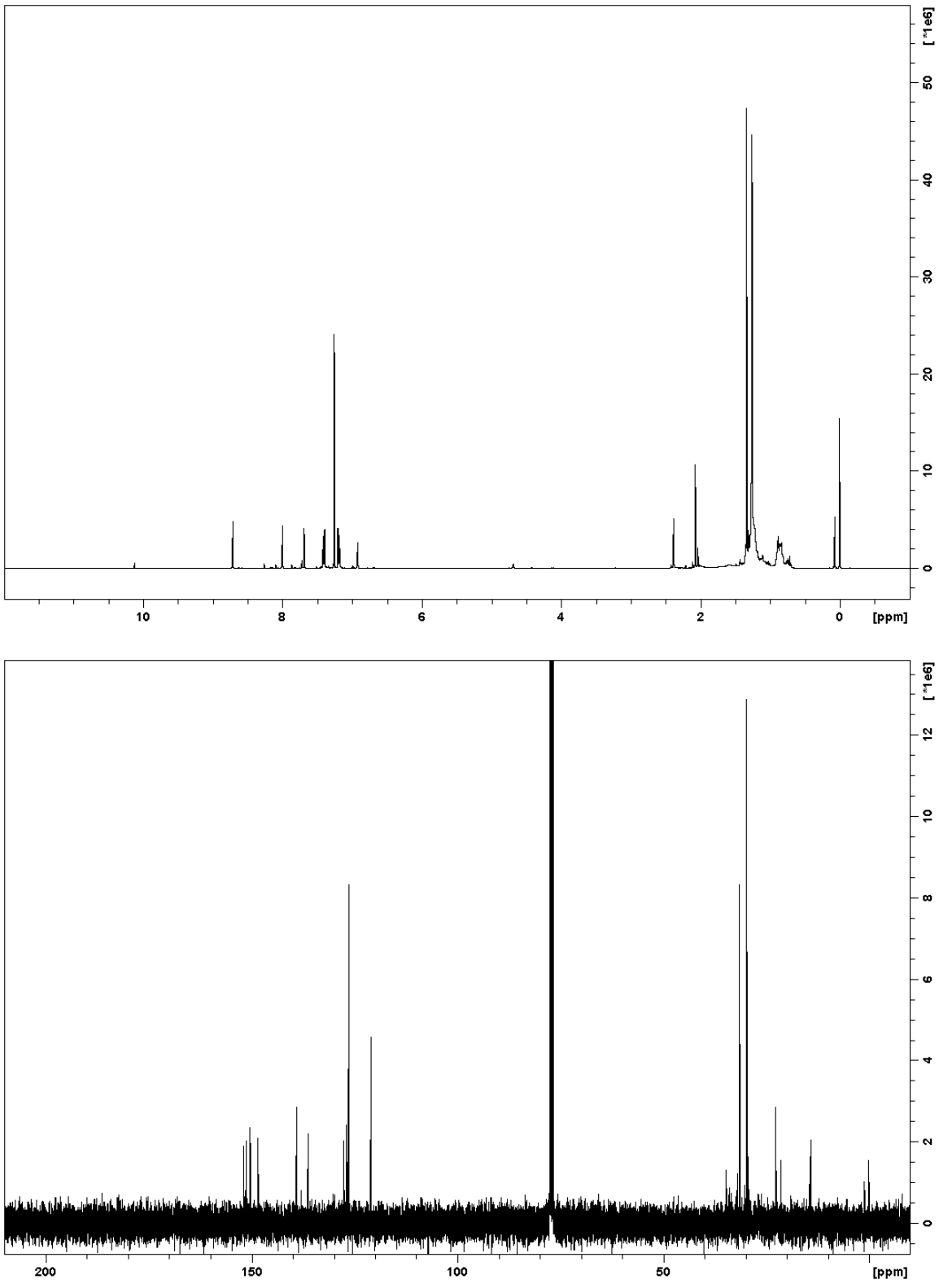

Figure A3.35. ^{1}H (400 MHz, $CDCl_3$) and ^{13}C NMR (100 MHz, $CDCl_3$) spectra for **2e**.

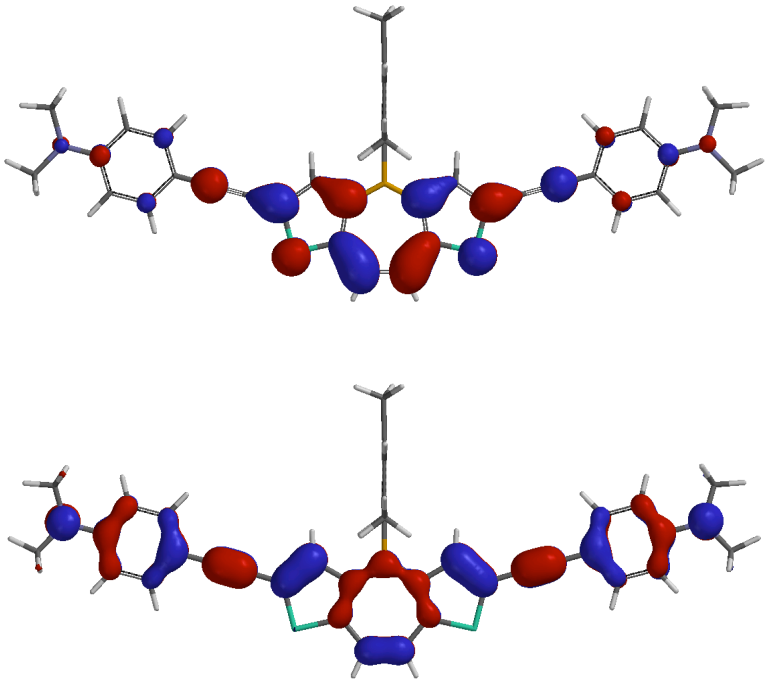

Figure A3.36. DFT calculated (B3LYP/6-31G*) LUMO (-1.92 eV; top) and HOMO (-4.64 eV; bottom) surfaces for **1a**.

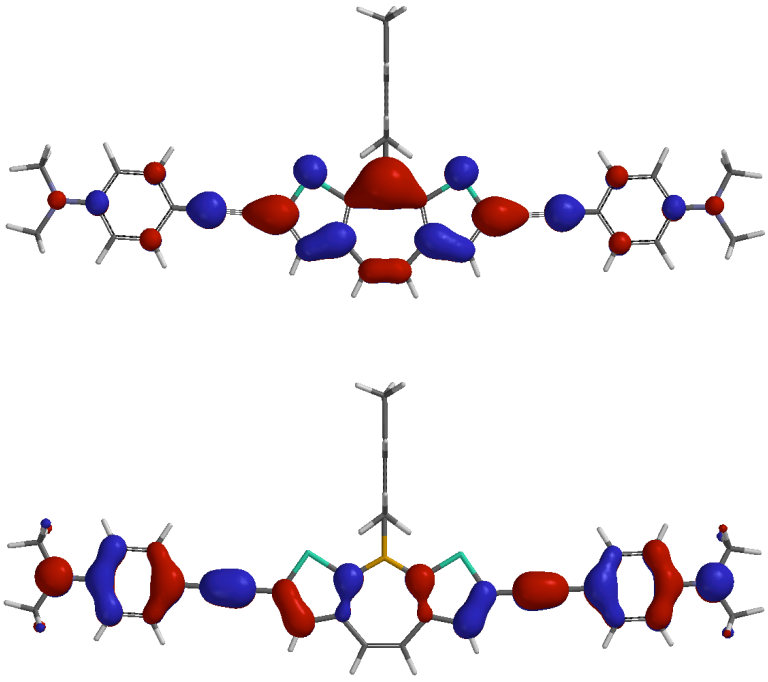

Figure A3.37. DFT calculated (B3LYP/6-31G*) LUMO (-1.76 eV; top) and HOMO (-4.81 eV; bottom) surfaces for **2a**.

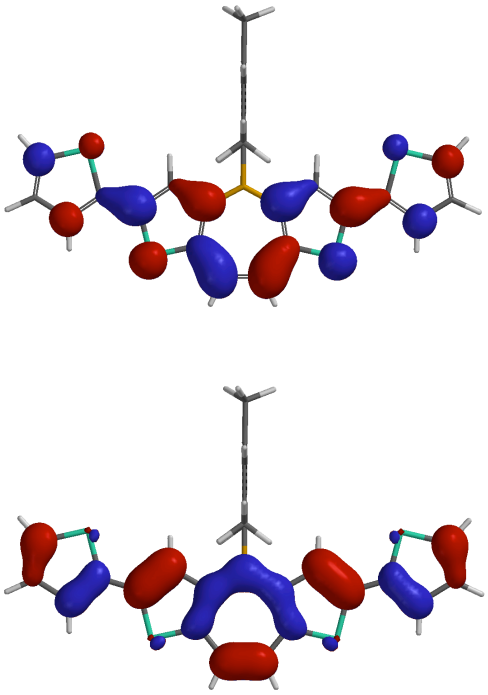

Figure A3.38. DFT calculated (B3LYP/6-31G*) LUMO (-2.17 eV; top) and HOMO (-5.17 eV; bottom) surfaces for **1b**.

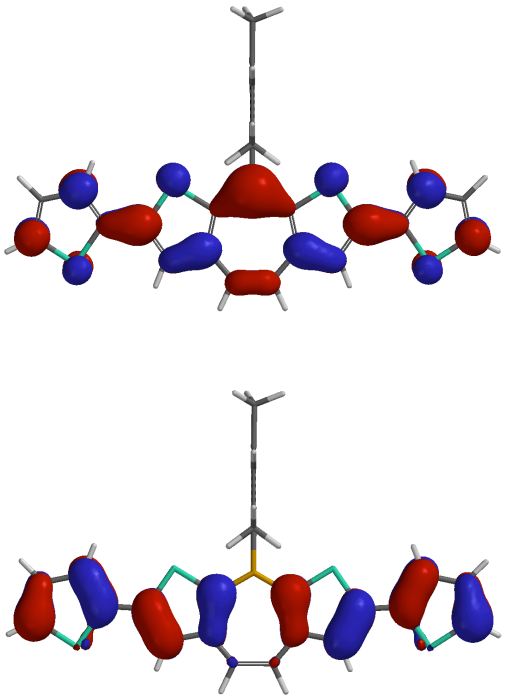

Figure A3.39. DFT calculated (B3LYP/6-31G*) LUMO (-2.02 eV; top) and HOMO (-5.54 eV; bottom) surfaces for **2b**.

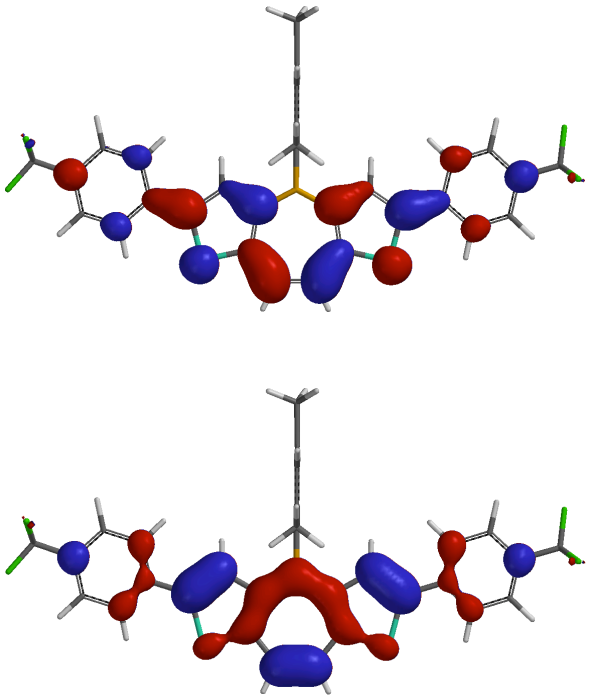

Figure A3.40. DFT calculated (B3LYP/6-31G*) LUMO (-2.50 eV; top) and HOMO (-5.67 eV; bottom) surfaces for **1c**.

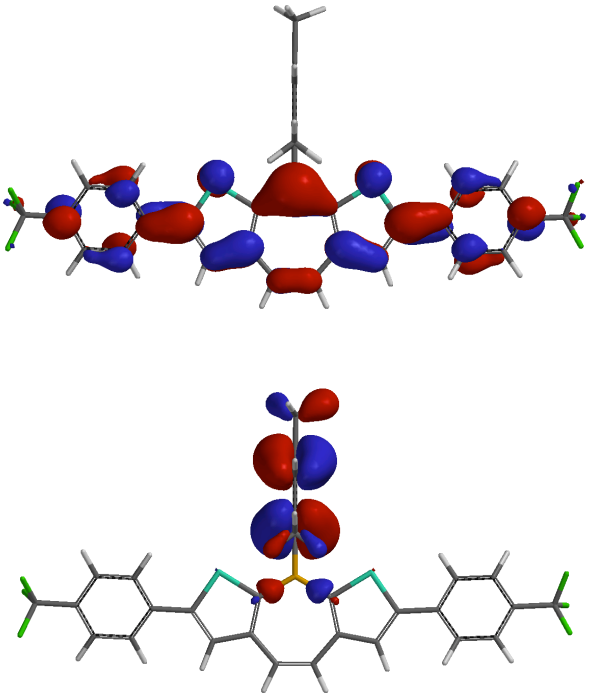

Figure A3.41. DFT calculated (B3LYP/6-31G*) LUMO (-2.28 eV; top) and HOMO (-6.04 eV; bottom) surfaces for **2c**.

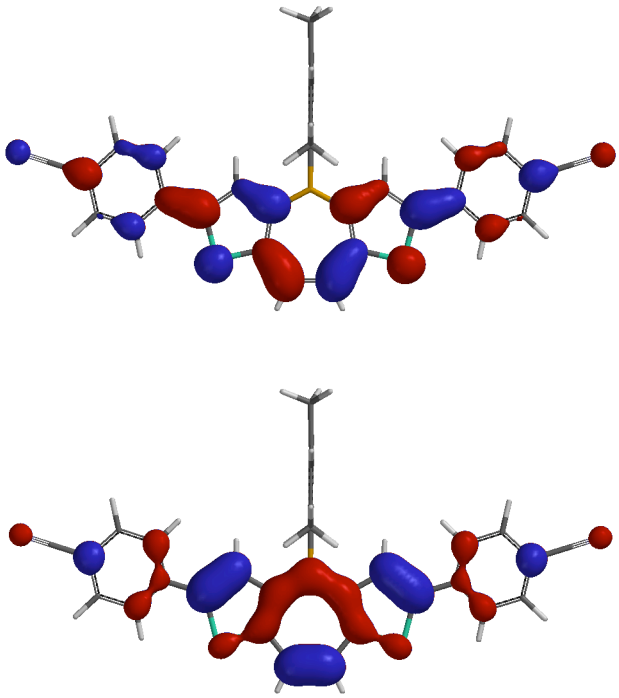

Figure A3.42. DFT calculated (B3LYP/6-31G*) LUMO (-2.78 eV; top) and HOMO (-5.85 eV; bottom) surfaces for **1d**.

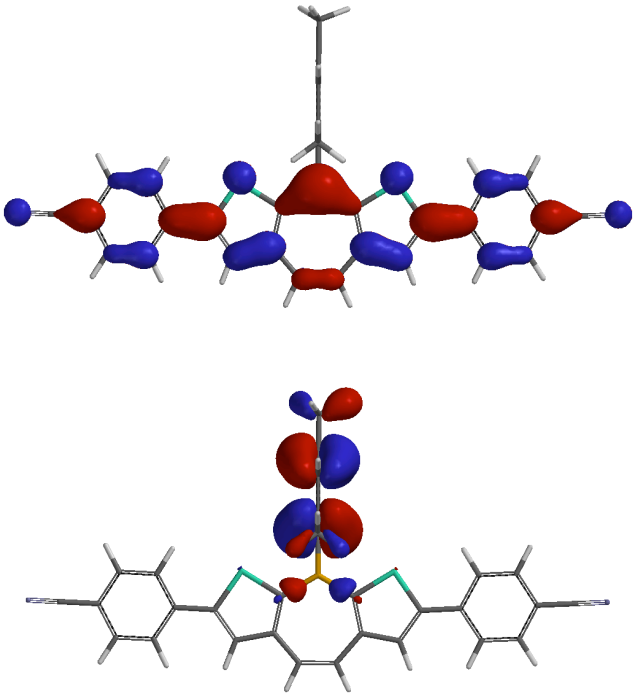

Figure A3.43. DFT calculated (B3LYP/6-31G*) LUMO (-2.66 eV; top) and HOMO (-6.18 eV; bottom) surfaces for **2d**.

Table A3.1. Cartesian coordinates (in Å) for optimized geometries of **1a**, **2a**, **1b**, **2b**, **1c**, **2c**, **1d**, and **2d** calculated at the DFT (B3LYP/6-31G*) level.

1a

	Atom		X	Y	Z
1	C	C2	1.3595700	1.7181446	-0.0865641
2	C	C5	0.6804040	4.2083154	-0.2084163
3	H	H2	1.1433338	5.1917781	-0.2622991
4	C	C6	-0.6927466	4.2058312	-0.1966026
5	H	H5	-1.1600683	5.1876268	-0.2418368
6	C	C8	-1.3612179	1.7130800	-0.0705144
7	B	B1	0.0007747	0.9883942	-0.0441512
8	C	C11	0.0034282	-0.5996809	0.0244347
9	C	C12	-0.0016020	-3.4399870	0.1362517
10	C	C13	-0.0182353	-1.2745410	1.2667688
11	C	C14	0.0205341	-1.3692869	-1.1600089
12	C	C15	0.0162653	-2.7669654	-1.0876998
13	C	C16	-0.0212620	-2.6723600	1.3048467
14	H	H7	0.0254433	-3.3439617	-2.0114917
15	H	H10	-0.0420203	-3.1745587	2.2711056
16	C	C17	0.0374910	-0.6911688	-2.5146997
17	H	H4	-0.8437647	-0.0519389	-2.6550845
18	H	H12	0.0518100	-1.4236731	-3.3285121
19	H	H13	0.9179574	-0.0460724	-2.6296360
20	C	C18	0.0201591	-4.9499691	0.1991750
21	H	H11	1.0264459	-5.3285102	0.4252519
22	H	H14	-0.2884849	-5.3942197	-0.7532111
23	H	H15	-0.6479362	-5.3298815	0.9810484
24	C	C19	-0.0446704	-0.4914211	2.5631643
25	H	H1	-0.0425194	-1.1577635	3.4320266
26	H	H16	-0.9373403	0.1434196	2.6309277
27	H	H17	0.8240331	0.1736101	2.6496313
28	C	C20	-5.0823850	1.3795251	-0.0205409
29	C	C21	5.0819248	1.3967646	-0.0956864
30	C	C22	6.2587716	1.0767045	-0.0879620
31	C	C23	-6.2580454	1.0564649	0.0068838
32	C	C24	7.6276218	0.7073502	-0.0811870
33	C	C25	10.3876516	-0.0224427	-0.0727719
34	C	C26	8.6431131	1.6814852	-0.1664196
35	C	C27	8.0273887	-0.6410881	0.0139040
36	C	C28	9.3663651	-0.9993542	0.0213310
37	C	C29	9.9838490	1.3323124	-0.1602885
38	H	H9	8.3646794	2.7289865	-0.2355772
39	H	H18	7.2678933	-1.4139242	0.0860770
40	H	H19	9.6202292	-2.0495277	0.1020044
41	H	H20	10.7232870	2.1211917	-0.2230629

42	C	C30	-7.6268636	0.6878446	0.0382649
43	C	C31	-10.3875896	-0.0378571	0.0975174
44	C	C32	-8.0288876	-0.6627248	0.0051133
45	C	C33	-8.6404089	1.6659454	0.0975233
46	C	C34	-9.9814191	1.3185651	0.1240951
47	C	C35	-9.3682751	-1.0190861	0.0298816
48	H	H3	-7.2710138	-1.4387618	-0.0455714
49	H	H22	-8.3602283	2.7149859	0.1197358
50	H	H23	-10.7192849	2.1102509	0.1648335
51	H	H24	-9.6237136	-2.0713363	-0.0044565
52	N	N1	-11.7256369	-0.3881471	0.1416088
53	N	N2	11.7249209	-0.3753583	-0.0840689
54	C	C36	-12.1155374	-1.7751521	-0.0493333
55	H	H25	-11.6708863	-2.4213599	0.7175119
56	H	H28	-11.8215932	-2.1656700	-1.0362709
57	H	H29	-13.2002360	-1.8556389	0.0400247
58	C	C37	-12.7442756	0.6443177	0.0476856
59	H	H21	-12.6868392	1.2098673	-0.8952006
60	H	H30	-12.6634202	1.3581138	0.8768992
61	H	H31	-13.7299770	0.1794761	0.1069675
62	C	C38	12.1110228	-1.7565028	0.1500831
63	H	H26	13.1970771	-1.8394226	0.0850023
64	H	H32	11.6807293	-2.4235603	-0.6071811
65	H	H33	11.7983073	-2.1205515	1.1409072
66	C	C39	12.7447888	0.6589960	-0.0373231
67	H	H27	13.7304738	0.1918686	-0.0699141
68	H	H34	12.6836770	1.2695033	0.8766582
69	H	H35	12.6676095	1.3320571	-0.9003879
70	C	C1	1.5793708	3.1127213	-0.1596733
71	C	C3	-1.5869247	3.1069226	-0.1350474
72	S	S1	3.2977340	3.4951694	-0.1910368
73	S	S2	-3.3068810	3.4835175	-0.1374478
74	C	C4	3.7366798	1.7927900	-0.1063125
75	C	C7	2.6018557	1.0105755	-0.0583745
76	H	H38	2.6572819	-0.0704091	-0.0045540
77	C	C9	-2.6003983	1.0008201	-0.0275855
78	H	H41	-2.6509463	-0.0806353	0.0214823
79	C	C10	-3.7384181	1.7791773	-0.0526644

2a

	Atom		X	Y	Z
1	S	S1	2.8189197	-0.2766232	0.0677924
2	C	C1	3.8069667	1.1726378	0.0626269
3	C	C2	1.3200259	0.6376492	0.0831250
4	C	C3	1.6092823	2.0206493	0.0852810
5	C	C4	3.0098660	2.2973505	0.0745046

6	H	H6	3.4186994	3.3021531	0.0735519
7	C	C5	0.6668568	3.1058798	0.0960783
8	H	H2	1.1297232	4.0915791	0.0995081
9	C	C6	-0.6956445	3.1004656	0.1009986
10	H	H5	-1.1663200	4.0824389	0.1077714
11	C	C7	-1.6295835	2.0078853	0.0961592
12	C	C8	-1.3297954	0.6271591	0.0913210
13	S	S2	-2.8217139	-0.2985428	0.0838155
14	C	C9	-3.8208446	1.1431340	0.0848126
15	C	C10	-3.0322879	2.2738597	0.0936783
16	H	H8	-3.4487208	3.2755226	0.0951012
17	B	B1	-0.0018546	-0.1276283	0.0895228
18	C	C11	0.0061788	-1.7171092	0.0916496
19	C	C12	0.0251786	-4.5570898	0.0975749
20	C	C13	0.0138116	-2.4373541	1.3099677
21	C	C14	0.0048496	-2.4411316	-1.1221966
22	C	C15	0.0131830	-3.8401129	-1.1008149
23	C	C16	0.0219376	-3.8346111	1.2948530
24	H	H7	0.0090289	-4.3829941	-2.0447645
25	H	H10	0.0249291	-4.3732930	2.2414649
26	C	C17	-0.0089778	-1.7163002	-2.4523311
27	H	H4	-0.8974905	-1.0808754	-2.5549848
28	H	H12	-0.0050507	-2.4219332	-3.2895065
29	H	H13	0.8647681	-1.0619870	-2.5627411
30	C	C18	0.0619808	-6.0678332	0.1044868
31	H	H11	1.0710289	-6.4425448	0.3239997
32	H	H14	-0.2355683	-6.4800447	-0.8655196
33	H	H15	-0.6069664	-6.4829275	0.8675186
34	C	C19	0.0103662	-1.7053123	2.6361740
35	H	H1	0.0171223	-2.4063327	3.4772002
36	H	H16	-0.8753349	-1.0662389	2.7405954
37	H	H17	0.8868942	-1.0532157	2.7376187
38	C	C20	-5.2225344	1.0637164	0.0721737
39	C	C21	5.2091110	1.1032468	0.0450758
40	C	C22	6.4256985	1.0259828	0.0265639
41	C	C23	-6.4386711	0.9794977	0.0557540
42	C	C24	7.8416082	0.9524715	0.0018900
43	C	C25	10.6913918	0.8096991	-0.0522373
44	C	C26	8.6331765	2.1189988	0.0166196
45	C	C27	8.5111859	-0.2873435	-0.0443524
46	C	C28	9.8946385	-0.3613691	-0.0733076
47	C	C29	10.0169206	2.0550374	-0.0114504
48	H	H9	8.1442679	3.0882268	0.0474489
49	H	H18	7.9269568	-1.2026278	-0.0602571
50	H	H19	10.3603223	-1.3386330	-0.1121107
51	H	H20	10.5792830	2.9810589	-0.0045236
52	C	C30	-7.8541394	0.8973127	0.0306197

53	C	C31	-10.7033489	0.7373390	-0.0304033
54	C	C32	-8.5155028	-0.3446436	-0.0560370
55	C	C33	-8.6535806	2.0573893	0.0803710
56	C	C34	-10.0368678	1.9850644	0.0482668
57	C	C35	-9.8984348	-0.4267082	-0.0896018
58	H	H3	-7.9254158	-1.2551405	-0.1019607
59	H	H22	-8.1714110	3.0285916	0.1408961
60	H	H23	-10.6047461	2.9071672	0.0817084
61	H	H24	-10.3569388	-1.4053004	-0.1639608
62	N	N1	-12.0834416	0.6590827	-0.0448495
63	N	N2	12.0710691	0.7406397	-0.0679971
64	C	C36	-12.7333859	-0.6208787	-0.2726676
65	H	H25	-12.4755198	-1.3445267	0.5112848
66	H	H28	-12.4626129	-1.0610340	-1.2442837
67	H	H29	-13.8155663	-0.4813461	-0.2518874
68	C	C37	-12.8773938	1.8743107	-0.0950938
69	H	H21	-12.6983731	2.4595441	-1.0105472
70	H	H30	-12.6682914	2.5210876	0.7665086
71	H	H31	-13.9360239	1.6114427	-0.0621326
72	C	C38	12.7321854	-0.5443911	-0.2199126
73	H	H26	13.8127660	-0.3925024	-0.2287567
74	H	H32	12.4503292	-1.0482494	-1.1562218
75	H	H33	12.4959018	-1.2203000	0.6129467
76	C	C39	12.8587210	1.9595851	-0.1183184
77	H	H27	13.9188484	1.7022246	-0.0961769
78	H	H34	12.6535741	2.6050370	0.7460210
79	H	H35	12.6688003	2.5449117	-1.0309942

1b

	Atom		X	Y	Z
1	C	C1	1.3577209	-1.4000131	0.0007810
2	C	C2	1.5798553	-2.7928683	0.0004550
3	C	C3	2.6015614	-0.6915148	0.0020304
4	C	C4	3.7356049	-1.4690635	0.0026993
5	S	S1	3.3015564	-3.1687846	0.0015786
6	C	C5	0.6860918	-3.8936114	-0.0008681
7	C	C6	-0.6868656	-3.8934972	-0.0018063
8	C	C7	-1.5804386	-2.7926016	-0.0017421
9	C	C8	-1.3580889	-1.3997730	-0.0013557
10	S	S2	-3.3021991	-3.1682221	-0.0027171
11	C	C9	-3.7359680	-1.4684177	-0.0025575
12	C	C10	-2.6018009	-0.6910679	-0.0021008
13	B	B1	-0.0000948	-0.6709348	-0.0005975
14	C	C11	0.0001153	0.9167017	-0.0017018
15	C	C12	0.0055177	3.7580167	-0.0038496
16	C	C13	-0.0023760	1.6400930	1.2132734

17	C	C14	0.0075328	1.6368178	-1.2161601
18	C	C15	0.0111714	3.0363701	-1.1993301
19	C	C16	0.0015152	3.0376598	1.1947371
20	C	C17	-0.0058058	0.9098791	2.5409010
21	C	C18	0.0151218	0.9062178	-2.5436178
22	H	H2	-0.8884259	0.2656675	2.6442359
23	H	H13	0.8733676	0.2614357	2.6470637
24	H	H12	-0.0055225	1.6110154	3.3815947
25	H	H6	2.6411133	0.3927550	0.0025212
26	H	H4	1.1516803	-4.8771161	-0.0011253
27	H	H1	-1.1526238	-4.8769212	-0.0026474
28	H	H7	-2.6410800	0.3932124	-0.0021912
29	H	H5	-0.8648097	0.2593267	-2.6528996
30	H	H15	0.0189026	1.6072187	-3.3844242
31	H	H10	0.0030881	3.5784887	2.1401176
32	H	H8	0.0203165	3.5760309	-2.1450124
33	C	C19	-0.0135690	5.2692886	-0.0003495
34	H	H16	0.6852968	5.6782211	0.7389127
35	H	H11	0.2576192	5.6751151	-0.9806847
36	H	H17	-1.0099246	5.6574965	0.2511493
37	H	H14	0.8970099	0.2605318	-2.6439047
38	C	C20	-6.2580777	-1.8442266	-0.0006523
39	C	C21	-5.1238985	-1.0586082	-0.0025420
40	C	C22	-7.4684588	-1.0975255	-0.0006744
41	C	C23	-7.2564710	0.2541483	-0.0026511
42	S	S3	-5.5668468	0.6410959	-0.0044460
43	C	C24	6.2576338	-1.8453349	0.0057572
44	C	C25	5.1236068	-1.0594794	0.0037715
45	C	C26	7.4681618	-1.0988834	0.0062510
46	C	C27	7.2563950	0.2528286	0.0047634
47	S	S4	5.5668963	0.6401293	0.0025042
48	H	H19	6.2215653	-2.9297845	0.0067981
49	H	H20	8.4544614	-1.5497061	0.0076778
50	H	H21	7.9889190	1.0488556	0.0047583
51	H	H9	-8.4548386	-1.5481755	0.0006252
52	H	H18	-7.9889787	1.0501981	-0.0030888
53	H	H3	-6.2222355	-2.9286844	0.0007406

2b

	Atom		X	Y	Z
1	C	C1	1.3218235	1.0389122	0.0066644
2	C	C2	1.6156370	2.4181841	-0.0024858
3	C	C5	0.6790041	3.5067723	-0.0115647
4	C	C6	-0.6840365	3.5058047	-0.0113943
5	C	C7	-1.6192096	2.4159211	-0.0020767
6	C	C8	-1.3235752	1.0370070	0.0069856

7	B	B1	-0.0006497	0.2754827	0.0098108
8	C	C11	0.0005993	-1.3113431	0.0171868
9	C	C12	-0.0025387	-4.1508675	0.0290860
10	C	C13	-0.0010201	-2.0386026	-1.1968949
11	C	C14	-0.0014178	-2.0269687	1.2356956
12	C	C15	-0.0041155	-3.4261298	1.2224922
13	C	C16	-0.0037885	-3.4355988	-1.1723496
14	C	C17	-0.0026486	-1.3176536	-2.5297657
15	C	C18	-0.0036225	-1.2965166	2.5633966
16	H	H2	-0.8807834	-0.6690426	-2.6382975
17	H	H13	0.8810452	-0.6775914	-2.6441910
18	H	H12	-0.0087941	-2.0268367	-3.3635675
19	H	H4	1.1449233	4.4908103	-0.0194946
20	H	H1	-1.1513183	4.4892003	-0.0191924
21	H	H5	-0.8827371	-0.6485489	2.6677381
22	H	H15	-0.0085831	-1.9999206	3.4020786
23	H	H10	-0.0086705	-3.9804629	-2.1153383
24	H	H8	-0.0090504	-3.9632398	2.1695685
25	C	C3	-3.0240278	2.6819963	-0.0047621
26	C	C10	3.0200843	2.6859909	-0.0054991
27	C	C4	-3.8143481	1.5574078	0.0029423
28	C	C9	3.8118357	1.5623852	0.0018500
29	H	H14	0.8793406	-0.6546787	2.6731702
30	S	S1	-2.8206888	0.1178762	0.0174974
31	S	S2	2.8200106	0.1215739	0.0167130
32	C	C19	0.0183518	-5.6618529	0.0305787
33	H	H3	-0.6784521	-6.0738192	-0.7088946
34	H	H16	1.0159080	-6.0488408	-0.2180619
35	H	H11	-0.2537485	-6.0650833	1.0116925
36	H	H7	-3.4255915	3.6907655	-0.0184372
37	H	H17	3.4204014	3.6952553	-0.0191811
38	C	C20	6.0582796	0.3575610	-0.0806304
39	C	C21	5.2582975	1.4780986	-0.0010618
40	C	C22	7.4504007	0.6487972	-0.0592233
41	C	C23	7.7098795	1.9888717	0.0363811
42	S	S3	6.2515344	2.9224310	0.1043418
43	C	C24	-6.0591767	0.3496262	-0.0796526
44	C	C25	-5.2606882	1.4711924	0.0004636
45	C	C26	-7.4516921	0.6389626	-0.0576254
46	C	C27	-7.7129450	1.9786097	0.0390896
47	S	S4	-6.2558538	2.9140965	0.1073459
48	H	H18	8.6695449	2.4868952	0.0726323
49	H	H9	8.2250538	-0.1080020	-0.1138068
50	H	H6	5.6558647	-0.6470075	-0.1577350
51	H	H19	-5.6554286	-0.6543344	-0.1576490
52	H	H20	-8.2253399	-0.1188437	-0.1125538
53	H	H21	-8.6732794	2.4752982	0.0759856

1c

	Atom		X	Y	Z
1	C	C2	1.3576884	-1.4621292	-0.0026485
2	C	C5	0.6790559	-3.9552823	-0.0052323
3	H	H2	1.1426867	-4.9396336	-0.0066723
4	C	C6	-0.6922661	-3.9515182	-0.0046370
5	H	H5	-1.1612333	-4.9333545	-0.0057494
6	C	C8	-1.3581437	-1.4546838	-0.0003155
7	B	B1	0.0013237	-0.7266106	-0.0007929
8	C	C11	0.0050818	0.8612837	0.0007725
9	C	C12	0.0022891	3.7035049	0.0033152
10	C	C13	-0.0046953	1.5853657	-1.2143933
11	C	C14	0.0117481	1.5819916	1.2156848
12	C	C15	0.0089369	2.9817254	1.1992861
13	C	C16	-0.0069999	2.9832605	-1.1958183
14	H	H7	0.0103383	3.5210717	2.1452214
15	H	H10	-0.0185132	3.5242067	-2.1410681
16	C	C17	0.0182236	0.8503960	2.5424295
17	H	H4	-0.8607955	0.2019318	2.6496367
18	H	H12	0.0207750	1.5496600	3.3846868
19	H	H13	0.9004308	0.2050335	2.6419469
20	C	C18	0.0232362	5.2146263	0.0003993
21	H	H11	1.0227684	5.6011252	-0.2402598
22	H	H14	-0.2571840	5.6209217	0.9777917
23	H	H15	-0.6665362	5.6248311	-0.7464062
24	C	C19	-0.0170544	0.8545345	-2.5414777
25	H	H1	-0.0193632	1.5541671	-3.3834252
26	H	H16	-0.9013481	0.2117388	-2.6391199
27	H	H17	0.8597913	0.2034826	-2.6507931
28	C	C1	1.5771133	-2.8550851	-0.0042326
29	C	C3	-1.5845366	-2.8465659	-0.0025104
30	S	S1	3.2937384	-3.2333091	-0.0053306
31	S	S2	-3.3028794	-3.2161916	-0.0021835
32	C	C4	3.7388552	-1.5353546	-0.0035370
33	C	C7	2.6048634	-0.7590380	-0.0024315
34	H	H38	2.6349349	0.3242101	-0.0012998
35	C	C9	-2.6018087	-0.7453999	0.0022316
36	H	H41	-2.6268054	0.3379907	0.0051170
37	C	C10	-3.7396607	-1.5160516	0.0014790
38	C	C20	5.1415880	-1.1099276	-0.0032162
39	C	C21	7.8336591	-0.2718294	-0.0024617
40	C	C22	5.4756976	0.2607533	-0.0056804
41	C	C23	6.1943089	-2.0420057	-0.0003107
42	C	C24	7.5240930	-1.6314055	-0.0000186
43	C	C25	6.8000613	0.6724771	-0.0052255

44	H	H3	4.6921667	1.0109223	-0.0081140
45	H	H6	5.9766054	-3.1061815	0.0019521
46	H	H8	8.3193004	-2.3687741	0.0021569
47	H	H9	7.0364844	1.7323847	-0.0071243
48	C	C26	-5.1406896	-1.0845544	0.0030595
49	C	C27	-7.8302421	-0.2377381	0.0057158
50	C	C28	-6.1972586	-2.0164532	0.0071124
51	C	C29	-5.4717716	0.2839670	0.0004406
52	C	C30	-6.7979020	0.7020348	0.0017776
53	C	C31	-7.5220000	-1.6016637	0.0083880
54	H	H19	-5.9814718	-3.0809772	0.0096161
55	H	H20	-4.6869733	1.0328890	-0.0029016
56	H	H21	-7.0310357	1.7610634	-0.0002015
57	H	H22	-8.3197341	-2.3384520	0.0117341
58	C	C32	-9.2737963	0.1814910	0.0061075
59	C	C33	9.2572409	0.2099886	-0.0026308
60	F	F1	10.1457151	-0.8058435	0.0005916
61	F	F2	9.5189653	0.9792243	1.0803841
62	F	F3	9.5204791	0.9735951	-1.0892695
63	F	F4	-9.4213312	1.5229562	0.0114116
64	F	F5	-9.9271656	-0.2928755	-1.0810062
65	F	F6	-9.9290489	-0.3019172	1.0880491

2c

	Atom		X	Y	Z
1	S	S1	2.8191492	-0.1905978	-0.0144627
2	C	C1	3.8127244	1.2464054	-0.0077916
3	C	C2	1.3230466	0.7237854	-0.0031325
4	C	C3	1.6163116	2.1038284	-0.0023407
5	C	C4	3.0225285	2.3693537	-0.0030008
6	H	H6	3.4213878	3.3781666	0.0273123
7	C	C5	0.6805759	3.1936061	0.0029900
8	H	H2	1.1470474	4.1774420	0.0067896
9	C	C6	-0.6825834	3.1933598	0.0009436
10	H	H5	-1.1494280	4.1770252	0.0027338
11	C	C7	-1.6177650	2.1031435	-0.0019414
12	C	C8	-1.3234192	0.7233004	-0.0054841
13	S	S2	-2.8187804	-0.1922825	-0.0060559
14	C	C9	-3.8131560	1.2439636	-0.0126969
15	C	C10	-3.0243717	2.3677572	-0.0064208
16	H	H8	-3.4244473	3.3762321	-0.0340696
17	B	B1	0.0000262	-0.0414720	-0.0023063
18	C	C11	0.0000555	-1.6288703	0.0017203
19	C	C12	-0.0063606	-4.4682106	0.0112409
20	C	C13	-0.0016279	-2.3468958	1.2215722
21	C	C14	-0.0033648	-2.3537754	-1.2117521

22	C	C15	-0.0078090	-3.7526507	-1.1882006
23	C	C16	-0.0061700	-3.7440528	1.2077389
24	H	H7	-0.0138032	-4.2967339	-2.1312699
25	H	H10	-0.0117784	-4.2816496	2.1547868
26	C	C17	-0.0036279	-1.6310132	-2.5432635
27	H	H4	-0.8771003	-0.9750789	-2.6467778
28	H	H12	-0.0176368	-2.3378433	-3.3790372
29	H	H13	0.8850539	-0.9976719	-2.6578988
30	C	C18	0.0140283	-5.9790537	0.0206520
31	H	H11	1.0163233	-6.3635666	0.2529083
32	H	H14	-0.2762458	-6.3896921	-0.9520171
33	H	H15	-0.6681564	-6.3853245	0.7764811
34	C	C19	-0.0038764	-1.6137684	2.5473435
35	H	H1	0.0021895	-2.3141034	3.3886658
36	H	H16	-0.8890512	-0.9740056	2.6529663
37	H	H17	0.8731780	-0.9623554	2.6495069
38	C	C20	-5.2794378	1.1688156	-0.0183469
39	C	C21	-8.0912240	1.0461610	-0.0276602
40	C	C22	-6.0513338	2.2425764	0.4640473
41	C	C23	-5.9516001	0.0328989	-0.5028910
42	C	C24	-7.3410220	-0.0306934	-0.5045041
43	C	C25	-7.4397308	2.1850881	0.4553847
44	H	H9	-5.5572365	3.1211715	0.8665004
45	H	H18	-5.3820753	-0.8026253	-0.8988642
46	H	H19	-7.8434690	-0.9119082	-0.8886989
47	H	H20	-8.0200972	3.0232846	0.8274318
48	C	C26	5.2791986	1.1745020	-0.0122928
49	C	C27	8.0913232	1.0612455	-0.0208056
50	C	C28	5.9576074	0.0244514	0.4335805
51	C	C29	6.0454205	2.2617634	-0.4686114
52	C	C30	7.4357687	2.2101363	-0.4664918
53	C	C31	7.3454663	-0.0338903	0.4259691
54	H	H3	5.3924254	-0.8265814	0.8017866
55	H	H22	5.5478100	3.1483564	-0.8484136
56	H	H23	8.0116508	3.0566965	-0.8238016
57	H	H24	7.8529811	-0.9298424	0.7700948
58	C	C32	9.5928603	0.9876581	0.0187944
59	C	C33	-9.5917647	0.9626987	0.0270171
60	F	F1	10.0480688	-0.1576923	-0.5393081
61	F	F2	10.1740892	2.0171771	-0.6329208
62	F	F3	10.0569350	1.0065320	1.2904477
63	F	F4	-10.0825805	0.0918429	-0.8815114
64	F	F5	-10.1691623	2.1634129	-0.2043490
65	F	F6	-10.0239375	0.5500634	1.2419854

1d

	Atom		X	Y	Z
1	C	C2	1.3581466	-1.4406325	-0.0021830
2	C	C5	0.6854046	-3.9358018	-0.0041668
3	H	H2	1.1513304	-4.9190115	-0.0052118
4	C	C6	-0.6857773	-3.9356303	-0.0037166
5	H	H5	-1.1519592	-4.9187186	-0.0045002
6	C	C8	-1.3577679	-1.4403186	-0.0006583
7	B	B1	0.0004563	-0.7075051	-0.0008432
8	C	C11	0.0003063	0.8796993	0.0006468
9	C	C12	-0.0067137	3.7216679	0.0031658
10	C	C13	-0.0070336	1.6035418	-1.2147822
11	C	C14	0.0021385	1.6002105	1.2158035
12	C	C15	-0.0026745	2.9999035	1.1992253
13	C	C16	-0.0115722	3.0013889	-1.1960574
14	H	H7	-0.0049584	3.5392907	2.1450711
15	H	H10	-0.0211276	3.5423602	-2.1412542
16	C	C17	0.0055257	0.8687738	2.5427017
17	H	H4	-0.8734055	0.2198263	2.6480485
18	H	H12	0.0053199	1.5681158	3.3848007
19	H	H13	0.8878485	0.2239810	2.6451855
20	C	C18	0.0123525	5.2327502	0.0002302
21	H	H11	1.0118035	5.6200532	-0.2392382
22	H	H14	-0.2697052	5.6388288	0.9771702
23	H	H15	-0.6767786	5.6420292	-0.7475896
24	C	C19	-0.0141358	0.8728250	-2.5420206
25	H	H1	-0.0171606	1.5725211	-3.3838164
26	H	H16	-0.8959486	0.2269410	-2.6420583
27	H	H17	0.8652481	0.2249337	-2.6500615
28	C	C1	1.5809746	-2.8332594	-0.0034031
29	C	C3	-1.5810427	-2.8328575	-0.0021711
30	S	S1	3.2977414	-3.2082622	-0.0040948
31	S	S2	-3.2979200	-3.2073221	-0.0017584
32	C	C4	3.7389691	-1.5092821	-0.0025445
33	C	C7	2.6028048	-0.7347478	-0.0018196
34	H	H38	2.6297306	0.3486008	-0.0008721
35	C	C9	-2.6021913	-0.7340082	0.0011205
36	H	H41	-2.6288945	0.3493387	0.0029249
37	C	C10	-3.7385961	-1.5081893	0.0008061
38	C	C20	-5.1386693	-1.0795195	0.0020928
39	C	C21	-7.8354081	-0.2354385	0.0040865
40	C	C22	-6.1940842	-2.0125208	0.0029118
41	C	C23	-5.4714173	0.2912883	0.0024147
42	C	C24	-6.7936645	0.7090435	0.0034187
43	C	C25	-7.5204868	-1.6040349	0.0038519
44	H	H3	-5.9767241	-3.0766036	0.0028025

45	H	H6	-4.6870621	1.0404507	0.0018077
46	H	H8	-7.0305357	1.7681084	0.0036559
47	H	H9	-8.3184153	-2.3394558	0.0043681
48	C	C26	5.1391959	-1.0811602	-0.0020275
49	C	C27	7.8362848	-0.2381506	-0.0008087
50	C	C28	5.4725021	0.2895089	-0.0023837
51	C	C29	6.1942500	-2.0145729	-0.0010251
52	C	C30	7.5208151	-1.6066182	-0.0004546
53	C	C31	6.7949105	0.7067405	-0.0017571
54	H	H19	4.6884183	1.0389565	-0.0031477
55	H	H20	5.9764685	-3.0785689	-0.0006162
56	H	H21	8.3184461	-2.3423621	0.0002718
57	H	H22	7.0322323	1.7657057	-0.0019809
58	C	C32	9.2022751	0.1904194	-0.0002327
59	N	N1	10.3123441	0.5397209	0.0002206
60	C	C33	-9.2012362	0.1936601	0.0049137
61	N	N2	-10.3111770	0.5433684	0.0055386

2d

	Atom		X	Y	Z
1	S	S1	2.8155154	-0.1217197	-0.0047580
2	C	C1	3.8119373	1.3153017	-0.0038463
3	C	C2	1.3207306	0.7914412	-0.0010962
4	C	C3	1.6127349	2.1715042	0.0005589
5	C	C4	3.0178343	2.4374769	-0.0009907
6	H	H6	3.4078381	3.4499139	0.0002025
7	C	C5	0.6761969	3.2610008	0.0035424
8	H	H2	1.1416217	4.2452507	0.0043583
9	C	C6	-0.6867148	3.2591812	0.0054601
10	H	H5	-1.1547509	4.2421884	0.0075881
11	C	C7	-1.6203986	2.1672259	0.0049890
12	C	C8	-1.3248292	0.7879154	0.0025566
13	S	S2	-2.8172882	-0.1290341	0.0026955
14	C	C9	-3.8174161	1.3054148	0.0061534
15	C	C10	-3.0261883	2.4296208	0.0070899
16	H	H8	-3.4187153	3.4410805	0.0094969
17	C	C11	0.0014693	-1.5636200	-0.0024768
18	C	C12	0.0035316	-4.4026753	-0.0065909
19	C	C13	0.0032269	-2.2871729	1.2141907
20	C	C14	-0.0016415	-2.2824859	-1.2196889
21	C	C15	-0.0017390	-3.6814171	-1.2026666
22	C	C16	0.0029116	-3.6842435	1.1934488
23	H	H7	-0.0075531	-4.2209572	-2.1482617
24	H	H10	0.0008008	-4.2264411	2.1378409
25	C	C17	-0.0082493	-1.5534514	-2.5477765
26	H	H4	-0.8916992	-0.9109719	-2.6515511

27	H	H12	-0.0087798	-2.2564153	-3.3868249
28	H	H13	0.8707579	-0.9058007	-2.6569984
29	C	C18	0.0291556	-5.9134019	-0.0045254
30	H	H11	1.0330995	-6.2951177	0.2249739
31	H	H14	-0.2605696	-6.3204496	-0.9788070
32	H	H15	-0.6506318	-6.3256802	0.7501339
33	C	C19	0.0023380	-1.5603622	2.5434823
34	H	H1	0.0031850	-2.2646303	3.3814357
35	H	H16	-0.8794295	-0.9161907	2.6510237
36	H	H17	0.8829898	-0.9145898	2.6507120
37	B	B1	-0.0011113	0.0229947	-0.0002048
38	C	C20	-5.2827960	1.2270204	0.0075775
39	C	C21	-8.1041212	1.0925203	0.0103038
40	C	C22	-5.9514487	-0.0123149	0.0123305
41	C	C23	-6.0663783	2.3983677	0.0041793
42	C	C24	-7.4521415	2.3377265	0.0056279
43	C	C25	-7.3376747	-0.0843565	0.0135884
44	H	H3	-5.3805236	-0.9359061	0.0152345
45	H	H9	-5.5869684	3.3711799	0.0001130
46	H	H18	-8.0389652	3.2505516	0.0030350
47	H	H19	-7.8340715	-1.0492089	0.0171156
48	C	C26	5.2775109	1.2407767	-0.0058335
49	C	C27	8.0992086	1.1136594	-0.0091581
50	C	C28	6.0580468	2.4141776	-0.0075153
51	C	C29	5.9494322	0.0031901	-0.0060234
52	C	C30	7.3358403	-0.0652209	-0.0076914
53	C	C31	7.4439641	2.3571578	-0.0090922
54	H	H21	5.5761364	3.3857686	-0.0076654
55	H	H22	5.3809528	-0.9219175	-0.0047527
56	H	H23	7.8347841	-1.0287671	-0.0077958
57	H	H24	8.0283882	3.2715236	-0.0102723
58	C	C32	9.5301214	1.0497169	-0.0105604
59	N	N1	10.6925935	0.9983805	-0.0116721
60	C	C33	-9.5348628	1.0248327	0.0115305
61	N	N2	-10.6971972	0.9704588	0.0125272

Appendix 4. Supporting Information for Chapter 5

List of Figures

List of Tables

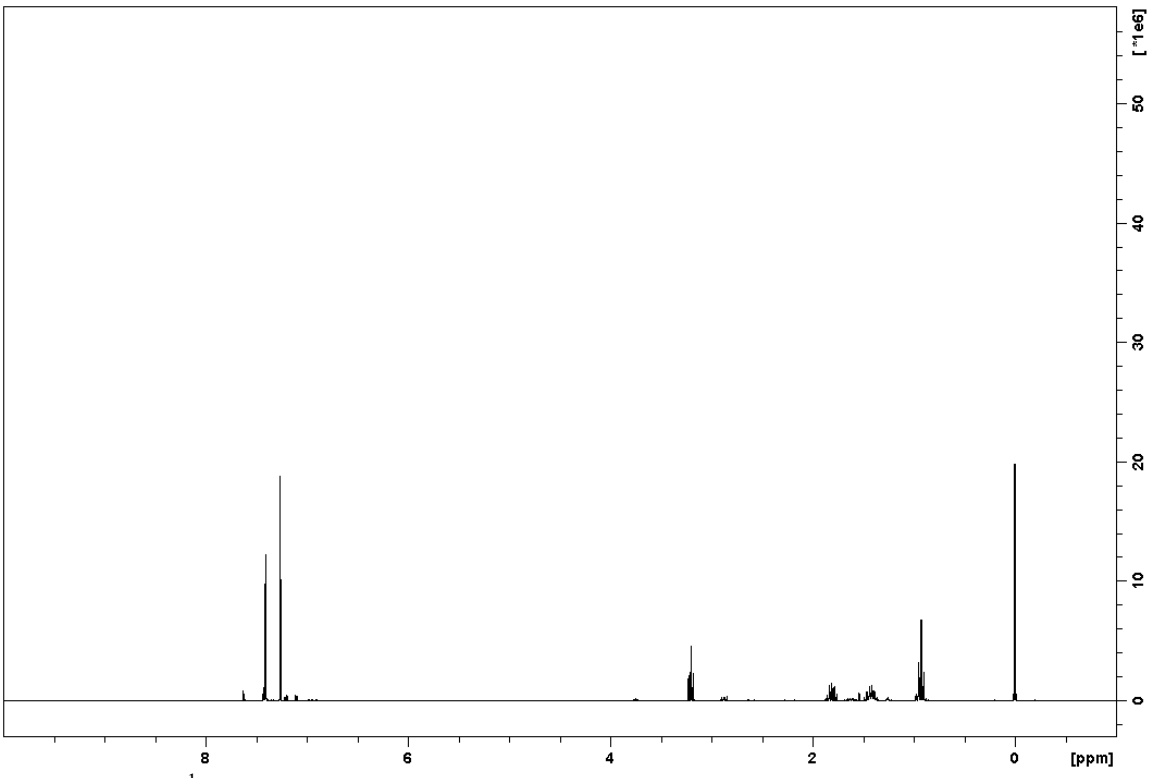

Figure A4.1. ^{1}H (400 MHz, CD_2Cl_2) spectrum for 3,4-diiodothiophene.

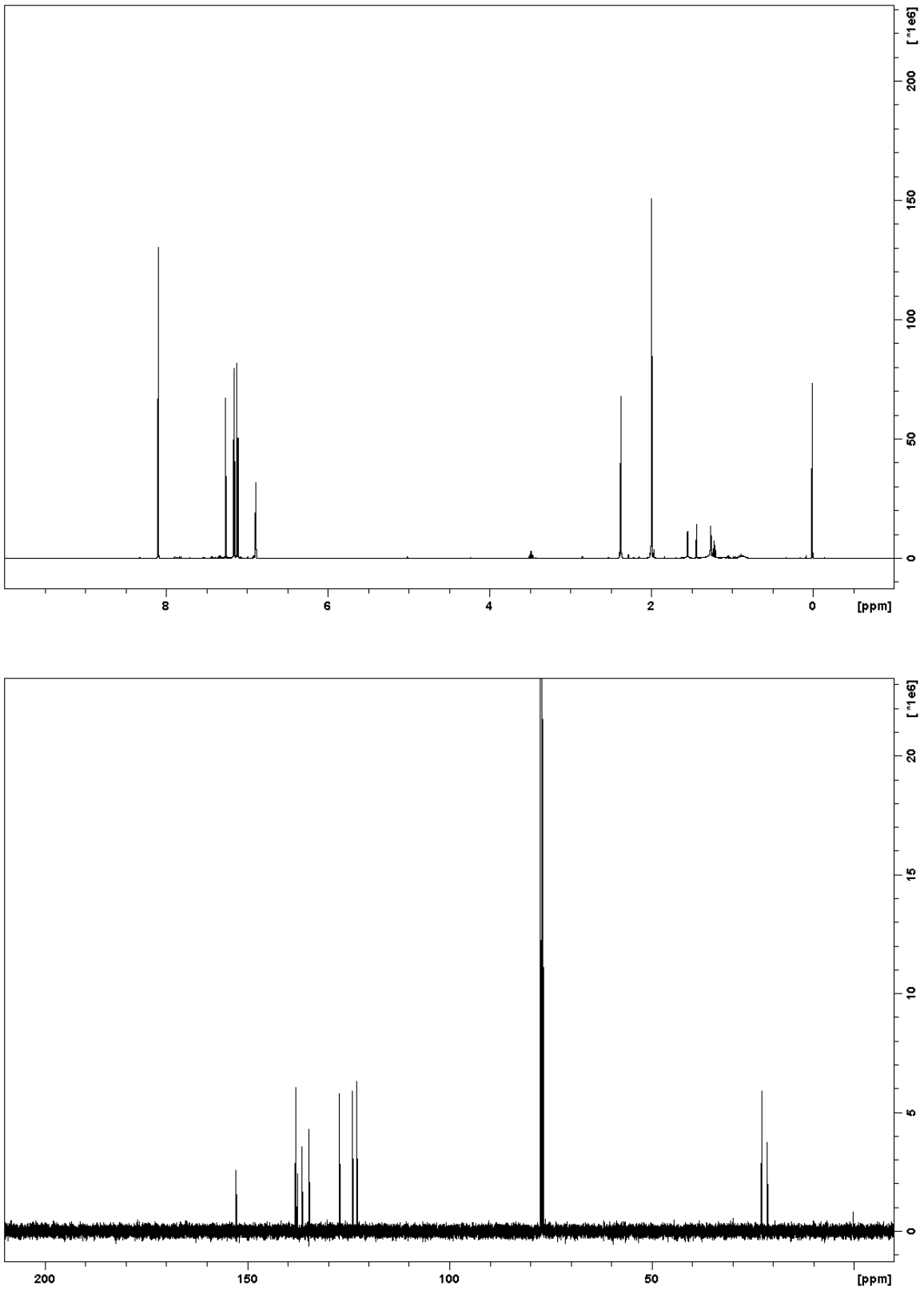

Figure A4.2. ^{1}H (400 MHz, CD_2Cl_2) and ^{13}C NMR (100 MHz, CD_2Cl_2) spectra for **1**.

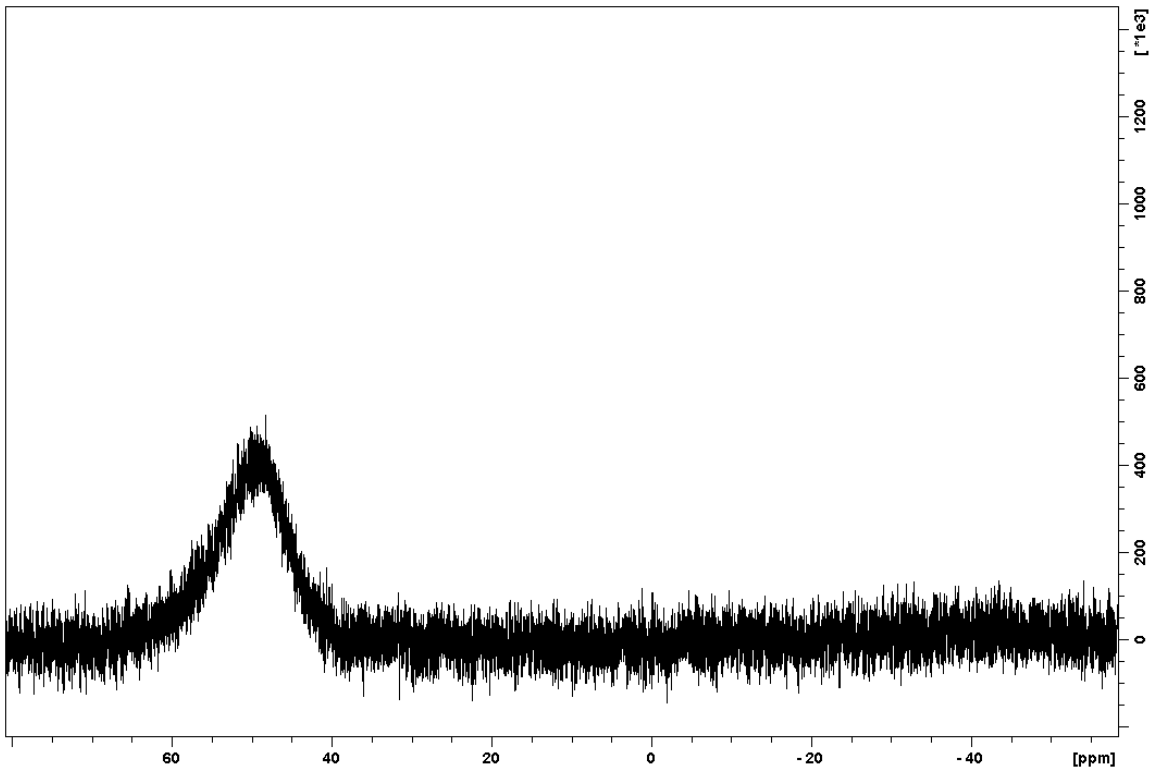

Figure A4.3. ^{11}B NMR (96 MHz, CD_2Cl_2) spectrum for **1**.

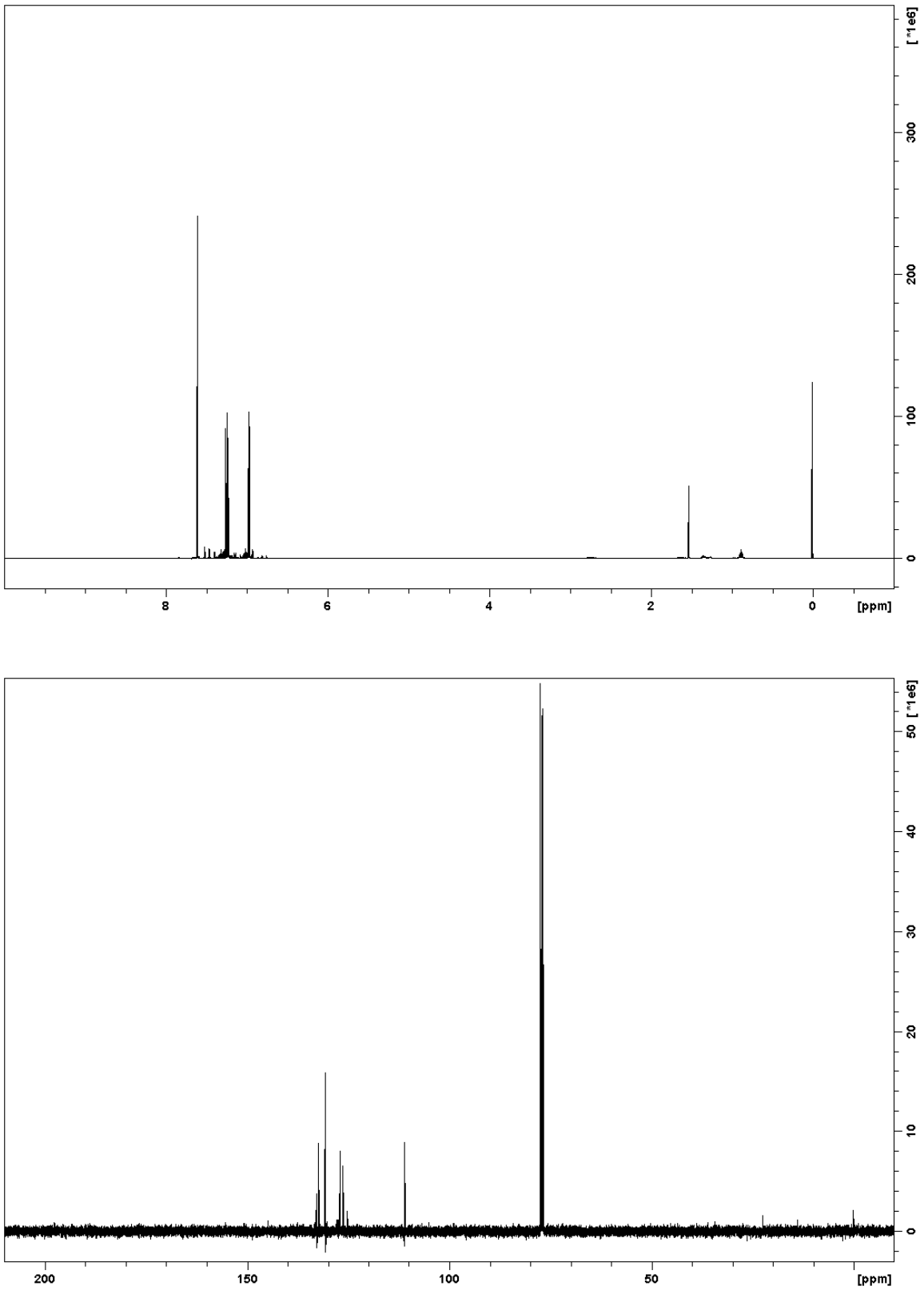

Figure A4.4. ^{1}H (400 MHz, CD_2Cl_2) and ^{13}C NMR (100 MHz, CD_2Cl_2) spectra for **2**.

Table A4.1. Atomic coordinates for the X-ray crystal structure of **1**.

Number	Label	Xfrac + ESD	Yfrac + ESD	Zfrac + ESD
1	C1	0.6138(2)	0.12072(5)	0.5229(2)
2	C2	0.7460(2)	0.08958(6)	0.5038(2)
3	H2	0.7199	0.0704	0.4093
4	C3	0.9100(3)	0.08992(6)	0.6314(2)
5	H3	1.0107	0.0712	0.637
6	C4	0.6906(2)	0.14514(5)	0.6700(2)
7	C5	0.6176(2)	0.18182(5)	0.7387(2)
8	C6	0.7299(2)	0.20542(5)	0.8762(2)
9	H6	0.8569	0.199	0.9323
10	C7	0.4157(2)	0.23536(6)	0.7770(2)
11	H7	0.3046	0.2514	0.7579
12	C8	0.4320(2)	0.19946(5)	0.6788(2)
13	C9	0.2759(2)	0.18456(5)	0.5353(2)
14	C10	-0.0411(3)	0.17988(7)	0.3234(3)
15	H10	-0.1675	0.1828	0.2553
16	C11	0.0771(2)	0.15120(6)	0.2912(2)
17	H11	0.0412	0.1316	0.1975
18	C12	0.2622(2)	0.15303(5)	0.4116(2)
19	C13	0.3593(2)	0.08651(5)	0.2495(2)
20	C14	0.3727(2)	0.09575(6)	0.0904(2)
21	C15	0.3289(2)	0.06332(6)	-0.0349(2)
22	H15	0.3395	0.0699	-0.1418
23	C16	0.2702(2)	0.02176(6)	-0.0074(2)
24	C17	0.2553(2)	0.01288(6)	0.1500(2)
25	H17	0.2144	-0.0153	0.1708
26	C18	0.2995(2)	0.04460(5)	0.2781(2)
27	C19	0.4357(3)	0.14043(7)	0.0550(3)
28	H19A	0.4605	0.1591	0.1556
29	H19B	0.3389	0.1539	-0.0407
30	H19C	0.5487	0.1374	0.0271
31	H19D	0.4382	0.1412	-0.0609
32	H19E	0.5598	0.1463	0.1353
33	H19F	0.35	0.1629	0.0676
34	C20	0.2253(2)	-0.01293(6)	-0.1443(2)
35	H20A	0.121	-0.0031	-0.2422
36	H20B	0.1927	-0.0405	-0.1006
37	H20C	0.3332	-0.0178	-0.1787
38	C21	0.2816(3)	0.03401(6)	0.4477(2)
39	H21A	0.4027	0.0366	0.5369
40	H21B	0.2352	0.0039	0.4457

41	H21C	0.1951	0.0547	0.4704
42	B1	0.4141(3)	0.12181(6)	0.3970(2)
43	S1	0.91430(6)	0.12828(2)	0.78241(5)
44	S2	0.61723(7)	0.24685(2)	0.93383(6)
45	S3	0.06526(6)	0.21024(2)	0.50159(6)

Table A4.2. Cartesian coordinates (in Å) for optimized geometry of **1** calculated at the DFT (B3LYP/6-311G**) level of theory.

	Atom		X	Y	Z
1	C	C2	-1.2344579	-1.3656295	0.1587950
2	C	C5	-3.7362035	-0.7293715	-0.0961292
3	C	C6	-3.7365415	0.7283324	-0.0938673
4	C	C8	-1.2356804	1.3635254	0.1664034
5	B	B1	-0.5147641	-0.0005907	0.0715910
6	C	C11	1.0690128	0.0012898	-0.0290816
7	C	C12	3.8995307	0.0145018	-0.2363972
8	C	C13	1.6990244	0.0087607	-1.2908047
9	C	C14	1.8753219	0.0024472	1.1292957
10	C	C15	3.2677660	0.0108718	1.0084857
11	C	C16	3.0940401	0.0157457	-1.3759248
12	C	C17	1.2474156	-0.0113791	2.5074428
13	C	C18	5.4056434	-0.0107450	-0.3448202
14	C	C19	0.8736170	0.0163253	-2.5596164
15	C	C1	-2.6067810	-1.6156179	0.1409592
16	C	C3	-2.6078113	1.6138675	0.1478044
17	S	S1	-2.9393436	-3.3221068	0.3879951
18	S	S2	-2.9403010	3.3194211	0.4021079
19	C	C4	-1.2507278	-3.7004573	0.4828787
20	C	C7	-0.4878772	-2.5871831	0.3428898
21	C	C9	-0.4891271	2.5840369	0.3582478
22	C	C10	-1.2517444	3.6967389	0.5023692
23	C	C20	-4.9973608	-1.2264450	-0.3650844
24	C	C21	-4.9979675	1.2252401	-0.3616617
25	S	S3	-6.1691882	-0.0005542	-0.6044773
26	H	H3	0.5919873	2.6018735	0.3932026
27	H	H6	-0.9393089	4.7164738	0.6702022
28	H	H8	0.5932847	-2.6059418	0.3740892
29	H	H9	-0.9383927	-4.7211297	0.6446414
30	H	H2	-5.2887751	-2.2609726	-0.4532743
31	H	H5	-5.2897906	2.2599943	-0.4476439
32	H	H17	0.2139265	-0.8559673	-2.6142117
33	H	H1	1.5108467	0.0075712	-3.4464901
34	H	H16	0.2346188	0.9037716	-2.6165040
35	H	H13	0.5371373	0.8112721	2.6371538
36	H	H4	2.0057102	0.0771427	3.2882201
37	H	H12	0.6933862	-0.9388978	2.6852678
38	H	H7	3.8740604	0.0170446	1.9106519
39	H	H10	3.5611546	0.0259169	-2.3569285
40	H	H15	5.7462475	0.4444744	-1.2778345
41	H	H11	5.7842474	-1.0387091	-0.3244571
42	H	H14	5.8741648	0.5250586	0.4845144

Table A4.3. Cartesian coordinates (in Å) for optimized geometries of **4** (singlet), **4** (triplet), **BDTQ** (singlet), **BDTQ** (triplet), **TMTQ** (singlet), **TMTQ** (triplet), **5** (singlet), and **5** (triplet) calculated at the DFT level of theory (RB3LYP/6-31G* for singlet states; UB3LYP/6-31G* for triplet states).

4 (singlet)

	Atom		X	Y	Z
1	C	C2	1.3673363	-1.5201366	-0.0021820
2	C	C5	0.7046429	-3.9994622	-0.0021959
3	H	H2	1.1418486	-4.9956802	-0.0031404
4	C	C6	-0.7177537	-3.9972893	-0.0004532
5	H	H5	-1.1580163	-4.9921637	-0.0003462
6	C	C8	-1.3729863	-1.5159276	0.0016830
7	B	B1	-0.0016564	-0.7671670	-0.0001577
8	C	C11	0.0009255	0.8068601	0.0012532
9	C	C12	0.0013197	3.6418374	0.0037640
10	C	C13	-0.0034393	1.5257707	-1.2171561
11	C	C14	0.0032920	1.5223880	1.2194325
12	C	C15	0.0020679	2.9207604	1.1999188
13	C	C16	-0.0042317	2.9222601	-1.1954891
14	H	H7	0.0003826	3.4605034	2.1447920
15	H	H10	-0.0111128	3.4635892	-2.1397519
16	C	C17	0.0045457	0.7922637	2.5473731
17	H	H4	-0.8757496	0.1455344	2.6579671
18	H	H12	0.0021053	1.4938985	3.3865449
19	H	H13	0.8889952	0.1512826	2.6584982
20	C	C18	0.0239750	5.1518221	-0.0002661
21	H	H11	1.0248674	5.5320852	-0.2435509
22	H	H14	-0.2539298	5.5590212	0.9769760
23	H	H15	-0.6669519	5.5599210	-0.7464948
24	C	C19	-0.0108916	0.7963046	-2.5454008
25	H	H1	-0.0102580	1.4981948	-3.3843570
26	H	H16	-0.8964510	0.1563809	-2.6536731
27	H	H17	0.8682152	0.1484643	-2.6590294
28	C	C1	1.5901475	-2.9499746	-0.0030171
29	C	C3	-1.6000759	-2.9451173	0.0012023
30	S	S1	3.3331171	-3.3241218	-0.0053845
31	S	S2	-3.3441264	-3.3141188	0.0036006
32	C	C4	3.7477488	-1.6242026	-0.0053938
33	C	C7	2.5582707	-0.8227603	-0.0035729
34	H	H38	2.6162124	0.2602565	-0.0032955
35	C	C9	-2.5618592	-0.8150236	0.0036264
36	H	H41	-2.6166674	0.2681707	0.0042064
37	C	C10	-3.7537078	-1.6129702	0.0050485
38	C	C20	-5.0554753	-1.1334135	0.0066410

39	C	C21	5.0509016	-1.1483956	-0.0068609
40	C	C22	5.3108629	0.2518221	-0.0069692
41	N	N1	5.5067845	1.4004676	-0.0068835
42	C	C23	6.1597411	-2.0396104	-0.0084566
43	N	N2	7.0449928	-2.7978386	-0.0099528
44	C	C24	-5.3117142	0.2674934	0.0084786
45	N	N3	-5.5050246	1.4165798	0.0099954
46	C	C25	-6.1668649	-2.0214743	0.0062702
47	N	N4	-7.0543544	-2.7770843	0.0061591

4 (triplet)

	Atom		X	Y	Z
1	C	C2	1.3536611	-1.5069810	-0.0012090
2	C	C5	0.6687249	-4.0025421	-0.0019047
3	H	H2	1.1277501	-4.9886487	-0.0026105
4	C	C6	-0.7032450	-3.9967238	-0.0009424
5	H	H5	-1.1706184	-4.9789216	-0.0010224
6	C	C8	-1.3675191	-1.4954125	0.0009139
7	B	B1	-0.0043467	-0.7608804	0.0003573
8	C	C11	0.0028011	0.8180621	0.0015913
9	C	C12	0.0119288	3.6549381	0.0037804
10	C	C13	0.0038701	1.5384555	-1.2155926
11	C	C14	0.0040915	1.5353315	1.2183521
12	C	C15	0.0074111	2.9338956	1.1999818
13	C	C16	0.0072974	2.9351351	-1.1954101
14	H	H7	0.0051014	3.4738781	2.1449017
15	H	H10	0.0047487	3.4764303	-2.1399023
16	C	C17	-0.0009705	0.8048050	2.5460244
17	H	H4	-0.8854113	0.1632543	2.6539726
18	H	H12	0.0007376	1.5058504	3.3860024
19	H	H13	0.8781633	0.1563725	2.6562885
20	C	C18	0.0392562	5.1652355	-0.0001355
21	H	H11	1.0411318	5.5437740	-0.2425687
22	H	H14	-0.2383242	5.5731260	0.9770726
23	H	H15	-0.6500588	5.5759827	-0.7465945
24	C	C19	-0.0020069	0.8083121	-2.5434439
25	H	H1	0.0007912	1.5094253	-3.3833639
26	H	H16	-0.8873913	0.1680500	-2.6514179
27	H	H17	0.8761231	0.1585025	-2.6536123
28	C	C1	1.5736542	-2.9059345	-0.0022380
29	C	C3	-1.5989757	-2.8925476	0.0001083
30	S	S1	3.2847357	-3.3100980	-0.0039999
31	S	S2	-3.3132272	-3.2828842	0.0009706
32	C	C4	3.7289678	-1.6134937	-0.0032112
33	C	C7	2.5866475	-0.8070217	-0.0017605

34	H	H38	2.6491291	0.2754394	-0.0009816
35	C	C9	-2.5948757	-0.7856020	0.0021277
36	H	H41	-2.6485309	0.2973433	0.0028120
37	C	C10	-3.7437154	-1.5827707	0.0022940
38	C	C20	-5.0932844	-1.1485973	0.0029312
39	C	C21	5.0819375	-1.1900948	-0.0040784
40	C	C22	5.3972954	0.1920600	-0.0033893
41	N	N1	5.6400984	1.3334395	-0.0027668
42	C	C23	6.1481860	-2.1219375	-0.0056275
43	N	N2	7.0068921	-2.9131284	-0.0067812
44	C	C24	-5.3978226	0.2359763	0.0049664
45	N	N3	-5.6318333	1.3791911	0.0062352
46	C	C25	-6.1669335	-2.0719294	0.0017034
47	N	N4	-7.0320423	-2.8561163	0.0011772

BDTQ (singlet)

	Atom		X	Y	Z
1	C	C2	0.7260151	0.0000000	-0.4578691
2	C	C5	0.7155700	0.0000000	-2.9227181
3	H	H2	1.2409698	0.0000000	-3.8723641
4	C	C6	-0.7155700	0.0000000	-2.9227181
5	H	H5	-1.2409698	0.0000000	-3.8723641
6	C	C8	-0.7260151	0.0000000	-0.4578691
7	C	C1	1.3991014	0.0000000	-1.7368404
8	C	C3	-1.3991014	0.0000000	-1.7368404
9	S	S1	3.1527295	0.0000000	-1.5281943
10	S	S2	-3.1527295	0.0000000	-1.5281943
11	C	C4	2.9721555	0.0000000	0.2260092
12	C	C7	1.5950167	0.0000000	0.6094650
13	H	H38	1.3042026	0.0000000	1.6540166
14	C	C9	-1.5950167	0.0000000	0.6094650
15	H	H41	-1.3042026	0.0000000	1.6540166
16	C	C10	-2.9721555	0.0000000	0.2260092
17	C	C20	-4.0565042	0.0000000	1.0938160
18	C	C21	4.0565042	0.0000000	1.0938160
19	C	C22	3.8501082	0.0000000	2.5022438
20	N	N1	3.6540410	0.0000000	3.6509845
21	C	C23	5.3923240	0.0000000	0.6060098
22	N	N2	6.4754708	0.0000000	0.1754411
23	C	C24	-3.8501082	0.0000000	2.5022438
24	N	N3	-3.6540410	0.0000000	3.6509845
25	C	C25	-5.3923240	0.0000000	0.6060098
26	N	N4	-6.4754708	0.0000000	0.1754411

BDTQ (triplet)

	Atom		X	Y	Z
1	C	C2	0.7147392	0.0000000	-0.4557222
2	C	C5	0.6924904	0.0000000	-2.9343847
3	H	H2	1.2384546	0.0000000	-3.8722062
4	C	C6	-0.6924904	0.0000000	-2.9343847
5	H	H5	-1.2384546	0.0000000	-3.8722062
6	C	C8	-0.7147392	0.0000000	-0.4557222
7	C	C1	1.3817670	0.0000000	-1.7050625
8	C	C3	-1.3817670	0.0000000	-1.7050625
9	S	S1	3.1209138	0.0000000	-1.5167087
10	S	S2	-3.1209138	0.0000000	-1.5167087
11	C	C4	2.9533496	0.0000000	0.2423387
12	C	C7	1.6151507	0.0000000	0.6364493
13	H	H38	1.3209626	0.0000000	1.6797668
14	C	C9	-1.6151507	0.0000000	0.6364493
15	H	H41	-1.3209626	0.0000000	1.6797668
16	C	C10	-2.9533496	0.0000000	0.2423387
17	C	C20	-4.0909978	0.0000000	1.0909337
18	C	C21	4.0909978	0.0000000	1.0909337
19	C	C22	3.9251485	0.0000000	2.4984952
20	N	N1	3.7605704	0.0000000	3.6538423
21	C	C23	5.4065316	0.0000000	0.5684537
22	N	N2	6.4820111	0.0000000	0.1138045
23	C	C24	-3.9251485	0.0000000	2.4984952
24	N	N3	-3.7605704	0.0000000	3.6538423
25	C	C25	-5.4065316	0.0000000	0.5684537
26	N	N4	-6.4820111	0.0000000	0.1138045

TMTQ (singlet)

	Atom		X	Y	Z
1	C	C1	1.9986696	0.8587529	0.1414890
2	C	C2	1.3327663	2.1387291	-0.0258954
3	C	C3	-0.0038215	2.3927703	-0.2227252
4	C	C4	-1.1122293	1.4675133	-0.2478056
5	C	C5	-1.1354751	0.2904510	0.4433840
6	C	C6	1.1354751	-0.2904510	0.4433840
7	C	C7	0.0000000	0.0000000	1.3823177
8	C	C8	-1.9986696	-0.8587529	0.1414890
9	C	C9	3.3753330	0.7543308	-0.0060351
10	C	C10	4.3032701	1.7607805	-0.4343003
11	C	C11	5.6107088	1.3726086	-0.4322583
12	C	C12	5.8085546	0.0164582	-0.0081070
13	S	S1	4.2702222	-0.7349647	0.3912614
14	C	C13	1.1122293	-1.4675133	-0.2478056

15	C	C14	0.0038215	-2.3927703	-0.2227252
16	C	C15	-1.3327663	-2.1387291	-0.0258954
17	H	H1	-0.2181782	-0.8624911	2.0172268
18	H	H7	0.2181782	0.8624911	2.0172268
19	H	H6	-1.9296372	1.7209019	-0.9187256
20	H	H2	-0.2470777	3.4188431	-0.4940916
21	H	H4	1.9844790	3.0045686	-0.0948740
22	H	H9	3.9825030	2.7467112	-0.7480408
23	H	H10	6.4443601	2.0033952	-0.7182081
24	H	H3	1.9296372	-1.7209019	-0.9187256
25	H	H11	0.2470777	-3.4188431	-0.4940916
26	H	H12	-1.9844790	-3.0045686	-0.0948740
27	C	C16	7.0191735	-0.6528780	0.0833640
28	C	C17	8.2320360	0.0097120	-0.2609686
29	C	C18	7.0832108	-2.0061654	0.5175729
30	N	N1	9.2103237	0.5748183	-0.5470870
31	N	N2	7.0982087	-3.1160286	0.8736656
32	C	C19	-3.3753330	-0.7543308	-0.0060351
33	C	C20	-4.3032701	-1.7607805	-0.4343003
34	C	C21	-5.6107088	-1.3726086	-0.4322583
35	C	C22	-5.8085546	-0.0164582	-0.0081070
36	S	S2	-4.2702222	0.7349647	0.3912614
37	H	H8	-3.9825030	-2.7467112	-0.7480408
38	H	H5	-6.4443601	-2.0033952	-0.7182081
39	C	C23	-7.0191735	0.6528780	0.0833640
40	C	C24	-8.2320360	-0.0097120	-0.2609686
41	C	C25	-7.0832108	2.0061654	0.5175729
42	N	N3	-9.2103237	-0.5748183	-0.5470870
43	N	N4	-7.0982087	3.1160286	0.8736656

TMTQ (triplet)

	Atom		X	Y	Z
1	C	C1	1.9134355	0.8349073	0.4148034
2	C	C2	1.3157731	2.1136474	0.3619413
3	C	C3	-0.0545307	2.4428339	0.2672738
4	C	C4	-1.1634105	1.5883370	0.2814492
5	C	C5	-1.1185786	0.2900581	0.8105632
6	C	C6	1.1185786	-0.2900581	0.8105632
7	C	C7	0.0000000	0.0000000	1.7581492
8	C	C8	-1.9134355	-0.8349073	0.4148034
9	C	C9	3.3007846	0.7106869	-0.0017841
10	C	C10	4.0162505	1.5455740	-0.8654201
11	C	C11	5.3596823	1.2021448	-1.0111564
12	C	C12	5.7301484	0.0737985	-0.2546274
13	S	S1	4.3555383	-0.5348154	0.6555752
14	C	C13	1.1634105	-1.5883370	0.2814492

15	C	C14	0.0545307	-2.4428339	0.2672738
16	C	C15	-1.3157731	-2.1136474	0.3619413
17	H	H1	-0.2209809	-0.8642626	2.3880618
18	H	H7	0.2209809	0.8642626	2.3880618
19	H	H6	-2.0591915	1.9376756	-0.2241174
20	H	H2	-0.2497315	3.4734659	-0.0221986
21	H	H4	1.9951942	2.9465046	0.1996129
22	H	H9	3.5485375	2.3632417	-1.4013062
23	H	H10	6.0624231	1.7233315	-1.6509612
24	H	H3	2.0591915	-1.9376756	-0.2241174
25	H	H11	0.2497315	-3.4734659	-0.0221986
26	H	H12	-1.9951942	-2.9465046	0.1996129
27	C	C16	7.0019855	-0.5331813	-0.1926965
28	C	C17	8.0846526	0.0128369	-0.9302164
29	C	C18	7.2353268	-1.6885113	0.5944006
30	N	N1	8.9568331	0.4827906	-1.5465137
31	N	N2	7.3985702	-2.6415198	1.2482418
32	C	C19	-3.3007846	-0.7106869	-0.0017841
33	C	C20	-4.0162505	-1.5455740	-0.8654201
34	C	C21	-5.3596823	-1.2021448	-1.0111564
35	C	C22	-5.7301484	-0.0737985	-0.2546274
36	S	S2	-4.3555383	0.5348154	0.6555752
37	H	H8	-3.5485375	-2.3632417	-1.4013062
38	H	H5	-6.0624231	-1.7233315	-1.6509612
39	C	C23	-7.0019855	0.5331813	-0.1926965
40	C	C24	-8.0846526	-0.0128369	-0.9302164
41	C	C25	-7.2353268	1.6885113	0.5944006
42	N	N3	-8.9568331	-0.4827906	-1.5465137
43	N	N4	-7.3985702	2.6415198	1.2482418

5 (singlet)

	Atom		X	Y	Z
1	C	C2	1.3632823	-1.7008270	-0.0003570
2	C	C5	0.7004813	-4.1841014	-0.0010132
3	H	H2	1.1459254	-5.1767077	-0.0025657
4	C	C6	-0.7067971	-4.1832817	0.0021158
5	H	H5	-1.1533386	-5.1754008	0.0031263
6	C	C8	-1.3674216	-1.6991769	0.0013853
7	B	B1	-0.0020938	-0.9563377	0.0018602
8	C	C11	-0.0001849	0.6230944	0.0075695
9	C	C12	0.0025520	3.4617094	0.0190931
10	C	C13	-0.0000851	1.3484341	-1.2075213
11	C	C14	-0.0015157	1.3375017	1.2269606
12	C	C15	-0.0013197	2.7364883	1.2131241
13	C	C16	0.0000024	2.7454921	-1.1826490
14	H	H7	-0.0055823	3.2730682	2.1600241

15	H	H10	-0.0033440	3.2897245	-2.1255050
16	C	C17	-0.0062456	0.6028589	2.5522790
17	H	H4	-0.8896656	-0.0404836	2.6562607
18	H	H12	-0.0059012	1.3008380	3.3948950
19	H	H13	0.8734202	-0.0451040	2.6595570
20	C	C18	0.0281626	4.9718866	0.0206334
21	H	H11	1.0317603	5.3516900	-0.2119120
22	H	H14	-0.2576485	5.3763641	0.9967480
23	H	H15	-0.6547948	5.3849763	-0.7302210
24	C	C19	-0.0033780	0.6227675	-2.5377885
25	H	H1	-0.0024904	1.3262662	-3.3757848
26	H	H16	-0.8864425	-0.0202663	-2.6467136
27	H	H17	0.8765392	-0.0243046	-2.6483699
28	C	C1	1.5878735	-3.1205269	-0.0024359
29	C	C3	-1.5931445	-3.1187570	0.0029544
30	S	S1	3.3253455	-3.4876691	-0.0062006
31	S	S2	-3.3308803	-3.4846075	0.0048298
32	C	C4	3.7472409	-1.7759025	-0.0052735
33	C	C7	2.5659905	-0.9978184	-0.0014432
34	H	H38	2.5994956	0.0869103	0.0001437
35	C	C9	-2.5696794	-0.9953418	0.0001686
36	H	H41	-2.6024613	0.0894299	-0.0008845
37	C	C10	-3.7515264	-1.7725658	0.0009964
38	C	C20	6.2565942	-2.0869868	-0.0115603
39	C	C21	5.0634660	-1.3157613	-0.0077742
40	S	S3	5.4583637	0.4129514	-0.0060830
41	C	C22	7.4112595	-1.3465111	-0.0128187
42	H	H6	8.4135305	-1.7586961	-0.0154670
43	C	C23	7.1835966	0.0638234	-0.0098565
44	C	C24	8.1500744	1.0651465	-0.0094946
45	C	C25	9.5307710	0.7213519	-0.0119674
46	N	N3	10.6542490	0.4100816	-0.0141242
47	C	C26	7.7913796	2.4403473	-0.0059850
48	N	N4	7.4630518	3.5592838	-0.0032603
49	H	H8	6.2381206	-3.1719600	-0.0132698
50	C	C27	-6.2607168	-2.0831256	0.0041319
51	C	C28	-5.0675350	-1.3119354	-0.0010122
52	S	S4	-5.4623551	0.4167826	-0.0121755
53	C	C29	-7.4152884	-1.3426659	-0.0007058
54	H	H3	-8.4175735	-1.7548132	0.0020065
55	C	C30	-7.1875754	0.0676579	-0.0100082
56	C	C31	-8.1543332	1.0686469	-0.0175653
57	C	C32	-9.5348989	0.7242281	-0.0151199
58	N	N1	-10.6582858	0.4126438	-0.0124806
59	C	C33	-7.7965165	2.4440330	-0.0279119
60	N	N2	-7.4692209	3.5632320	-0.0369773
61	H	H9	-6.2422881	-3.1680744	0.0113927

5 (triplet)

	Atom		X	Y	Z
1	C	C2	1.3573295	-1.6641604	-0.0022854
2	C	C5	0.6837054	-4.1589658	-0.0037276
3	H	H2	1.1466921	-5.1434000	-0.0045492
4	C	C6	-0.6895126	-4.1583260	-0.0014664
5	H	H5	-1.1534262	-5.1423234	-0.0004822
6	C	C8	-1.3609900	-1.6629657	-0.0011005
7	B	B1	-0.0009324	-0.9258280	0.0023886
8	C	C11	0.0001617	0.6573793	0.0088245
9	C	C12	0.0009219	3.4972479	0.0216693
10	C	C13	-0.0012737	1.3842696	-1.2049149
11	C	C14	-0.0005632	1.3721742	1.2274865
12	C	C15	-0.0013708	2.7713712	1.2152466
13	C	C16	-0.0021363	2.7815153	-1.1803390
14	H	H7	-0.0051940	3.3074896	2.1625746
15	H	H10	-0.0067298	3.3262059	-2.1231001
16	C	C17	-0.0038681	0.6362102	2.5519851
17	H	H4	-0.8866415	-0.0082560	2.6549918
18	H	H12	-0.0031785	1.3332191	3.3956529
19	H	H13	0.8758645	-0.0120996	2.6568712
20	C	C18	0.0252061	5.0076938	0.0240035
21	H	H11	1.0272443	5.3896662	-0.2120914
22	H	H14	-0.2573750	5.4112708	1.0015581
23	H	H15	-0.6611831	5.4209479	-0.7237916
24	C	C19	-0.0052975	0.6586738	-2.5351252
25	H	H1	-0.0055425	1.3620748	-3.3734611
26	H	H16	-0.8878387	0.0145705	-2.6423435
27	H	H17	0.8746128	0.0115092	-2.6455484
28	C	C1	1.5808916	-3.0597106	-0.0050629
29	C	C3	-1.5857158	-3.0582984	-0.0010505
30	S	S1	3.2981018	-3.4429258	-0.0096944
31	S	S2	-3.3031658	-3.4399294	-0.0015230
32	C	C4	3.7350603	-1.7407687	-0.0075592
33	C	C7	2.5936908	-0.9577321	-0.0034731
34	H	H38	2.6313305	0.1266845	-0.0012082
35	C	C9	-2.5966480	-0.9552303	-0.0018213
36	H	H41	-2.6332944	0.1292321	-0.0004658
37	C	C10	-3.7386792	-1.7373254	-0.0016015
38	C	C20	6.2526412	-2.1197771	-0.0145236
39	C	C21	5.1015113	-1.3222163	-0.0096844
40	S	S3	5.5286262	0.3859732	-0.0059384
41	C	C22	7.4410089	-1.3982321	-0.0147326
42	H	H6	8.4310233	-1.8392019	-0.0176102
43	C	C23	7.2451908	-0.0002861	-0.0100674

44	C	C24	8.2377188	0.9967484	-0.0068387
45	C	C25	9.6095297	0.6292512	-0.0087016
46	N	N3	10.7281885	0.2987081	-0.0111430
47	C	C26	7.9068039	2.3758983	-0.0003958
48	N	N4	7.6049283	3.5030781	0.0039653
49	H	H8	6.2101765	-3.2037325	-0.0175550
50	C	C27	-6.2562615	-2.1151241	0.0166819
51	C	C28	-5.1049542	-1.3180290	-0.0016688
52	S	S4	-5.5316191	0.3900590	-0.0276978
53	C	C29	-7.4444290	-1.3932894	0.0111717
54	H	H3	-8.4345335	-1.8338922	0.0235597
55	C	C30	-7.2482596	0.0044029	-0.0128470
56	C	C31	-8.2406936	1.0014752	-0.0254042
57	C	C32	-9.6125062	0.6341055	-0.0140474
58	N	N1	-10.7311630	0.3037093	-0.0036583
59	C	C33	-7.9100711	2.3804683	-0.0510299
60	N	N2	-7.6090382	3.5076813	-0.0723703
61	H	H9	-6.2140745	-3.1989386	0.0350695

Appendix 5. Supporting Information for Chapter 6

List of Figures

List of Tables

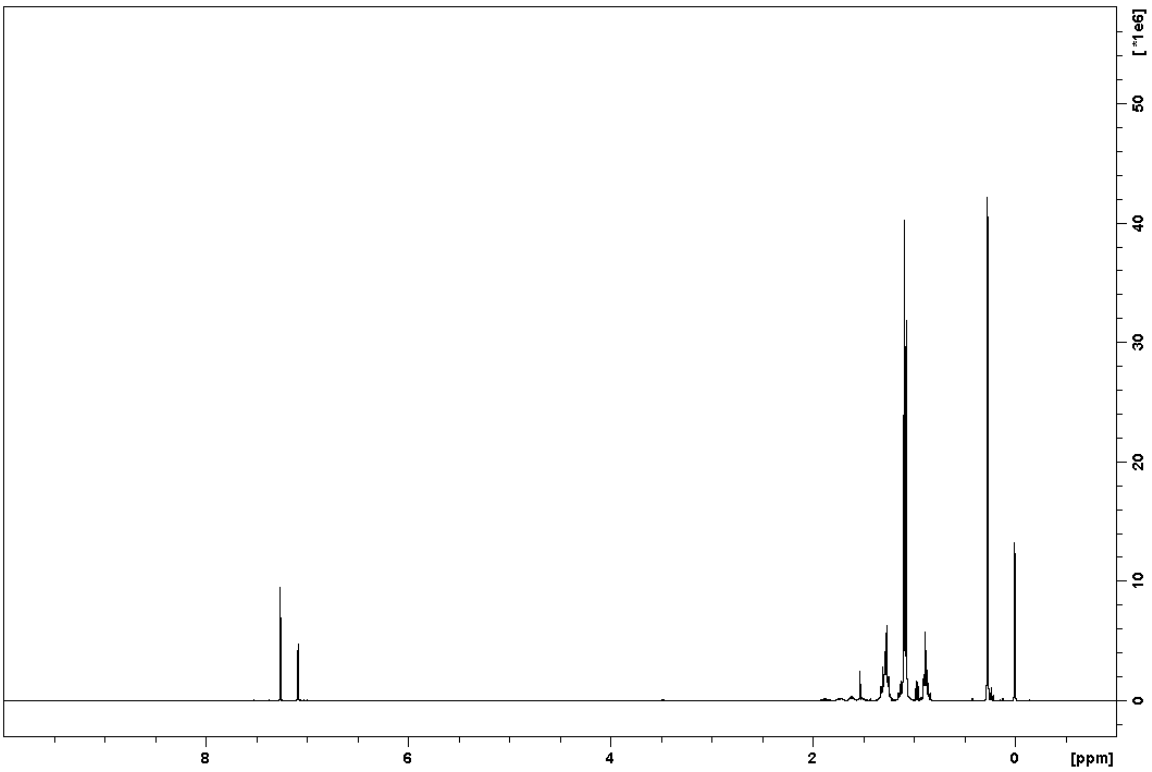

Figure A5.1. ^{1}H (400 MHz, $CDCl_3$) spectrum for **S1**.

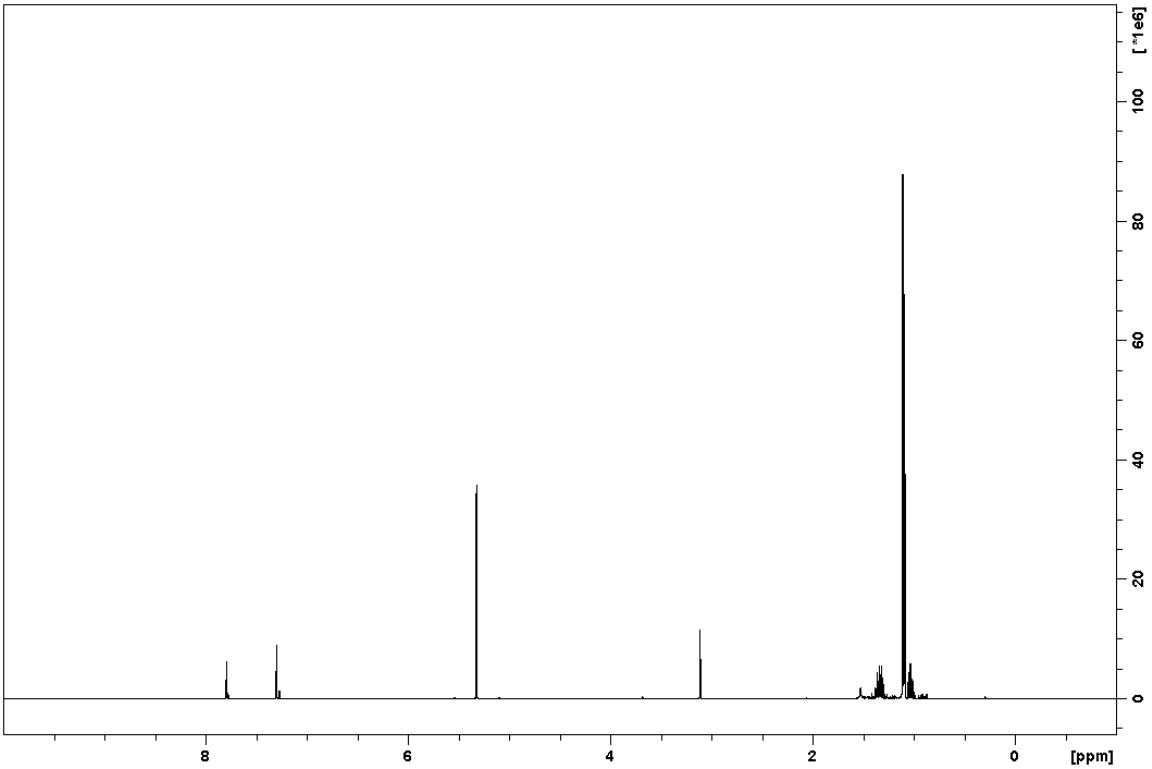

Figure A5.2. ^{1}H NMR (400 MHz, CD_2Cl_2) spectrum for **S3**.

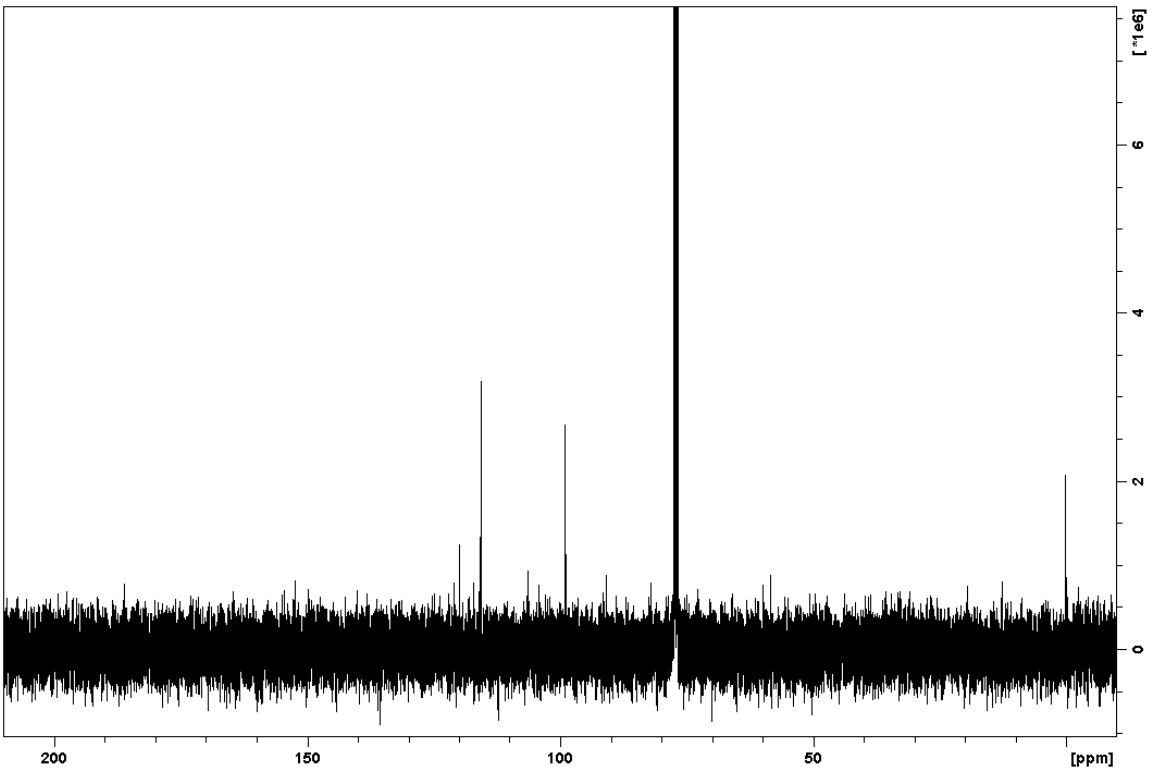

Figure A5.3. ^{13}C NMR (100 MHz, $CDCl_3$) spectrum for **2**.

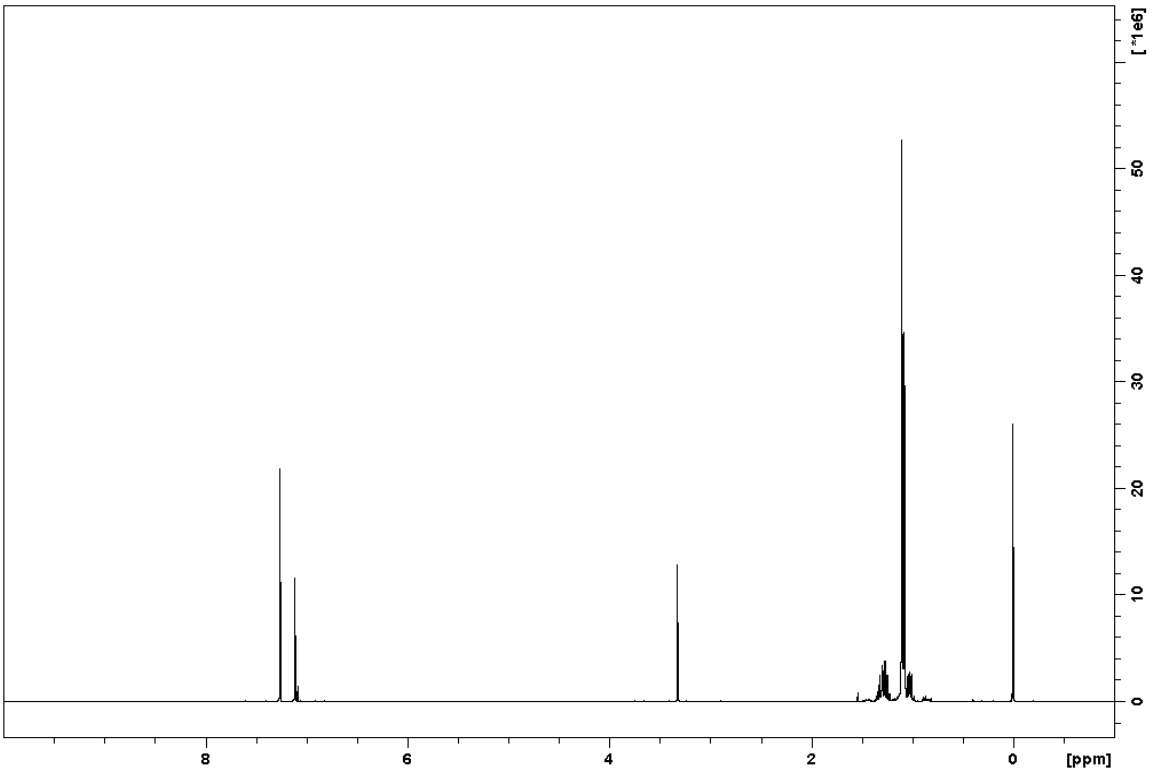

Figure A5.4. ^{1}H (400 MHz, $CDCl_3$) spectrum for **3**.

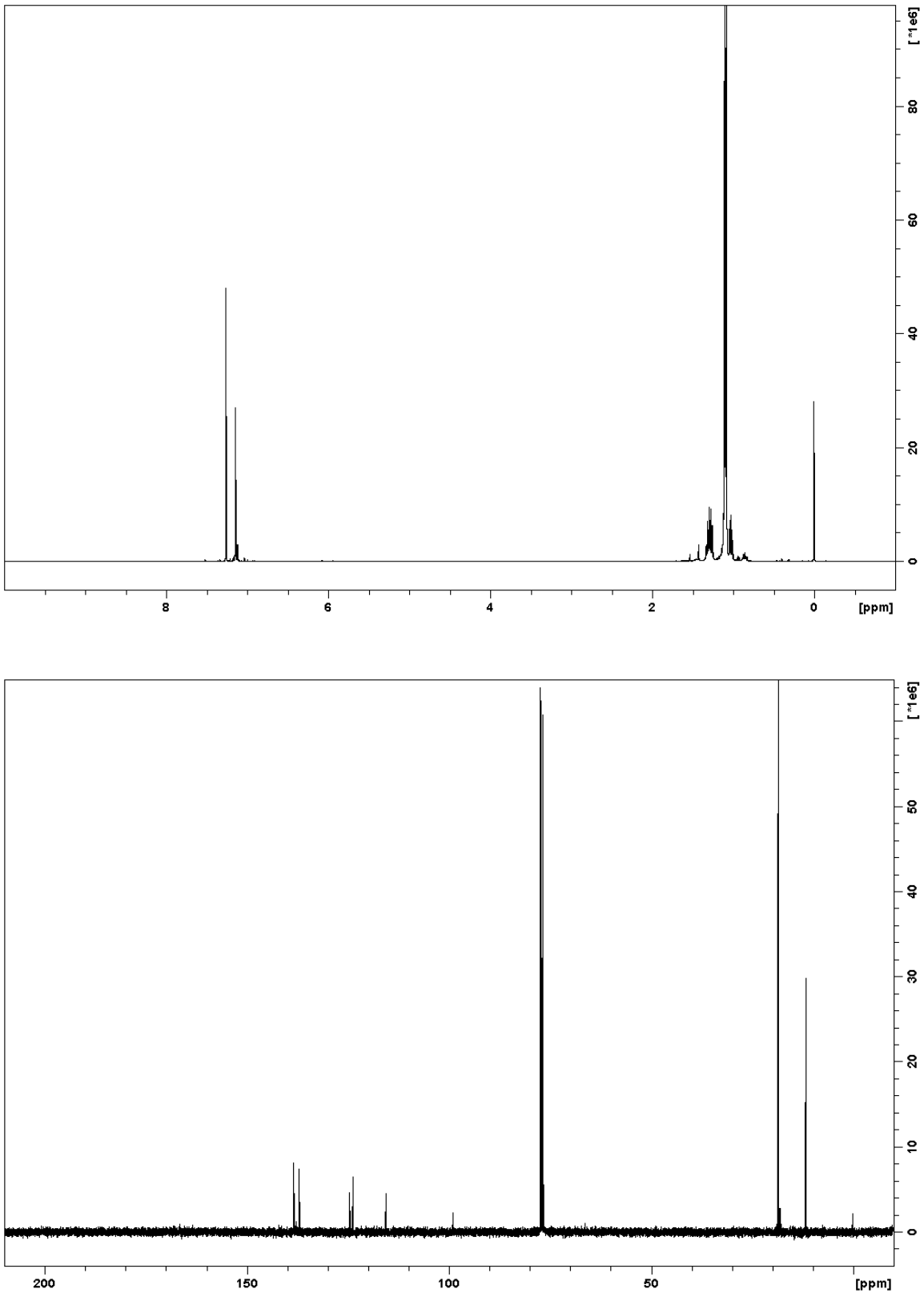

Figure A5.5. ^{1}H (400 MHz, $CDCl_3$) and ^{13}C NMR (100 MHz, $CDCl_3$) spectra for **5**.

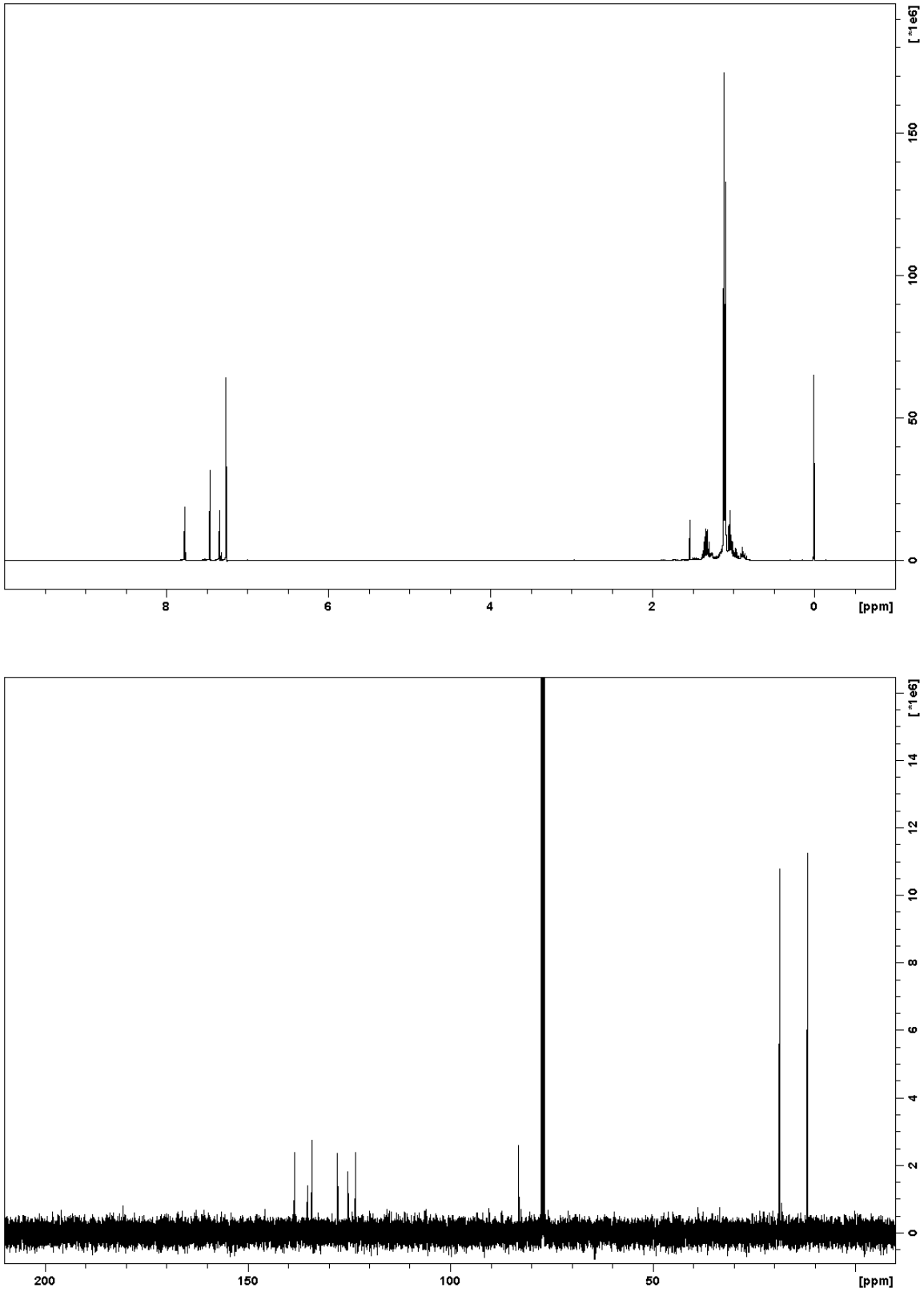

Figure A5.6. ^{1}H (400 MHz, $CDCl_3$) and ^{13}C NMR (100 MHz, $CDCl_3$) spectra for **6**.

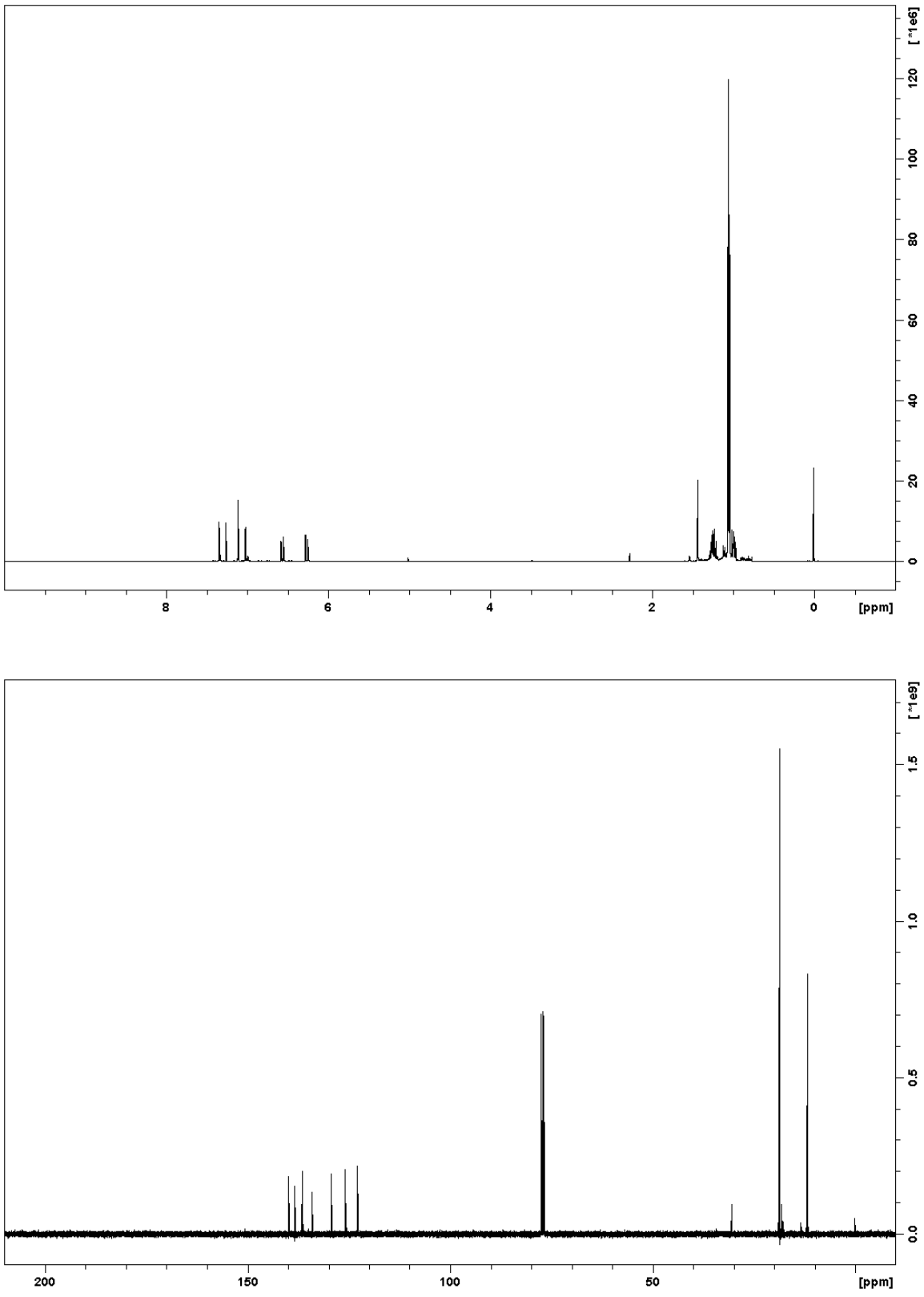

Figure A5.7. ^{1}H (400 MHz, $CDCl_3$) and ^{13}C NMR (100 MHz, $CDCl_3$) spectra for **7**.

Table A6.1. Cartesian coordinates (in Å) for optimized geometries of **I-Mes**, **II-Mes**, **IV-Mes**, and **V-Mes** calculated at the DFT (B3LYP/6-31G*) level.

I-Mes

	Atom		X	Y	Z
1	S	S1	0.0000000	0.0000000	0.2473175
2	C	C2	-1.2757917	0.0029207	1.4323489
3	C	C3	-0.7340024	0.0032035	2.7320178
4	C	C5	-1.4974050	0.0093052	3.9491972
5	H	H2	-0.9126320	0.0071011	4.8625220
6	C	C6	-2.8445682	0.0196557	4.1745958
7	H	H5	-3.1325573	0.0241001	5.2248370
8	C	C7	-3.9575024	0.0255840	3.2719944
9	C	C8	-3.9032031	0.0171841	1.8638191
10	S	S2	-5.5359434	0.0269199	1.2128109
11	C	C9	-6.2444816	0.0415980	2.7892471
12	C	C10	-5.3027746	0.0394081	3.7753353
13	H	H8	-5.5382655	0.0472774	4.8348574
14	C	C11	-2.9828895	-0.0190297	-0.6609224
15	C	C12	-3.4559522	-0.0654754	-3.4606855
16	C	C13	-3.1186377	-1.2478511	-1.3503066
17	C	C14	-3.0914314	1.1842818	-1.3940199
18	C	C15	-3.3263985	1.1425137	-2.7729716
19	C	C16	-3.3535577	-1.2517618	-2.7275525
20	H	H7	-3.4096599	2.0784597	-3.3231410
21	H	H10	-3.4586505	-2.2057547	-3.2423697
22	C	C17	-2.9534241	2.5259895	-0.7040999
23	H	H4	-3.6937372	2.6486664	0.0961936
24	H	H12	-3.0894716	3.3505666	-1.4112540
25	H	H13	-1.9631240	2.6430697	-0.2462228
26	C	C18	-3.6769781	-0.0970814	-4.9551546
27	H	H11	-2.7569396	-0.3745715	-5.4868884
28	H	H14	-3.9929115	0.8801773	-5.3348289
29	H	H15	-4.4420089	-0.8314115	-5.2336703
30	C	C19	-3.0103343	-2.5654319	-0.6105008
31	H	H1	-3.1427714	-3.4129150	-1.2907868
32	H	H16	-3.7675506	-2.6511368	0.1788113
33	H	H17	-2.0311028	-2.6775470	-0.1282887
34	H	H32	-7.3207569	0.0516927	2.9072565
35	B	B1	-2.7211401	0.0020858	0.9041617
36	C	C1	1.2757917	-0.0029207	1.4323489
37	C	C4	0.7340024	-0.0032035	2.7320178
38	C	C20	1.4974050	-0.0093052	3.9491972
39	H	H3	0.9126320	-0.0071011	4.8625220
40	C	C21	2.8445682	-0.0196557	4.1745958
41	H	H6	3.1325573	-0.0241001	5.2248370

42	C	C22	3.9575024	-0.0255840	3.2719944
43	C	C23	3.9032031	-0.0171841	1.8638191
44	S	S3	5.5359434	-0.0269199	1.2128109
45	C	C24	6.2444816	-0.0415980	2.7892471
46	C	C25	5.3027746	-0.0394081	3.7753353
47	H	H18	5.5382655	-0.0472774	4.8348574
48	C	C26	2.9828895	0.0190297	-0.6609224
49	C	C27	3.4559522	0.0654754	-3.4606855
50	C	C28	3.1186377	1.2478511	-1.3503066
51	C	C29	3.0914314	-1.1842818	-1.3940199
52	C	C30	3.3263985	-1.1425137	-2.7729716
53	C	C31	3.3535577	1.2517618	-2.7275525
54	H	H19	3.4096599	-2.0784597	-3.3231410
55	H	H20	3.4586505	2.2057547	-3.2423697
56	C	C32	2.9534241	-2.5259895	-0.7040999
57	H	H21	3.6937372	-2.6486664	0.0961936
58	H	H22	3.0894716	-3.3505666	-1.4112540
59	H	H23	1.9631240	-2.6430697	-0.2462228
60	C	C33	3.6769781	0.0970814	-4.9551546
61	H	H24	2.7569396	0.3745715	-5.4868884
62	H	H25	3.9929115	-0.8801773	-5.3348289
63	H	H26	4.4420089	0.8314115	-5.2336703
64	C	C34	3.0103343	2.5654319	-0.6105008
65	H	H27	3.1427714	3.4129150	-1.2907868
66	H	H28	3.7675506	2.6511368	0.1788113
67	H	H29	2.0311028	2.6775470	-0.1282887
68	H	H30	7.3207569	-0.0516927	2.9072565
69	B	B2	2.7211401	-0.0020858	0.9041617

II-Mes

	Atom		X	Y	Z
1	C	C2	3.6074194	2.7934767	-0.2096830
2	C	C5	1.6465799	4.4670321	-0.2873941
3	H	H2	1.4693657	5.5387977	-0.3517147
4	C	C6	0.5223442	3.6861948	-0.2232012
5	H	H5	-0.4213761	4.2284157	-0.2442860
6	C	C8	1.3748672	1.2489358	-0.0856001
7	B	B1	2.9053962	1.4240845	-0.1090272
8	C	C11	3.8327458	0.1367108	-0.0256909
9	C	C12	5.5226859	-2.1426040	0.1181793
10	C	C13	4.2583834	-0.3695162	1.2250528
11	C	C14	4.2758516	-0.5088478	-1.2019239
12	C	C15	5.1067981	-1.6316585	-1.1133304
13	C	C16	5.0906379	-1.4909786	1.2781279
14	H	H7	5.4394153	-2.1164935	-2.0298061
15	H	H10	5.4108802	-1.8654671	2.2494923

16	C	C17	3.8648622	0.0104380	-2.5644650
17	H	H4	4.2225490	1.0352811	-2.7265910
18	H	H12	2.7734405	0.0325813	-2.6769693
19	H	H13	4.2683582	-0.6149217	-3.3673978
20	C	C18	6.4004605	-3.3700120	0.2014555
21	H	H11	7.2071691	-3.2385632	0.9322574
22	H	H14	6.8565488	-3.6027097	-0.7664677
23	H	H15	5.8258029	-4.2521989	0.5142773
24	C	C19	3.8172119	0.2952784	2.5125482
25	H	H1	4.2514205	-0.2022026	3.3858172
26	H	H16	2.7257836	0.2699029	2.6248405
27	H	H17	4.1158114	1.3506742	2.5460566
28	C	C1	3.0097242	4.0672719	-0.2831327
29	C	C3	0.4002969	2.2729817	-0.1358859
30	S	S1	4.2203469	5.3434394	-0.3862603
31	S	S2	-1.2590225	1.6634321	-0.0817941
32	C	C4	5.5117120	4.1876414	-0.3316822
33	C	C7	5.0427316	2.9115430	-0.2402599
34	H	H38	5.6930470	2.0454635	-0.1949276
35	C	C9	0.6956227	-0.0144617	-0.0068464
36	C	C10	-0.6953847	0.0147358	0.0051276
37	H	H18	6.5403397	4.5219911	-0.3703379
38	C	C20	-1.3746469	-1.2487976	0.0815912
39	C	C21	-0.5220103	-3.6863170	0.2138874
40	H	H3	0.4217422	-4.2283470	0.2352624
41	C	C22	-1.6462402	-4.4676639	0.2721233
42	H	H6	-1.4689914	-5.5395793	0.3328504
43	C	C23	-3.6073795	-2.7942919	0.1933626
44	B	B2	-2.9051993	-1.4242120	0.1030680
45	C	C24	-3.8323685	-0.1361918	0.0287695
46	C	C25	-5.5218194	2.1444779	-0.0968880
47	C	C26	-4.2618704	0.3771193	-1.2177651
48	C	C27	-4.2712692	0.5030750	1.2100088
49	C	C28	-5.1021026	1.6265108	1.1304727
50	C	C29	-5.0937294	1.4993140	-1.2618480
51	H	H8	-5.4320390	2.1059264	2.0508262
52	H	H9	-5.4172771	1.8792261	-2.2299181
53	C	C30	-3.8581207	-0.0258274	2.5681000
54	H	H19	-4.2438510	0.6051934	3.3752588
55	H	H21	-2.7665136	-0.0679685	2.6717698
56	H	H22	-4.2332128	-1.0442248	2.7313080
57	C	C31	-6.3993021	3.3727416	-0.1697652
58	H	H23	-7.1966093	3.2537277	-0.9128915
59	H	H24	-5.8215834	4.2609226	-0.4594675
60	H	H25	-6.8675209	3.5881547	0.7964250
61	C	C32	-3.8258927	-0.2814982	-2.5102217
62	H	H26	-4.1327617	-1.3343620	-2.5512082

63	H	H27	-2.7343525	-0.2638353	-2.6224604
64	H	H28	-4.2564769	0.2256564	-3.3798056
65	C	C33	-0.4000269	-2.2729211	0.1305616
66	C	C34	-3.0095343	-4.0682988	0.2636721
67	S	S3	1.2593084	-1.6631760	0.0792074
68	S	S4	-4.2202577	-5.3453869	0.3539778
69	C	C37	-5.0428859	-2.9130706	0.2154063
70	C	C38	-5.5118697	-4.1898320	0.2974496
71	H	H30	-5.6935374	-2.0471161	0.1703247
72	H	H31	-6.5406249	-4.5247962	0.3279983

IV-Mes

	Atom		X	Y	Z
1	C	C2	1.6894923	-1.3532606	-0.0000605
2	C	C3	3.0782230	-1.5831923	-0.0004951
3	C	C5	4.1883460	-0.6899948	0.0005018
4	H	H2	5.1698008	-1.1580762	0.0000166
5	C	C6	4.1905112	0.6771086	0.0022002
6	H	H5	5.1733896	1.1421649	0.0030784
7	C	C7	3.0831976	1.5737326	0.0030264
8	C	C8	1.6937526	1.3480262	0.0022754
9	C	C11	-0.6370833	0.0010013	-0.0007004
10	C	C12	-3.4734284	0.0103458	-0.0040661
11	C	C13	-1.3570520	0.0026536	1.2124316
12	C	C14	-1.3527521	0.0065511	-1.2139885
13	C	C15	-2.7513836	0.0122252	-1.1990481
14	C	C16	-2.7537153	0.0084855	1.1945847
15	H	H7	-3.2900499	0.0197765	-2.1455685
16	H	H10	-3.2943713	0.0133717	2.1402822
17	C	C17	-0.6176450	0.0101520	-2.5376213
18	H	H4	0.0277074	0.8930481	-2.6365140
19	H	H12	-1.3144790	0.0142412	-3.3822972
20	H	H13	0.0246058	-0.8742987	-2.6426019
21	C	C18	-4.9847072	-0.0082289	-0.0015557
22	H	H11	-5.3744611	-1.0065537	0.2402672
23	H	H14	-5.3898481	0.2721056	-0.9797882
24	H	H15	-5.3944098	0.6843505	0.7433831
25	C	C19	-0.6233956	0.0022552	2.5368157
26	H	H1	-1.3209770	0.0028242	3.3808722
27	H	H16	0.0211513	0.8853626	2.6391408
28	H	H17	0.0196214	-0.8819552	2.6390827
29	B	B1	0.9404840	-0.0014465	0.0013673
30	N	N1	0.9365744	-2.5261072	-0.0008954
31	N	N2	0.9444200	2.5231010	0.0032441
32	C	C1	1.6733029	-3.5878062	-0.0028709
33	H	H3	1.2817543	-4.5996390	-0.0039951

34	C	C4	1.6843460	3.5825674	0.0040424
35	H	H9	1.2958032	4.5955660	0.0045475
36	S	S1	3.4116481	3.3003462	0.0047955
37	S	S2	3.4016268	-3.3108036	-0.0038889

V-Mes

	Atom		X	Y	Z
1	S	S1	-0.7559931	-2.8487709	-0.0036038
2	C	C1	-2.2742304	-3.6962134	-0.0059343
3	C	C2	-1.6218618	-1.3218357	-0.0019373
4	C	C3	-2.9997466	-1.6082319	-0.0031356
5	C	C5	-4.0967017	-0.6871557	-0.0024123
6	H	H2	-5.0638511	-1.1820905	-0.0034019
7	C	C6	-4.0986278	0.6762061	-0.0009313
8	H	H5	-5.0671739	1.1684035	-0.0008122
9	C	C7	-3.0042582	1.6003440	0.0008405
10	C	C8	-1.6255985	1.3177150	0.0009393
11	S	S2	-0.7638834	2.8469784	0.0038107
12	C	C9	-2.2844183	3.6902583	0.0044270
13	C	C11	0.7310375	0.0013588	0.0012697
14	C	C12	3.5689575	0.0107621	0.0040733
15	C	C13	1.4530100	0.0075520	-1.2156230
16	C	C14	1.4493492	0.0020750	1.2180222
17	C	C15	2.8481856	0.0080456	1.2000819
18	C	C16	2.8498901	0.0134141	-1.1952546
19	H	H7	3.3881913	0.0123314	2.1453614
20	H	H10	3.3916089	0.0216076	-2.1398427
21	C	C17	0.7219014	-0.0002375	2.5473934
22	H	H4	0.0736666	0.8783076	2.6574770
23	H	H12	1.4267625	0.0021698	3.3846855
24	H	H13	0.0802212	-0.8836547	2.6571093
25	C	C18	5.0797840	-0.0075593	0.0004997
26	H	H11	5.4664028	-1.0052264	-0.2477196
27	H	H14	5.4861520	0.2667418	0.9795770
28	H	H15	5.4878710	0.6883110	-0.7418150
29	C	C19	0.7264800	0.0106382	-2.5454426
30	H	H1	1.4317437	0.0187672	-3.3823562
31	H	H16	0.0764533	0.8883875	-2.6511021
32	H	H17	0.0866005	-0.8735001	-2.6599686
33	H	H32	-2.3199635	4.7748955	0.0060325
34	H	H40	-2.3068169	-4.7809431	-0.0075606
35	B	B1	-0.8532807	-0.0010167	-0.0002256
36	N	N1	-3.3480299	2.9464278	0.0027807
37	N	N2	-3.3398333	-2.9552623	-0.0053020

intended to be blank.

Curriculum Vitae

David Robert Levine was born in New Hyde Park, New York on March 21st, 1980. He attended Vassar College in Poughkeepsie, New York for undergraduate studies, where he majored in chemistry and conducted research with Professor Christopher J. Smart on the synthesis and characterization of fullerene – transition metal complexes. He also served as a laboratory intern, assisting in the instruction and administration of organic chemistry laboratory classes. After graduating in the spring of 2002, David took a position as an engineering aide in the research and development division at the Pall Corporation in Port Washington, New York, where he worked on the chemical surface modification of fluorinated polymer membranes for applications in the microelectronics industry. In the fall of 2008 he returned to academia to pursue his graduate degree in chemistry at the Johns Hopkins University, joining the research group of Professor John D. Tovar. His doctoral research focused on the design, synthesis, and characterization of novel polycyclic aromatic compounds featuring formally Hückel-aromatic borepin rings as electron-deficient, stimuli-responsive π-conjugated materials. While at Johns Hopkins, he served as a graduate teaching assistant from 2008 to 2013, covering lecture courses in introductory and advanced organic chemistry, spectroscopic methods of organic structure determination, and intermediate organic chemistry laboratory.

DAVID R. LEVINE

300-A E. University Parkway, C-2, Baltimore, MD, 21218 • (516) 319-6749 • dlevin17@jhu.edu

RESEARCH INTERESTS

Synthetic and physical organic chemistry, organic electronic materials, molecular machines, supramolecular chemistry, chemical sensors, catalysis, aromaticity

EDUCATION AND RESEARCH EXPERIENCE

The Johns Hopkins University, Baltimore, MD
Ph. D., Chemistry **2016**
M.A., Chemistry **2012**
Research advisor: Prof. John D. Tovar
Design, synthesis, and characterization of novel boron-containing π-conjugated organic materials

Pall Corporation, Port Washington, NY
Research and Development - Engineering Aide **2003 – 2007**
Chemical surface modification and performance testing of fluorinated polymer membrane materials for use in the microelectronics industry

Vassar College, Poughkeepsie, NY
B.A., Chemistry **2002**
Research Advisor: Prof. Christopher J. Smart
Synthesis of fullerene – transition metal complexes

PUBLICATIONS

Original Research:

Levine, D. R.; Tovar, J. D. "Unsymmetrical dithienoborepins: perturbations of conjugation and aromaticity *en route* to property tuning in boron-containing polycyclic aromatics". In preparation.

Levine, D. R.; Siegler, M. A.; Tovar, J. D. "Thiophene-fused borepins as directly functionalizable boron-containing π-electron systems". *J. Am. Chem. Soc.,* **2014**, *136*, 7132-7139
(Highlighted in *Synfacts:* Swager, T. M.; Zhao, Y. *Synfacts* **2014**, *10*, 698.)

Levine, D. R.; Caruso Jr., A.; Siegler, M. A.; Tovar, J. D. "*Meta-B*-Entacenes: new polycyclic aromatics incorporating two fused borepin rings." *Chem. Commun.,* **2012**, *48*, 6256-6258 (part of a special web-themed issue on aromaticity)

Book Chapters:

Levine, D. R.; Tovar, J. D. "Boron-containing polycyclic aromatics". In *Polycyclic Arenes and Heteroarenes: Synthesis, Properties, and Applications;* Miao, Q., Ed. Wiley – VCH, 2015; pp 251–276.

PRESENTATIONS

"Development of synthetically versatile, tunable, polycyclic π-electron systems based on formally aromatic borepin rings." Oral presentation and poster presentation, *15th Boron in the Americas conference (BORAM XV)*, Newark, NJ. June 15 – 19, 2014

"Synthetically versatile polycyclic π-electron systems based upon formally aromatic borepin cores." Poster presentation, *15th International Symposium on Novel Aromatic Compounds (ISNA-15)*, Taipei, Taiwan. July 28 – August 2, 2013

"Synthetically versatile, tunable π-electron systems based on formally aromatic borepin rings." Oral presentation and poster presentation, *Gordon Research Seminar / Gordon Research Conference – Physical Organic Chemistry*, Holderness, NH. June 22 – 28, 2013

HONORS AND AWARDS

Sarah and Adolph Roseman Achievement Award (outstanding accomplishment in graduate chemistry research) – *Johns Hopkins University*, 2015

First prize, outstanding short oral presentation – *15th Boron in the Americas conference*, 2014

Best poster award - *15th International Symposium on Novel Aromatic Compounds*, 2013

Outstanding poster award / invited oral presentation - *Gordon Research Conference: Physical Organic Chemistry*, 2013

TECHNICAL AND RESEARCH PROFICIENCY

Synthetic organic chemistry

- Rational design of organic/ organo-main group materials with targeted properties
- Extensive experience in retrosynthetic planning and execution of multistep organic syntheses, including standard organic purification methods
- Expertise in air-free Schlenk line techniques
- Expertise in employing a variety of classical (e.g. carbonyl olefinations, metalation chemistry) and modern methods (e.g. - transition metal catalyzed cross-couplings, direct arylations) for the construction and functionalization of complex π-conjugated and heteroaromatic systems.

Characterization/Instrumentation methods

- 1-D NMR (^{1}H, ^{11}B, ^{13}C) and 2-D correlation spectroscopy (COSY, NOESY, HSQC)
- UV-Vis and photoluminescence spectroscopy (steady state and time resolved)
- Electrochemical characterization (cyclic voltammetry)
- Theoretical calculations (DFT, TD-DFT)
- Mass spectrometry (MALDI-TOF)
- HPLC, GPC
- Analysis of X-ray structural data (single crystal)

Software

- Computational/ chemical modeling software (Spartan, Gaussian, Mercury)
- Apple iWorks (Keynote, Pages) and Microsoft Office (Word, Excel, Powerpoint)
- Graphing software (Kaleidagraph)

Mentorship

- Training of several graduate and undergraduate level lab members

TEACHING EXPERIENCE

The Johns Hopkins University, Baltimore, MD

Teaching Assistant **2008-2013**

Development of instructional material and teaching/administration of undergraduate and graduate courses

Courses: Introductory Organic Chemistry I / II, Advanced Mechanistic Organic Chemistry II, Spectroscopic Methods of Organic Structure Determination, Intermediate Organic Chemistry Laboratory

Vassar College, Poughkeepsie, NY

Laboratory Intern **2000-2001**

Assisted in the instruction and administration of Introductory Organic Chemistry Laboratory courses